NASA-CR-189744
19920010064

1991 RESEARCH REPORTS

NASA/ASEE SUMMER FACULTY FELLOWSHIP PROGRAM

JOHN F. KENNEDY SPACE CENTER
AND
UNIVERSITY OF CENTRAL FLORIDA

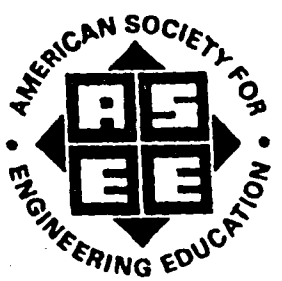

National Aeronautics and
Space Administration

1991 RESEARCH REPORTS

NASA/ASEE SUMMER FACULTY FELLOWSHIP PROGRAM

JOHN F. KENNEDY SPACE CENTER

UNIVERSITY OF CENTRAL FLORIDA

EDITORS:

Dr. E. Ramon Hosler
Professor of Engineering
University of Central Florida

Dr. Mark A. Beymer
Mr. Dennis W. Armstrong
Systems Training and Employee Development Branch
Kennedy Space Center

PREPARED FOR:

John F. Kennedy Space Center
Merritt Island, Florida

NASA Grant NGT-60002 Supplement: 6

Contractor Report No. CR-189744

November 1991

PREFACE

This document is a collection of technical reports on research conducted by the participants in the 1991 NASA/ASEE Summer Faculty Fellowship Program at Kennedy Space Center (KSC). This was the seventh year that a NASA/ASEE program has been conducted at KSC. The 1991 program was administered by the University of Central Florida in cooperation with KSC. The program was operated under the auspices of the American Society for Engineering Education (ASEE) with sponsorship and funding from the Office of Educational Affairs, NASA Headquarters, Washington, D.C. The KSC program was one of nine such Aeronautics and Space Research Programs funded by NASA Headquarters in 1991. The basic common objectives of the NASA/ASEE Summer Faculty Fellowship Program are:

a. To further the professional knowledge of qualified engineering and science faculty members;

b. To stimulate an exchange of ideas between participants and NASA;

c. To enrich and refresh the research and teaching activities of participants' institutions; and,

d. To contribute to the research objectives of the NASA centers.

The KSC Faculty Fellows spent ten weeks (June 3 through August 9, 1991) working with NASA scientists and engineers on research of mutual interest to the University faculty member and the NASA colleague. The editors of this document were responsible for selecting appropriately qualified faculty to address some of the many problems of current interest to NASA/KSC. A separate document reports on the administration aspects of the 1991 program. The NASA/ASEE program is intended to be a two-year program to allow in-depth research by the University faculty member. In most cases a faculty member has developed a close working relationship with a particular NASA group that has provided funding beyond the two-year limit.

TABLE OF CONTENTS

1991 NASA/ASEE SUMMER FACULTY FELLOWSHIP PROGRAM

JOHN F. KENNEDY SPACE CENTER
UNIVERSITY OF CENTRAL FLORIDA

DEVELOPMENT OF AN ACCELERATED TEST METHOD FOR THE DETERMINATION OF SUSCEPTIBILITY TO ATMOSPHERIC CORROSION

PREPARED BY:	John R. Ambrose, Ph.D., P.E.
ACADEMIC RANK:	Associate Professor
UNIVERSITY AND DEPARTMENT:	University of Florida Department of Materials Science and Engineering
NASA/KSC	
DIVISION:	Materials Science Laboratory
BRANCH:	Failure Analysis and Materials Evaluation
NASA COLLEAGUE:	Coleman J. Bryan
DATE:	July 26, 1991
CONTRACT NUMBER:	University of Central Florida NASA-NGT-60002 Supplement: 6

ACKNOWLEDGEMENTS

I would like to express my appreciation for being selected to participate in the 1991 NASA/ASEE Summer Faculty Fellowship program, to Ray Hostler [University of Central Florida] and Mark Beymer [NASA] for their capable administration of the program, and to my NASA colleagues Cole Bryan and Rupert Lee for their assistance and encouragement. Special thanks must go to Jim Jones for his assistance in expediting the various chemical analyses which I requested and to Helein Hitchcock, Hae Soo Kim, Stan Young and Bill Carman for their capable technical assistance. And to Lee Underhill, without whose assistance in finding the various apparatus with which to set up my experiments I would never have even begun this project, I offer a nomination for the "Golden Scrounge" award.

And most of all, my gratitude to the Materials Testing Laboratory staff - to Steve McDanel, whose progress from a former student to a capable failure analyst makes this teacher proud, to Scott Murray for his patience and cooperation in allowing this curious child of 51 years to tag along, seeing things again for the first time, and most especially to Peter Marciniak, whose instruction and encouragement allowed me to find satisfaction in doing things undone for some 25 years. May Scott always find one last jelly doughnut each morning and Peter his film for "just one more".

...and to KSC and its surrounding Merritt Island Wildlife Refuge for being what and where they are. I can sincerely say that no summer has meant more to me or will mean more as time goes by. Even though endless summers must always end, thanks for the memories...

ABSTRACT

The theoretical rationale is presented for utilization of a repetitive cyclic current reversal voltammetric technique for characterization of localized corrosion processes, including atmospheric corrosion. Applicability of this proposed experimental protocol is applied to characterization of susceptibility to crevice and pitting corrosion, atmospheric corrosion and stress corrosion cracking. Criteria upon which relative susceptibility is based have been determined and tested using two iron-based alloys commonly in use at NASA/KSC - A36, a low carbon steel and 4130, a low alloy steel.

Practicality of the procedure has been demonstrated by measuring changes in anodic polarization behavior during high frequency current reversal cycles of 25 cycles per second with 1 mA/cm^2 current density amplitude in solutions containing Cl^{-1}. The results demonstrated that, due to excessive polarization which affects conductivity of barrier corrosion product layers, A36 was less resistant to atmospheric corrosion than its 4130 counterpart - behavior which has also been demonstrated during exposure tests.

SUMMARY

Based on an analysis of factors which are known to contribute to the overall corrosion process, galvanostatic electrochemical procedures show greater promise for creating an environment during accelerated testing which more closely simulates natural environments than do conventional potentiostatic methods. Similarly, since both anodic and cathodic reactions occur simultaneously on the surfaces of freely corroding metals, it is necessary to periodically reverse the direction of current flow. On the basis of these modelling simulation requirements, the Repetitive Current Reversal Voltammetry technique has been developed.

Using a galvanostat to supply current, and a storage oscilloscope to measure potential transients as a function of time, a methodology and associated predictive criteria have been generated using two representative alloys found in common use at NASA\KSC - A36 steel and 4130 low alloy steel. By trial and error, the optimum combination of impressed current amplitude and current reversal cycle frequency has been found which will differentiate environmental degradation behavior for these two metals - +/- 2 milliamperes current amplitude with a 25 cycles per second current reversal frequency.

Results to date suggest that susceptibility to various localized corrosion forms of attack may be associated with "over-polarization", that is, too high an electrical resistivity for insoluble corrosion product barrier layers which form at the metal/environment interface. In the presence of aggressive ions such as the chloride ion, these high potential drops or fields across the barrier layers "draws" these aggressive anions into the film, causes its decrease in resistivity and eventually leads to the inability of passivity being maintained.

This report summarizes many of the insights, opinions and perspectives of the author which may prove useful to others as they contemplate developing experimental procedures for the study of environmental degradation of materials.

TABLE of CONTENTS

LIST OF ILLUSTRATIONS

1.0 INTRODUCTION

The vast majority of electrochemical test methods used in corrosion science experimentation derive from potentiostatic polarization techniques - i.e. a measurement of current required to maintain the potential of a metal at some reference value. As the name implies, the electronic instrumentation fixes potential by regulation of current. As a consequence of this functionality, corrosion rates [current] vary with time as the externally maintained potential remains fixed [potentiostatic] or is varied [potentiodynamic sweep] during the course of the experiment.

A number of "accelerated" corrosion test procedures are based upon potentiostatic polarization procedures - linear current versus applied potential relationships or "polarization curves", low amplitude linear polarization for determination of "polarization resistance", low amplitude cyclic polarization or "AC impedance" and linear cyclic voltammetry or "LCV" to name but a few. Although a great deal of information has been obtained through such experimentation, some of it even useful, attempts to correlate long term corrosion behavior with the results of such procedures have often been fraught with inconsistencies, irreproducibilities and difficulties with interpretation. The problem, as I see it, is that the basis for these techniques - potential or polarization control - is not a suitable or accurate model for the way metals behave in "real life" situations. The true basis is, in fact, just the opposite.

When a metallic material is exposed to a corrosive environment, there develops, rather quickly, an electrochemical potential across the metal/environment interface which serves to drive those chemical reactions which contribute to that particular electrochemical potential. Corrosion processes consist of one or more anodic or oxidation reactions which, in a physical sense, carry current out from the surface of the metal and into the environment. Anodic current is balanced by a cathodic current of equal amplitude which flows into the metal from the environment, carried by one or more reduction reactions. The respective current flows produce, due to a electrical resistance which opposes the flow of current [polarization resistance], a shift in potential or polarization equal to the product of the current flow and the resistance through which that current flows. The resulting so-called "mixed" or corrosion potential of the material is positioned between the reversible potentials for the various electrochemical processes, the displacement being dependent upon the polarization resistance for the various contributing electrochemical reactions. Mathematical models of electrochemical kinetics [e.g. Butler-Volmer equation] have been used to characterize the relationship between current and applied potential, resulting in what have come to be known as "Evans Diagrams". A schematic representation of current flow across the metal/environment interface is shown in Figure 1.

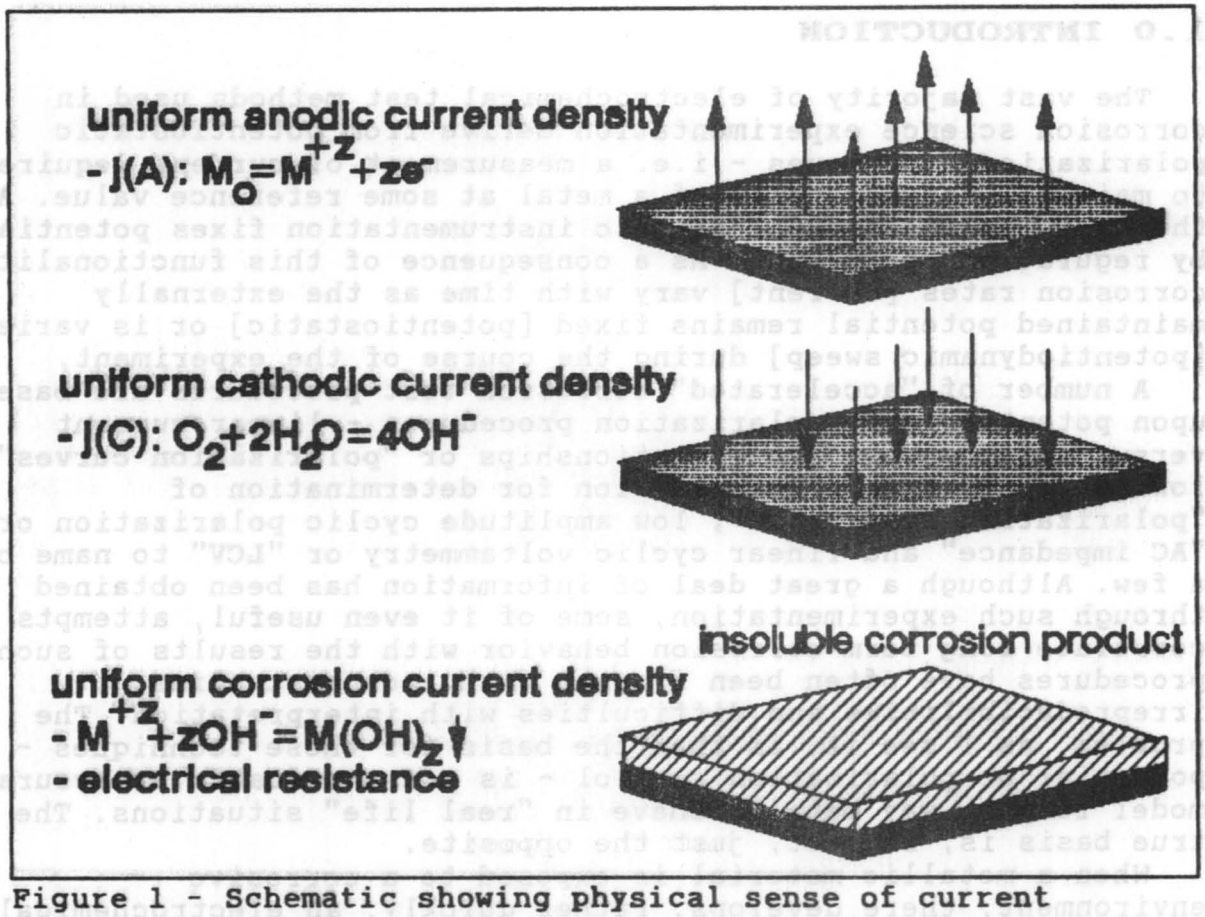

Figure 1 - Schematic showing physical sense of current direction - anodic current leaving metal and cathodic current entering it.

The point to be made is simply this: Since the corrosion potential of the material is determined by polarization, specifically polarizibility of the material as influenced by the contributing electrochemical reactions, then it is the flow of current which controls potential, not the other way around. Fixing or controlling the potential of the material will cause current flow to conform to the degree of polarization - if there is any change in resistance to current flow which occurs as a natural consequence of the chemical reactions taking place during service exposure, then current will change accordingly. One such occurrence, the evolution of insoluble reaction products which block the flow of current across the interface, is also shown in Figure 1. Under "natural", free corroding conditions, it would seem that development of insoluble corrosion products with whatever inherent intrinsic electrical and ionic transport resistivity they possess would cause the corrosion potential to shift in one direction or another with respect to a film-free metal/electrolyte interface. Since many metal oxides and hydroxides [iron based, e.g.] provide greater resistance to the anodic current flow [ion transport control], the corrosion

potential under natural conditions tends to shift toward more positive values. When experimental simulation of corrosion processes are under potentiostatic control, the potential, of course, is fixed. There are two consequences of this control. One, the corrosion current would not be expected to be the same as under natural control conditions, resulting in lack of correspondence with long term corrosion rates. Secondly, since the potential of the metal determines what electrochemical reactions can occur, differences in potential may result in altogether different reaction products being generated. Since it is the reactions products which determine the nature of insoluble reaction products, and it is the insoluble reaction products which affect both degree of polarization and amplitude of the corrosion current, the end result is most likely a continual divergence of experimental corrosion rates from the real ones.

A second negative characteristic associated with potentiostatic control of electrochemical processes derives from the configuration of the system used to control the process being studied. Under anodic polarization - when the potential of the material is driven to higher [more positive] values than its corrosion or steady-state value - the current which produces this polarization leaves the material [working electrode], flows through the electrolyte and enters a remote auxiliary [counter] electrode. In a freely corroding metal, on the other hand, current leaves and enters the same exposed surface, albeit not necessarily at the same point on that surface. What this means is that cathodic and anodic reactions do not occur concurrently on the same metal surface - more significantly, the reaction products of these electrochemical processes are not produced at a common surface. Since most insoluble corrosion products which form in aqueous environments contain metal cations, hydroxide ions and other constituent anions [SO_4^{-2}, Cl^{-1}, CO_3^{-2}, etc.], isolating anode from cathode in the electrochemical cell changes the localized chemistry associated with the natural or free corrosion process [Figure 2].

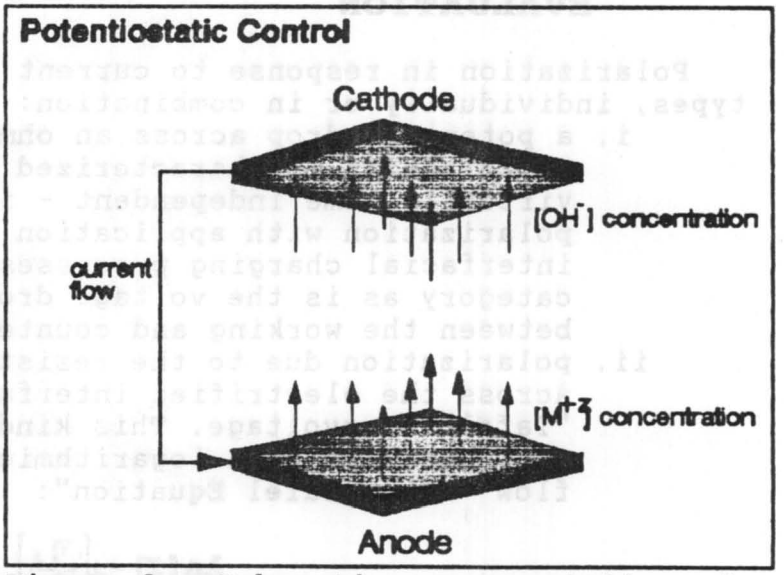

Figure 2 - Schematic representation of the separation of anode and cathode in an electrochemical cell utilizing potentiostatic control.

1.1 THEORETICAL BASIS for PROPOSED EXPERIMENTAL PROCEDURE

Measurement of degree of polarization which result from impressed current is not a new technique, having been used for some time as an analytical chemistry technique - chronopotentiometry, stripping voltammetry, etc. It has not been used to any great extent in corrosion science applications. It would seem, however, to be most appropriate in measuring the behavior of a material in response to flow of current across the metal/environment interface. By impressing a constant [galvanostatic] current between an inert electrode [platinum counter] and the material being characterized [working electrode], the potential change or polarization can be measured as a function both of time and of the amplitude of the impressed current. In order to simulate "natural" conditions, the current direction should be regularly reversed in order to develop concentrations of both kinds of reaction products at the metal interface - anodic and cathodic. Thus evolves the name of the technique - "CYCLIC CURRENT REVERSAL VOLTAMMETRY". The experimental variable to be measured will be the rate of change in material potential, or "polarization rate".

1.1.1 CRITERIA for CORROSION SUSCEPTIBILITY EVALUATION

Polarization in response to current flow can be of three types, individually or in combination:

i. a potential drop across an ohmic resistance. This polarization is characterized by a V=IR response, and is virtually time independent - i.e. instantaneous polarization with application of current. Capacitance or interfacial charging processes are included in this category as is the voltage drop across the electrolyte between the working and counter electrodes.

ii. polarization due to the resistance to charge transfer across the electrified interface - i.e. so-called "Tafel" overvoltage. This kind of polarization is characterized by a logarithmic dependence upon current flow - the "Tafel Equation":

$$\ln[I] = \pm\left[\frac{\eta_i}{\beta_i}\right]$$

where n_i = degree of polarization produced by current I
and β_i = charge transfer resistance.

iii. the potential drop across an insoluble reaction product or film which forms at the metal/electrolyte interface. The degree of polarization is a function of the resistivity of the reaction product, the polarization rate is a function of the nucleation/growth kinetics of the deposition process. It is this polarization process with which we will be most interested.

A schematic representation of the polarization extremes - polarization resistance during active metal dissolution versus IR resistance across an insoluble corrosion product - is shown in Figure 3.

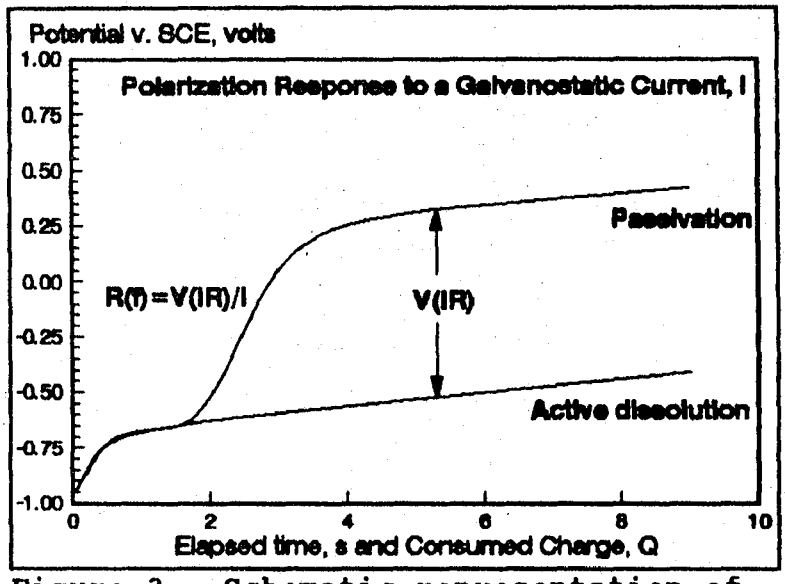

Figure 3 - Schematic representation of limiting cases in polarization behavior - metal dissolution v. insoluble corrosion product.

Under conditions of repetitive current reversal, any change in either degree or in rate of polarization signifies changes in the one of the three processes enumerated above. Of the three, only the third should provide any significant contribution. Thus, by evaluating such changes, we should be able to establish criteria for evaluating the environmental stability of a particular material in a given environment.

As "protective" films grow on bare or air-formed film covered metal substrates, there should be a regular increase in degree of polarization with each consecutive anodic cycle. Furthermore, the degree of polarization should progressively decrease as well, if the protective film is becoming more and more protective. Any change in this trend will be interpreted as an indication of development of instability in the system - a loss in ability of the system to resist the corrosive actions of the environment.

1.1.2 EXAMPLES of HOW CRITERIA ARE APPLIED

NASA/KSC is interested in predictive capability with respect to a large number of environmental degradation of materials problems. Specifically, accelerated test methods for predicting long term resistance of coated and uncoated metals to atmospheric

corrosion are needed for rapid, early screening of candidate materials. Susceptibility to crevice corrosion, pitting and stress corrosion cracking - all localized forms of corrosion attack - is another area to which this approach can be applied in developing accelerated test methodology.

1.1.2.1 ATMOSPHERIC CORROSION

Atmospheric corrosion can occur in two forms - at elevated temperatures by direct reaction between material and corrosive gasses, and through electrochemical means by interaction between material and condensed aqueous liquid films. KSC is considered one of the most, if not the most, severe locations for atmospheric corrosion in the world. This is due to its proximity to the ocean and to the corrosive nature of combustion products from Space Shuttle solid fuel rocket boosters [SRBs].

During atmospheric corrosion under condensed moisture films, the actual corrosion process naturally takes place only when the film is present upon the surface - long term exposure testing as, for instance, is performed at NASA-KSC's seaside test site, provides an integrated measure of atmospheric corrosion behavior under those conditions where condensation is present. Ocean spray, rain, condensation of dew, etc. provide the natural environment. The process of condensation and evaporation actually increases the severity of the attack over what it would be under constant exposure conditions - and, as such, provides a clue as to an appropriate acceleration procedure.

As Figure 4 demonstrates, although initial, as-condensed electrolyte concentrations may fall below a critical level to initiate corrosive attack [$<5x10^{-3}$M Cl^{-1} for carbon steels, e.g.], a critical level can be achieved during evaporation. During test site exposures, this condition is only reached during some fraction of the total exposure times. Rainwater and dew condensation tend to return the process back to square one.

It is therefore proposed that one possible acceleration test would be to increase chloride [or any other aggressive species] by aliquot additions to a stock solution while the metal undergoes repetitive current reversal voltammetry. The time or number of cycles to a point where polarization behavior is affected would be a criteria for comparison of material susceptibility.

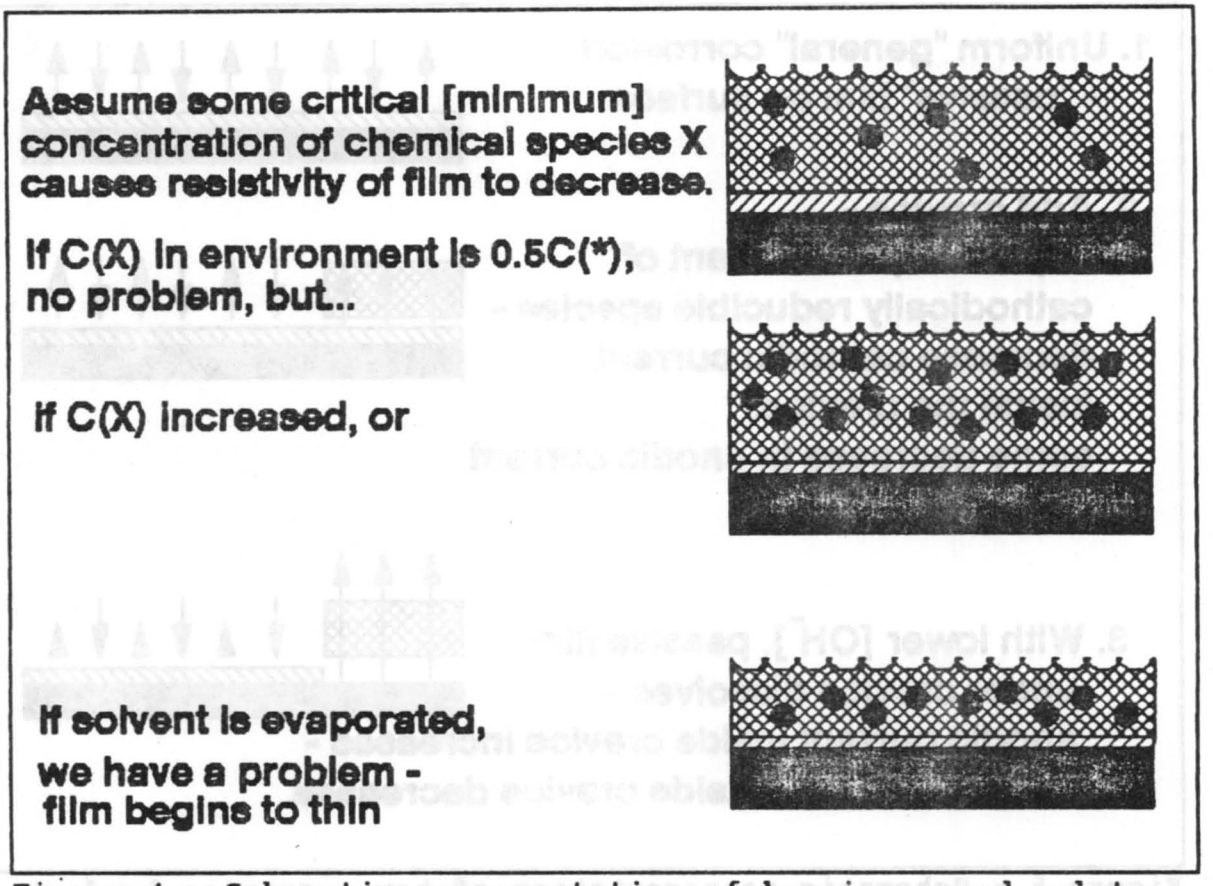

Figure 4 - Schematic representation of how increased solute concentrations can be used to simulate evaporation of condensed moisture layers.

1.1.2.2 CREVICE CORROSION

Metals with the capacity to passivate themselves with barrier surface films [aluminum, stainless steels, nickel and titanium alloys] require a finite hydroxide ion concentration [from the cathodic reduction of oxygen] to retain their passivity. Occluding any area of a passive metal surface - with a crevice, for example, restricts oxygen transport to the creviced area, and leads to breakdown of passivity and active corrosion [Figure 5]. Degree of susceptibility of a material to this form of localized corrosion might also be rapidly characterized by an accelerated test combining Repetitive Current Reversal Voltammetry [RCRV] with oxygen depletion from the electrolyte.

It is proposed that an accelerated method for determination of susceptibility to crevice corrosion would involve the effect of oxygen depletion on RCRV while deaerating the electrolyte.

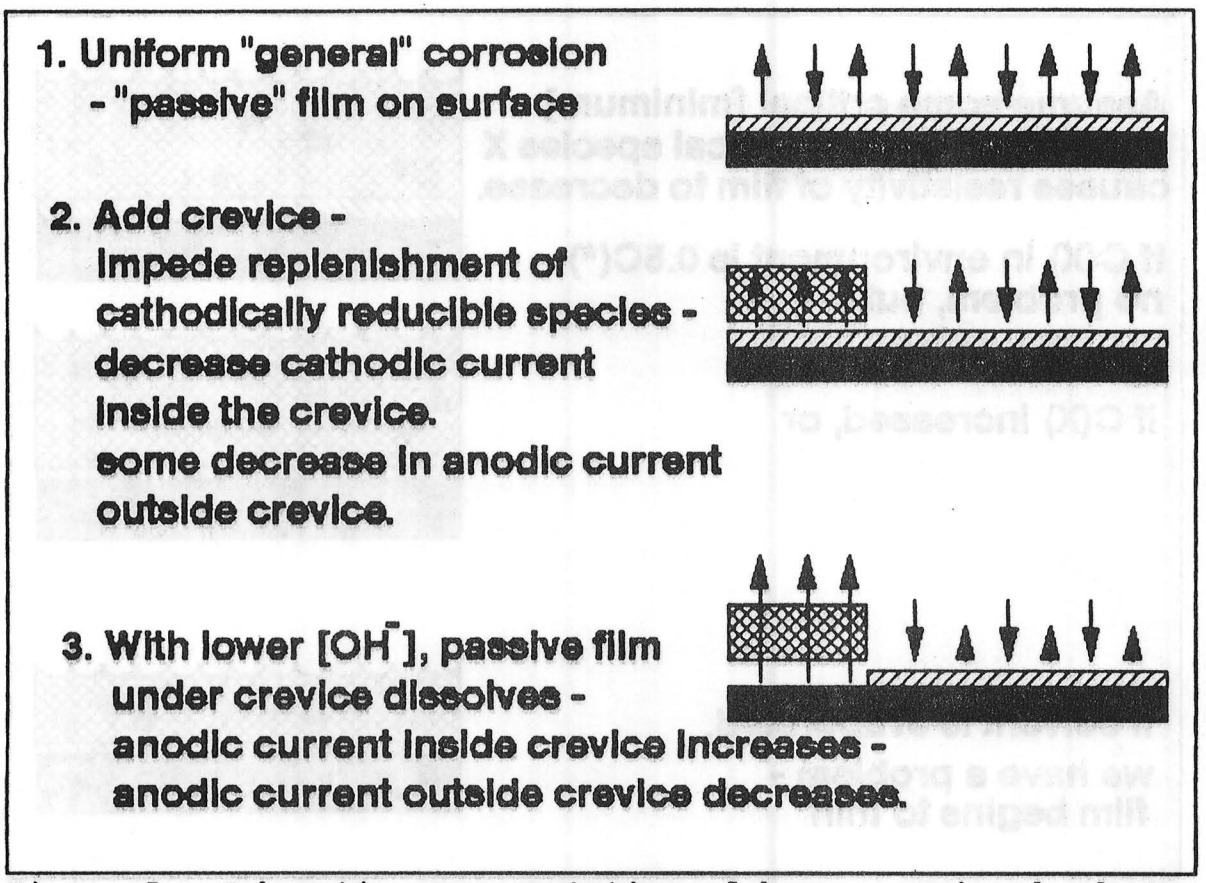

Figure 5 - Schematic representation of how a crevice leads to localized breakdown of passivity.

1.2 PROPOSED EXPERIMENTAL PROTOCOL

a. Reversal frequency and current amplitude experimental operational variables.
b. Determination of the effect of oxygen depletion on RCRV kinetics.
c. Determination of the effect of increased chloride ion concentration on RCRV kinetics.
d. Comparison of RCRV kinetics for two different materials for the purposes of distinguishing behavior - procedural feasibility determination.
e. Determination of effects of other atmospheric contaminants on RCRV kinetics.
f. Development of a "standard" test medium composition and methodology for characterization of atmospheric corrosion resistance.

2.0 EXPERIMENTAL - MATERIALS and EQUIPMENT

Feasibility studies were performed using two relatively common ferrous-based alloys in use at NASA/KSC - A36 [basically a carbon steel] and 4130 [a low alloy steel]. Their compositions are given in Table I.

Based upon these compositions, the A36 alloy would be expected to show the lesser degree of resistance toward atmospheric corrosion attack.

Table I - Elemental Compositions of Iron Alloys Selected for this Study.

A36:	0.29 C(max), 0.8-1.20 Mn, 0.20Cu
4130:	0.28-0.33 C, 0.40-0.60 Mn, 0.15-0.30 Si, 0.8-1.10 Cr, 0.15-.25 Mo

Specimens of the two materials were machined into rectangular configurations, then assembled into the electrode configuration shown in Figure 6. This particular assembly configuration was selected for a number of reasons - immersion of the tip end of the assembly beneath the electrolyte precludes the need for isolation coating and their inherent tendency of providing crevices for crevice corrosion attack; multiple material

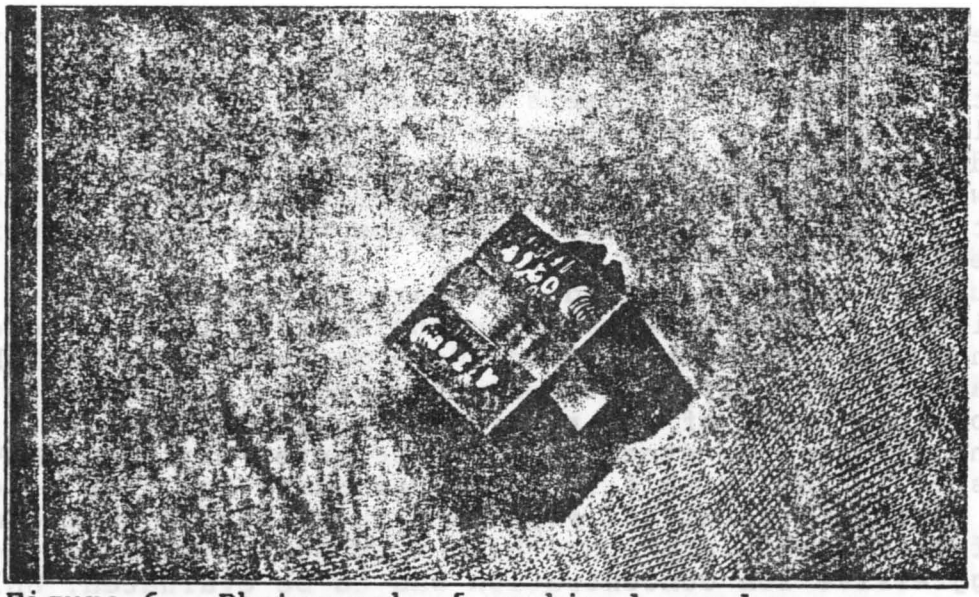

Figure 6 - Photograph of machined samples assembled into the bi-specimen electrode configuration.

experimental runs can be made consecutively in the same

electrolyte without concern for changing, cleaning and repositioning electrodes between experiments.

The electrochemical cell used in these studies was designed and constructed prior to my arrival at KSC - it is shown in Figure 7. It features, in addition to conventional items

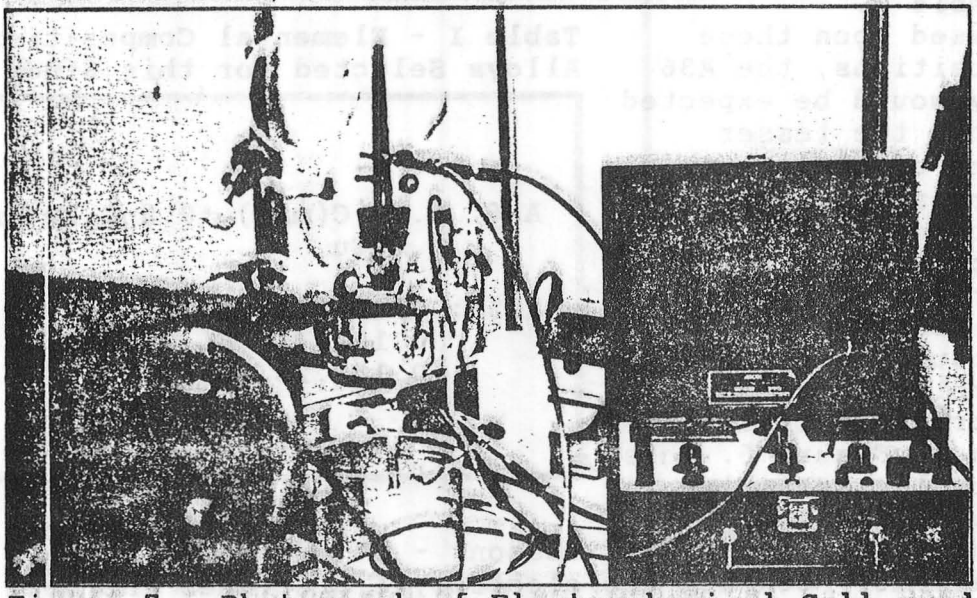

Figure 7 - Photograph of Electrochemical Cell used in these studies.

[reference electrode well/luggin capillary, isolated counter electrode well, working electrode access and gas dispersion tube input], two separate vessels for addition of test solutions.

Electrochemical measurements were obtained using a Tacussel BiPad potentiostat/galvanostat coupled with a signal generator. The waveform selected for these experiments was a square wave function in which the input variables were current amplitude and cycle frequency [Figure 8].

Current amplitudes used here were as high as +/- 2 milliamperes with reversal frequencies from 10 milliseconds to 10 seconds. Polarization kinetics were measured using a Tektronics storage oscilloscope. Data was obtained by analysis of photographs taken of the retained screen image.

The standard or stock solution selected was 0.1M KH_2PO_4 adjusted to pH=7 with 0.1M NaOH. The basis for this selection was that phosphate solutions represent in innocuous environment insofar as steels are concerned. 0.1M NaCl was added when effect of aggressive ion concentration was to be evaluated. Unless otherwise noted, all solutions used were air-saturated and stagnant.

Prior to running any experiment, specimens were mechanically polished using 100 grit silicon carbide paper, rinsed with distilled water, then dried with absolute ethanol rinse and a blast of warm air before assembling the electrode and placing the

assembly in the electrochemical cell. Solution was added from one of the reservoirs to a level just above the bottom of the electrode assembly. Rest or corrosion potentials were recorded once they had reached some steady state value.

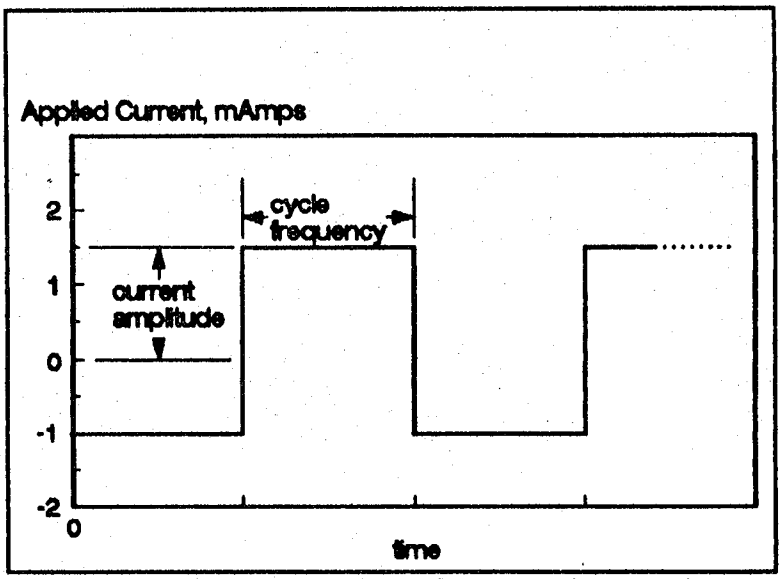

Figure 8 - Schematic of Experimental Procedure with respect to the RCRV control variables.

3.0 EXPERIMENTAL RESULTS and DISCUSSION

In Figure 9, for those who derive comfort from conventional polarization curves, appears a pair of polarization curves describing potentiostatic polarization behavior for A36 steel in air-saturated and deaerated [with N_2] KH_2PO_4 solution [pH 7]. The only feature of interest is the graphic demonstration of the ability of the A36 alloy to passivate in this solution, whether O_2 is present or not. Notice that the potentiostatic method requires a critical anodic current of better than 500 mA to achieve passivation at potentials around -600 mV v SCE. Also note that the critical current requirements are higher in the

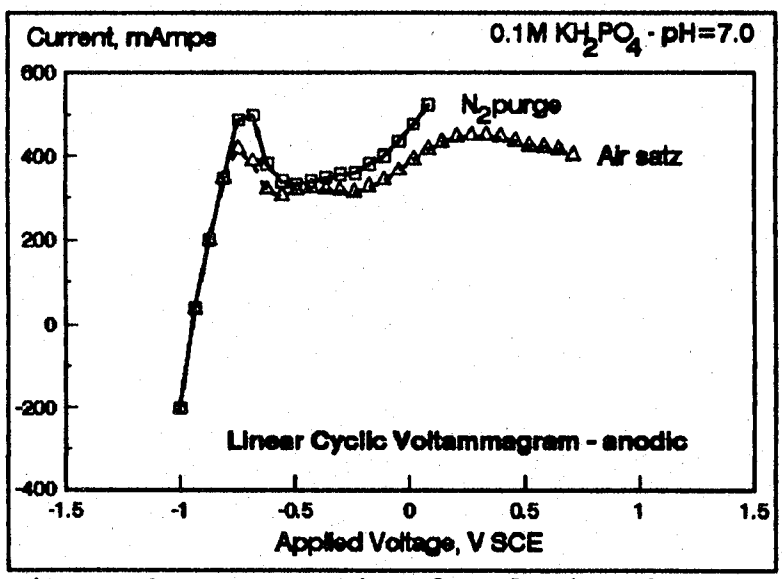

Figure 9 - Conventional Polarization Plot [I v. V] showing the Effects of Oxygen Depletion on Corrosion Kinetics of A36 Alloy.

deaerated solution.

When the same experiment is performed using the low frequency RCRV method, with a +/- 10 second frequency and a +/- 1.25 mA current amplitude, passivation is produced by the 5th cycle with one four hundredth [1/400] of the anodic current required for the potentiostatic polarization method [Figure 10].

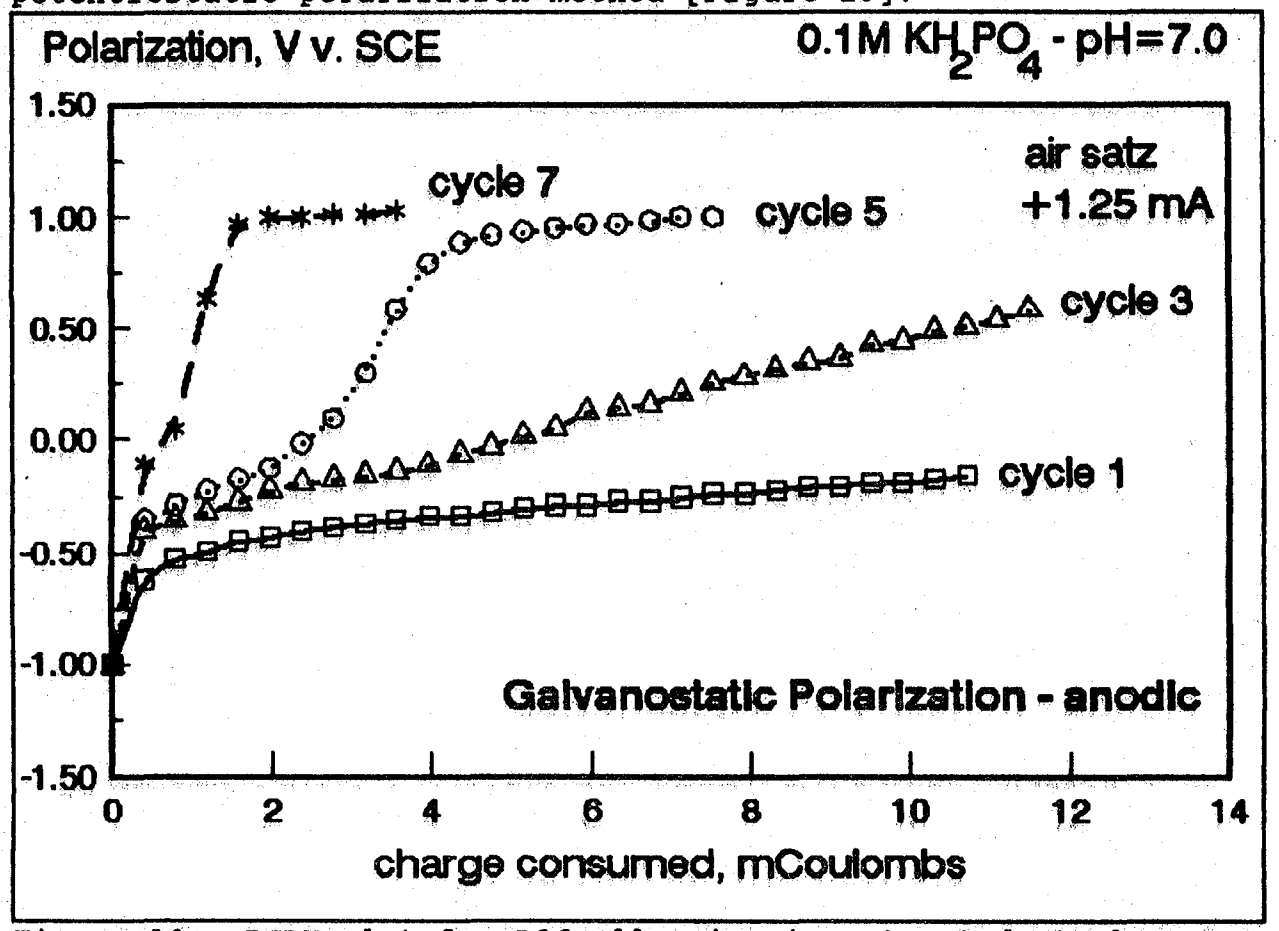

Figure 10 - RCRV plot for A36 alloy in air-saturated stock solution.

These results, as contained within Figures 9 and 10, serve to endorse my argument criticizing the reliance on potentiostatic polarization procedures for prediction of corrosion behavior. Their use, particularly in determining , from Tafel slope measurements, corrosion current densities are misleading to say the least.

RCRV measurements of the 4130 alloy in the stock solution using low frequency current reversals were similar to the results displayed in Figure 10, only the number of cycles to produce passivity were noticeably less - by the 2nd cycle. However, experimental results for both alloys in this stock solution were extremely irreproducable. The problem lies with the electrochemical history of the process. Length of time at open

circuit was of prime consideration - after passivation was achieved with either alloy, it became impossible to distinguish behavior between the two alloys. Specimen pretreatment prior to the experiments was also an influencing factor - surface preparation and finish would affect the results.

Addition of solutions containing chloride ion resulted in inability of both alloys to achieve passivation - the film resistance appeared, however, slightly greater for the 4130 alloy than for the A36. These results also were difficult to reproduce. The point is, unless a definitive criteria can be developed which is independent of operator procedure, the technique will never be applicable as a standard test method.

One problem with the electrochemical cell was that, with its present design, aliquots of solutions containing the aggressive species could not be rapidly mixed with the stock solution. This suggests a design change such that second solution aliquots be added through the gas dispersion valve circuit - in this way, solutions can be rapidly mixed during RCRV sequences.

3.1 HIGH FREQUENCY CURRENT REVERSAL CYCLING

Increasing the cycle frequency increases the stability of the system - at least with respect to reproducibility in measurement. In Figure 11 is plotted polarization kinetics for a single typical cycle when a ±10 mA amplitude current is impressed for 10 mS cycles. A number of relevant observations are worth noting - When forward and reverse current amplitudes are equal [current balanced], the median potential read from a slow response high impedance voltmeter is remarkably constant. So constant, in fact, this procedure might be considered as a standard test method for measurement of corrosion potentials. Changes in current amplitude results in a shift in median potential to higher or lower values, respectively.

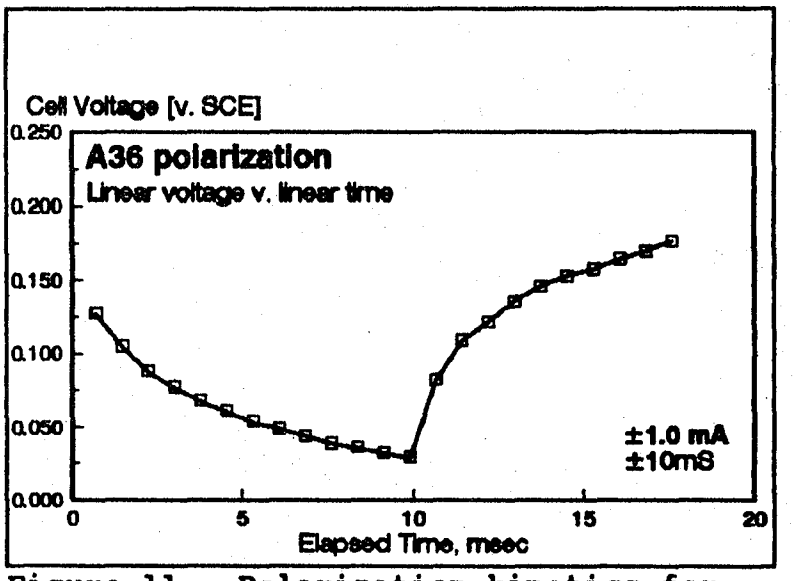

Figure 11 - Polarization kinetics for A36 alloy in the stock solution; experimental parameters shown on graph.

When current amplitudes are unbalanced, the median potential shifts in the direction of the current imbalance. This procedure should also be studied further in that the rate of polarization

shift appears to reflect the degree of control of the contributing anodic and cathodic electrochemical kinetics on the overall corrosion process.

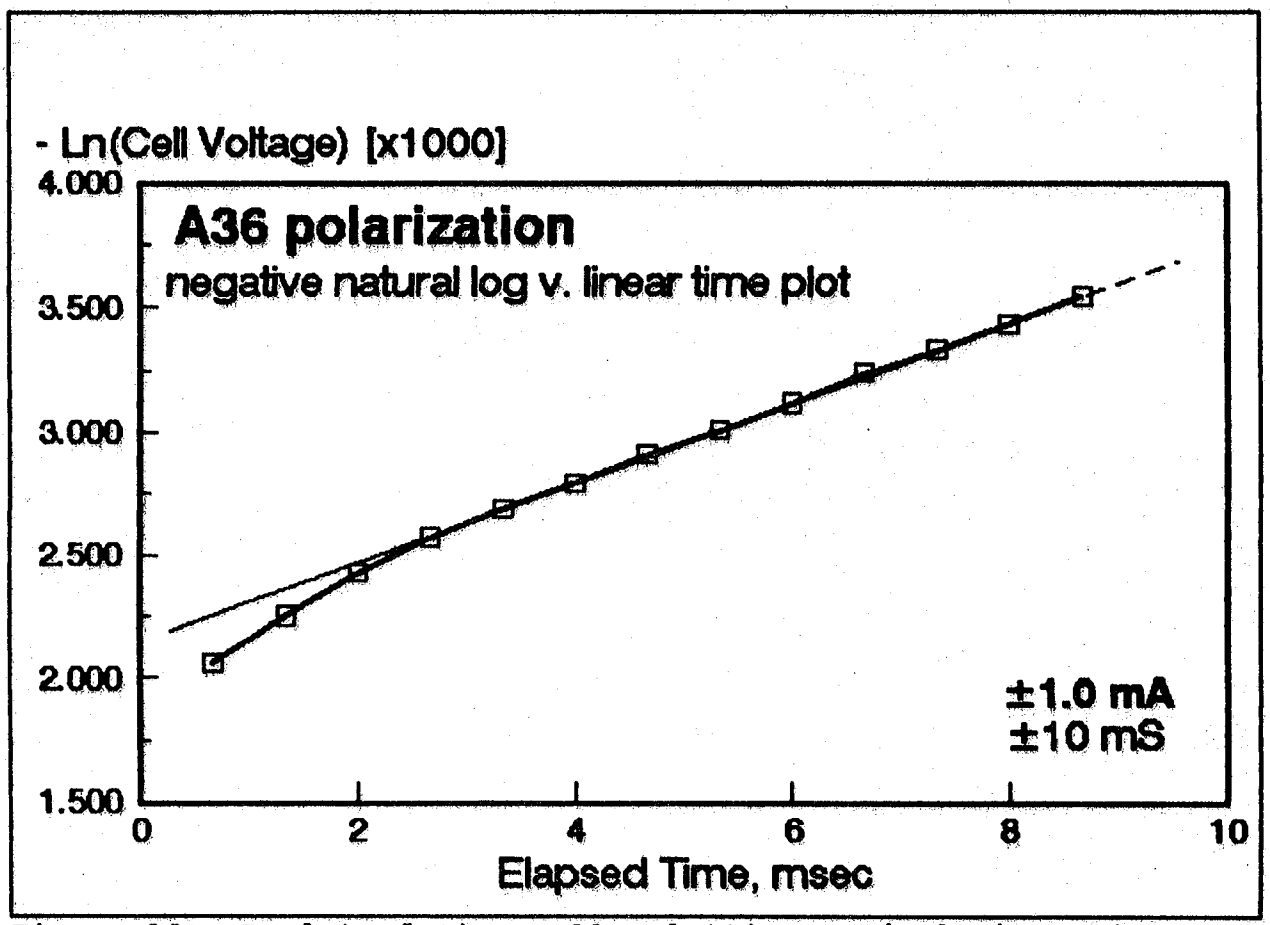

Figure 12 - Replot of Figure 11, plotting -Ln(volts) v. time.

Replotting the data of Figure 11 using the negative natural logarithm of the cell voltage, produces the graph shown in Figure 12. Only the anodic polarization portion of the overall cycle is shown. Although the plot is not a linear function of the plotting variables over the whole range, it fits the later portion of the cycle quite well. Neither an exponential or parabolic plot would do as well. Without drawing any conclusions as to the mechanistic implications to be derived from this, experimental results will be presented in this format, since it is easier to see variations when comparing different alloys and when chloride ion solutions are introduced into the stock solution.

3.2.1 POLARIZATION BEHAVIOR IN 0.1M KH_2PO_4

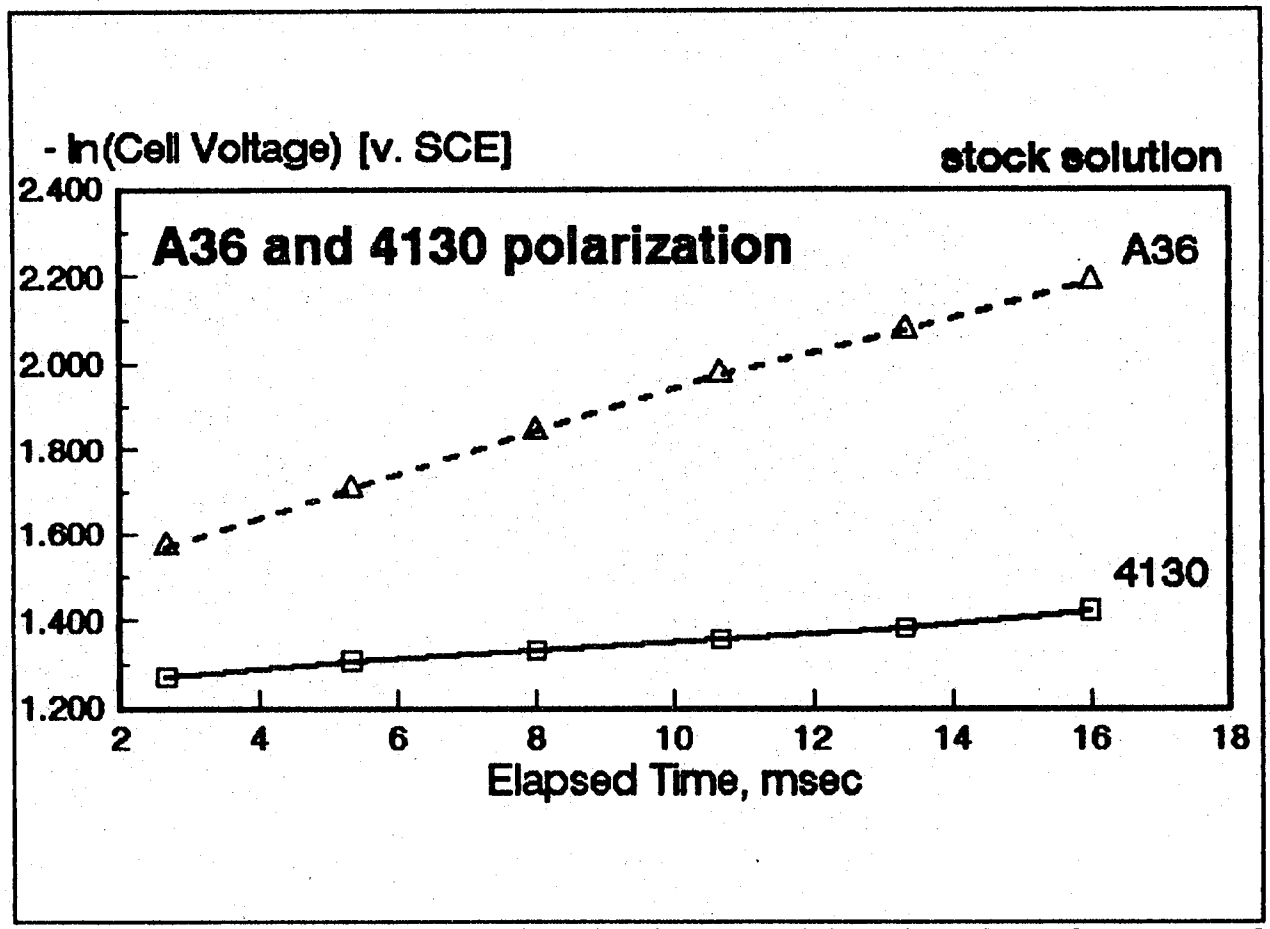

Figure 13 - A comparison of polarization kinetics for the A36 and 4130 alloy steels in the stock solution [0.1 KH_2PO_4, pH 7]. Current amplitude was ±2 mA, cycle reverse frequency was ±20 mS.

In Figure 13 are compared polarization kinetics for our two reference materials, the A36 carbon steel and the 4130 low alloy steel. The operational variables were selected by trial and error to produce the optimum conditions for producing the greatest difference in behavior between the two - 20 mS current reversal frequency with a 2 mA current amplitude. What is interesting to note is that the A36 alloy evidences a larger degree of polarization than does the 4130 steel. Remember, now, the 4130 is more resistant to atmospheric corrosion than the A36. Furthermore, the IR drop [film electrical resistance] is substantially greater for the A36 material. Intuitively, you might think that this is contradictory in terms of the known corrosion resistance of the low alloy steel. It must be emphasized that corrosion resistance lies not necessarily with electrical resistivity, but with passivity - with the resistance

to ion transport through the barrier layer. The proof of the pudding, so to speak, will lie with ability of a barrier layer to retain its ionic resistivity in the presence of aggressive or corrosive chemical species. Whatever, we can say at this point that polarization behavior of the A36 alloy is distinguished by a larger electrical resistance which, in the presence of impressed anodic currents, results in larger [more positive] degrees of polarization - larger electrical fields or potential drops across the barrier corrosion product layer.

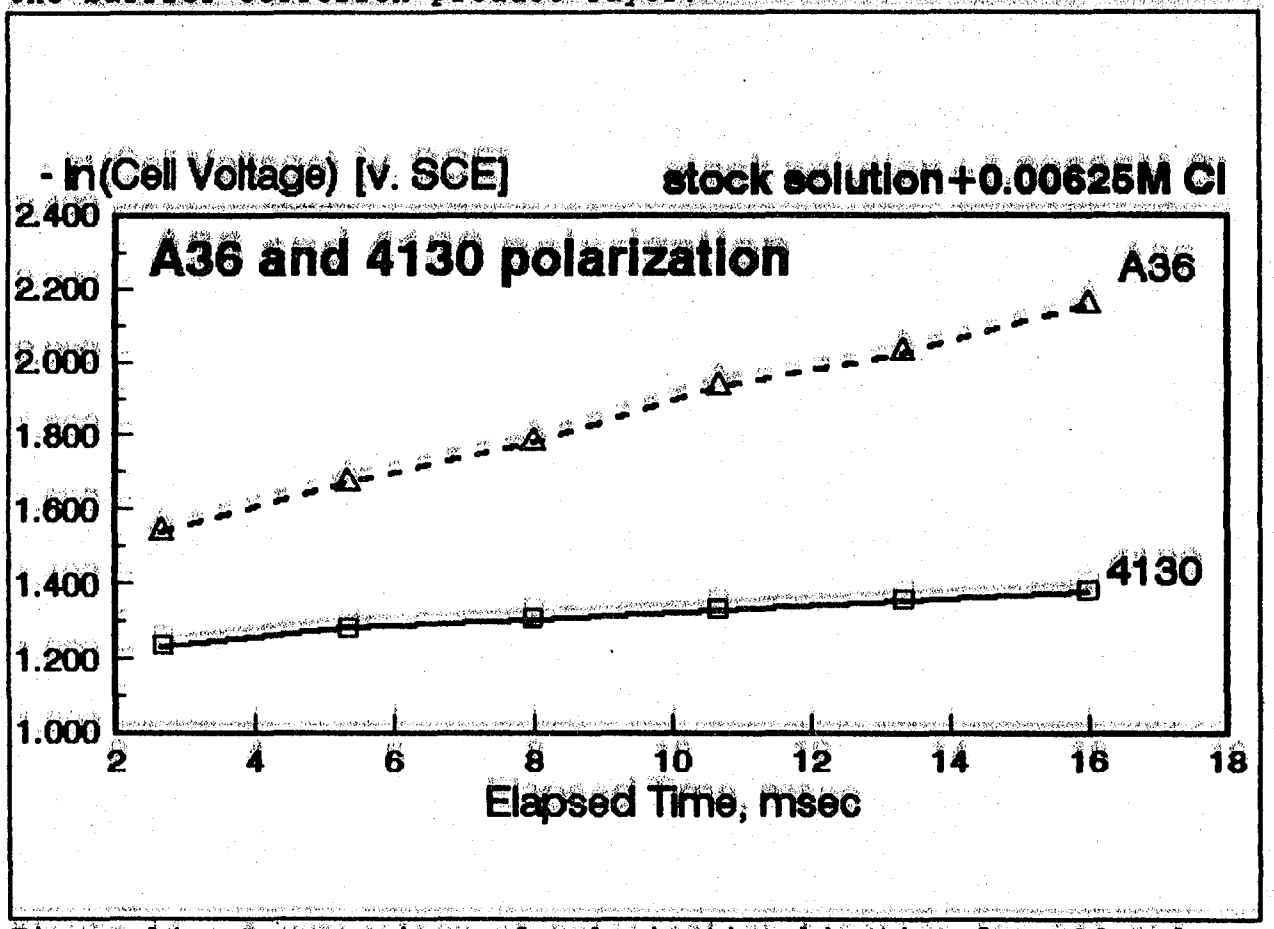

Figure 14 - A comparison of polarization kinetics for A36 and 4130 steels in the stock solution to which has been sufficient chloride ion to bring the overall Cl^{-1} concentration to 6.25×10^{-3} M.

Immediately upon addition of chloride ions, here producing a concentration in the stock solution of 6.25×10^{-3} M, just above the minimum concentration required to produce pitting in low carbon steels, there are changes in polarization behavior between the two metals. These results are shown in Figure 14. There is little apparent difference between polarization kinetics for the two materials. However, there are differences in polarization degree.

In order to better visualize what the differences are, the

data contained in Figures 13 and 14 are compared by replotting and comparing the polarization behavior of each alloy with, and without, chloride ions being present.

Notice that there is little change in the kinetics of polarization, but a noticeable decrease in the IR drop across the film - the film has become more electrically conductive [Figure 15]. Similarly, when the behavior of the 4130 alloy is compared in stock and chloride containing solution, there is also a decrease in IR drop across the corrosion product, but the relative amount of the decrease is far less [Figure 16].

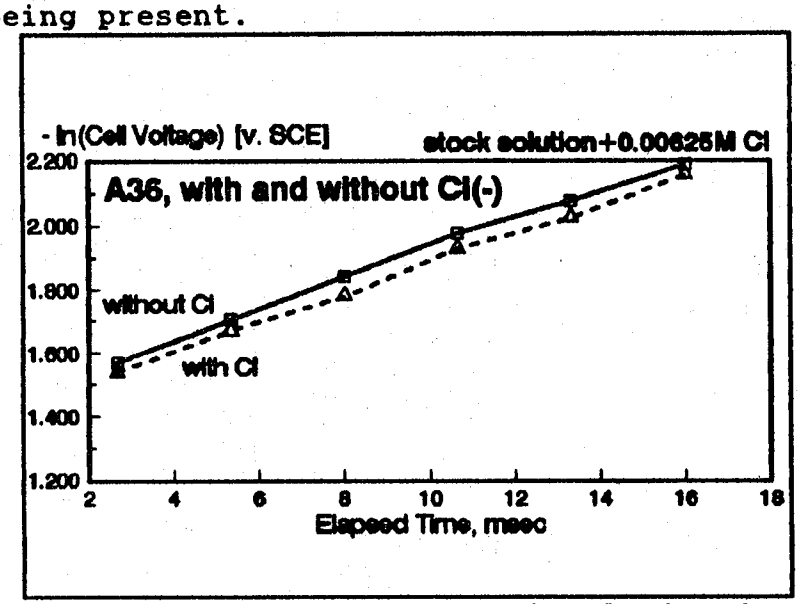

Figure 15 - A comparison of polarization behavior for A36 with, and without, chloride ions being present [from Figures 13 and 14].

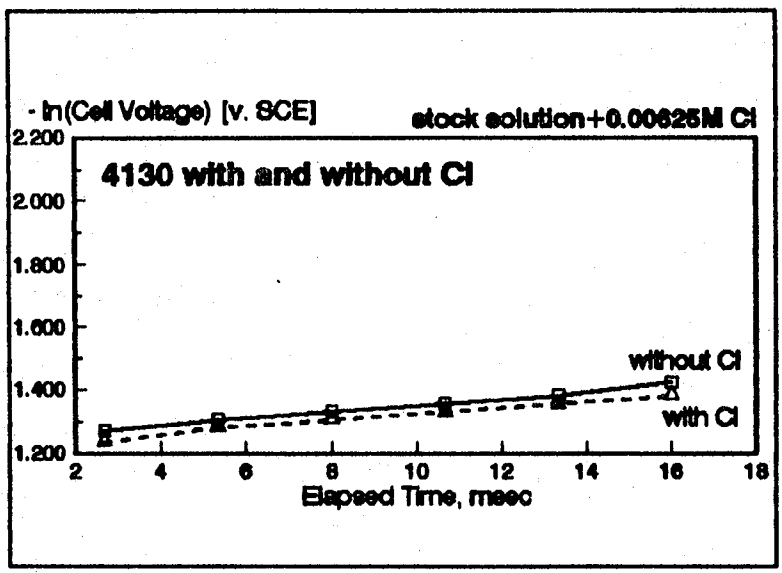

Figure 16 - Polarization behavior of 4130 with and without Cl^{-1}.

There is little other than speculation as to the interpretation of this behavior. The fact that the degree of polarization is so much greater for the A36 alloy indicates that there is a greater driving force for migration of negatively charged anionic species into the film toward the metal/film interface. This, by itself, does not necessarily result in increased electronic conductance - unless, the chloride ion somehow leads to the production of electronic charge carriers within the corrosion product. Perhaps, just perhaps, chloride ions within the corrosion product lead to an increased concentration of negative charge carriers, increasing the n-type extrinsic semiconductivity

of the barrier layer.

Whatever the explanation, within a few minutes, the IR drop decrease trend continues, until, after 5 minutes, the A36 has completely lost its capacity for producing a electrically resistive barrier layer completely [Figure 17].

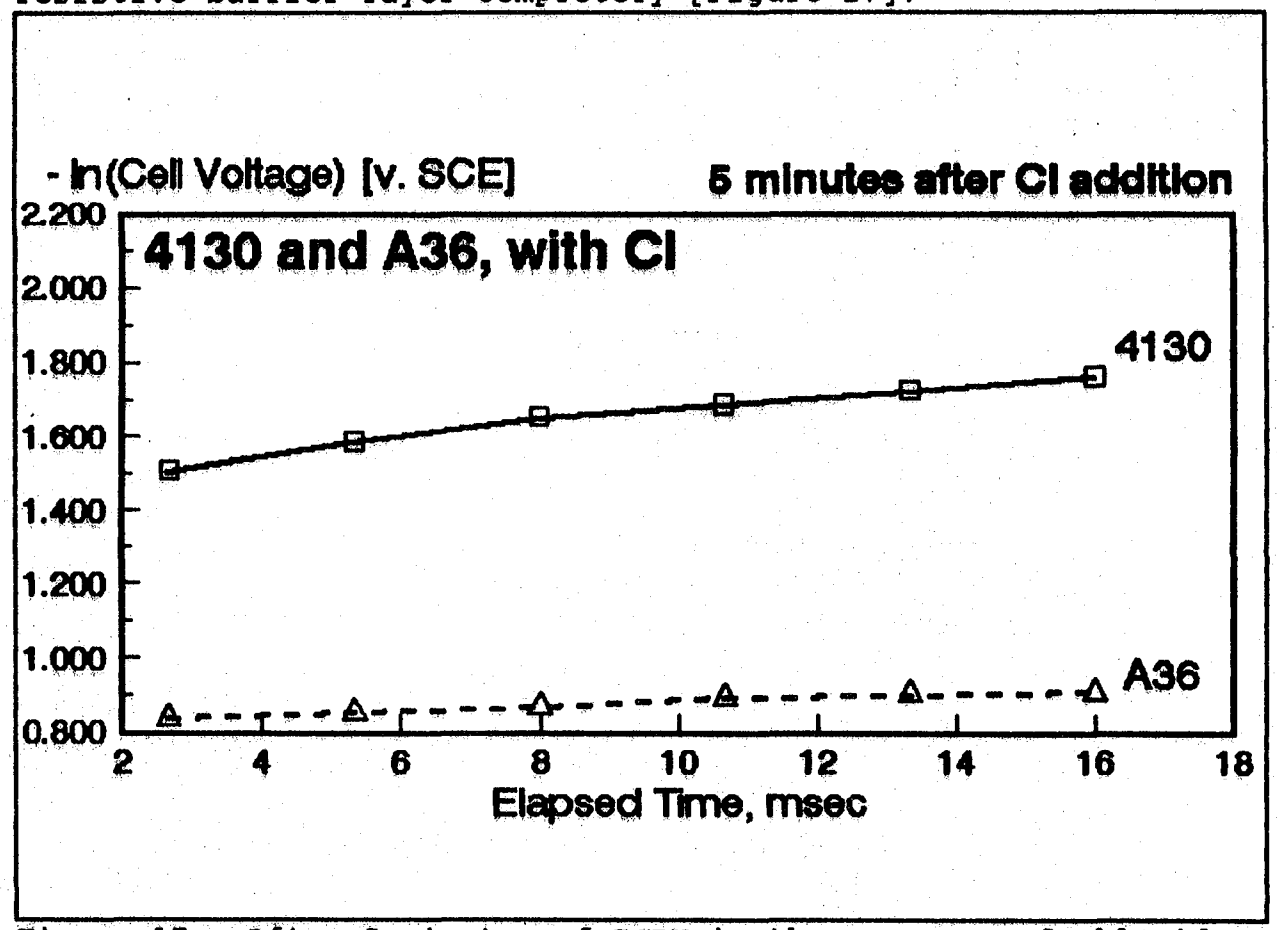

Figure 17 - After 5 minutes of RCRV in the presence of chloride ion, A36 has lost its capacity for production of electrically resistive corrosion products while 4130 is hardly affected at all.

Notice that the 4130 is hardly affected at all.

Bear in mind that this behavior has been measured without the occurrence of noticeable corrosion attack on the A36 alloy - only the tendency has been measured.

4.0 CONCLUSIONS

a. Galvanostatic measurements represent a more natural approach to the modelling and development of accelerated test methods than do conventional potentiostatic methods.

b. Periodic or cyclic current reversal tends to simulate concurrent anodic and cathodic reactions on a freely corroding metal surface better than do potentiostatic methods where anodic and cathodic processes occur on separate electrode surfaces.

c. Development of highly resistive barrier layers which result in large degrees of polarization during anodic current cycles appear to be directly associated with susceptibility to atmospheric corrosion.

d. Repetitive Current Reversal Voltammetry [RCRV] has been demonstrated to be a highly sensitive means with which to differentiate relative susceptibility to localized corrosion attack.

5.0 RECOMMENDATIONS FOR FUTURE WORK

a. Experimentation must be continued with attention focussed on variations in polarization behavior as a function of solution composition. This would require modification to the existing electrochemical cell used in these studies.

b. Development of a standard test solution and procedure to be applied to a larger list of candidate materials. Emphasis must be placed on establishing experimental methodology which is not limited by the experience or skill of the operator - "idiot proof".

c. For scientific purposes, parallel studies of mechanistic implications of polarization kinetics should be accomplished. This will require "up-grading" of the equipment used - a digital oscilloscope with computer interfacing would speed up the data acquisition and interpretation process.

d. The relationship between polarization behavior and both current amplitude and frequency needs to be established in more detail than has been done for these feasibility studies. It is possible that the results of these experiments may be integrated with experimentation using AC impedance techniques thus permitting more meaningful interpretation of alternating current methods than has been achieved to date.

1991 NASA/ASEE SUMMER FACULTY FELLOWSHIP PROGRAM

JOHN F. KENNEDY SPACE CENTER
UNIVERSITY OF CENTRAL FLORIDA

HAZARDOUS GAS LEAK ANALYSIS IN THE SPACE SHUTTLE

PREPARED BY:	Ronald G. Barile
ACADEMIC RANK:	Professor
UNIVERSITY AND DEPARTMENT:	Florida Institute of Technology Chemical Engineering
NASA/KSC	
DIVISION:	Engineering Design Lab
BRANCH:	Instrumentation & Hazardous Gas
NASA COLLEAGUE:	Rick Adams
DATE:	August 22, 1991
CONTRACT NUMBER:	University of Central Florida NASA-NGT-60002 Supplement: 6

ACKNOWLEDGEMENTS

Every person below was a terrific help to me. This summer was a wonderful experience because of them.

The NASA persons who conceived and directed the project:

Rick Adams, who guided me with skill and patience, and his superiors, Bill Helms and Dave Collins.

Other NASA persons who kindly gave of their time on a daily basis to help me along:

Mat Verdier, Bill Larson, Peggy Eberhardt, Curtiss Ihlefeld, and Lorri Carr.

The Boeing Haz Gas Lab personnel who put in a major amount of time and made all my computer and experimental work possible:

Larry Lingvay, Rich Hritz, Guy Naylor, and Terry Hammond.

The Transducer Lab and the Optics Lab personnel who helped substantially and loaned important equipment:

Drew Schmidt, Dick Deyoe, and Dr. Bob Youngquist.

The KSC library staff gave efficient and kindly support.

My former graduate instructor from the U. of Illinois, still doing a great job:

Prof. Ray Hosler, UCF.

THANKS!

ABSTRACT

This study focuses on helium tests of the main propulsion system in the space shuttle and on hydrogen leaks. The hazardous gas detection system (HGDS) in the mobile launch pad uses mass spectrometers to monitor the shuttle environment for leaks. The mass spectrometers are fed by long tubes to sample gas from the payload bay, mid body, aft engine compartment and external tank. The overall purpose of this study is to improve the HGDS, especially in its potential for locating cryogen leaks.

Pre-existing leak data was analyzed for transient information to determine if the leak location could be pinpointed from test data. Then, a rapid-response leak detection experiment was designed, built, and tested. The apparatus included a Perkin Elmer MGA-1200 mass spectrometer, an air velocity transducer, and a pressure transducer, all monitored by a Macintosh IIFX computer using LabVIEW software. A jet of helium flowing into the lab air simulated a gas leak. Schlieren imaging and video recordings were also employed to study the jet flow phenomena. Steady and pulsed jets were logged for concentration, velocity, and pressure, and the power spectral density of each was computed.

Large eddies and vortices were visually seen with Schlieren imaging, and they were detected in the time plots of the various instruments. The response time of the MGA-1200 was found in the range of 0.05 to 0.1 sec. Pulsed concentration waves were clearly detected at 25 cycles per sec. by spectral analysis of MGA data. One practical consequence of this study is to suggest that the backup HGDS sampling frequency should be increased above the present rate of 1 sample per second.

SUMMARY

This study focuses on helium tests of the cryogenic propellant system in the space shuttle and on hydrogen leaks. The hazardous gas detection system (HGDS) in the mobile launch pad uses mass spectrometers fed by long gas sampling tubes to monitor the payload bay, mid body, aft engine compartment and external tank. The mass spectrometers continuously assay the shuttle environment for hydrogen, helium, oxygen and argon. The overall purpose of this study is to improve the HGDS, especially in its potential for locating cryogen leaks.

Specifically, the present HGDS was reviewed and pre-existing leak data was analyzed for transient information to determine if the leak location could be pinpointed from test data. Spectral analysis was performed on earlier data measured at the OPF and in the Hazardous Gas Detection Lab. Then, a rapid-response leak detection experiment was designed, built, and tested. The apparatus included a Perkin Elmer MGA-1200 mass spectrometer, an air velocity transducer, and a pressure transducer, all monitored by a Macintosh IIFX computer using LabVIEW software. A jet of helium flowing into the lab air simulated a gas leak. Schlieren imaging and video recordings were also employed to study the flow phenomena. Experiments on leak jet characterization included velocity, pressure and concentration profiles and in particular on rapid fluctuations of these variables. Steady and pulsed jets were logged for concentration, velocity, and pressure, and the power spectral density was computed for each observation.

The LabVIEW software performed well in both analysis of earlier data and in real-time data acquisition and reduction. The air velocity transducer (TSI) and the pressure transducer (Rosemount) were capable of measuring rapid transients in helium jet phenomena, and it has the versatility and potential to be applied to leak detection and location. Particular emphasis was centered on large eddies and vortices in the jet-air mixing

zone. Large eddies and vortices were visually seen with Schlieren imaging, and they were detected in the time plots of the various instruments. The response time (63.2%) of the MGA-1200 was found in the range of 0.05 to 0.1 sec., and possibly lower. Pulsed concentration waves were clearly detected at 25 cycles per sec. by spectral analysis of MGA data. For certain, the MGA is fast enough to detect transients such as hydrogen or helium eddies in the time trace data, if sampled at say 50 Hz. Spectral analysis showed some evidence of correlated power in the 0.1 to 20 Hz. region, but visual and transient concentration observations indicated that eddy shedding from the leak jet is somewhat irregular in time. Thus, such events may not correlate well as a definite peak in a power spectral density plot. One practical consequence of this study is to suggest that the backup HGDS sampling frequency should be increased above the present rate of 1 sample per second.

TABLE OF CONTENTS

LIST OF ILLUSTRATIONS

Figure

I INTRODUCTION

In the space shuttle, hydrogen and oxygen are the main engines propulsion gases, as well as the fuel-cell power system gases. Leaks of these gases may be found in the aft fuselage, the mid body, and other areas. Other hazardous gases in the shuttle include nitrogen tetroxide, monomethyl hydrazine, and hydrazine. Various forms of leak detection equipment are employed in and around the shuttle wherever hazardous materials are present. The hazardous gas detection system (HGDS) uses mass spectrometers fed by long gas sampling tubes to monitor the payload bay, mid body, aft engine compartment, and external tank. The mass spectrometers in the HGDS system continuously monitor the environment for hydrogen, helium, oxygen and argon. A detailed account of the HGDS including development of the helium signauture test for the orbiter main propulsion system was presented by Bilardo and Izquierdo in 1987 (1).

This study will focus on helium tests of the cryogenic propellant system and on hydrogen leaks. Helium signature tests are routinely performed to determine the shuttle's cryogenic system integrity. These tests are scheduled at the OPF and the launch pad previous to the start of countdown. Also, catalytic hydrogen detectors inside and around the shuttle are monitored for possible leaks during the countdown period.

Main Goals of Present Study:

1. Assess the present HGDS and analyze earlier leak data to determine if the leak location can be pinpointed from test data.
2. Analyze lab test and OPF helium leak data with LabVIEW software to determine if frequency analysis has meaningful information.
3. Design, build, and test a rapid-response leak detection experiment which focuses on leak characterizaton including velocity, pressure and concentration profiles and in particular on rapid fluctuations of these variables.
4. For a longer-term objective: Predict an improved placement of sample tubes and improved data analysis for special tests (leak events, etc.) so that leak source locations can be identified from frequency analysis of mass spectrometer data.

II BACKGROUND

2.1 PRESENT SYSTEM DEFINITION

The backup hazardous gas detection system draws gas samples in 0.18-in. ID tubes to a Perkin Elmer MGA-1200 mass spectrometer (MS). The MS is a magnetic sector, fixed collector, turbo-pumped instrument, performing 1-sec. per channel analysis (but capable down to 0.02 sec. samples). The MS is situated about 200 ft. away on the mobile launch platform. Five gas samples are sequentially assayed for hydrogen, helium, oxygen and argon. The five samples arrive in separate tubes: three from the shuttle, one from the tail service mast, and one from the external tank.

When cryogenic propellants are on board, about 180 lb/min. of gaseous nitrogen purge gas passes from the mid fuselage, including the payload bay (PB) and the mid body (MB), through the 1307 bulkhead into the aft fuselage (Figs. 1 and 2). Sample gases are drawn into 0.23-in. ID SS tubes distributed in the aft area. The payload bay and mid body tubes are located just aft of the 1307 bulkhead. Four tubes which sample the payload bay purge are connected through tees into one tube which is routed through the umbilical disconnect panel (UDP, line 2). Two SS tubes which sample the mid body purge are connected into one tube leading to the UDP (line 4). The pair of aft sample tubes are mixed together and routed to the UDP. The aft sample tubes are located several feet aft of the 1307 BH at the #9 vent doors, thus the aft sample could reflect upstream leaks from the MB and PLB.

The nitrogen purge is flowing at the pad when the cryogenic propellants are loaded into the vehicle. Both hydrogen and oxygen flow inside separate piping systems from the tail service mast to the shuttle aft compartment to the external tank. Before loading cryogens, helium is injected in this piping system with air purge on the outside (1). This type of test is performed once at the OPF and once at the launch pad to determine whether the system is sealed before loading cryogens.

Hence, leaks in the cryogenic piping can be detected via helium tests before loading cryogens, and by hydrogen and oxygen detection during and after these are loaded on board. Due to safety considerations, the present study was done exclusively with helium, although hydrogen can be easily implemented in future work.

2.2 EARLIER KSC WORK RELATED TO HAZARDOUS GAS DETECTION

In 1990, Schleier studied gas leaks of helium, nitrogen, and argon by flowing the gases through a slightly cracked gate valve (2). Using helium at 68 psig and 105 sccm as the reference condition, flows of helium, nitrogen, and argon correlated well as predicted vs. observed flows. However, the correlation had a slope of 0.9 and an intercept of 15 sccm, which means the predictions will be high at leaks aroung 15 sccm. Further analysis by the present author showed that the individual gas curves for predicted vs. observed were quite different. The end result is that the correlation could give false predictions, either high or low, on the order of 50% error in the range of the flows observed in the lab, and possibly worse errors outside of the data range.

Mehta characterized a turbomolecular-pumped magnetic sector mass spectrometer in 1988 working with the HGDL (3). The model was Perkin Elmer MGA-1200, the same type which is proposed for the present study (H2S2). Linearity, precision, drift, detection limits and accuracy were found to be acceptable for quantitative analytical determination of hydrogen, helium, oxygen and argon in nitrogen or helium background gases. The 90% rise times for pulse inputs were on the order of one-half second. Kachnic and Raisin in 1988 (4) put a one-second pulse of nitrogen into helium into the Perkin Elmer 17" disconnect mass spectrometer resulted in an 84% peak on nitrogen and a dead time of less than 0.1 sec on the upswing. The downswing started about 0.2 sec late, and took another 0.8 sec. to drop to zero. A one-second pulse of helium into nitrogen rose quickly to 98% in less than 0.1 sec., but it did not fall off from 98% until 3 sec. and it zeroed after another second (4 sec. total). This reference was not thoroughly documented to the extent that the response can be

considered accurate, but it gives an idea of one MS observed in the field. A recent internal HGDL study (5) on noise in MGA-1200 reported that the unfiltered 60-cycle and related harmonic rms noise level was on the order of 100 mV, which is consistent with noise observed in the present study (both magnitude and frequency). Both noise and time response will be addressed below.

2.3 LITERATURE SURVEY OF MASS SPECS, JETS AND LEAKS

The following brief literature survey gives an indication that much useful information is available to guide researchers and practitioners in leak detection. Only the highlights are presented since the body of literature is beyond the scope of a short-term project. The information on free jets will prove especially valuable in a longer-term study.

2.3.1 MASS SPECTROMETERS. Mentioned earlier, Mehta made substantial observations in characterizing the MGA-1200 turbo-pumped mass spectrometer (3). Another series of tests with a Leybold helium leak detector are reviewed below (6). In a 1977 KSC report (7), details are given of the UTHE Technology International (UTI) mass spectrometer and related sampling equipment which monitors the main propulsion fuel loading in the space shuttle. This system is the Hazardous Gas Detection System (HGDS) located in the mobile launch pad, also known as the "Prime" mass spectrometer. Of several mass spectrometer texts available at KSC, a good treatment of basic concepts and practical applications is given by J. Roboz (8).

2.3.2 FREE JETS. A thorough survey of free jet literature was performed because a gas leak is likely to behave in a similar manner to a jet with regard to velocity decay, pressure profile, concentration decay, sonic waves, etc. The rapid, perhaps periodic fluctuations seen in mass spectrometer test data (e.g., Figs. 4 and 5 discussed below) are reminiscent of vortices or large scale eddies which form at the edge of the jet-air mixing zone (9-14). These swirling structures which travel with the jet at roughly the local centerline velocity could give rise to

the type of concentration fluctuations which are observed in MS tests of concern here.

Measurements of the mixing of two coaxial hydrogen-air jets are reported by Chriss (15), including centerline decay and radial profile shapes of composition, velocity, and total enthalpy. The striking result is that velocity and composition decay almost identically on dimensionless plots, Fig. 3. Becker et al. (9) worked with an air-air jet marked with oil smoke. Turbulent concentration fluctuations of the nozzle gas diffusing into the stagnant gas were on the order of 25% of the centerline value (lateral distance from centerline about 1/3 of jet radius). Heat transfer and flow measurements including frequency and intermittency data are given by Chua and Antonia (10). Turbulent fluctuations ranged from 10Hz for large peaks to 100 Hz for small variations. Other relevant papers on jets include flow field (16), mixing (17), text-book development and experimental data (18), and imaging of a methane jet (19).

2.3.3 GAS LEAKS. Researchers in the natural gas industry are quite expert on gas leaks. A review of their techology is helpful in understanding leak and gas phenomena. Examples of publications include AGA Gas Handbook (20), diffusion leak artifacts (21), and Nondestructive Testing Handbook/Leak Testing (22).

III ANALYSIS OF EARLIER TESTS

3.1 LabVIEW SOFTWARE

LabVIEW programs (VI's) writen by Larry Lingvay (Boeing HGDL) were used to analyze existing helium leak data. Most of the data were stored in data files such as Cricket Graph documents which were not compatible with LabVIEW. This problem was solved by reading and editing the data with Microsoft Excel and saving the file as an Excel text file. In this form, the data could be read and processed directly by LabVIEW. (Note that any control headers or column labels must be removed in the editor.) The LabVIEW programs were entitled:

ASCII two 1D arrays2

and *Filtered FFT Read*

The first program opened, read and closed a data file, followed by several operations which created an array from the original data table. This array was transfered to the second program where the data were filtered, the power spectral density (PSD) was computed, and the results were graphed. A number of signal-processing references proved helpful in this phase of the work (23-26). One of particular interest concerned how the eye distinguishes a continuous spectrum of colors with only three types of receptors (cones). Detecting a gas leak with a few sparsely configured sensors is a problem which is similar to the eye mechanism. The key to determining the leak location would be to analyze the time and frequency history of separate sensor locations and overlay the data with logic computations (25).

3.1.1 TEST WAVE. The LabVIEW programs were validated by running a 1 KHz sine wave as the data file. The results are shown in Fig. 4 for a 1 KHz, 0.1 v peak-to-peak sine wave. The upper plot is the input wave, and the lower plot is the PSD, Watts/Ohm, vs. frequency in Hz. The PSD peak at 1 KHz. indicates that the programs have correctly analyzed the data file. Note that the sampling interval, designated on the lower

left part of the plot by "S.INT-delt(sec)" must be entered manually into the control box to the left of this label. In this case the sampling interval is 20 microseconds.

3.2 RESULTS: EXISTING HGDL DATA

3.2.1 SIMULATED LEAKS IN LAB. Helium experiments were performed in March, 1990 in the EDL building. Data were selected from these tests and analyzed with LabVIEW programs discussed above. Two cases were selected to show the capability of the programs to analyze mass spectrometer data. The first was "BLDG FILL" which involved measurements of helium leaking from a jet into rooms 115 and 116 in EDL (DE Haz Gas Lab). The raw data and the PSD are shown in Fig. 5 for a band of data between 1650 and 2200 sec. The initial 500 sec of data were taken in room 116 where the level of helium was 9 to 11 ppm. Later, a fan was set up to mix the helium at the jet orifice with air in room 115. The level of helium there was 35 to 45 ppm. A better picture of the data is obtained if they are separated into three bands, roughly 0-500, 1000-1500,1500 to 2000 sec. Another reason to separate data into bands is to keep them in band widths which have constant sampling frequency. Data such as "BLDG FILL" were sampled at 1.05-sec. intervals but other data are reported at mixed periods from 1.05 to to 21.2 sec. (e.g., "ROOM FILL").

Fig. 6 shows band 1 of "BLDG FILL" in an unfiltered condition. The PSD appears to have some significant peaks from 0.01 to 0.1 Hz. A large amount of data was analyzed, both unfiltered and filtered, but space does not permit including them here. Other data obtained in the HGDL, the ROOM FILL series was analyzed as well. An example of the data in band 4 is shown in Fig. 7 where a small peak at 0.05 Hz appears.

3.2.2 OPF-SHUTTLE HELIUM LEAK SIGNITURE TESTS. An attempt was made (6) in 1990 to show that modified Leybold helium leak detectors could be capable of performing the OPF portion of the orbiter aft helium signiture leak test, *V1201*. If successful, this might eliminate the need for this procedure at the pad,

test *V1202*. If *V1202* is still required at pad, the Leybold leak detectors would eliminate the requirement to use the HGDS (U72-1186) to perform the test, reducing manpower and MS service problems caused by excessive oxygen and water in the pad test.

Testing was performed in HB1 of the OPF using the prototype system to characterize helium background in and around the orbiter and at ground level. Also, a demonstration was given in the DE/Haz Gas Lab. Stability and resolution at sub-ppm levels of helium have been shown to be adequate to allow a production version to replace the HGDS (prime) when performing *V1201* or *V1202*, either at the OPF or the pad. The system was relocated to the OPF HB1 for OPF background evaluation testing by ESC personnel.

Frequency analysis of earlier OPF data were also performed as described above for the HGDL data. Fig. 8 depicts a filtered version of helium data from an OPF test on Feb. 23, 1990, taken at a sample period of about 5.4 sec. The low-pass Bessel filter had a cutoff at 0.09 Hz and a frequency resolution of 0.0003 Hz. Again, there does not appear to be a correlated peak on the PSD, with the exception of events around and below 0.011 Hz.

3.2.3 LAUNCH PAD-SHUTTLE HELIUM LEAK SIGNATURE TESTS. The HGDL files contain results of many helium signature tests on the launch pad. These data can be handled in the same way as discussed above. The results would show periodic events below 1 Hz due to the slow sampling speed of the measurements.

3.3 DISCUSSION OF ANALYSIS RESULTS

The test sine wave showed that the digital computation of power spectral density was accurate, as shown in Fig. 4. Applying this method to data measured in the HGDL and the OPF with the Leybold detector did not result in any obvious characteristic frequencies. Comparing the power spectra in Figs. 5-8 (where *T-Domain Amplitude* is in ppm helium), there are some peaks at frequencies below 0.1 Hz that have correlated power, but the peaks do not stand out above the remainder of the spectra as

expected (compare Fig. 4). Furthermore, events at these frequencies represent concentration waves of very long periods, 10 to 500-sec. Since the data were measured in 1-sec. intervals, there can be no meaningful frequencies represented in them above 1 Hz, and to eliminate aliasing, the analysis must be at frequencies below the Nyquist value of one-half of the sampling frequency, or 0.5 Hz.

Data from the OPF have similar characteristics to the above. The only significant power peaks occur at event times between 100 and 400 sec. (i.e., 0.011 to 0.0025 Hz.). Events of such low frequencies could be construed as instrument drift. From another point of view, there may well be slow concentration oscillations due to vorticies shedding off of a jet leak. These events were noticed in new data reported below using Schlieren imaging. The striking thing about Schlieren images is that large, lumbering vortices do in fact peel off from the jet stream, but not at precisely regular intervals. Irregular concentration jumps detected by a sampling tube leading to a mass spectrometer could remain intact and be detected, but the power spectral density would not always show these events as high-dB peaks beacuse they don't occur at regular intervals. Such events occuring at low frequencies below 1 Hz may be more easily detected by observing the time-concentration plot instead of the power density. Another method of analysis would be to take moments of the power such as the product of frequency and PSD. This technique has proved fruitful in other jet studies reported in the literature. A final consideration is that concentration fluctuations caused by flow events such as vortices will occur at frequencies depending on the source-stream velocity, orifice geometry, and macroscale flows such as nitrogen purging. In general, fluctuations caused by jet mixing would be expected to be in the frequency range of 1 Hz or above (c.f., ref. 10).

IV NEW EXPERIMENTS

4.1 SIMULATED HELIUM LEAKS

A helium leak was simulated in the HGD Lab by a pure helium stream (KSC grade) flowing from the lab-service panel through 1/4-in. Tygon tubing, and exiting through a small nozzle. The gas exited the nozzle from a circular orifice, 0.05 cm. diameter, recessed in a short tube, 0.5 cm long and 0.4 cm. diameter. In effect, the jet was actually emerging from the 0.4-cm. tube, at velocities of 10,000 FPM and above.

4.1.1 APPARATUS AND PROCEDURE. A schematic drawing of the equipment used in the HGDL is shown in Fig. 9. A Rosemount pressure transducer was used to measure pressure fluctuations in the jet field (Minneapolis, MN). This device is capable of measuring pressure from 22 to 32 inches of mercury absolute. Velocity and its fluctuations were detected by a TSI Inc. air velocity transducer with a range of 0 to 10,000 fpm (St. Paul, MN). These probes were mounted on a calibrated X-Y vise which provided an accurate measure of the probe tips in relation to the jet origin.

The jet stream representing the leak was measured and controlled by a Sierra Instruments 840 SideTrak mass flow meter/controller. The instrument was calibrated for nitrogen gas flow, but was correctable to helium gas by multiplying the reading by 1.453 (for units of standard liters per minute). An independent check on the frequency response of velocity, pressure, and concentration measurements was provided by installing in the leak jet a solenoid valve driven by a square wave generator and power supply. Most experiments were done with a steady flow in the leak jet, but selected experiments were done with various pulsed frequencies as noted elsewhere in the text.

In order to observe the leak jet, a Schlieren grating and TV video system was set up. Most experiments were performed with the assistance of this equipment to locate the jet and large vortices which rolled off of the jet. Video recordings were

made of the major jet phenomena associated with experiments reported here.

A Perkin Elmer MGA-1200 (H2S2) was employed as the gas analyzer. A sample pump drew 0.2 to 1 liter per minute past a SS tube connector which was specially fitted with a capillary tube to provide a 200 Torr leak to the MS input. The helium jet was sampled with a 0.2-cm. nozzle probe with 7.5 ft.of 1/4-in. ID Tygon tubing leading to the MGA valve #2. Samples were taken at various locations in accordance with the velocity and pressure sampling (x=axial, y=horizontal, z=vertical). Later, a 15-ft. length of 1/32-in. ID SS capillary tubing was fitted to the MGA inlet valve #2. This sample line, excluding the earlier short length of fine capillary tube, was pumped directly with the MGA roughing pump. It turned out that the sampling dead time dropped drastically, as discussed below.

All three sensors were fed into a National Instruments data acquisition board (NB-MIO-16XL-42) plugged into a MacIntosh IIFX computer. A LabVIEW VI called *Super Spectrum Analyzer w/0* sampled, plotted and analyzed the data from each sensor. The analysis routine was to sample during a given time window with a specified number of samples, e.g., 1024, 2048, etc., and then find the mean, standard deviation, and power spectral density. Another version of this VI, *Ultra Spectrum Analyzer/Ave*, was implemented to sum multiple replicate data bands and average the PSD. Specific results of spectrum averaging are not included in this report.

V RESULTS-CHARACTERIZATION OF A HELIUM JET

5.1 FLOW VELOCITY AND VISUALIZATION

Velocity measurements were made first to establish the jet location. The air velocity transducer (AVT) had a very rapid response to flow variations. A typical helium jet of 2.9 SLM flow into air issued from the 0.4-cm. leak orifice at 827 FPM and decayed to 692 FPM at x = 8 cm downstream on the horizontal centerline. Fig. 10 shows the velocity and PSD traces at this point (where velocity in ft/min is equal to 2000 times volts). For comparison, a hydrogen jet (15) under these conditions would decay to about 20% of the initial velocity, or 270 FPM, within 20 orifice diameters (i.e., in this case, 8 cm.). The unsteady nature of the velocity curve indicates the eddy fluctuations in the stream which give rise to +/- 60 FPM changes. Note that this jet, being horizontal, is strongly buoyant. Thus, a measurement on the horizontal centerline is likely to be below the main jet body. In another run, a 1.2 SLM helium jet was pulsed at 5 Hz. (top Fig. 11) and 20 Hz (bottom Fig. 11) to observe the frequency response of the AVT located at x = 2.5 cm on the centerline. Both PSD curves show strong peaks at the forcing frequencies of 5 and 20 Hz., respectively, showing that the AVT had the capability of seeing velocity fluctuations. In a third run, with x = 22 cm., the lateral velocity profile from y = 0.0 to 2.5 cm. showed large fluctuations, on the order of 10 to 100% of the axial flow (e.g., Fig. 12). Meanwhile, the axial velocity decayed from 230 FPM at y = 0, to 26 FPM at y = 2.5 cm. These later data were observed with a jet of 7.4 SLM. A video cassette recording was made in the above experiments as well as others discussed below.

5.2 PRESSURE FIELD

The pressure field in the jet vicinity was sampled at a few locations, mainly in connection with pulsed helium jets. A pressure pulse of 25 Torr was observed 2.5 cm. downstream from a helium jet cycled at 1 Hz. The power spectrum was quite distinctive for pulsed tests of 1, 1.5, and 2 cps. A map of the

steady jet field is definitely of interest, but perhaps a more sensitive transducer would be necessary, e.g., full scale range of 50 instead of 250 Torr in the present instrument. In one test at 1.5 cps, the data system was pushed to the upper limit of 50,000 Hz. Fig. 13 shows the time trace expanded and the power density extended to 22,000 Hz. Several significant peaks are evident, at 6K, 12K, 15K, and 20K Hz., which seem to suggest that ultrasound signals found by others near 40K Hz. might be detected with this transducer.

5.3 CONCENTRATION FIELD AND FREQUENCY ANALYSIS

The average helium concentrations vs. distance measured by the MGA-1200 are given in Fig. 14. The standard deviation for these data are on the order of 1% helium due to the noise in the MGA-Macintosh system. As for detecting helium vortices by frequency analysis of the concentration-vs.-time data, the question of response time arises for the sample tube and the MGA-1200. An indication of the mass system response was determined by rapidly thrusting the sample tube from room air into the helium jet. The response curve is shown in Fig. 15. The total sample dead time is not shown on the graph, but it was separately measured at 10 sec. in the 1/4-in Tygon tube of 7.5 ft. The figure shows a 90% rise time of 1 sec., or a peak-to-peak time of 1.3 sec. Because this was considered too slow, modifications were made to incorporate the 1/32-in. capillary sample tube. The helium concentration rise and fall times for a square wave input to the 1/32-in. tube are shown in Fig. 16. The procedure was to place the sample tube at x = 2.5 cm. in the helium jet, then block the tube with a ruler, quickly remove the ruler at time zero, and replace it at 3 sec.

VI DISCUSSION OF NEW EXPERIMENTS

Velocity and Flow Visualization The air velocity transducer was simple and versatile, yielding fast response and easy mapping of the helium jet field. Its frequency response was directly seen by pulsing the jet in selected runs. In steady-jet runs, the PSD showed some 60 Hz. noise and associated harmonics. Schlieren images of the jets indicated that the large eddies or vortices do give rise to large velocity fluctuations, but these do not occur at precisely regular intervals. For this reason, there were no standout PSD peaks, but the vorticies could be seen quite clearly in the time trace of the AVT. Thus, the AVT could be applied to leak detection and to pinpointing leak location if the environment were not overwhelmed by purge gas or physical obstructions.

Pressure The Rosemount pressure transducer was also simple and versatile, with extremely fast frequency response. It was capable of sensing vortices around 1 to 10 Hz., and also able to pick up ultrasound, although in the latter measurements, artifacts of electronic noise could not be ruled out.

Concentration Using Mass Spectrometer From knowledge of the dissipation of a hydrogen jet into air (15), it is reasonable to expect a rapid dissipation of helium jets as well. Our measurements show that the helium jet in terms of velocity persists several times longer downstream than a hydrogen jet, as measured by the variable x/D, the downstream length coordinate divided by the leak orifice diameter. Fig. 15 gives a rough measure of the MGA response, but it contains an error of 0.1 or 0.2 sec which is the time required to move the sample nozzle into the helium jet. Although this appears to be slow for frequency analysis, modifications were made in the sample plumbing which significantly increased the system response. The lower curve, PSD vs. frequency, shows 60 cycle noise and its many harmonics. The substitution of the smaller sample tube decreased the total system dead time (Fig. 16) to roughly 0.2 sec., which is likely to be mainly the sample-tube dead time. The MGA-1200 time constant can be estimated from this figure.

The rise time constant is on the order of 0.05 sec., and the fall time constant is about 0.1 sec. These numbers suggest that the MGA-1200 is capable of detecting fluctuations at or below about 20 Hz. At this writing, another experiment with a pulsed jet resulted in a significant PSD peak at 25 cps which was the pulsing frequency. The 1/32-in. sample tube was situated 2.5 cm. downstream from the jet nozzle within the free jet stream. This again underscores the rapid response of the MGA-1200.

VII CONCLUSIONS AND RECOMMENDATIONS

Conclusions

* The LabVIEW software developed for this work was capable of reading, plotting, and calculating power spectra of digital data. These included earlier helium data at the OPF and HGDL stored on hard disks, and new data acquired and analyzed in real time in the present work. This capability was applied to mass spectrometer, air velocity transducer, and pressure transducer data reported in this work.

* An air velocity transducer (TSI) was capable of measuring rapid transients in helium jet phenomena, and it had the versatility and potential to be applied to leak detection and location.

* An ambient pressure transducer (Rosemount) was capable of sensing rapid pressure phenomena in the helium leak jet, including pressure fluctuations, sound, and ultrasound up to the maximum frequency capability of our present data acquisition system, 25,000 Hz. This may correlate with other reports of ultrasound leak detection near 40,000 Hz. Thus, it may be possible to do leak detection and location with this simple device.

* The response time (63.2%) of the MGA was shown to be 0.05 to 0.1 sec., and possibly lower. Pulsed concentration waves were detected at 25 cycles per sec. using spectral analysis (but no experiment was run above this frequency).

* Vortices and large eddies were visually seen with Schlieren imaging. The MGA-1200 is fast enough to detect transients such helium eddies in the time trace data, if sampled at say 50 Hz. Spectral analysis showed some evidence of correlated power in the 0.1 to 20 Hz. region, but visual and transient concentration observations indicated that eddy shedding from the leak jet is somewhat irregular in time. Thus, such events may or may not correlate well as definite peaks in a power spectral density

plot.

Recommendations

* One practical consequence of this study is to suggest that the backup HGDS sampling frequency should be increased above the present rate of 1 sample per second.

* Also, it would be interesting to do tests like the above using two or more mass spectrometer sample tubes at different locations. These could be monitored sequentially by switching a solenoid valve between tubes. Then, spectral analysis of different tube locations would be analyzed for transient events pointing to the leak location. Such a system could be implemented with the present HGDS sample tubes in the shuttle.

REFERENCES

1. Bilardo, V. J., Jr., and Izquierdo, F., "Development of the Helium Signature Test for Orbiter Main Propulsion System Revalidation Between Flights," AIAA 25th Aerospace Sciences Meeting, Jan., 1987.

2. Schleier, H., "Correlation of Leak Rates of Various Fluids with the Leak Rate of an Inert Gas in the Same Configuration," NASA/ASEE Summmer Faculty Fellowship Program, 308-338, 1990.

3. Mehta, N. K., "Characterization of a Turbomolecular-Pumped Magnetic Sector Mass Spectrometer," NASA/ASEE Summer Faculty Fellowship Program, KSC/UCF, 1988.

4. Kachnic, J., and Raisin, P., "The 17" Disconnect Mass Spectrometer with Turbomolecular Turbo Pump," Internal Report from Boeing to Dave Collins, NASA-KSC, DL-ESS-24, 4-12-88.

5. Hazardous Gas Detection Lab, Internal Report, "Overview of MGA-1200 Electrometer Card Testing," 1990.

6. "OPF/Orbiter Aft Helium Background Environment," DL-ESS-24, Mar., 1990.

7. PRC, "Space Shuttle Technical Manual, Operation and Maintenance, Hazardous Gas Detection System, KSC Prototype (U72-1186)," KSC TM-680, April, 1977.

8. Roboz, J., Introduction to Mass Spectrometry: Instrumentation and Techniques, Interscience, 1968.

9. Becker, H. A., Hottel, H. C., and Williams, G. C., "The Nozzle Fluid Concentration Field of the Round Turbulent Free Jet," J. Fluid Mech., 30, 285-303 (1967).

10. Chua, L. P., and Antonia, R. A., "Flow Reversal and Intermittency of a Turbulent Jet," AIAA J., 27, (11), 1494-1499 (1989).

11. Ghoniem, A. F., Chen, D. Y., and Oppenheim, A. K., "Formation and Inflammation of a Turbulent Jet," AIAA J., 24, (2), 224-229 (1986).

12. Lam, K. M., and Ko, N. W. M., "Investigation of Flow Structures of a Basic Annular Jet," AIAA J., 24, (9), 1488-93 (1986).

13. Birch, A. D., Brown, D. R., Dodson, M. G., and Thomas, J. R., "The Turbulent Concentration Field of a Methane Jet," J. Fluid Mech., 88, (3), 431-449 (1978).

14. Yule, A. J., "Observations of Late Transitional and Turbulent Flow in Round Jets," in Turbulent Shear Flows, Durst (Editor), Univ. Park, PA, Apr. 18-20, 1977.
15. Chriss, D. E., "Experimental Study of Turbulent Mixing of Subsonic Axisymmetric Gas Streams," Arnold Engineering Development Center, AEDC-TR-68-133, Aug. 1968.
16. Benedict, R. P., "The Flow Field of a Free Jet," in R. B. Dowdell, Ed., Flow-Its Measurement and Control in Science and Industry, Vol. 1, ISA, 1974.
17. Schetz, J.A., Injection and Mixing in Turbulent Flow, Progr. in Astronautics and Aeronautics, 68, AIAA, 1980. (pp. 19-52.)
18. Schlichting, H., Boundary Layer Theory, McGraw-Hill, 1960.
19. Vranos, A., and Liscinsky, D. S., "Planar Imaging of a Turbulent Methane Jet," AIAA J., 24, (9), 1564-65 (1986).
20. Ahlberg, K., Ed., AGA Gas Handbook, Almqvist & Wiksell, Sweden, 1985.
21. Jitschin, W., "Diffusion Leak Artifacts as a Secondary Standard for Gas Flow," Vacuum, 38, (8-10), 883-886 (1988).
22. McMaster, R. C., Ed., Nondestructive Testing Handbook, 2nd Edn., Vol. 1, Leak Testing, Amer. Soc. for Nondestruct. Testing, Inc., 1982.
23. Brigham, E. O., The Fast Fourier Transform and Its Applications, Prentice Hall, 1988.
24. Blackburn, J. A., Ed., Spectral Analysis: Methods and Techniques, Marcel Dekker, 1970.
25. Erickson, R. P., "On the Neural Bases of Behavior," American Scientist, 72, May-June, 233-241 (1984).
26. Katys, G. P., Continuous Measurement of Unsteady Flow, Pergamon Press, 1964.

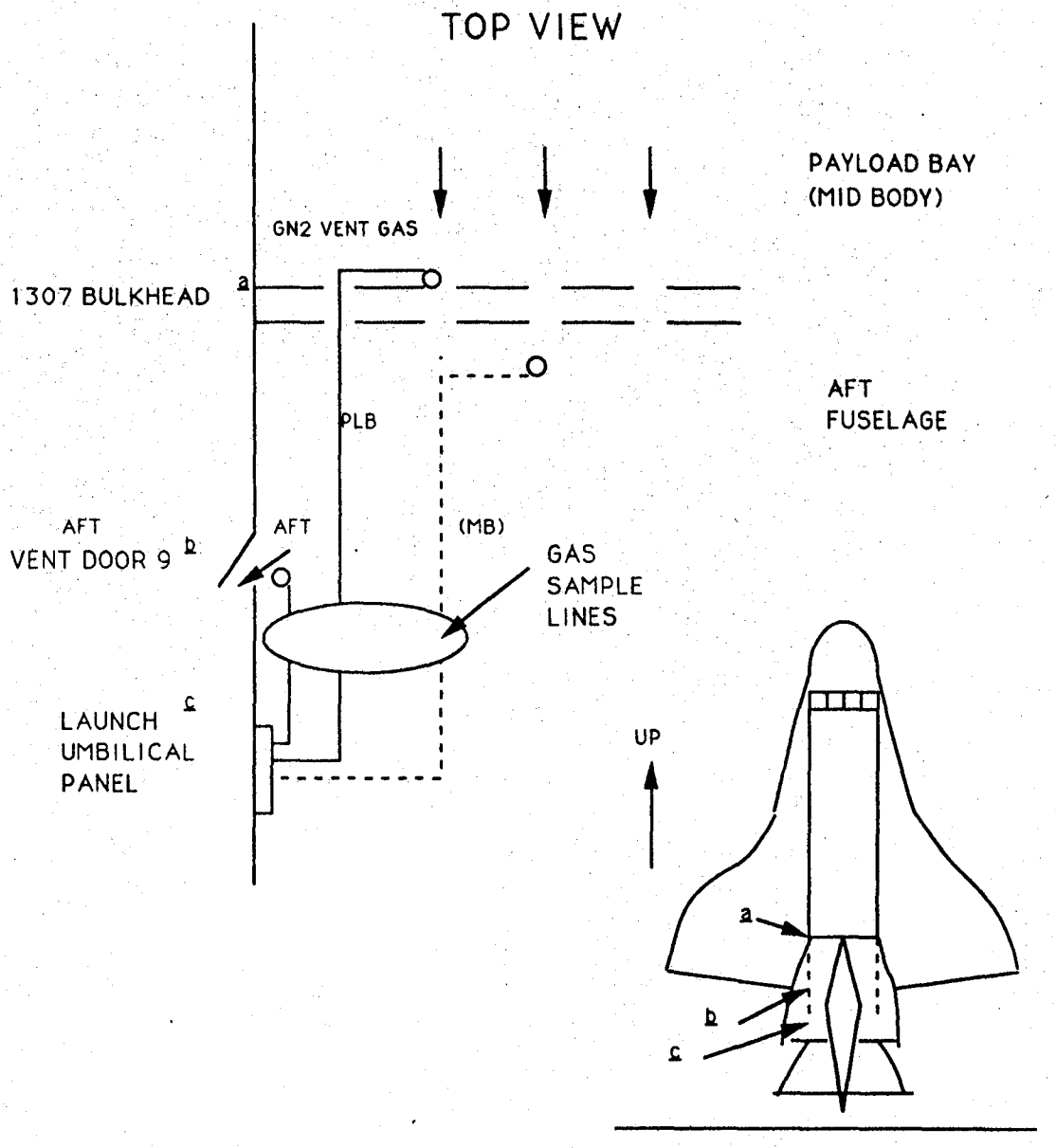

Figure 1. Top view of shuttle showing nitrogen purge areas and HGDS sample tubes

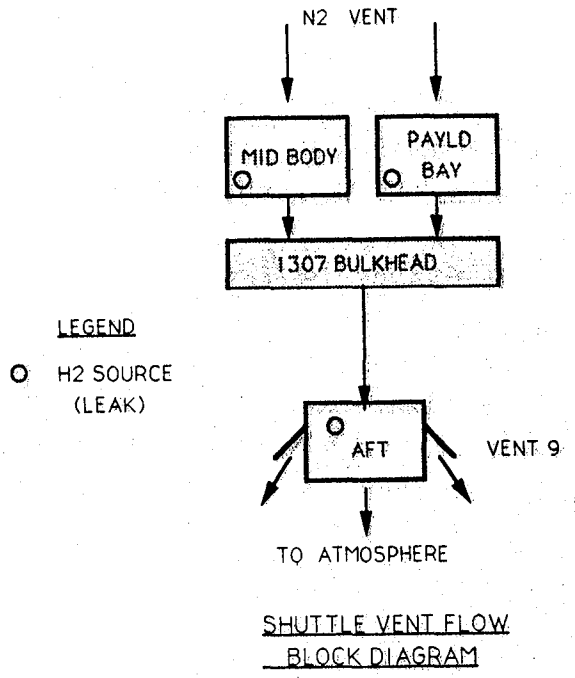

Figure 2. Block diagram of nitrogen purge flow in the space shuttle

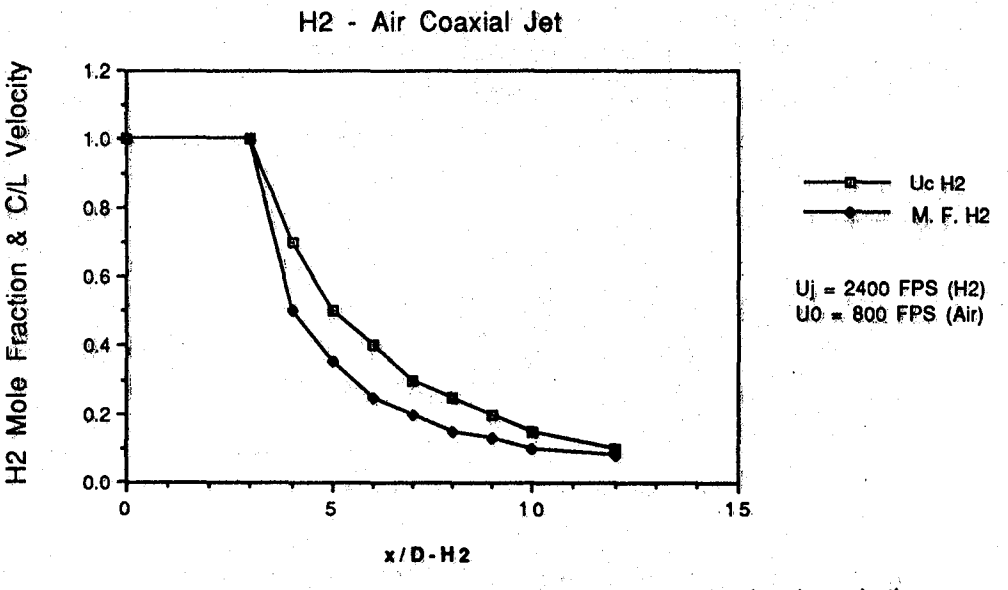

Figure 3. Hydrogen-air coaxial jet showing velocity and concentration decay in the centerline, by Chriss

't Panel

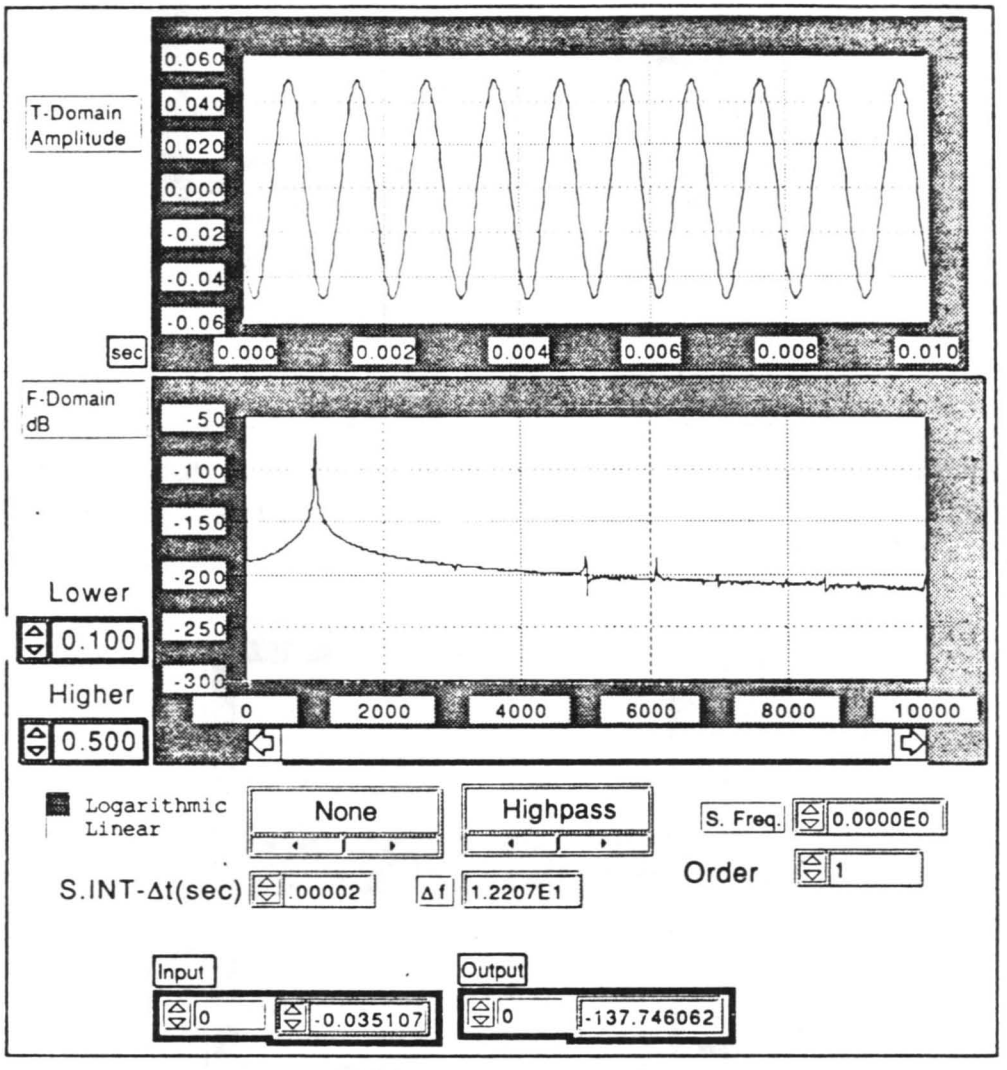

Figure 4. Analysis of a test wave by LabVIEW software "Filtered FFT Read" developed for this study: 1000 Hz. sine wave, 100 mv peak-to- peak amplitude, 4096 samples, 20 microsec. sampling increments; PSD on lower curve shows main frequency peak of 1000 Hz., using no filtering.

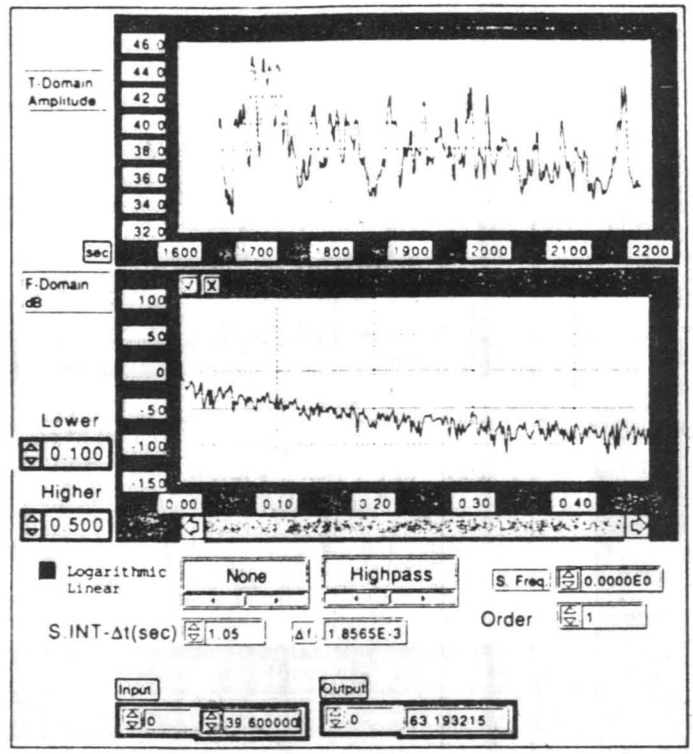

Figure 5. Example of HGD Lab helium test data, "BLDG FILL" band 3, spectral analysis using LabVIEW software; data were stored originally at 1.05-sec. intervals, and presently analyzed at this same sample frequency, with no filtering.

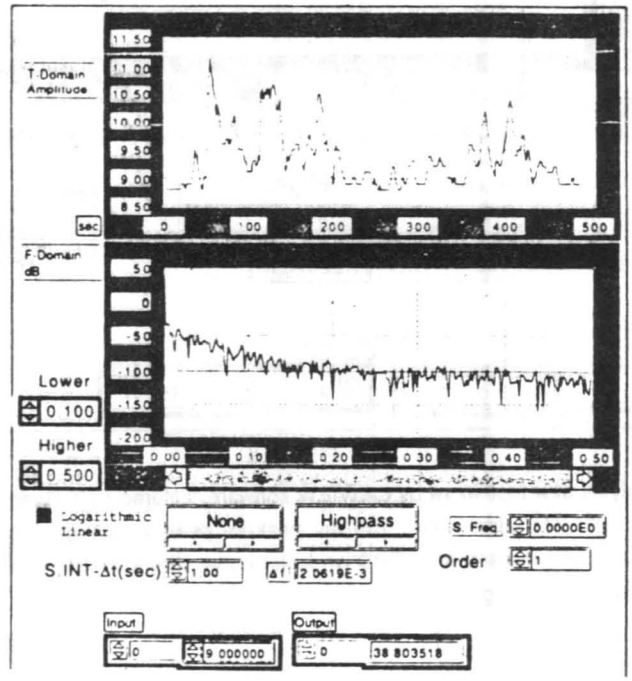

Figure 6. Example of HGD Lab test data "BLDG FILL", band 1, spectral analysis for 1.0-sec. sample frequency, with no filtering

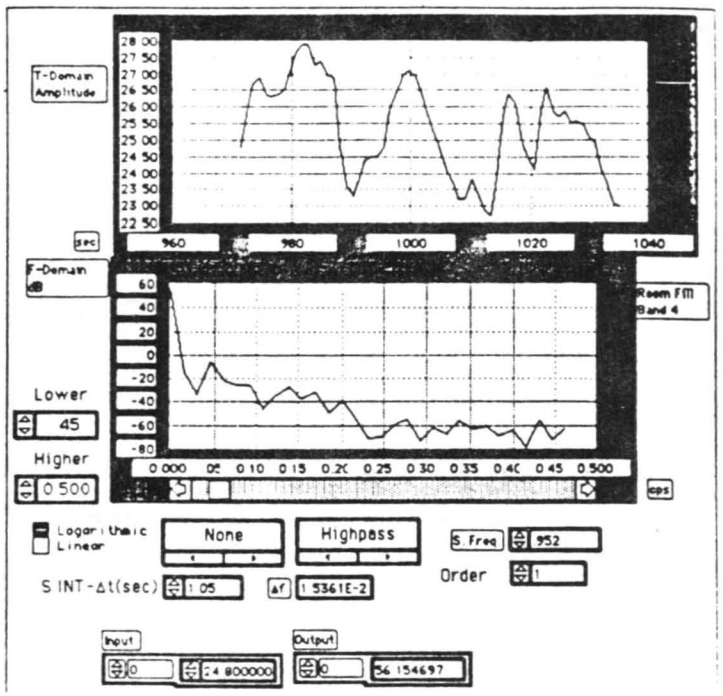

Figure 7. Example of HGD Lab test data "ROOM FILL", band 4, spectral analysis for 1.05-sec. sample frequency, with no filtering

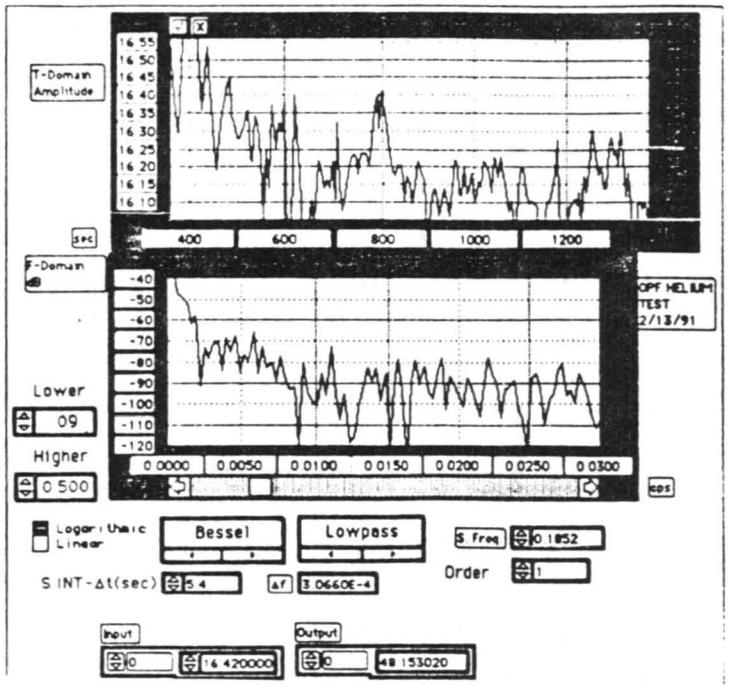

Figure 8. Example of OPF test data spectral analysis for 5.4-sec. sample frequency, with Bessel lowpass filtering

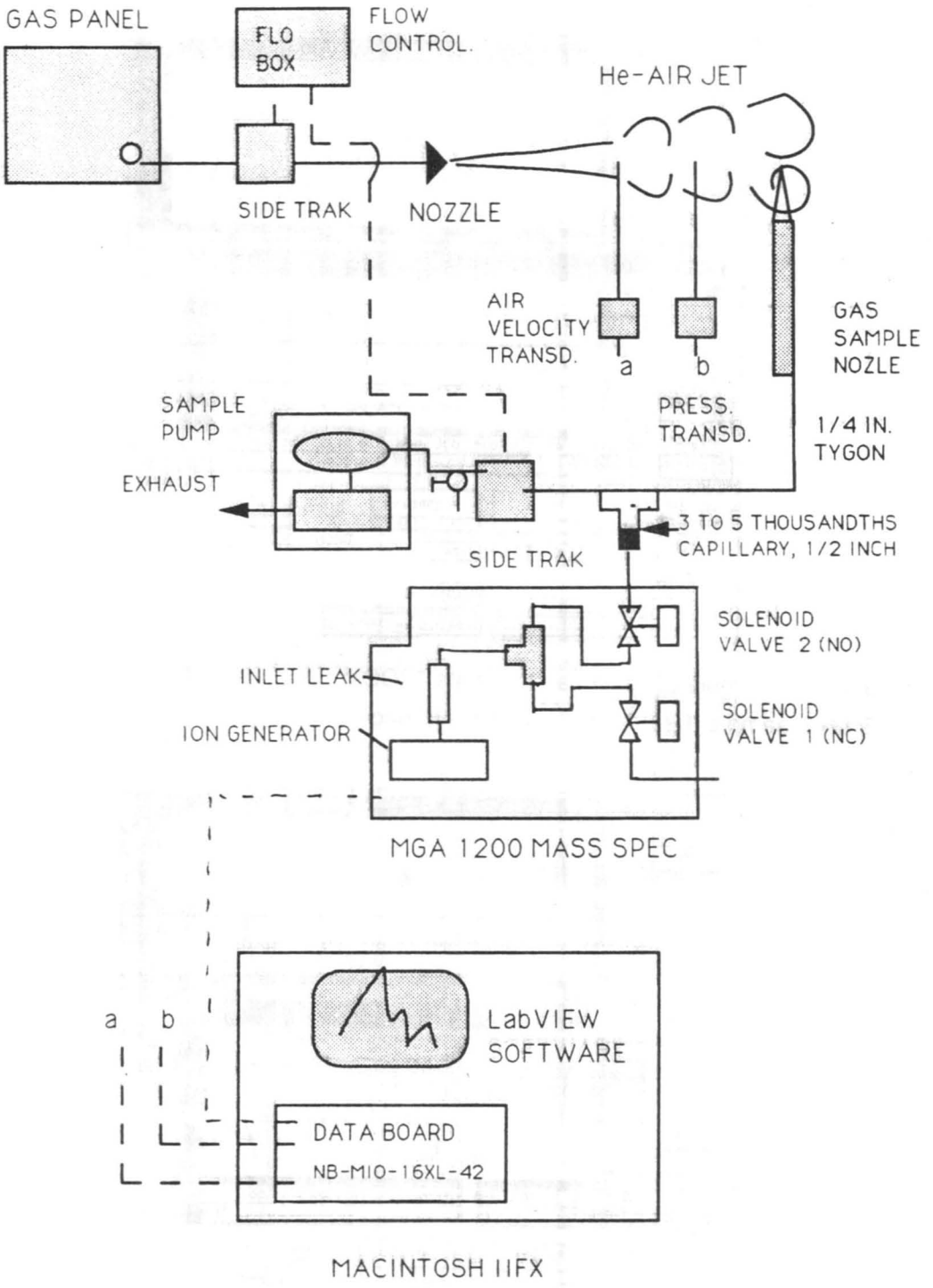

Figure 9. Present experimental setup featuring 1/4-in., 7.5-ft. sample tube and 1/2 in long capillary leak tube

Front Panel

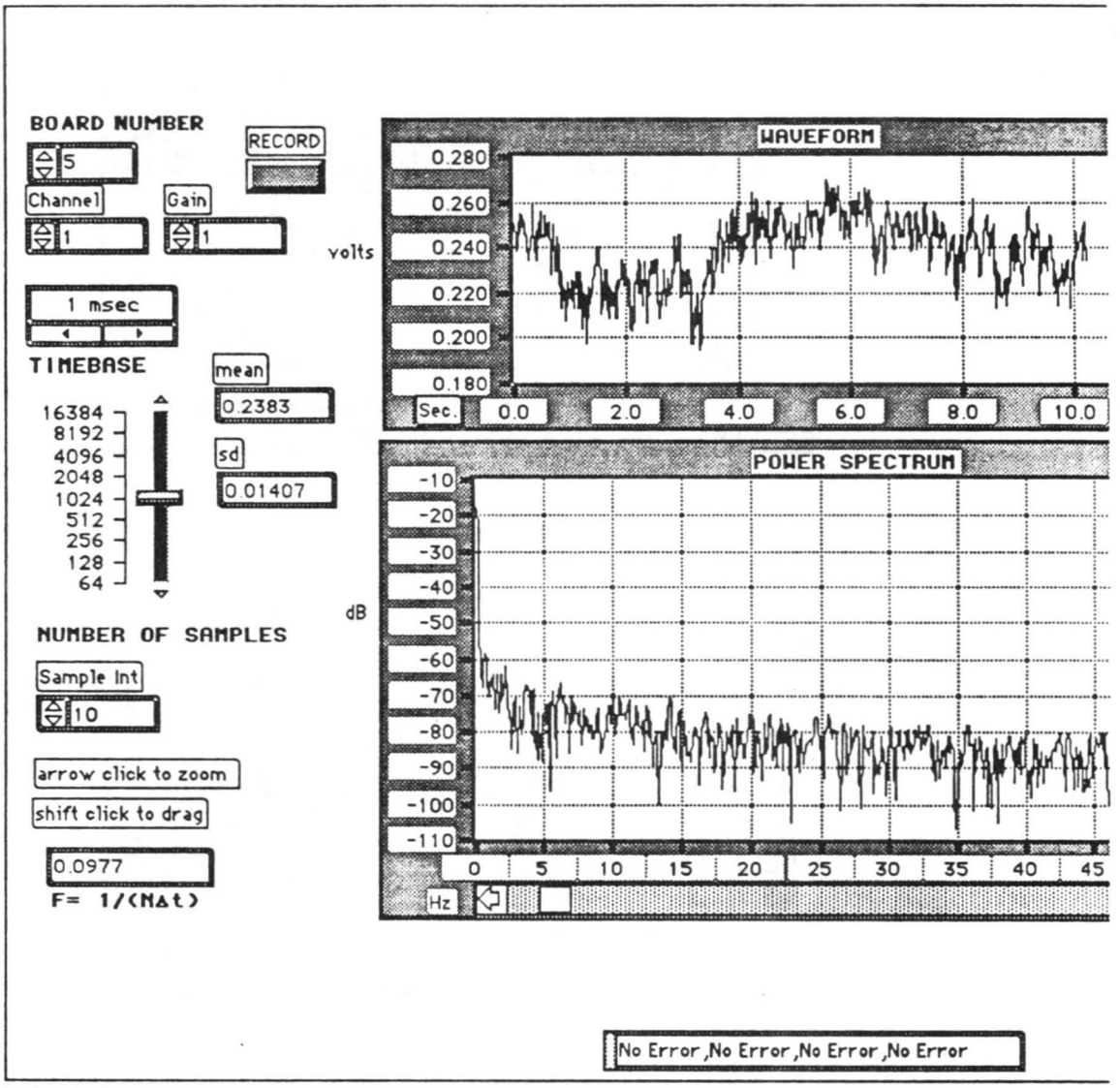

Figure 10. · Air velocity transducer response to a 2.9 SLM steady helium jet with probe at x = 8 cm., y = 0; local velocity is 692 FPM; initial jet velocity is 760 FPM.

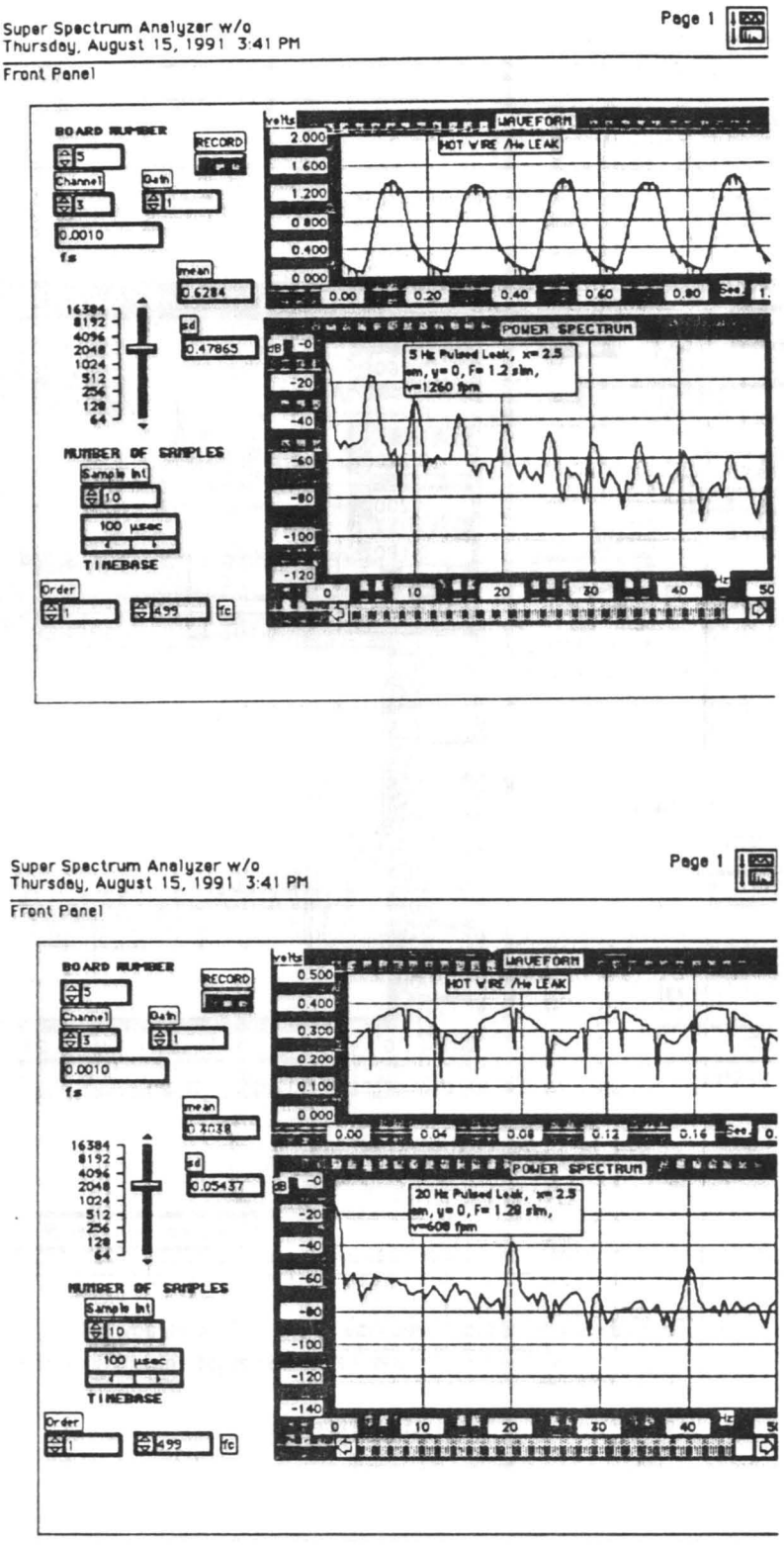

Figure 11. Response of air velocity transducer to pulsed helium jet; probe at 2.5 cm downstream in centerline. Top: 5 Hz, helium flow at 1.24 SLM, local velocity at 1260 FPM; bottom: 20 Hz, helium flow at 1.28 SLM, local velocity at 608 FPM

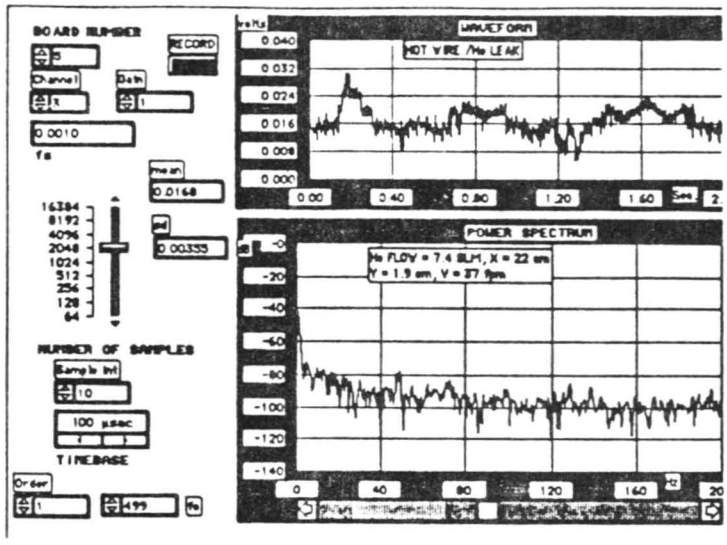

Figure 12. Air velocity transducer in helium jet flowing into room air; probe at 22 cm downstream offset from centerline (x = 22, y = 1.9 cm.). Helium flow is 7.4 SLM, local velocity is 37 FPM, initial jet is 1930 FPM.

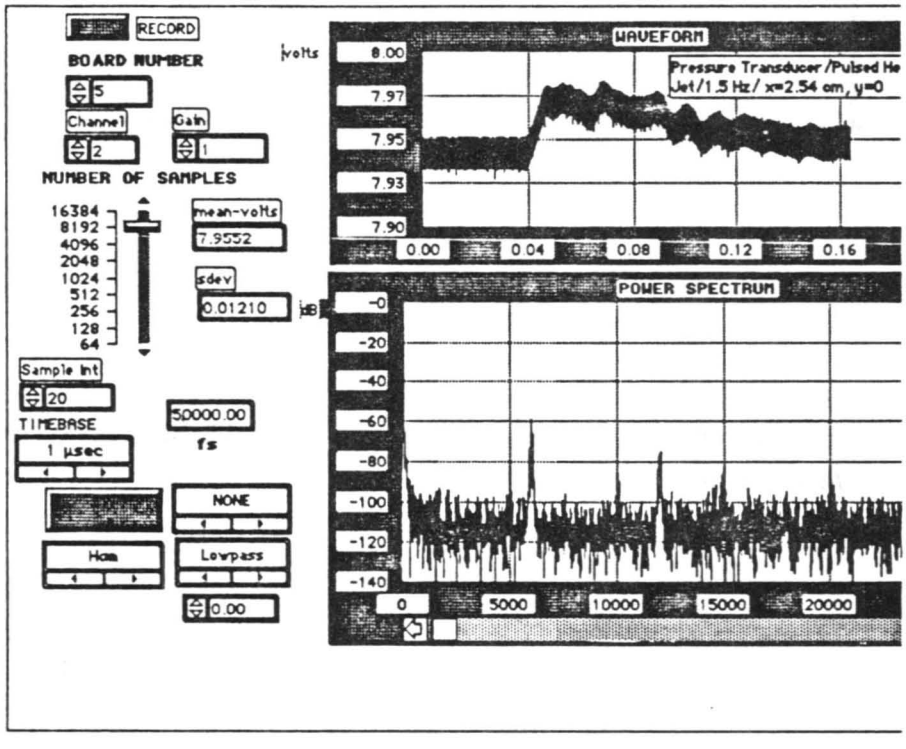

Figure 13. High frequency response of the Rosemount pressure transducer to a 1.5 cycle pulsed helium jet

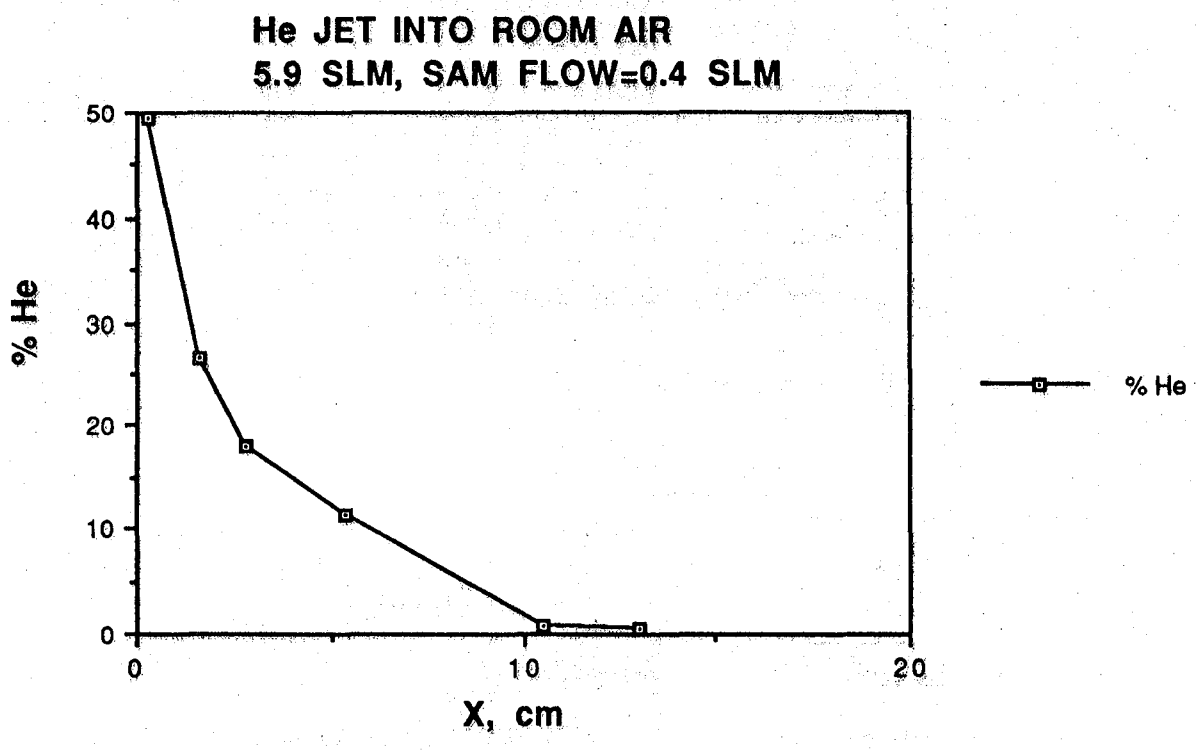

Figure 14. Helium concentration decay in a steady jet of 5.9 SLM using time-averaged data with 1/4-in., 7.5-ft. sample tube

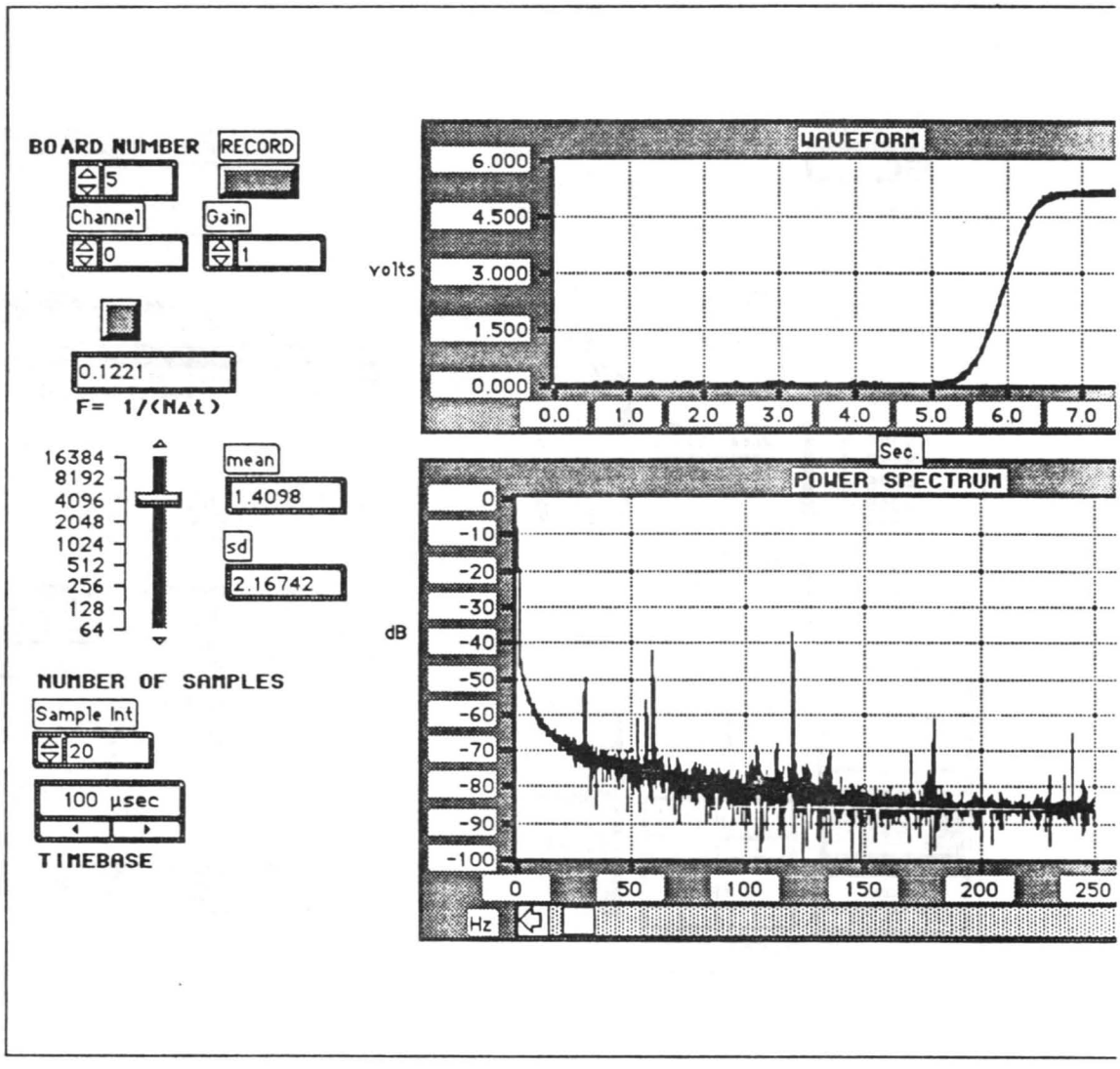

Figure 15. Response of 1/4-in., 7.5-ft. sample tube and MGA-1200 to a step input of helium

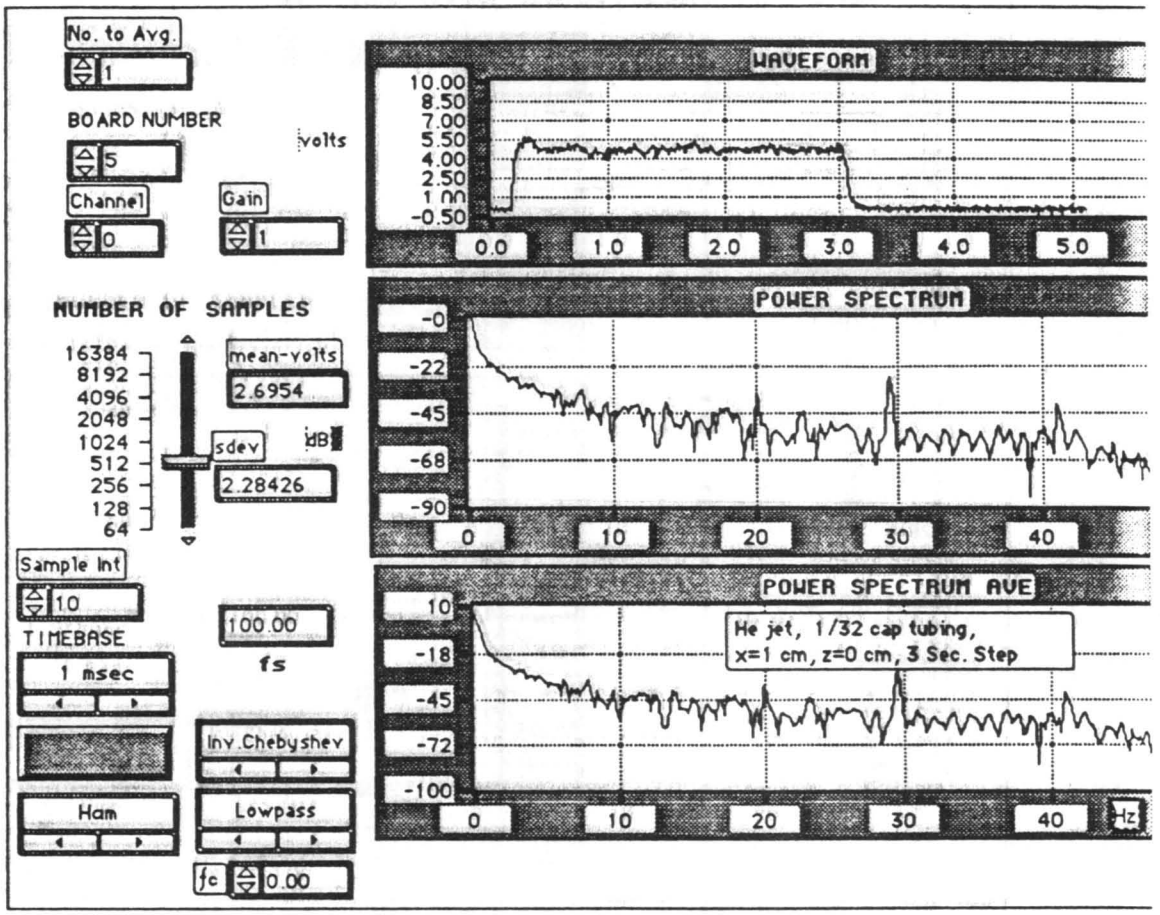

Figure 16. Response of 1/32-in., 15-ft. sample tube and MGA-1200 to a square wave input of helium

1991 NASA/ASEE SUMMER FACULTY FELLOWSHIP PROGRAM

JOHN F. KENNEDY SPACE CENTER
UNIVERSITY OF CENTRAL FLORIDA

REFLECTION EFFECTS IN MULTIMODE FIBER SYSTEMS UTILIZING LASER TRANSMITTERS

PREPARED BY:	Harry E. Bates
ACADEMIC RANK:	Professor
UNIVERSITY AND DEPARTMENT:	Towson State University Department of Physics
NASA/KSC	
DIVISION:	Electronic Systems
BRANCH:	Communications
NASA COLLEAGUE:	Po T. Huang
DATE:	August 20, 1991
CONTRACT NUMBER:	University of Central Florida NASA-NGT-60002 Supplement: 6

ACKNOWLEDGEMENTS

This research effort would not have been possible with out the assistance, cooperation and careful planning of a number of people. Larry Hand and Po Huang suggested the program and provided valuable support along the way. Po Huang was always available to answer questions provide literature references. He also gave guidance and support in more ways than can be described here. All levels of Engineering management above Po and Larry beginning with Perry Rogers provided valuable assistance and showed genuine interest in the project. Everyone was willing to listen and suggest solutions to problems. Special thanks to Fred MacKenzie,Richard Hall and Otto Variossi for helping to provide computers and software to use at Headquarters Building and introductions to people who could help with other problems in the area of data analysis. Mark Nurge was also especially helpful in assisting with ideas and equipment needed to interface the Macintosh in the laboratory to the optical spectrum analyzer. Boeing personnel were also most helpful in the laboratory. Special thanks to Houston Galloway and Bob Swindel who worked closely in all phases of this project including, but not limited to, design and acquisition of necessary equipment, shop work, and data collection. Brent Yates a coop from Georgia Tech. provided excellent assistance in the laboratory and with computer work especially in creating a model of a low pass filter to use in testing the RF spectrum analyzer and in transfering data files to the VAX.Thanks to Dr. Bob Youngquest who was willing to provide optical parts, filters and most of all ideas and approaches to technical problems.

ABSTRACT

A number of optical communication lines are now in use at the Kennedy Space Center (KSC) for the transmission of voice, computer data and video signals. At the present time all of these channels utilize a single carrier wavelengths centered near 1300 nm or 1550 nm. Engineering tests in the past have given indications of the growth of systematic and random noise in the RF spectrum of a fiber network as the number of connector pairs is increased. This noise seems to occur when a laser transmitter is utilized instead of a LED. It has been suggested that the noise is caused by back reflections created at connector fiber interfaces. Experiments were performed to explore the effect of reflection on the transmitting laser under conditions of reflective feedback.. This effort included, computer integration of some of the instrumentation in the fiber optic laboratory utilizing the Lab View software recently acquired by the laboratory group. The main goal was to interface the Anritsu Optical and RF spectrum analyzers to the Macintosh II computer so that laser spectra and newtork RF spectra could be simultaneously and rapidly acquired in a form convenient for analysis. Both single and multimode fiber is installed at the Space Center. Since the great majority is multimode, this effort concentrated on multimode systems.

SUMMARY

A number of optical communication lines are now in use at the Kennedy Space Center (KSC) for the transmission of voice, computer data and video signals. At the present time all of these channels utilize a single carrier wavelengths centered near 1300 nm or 1550 nm. Engineering tests in the past have given indications of the growth of systematic and random noise in the RF spectrum of a fiber network as the number of connector pairs is increased. This noise seems to occur when a laser transmitter is utilized instead of a LED.

It has been suggested that the noise is caused by back reflections created at connector fiber interfaces. Experiments were performed to explore the effect of reflection on the transmitting laser under conditions of reflective feedback and on the modulatation transmitted by the fiber optic link.

A major part of this effort included, computer integration of some of the instrumentation in the fiber optic laboratory utilizing the Lab View software recently acquired by the laboratory group. The main goal was to interface the Anritsu Optical and RF spectrum analyzers to the Macintosh IIx computer so that laser spectra and newtork RF spectra could be simultaneously and rapidly acquired in a form convenient for analysis. This goal was achieved. So much data was accumulated during these experiments that additional work will be required to do a complete detailed statistical analysis. At this point, only preliminary qualitative observations can be made through the use of 3D surface plots of data.

It was confirmed that connector reflections cause the RF spectrum to become perturbed. The more connectors in a network, the greater the perturbation. The optical spectrum also seems to be perturbed but this effect is not as easy to correlate to the connector number based on a quick look at the data. A more detailed analysis is required.

Some surprising results were also obtained. These include a chirp in the transmitter laser spectrum observed by utilizing a high speed spectral technique involving the use of a Fabry Perot interferometer. The success of this experiment suggests an experimental setup utilizing a boxcar signal averager for future work.

It was found that low frequency large amplitude motions and vibrations could adversely affect the optical spectrum and the RF spectrum. These results have significant implications when considering the design of any fiber optic system where fiber is likely to be subjected to such mechanical perturbations. For example in applications where a fiber data transmission link is located in a joint that can move while data is transmitted. Also in the case of large amplitude vibrations that might be encountered in the area of a launch beyond T + 0.

Both single and multimode fiber is installed at the Space Center. Since the great majority is multimode, this effort concentrated on multimode systems.

TABLE OF CONTENTS

LIST OF ILLUSTRATIONS

ABBREVIATIONS AND ACRONYMS LIST

CDSC	Communications Distribution and Switching Center
OSA	Optical Spectrum Analyzer
OTDR	Optical Time Domain Reflectometer
LED	Light Emitting Diode
KSC	Kennedy Space Center
TX	Transmitter
RMODE	Reflection Mode
TMODE	Transmission Mode
RX	Receiver
LID	Laser Diode

I. INTRODUCTION

A number of optical communication links are now in use at the Kennedy Space Center (KSC) for the transmission of voice, computer data and video signals. At the present time all of these channels utilize a single carrier wavelengths centered near 1300 nm or 1550 nm. Engineering tests in the past have given indications of the growth of systematic and random noise in the RF spectrum of a fiber network as the number of connector pairs is increased. This noise seems to occur when a laser transmitter is utilized instead of a LED. It has been suggested that the noise is caused by back reflections created at connector fiber interfaces. These perturbations may have both systematic and non systematic components. Therefore, repetitive observations must be made. Computer controlled experiments were performed to explore the effect of reflection on the transmitting laser under conditions of reflective feedback. The first step in this effort was to interface the Anritsu Optical and RF spectrum analyzers to the Macintosh IIx computer so that laser spectra and newtork RF spectra could be simultaneously and rapidly acquired in a form convenient for analysis. Experiments were conducted using this setup as well as several others. The experimental configurations and computer integration system is first presented. A brief description of experimental conditions is given, results and conclusions summarized, and finally data in the form of graphs are given in Appendices.

II. INTEGRATED LABORATORY SPECTRAL ANALYSIS SYSTEM

2.1 OPTICAL SPECTRUM ANALYZER

An Anritsu optical spectrum analyzer was available in the laboratory to be used to perform spectral analysis of coherent and incoherent sources. This piece of test equipment was equipped with an IEEE 488 computer interface which provides for bidirectional computer communication. A portion of the work done under this research effort was to interface the OSA with a Macintosh IIx computer to enable the efficient collection of spectral data in machine readable form. It was envisioned that the operator would manually set up the spectrum analyzer for any given experiment and when a spectrum was collected, activate the computer interface system and acquire a sequential data file containing the maximum wavelength, the minimum wavelength of the scan and 501 data points of optical spectral power density expressed in dBm or mW evenly distributed over the spectral interval.

2.2 RF NETWORK/SPECTRUM ANALYZER

An Anritsu radio frequency spectrum/ network analyzer was available in the laboratory to be used to perform analysis of the information channel of fiber optic networks. By using a computer to serve as an integrated data collection system, the RF spectra generated by this analyzer could be collected almost simultaneously with the optical spectrum allowing a correlation of data between the two instruments. The laboratory's Macintosh computer allowed this integration to be accomplished.

2.3 COMPUTER ANALYSIS AND DATA COLLECTION

2.3.1 THE MACINTOSH IIX COMPUTER

The Macintosh IIx Computer utilized a IEEE-488 National Instruments GPIB interface board which permitted the Macintosh computer to be coupled with the optical spectrum analyzer and the RF spectrum/network analyzer. Labview software system was chosen as a medium in which to develop an application program to integrate the collection of data by these two instruments.

The program created to connect the Macintosh with the spectrum analyzers displays one window. The window contains two graphic elements the permit the real time observation of collected spectra while an experiment is in progress. Parameter inputs are available to provide for specifying the number of runs the time in seconds between runs, the data storage disk name, the file name and experimental parameter notes to be saved in a text file. When the program is run, the optical spectrum analyzer and RF network/spectrum analyzers are triggered. The computer pauses to wait for data to be collected and spectra are displayed and written to two data files. The program assumes that experimental parameters are setup on the front panel of each instrument. Also, no error checking is performed on the data file name, volume name, or time between run parameters. Further work would need to be performed to make a more user friendly interface. Optical power vs wavelength and RF network transmission in dB vs frequency are stored on the designated disk for each data run made. The files are suitable for direct input to spread sheet and graphics programs. A series of VAX IMSL-based fortran programs have been written to assist in the analysis of multiple data runs. It was found that 15 seconds between runs and 40 total experimental runs would create a ten minute total test time and almost fill one double density (not high density) floppy disk with data. A total of 81 files are created, one not file and 20 files of optical and RF spectra.

2.3.2 VAX COMPUTER DATA ANALYSIS

The VAX support group created a set of graphics programs that could be used to display the data generated using the laboratory computer in a 3D spectrum/parameter axis plot. This set of programs can directly access the data files generated by the Labview application. In this stage of the analysis of the fiber optic systems, this 3D technique is used as the primary means of getting a first look at the data. Most of the conclusions drawn to date are based on this type of analysis. Further efforts will permit a more detailed statistical analysis to be performed. Some difficulty in preparing the plots resulted in no axis labels being printed in some cases. A summary of the experimental parameters for each run presented is given at the bottom of the plot. This should allow a reasonable interpretation of the results.

2.4 DESIGN OF FIBER TO FREE SPACE TO FIBER SYSTEM

In order to provide a means of inserting optical components such as wave plates, polarizers and a Fabry Perot interferometer into the optical beam path of a communication system, a means of connecting fiber optics to free space optics was required. Such a system was constructed using fiber holders, SLS-2.0-0.25-1.3 GRIN lenses selected from a laboratory set, precision translation stages to hold optical fiber and lenses, and an optical table for the assembly of components. The optical design of one configuration of the system is shown in the diagram below.

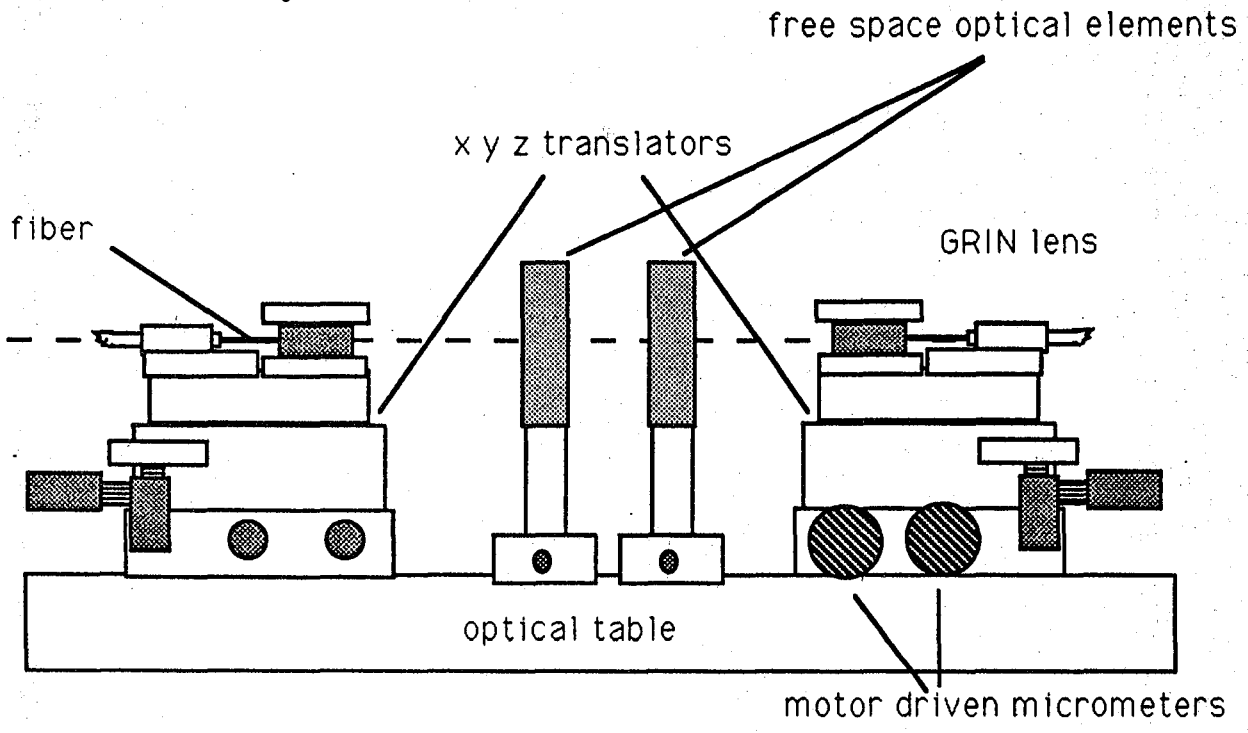

Figure 2.4-1. Concept Drawing Fiber to Free Space to Fiber system (not to scale and fiber V block detail not shown here.)

Experiments were conducted to determine the attenuation of the system. It was found that with an air gap spacing of 6.5", sufficient to permit introduction of the Fabry Perot system. Under these conditions a 10 dB loss was sustained in going from fiber to air to fiber.

2.5 Fabry perot interferometer

A Fabry Perot interferometer was set up to be used to obtain high resolution spectra as well as allowing the study of transient spectral phenomena of the laser transmitters. This device consists of two high quality mirrors having very high reflectivity and held in stable mounting hardware that includes piezoelectric electromechanical translators. The mechanical system is shown in the figure below:

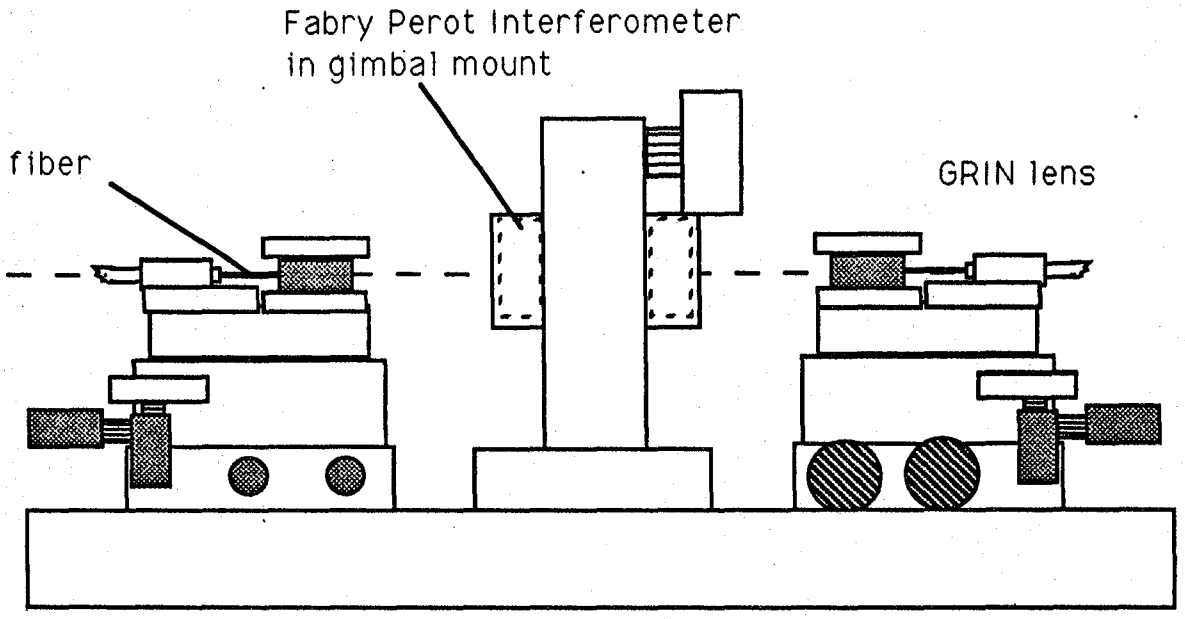

Figure 2.5-1. Concept Drawing Fabry Perot Interferometer system (not to scale and fiber V block detail not shown here.)

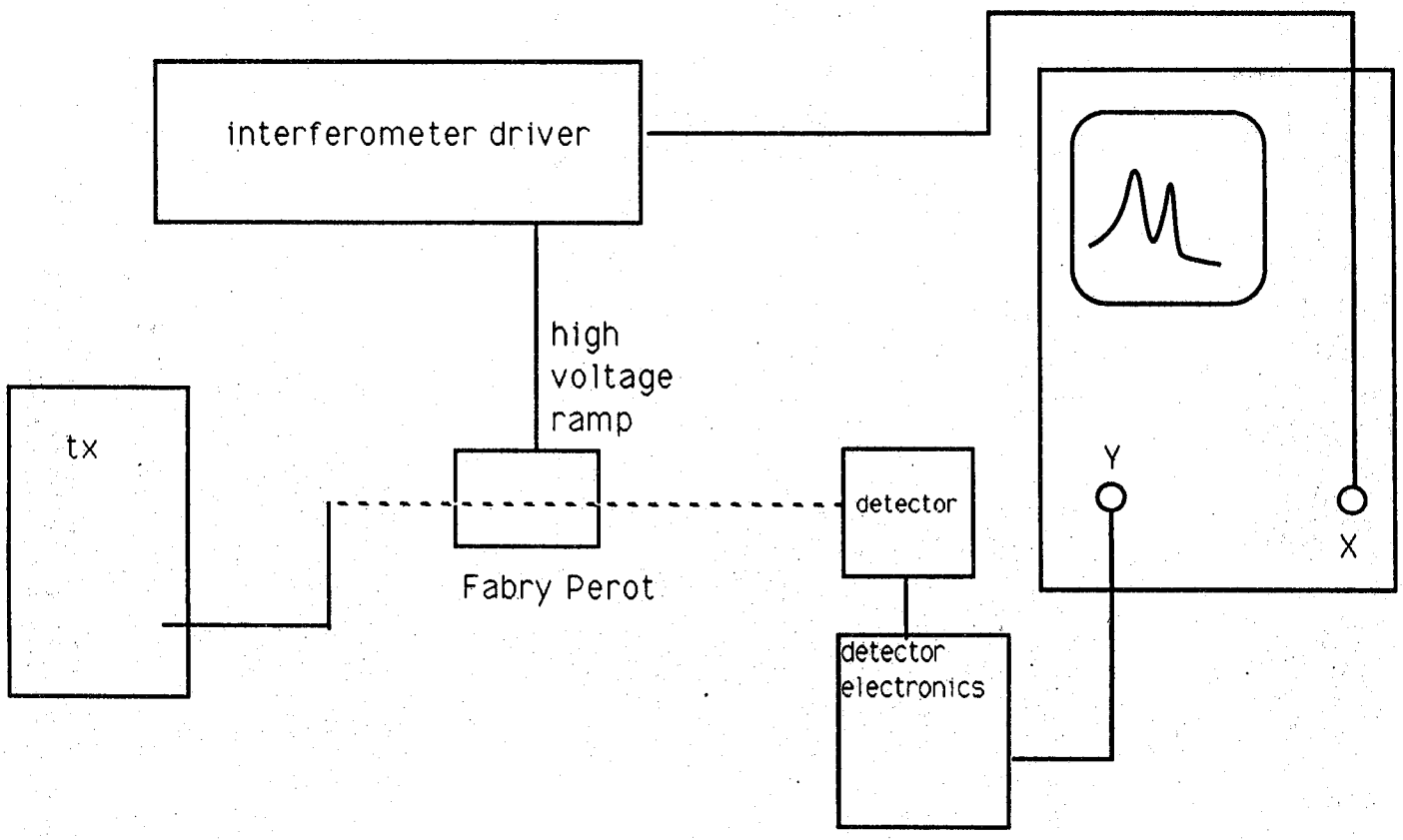

Figure 2.5-2. Block Diagram Illustrating Method of Utilizing Fabry Perot Interferometer to Collect Spectrum.

The Fabry Perot was calibrated by using the Anritsu optical spectrum analyzer as a standard. The results of this calibration are shown in the graph that follows.

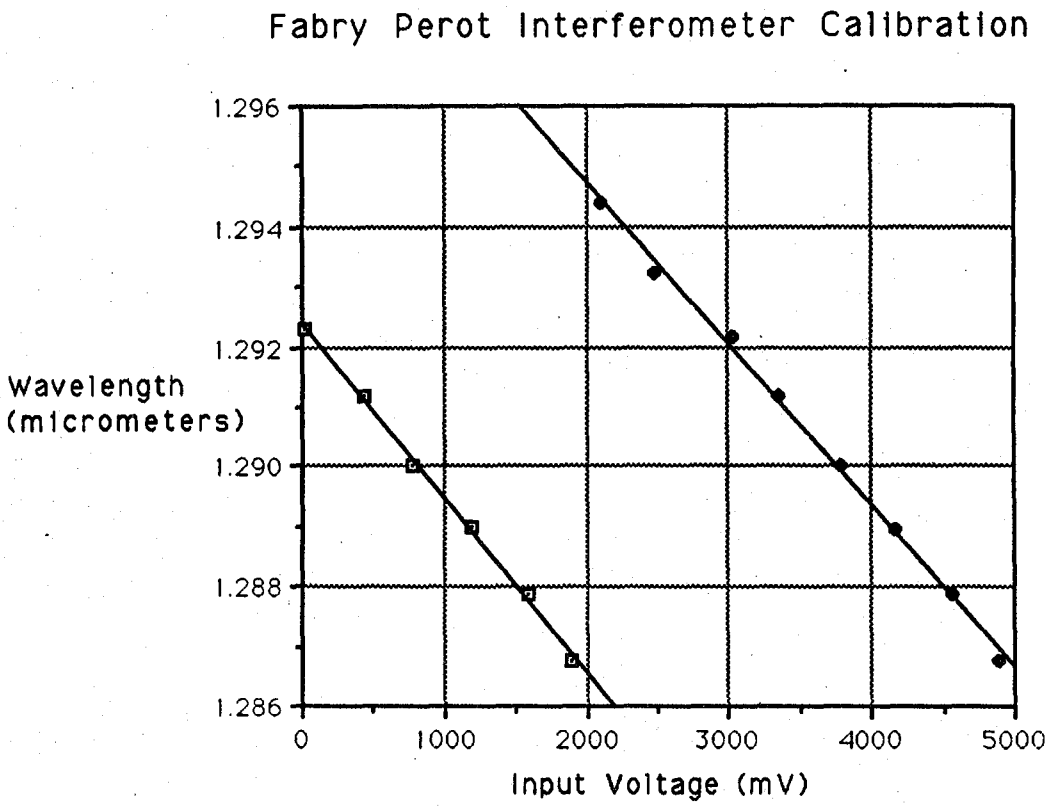

Figure 2.5-3. Fabry Perot Transmission Wavelength vs. Applied Voltage

A linear least squares fit to the above data in each of the two regions yielded the following equations:

$$L_a = 1.2924 - (2.92 \times 10^{-6})\, v$$

$$L_b = 1.3001 - (2.70 \times 10^{-6})\, v$$

Where the wavelength L for the two regions is given in micrometers and the voltage is given in mV.

The free spectral range can be obtained from the above by taking the difference between the y intercepts. This gives a measured free

spectral range of about 7.7 nm. Close to that calculated from the manufactures specifications of 8 nm.

The finesse of the system can be roughly estimated by observing that two adjacent modes can just be resolved. The laser modes are separated by 1.0 nm for the laser used in the tests. Thus the finesse is about 7.7nm/1.0nm or about 8. This is 1/5 that the expected value. This could be caused by modulation on the laser or poor alignment and filling of the aperture of the Fabry Perot. Additional time should be spent in resolving this issue.

Because of the limited time available to work with this instrument, the author was unable to use it to obtain high resolution spectra of the laser sources. However valuable experiments were undertaken to observe the temporal behavior of the transmitter sources at fixed wavelengths. The results of these experiments are discussed in a later section.

III EXPERIMENTS PERFORMED

3.1 BASIC NETWORK CONFIGURATIONS STUDIED

3.1.1 TRANSMISSION MODE

Transmission mode studies analyze the modulation and light spectra transmitted through the test loop. Experiments were conducted using a laboratory spool of test fiber, with various numbers of connector pairs on short jumpers added after the test spool and through one and two loop actual data links from the EDL to the CDSC. The experimental configuration is shown in the Fig. below. Each group of similar experiments included a base line configuration that only utilized the 1 km laboratory spool of fiber.

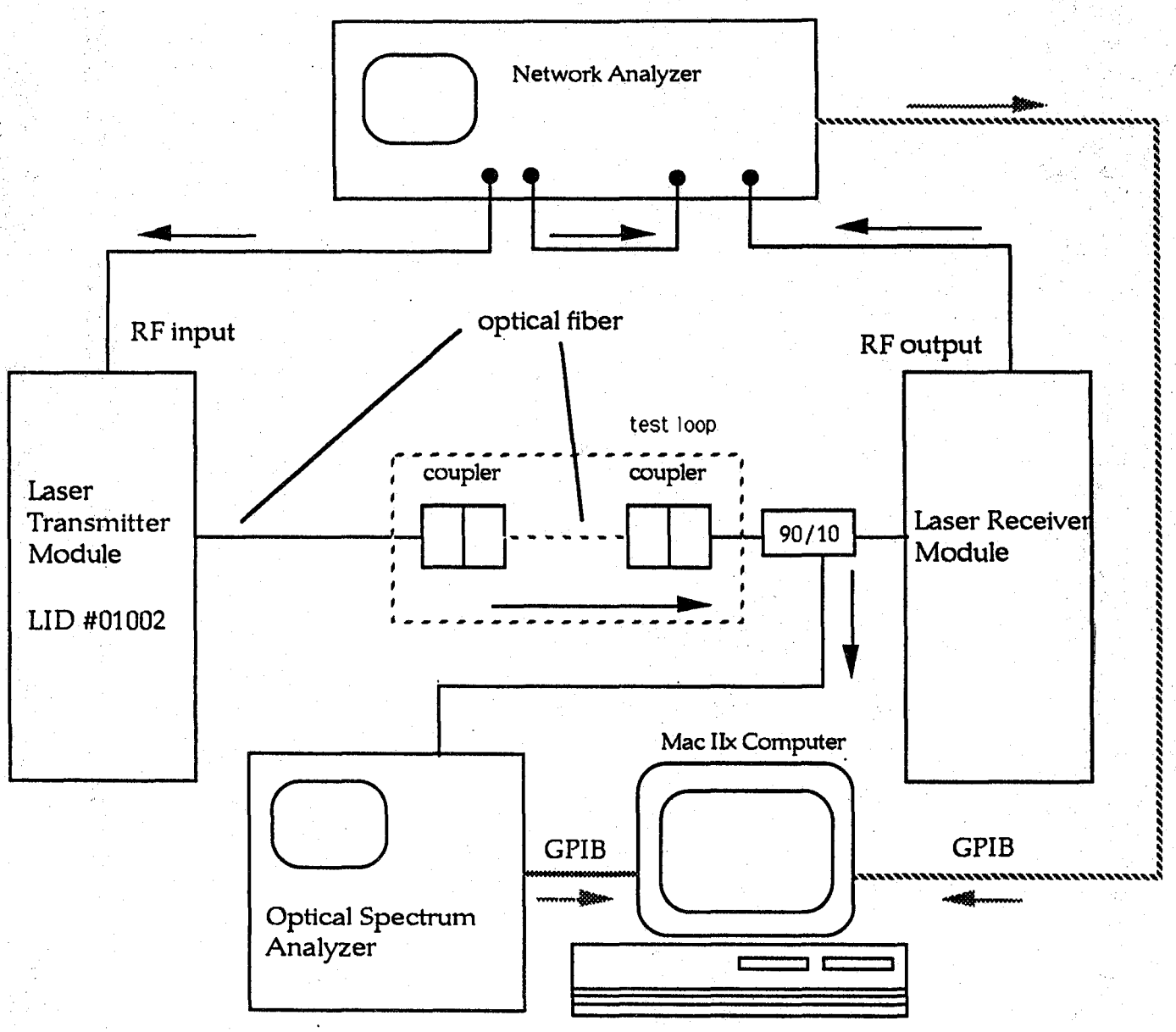

Figure 3.1.1-1 Transmission Mode Experimental Setup.

Appendix A shows selected output data from TMODE experiments.

3.1.2 REFLECTION MODE

Reflection mode studies analyze the modulation spectra transmitted through the test loop and light spectra collected directly at the laser source.. Experiments were conducted using a laboratory spool of test fiber, with various numbers of connector pairs on short

jumpers added after the test spool and through one and two loops actual data links from the EDL to the CDSC. Each group of similar experiments included a base line configuration that only utilized the 1 km laboratory spool of fiber. The experimental setup is shown in the Fig. below.

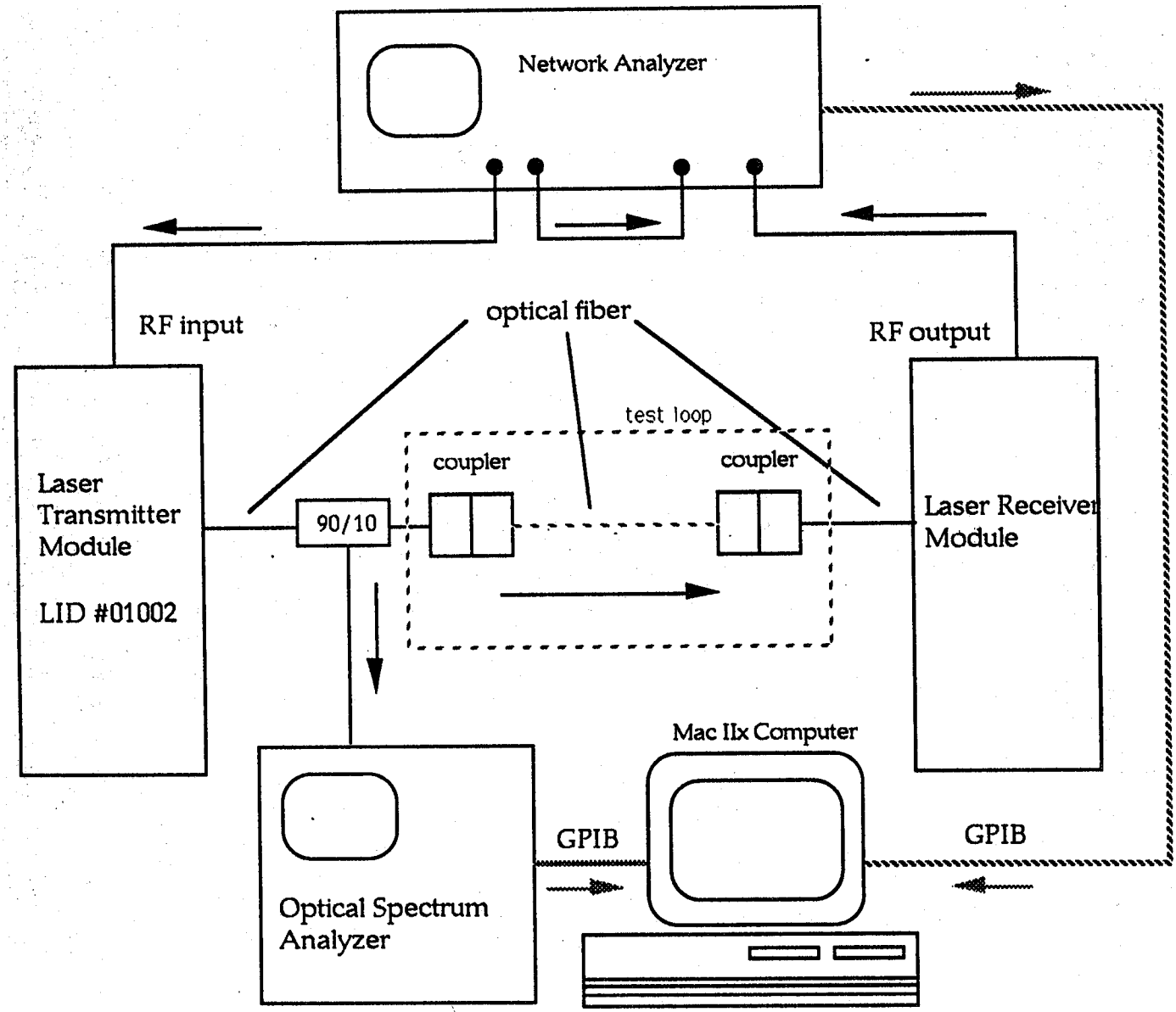

Figure 3.1.2-2 Reflection Mode Experimental Setup

Appendix B shows a selected collection of output data from these reflection mode experiments.

3.2 RESULTS OF STUDIES WITH FREE SPACE LINK IN NETWORK

A study was conducted to explore the effects of quarter wave plates and polarizers in the test link. A test section was constructed that consisted of a free space link with a polarizer and a quarter wave plate oriented at 45 degrees to the axis of the polarizer. The basic setup is shown below:

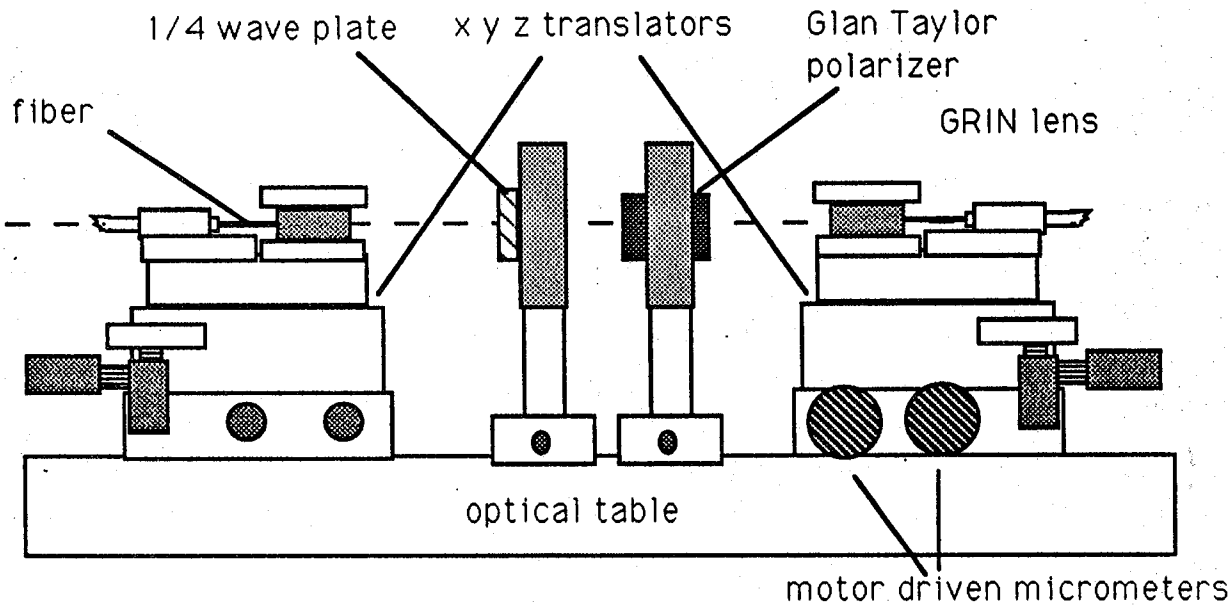

Figure 3.2-1. Free Space Test Link.

RF and optical spectra were collected with this free space section in the optical link and with out in order to compare. A sample of a spectrum taken with the polarizer and 1/4 wave plate is shown below. Eighteen connector pairs were utilized in both setups to create perturbations in the network transmission.

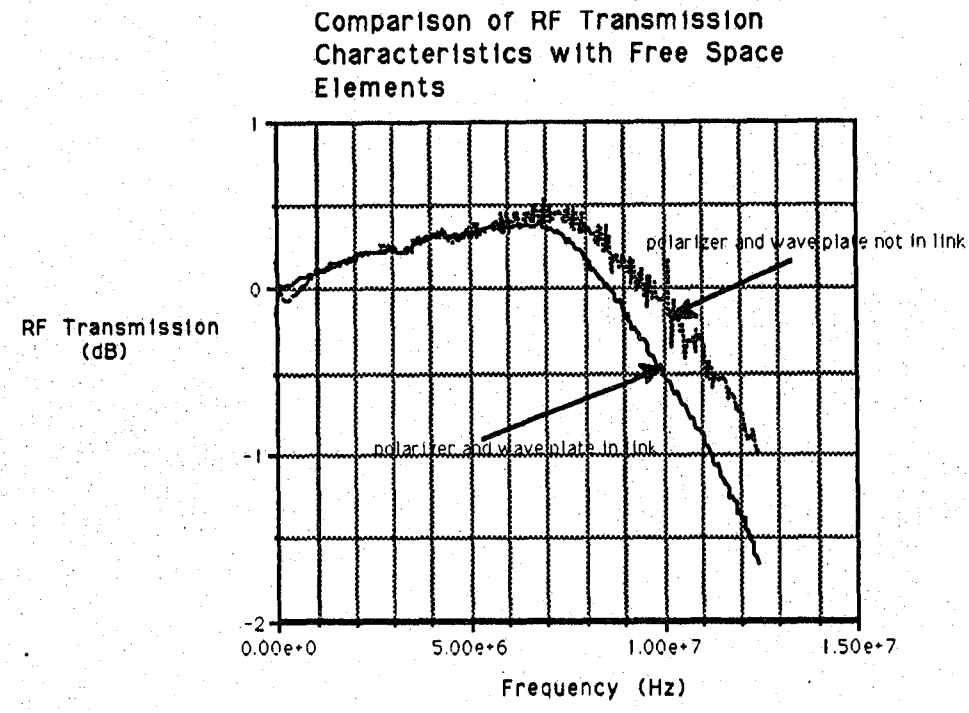

Figure 3.2-2. The effects of elements in Free Space Link on RF Spectrum

This interesting result is just a preliminary view of the kind of things that can be accomplished by studying the insertion of various combinations of free space optical elements into a fiber optic link. It suggests that many further experiments need to be done to try to optimize link performance and help minimize the adverse effects of reflections at connectors.

3.3 RESULTS OF STUDIES USING THE FABRY-PEROT INTERFEROMETER

A limited number of experiments were conducted with the Fabry Perot interferometer. One significant result was the observation of chirp in the modal frequency of the transmission laser with a repetition rate equal to the modulation frequency of the laser. This was observed by setting the Fabry Perot at a fixed transmission frequency thereby selecting one mode of the transmitter laser. Graphs taken from the sampling oscilloscope are shown in Appendix C. The shape of the peak of the modulated waveform could be set by

changing the bias on the piezoelectric element of the interferometer. This conclusively proves that a small chirp is present in the laser output frequency during the time the carrier pulse is on. an estimate of the magnitude of this chirp could be made given time for further experiments and analysis.

4.0 CONCLUSIONS AND RECOMMENDATIONS FOR FURTHER WORK

This work has both answered questions and suggested new ones. The experiments performed show conclusively that connectors in a fiber optic network do effect the performance of the network if a laser source is utilized. The perturbations increase as more connector pairs are introduced. While a frequency chirp was observed with the Fabry Perot setup, the amount of the chirp is small compared to the spacing between the modes. This conclusion is supported by the many spectra collected over time. Laser modes remained locked in place and modal spacing did not change. Large shifts in energy distribution between modes was noticed. In some cases this was seen when a fiber in the test link was moved several centimeters. Small vibrations did not produce as noticeable an effect. More work needs to be done to quantify these effects especially if fibers are to be employed in systems subject to vibrations, thermal stress or large amplitude mechanical motion during normal operations.

The presence of optical elements such as polarizers, GRIN lenses and wave plates can effect both bandwidth and perturbations caused by connector reflections. Only preliminary experiments have been conducted in the limited time available. The author recommends that these experiments be continued and theories developed to account for such effects in multimode systems. The results of such research could have an impact on the design and implementation of fiber systems at KSC and for the Space Station Project where it is anticipated that large diameter optical fiber will be used.

A considerable effort was made during this project to link the Macintosh IIx computer to the optical spectrum analyzer and the RF spectrum analyzer. As a result of the success of this effort a large amount of data has been collected. More data in fact than can be completely analyzed in the short period of time available during a Summer Faculty Fellowship. It is therefore recommended that data analysis be continued so as to develop more quantitative statistical results of the experiments completed to date.

Appendix A SELECTED DATA OUTPUT FROM TMODE EXPERIMENTS

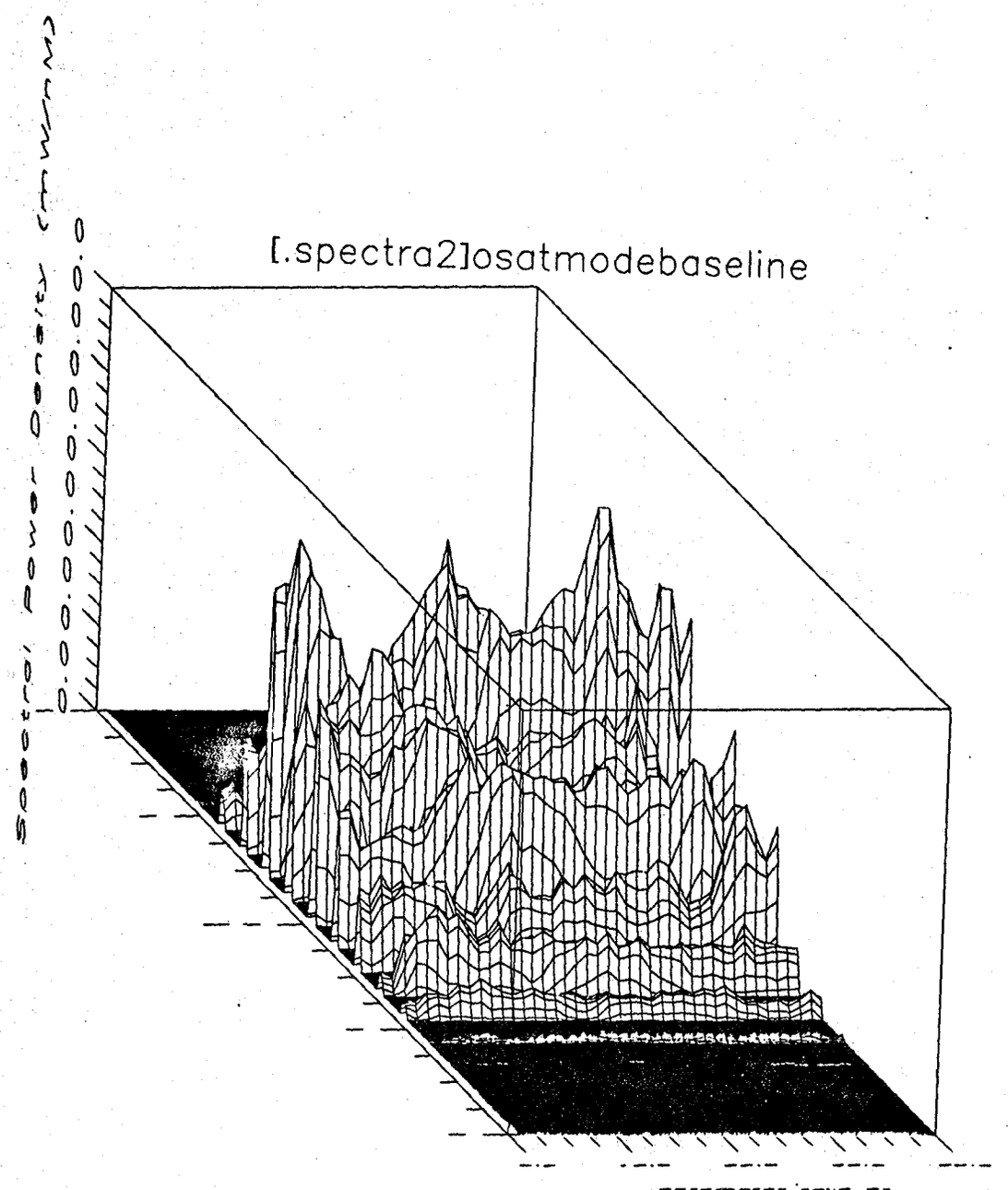

TMODEBASELINE

Tmode no connector pairs added to system. OSA 500 nW, 1.28-1.3 micrometers span. RF 10 Hz to 12.5 MHz .1 dB/div VBW 300 Hz RBW 100Hz. 35 dB variable ATTENUATOR IN LINE. 15 sec betweeh runs.

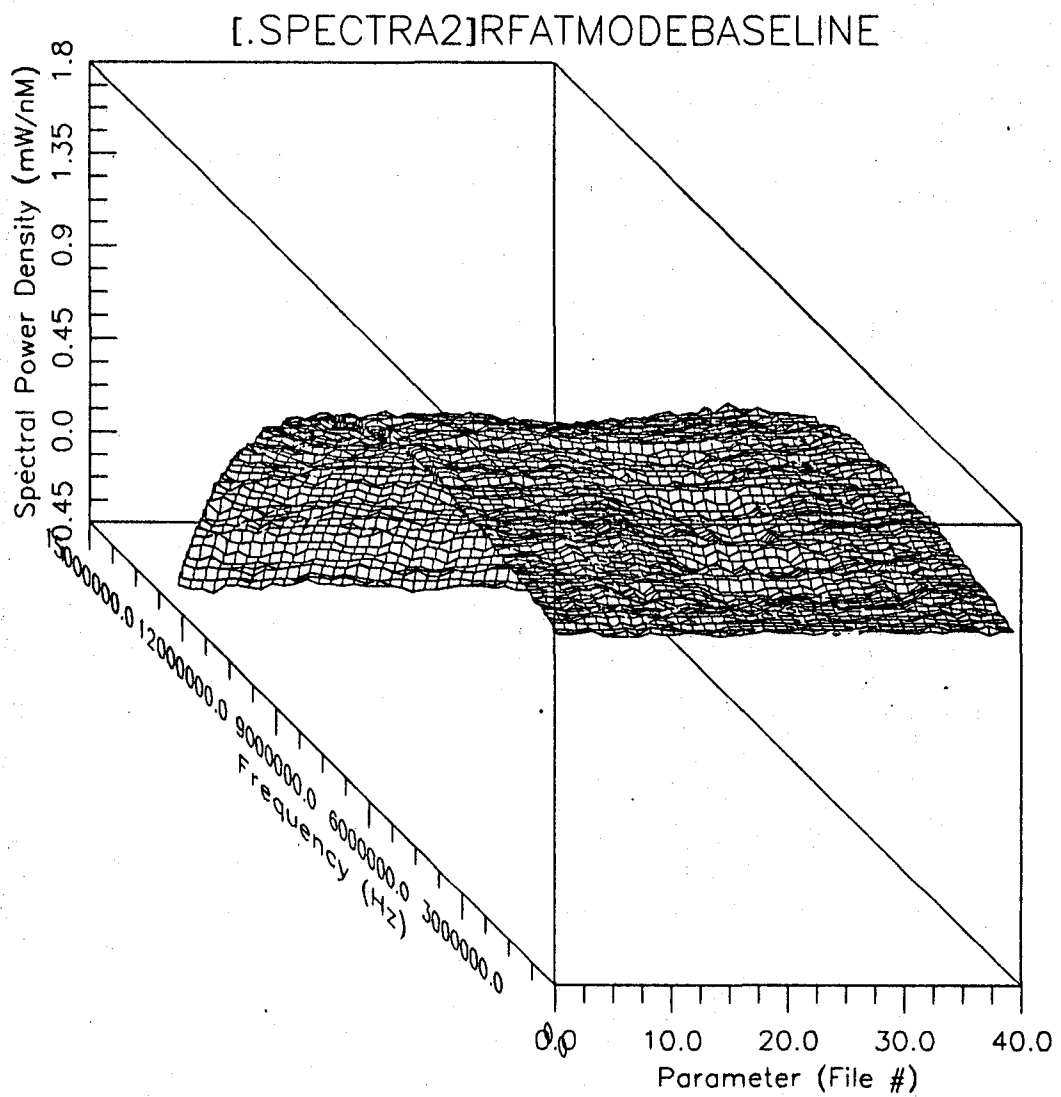

TMODEBASELINE

Tmode no connector pairs added to system. OSA 500 nW, 1.28-1.3 micrometers span. RF 10 Hz to 12.5 MHz .1 dB/div VBW 300 Hz RBW 100Hz. 35 dB variable ATTENUATOR IN LINE. 15 sec between runs.

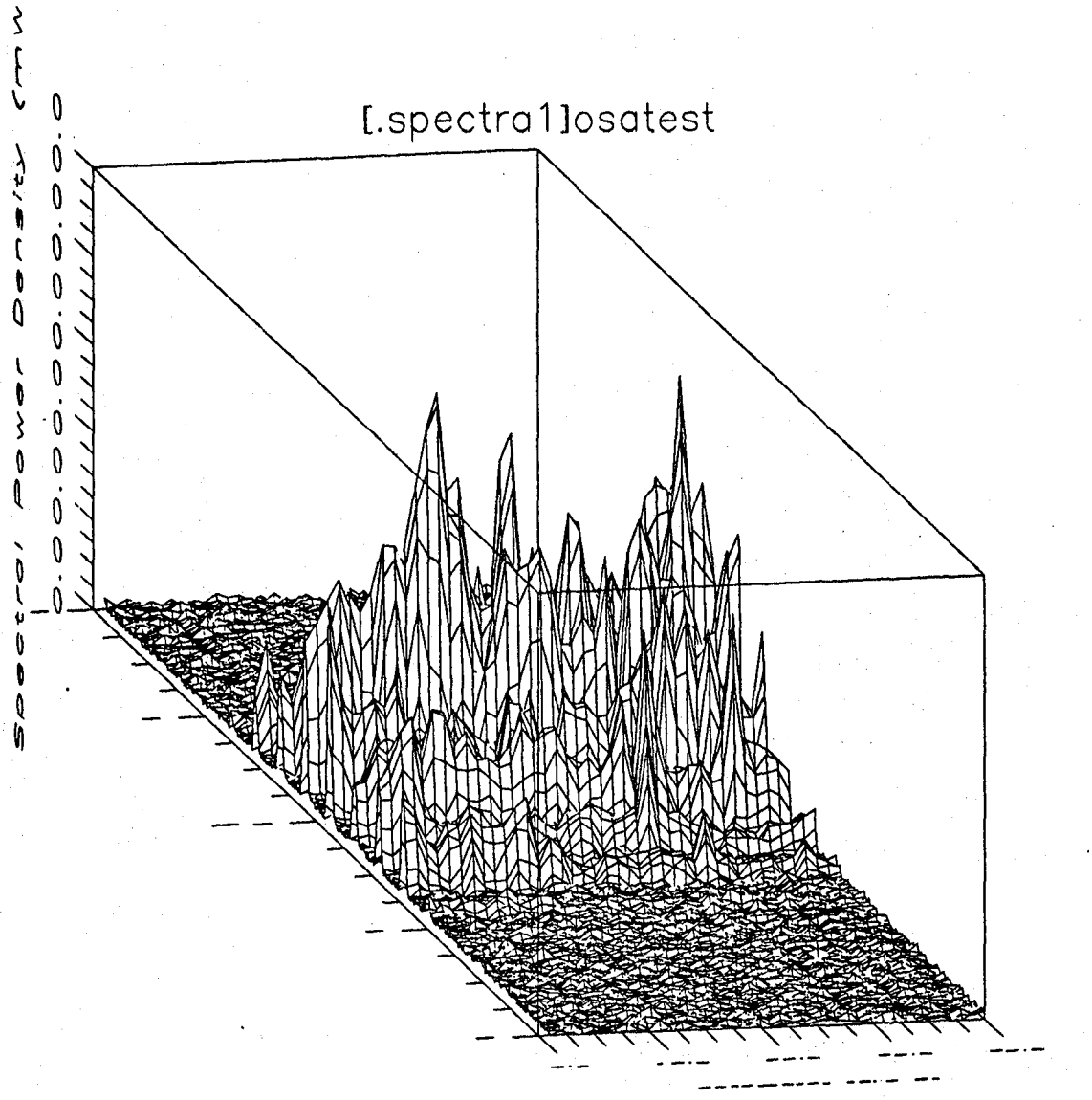

RFATEST

Tmode 20 connector pairs added to system. OSA 2.5 nW, 1.28-1.3 micrometers span. RF 10 Hz to 12.5 MHz .1 dB/div VBW 300 Hz RBW 100Hz. NO ATTENUATOR IN LINE.

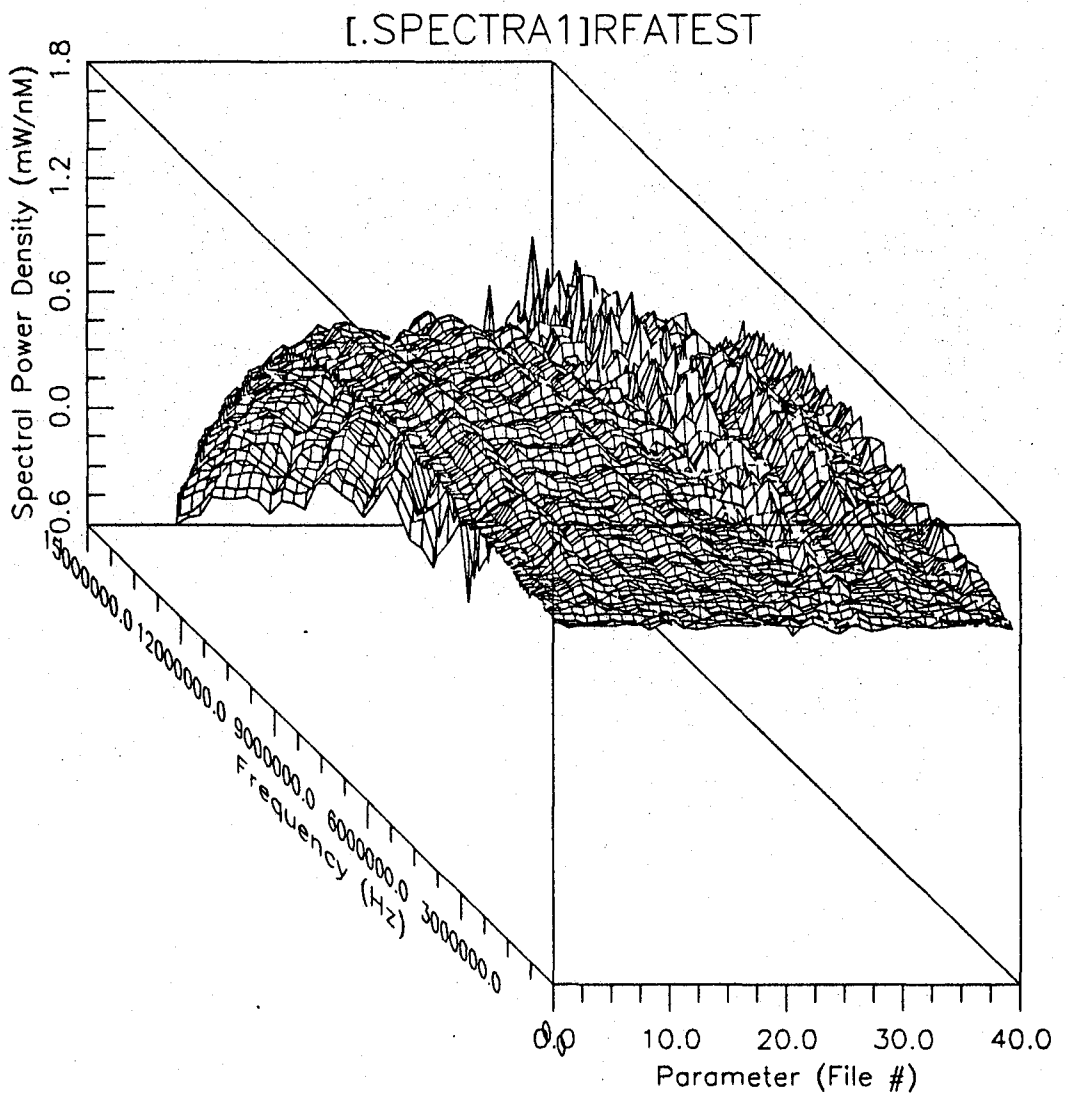

RFATEST

Tmode 20 connector pairs added to system. OSA 2.5 nW, 1.28-1.3 micrometers span. RF 10 Hz to 12.5 MHz .1 dB/div VBW 300 Hz RBW 100Hz. NO ATTENUATOR IN LINE.

Appendix B SELECTED DATA OUTPUT FROM RMODE EXPERIMENTS

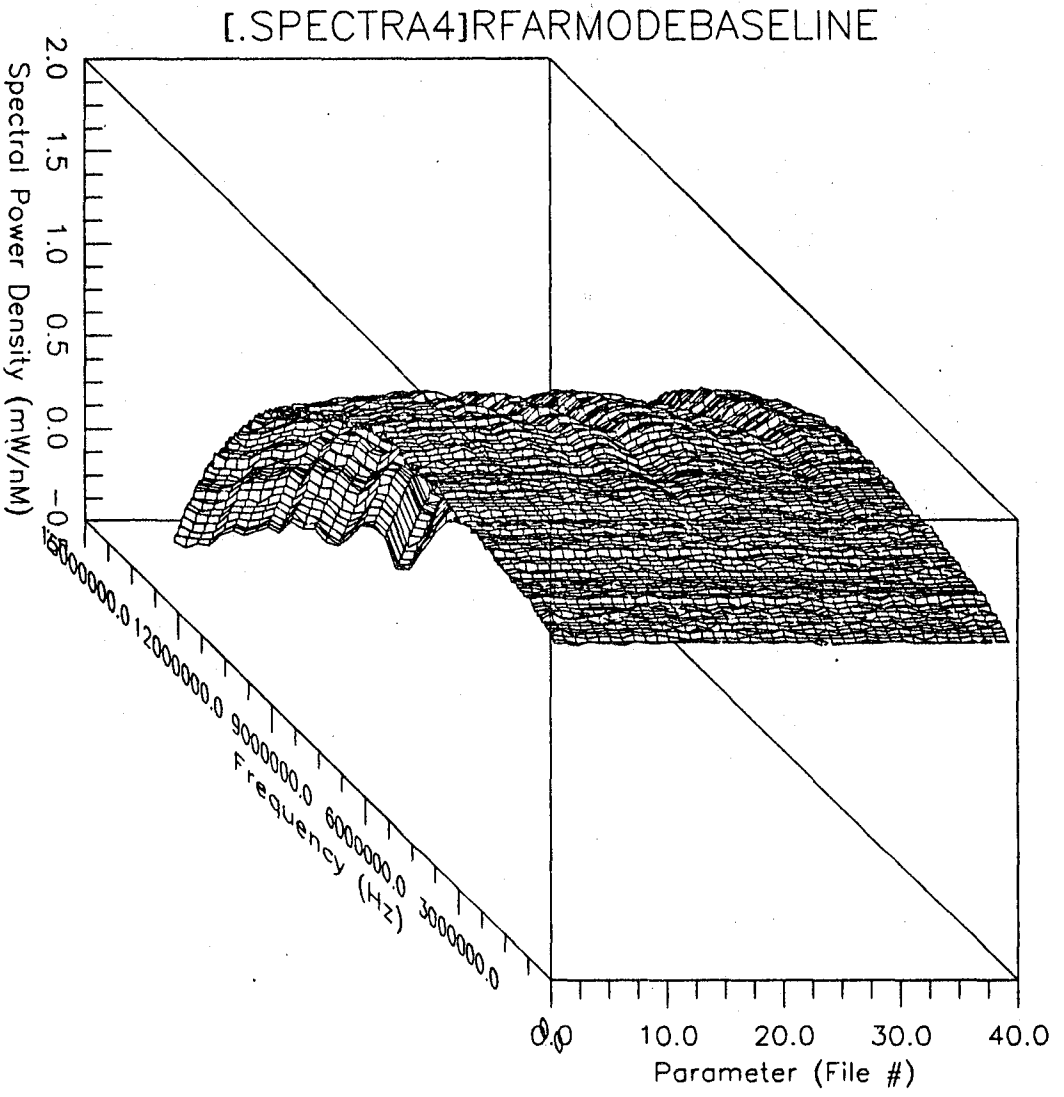

RMODE BASELINE

Rmodebaseline system no extra connectors AS WELL AS 20 dB variable ATTENUATOR IN LINE. OSA 500 nW, 1.28-1.3 micrometers span. RF 10 Hz to 12.5 MHz .1 dB/div VBW 300 Hz RBW 100Hz. 15 sec between runs.

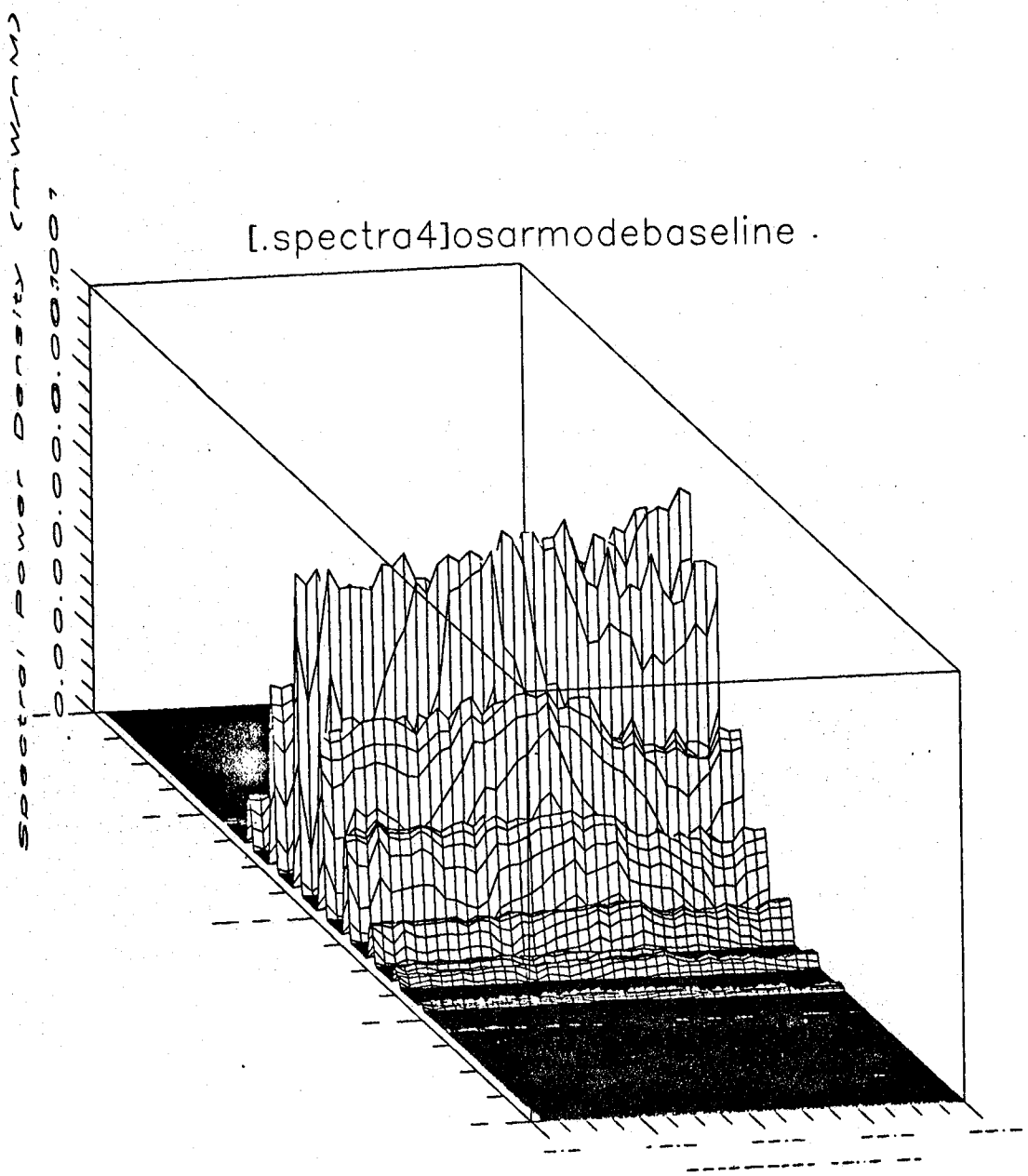

RMODE BASELINE

Rmodebaseline system no extra connectors AS WELL AS 20 dB variable ATTENUATOR IN LINE. OSA 500 nW, 1.28-1.3 micrometers span. RF 10 Hz to 12.5 MHz .1 dB/div VBW 300 Hz RBW 100Hz. 15 sec between runs.

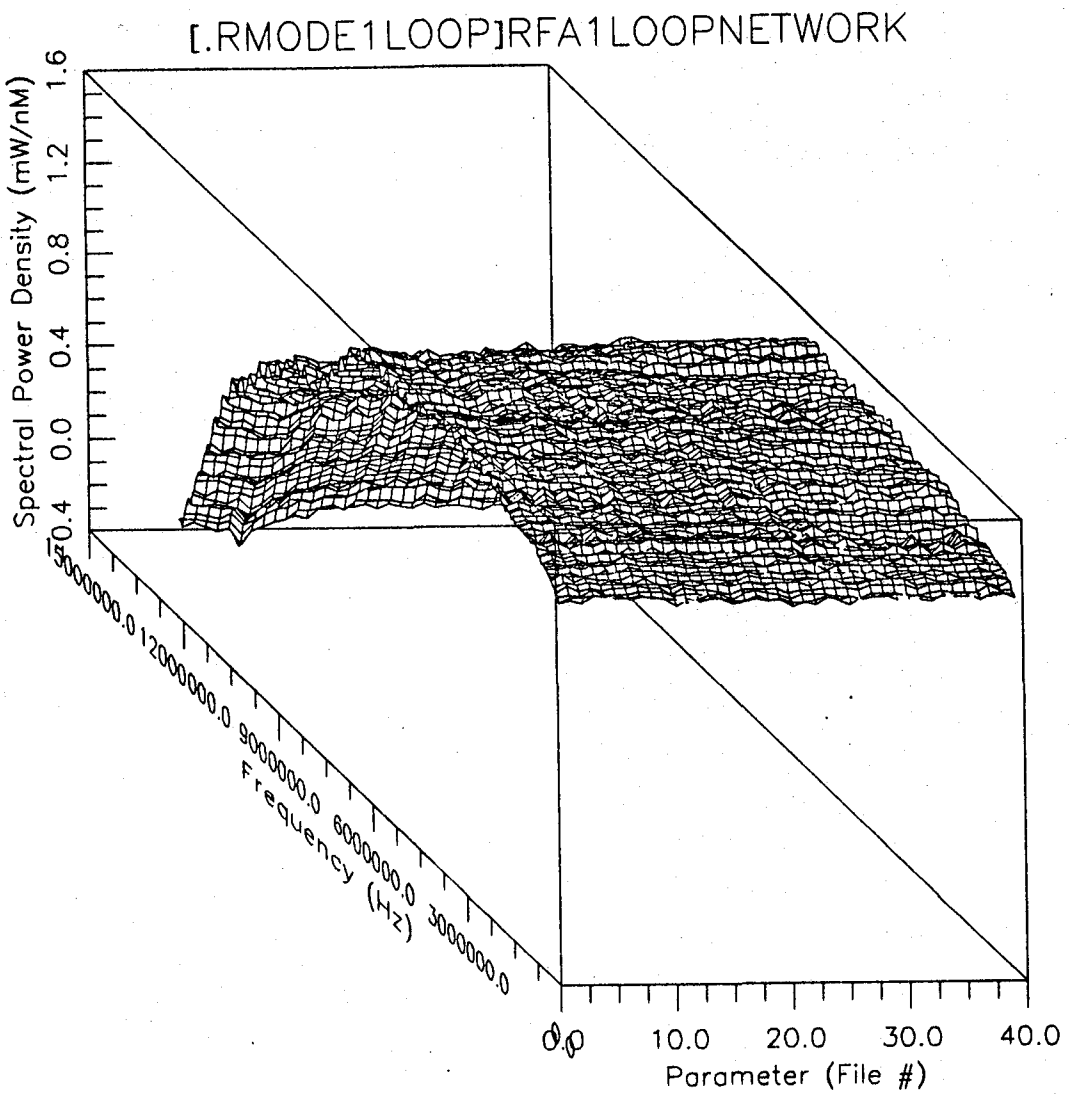

RMODE1LOOP

Rmode system 1 loop network CDSC and back. OSA 500 nW, 1.28-1.3 micrometers span. RF 10 Hz to 12.5 MHz .2 dB/div VBW 300 Hz RBW 100Hz. 15 sec between runs.

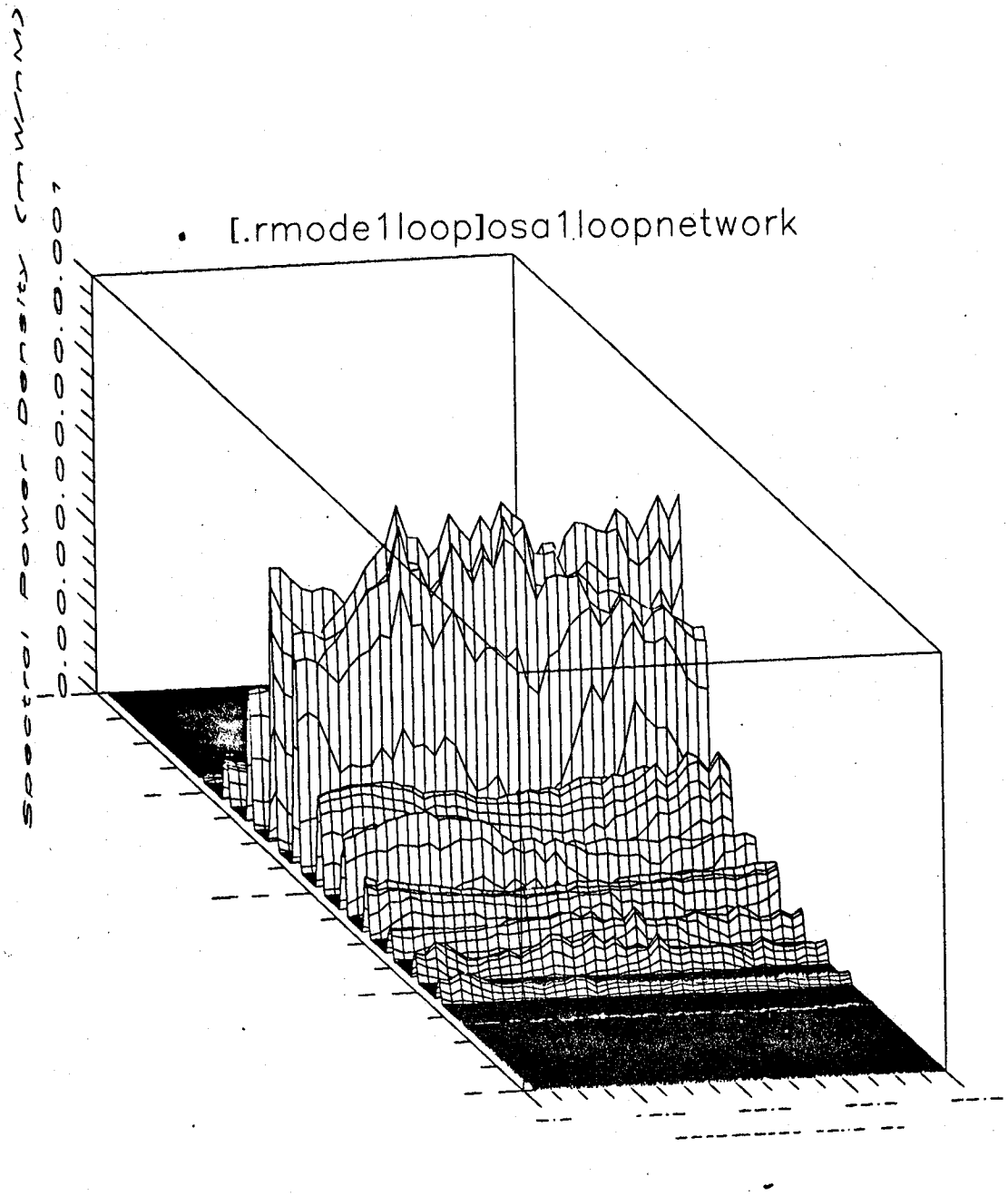

RMODE1LOOP

Rmode system 1 loop network CDSC and back. OSA 500 nW, 1.28-1.3 micrometers span. RF 10 Hz to 12:5 MHz .2 dB/div VBW 300 Hz RBW 100Hz. 15 sec between runs.

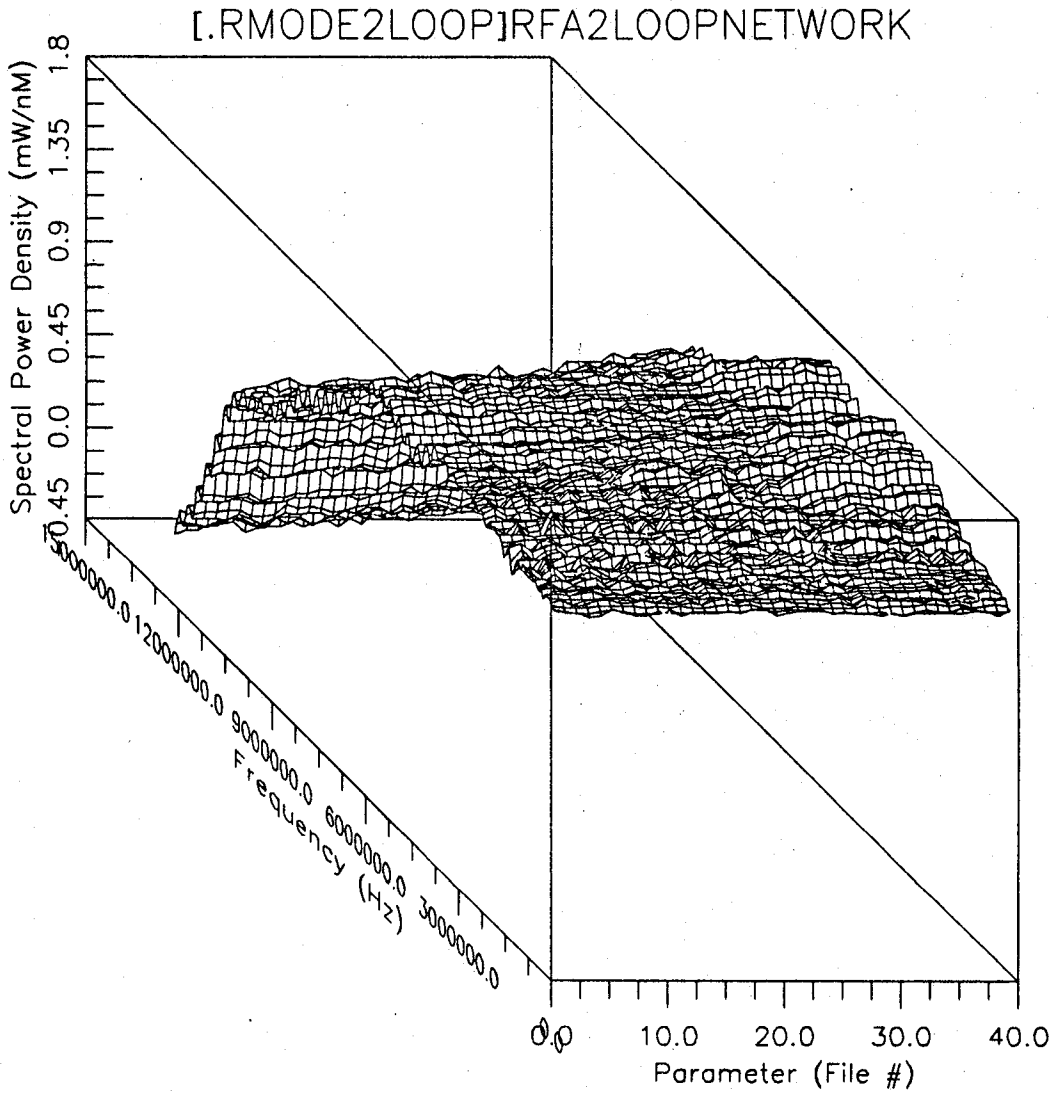

RMODE2LOOP

Rmode system 2 loop network CDSC and back. OSA 500 nW, 1.28-1.3 micrometers span. RF 10 Hz to 12.5 MHz .2 dB/div VBW 300 Hz RBW 100Hz. 15 sec between runs. 6-7 13.5 dB and 7-8 12.5 dB attenuation 1loop run was 6-7 only. RF referenced to short cable.

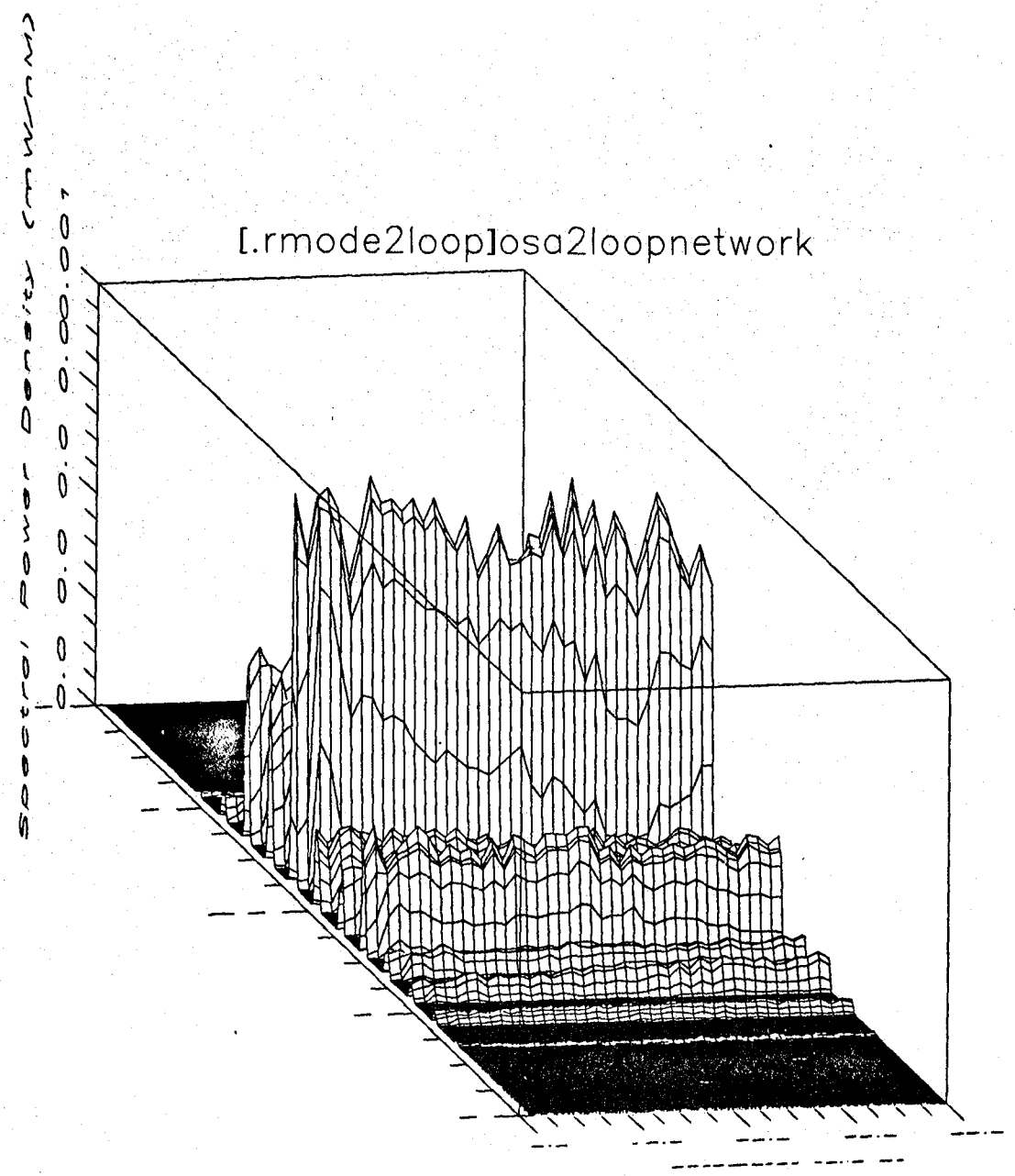

RMODE2LOOP

Rmode system 2 loop network CDSC and back. OSA 500 nW, 1.28-1.3 micrometers span. RF 10 Hz to 12.5 MHz .2 dB/div VBW 300 Hz RBW 100Hz. 15 sec between runs. 6-7 13.5 dB and 7-8 12.5 dB attenuation 1loop run was 6-7 only. RF referenced to short cable.

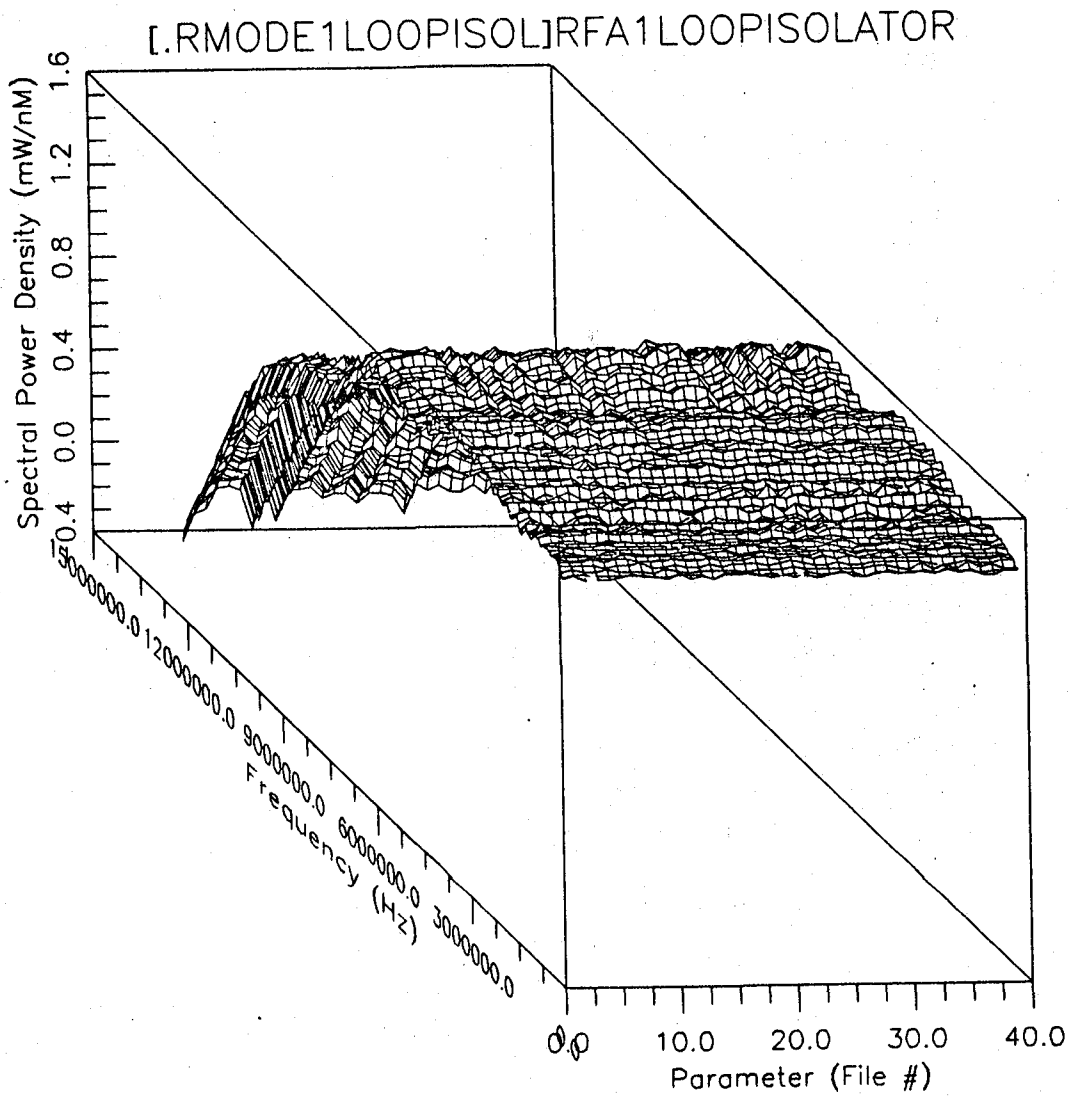

1LOOPISOLATOR

Rmode system 1 loop network CDSC and back WITH OPTICAL ISOLATOR ISOWAVE 113 POZ S/N 0391. AT TX SIDE. OSA 500 nW, 1.28-1.3 micrometers span. RF 10 Hz to 12.5 MHz .2 LOOP TOO MUCH ATTENUATION FOR RX dB/div VBW 300 Hz RBW 100Hz. 15 sec between runs. 6-7 13.5 dB and 7-8 12.5 dB .2attenuation 1loop run was 6-7 only. RF referenced to short cable.

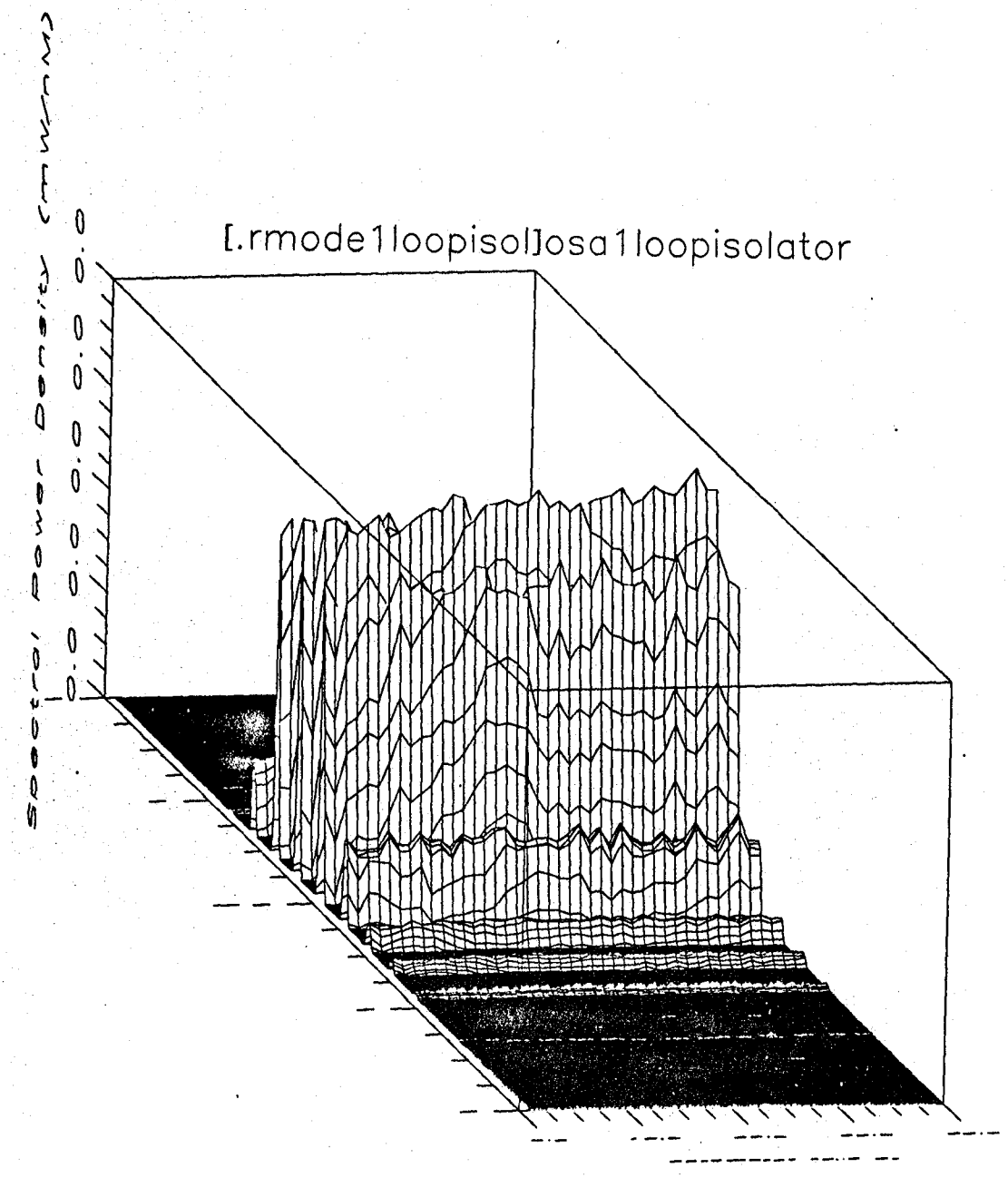

1LOOPISOLATOR

Rmode system 1 loop network CDSC and back WITH OPTICAL ISOLATOR ISOWAVE 113 POZ S/N 0391. AT TX SIDE. OSA 500 nW, 1.28-1.3 micrometers span. RF 10 Hz to 12.5 MHz .2 LOOP TOO MUCH ATTENUATION FOR RX dB/div VBW 300 Hz RBW 100Hz. 15 sec between runs. 6-7 13.5 dB and 7-8 12.5 dB .2attenuation' 1 loop run was 6-7 only. RF referenced to short cable.

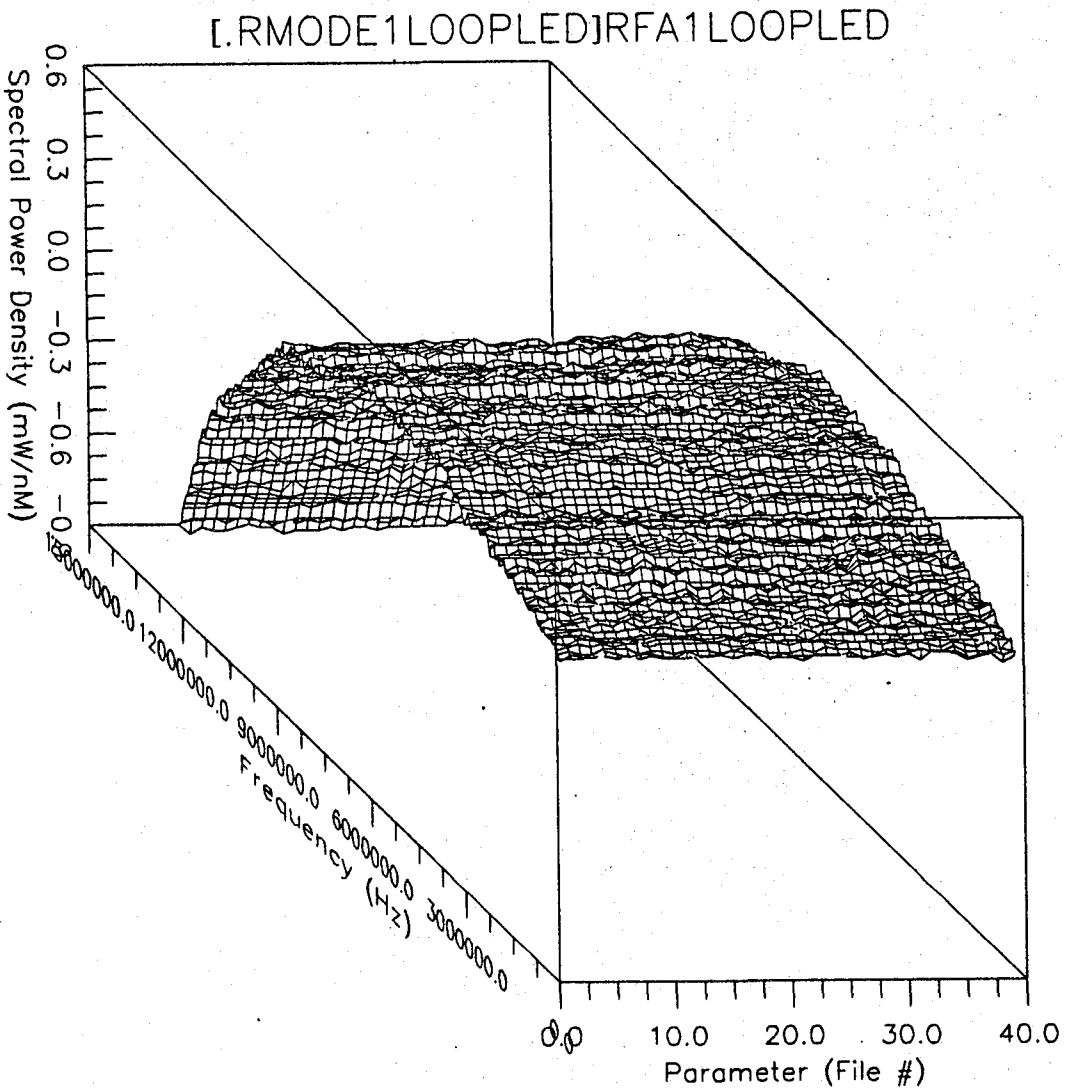

1LOOPLED

LED 01400 . Rmode system 1 loop network CDSC and back one connector removed in frame room. OSA 1 nW, 1.0-1.5 micrometers span. RF 10 Hz to 12.5 MHz .2 LOOP TOO MUCH ATTENUATION FOR RX dB/div VBW 300 Hz RBW 100Hz. 15 sec between runs. 6-7 13.5 dB and 7-8 12.5 dB .2attenuation 1loop run was 6-7 only. RF referenced to short cable.

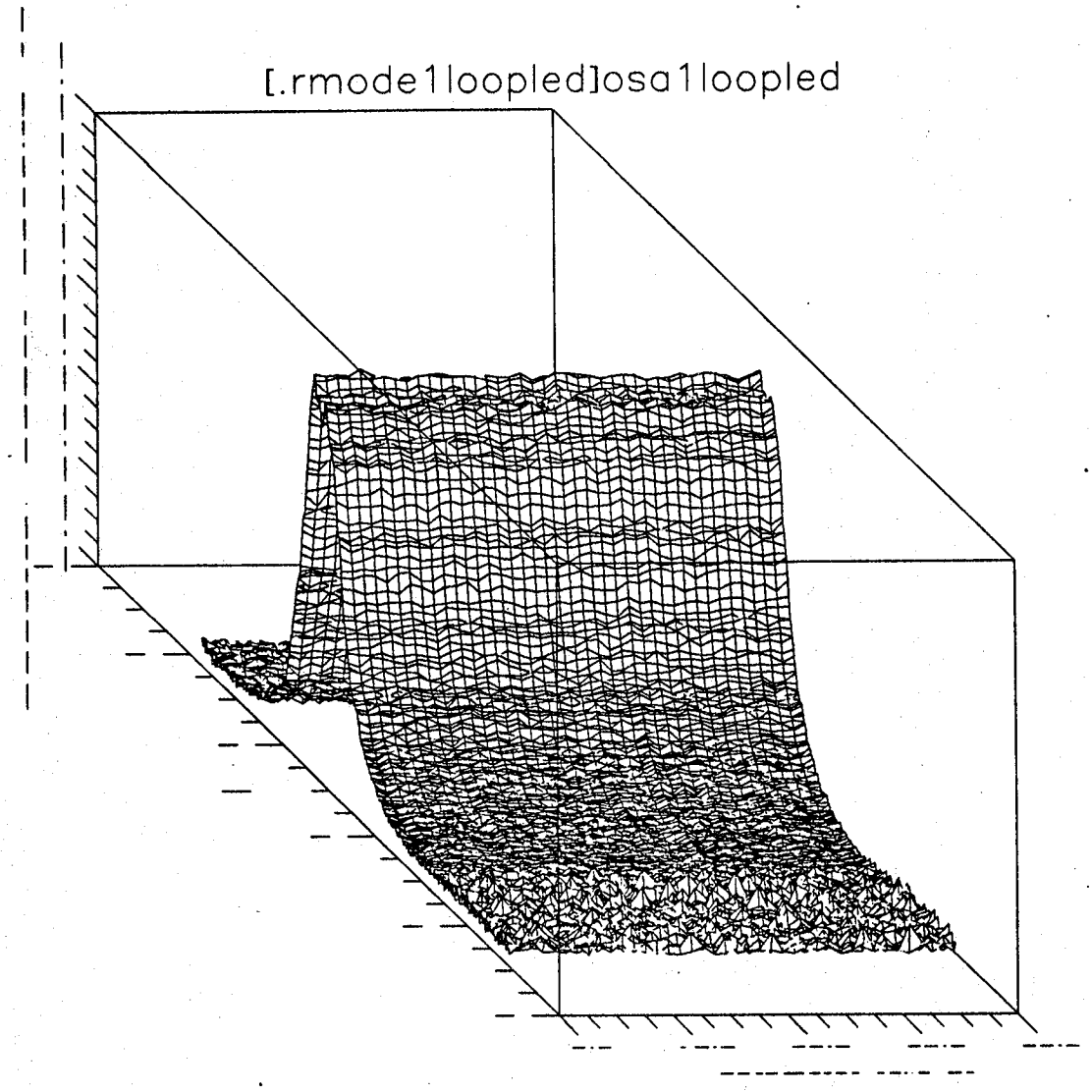

1LOOPLED

LED 01400 . Rmode system 1 loop network CDSC and back one connector removed in frame room. OSA 1 nW, 1.0-1.5 micrometers span. RF 10 Hz to 12.5 MHz .2 LOOP TOO MUCH ATTENUATION FOR RX dB/div VBW 300 Hz RBW 100Hz. 15 sec between runs. 6-7 13.5 dB and 7-8 12.5 dB .2attenuation 1loop run was 6-7 only. RF referenced to short cable.

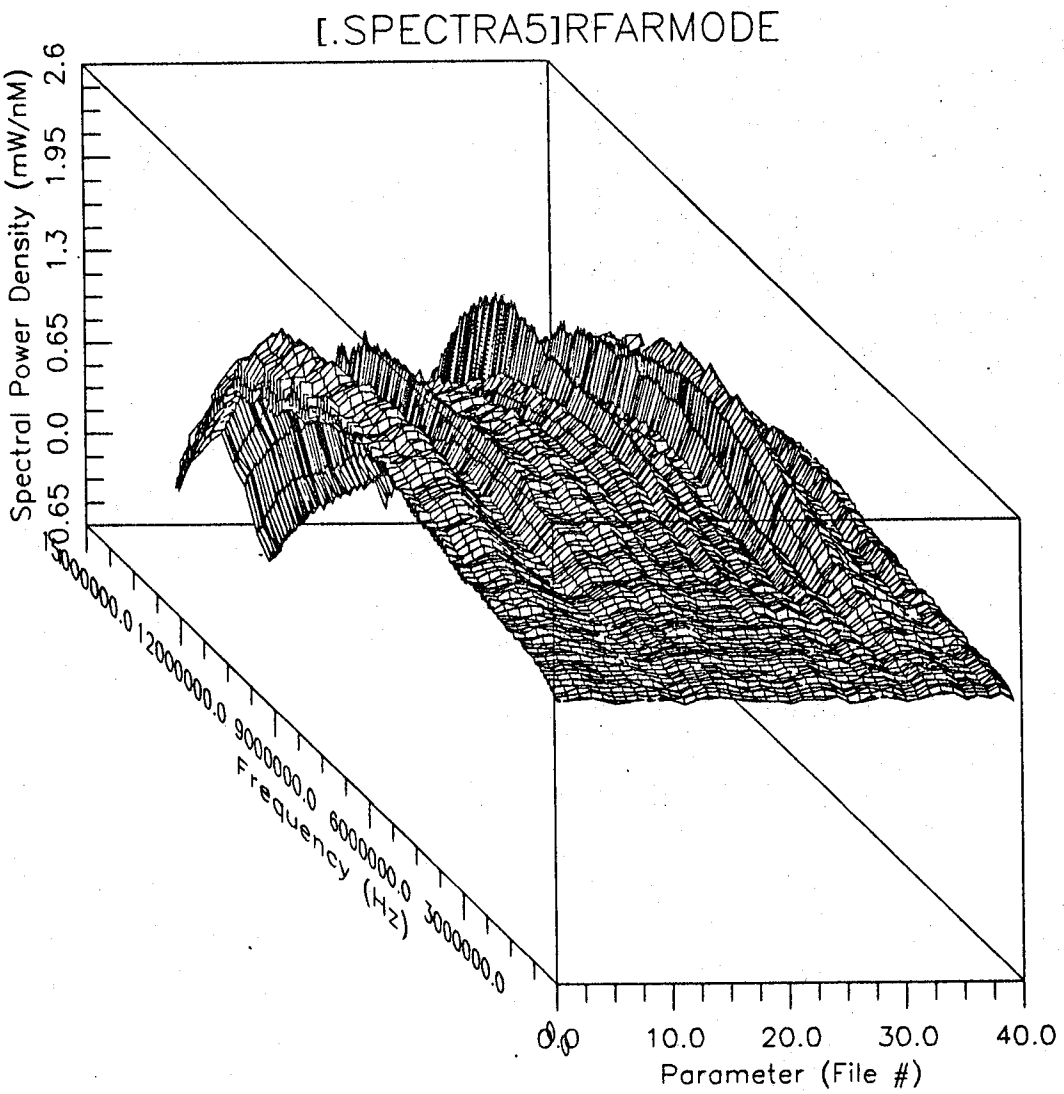

RMODE

Rmode system 20 extra connectors AS WELL AS 0 dB variable ATTENUATOR IN LINE. OSA 500 nW, 1.28-1.3 micrometers span. RF 10 Hz to 12.5 MHz .1 dB/div VBW 300 Hz RBW 100Hz. 15 sec between runs.

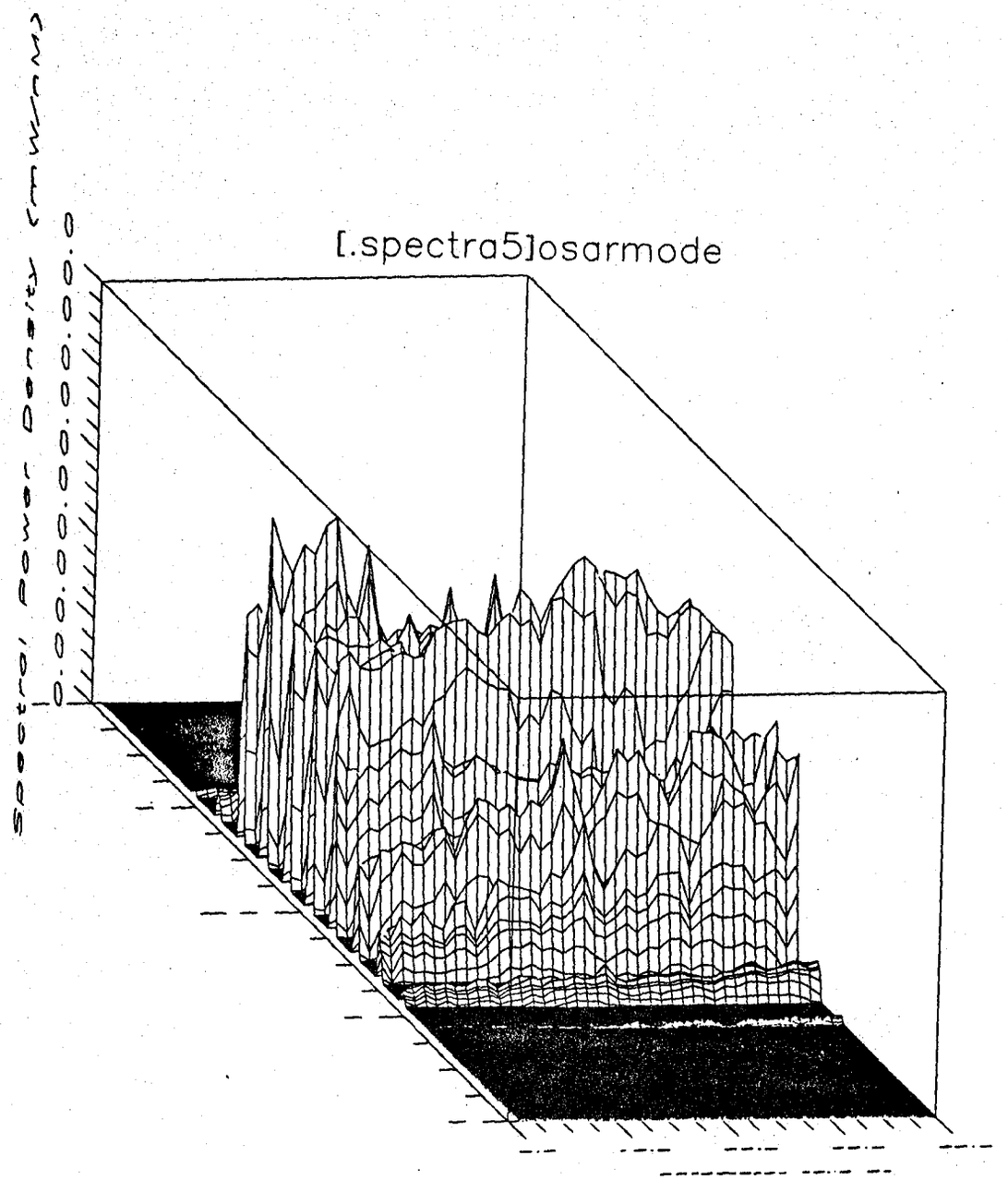

RMODE

Rmode system 20 extra connectors AS WELL AS 0 dB variable ATTENUATOR IN LINE. OSA 500 nW, 1.28-1.3 micrometers span. RF 10 Hz to 12.5 MHz .1 dB/div VBW 300 Hz RBW 100Hz. 15 sec between runs.

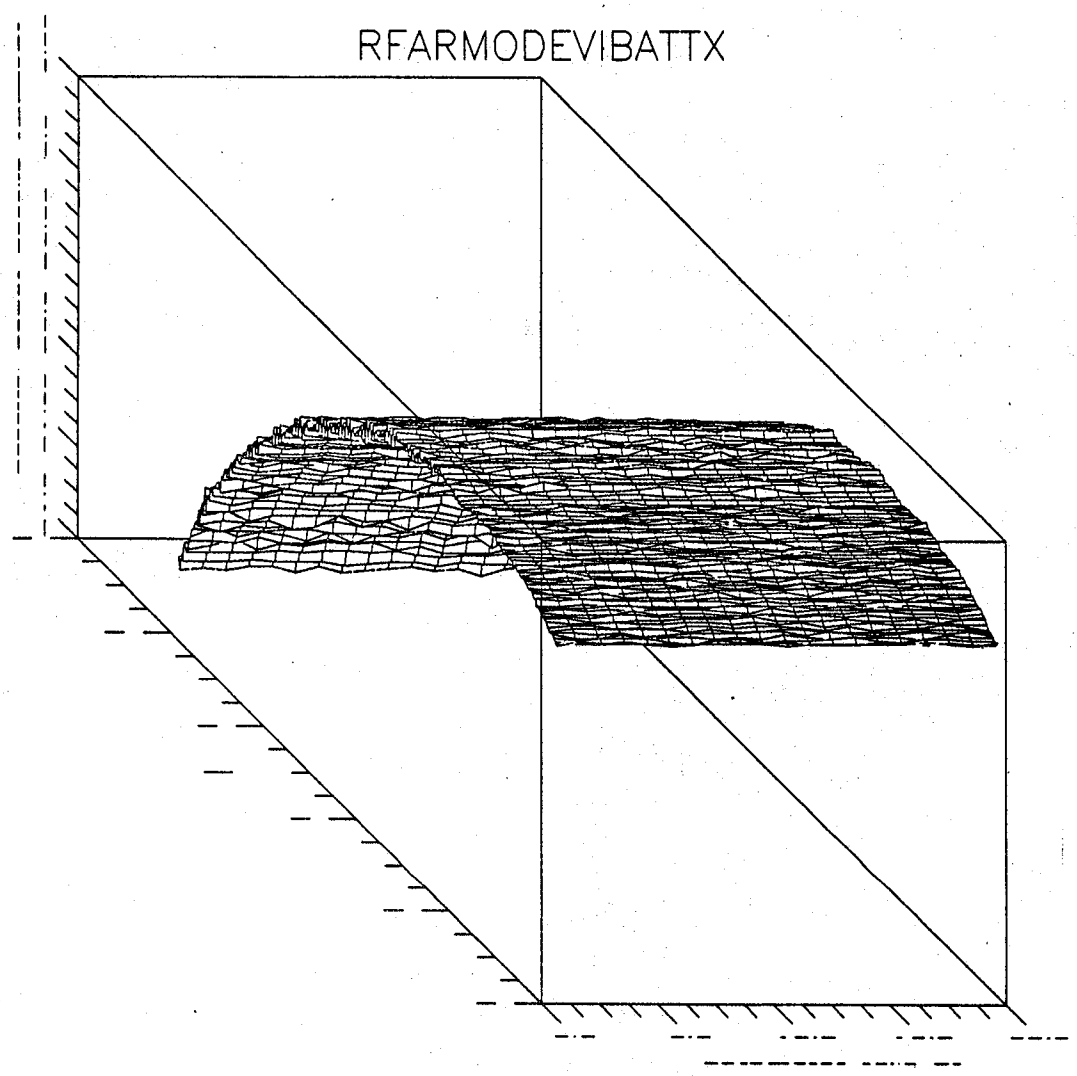

RMODEVIBATTX

Reflection mode. TX to fiber jumper connected to speaker to 90 10 splitter to 15 dB atten to 1km spool to RX . OSA 1.28 micormeters to 1.3 micrometers 500 nW. RFA 100 TO 12.5 MHz. .2dB /div RBW 100 VBW 300. Speaker driven 100 Hz +12dBm.

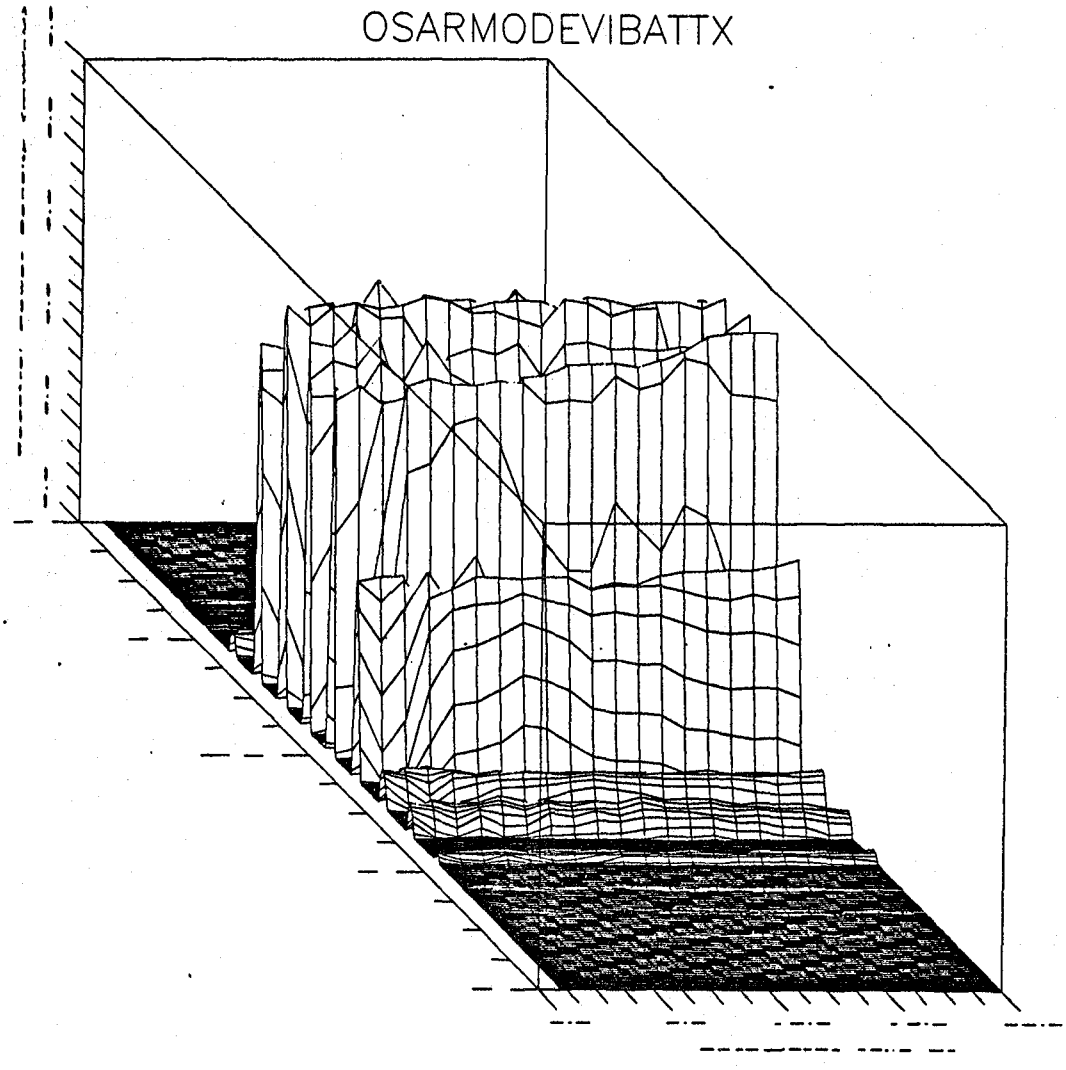

RMODEVIBATTX

Reflection mode. TX to fiber jumper connected to speaker to 90 10 splitter to 15 dB atten to 1km spool to RX . OSA 1.28 micormeters to 1.3 micrometers 500 nW. RFA 100 TO 12.5 MHz. .2dB /div RBW 100 VBW 300. Speaker driven 100 Hz +12dBm.

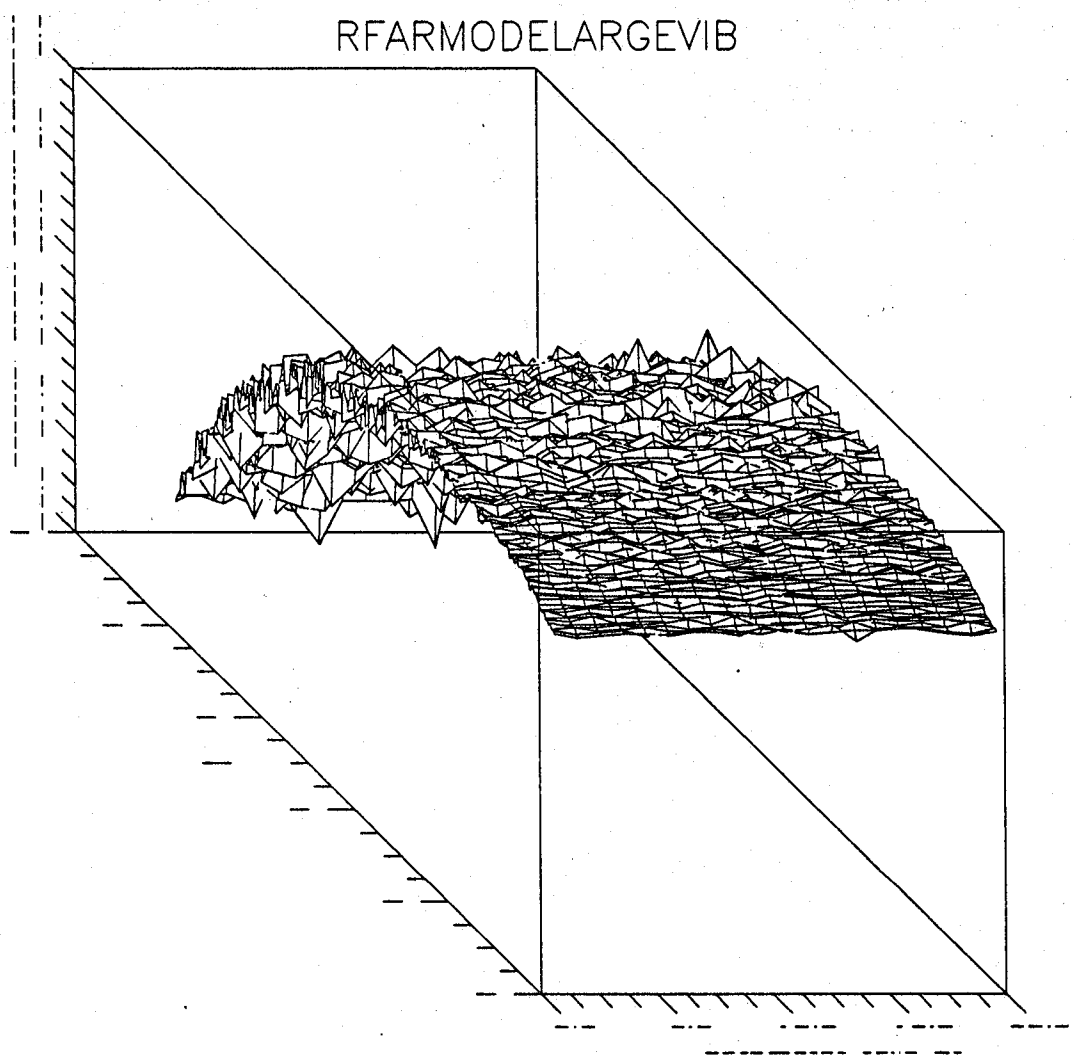

RMODELARGEVIB

Reflection mode. Manual vibration (10-20cm) of jumper connected to 90 10 splitter to 15 dB atten to 1km spool to RX . OSA 1.28 micormeters to 1.3 micrometers 500 nW. RFA 100 TO 12.5 MHz. 0.2dB /div RBW 100 VBW 300.

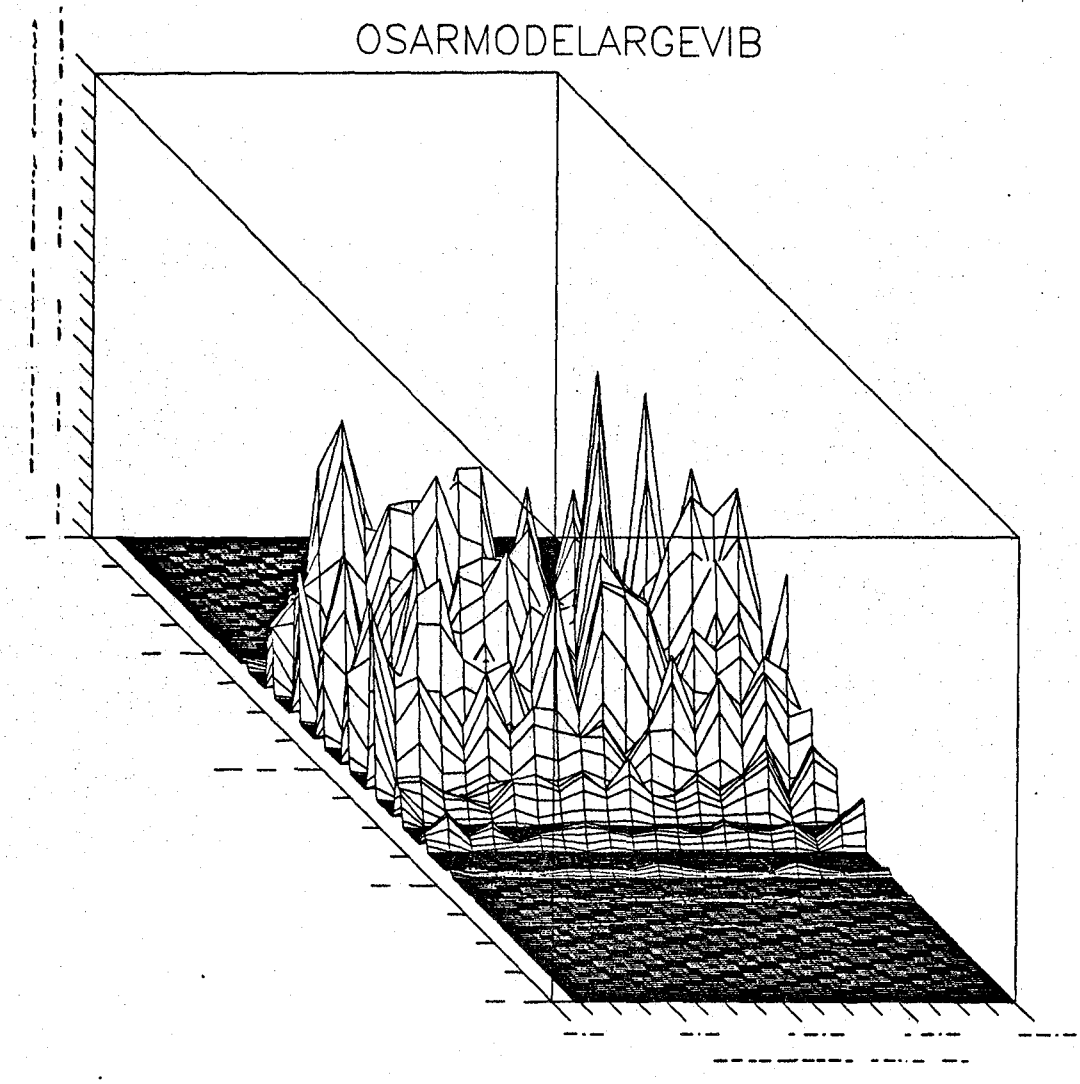

RMODELARGEVIB

Reflection mode. Manual vibration (10-20cm) of jumper connected to 90 10 splitter to 15 dB atten to 1km spool to RX . OSA 1.28 micormeters to 1.3 micrometers 500 nW. RFA 100 TO 12.5 MHz. 0.2dB /div RBW 100 VBW 300.

Appendix C HIGH SPEED VARIATIONS IN CARRIER OBSERVED USING FABRY PEROT INTERFEROMETER

11802 DIGITIZING SAMPLING OSCILLOSCOPE
date: 16-AUG-91 time: 14:55:57

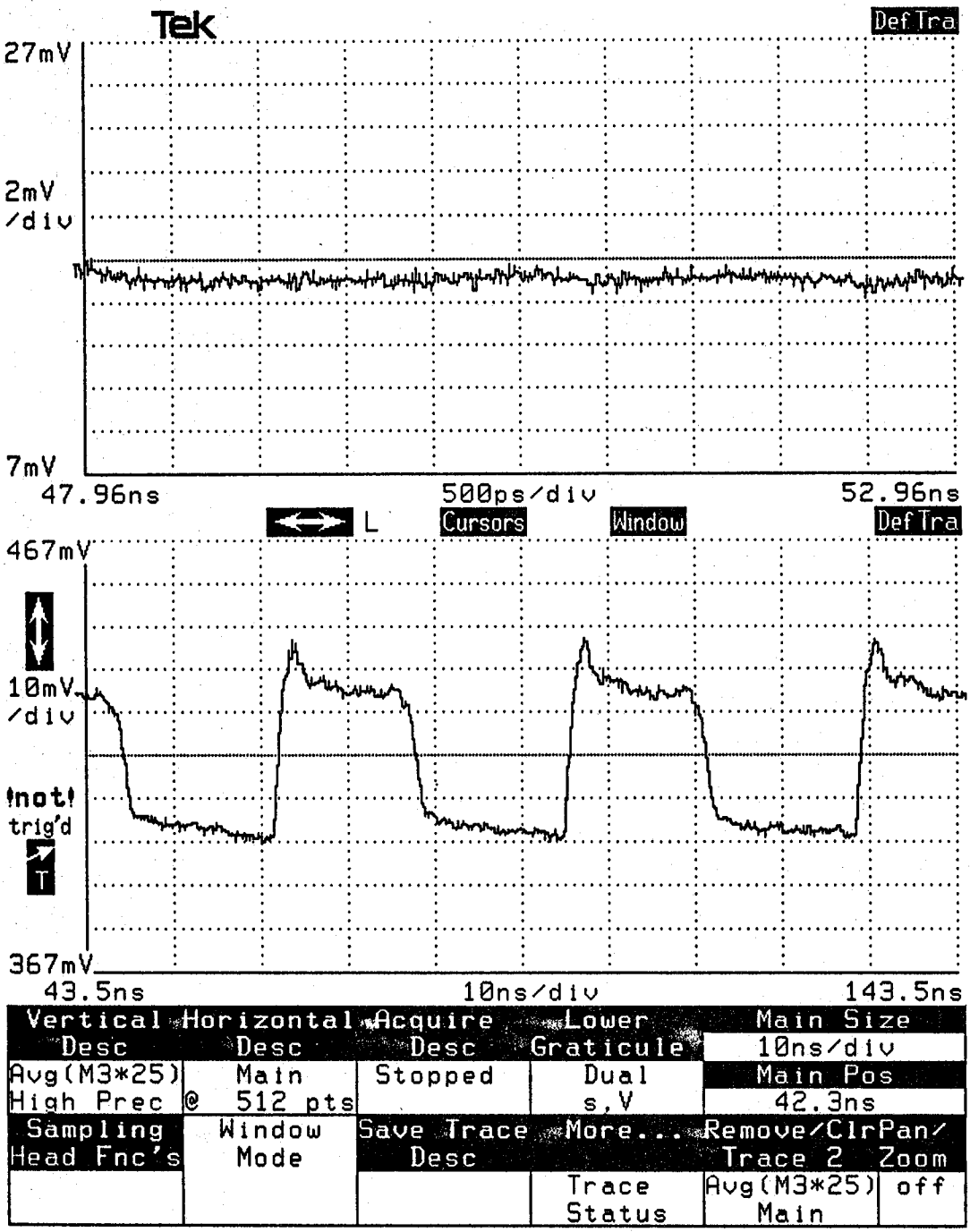

LASER MODULATION FABRY PEROT VOLTAGE 3.0201
BASELINE NETWORK

11802 DIGITIZING SAMPLING OSCILLOSCOPE
date: 16-AUG-91 time: 15:24:14

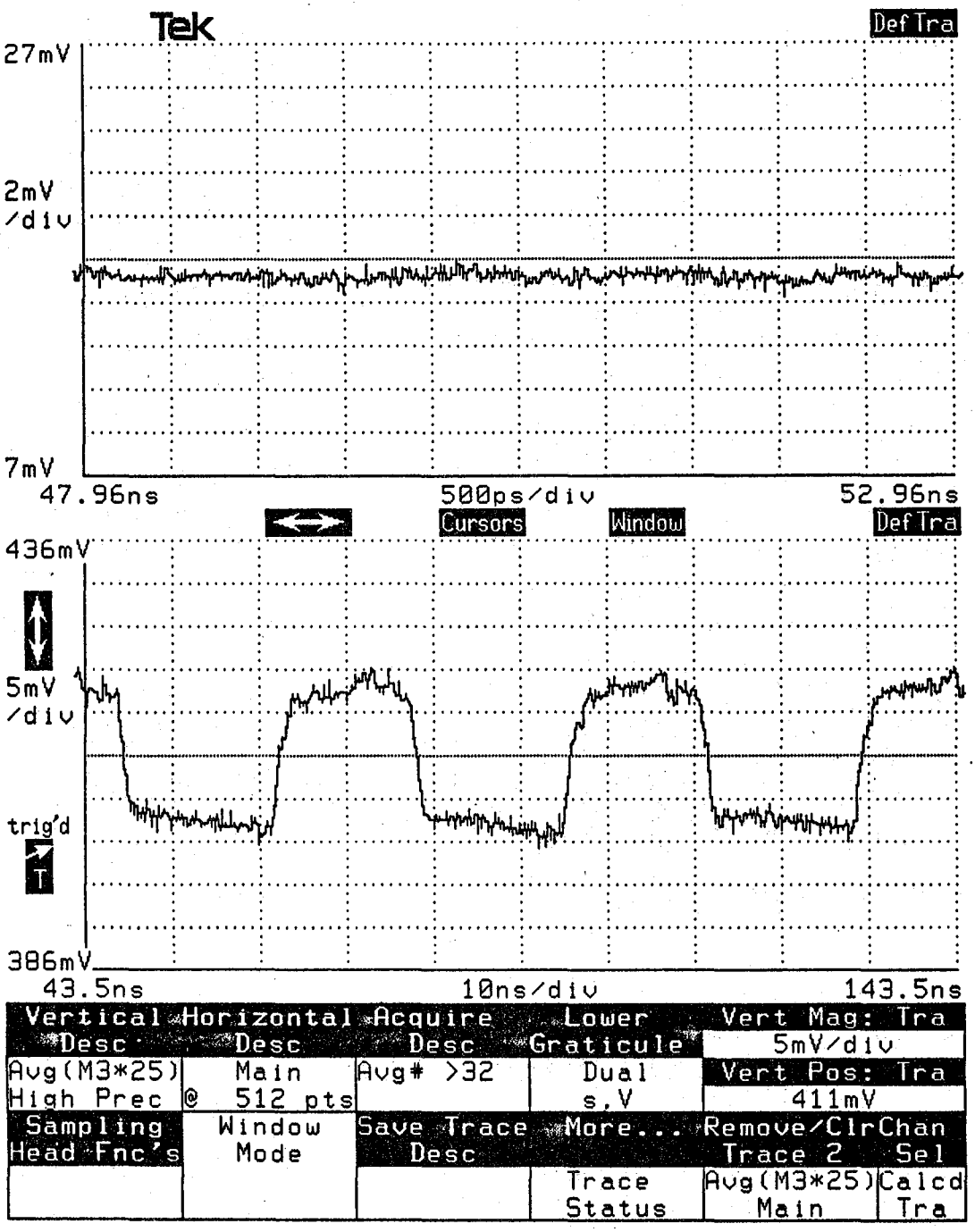

LASER MODULATION FABRY PEROT VOLTAGE 3.4389 V
BASELINE NETWORK

Appendix D OTDR OBSERVATIONS OF LINKS USED IN TESTS

LINK 5→6

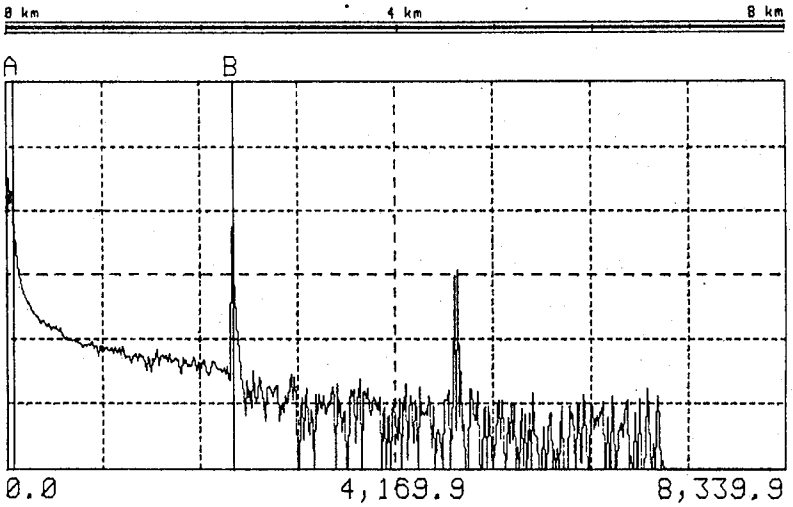

Optics: TD-861 1300nm HR Multimode
Scan Mode: INCOMPLETE
Pulse Width: SHORT

LINK 7-8

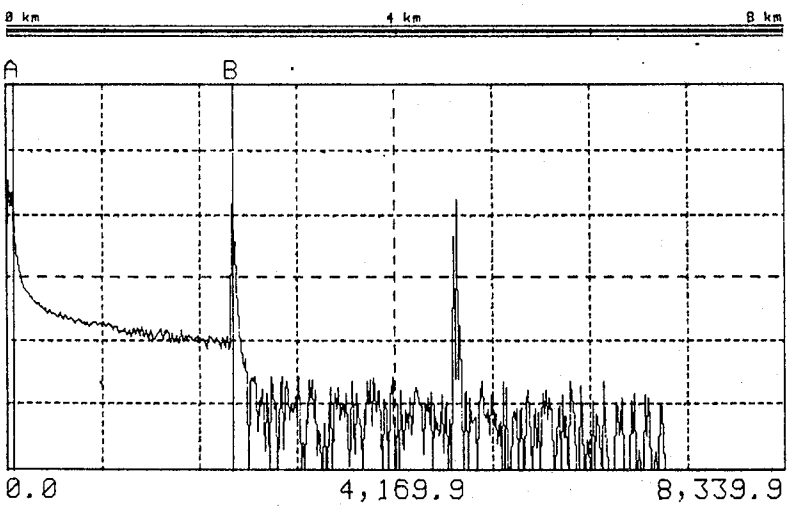

Optics: TD-861 1300nm HR Multimode
Scan Mode: INCOMPLETE
Pulse Width: SHORT

OPTICAL TIME DOMAIN REFLECTOMETRY ON FIBER TEST LINKS USED

LAB FIBER SPOOL

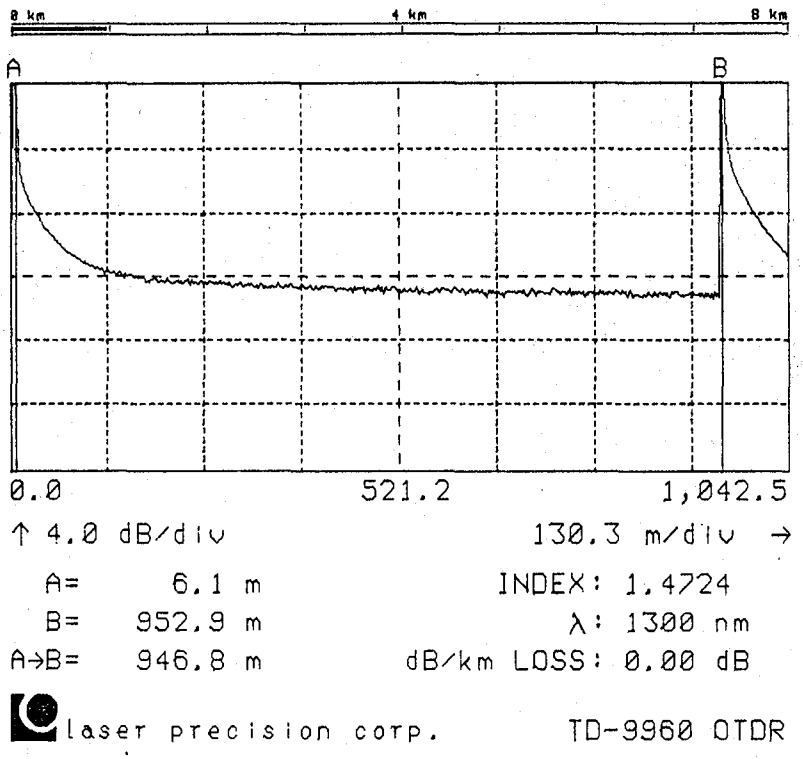

Optics: TD-861 1300nm HR Multimode
Scan Mode: FAST
Pulse Width: SHORT

OPTICAL TIME DOMAIN REFLECTOMETRY ON FIBER TEST LINKS USED

1991 NASA/ASEE SUMMER FACULTY FELLOWSHIP PROGRAM

JOHN F. KENNEDY SPACE CENTER
UNIVERSITY OF CENTRAL FLORIDA

INFORMATION FLOW ANALYSIS OF LEVEL IV PAYLOAD PROCESSING OPERATIONS

PREPARED BY:	Mary E. Danz
ACADEMIC RANK:	Assistant Professor
UNIVERSITY AND DEPARTMENT:	University of Central Florida Department of Industrial Engineering and Management Systems
NASA/KSC	
DIVISION:	Payload Processing Operations
BRANCH:	CS-EED
NASA COLLEAGUE:	Rey Diaz
DATE:	August 7, 1991
CONTRACT NUMBER:	University of Central Florida NASA-NGT-60002 Supplement: 6

Acknowledgments

I appreciate the opportunity to participate in the NASA/ASEE summer program and gratefully acknowledge the assistance and support of my NASA colleague, Rey Diaz (CS-EED Project Engineer) and Bill Williams (Advanced Projects Office), as well as the friendly guidance of Ramon Hosler (program administrator) and Kari Stiles (administrative assistant).

Abstract

The Level IV Mission Sequence Test (MST) was studied to develop strategies and recommendations to facilitate information flow. Recommendations developed as a result of this study include revised format of the TAP document and a conceptualized software-based system to assist in the management of information flow during the MST.

Summary

The Level IV Mission Sequence Test (MST) was studied to develop strategies and recommendations to facilitate information flow. Since payloads are becoming more complex, and the need for efficient processing continues, the MST which tests the payload at Level IV is a complex procedure which integrates technical equipment and personnel. The Test and Assembly Procedure (TAP) is the basis for information flow during the MST, and as such, the document should support its navigation in an optimum manner. Due to the relationship between the structure of the TAP and how it was used during the MST, suggested format changes were recommended.

Also, to support the information requirements of the MST personnel, an information support system was conceptualized. The progress to date on the system is identification of the desirable supporting functions in a series of screens which illustrate how a number of possible information areas could be supported.

The team members have developed successful strategies to compensate for the current TAP document and information support procedures. In this study, methods to further improve the TAP document and provide information support were researched with the aim of facilitating team dedication to the test and trouble-shooting functions of the Level IV MST.

Table of Contents

Acronyms List

CMD Commander (for call signs)
EE Experiment Engineer
K4TC Level IV Test Conductor
MET Mission Elapsed Time
MST Mission Sequence Test
O&C Operations and Checkout Building
OMI Operation and Maintenance Instructions
PE Project Engineer
PI Principal Investigator
RESP Recipient of command (for call signs)
SEQ Sequence (in TAP)
STS Space Transportation System
TAP Test and Assembly Procedure
TQ Multiple Inspection Verifications by Technician and Quality (in TAP)
WAD Work Authorization Document

I. INTRODUCTION

1.1 MISSION SEQUENCE TEST (MST) BACKGROUND. The purpose of this study was to analyze the flow of information during the Level IV Mission Sequence Test (MST). The study of human-human communication is not new. However, the study of information flow, including documentation, is a relatively new field of research in the area of the human factors study of systems. This topic is attracting interest from various researchers, for example, Schmager (1991) recently reported a study of the information flow of batch production control in manufacturing.

The MST is a testing procedure which involves communication of numerous personnel and the generation of documents and forms. Actually, the information flow between the processing team members begins several months before the MST, when the procedures are being developed for each individual experiment of the payload. The project engineer (PE) assigned to the payload follows its progress throughout the integration process. The written procedures followed during the MST, called Test and Assembly Procedure (TAP), are authored by the PE as he/she combines input from the experiment principal investigators (PIs) and the experiment engineers (EEs). After the MST is completed, the team continues to work on trouble-shooting issues in the ongoing effort to prepare the payload for advancement to Level III/II. Since the TAP is the baseline for information flow during the MST, the process of generating the TAP was

also studied.

1.2 PURPOSE OF STUDY. For the purpose of this study, three areas related to the MST were studied. The first area was preparation of the TAP by the PE. The second area was the design of the physical format of the TAP document with respect to its function of supporting the steps to be executed during the MST. The last area was a study of the MST in terms of overall information support. It was found that studying the MST in this progression was the best approach to identify attributes which make the team successful over the Level IV stage.

1.3 LEVEL IV BACKGROUND. Horizontal payloads are integrated in the Operations and Checkout Building (O&C). The payloads are delivered to KSC and are individually tested in Pre-Level IV. At Level IV, the experiments are integrated into racks or pallets for the first time. This is the first time the experiments are operated together, using the same power sources and the same computer data handling systems. The team concentrates its efforts on ensuring that the electrical and mechanical interfaces are error free, as well as confirming that the experiments are operating within specifications. Although each team member is a specialist in certain areas, many situations are first time encounters and must be solved without prior experience with similar solutions.

During development of the TAP to be used during the MST, the PE receives input from each of the specialists and PIs regarding their specific experiments. So during

the time he/she prepares for the MST, the PE is becoming familiarized with the TAP. He/She and the counterpart develop an expert knowledge of the TAP content.

The Level IV MST usually spans one week. Three days are reserved for actual testing and two days in between are used from trouble-shooting. There are various participants in the MST and they are in different locations within the O&C. During an MST the PE and counterpart are now referred to as K4TC (test conductor). Depending on the type of payload, K4TC will be located in the Control Room or the Users Room. The mission and payload specialists are located in the payload within the bay, as are some technicians. The supporting engineers and personnel are in the Control Room, and the PIs and EEs are in the Users Room. A group of visitors may also observe the MST from a conference room. Quality are located in yet another room.

All personnel are interfaced with the audio network (net) which allows them to monitor active channels during the MST. The participating personnel have different levels of involvement and knowledge about the MST and the TAP content. Variations in the TAP and equipment problems are resolved as they are encountered, along with generation of the appropriate paperwork. These conditions challenge the K4TC to lead the team through a successful MST in a timely manner.

II. METHODOLOGY

2.1 DATA COLLECTION AND ANALYSIS. Due to the dependence of the MST on

previous team work and information flow, the study was approached from a systems viewpoint. Approximately the first five weeks were used to learn and observe the MST. Two MSTs were directly observed. Several documents were reviewed to familiarize the investigator with the background of Level IV activities. These documents included, but were not limited to: the STS Investigator's Guide (1989), the User's Guide to Spacelab Payload Processing (1986), the CS-EED Employee Reference Handbook, and the Spacelab News Reference. Engineers representing a variety of specialties were also interviewed and questioned to clarify questions and details. Successful team strategies were noted during the MST observation and interviews. During this time, the systems approach to investigating information flow during the MST was formulated and planned to be initiated during the next five weeks of the period.

2.2 DEVELOPMENT OF RECOMMENDATIONS. During these five weeks, the paper communication related to the MST was studied, including pre-TAP documents and deviations. The format of the TAP document was also reviewed based on observations during the MSTs and successful team strategies. Finally, a software-based information support system was conceptualized, using a simple prototyping method. During this five week period, the investigator also participated in a Workshop hosted by the Crew Factors Group of the Human Factors Division at NASA Ames Research Center. At this workshop, the work to date was presented to other investigators working in the areas of team performance and information flow.

III. RESULTS AND DISCUSSION

3.1 DOCUMENT FINDINGS. Observations of the MST were the bases for recommendations on the format of the TAP document. The specifications were examined which define the format of a TAP document. The relationship of the document structure to how it was used on line was studied.

3.1.1 The TAP Specifications. The Work Authorization Document (WAD) says that a TAP is similar to an OMI, and is formatted to provide for easy development and processing during the Level IV tasks. It is specified that the TAP be organized in five sections. Section I should cover the test objective, special equipment, special instructions, acronyms, and call signs. Section II covers the pre-operation setup instructions which lists any special configurations required prior to beginning the operation instructions. Section III lists the operation support set up instructions. Section IV has the operation instructions which include call to stations, power up and down, as well as specific task instructions. Section V covers the post operation instructions, which are performed after Section IV is complete.

3.1.2 The TAP Currently Used in the MST. The following is a discussion on the format of the TAP with respect to the MST. It is recognized that there are at least three types

of TAPs, and that numerous TAPs are developed in many organizations at KSC. However, the comments here are only applicable to Level IV MST and were specifically based on case study.

Given that the MST is a complex procedure integrating technical equipment and personnel, it is desirable that the document support its navigation in an optimum manner. This is becoming more important as the payloads become more complex and the need for more efficient processing increases. Increasing complexity was also cited by Wright and Aitken (1991) as motivation to develop a software based semi-automated network scheduling system for satellite payloads.

The team spent a considerable amount of audio time receiving inquiries and sending responses as to the current step in the document. During MST observation, navigation of the document was difficult and awkward. Even experts in the TAP used sticky notes to identify specific sections, as there was skipping and jumping around between steps and sections.

The PE has the task of editing and integrating the TAP as well as conducting the MST. If the document could better support personnel navigation during the test, this may relieve the team from answering the many inquiries of what is the current step in the test, and perhaps improve on the efficiency and interaction between test personnel, such as buy offs and generation of deviations.

By its nature, the TAP document guides the personnel through a first-time testing procedure which involves trouble-shooting activity on demand. Although the K4TC is

acquainted with all the steps, and the engineers are familiar with their specific experiments, the steps have not actually been executed before. Thus, the TAP may be likened to a learning situation. This situation is in contrast to an Operations and Maintenance Instruction (OMI) which is a more established set of procedures and have been modified, but not extensively, for each session. In this case the personnel participating in the OMI have the advantage of instruction rehearsal. Due to the fundamental differences between the activities which the TAP and the OMI support, it is recommended that the format of the documents reflect the differences between the document functions.

3.1.3 Format Recommendations. The specific format recommendations are discussed below, and are suggested to enhance the readability, legibility, and navigation qualities of the TAP. Pages of the TAP in the old format, Tables 1 and 3, and in the new suggested format, Tables 2 and 4, have been included for comparison. The lettered areas of each page correspond to the following lettered points.

A. Upper and lower case letters are recommended for text. Upper case letters should be reserved for acronyms and call signs, or cases where emphasis is needed (Zimmerman & Campbell, 1988). Upper and lower case text is more readable than upper case only because upper case letters are indicators of the start of a new instruction, acronym, call sign or code. Also, upper case text is already used as a heading level in the TAP document. Utilizing lower and upper case in the general text reserves

the upper case text as an important heading level. This is applicable to the TAP because much of the reading is quick scanning over the steps, yet must be performed with accurate attention to detail.

B. The 11 x 8 1/2 " landscape orientation of the page was selected to allow addition of another column, called type, and to allow the text lines of each step to be longer. This modification was made to facilitate the reading of the TAP by providing the sequence information in columns which are read consistently from left to right.

B.1. The column, type, was added so that notes, cautions and warnings could be designated without being embedded in the text. This change also saves a line of space for each note.

B.1.1. The warning notes are still set off by asterisks, although it is not necessary that the asterisks form an entire border around the message.

B.2. The procedures are written in the same style, but more space is available for a longer line of text. This should aid the reader so that the listener hears a more complete message. This is especially important if the respondent is not able to read the TAP while executing the steps.

B.2.1. The beginning of each phrase is a new line. This aids in distinguishing substeps within a step, and facilitates quick scanning of the text.

C. The detailed header of each page was removed and changed to a footer with section information only. It is suspected that the detailed header was necessary with the old format due to the frequent skipping of sections. However, with the new format the

header is trimmed to the minimum necessary information and this results in additional space savings, as well. To make navigation easier footer noting the specific task being performed appears at the bottom left of the page, allowing the user to thumb through the document quickly.

D. The levels of heading in the old format were difficult to distinguish from the text. Since all text was in upper case letters, the level was limited. The main header was bold underlined upper case, the notes were bold upper case with a colon, and other levels were also underlined upper case text. The new format utilizes three levels of headings: (1) all bold upper case for header and remarks, (2) underlined text for emphasis within instructions and (3) asterisk notation with bold upper case for warnings.

E. The new format is arranged by the order in which the steps will be performed, instead of by the 5 standard sections (information, pre-operation setup, pre-operations, operations, and post-operations). The new document is subdivided by time slice. Each time slice has the pertinent sections included. The time slices are separated by colored title pages. The advantage of this organization is that it follows the actual itinerary of MST activity more closely, and will reduce the amount of page turning and step skipping since all activities occurring on the same day are located in the same section of the document. It is also suggested that text be copied and inserted where appropriate if the same steps must be repeated on another day.

F. The zero number and "oh" letter should be distinguishable so that codes will entered in without mistaken identities. On occasion personnel misread the code and an

error message was received. Thus, it is recommended that at least in the codes to be entered, these characters be readily distinguishable.

These are formatting suggestions which have been developed without in depth analysis of the content of the steps. Currently audio tapes of the MST are being analyzed to identify the successful strategies of the team and altering the procedural content to reflect this. For example, in one MST the written TAP required verification of the illumination of two indicators in two separate steps. Although written as two steps, the respondent chose to verify both indicators in the same step. Perhaps the document content will be revised to accommodate the efficiency of the personnel responses.

3.2 INFORMATION SUPPORT SYSTEM. Next, the information flow of the MST was considered. A software-based system to support information management was conceptualized. The progress to date on this system is the identification of desirable supporting functions, and a series of screens which illustrate a number of possible areas which could be supported. The initial work has emphasized the development of the human computer interface, which is a key factor to the potential success of a system. O'Neal and Manahan (1991) also used the prototype method in the process of developing a human comuputer interface for a system which will provide computer supported procedures to the astronauts while on board spacecraft.

The process of collecting feedback on the functions has begun and the resulting

recommendations are continuously being considered. It is envisioned that the information would be available to the MST participants with varying levels of interaction. The system would allow personnel to access current changes and status of MST, including deviations, quality activity and overall progress of the time slice. The purpose of the system is to improve information available to the participants and automate some low level functions.

3.2.1 Proposed Features of the System. The basic screen is shown in Figure 1, and the following points of discussion correspond to the items labelled in the figure.

A. The menu is shown in the right side of the screen and coexists with a window showing the current step of the TAP. The screen view of the TAP could be updated to show recent deviations and buy-offs as shown in A.1. It is suggested that the five digit identification numbers of the quality engineer and technician be entered by keyboard, perhaps in password format.

B. Another potentially useful feature is the status option of the menu. With this option, the team personnel could refer to the status of the activities for a slice, as well as find start and end times for power ups. Also available is a time slice status indicator to show the overall progress of the time slice.

C. The help button supplies general navigational instructions for using the system.

D. Color code information summary is shown under the help menu. Red indicates that a deviation has been initiated against that particular step. The specific

deviation can also be viewed using the deviation selection. Any text in yellow is used to reference a figure, or to indicate quality activities.

E. The support includes applicable documents such as call signs, acronyms and safety requirements.

F. The display defaults would allow the user to display only the sequences or steps of interest by experiment, commander, responder or steps where quality is involved.

G. Print screen would provide printout of information on the screen.

H. The deviation button would allow review of the written deviations, or authoring of new ones right on the screen.

3.3 SUCCESSFUL STRATEGIES. Audiotapes are currently being analyzed to further develop details of successful team strategy. Successful strategy is dependent on team communication during the MST as well as throughout the Level IV processing operations. During the MST, the team is successful in communicating with team members in the trouble-shooting mode. The team uses a look-ahead strategy to point out future problems and events which are potentially difficult. Personnel offer to take duties which are not necessarily theirs (such as time keeping and monitoring) and the team cross checks and monitors each other. During the MST, the team behavior has evolved to include efficient responses over the net, and successful strategies for authoring and processing forms. These relationships begin to develop before the MST through communication which is fostered by the accessibility between team members and PIs.

The team develops confidence since the EEs are trusted and accept the responsibility for the well-being of the experiments.

3.4 FURTHER RECOMMENDATIONS. Introductory analysis of the preparation procedure showed that there would be a use for an improved method of incorporating suggested changes into the TAP drafts. Currently, the changes are reported by fax, letter, computer mail, red-lines and the change request form. This suggests that the form should be analyzed for its format with respect to what the team requires. The form could probably be designed so that it would be readily used and incorporated into the draft. Also, technologies and organizational methods for incorporating the changes should be researched. A similar situation exists with the deviation form. The deviations were reported consistently in a format which was not necessarily defined by the deviation form. Since the style of the deviation report has evolved to this format, perhaps the form should be changed to accommodate it.

IV. CONCLUDING REMARKS

In general, team members have adapted successful strategies in spite of the TAP format. This investigation has researched ways to further improve the TAP document and associated forms so that the team can be dedicated their true testing trouble-shooting functions, rather than navigational attention required to track steps in the TAP. Further

work is being done to incorporate successful strategies into recommendations for the actual procedural content of the TAP.

References

European Space Agency. *Spacelab News Reference.*

NASA, KSC. *CS-EED Employee Reference Handbook.* Payload Processing Operations.

NASA, KSC. *User's Guide to Spacelab Payload Processing,* (October 1986).

NASA, KSC. *Work Authorization Documentation Handbook.* #KCA-HB-0018.0

NASA, MSFC. *STS Investigator's Guide.* (October 1989).

O'Neal, M. and Manahan, M. (1991). Spacecraft crew procedures from paper to computers. *Fourth Annual Workshop on Space Operations, Applications, and Research.* #3103, Volume II.

Schmager, B. (1991). The importance of human interaction in batch production control. In: *Designing for Everyone.* Bristol, PA: Taylor and Francis.

Wright, C. and Aitken, D. (1991). A human factors approach to range scheduling for satellite control. *Fourth Annual Workshop on Space Operations, Applications, and Research.* #3103, Volume II.

Zimmerman, C. and Campbell, J. (1988). *Fundamentals of Procedure Writing.* Columbia, MD: GP.

Table 1. TAP Excerpt

DATE: 04-04-91 REV. BASIC T1-IML-1-0050

SECTION IV

OPERATION INSTRUCTIONS

SEQ	CMD	RESP	(MET)	DESCRIPTION	VERIF
19-000				EXP 10 - MVI OPERATIONS	
				NOTE:	
				THE MVI OPERATIONS WILL BE PERFORMED DURING LVL III/II MST SLICE 1.	
				MVI TEST PREPARATIONS	
19-001		PS2		UNSTOW/CONFIGURE CASSETTE RECORDER FOR SUBJECT:	
				A. UNSTOW CASSETTE RECORDER AND SEVERAL UNUSED TAPES FROM CREW KIT - TEMP STOW EXTRA TAPES IN POCKETS.	
				B. LABEL TAPE WITH SUBJECT ID AND MET LOAD TAPE IN RECORDER.	
				NOTE:	
				CHANGEOUT BATTERY IF RECORDER DOES NOT WORK.	
				C. VOICE RECORD SUBJECT ID AND MET. PLAY BACK FOR VOICE CHECK. TEMP STOW RECORDER IN POCKET.	
				D. UNSTOW INDIVIDUAL NOSEPIECE FROM CREW KIT (IF DESIRED). TEMP STOW.	

Table 2. Recommended TAP Format.

B.1

EXPERIMENT 10 - MVI OPERATIONS

SEQ	CMD	RESP (MET)	REMARK	DESCRIPTIONS	VERIF
11-000			**NOTE**	The MVI Operations will be performed during LVL III/II MST Slice 1.	
				MVI TEST PREPARATIONS (B.2)	
11-001		PS2	(D)	Unstow/Configure cassette recorder for subject: A. Unstow cassette recorder and several unused tapes from crew kit temp stow extra tapes in pockets. B. Label tape with subject ID and MET load tape in recorder.	
			NOTE	Change out battery if recorder does not work.	
				C. Voice record subject ID and MET. Play back for voice check. Temp stow recorder in pocket. D. Unstow individual nosepiece from crew kit (if desired). Temp stow.	
11-002		PS2		Install TPL liner in helmet, if required.	
			NOTE	The following MVI preparations must be completed at least 20 minutes prior to the start of MVI MST Slice 1 Operations.	
			NOTE	If skin is very sensitive alcohol wipes may be substituted for Omniprep.	
11-003		PS2		Prepare skin at electrode sites with Omniprep (or alcohol) and dry gauze. Remove electrodes from package in service kit, check electrode paste is on electrodes, and apply to the buffed areas.	

C

Table 3. TAP Excerpt

DATE: 04-04-91 REV. BASIC T1-IML-1-0050

SECTION IV

OPERATION INSTRUCTIONS

SEQ	CMD	RESP (MET)	DESCRIPTION	VERIF
19-019		MS3	ROUTE EOG ELECTRODE CABLE THROUGH HOLE IN HRD, PLUG INTO HIB J4 CONNECTOR (GREEN/BLACK COLOR CODE), AND SECURE EXCESS CABLE WITH VELCRO STRAP(S).	
19-020		PS2	CONFIGURE/POSITION POWER KILL SWITCH ON CHAIR RAIL.	

WARNING

```
**********************************
* IF A WARNING TONE IS SOUNDED   *
* AT ANY TIME DURING MVI         *
* OPERATIONS, THE OPERATOR       *
* SHOULD IMMEDIATELY STOP        *
* PROCEDURES, SHUT DOWN CHAIR    *
* OPERATIONS BY FLIPPING         *
* ROTATOR SW, AND ASSIST         *
* SUBJECT FROM CHAIR.            *
**********************************
```

19-021		PS2	OPEN HELMET BLADDER VALVES, LOWER HRD/HELMET, CLOSE	
		MS3	INFLATE BLADDERS AS NEEDED (FRONT BULB = SIDE BLADDERS, BACK BULB = TOP BLADDERS	
19-022		MS3	CHECK HELMET VISORS ARE COMPLETELY LOWERED AND SUBJECT'S EYES CENTERED IN OPENINGS.	

Table 4. Recommended TAP Format.

Date: 04-04-91 Rev. Basic T1-IML-1-0050

SEQ	CMD	RESP (MET)	REMARK	DESCRIPTIONS	VERIF
11-020		PS2		Configure/position power kill switch on chair rail.	
			B.1.1	**********	
				WARNING If a warning tone is sounded at any time during MVI operations, the operator should immediately stop procedures, shut down chair operations by flipping rotator SW, and assist subject from chair.	
				**********	
11-021		PS2 MS3		Open helmet bladder valves, lower HRD/Helmet, close Inflate bladders as needed (front bulb = side bladders, back bulb = top bladders)	
11-022		MS3		Check helmet visors are completely lowered and subject's eyes centered in openings.	
11-023		MS3 PS2		Adjust shoulder and hip pads, and tighten 4 point harness restraint (knee and root restraints).	
11-024		MS3		Verify EOG signal polarity by having subject move eyes up, down, right, left (signal + for up and right, signal - for down and left). Scale display as necessary.	
11-025		MS3		Verify/Power-on SL Rack 4 Monitor.	
11-026		MS3		Confirm proper eye position: A. Entire eye in video field B. Helmet liner not visible C. Video overlay or header information not covering any portion of the eye. If proper eye position can not be attained, subject should attempt to adjust by inflating or deflating bladders.	

140

1991 NASA/ASEE SUMMER FACULTY FELLOWSHIP PROGRAM

JOHN F. KENNEDY SPACE CENTER
UNIVERSITY OF CENTRAL FLORIDA

MODELING AND CONTROL OF THE AUTOMATED RADIATOR INSPECTION DEVICE

PREPARED BY:	Darren Dawson, Ph.D.
ACADEMIC RANK:	Assistant Professor
UNIVERSITY AND DEPARTMENT:	Clemson University Electrical & Computer Engineering
NASA/KSC	
DIVISION:	Mechanical Engineering
BRANCH:	Special Projects (RADL)
NASA COLLEAGUE:	V. Leon Davis, Chief Robotics and Automation
DATE:	July 27, 1991
CONTRACT NUMBER:	University of Central Florida NASA-NGT-60002 Supplement: 6

Acknowledgments

I would like to thank NASA and ASEE for the opportunity to participate in this program. My professional knowledge of launch operations and shuttle support has increased greatly based on my interactions with the robotics group at NASA and the employees of Boeing Aerospace Organization, the engineering contractor for the Robotics Applications Development Laboratory. A special thanks to Leon Davis, my NASA colleague, for giving me the freedom to pursue interesting and challenging problems.

ABSTRACT

Many of the operations performed at Kennedy Space Center (KSC) are dangerous and repetitive tasks which make them ideal candidates for robotic applications. For one specific application, KSC is currently in the process of designing and constructing a robot, called the Automated Radiator Inspection Device (ARID), to inspect the radiator panels on the orbiter. In this report, the following related aspects of the ARID project are discussed: 1) Modeling of the ARID, 2) Design of control algorithms for the ARID, and 3) Nonlinear-Based simulation of ARID control algorithms. Based on the information delineated in this report, recommendations are then made to assist KSC personnel in the successful completion of the ARID project.

Summary

To automate the inspection of the radiator panels on the orbiter, Kennedy Space Center (KSC) is designing and constructing the Automated Radiator Inspection Device (ARID). Utilizing a vision-based system, the ARID will be capable of inspecting the entire surface of the radiator panels. Due to accuracy requirements imposed by the vision system, the ARID robot must be precisely controlled to ensure that the end-effector mounted camera is maintained at the proper distance from the radiator panels. To aid KSC personnel in the successful completion of the ARID project, a study was done to examine the associated modeling and control aspects of the ARID robot.

With regard to modeling, several separate sub-areas are analyzed and investigated. The rigid body statics and dynamics are formulated to describe the geometry and dynamic motion of the ARID. Since the ARID is a large robot that utilizes harmonic drives, a model including the effects of dominant mode structural vibrations and joint flexibilities are incorporated into the rigid-body dynamics. Since the ARID utilizes a redundant actuation system, a model including redundant actuators is also formulated.

With regard to control, several separate sub-areas are analyzed and investigated. For the rigid-body model, the performance of a PD controller is compared to a robust saturation controller. For the inclusion of joint flexibilities and dominant mode vibrational effects into the rigid body dynamics, the performance of a PD motor controller is compared to a nested PD motor/link controller and a nested PD motor/link/tip controller. To investigate the effects of redundant actuation on the control system performance, an independent torque controller is compared to a coupled torque controller.

TABLE OF CONTENTS

LIST OF ILLUSTRATIONS

I. INTRODUCTION

1.1 Robotics at Kennedy Space Center

The mission of Kennedy Space Center (KSC) is to provide manpower and support for fast, efficient, and safe preparation of launch vehicles. Robotics can be a key ingredient to satisfy this mission. Many of the operations performed at KSC are dangerous and repetitive which make them ideal candidates for robotic applications. The design and servicing procedures of present space vehicles and launch procedures make it difficult to implement robotic applications; however, the next generation space vehicles will no doubt be designed with robots in mind. Therefore, KSC personnel will have to become increasingly familiar with robots and related hardware such as sensors and control systems. The Robotics Applications Development Laboratory (RADL) provides this experience to KSC personnel and its contractors.

1.2 Description of the Automated Radiator Inspection Device

KSC is currently in the process of designing and constructing a robot, called the Automated Radiator Inspection Device (ARID), to inspect the radiator panels on the orbiter (See Figure 1.1). These panels, located on the inside of the cargo bay doors, are inspected when the orbiter is horizontally parked in the Orbiter Processing Facility (OPF). After the cargo bay doors are opened to expose the radiator panels, the inspection is presently performed by workers in a crane-assisted bucket over the radiator surface. The radiator surface is divided into grids, and surface defects are cataloged by location in the grid. These surface defects are monitored periodically to determine when repair is needed.

To automate this inspection process, the ARID robot is being constructed to move along the orbiter on a long track. Utilizing a vision-based system, the ARID will be capable of inspecting the entire surface of the radiator panels. The associated vision system will be able to divide the radiator panels into smaller grids and thus provide better cataloging of defects.

1.3 Objective of this Research Project

The objective of this research project is to assist KSC personnel in three areas: 1) Modeling of the ARID, 2) Design of control algorithms for the ARID, and 3) Nonlinear-based simulation of ARID control algorithms. The body of this report is dividing among these three areas.

With regard to modeling, several separate sub-areas are analyzed and investigated. The rigid body statics and dynamics [1] are formulated to describe the geometry and dynamic motion of the ARID. Specifically, the ARID kinematics, inverse kinematics, manipulator jacobian, and manipulator dynamics are given. Since the ARID utilizes harmonic drives, a model including effects of joint flexibilities [2] is incorporated into the rigid-body dynamics. Because of the large size of the ARID, structural

vibrations [3] are considered to be a potential problem; therefore, a model including the effects of "dominate mode" vibrations are incorporated into the rigid body/flexible joint model. Since the ARID utilizes a redundant actuation system, motor synchronization is considered to be a potential problem; therefore, a model including the effects of redundant actuators is formulated.

With regard to control, several separate sub-areas are analyzed and investigated. A proportional-derivative (PD) controller [1] and a robust saturation controller [4] are both designed for the rigid-body dynamics. For the inclusion of joint flexibilities into the rigid body dynamics, a PD motor controller [1] and nested PD motor/link controller [5] are formulated. For the inclusion of vibrational effects into the rigid body/joint flexibility model, a PD motor controller [1] and nested PD motor/link/tip controller [6] are formulated. To study the effects of redundant actuation on the control system performance, an independent torque controller [7] and a coupled torque controller [7] are formulated.

With regard to simulation, several separate sub-areas are analyzed and investigated. For the rigid-body model, the performance of a PD controller is compared to a robust saturation controller. For the inclusion of joint flexibilities into the rigid body dynamics, the performance of a PD motor controller is compared to a nested PD motor/link controller. For the inclusion of vibrational effects into the rigid body/joint flexibility model, the performance of a PD motor controller is compared to a nested PD motor/link/tip controller. To investigate the effects of redundant actuation on the control system performance, an independent torque controller is compared to a coupled torque controller.

II. RIGID BODY STATICS AND DYNAMICS

In this section, we present the static and dynamic rigid body relationships for the ARID robot. The terminology rigid body is used to emphasize that flexibilities due to link and drive transmissions have been neglected. In subsequent subsections, we will discuss modifications of the dynamic model due to link and joint flexibilities.

From Figure 1.1, we can see that the prismatic joint moves perpendicular to the direction of the three revolute joints; therefore, the motion of the prismatic joint is decoupled from the motion of the revolute joints. Since the prismatic motion is decoupled from the motion of the revolute joints, the static and dynamic relationships for the prismatic joint are relatively simple; therefore, in this section, we will only discuss the static and dynamic relationships for the revolute joints. Specifically, we will present the kinematics, inverse kinematics, manipulator jacobian, and the manipulator dynamic relationships for the three revolute joints.

2.1 Kinematics

The kinematics [1] (i.e. forward kinematics) problem is associated with finding the end-effector position and orientation given the three joint

angles. The end-effector position and orientation is sometimes called the task space coordinate set. From the geometric description given in Figure 2.1, we define the task space coordinate set as

$$X = \begin{bmatrix} x \\ y \\ \theta \end{bmatrix} \tag{2.1}$$

where X is a 3x1 vector, x denotes the position of the end-effector in the x-direction, y denotes the position of the end-effector in y-direction, and θ denotes the end-effector angle of orientation measured off the x-axis. Note that the coordinate set {x,y} defined in Figure 2.1 is a non-rotating coordinate set.

Utilizing a geometric approach, it is easy to show that the relationships between the task space variables and the joint space variables are given by

$$X = \begin{bmatrix} x \\ y \\ \theta \end{bmatrix} = h(q) = \begin{bmatrix} L_3c_{123} + L_2c_{12} + L_1c_1 \\ L_3s_{123} + L_2s_{12} + L_1s_1 \\ q_1 + q_2 + q_3 \end{bmatrix} \tag{2.2}$$

where q_1, q_2, q_3 are the joint variables defined in Figure 2.1; h(q) is the 3x1 vector of kinematic functions; L_1, L_2, L_3 are the link lengths defined in Figure 2.1; and c_1, s_{12}, c_{123} are used as abbreviations for $\cos(q_1)$, $\sin(q_1 + q_2)$, and $\cos(q_1 + q_2 + q_3)$, respectively.

2.2 Inverse Kinematics

The inverse kinematics [1] problem is associated with finding the three joint angles given the end-effector position and orientation. From the geometric description given in Figure 2.1, we define the joint space variable set as

$$q = \begin{bmatrix} q_1 \\ q_2 \\ q_3 \end{bmatrix} \tag{2.3}$$

where q is a 3x1 vector composed of the joint variables.

Utilizing a geometric approach, it is easy to show that the relationship between the joint space variables and the task space variables are given by

$$q_1 = \text{Atan2}\left[\frac{y - L_3s_\theta}{x - L_3c_\theta}\right] \pm \text{Acos}\left[\frac{(x - L_3c_\theta)^2 + (y - L_3s_\theta)^2 + L_1^2 - L_2^2}{2L_1\sqrt{(x - L_3c_\theta)^2 + (y - L_3s_\theta)^2}}\right], \tag{2.4}$$

$$q_2 = \text{Atan2}\left[\frac{c_1 y - s_1 x - L_3(c_1 s_\theta - s_1 c_\theta)}{c_1 x + s_1 y - L_3(c_1 s_\theta + s_1 s_\theta) - L_1}\right], \tag{2.5}$$

and

$$q_3 = \theta - q_1 - q_2 \tag{2.6}$$

where Acos(.) is used to denote the inverse cosine operation, Atan2(.) is used to denote the inverse tangent operation with quadrant checking operation, and the positive/negative operation (i.e. $\pm$ in (2.4)) is used to specify the up/down configuration of the ARID elbow.

2.3 Manipulator Jacobian

The manipulator jacobian matrix [1] is used to relate the joint space velocity vector to the task space velocity vector. The jacobian matrix is obtained by taking the time derivative of the forward kinematics given in (2.2). That is, the 3x3 Jacobian matrix (i.e. J(q)) satisfies the relationship

$$\dot{X} = \begin{bmatrix} \dot{x} \\ \dot{y} \\ \dot{\theta} \end{bmatrix} = J(q)\dot{q} = J(q)\begin{bmatrix} \dot{q}_1 \\ \dot{q}_2 \\ \dot{q}_3 \end{bmatrix} \tag{2.7}$$

where

$$J(q) = \begin{bmatrix} -L_1 s_1 - L_2 s_{12} - L_3 s_{123} & -L_2 s_{12} - L_3 s_{123} & -L_3 s_{123} \\ L_1 c_1 + L_2 c_{12} + L_3 c_{123} & L_2 c_{12} + L_3 c_{123} & L_3 c_{123} \\ 1 & 1 & 1 \end{bmatrix}. \tag{2.8}$$

One of the advantages of calculating the jacobian matrix online is that it can be used to avoid online calculation of the inverse kinematics. For example, one can utilize the task-space PD control [1]

$$\tau = J^T(q)\left[K_v(\dot{x}_d - J(q)\dot{q}) + K_p(x_d - h(q))\right] \tag{2.9}$$

where K_v, K_p are positive definite 3x3 gain matrices, x_d is a 3x1 vector used to represent the desired task space trajectory that we wish to track, and τ is the 3x1 vector used to represent the input torque to each link.

Note that (2.9) does not depend on the calculation of the inverse kinematics. It should also be noted that the task space coordinate set defined in this report is a nonrotating coordinate frame. For actual implementation of the ARID robot, a task space formulation can be used that

ensures that the ARID camera is always perpendicular to the radiator surface. This task-space coordinate set can be formulated if an analytical function of the radiator surface can be obtained.

2.4 Manipulator Dynamics

A robot is basically a positioning device. To control the end effector position we must know the dynamic properties of the manipulator in order to know how much force to exert on it to cause it to move. Too little force and the manipulator is slow to react. Too much force and the manipulator may oscillate about the desired position.

In this section, we give the dynamics of the ARID robot in the Lagrange Euler form [1]. The rigid body dynamics for the 3-link revolute ARID robot arm are

$$\tau = M(q)\ddot{q} + V(q,\dot{q}) + G(q) + F(\dot{q}) \tag{2.10}$$

where $M(q)$ is a 3×3 link inertia matrix, $V(q,\dot{q})$ is a 3×1 vector containing the centripetal and Coriolis terms, $G(q)$ is a 3×1 vector containing the gravity terms, $F(\dot{q})$ is a 3×1 vector containing the static and dynamic friction terms, $\ddot{q}$ is a 3×1 vector representing the link accelerations, and τ is the 3×1 control vector used to represent the torque provided by the actuators in each joint. With regard to ARID robot, we now explicitly define each term associated with (2.10). First, the inertia matrix $M(q)$ is given by

$$M(q) = \begin{bmatrix} M_{11} & M_{12} & M_{13} \\ M_{21} & M_{22} & M_{23} \\ M_{31} & M_{32} & M_{33} \end{bmatrix} \tag{2.11}$$

where

$$M_{11} = m_1 L_{c1}^2 + m_2(L_1^2 + L_{c2}^2 + 2L_1 L_{c2} c_2) + I_1 + I_2 + I_3 + m_3(L_1^2 + L_2^2 + L_{c3}^2 + 2L_1 L_2 c_2 + 2L_1 L_{c3} c_{23} + 2L_2 L_{c3} c_3),$$

$$M_{12} = M_{21} = m_2(L_{c2}^2 + L_1 L_{c2} c_2) + I_2 + I_3 + m_3(L_2^2 + L_{c3}^2 + L_1 L_2 c_2 + L_1 L_{c3} c_{23} + 2L_2 L_{c3} c_3),$$

$$M_{13} = M_{31} = I_3 + m_3(L_{c3}^2 + L_1 L_{c3} c_{23} + L_2 L_{c3} c_3),$$

$$M_{22} = m_2 L_{c2}^2 + I_2 + I_3 + m_3(L_2^2 + L_{c3}^2 + 2L_2 L_{c3} c_3),$$

$$M_{23} = M_{32} = I_3 + m_3(L_{c3}^2 + L_2 L_{c3} c_3),$$

$$M_{33} = m_3 L_{c3}^2 + I_3,$$

I_1, I_2, I_3, are the moments of inertia of links L_1, L_2, L_3, respectively; L_{c1}, L_{c2}, L_{c3}, are the distances to the center of mass of links L_1, L_2, L_3, respectively; and m_1, m_2, m_3, are the masses of links L_1, L_2, L_3, respectively (See Figure 2.1). Second, the Coriolis/centripetal terms $V(q,\dot{q})$ are given by

$$V(q,\dot{q}) = \begin{bmatrix} V_1 \\ V_2 \\ V_3 \end{bmatrix} \tag{2.12}$$

where

$$\begin{aligned} V_1 = {} & (-m_2 L_1 L_{c2} - m_3(L_1 L_2 s_2 + L_1 L_{c3} s_{23}))\dot{q}_2^2 + (-m_3(L_1 L_{c3} s_{23} + L_2 L_{c3} s_3))\dot{q}_3^2 \\ & + (-m_2 L_1 L_{c2} - m_3(L_1 L_2 s_2 + L_1 L_{c3} s_{23}))\dot{q}_1\dot{q}_2 \\ & + 2(-m_3(L_1 L_{c3} s_{23} + L_2 L_{c3} s_3))(\dot{q}_1\dot{q}_2 + \dot{q}_2\dot{q}_3), \end{aligned}$$

$$\begin{aligned} V_2 = {} & (m_2 L_1 L_{c2} + m_3(L_1 L_2 s_2 + L_1 L_{c3} s_{23}))\dot{q}_1^2 + (-m_3 L_2 L_{c3} s_3)\dot{q}_3^2 \\ & + 2(-m_3 L_2 L_{c3} s_3)(\dot{q}_1\dot{q}_2 + \dot{q}_2\dot{q}_3), \end{aligned}$$

and

$$V_3 = (m_3(L_1 L_{c3} s_{23} + L_2 L_{c3} s_3))\dot{q}_1^2 + (m_3 L_2 L_{c3} s_3)\dot{q}_2^2 + 2(m_3 L_2 L_{c3} s_3)\dot{q}_1\dot{q}_2.$$

Third, the gravity terms $G(q)$ are given by

$$G(q) = \begin{bmatrix} G_1 \\ G_2 \\ G_3 \end{bmatrix} \tag{2.13}$$

where

$$G_1 = m_1 g L_{c1} c_1 + m_2 g(L_1 c_1 + L_{c2} c_{12}) + m_3 g(L_1 c_1 + L_2 c_{12} + L_{c3} c_{123}),$$

$$G_2 = m_2 g L_{c2} c_{12} + m_3 g (L_2 c_{12} + L_{c3} c_{123}),$$

$$G_3 = m_3 g L_{c3} c_{123},$$

and

g is used to denote the gravitational constant (i.e. 9.81 m/s^2). Lastly, the friction terms $F(\dot{q})$ are given by

$$F(\dot{q}) = \begin{bmatrix} F_1 \\ F_2 \\ F_3 \end{bmatrix} \tag{2.14}$$

where

$$F_1 = v_{f1}\dot{q}_1 + k_{f1}\mathrm{sgn}(\dot{q}_1),$$

$$F_2 = v_{f2}\dot{q}_2 + k_{f2}\mathrm{sgn}(\dot{q}_2),$$

$$F_3 = v_{f3}\dot{q}_3 + k_{f3}\mathrm{sgn}(\dot{q}_3),$$

v_{f1}, k_{f1} are positive scalar constants used to denote the static and dynamic coefficients of friction for joint 1; v_{f2}, k_{f2} are positive scalar constants used to denote the static and dynamic coefficients of friction for joint 2; v_{f3}, k_{f3} are positive scalar constants used to denote the static and dynamic coefficients of friction for joint 3; and the sgn(.) is used to represent the signum function.

III. SIMULATION OF CONTROLLERS FOR THE RIGID BODY DYNAMICS

Utilizing the rigid body dynamics developed in Section II, controllers can be developed and tested. Specifically, the dynamic in (2.10) can be rewritten in the form

$$\ddot{q} = M^{-1}(q)[\tau - V(q,\dot{q}) - G(q) - F(\dot{q})]. \tag{3.1}$$

Utilizing a integration package such as SIMNON, the dynamics given by (3.1) can now be integrated over any desired simulation interval for any postulated control input τ.

Typically, the robot control objective is formulated as the tracking problem. That is, we wish to follow a desired trajectory for each joint with as small as deviation possible. To quantify the measure of success, we often

examine the tracking error which is defined by

$$e = q_d - q \tag{3.2}$$

where the 3x1 vector q_d is used to represent the desired trajectory for each joint. From (3.2), we can see that if tracking error (i.e. e) is small then we can be reasonably assured that the robot is performing as desired.

3.1 PD Control

As a starting point, we first simulated the simple PD controller [14] given by

$$\tau = K_v\dot{e} + K_p e \tag{3.3}$$

where K_v, K_p are 3x3 diagonal, positive definite matrices. The details of the program are given in the SIMNON file ARID1.T [8]. From Figure 3.1, we can see that the PD controller performs poorly, that is, the position and velocity tracking errors are relatively large.

3.2 Robust Saturation Control

To illustrate how an advanced control algorithm can improve tracking performance, we proposed the robust saturation controller [4]

$$\tau = K_v\dot{e} + K_p e + \frac{(e + \dot{e})\rho^2}{\|e + \dot{e}\|\rho + \epsilon} \tag{3.4}$$

where ϵ is a scalar positive constant, $\|\cdot\|$ is the standard Euclidean norm, and ρ is a scalar function that bounds the uncertainty. The details of the program are given in the SIMNON file ARID2.T [8]. From Figure 3.1 and 3.2, we can see that the robust saturation controller outperforms the PD controller by a wide margin. The reason for this improvement in performance is that the robust saturation controller compensates for any "uncertainty" with regard to the manipulator dynamics.

IV. MODELING AND CONTROL FOR JOINT FLEXIBILITIES

Since the ARID robot is a rather massive robot, the torque delivered to each link must be relatively large. To provide the necessary torque amplification, the ARID robot's actuation system utilizes harmonic drives. While the harmonic drives amplify the torque by a factor of approximately 200, the harmonic drives introduce flexibility at each joint. In order to move the robot accurately, the control strategy must compensate for the "joint flexibility" introduced by the harmonic drive. This very fact was confirmed in a presentation to KSC personnel by ROBOTICS RESEARCH INC.

4.1 Model of Joint Flexibilities

The joint flexibilities introduced by the harmonic drives can be modeled by placing springs at each joint (See Figure 4.1). Similar to [2], the rigid body dynamics for the 3-link revolute ARID robot arm with joint flexibilities can then be shown to be

$$M(q)\ddot{q} + V(q,\dot{q}) + G(q) + F(\dot{q}) = K(\Gamma q_m - q) \tag{4.1}$$

and

$$J\ddot{q}_m + B\dot{q}_m + \Gamma K(\Gamma q_m - q) = \tau \tag{4.2}$$

where $q_m(t)$ is a 3×1 vector representing the actuator displacements, K is a constant diagonal 3×3 matrix used to denote the joint flexibilities, J is a 3×3 positive-definite constant diagonal actuator inertia matrix, B is a positive-definite constant diagonal 3×3 matrix used to represent the actuator damping, Γ is a 3×3 positive-definite constant diagonal matrix used to represent the gear ratio in each harmonic drive, and all other quantities are the same as those defined in (2.10).

4.2 PD Motor Control and Simulation

To illustrate the pitfalls of local feedback (i.e. motor encoder feedback only), we simulated a simple PD motor controller [1] given by

$$\tau = K_v(\dot{q}_d - \dot{q}_m) + K_p(q_d - q_m) \tag{4.3}$$

where K_v, K_p are 3x3 diagonal, positive definite matrices. The details of the program are given in the SIMNON file ARID3.T [8]. From Figure 4.2, we can see that the PD controller performs poorly. The information delineated by Figure 4.2 makes sense since if we use motor feedback only, we not even attempting to control the robot end-effector (i.e. link position). That is, we are only controlling the motor.

4.3 Nested PD Motor/Link Control and Simulation

To illustrate the improvement in performance of including link encoder feedback along with motor encoder feedback, we simulated a nested PD motor/link controller [5] (i.e. nested feedback control means one feedback loop is inside another feedback loop) given by

$$\tau = K_{mv}K_{mp}[K_v\dot{e} + K_p e - K(q_m - q)] - K_{mv}K(\dot{q}_m - \dot{q}) \tag{4.4}$$

where K_v, K_p, K_{mv}, K_{mp} are 3x3 diagonal, positive definite matrices, and K is the joint flexibility matrix defined in (4.1). The details of the program

are given in the SIMNON file ARID5.T [8]. From Figure 4.3, we can see that the nested PD motor/link controller performs very well. The information delineated by Figure 4.3 also makes sense since if we use link feedback, we are actually measuring the quantity that we attempting to control. Note that in addition to using the motor resolver for motor position information, we must mount a position encoder on each link to implement the controller given in (4.4).

V. MODELING AND CONTROL FOR VIBRATIONAL EFFECTS

KSC personnel have often stated that the ARID will inspect the radiator panel along the prismatic joint axis [9]. That is, the gross motion of the ARID will be along the track while the revolute joints will move in small increments. Since the ARID is a long slender robot, it has been postulated that link vibrations along the prismatic joint axis may be a potential problem; therefore, the ARID control algorithm may have to be designed to actively compensate for these vibrations. Since these vibrations are the only ones considered in this report, we will refer to these gross motion vibrations as "dominant" vibrations.

5.1 Model of Dominant Vibrations

To compensate for the vibrations along the prismatic joint axis, a model for these vibrations must first be formulated. As shown in Figure 5.1, we have selected a lumped model [3] as a first attempt at proposing a possible solution to this problem. It should be emphasized that this problem of link flexibilities or link vibrations is still considered a research area.

From Figure 5.1, the dominant vibration model including joint flexibility is given by

$$m_e\ddot{q}_e + b_v(\dot{q}_e - \dot{q}_L) + k_v(q_e - q_L) = 0, \tag{5.1}$$

$$m_L\ddot{q}_L + b_v(\dot{q}_L - \dot{q}_e) + k_v(q_L - q_e) = k_m(\gamma q_m - q_L), \tag{5.2}$$

and

$$m_m\ddot{q}_m + b_m\dot{q}_m + \gamma k_m(\gamma q_m - q_L) = \tau \tag{5.3}$$

where m_e, m_L, m_m are positive scalar constants used to represent the lumped mass of the end-effector, link, and motor, respectively; b_v, b_m are positive scalar constants used to represent the lumped damping for the vibrational effects and the motor, respectively; q_e, q_L, q_m are used to represent the position of the end-effector, link, and motor, respectively; k_v, k_m are positive scalar constants used to represent the lumped spring constant for the vibrational effects and the joint flexibilities, respectively; γ is used

to represent the gear ratio, and τ is used to represent the control input.

5.2 PD Motor Control and Simulation

To illustrate the pitfalls of local feedback (i.e. motor encoder feedback only), we simulated a simple PD motor controller [1] given by

$$\tau = K_v(\dot{q}_d - \dot{q}_m) + K_p(q_d - q_m) \tag{5.4}$$

where K_v, K_p are 3x3 diagonal, positive definite matrices. The details of the program are given in the SIMNON file FLEX4.T [8]. From Figure 5.2, we can see that the PD controller performs very poorly. The information delineated by Figure 5.2 makes sense since if we use motor feedback only, we not even attempting to control the robot end-effector (i.e. end-effector position). That is, we are only controlling the motor.

5.3 Nested PD Motor/Link/Tip Control and Simulation

To illustrate the improvement in performance of including link encoder feedback and end-effector measurements along with motor encoder feedback, we simulated a nested PD motor/link/tip controller [6] given by

$$\tau = K_{p3}K_{p2}K_{v1}[K_p\dot{e} - (\dot{q}_L - \dot{q}_e)] + K_{p3}K_{p2}K_{p1}[K_p e - (q_L - q_e)] \tag{5.5}$$

$$- K_{p3}K_{p2}(q_m - q_L) - K_{p3}(\dot{q}_m - \dot{q}_L)$$

where K_{p3}, K_{p2}, K_{v1}, K_p, K_{p1} are positive controller gains. The details of the program are given in the SIMNON file FLEX3.T [8]. From Figure 5.3, we can see that the nested PD motor/link/tip controller performs very well. The information delineated by Figure 5.3 also makes sense since if we use end-effector feedback, we are actually measuring the quantity that we are attempting to control.

As we have already stated the controller given in (5.5) requires measurement of end-effector position as well as link and motor position; therefore, if vibrations become a problem, we must have a way of measuring end-effector position. A common method for measuring end-effector position for a vibrating robot is to mount an accelerometer on the end of the robot. The signal from the accelerometer can be integrated once to obtain end-effector velocity, that is

$$\dot{q}_e(t) = \int_0^t \ddot{q}_e(t)\, dt + \dot{q}_e(0). \tag{5.6}$$

The end-effector position can then be obtained by integrating (5.6) to obtain

$$q_e(t) = \int_0^t \dot{q}_e(t)\, dt + q_e(0). \tag{5.7}$$

VI. SYNCHRONIZATION OF REDUNDANT MOTORS

Since the ARID robot is the first robot to be installed next to flight hardware, the reliability of the ARID robot and associated control system is extremely important. That is, the ARID robot should be designed to minimize the chance of damaging the orbiter. To enhance reliability of the ARID robot, the electromechanical design of each joint includes redundant drive shafts, bearings, harmonic drives, brakes, transmission chains, motors, and computer control systems.

As pointed out in [9], two motors in parallel could cause a potential problem in that the motors might "fight" each other. That is, since the two motor/control systems will not have exactly the same dynamic characteristics, the torque delivered by each motor to the corresponding link will not be exactly the same at any instant of time. In this section, we develop a model and some control strategies to examine this motor synchronization problem.

6.1 Model of Motor Synchronization Problem

The model used to study the motor synchronization problem was based on the same model that was used to study the joint flexibility effects. For simplicity, we will only consider a one-link problem as illustrated in Figure 6.1. From Figure 6.1, we can see that the model is composed of two motors connected to the same link. The associated dynamic equations for this system are given by

$$mL^2\ddot{q} + mgL\sin(q) + v_f\dot{q} + k_f\,\mathrm{sgn}(\dot{q}) = K_1(\Gamma_1 q_{m1} - q) + K_2(\Gamma_2 q_{m2} - q), \tag{6.1}$$

$$J_1\ddot{q}_{m1} + B_1\dot{q}_{m1} + \Gamma_1 K_1(\Gamma_1 q_{m1} - q) = \tau_1, \tag{6.2}$$

and

$$J_2\ddot{q}_{m2} + B_2\dot{q}_{m2} + \Gamma_2 K_2(\Gamma_2 q_{m2} - q) = \tau_2 \tag{6.3}$$

where $q_{m1}(t)$, $q_{m2}(t)$ represent the actuator displacements of motors 1 and 2, respectively; τ_1, τ_2 represent the torque delivered by motors 1 and 2, respectively; K_1, K_2 are positive constants used to denote the joint flexibilities of harmonic drives 1 and 2, respectively; J_1, J_2 are positive constants used to represent the inertia of motors 1 and 2, respectively; B_1, B_2 are positive constants used to represent the damping in motors 1 and 2, respectively; Γ_1, Γ_2 are positive constants used to represent the gear ratio

of harmonic drives 1 and 2, respectively; and all other quantities are the same as those defined in (4.1) and (4.2).

6.2 Independent Torque Control and Simulation

To simulate the effects of redundant motors, we first simulated the nested PD motor/link controller given in Section 4.3 for each redundant system. That is, each control system, designated control system 1 and 2, has no sensory input based on its counterpart's performance. From Section 4.3, the two "independent" torque controllers are given by

$$\tau_1 = K_{mv1}K_{mp1}[K_{v1}\dot{e} + K_{p1}e - K_1(q_{m1} - q)] - K_{mv1}K_1(\dot{q}_{m1} - \dot{q}) \qquad (6.4)$$

and

$$\tau_2 = K_{mv2}K_{mp2}[K_{v2}\dot{e} + K_{p2}e - K_2(q_{m2} - q)] - K_{mv2}K_2(\dot{q}_{m2} - \dot{q}) \qquad (6.5)$$

where K_{v1}, K_{p1}, K_{mv1}, K_{mp1}, K_{v2}, K_{p2}, K_{mv2}, K_{mp2} are positive controller gains; K_1, K_2 are the joint flexibility constants defined in (6.1); and the link tracking error is defined in (3.2).

To simulate a possible failure of control system 2, τ_2 was set to zero at 4 seconds. To simulate mismatch in the redundant systems, the parameters representing the two motors/drives were assumed to be mismatched by 50%. The details of the program are given in the SIMNON file SYC1.T [8]. From Figure 6.2, we can see that the independent nested PD motor/link controllers perform very well. Even after motor 2 is shut completed down at 4 seconds, controller 1 compensates for this failure. Figure 6.2 seems also to confirm that the motor fighting problem may not be a problem if a proper torque based controller is utilized.

6.3 Coupled Torque Control and Simulation

To simulate the effects of coupled control of redundant motors, we simulated a "coupled" nested PD motor/link controller similar to that given in Section 4.3. That is, each control system has sensory input based on its counterpart's performance. The two coupled torque controllers are given by

$$\tau_1 = \tau_2 = K_{mv}K_{mp}[K_v\dot{e} + K_pe - K(q_{m1} + q_{m2} - 2q)] \qquad (6.6)$$

$$- K_{mv}K(\dot{q}_{m1} + \dot{q}_{m2} - 2\dot{q})$$

where K_v, K_p, K_{mv}, K_{mp} are positive controller gains; and K is the average joint flexibility constant (i.e. $(K_1 + K_2)/2$.

To simulate a possible failure of control system 2, τ_2 was set to zero at 4 seconds. To simulate mismatch in the redundant systems, the parameters representing the two motors/drives were assumed to be mismatched by 50%. The details of the program are given in the SIMNON file SYC2.T [8]. From Figure 6.3, we can see that the coupled nested PD motor/link controllers perform very well. Even after motor 2 is shut completed down at 4 seconds, controller 1 compensates for this failure. Figure 6.3 seems also to confirm that the motor fighting problem may not be a problem if a proper torque based controller is utilized.

It should be noted that the coupled torque control approach can be designed to maintain the redundant concept by installing redundant motor encoders at each motor shaft. In this way, the coupled torque control approach can be used without requiring that control systems 1 and 2 have any electrical connections that violate the integrity of the redundant channels.

VII. CONCLUSIONS AND RECOMMENDATIONS

In this report, the following related aspects of the ARID project have been discussed 1) Modeling of the ARID, 2) Design of control algorithms for the ARID, and 3) Nonlinear-based simulation of ARID control algorithms. Based on the information delineated in this report, conclusions and recommendations are now made to assist KSC personnel in the successful completion of the ARID project

7.1 Conclusions

To aid KSC personnel in the successful completion of the ARID project, a study was done to examine the associated modeling and control aspects of the ARID robot. With regard to modeling, the rigid body statics and dynamics were formulated to describe the geometry and dynamic motion of the ARID. A model including the effects of joint flexibilities and dominant vibrations were then incorporated into the rigid-body dynamics. Since the ARID utilizes a redundant actuation system, a model including redundant actuation was formulated.

With regard to control, a robust saturation controller was shown to outperform a PD controller for the rigid body dynamics. For the inclusion of joint flexibilities and dominant vibrational effects into the rigid body dynamics, a nested PD motor/link controller and a nested PD motor/link/tip controller were both shown to outperform a PD motor controller. To investigate the effects of redundant actuation on the control system performance, an independent nested PD motor/link torque controller and a coupled nested PD motor/link torque controller were both shown to give good performance inspite of a single motor failure.

7.2 Recommendations

Since it is widely recognized by robotic engineers that the robot control problem must be solved at the torque input level, it is suggested that the motor drive units be changed to accommodate torque based control development.

It is important to note that the synchronization of the redundant motors appears not to be a potential problem if a proper torque based control is used.

To compensate for joint flexibilities induced by the harmonic drives, it is suggested that redundant "base-mounted" link encoders be added to the design. Simply stated, if you do not measure link position, you can not control link position.

If link flexibilities (i.e. vibrations) are noted to be a problem during the initial testing phase, it is suggested that redundant link tip measurement devices (such as accelerometers) be added to the design.

Determine the failure mode of each motor to see if it continues to turn if it stops running due to a failure.

Since the host computer for the ARID control system is a relatively slow computer, it is suggested that a high speed DSP expansion board be added to the design to speed up online transmission and collection of data.

To reduce the time spent writing code and doing hardware interfacing, it is suggesting that a high level software system (for example LABVIEW) be used. Moving the robot accurately is a hard enough task as it is; therefore, re-design of low-level software and hardware should be avoided. It should also be noted that National Instruments sells a high-speed DSP expansion board (i.e. NB-DSP2300, 32-bit, 33 MFLOPS, high speed data transfer) for LABVIEW applications.

Utilize Jacobian matrix in conjunction with task-space formulation to avoid solving the inverse-kinematics online.

Since large movements of the prismatic joint may cause excessive vibration, KSC personnel should plan to make large movements with the revolute joints as a backup mode of operation.

Since exact position of the radiator is not known, it suggested that the controller incorporate feedback (i.e. range sensors) to accurately place the ARID end-effector. If the radiator panel does warp, it is believed that no "warping model" will model these nonlinear effects accurately enough to move the camera at 24" $\pm$ 1/8" tolerance in an open loop configuration.

Since it would be desirable for computer system 1 to know the position and velocity of motor 2, it is suggested that redundant motor encoders be added to the the design (This concept maintains the validity of the redundant specification). Note that redundant motor encoders will be needed if the ARID robot requires a coupled control approach.

If the ARID can not be accurately moved with simple nested PD control laws as the ones given in this report, KSC personnel should use advanced control techniques such as the ones given in [5] and [6].

To make the programs written in this report more useful, the following steps should be taken: 1) the prismatic program should be combined with the revolute program, 2) the redundant motor model should then be included, and 3) actual task space desired trajectories related to the radiator surface should then be included. If all these steps are taken, one program can then be used to evaluate the overall system performance.

If the PC23 indexer is used and a torque based controller is not used then vibration can be reduced by using the S-curve velocity profiling algorithm that comes with the indexer.

VIII. FIGURES

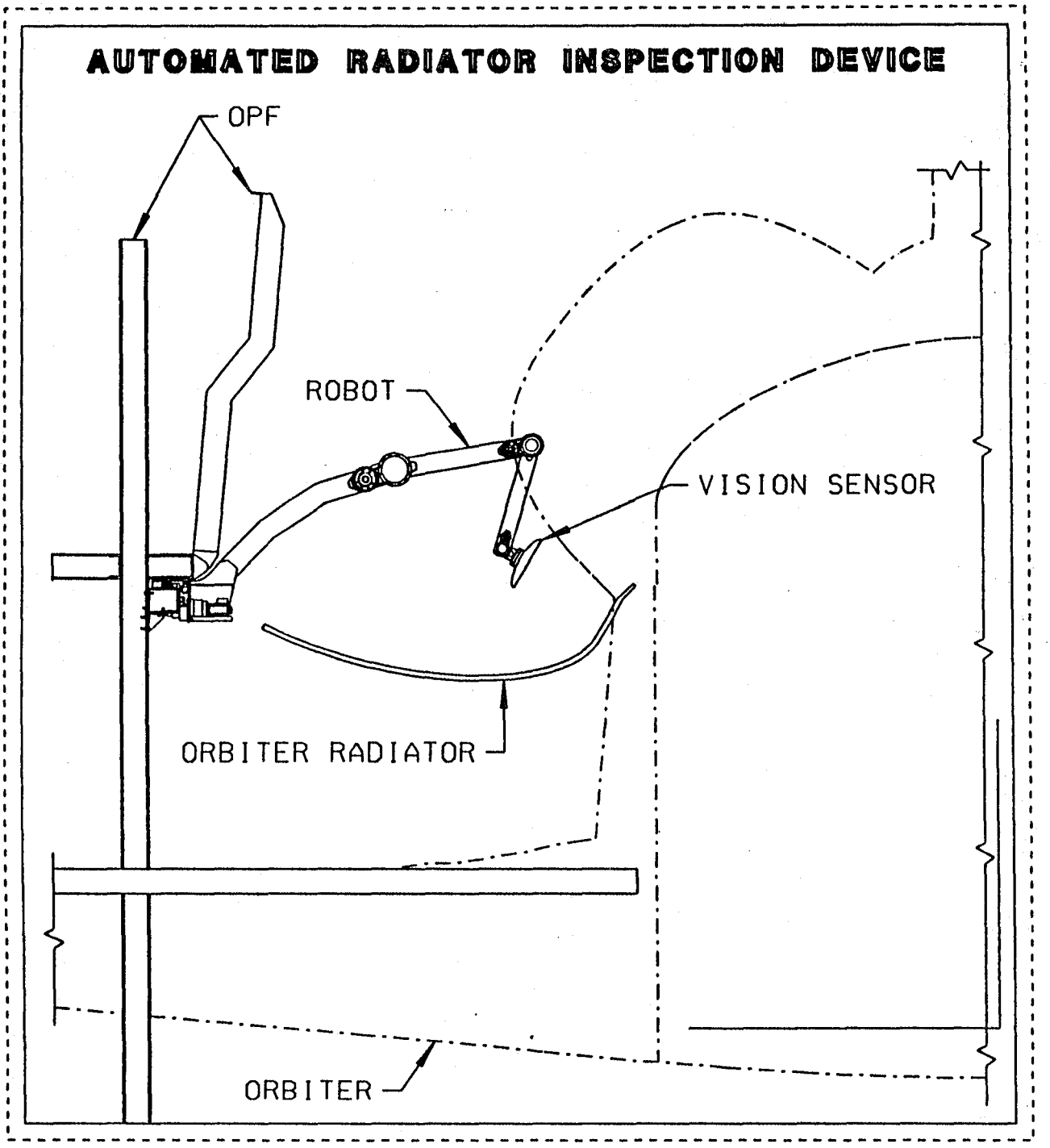

Figure 1.1 Diagram of the ARID Robot

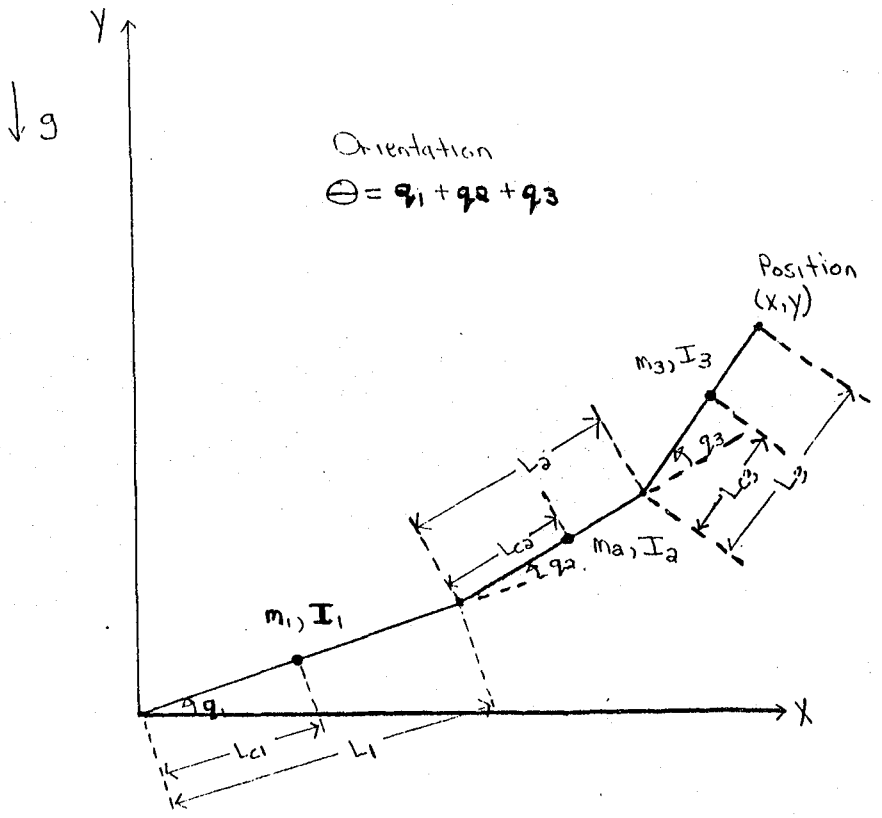

Figure 2.1 3-Link Robot Freebody Diagram

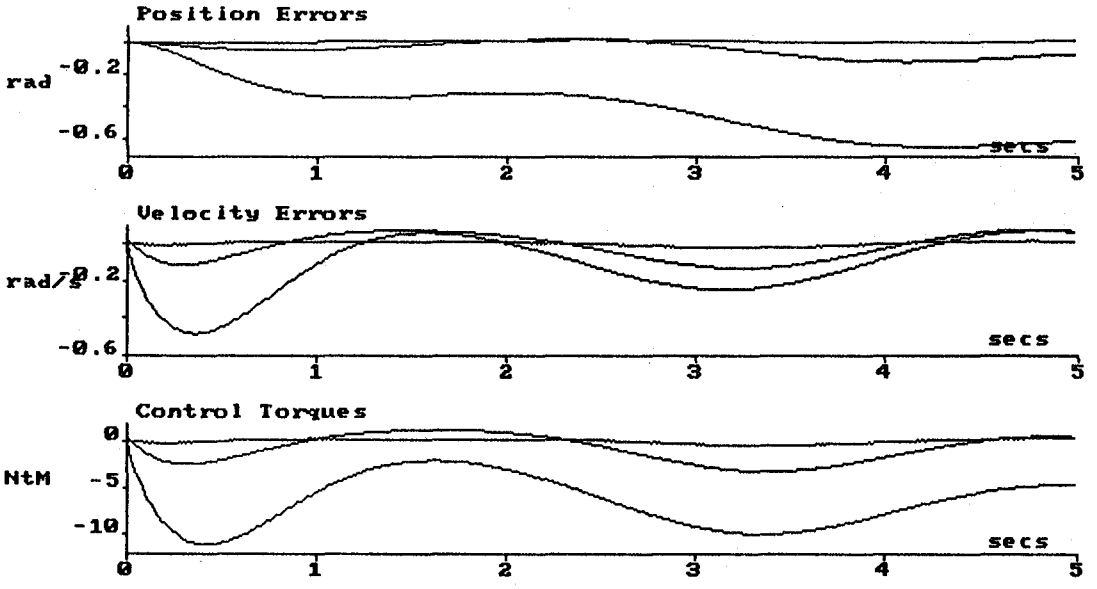

Figure 3.1 Rigid-Link PD Control Simulation

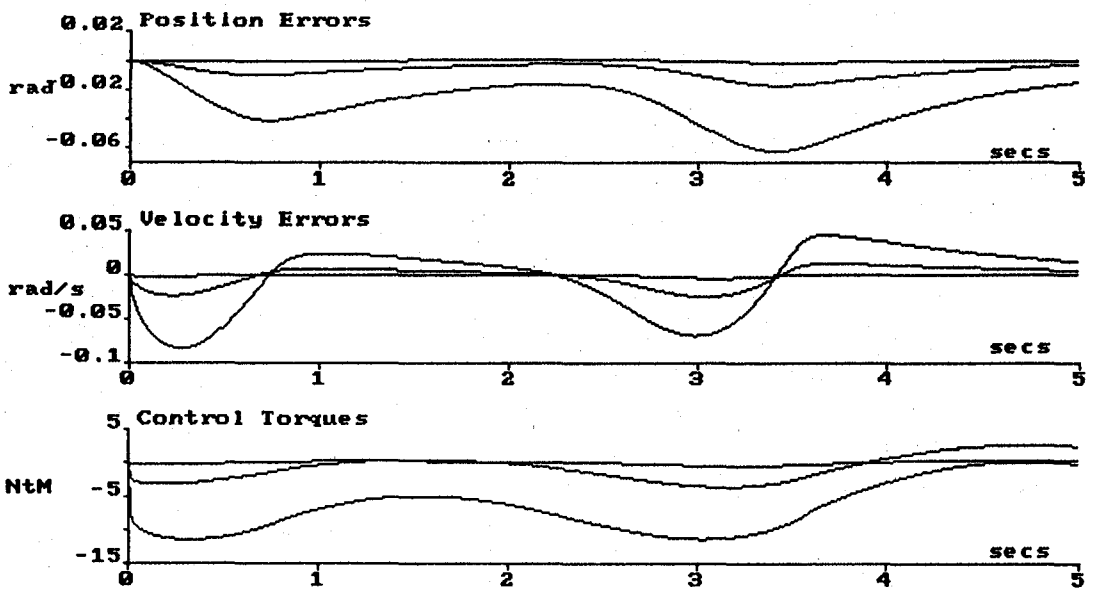

Figure 3.2 Rigid-Link Robust Saturation Control Simulation

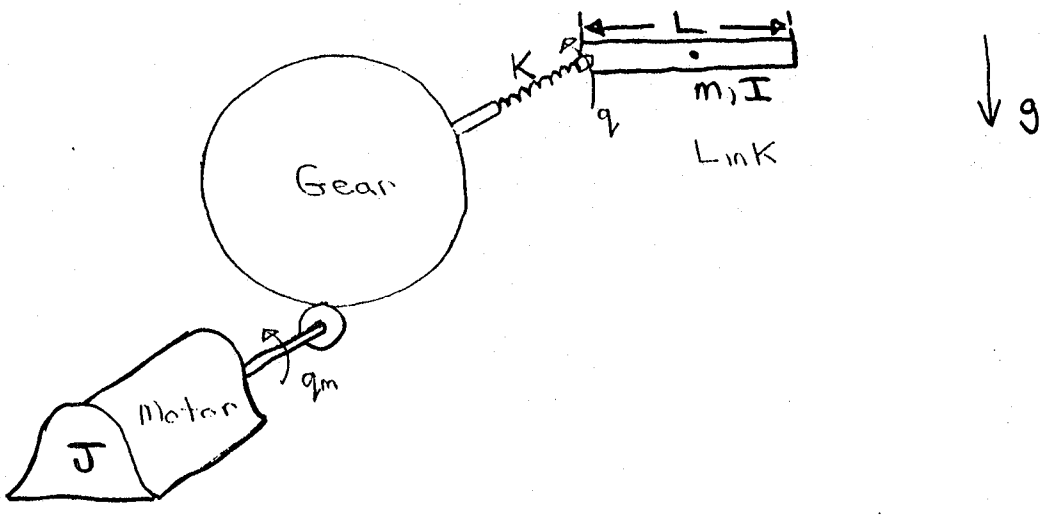

Figure 4.1 Model of Joint Flexibilities

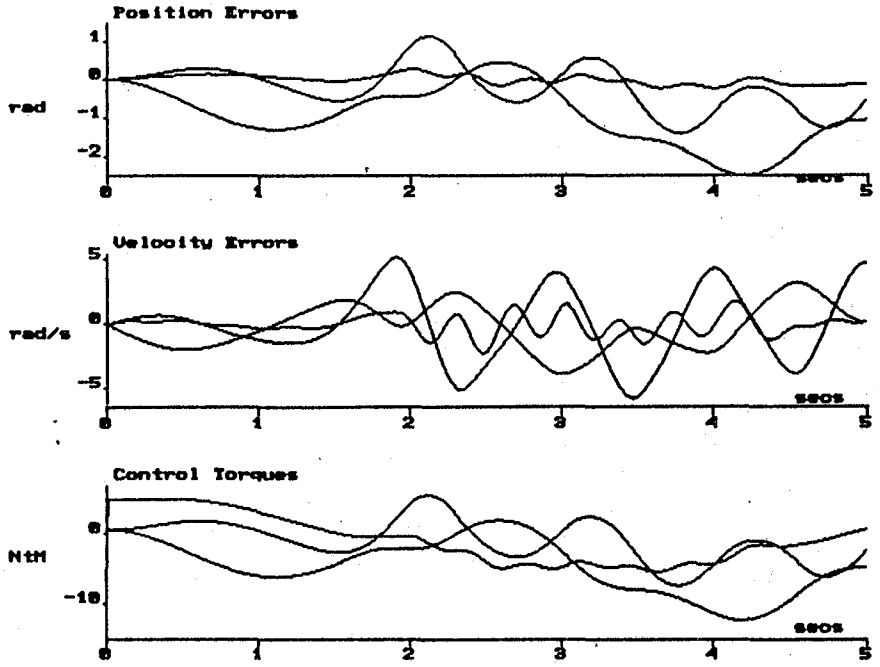

Figure 4.2 PD Motor Control Simulation

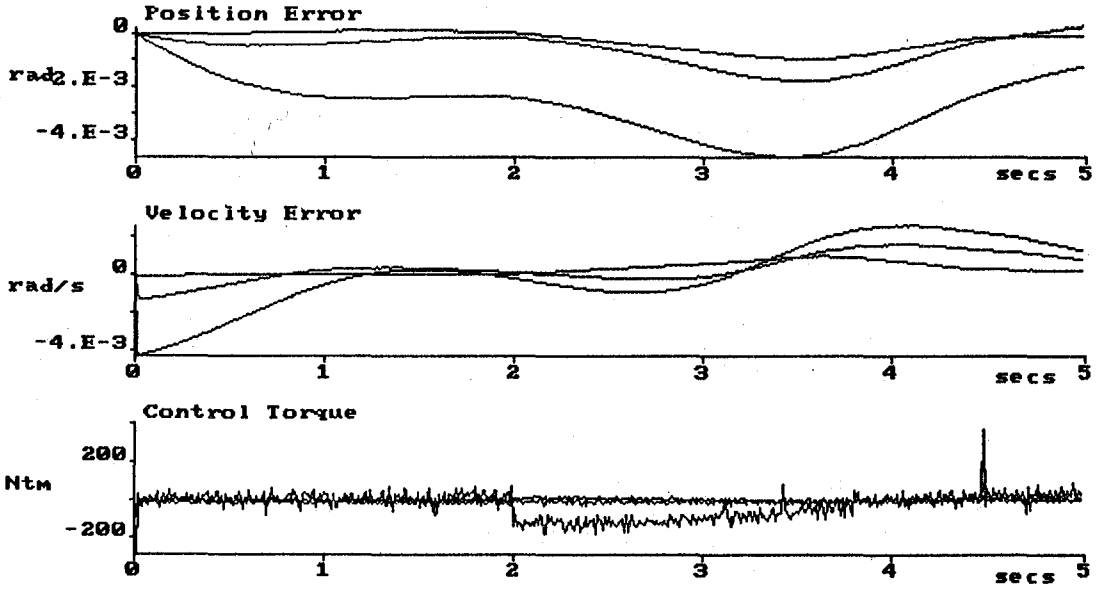

Figure 4.3 Nested PD Motor/Link Control Simulation

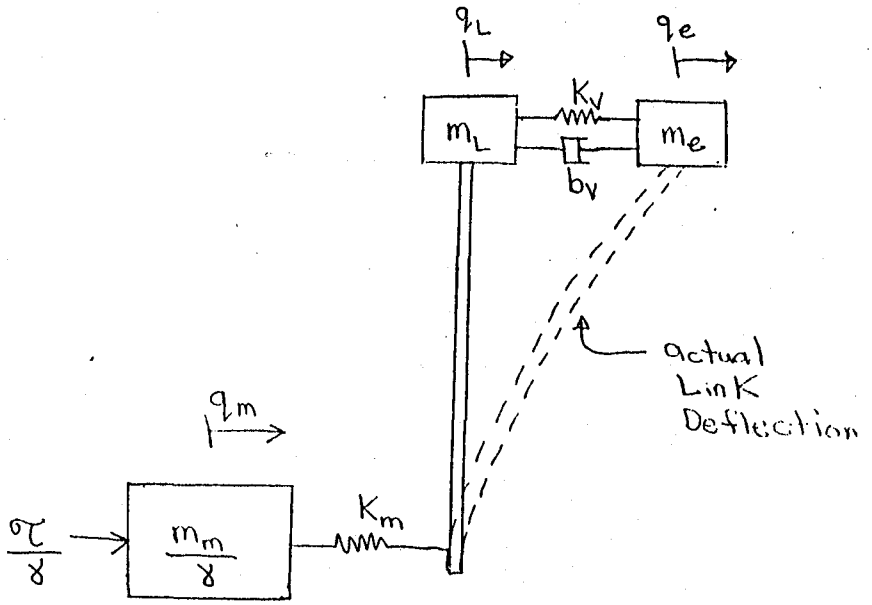

Figure 5.1 Model of Dominant Vibrations

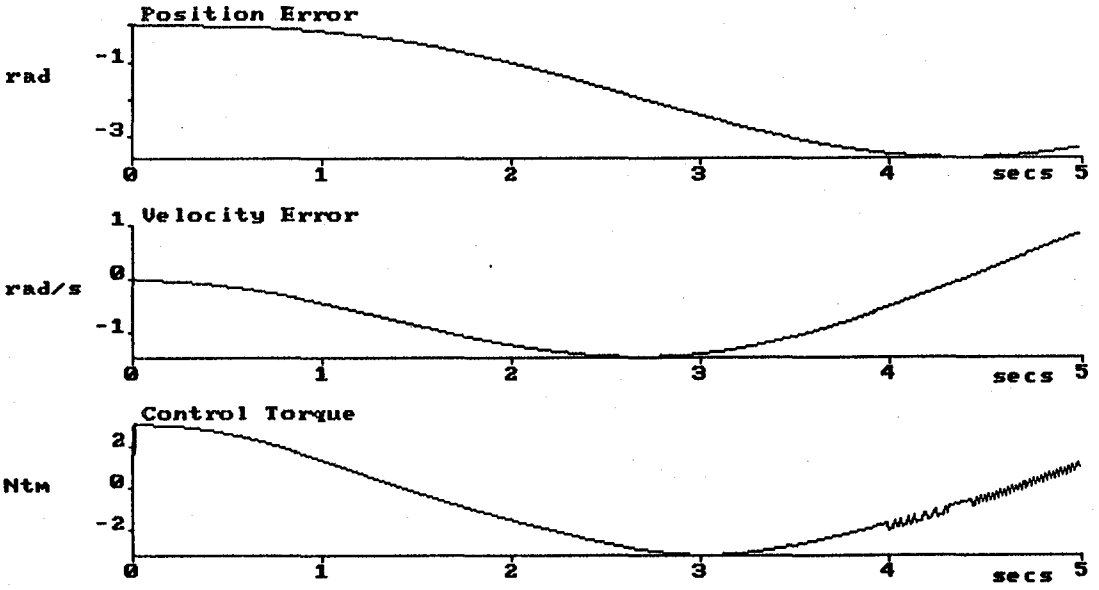

Figure 5.2 PD Motor Control Simulation

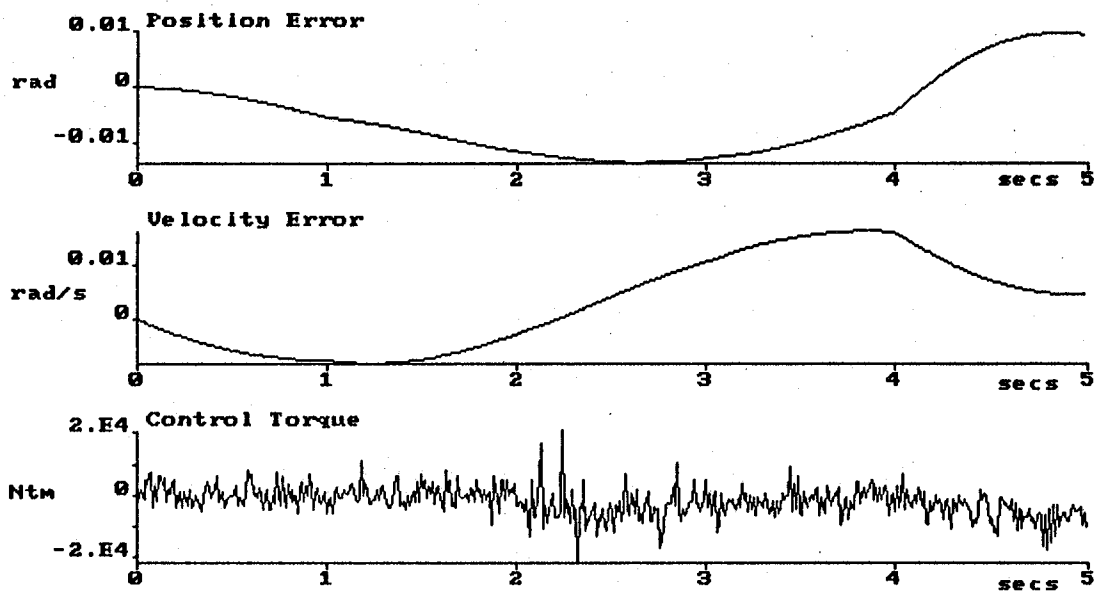

Figure 5.3 Nested PD Motor/Link/Tip Control Simulation

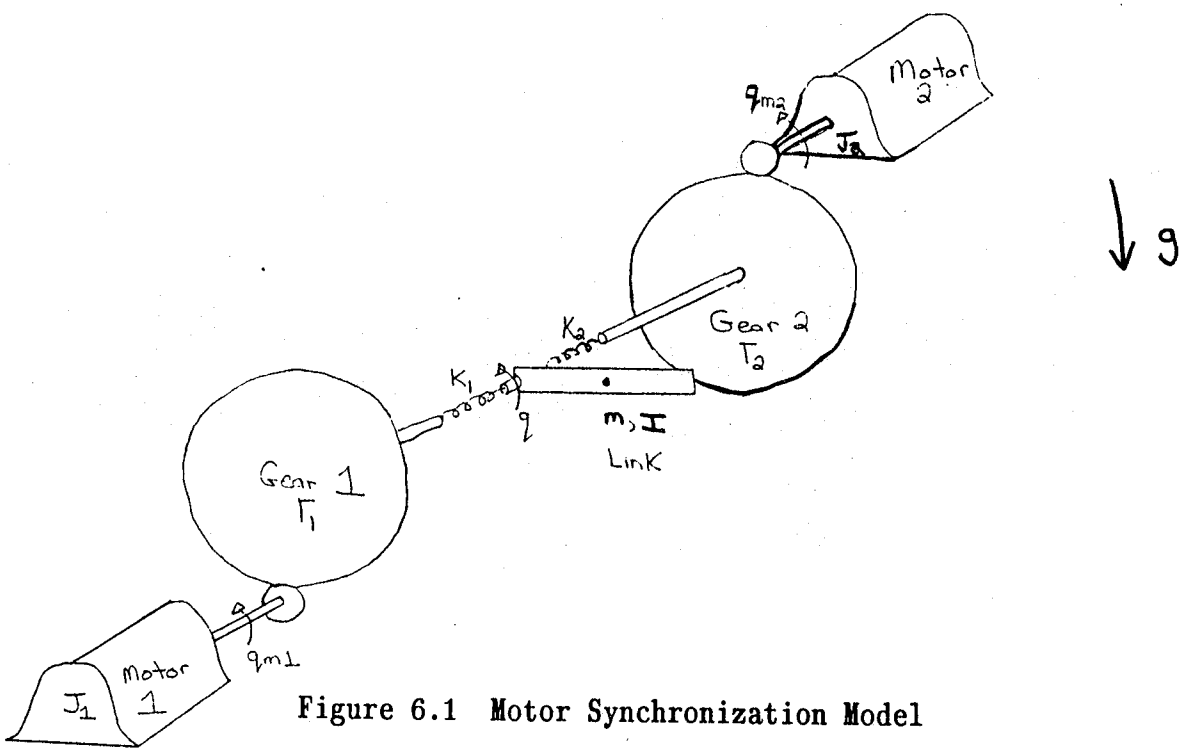

Figure 6.1 Motor Synchronization Model

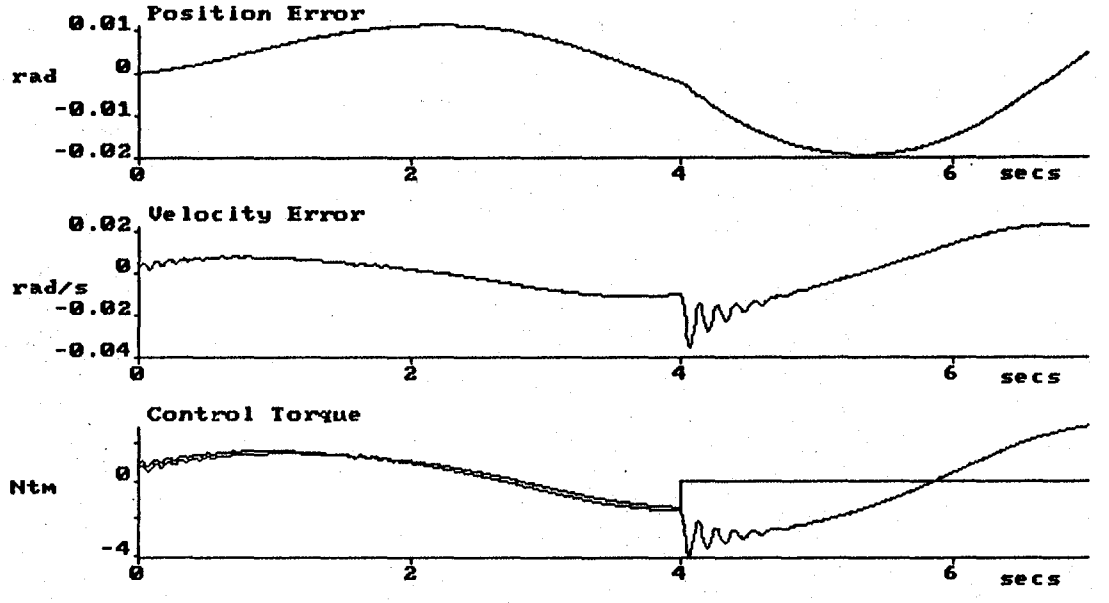

Figure 6.2 Independent Torque Control Simulation

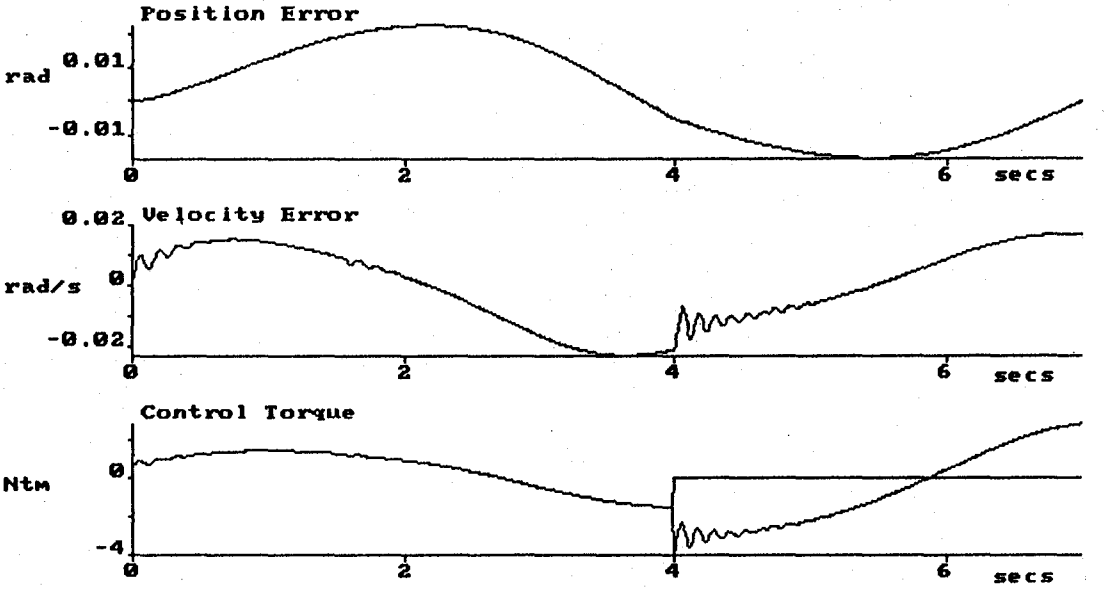

Figure 6.3 Coupled Torque Control Simulation

IX. REFERENCES

[1] M. Spong and M. Vidyasagar, Robot Dynamics and Control, New York: John Wiley and Sons, Inc., 1989.

[2] M. Spong, "Modeling and Control of Elastic Joint Robots", Journal of Dynamic Systems, Measurement, and Control, Vol. 109, Dec. 1987, pp 310-319.

[3] R. R. Craig, Jr., Structural Dynamics: An Introduction to Computer Methods, New York: John Wiley and Sons, Inc., 1981.

[4] D. Dawson, Z. Qu, F. Lewis and J. Dorsey, "Robust Control for the Tracking of Robot Motion", International Journal of Control, 1990, Vol. 52, No. 3, pp 581-595.

[5] D. Dawson, Z. Qu, and M. Bridges, "Robust Tracking of Rigid-Link Flexible-Joint Robots", Automatica, June 1991, submitted for publication.

[6] D. Dawson, Z. Qu, and S. Deepak, "Robust Tracking Control of Vibrating Robots", American Controls Conference, June 1992, in preparation.

[7] D. Dawson, Z. Qu, and M. Bridges, "Robust Sychronization of Redundantly-Driven Rigid-Link Flexible-Joint Robots", American Controls Conference, June 1992, in preparation.

[8] D. Dawson, "Simulation and Control Routines for the Automated Radiator Inspection Device", Informally submitted to KSC Robotics Group.

[9] V. Davis, "Robotic Control and Inspection Verification", KSC internal report.

1991 NASA/ASEE SUMMER FACULTY FELLOWSHIP PROGRAM

JOHN F. KENNEDY SPACE CENTER
UNIVERSITY OF CENTRAL FLORIDA

FRAME SHIFT/WARP COMPENSATION FOR THE ARID ROBOT SYSTEM

PREPARED BY:	Dr. Carl D. Latino
ACADEMIC RANK:	Associate Professor
UNIVERSITY AND DEPARTMENT:	Oklahoma State University Electrical & Computer Engineering
NASA/KSC	
DIVISION:	Mechanical Engineering
BRANCH:	Special Projects (ARID)
NASA COLLEAGUE:	Mr. V. Leon Davis
DATE:	August 9, 1991
CONTRACT NUMBER:	University of Central Florida NASA-NGT-60002 Supplement: 6

ACKNOWLEDGEMENTS

I would like to sincerely thank V. Leon Davis for the opportunity of working on the Automatic Radiator Inspection Device (ARID) project. I would like to add that his hospitality and friendship went beyond those of a supervisor and will long be remembered. I also want to acknowledge Chau Le, Todd Graham, and many other NASA and Boeing staff who have been very helpful and who helped make my stay here both productive and enjoyable.

Dr. Ramon Hosler and Kari Stiles need special mention for all their hard work which produced many well planned exciting and informative programs. I wish to applaud their genuine interest, efficency, friendliness and professionalism.

ABSTRACT

The inspection of an orbiter radiator panel is a time intensive tedious chore. The Automatic Radiator Inspection Device (ARID) is a system aimed at automating this procedure. The ARID must have the ability to aim a camera accurately at the desired inspection points which is in the order of 13000. The ideal inspection points are known. The panel may, however, be relocated due to inaccurate parking and warpage. A method of determining the mathematical description of a translated as well as warped surface by accurate measurement of only a few points on this surface is developed here.

The method developed uses a linear warp model whose effect is superimposed on the rigid body translation. Due to the angles involved, small angle approximations are possible which greatly reduces the computational complexity. Given an accurate linear warp model, all the desired translation and warp parameters can be obtained by knowledge of the ideal locations of four fiducial points and the corresponding measurements of these points on the actual radiator surface. The method uses three of the fiducials to define a plane and the fourth to define the warp. Given this information, it is possible to determine a transformation that will enable the ARID system to translate any desired inspection point on the ideal surface to its corresponding value on the actual surface.

SUMMARY

The orbiter radiators which are located on the inner surfaces of the payload doors need to be inspected for damage just before and just after each flight. This is a very time consuming, tedious and boring task which makes it an ideal application for a robot system. The Automatic Radiator Inspection Device (ARID) is a robot system being developed by NASA to address this problem. The device is a computer controlled four degree of freedom robot with a camera. It is designed to greatly reduce the inspection time and manpower needed. In addition it will improve the accuracy of data collection and processing.

To be effective, the robot must be capable of accurately positioning the camera relative to desired inspection points on the radiator panel. The system is to operate open loop, so it is essential that it knows precisely the positioning and orientation of the panel being inspected. Although the ideal position is known, the orbiter will not always be parked the same way and the door panel may not be open the same amount. Even though they are mechanically constrained, the doors may be warped. It was therefore essential to develop a method to deal with this problem.

The main objectives of this project were to evaluate methods under consideration and, if necessary, develop one capable of meeting the rigid constraints. To meet these constraints, it seemed necessary to develop an accurate warp model. Without a valid warp model it seems impractical to operate the system open loop. Warp was measured to be in the order of 2 inches over a 15 foot run. The warp needed to be mathematically descrivable. A first order warp approximation was assumed. Assuming that this model is true, it is possible to know the orientation and warpage of any panel by simply measuring four points whose ideal positions are known and their position independently verified (these points are called fiducials).

If a higher order warp modeling is needed, the procedure works, but requires that at least n+1 fiducial points be measured. A positive verification of the order needed for an acceptable model requires that more data be collected and evaluated. The data collected so far seems to indicate that a linear warp model will suffice to meet the requirements. If the warp is actuallu random the system may not be able to be operated in open loop.

TABLE OF CONTENTS

LIST OF ILLUSTRATIONS

I. INTRODUCTION

The Automatic Radiator Inspection Device (ARID) is a robot system that will be used in the inspection of the orbiter radiator panels for mission damage and for pre flight inspection. The data collected is to be stored so that comparisons between present and prevous data can be made for damage assessment. For inspection purposes each panel is subdivided into a tiling of four inch square sections. The center of these squares defines an inspection point. These points are known in some xyz coordinate system, but there are no visual clues of these on the panel surfaces.

The robot will have within its memory the ideal xyz coordinates of all the desired inspection points but no means of feedback to verify these during normal operation. The ideal position of each inspection point is known to the robot but the actual xyz coordinate of the point on the actual surface must be determined. The robot will move a camera that is to take photographs of the entire radiator surface by taking a series of 4 in. by 4 in. pictures. The center of each of these pictures is an inspection point. The data obtained at these points may then be compared to data obtained from previous inspections. In this way any new damage wether it be from flight or handling can be determined.

In order to make a proper assessment, the position and orientation of each inspection point must be known accurately. If the orbiter is parked with a different attitude and the doors are open different amounts at each inspection accurate comparisons cannot be made without complex image processing capabilities. The difference in parking attitude, door opening angle and warpage in the doors needs to be known precisely so that the robot can locate the intended inspection points accurately in order to position the camera at the proper focal distance.

To this end a method was needed which would provide the necessary information to the ARID system so that it could make the proper adjustments to compensate for inaccurate parking. Rigid body translation, also known as frame shift is a well known way of handling such a problem. The ideal as well as actual positions of points whose coordinates are known and whose position can be separately verified (these will be referred to as the fiducial points)

must be provided to the ARID system. If the panel is rigid, three points whose ideal and their corresponding measured points are known, suffice to accurately determine all six values of rotation and tranlation. It was found, however, that the panels could not be assumed rigid. In an effort to solve this problem a variety of methods and models were being considered.

There was one that was already being developed by Boeing. Part of the task was to evaluate the merits and accuracy of the method under consideration as well as develop a better one if needed. It should be noted that there are only twelve fiducial points on each of the four aft panels and only eight on the four fore panels. Any solution to this problem while maintaining the open loop option could only rely on these and no other points on the panels.

II. THE ARID SYSTEM

2.1 THE RADIATOR PANELS

The orbiter payload bay is enclosed by eight doors arranged in four groups of two. The inner side of these doors have radiator panels used to cool the on board electronics. Each panel is a smooth surface with eight bolts for each of the forward doors and twelve bolts for each of the aft doors (See Figure 2-1.). These are the only clearly distinguishing marks on the otherwise smooth surface of the radiators. These points will be referred to as fiducials.

Each radiator is inspected by the robot in 4 in. by 4 in. squares. This translates into over 1600 inspection points per panel or almost 13000 total points. It is therefore clear that visual feedback would be quite difficult as well as computationally taxing on the system. The doors were designed to operate in space at zero g's, therefore in the one g environment on earth they are supported by a structure called the strongback. These supports make the door more rigid but may at the same time introduce some unexpected warp.

The radiator panels have some complex curves to conform with the orbiter shape. The two forward panels have the most difficult curves for ARID to negotiate, but even the aft six doors require the use of a multidegree of freedom robot for proper camera placement and orientation. The panels are hinged to the orbiter and at this edge are quite straight. At other points a noticeable warp was detected. For a 15 foot door panel, with three corners properly located, the fourth was found to differ in placement by as much as 2 inches.

Restrictions on focal distance of the camera state that the distance from the panel surface must be 24 inches with a plus or minus 0.125 inches. Although a 2 inch warp on a 15 foot run may be considered small, it is sixteen times too large for the ARID system to tolerate.

2.2 THE ARID ROBOT

The ARID robot, see Figure 2-2, is a four degree of freedom device. It has one prismatic and three revolute joints. this robot will be mounted in the Orbiter Processing Facility (OPF) on a track parallel to the longitudinal axis of the orbiter. Ideally, the robot will use its revolute joints to position and aim the camera at the panel,

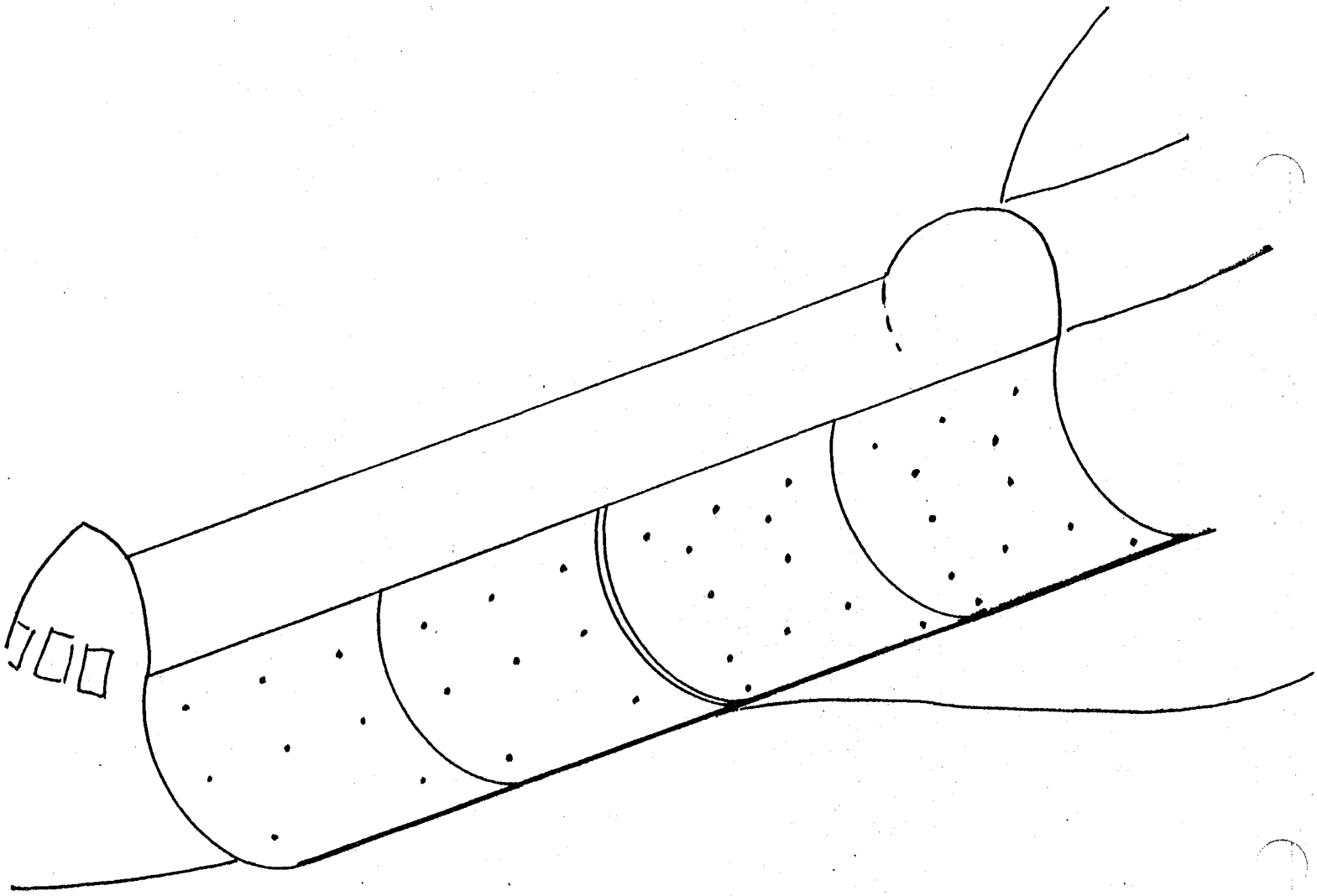

Figure 2-1 Fiducial Points on the Radiator Panels

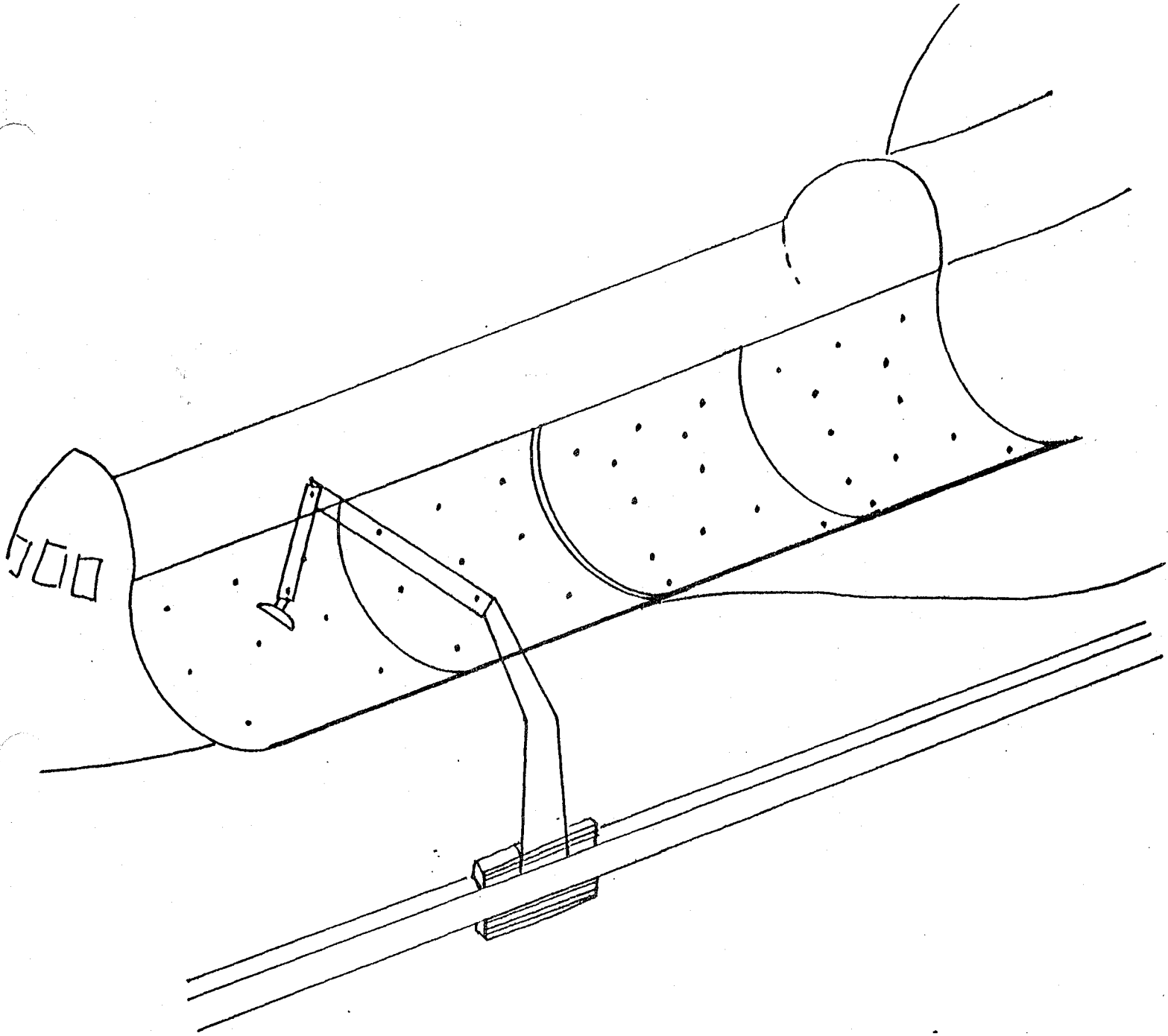

Figure 2-2 The ARID Robot With Radiator Panels

perpendicular to the surface, near one end of the track. It will then use the prismatic joint to move in a path parallel to a long series of inspection points and photograph them. At the end of one such inspection, at the end of the track, the revolute joints adjust to reposition the camera to the next inspection row. The robot then reverses didrection and repeats the procedure in the opposite direction.

It is in fact not possible to do this since the orbiter may be parked in a slightly different attitude every time. To make things even worse, the panels may be warped. The robot must be able to compensate for these and guide the camera accurately therefore must articulate the revolute joints as well as the prismatic one. Compensation can be accomplished if the panel shape can be effectively reported to the robot without the need to identify every inspection point. It is therefore necessary to be able to mathematically define the position of the fiducial points on the panel under test as well as their ideal locations.

With this information the robot would have to be able to generate a transfer function. This function would enable the robot to find the actual location of each inspection point given its ideal location. Since there are only a limited number of fiducial points, any method which is to be viable for an open loop solution, must do it reliably with these. If the order of the model exceeds the minimum number of fiducials needed, another method or a closed loop solution must be found.

III. THE FRAME SHIFT/WARP COMPENSATION PROBLEM

3.1 METHOD TO BE EVALUATED

Boeing was working on the frame shift/warp compensation problem and identified a method which showed promise. The method utilized two coordinate systems to identify the inspection points in redundant fashion. The method is described in greater detail in Appendix A.

IThe method employs the use of two coordinate systems each having a complete set of inspection points defined relative to its coordinate axes. It then generates two vectors, from the robot origin to the origins of the two coordinate axes. The relative orientations of the coordinate systems and the robot origin can and must be determined. The vector used for inspection is composed of the average of the two different vectors, from the robot origin, used to identify the inspection point.

In an unwarped system, the average vector will point to the exact inspection point since both vectors identify the point exactly. In a warped system it is hoped that the average, or weighted average of the vectors, gives a close approximation of the exact inspection point. The method requires the selection of four fiducial points (points whose coordinate positions can be verified) located in a rectangular layout on the radiator surface. Two dimetrically opposed points will be used as the origins of the two coordinate systems.

Each of the coordinate systems is defined by a vector from the origin to one of the adjacent points and another vector, also beginning at the origin, perpendicular to the first and pointing in the direction of the other adjacent point. The third coordinate is defined by the cross product of the two vectors. Each of these two coordinate systems must relate to the robot origin. Handling this step, especially in view of the fact that it must be done twice for every inspection point, will require a considerable amount of computing.

Every inspection point in the unwarped surface is known in terms of the two coordinate systems. It is therefore necessary to store two different values for each inspection point. The two different

vectors needed to define each inspection point must be known to the robot. When the surface is warped, two new vectors from the robot origin to the origins of the two coordinate systems must be known. The inspection point location is approximated by using the average of the two different vectors defining the point through the two coordinate systems. The procedure was being evaluated by considering it as it applied to the actual radiator panel. This approach proved too cumbersome to give any useful results.

To evaluate and determine if the method is viable a simple method that gave absolute results was needed. As part of the project we were asked to develop a way of verifying or rejecting the method. The method was evaluated for a simplified surface (see Appendix A) and was found to have errors as large as half the maximum induced warp. That is to say that if one corner of a linearly warped panel is displaced from ideal by some value W it is possible to have errors as great as W/2. Since it is essential to keep absolute error to less than 0.125 inches, W could not be allowed to exceed 0.25 inches.

Empirical measurements show that W is in fact in the order of inches. There is no reason to assume that the method is more applicable to curved surfaces, it was, therefore, concluded that a more accurate method was needed.

3.2 CURVE FITTING

If two non coincident points are on the xy plane, a unique line $y=mx + b$ can be drawn through them. For three points in the xy plane, a continuous function $y = ax^2 + bx + c$ can be found to exactly go through these points (assuming every x has only one y value). It is well know that in general, an n^{th} order function can be uniquely found for any n+1 points.

It therefore may seem reasonable to sample all the fiducials and use the displacements of each from its ideal position to find the warp of the radiator surface. It also may seem reasonable to sample more points in order to get a "better model". This, however, is not so. The sampling of many points is useful in verifying a model. A model may be developed from the statistics obtained from the sampling of a very large number of points. When only a small number of points is available, it is essential to know what kind of warping the panel may undergo. If warp is truly linear, sampling more than two points

and computing their displacement from ideal should result in a linear progression of error values.

If the ideal xyz locations of three colinear points is known and the actual positions are measured there may be some error in all the readings. A best fit line may be drawn using these points to help minimize this error. If frame shift was already taken into account, and measurements are accurate, the only discrepancy is due to warp. Warp can be measured by aligning one of the ideal end points with the corresponding measured point. All the other points must then be translated by the same vector. This results in an error vector of zero length for one point. Finding the error vector for the other points should result in a monotonically increasing error function as the measurements are taken farther from the first point.

If the points are equally spaced, the error vector should have approximate lengths l, 2*l, 3*l etc. If the plotting of the vector length versus distance is not a straight line it will be necessary to decide how to proceed. If a linear model is valid, a straight line best fit should be used. Trying to use all the points and fitting a curve to them will result in the problem of oversampling. Oversampling is the condition where a curve is assumed higher order than it actually is. The order of the curve should not be based solely on the samples taken. If a line is expected, when points are read with a certain degree of error, then fitting a straight line in conjunction with these points is the way to proceed. Fitting a second order curve to fit these points will not accurately depict what is actually occurring even if the curve seems to fit better.

It must be stressed that the model should dictate the order of the polynomial and not the number of points being considered. If more points are collected the negative effects of noisy readings will be filtered out when some method of curve fitting is applied. It should therefore be stressed that if the method used bases all the calculations on only four fiducials, these must be read as accurately as possible. Additional points may be read to reduce the effects of noisy readings but the order of the curve must be kept fixed. In order to have confidence in the model selected, data must be taken on orbiter panels (or accurate mock-ups) and based on these data, select a suitable model.

Some examples are illustrated in Figure 3-1. The first case shows two points. There is only one way of drawing a line through these.

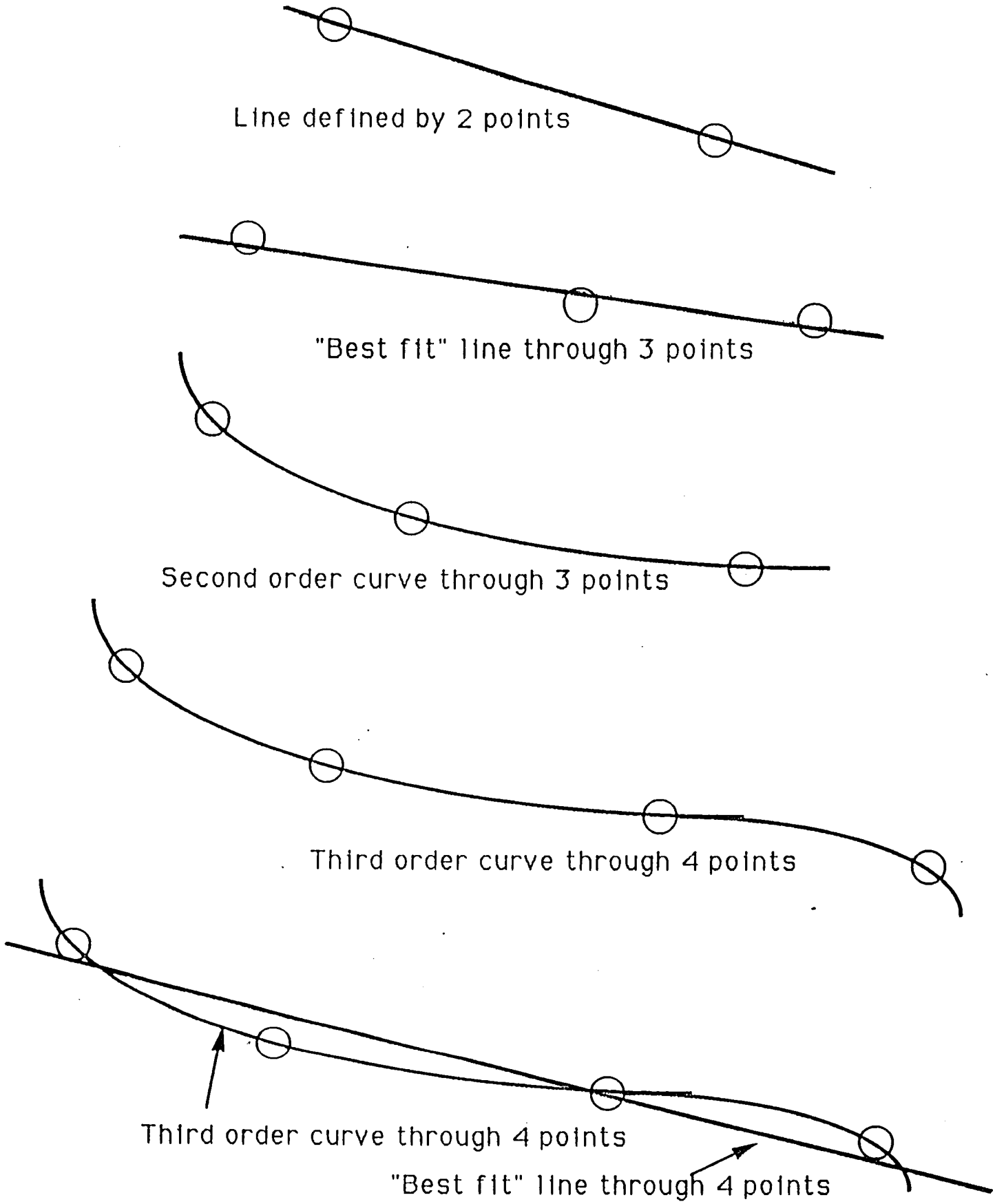

Figure 3-1 Curve Fitting Examples

the second and third show three points each. If it is known that the actual curve is a line, a best fit must be tried. If, however, the points are known to be exact, the curve must be of at least second order. The bottom two illustrate how with four points, a third order curve can be determined, for second or first order, some curve fitting is necessary.

3.3 METHOD DEVELOPED

Before and after each mission, the orbiter will be parked and inspected. The orbiter may be rotated and translated about three axes, the doors might be open at different angles and be warped as well. The rotation, translation and warp are relatively small in terms of radiator dimensions, but unacceptably large for accurate robotic inspection especially when the system is to operate in open loop. Several methods were considered for solving the warping problem including a variety of curve fitting approaches. All methods that were tried had a variety of shortcomings therefore it was decided to develop a totally new method.

The ARID system knows the ideal xyz coordinates of each inspection point. The actual inspection point is at some location x'y'z'. To inspect this point, it must be given information about the orbiter orientation and panel warp. It is desired to have an effective, accurate way of performing the proper conversion from an ideal inspection point to the actual orbiter surface. The radiators are effectively straight and rigid along the hinge line. If the edge farthest from the hinges is also found to be straight, the linear warp model seems reasonable.

If warp can be modeled, then it is possible to obtain the exact mathematical equations that govern the effects of translation, rotation and warp. By assuming that superposition holds and that warp is linear, it is possible to consider warp and translation separately then combine their effects. Translation includes rotation about the three axes. The problem is thus greatly simplified by separately considering the rigid body rotation, translation then the effects of warp. Without warp, knowing the ideal as well as displaced coordinates of three fiducials, displacements and angular rotations can be determined. This is true since it is simply the displacement of a rigid body in space.

By using only three points to determine a surface, noise in the readings could cause problems. To avoid this, it may be desirable to measure various points and use a curve fitting tecnique to make a best fit. Answers to these questions are, however, not within the scope of this report. It will be assumed that the fiducials are precisely located, are read accurately, and the linear warp model accurately defines the surface in question. The measured angles of

rotation were found to be less than one degree around any axis. Based on empirical data, warp of the doors is of the order of 2 inches for a linear distance of 15 feet. This is a small angle and permits the use of several approximations which greatly reduces necessary computations.

As an example, a system of four points will be used to illustrate the linear warp model method, see Figure 3-2. The points are considered to be at the corners of a rectangle, and reside on the xz plane. These simplifications make the method easier to understand and do not invalidate the fact that it works with some restrictions in a non coplanar point system.

Computer programs were written to evaluate the effectiveness of the procedure. A computer program was written in C++ to take a point in an xyz coordinate system, rotate and translate it. This and other programs were used as tools to make qualitative and quantitative measurements on the effects of small angle approximations on the error. It was found that first order approximations were accurate to much less than 1% error for values being considered. This allowed for many simplification to be used while keeping the results very accurate.

Theoretically, if the shape of the orbiter door is known, an accurate model for warpage is known and information about four of the ideal and actual fiducial points is known, the rotation translation and warpage can be obtained. For simplicity of explanation of the procedure, warpage has been assumed linear. Higher order warp can be handled in similar fashion, but will not be discussed here since the need has not been shown. The method will, however, be equally valid for more complex warp models provided that they are accurate representations of reality, there are a sufficent number of fiducials and superposition holds. This assumption is valid if the warp can be linearly superimposed on a surface of any shape.

This is not exactly correct, however, it is very close and well within our acceptable tolerances. Linear warp will be considered throughout this report unless it is otherwise stated.

EXAMPLE: Refer to Figure 3-2. Consider a rectangle in the xz plane. If the corner farthest from the origin is lifted in the z direction by a small amount, and if linearity is asssumed, the vertical displacement of any point on the surface may be calculated. The

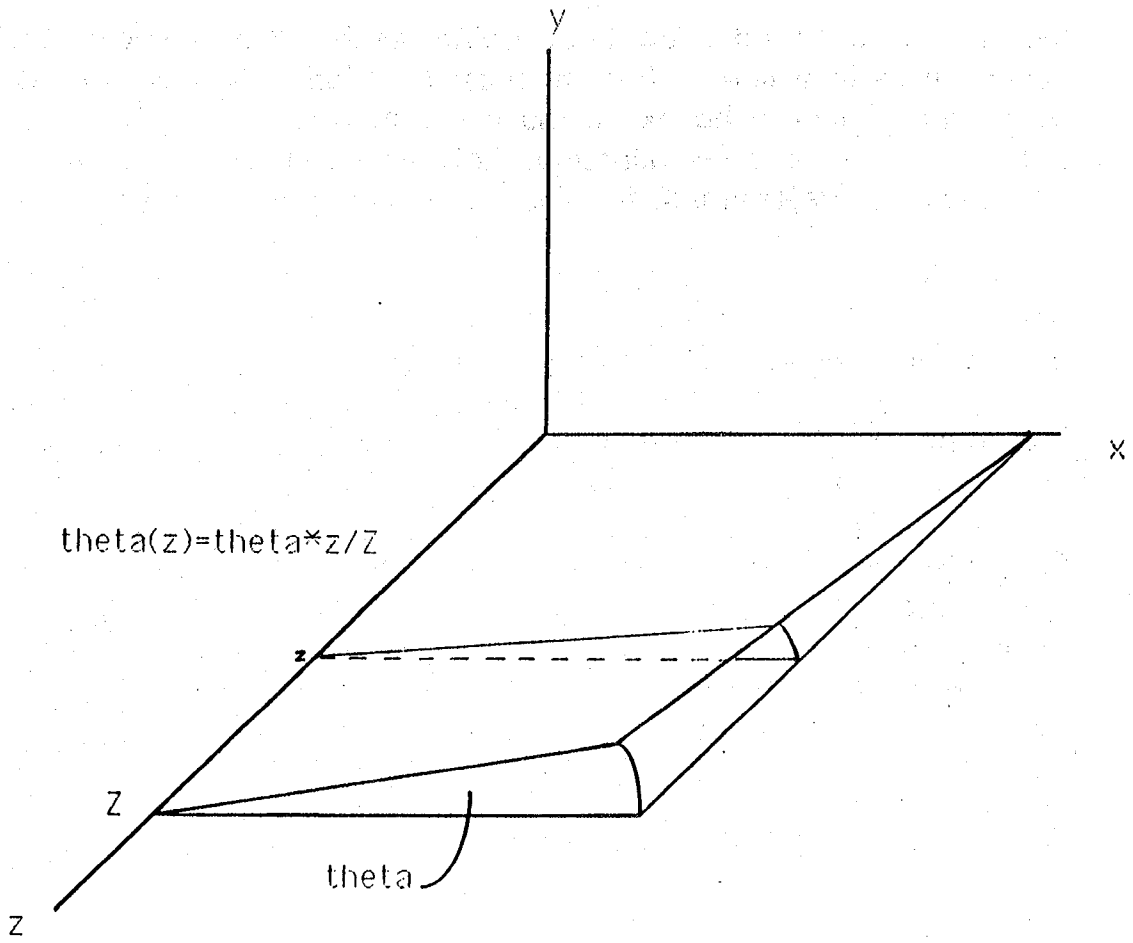

Figure 3-2 Planar Surface With Linear Warp

angle of any line formed by the intersection of the surface and a plane parallel to the xy plane is also easily determined. Assuming the four points in the xyz coordinate system are: (0,0,0), (X,0,0), (X,Y,0), and (0,Y,0). For this example the points are all coplanar.

Warping may be modeled by the lifting of one of the corners in the positive z direction, say delta z. Appllying it at the (X,Y,0) corner, moves the point to (X,Y,delta z). Actually if a corner is lifted the effected sides actually rotate, however, since the rotation is so slight, typically less than one degree, it may be modeled as a linear translation perpendicular to the xz plane. Given the linear warp assumption, the vertical displacement at any point (x,y) is:

$Z(x,y) = (x/X)*(y/Y)*(\text{delta } z)$

Therefore given four points allows the calculation of the vertical displacement at any point

3.4 LINEAR WARP

The assumptions are that with this warp, all planes parallel to the xz planes that intersect the warped surface are straight lines. The same is true for planes parallel to the yz plane. To define the warped surface it suffices to define the plane and the displacement at one corner. For the previous example three points are on the xz plane. The fourth corner is lifted by some value delta z.hat is if three points define the plane, finding how high above the plane the fourth point is defines the warp.

Given the same linear warp assumptions on any curved surface the same principle may be applied. Three of the fiducial points are used for defining a plane, then the height above (or below) the plane is established for the unwarped surface. With warp, the same plane is defined and the new displacement is obtained. The difference in the two numbers in conjunction with distance between the "warped" point and the fiducial is the warp.

The intersection of a plane perpendicular to the defined plane and parallel to one of the vectors (see Fig. 3-3) shows that the intersection of the surface is an undistorted curve that is rotated. Since warp is considred linear, the "angle of warp" is approximated by the inverse tangent of the warp divided by the linear dimension (call this theta). With this assumption, the angle of rotation of the

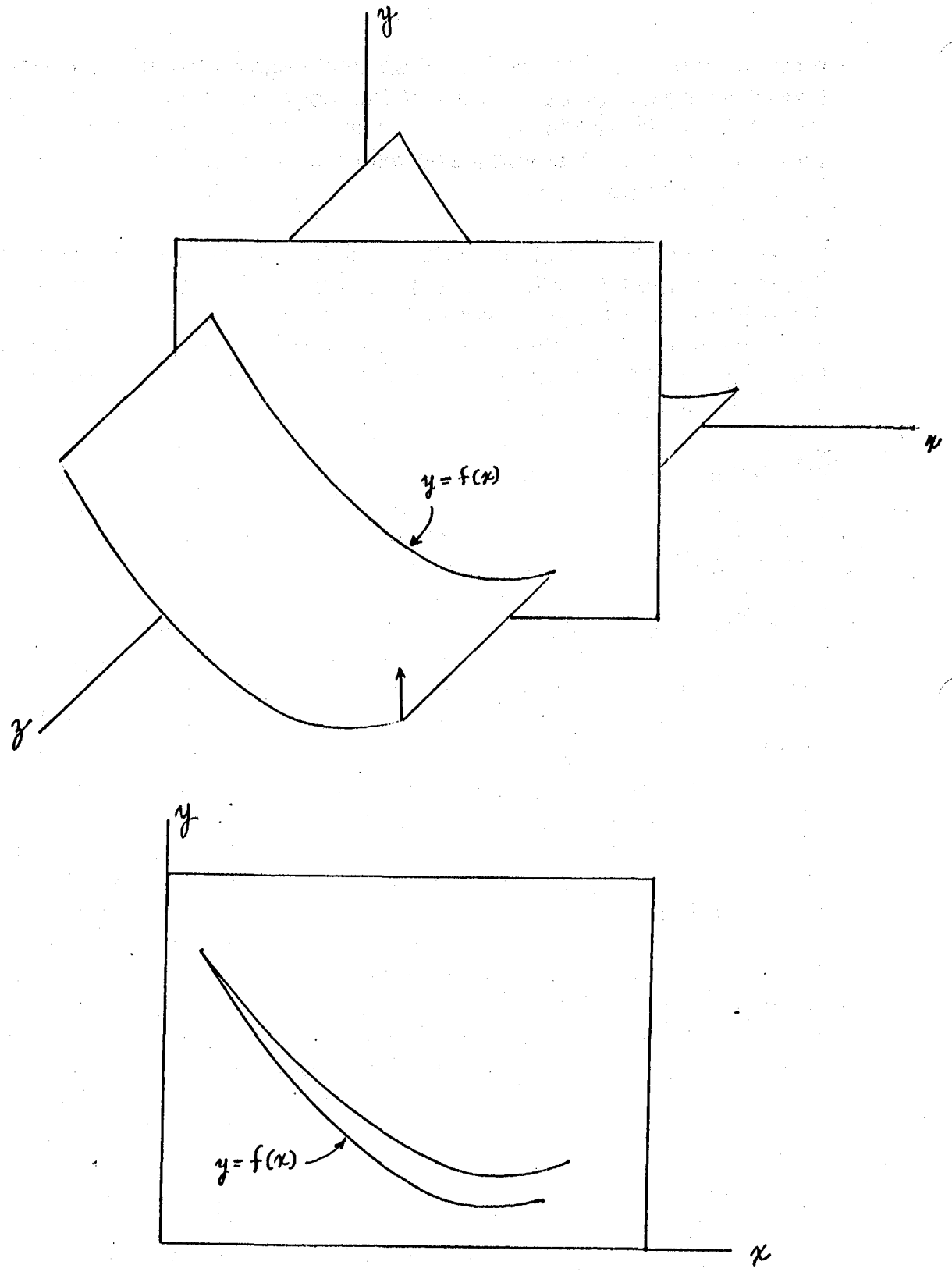

Figure 3-3 Warping With No Distortion

curve in question is theta at one extreme, 0 at the other and theta*x/X in between.

It should be stressed that as long as linear warp is assumed any shape surface can be handled this way with minimal amout of math necessary for the location of the inspection points. If linear warp cannot be assumed, a model must be selected that accurately defines the warping. This could be a second, third or some higher order system. the priciple should still hold.

3.5 COORDINATE TRANSFORMATION

When considering different coordinates to identify a given point in space it is often essential to convert between the two systems. Although most texts dealing with introductory robotics topics cover this in detail, a brief description is included here for convenience.

Given a point described in a rectangular coordinate system, the point may be displaced along the three axes or rotated about them. The order that these operations are performed matters, as well as to know relative to which system the operations are being performed. Given a general point P in space xyz, translating this point by some vector v then rotating the new point by some angles thetax, thetay and thetaz about the thee coordinate axes in turn, becomes a new point P'. To return to the original point, P' must first be rotated by minus thetaz, minus thetay, minus thetax, then translated by minus v in that order. For very small angles and an approximate solution, the order of angular rotations is unimportant.

To translate any arbitrary point Pi = (x, y, z) by an arbitrary vector v = ai + bj + ck results in a new point Pi' = (x+a, y+b, z+c).
Let $Vi = [x\ y\ z]^T$ be the vectorial representation of point Pi
Rotating Pi about the x axis by angle a is accomplished by multiplying Vi by Rot(x,a)
Where

$$Rot(x,a) = \begin{bmatrix} 1 & 0 & 0 \\ 0 & \text{Cos } a & \text{-Sin } a \\ 0 & \text{Sin } a & \text{Cos } a \end{bmatrix}$$

Similarly

$$Rot(y,a) = \begin{bmatrix} \text{Cos } a & 0 & \text{Sin } a \\ 0 & 1 & 0 \\ \text{-Sin } a & 0 & \text{Cos } a \end{bmatrix}$$

$$\text{Rot}(z,a) = \begin{bmatrix} \text{Cos a} & \text{-Sin a} & 0 \\ \text{Sin a} & \text{Cos a} & 0 \\ 0 & 0 & 1 \end{bmatrix}$$

By using these matrices it is possible to move any arbitrary point Pi, represented by vector Vi, by two distinct rotations so that the vector will point in any desired direction. Figure 3-4 depicts an arbitrary vector in space with convention of positive angle rotations. Similarly three rotations about the three axes can align any arbitary plane into one parallel to any desired orientation. Figure 3-5 illustrates how a rectangle in the xy plane can be rotated into any arbitrary orientation. Reversing the steps can take a rectangle, with one corner at the origin, and rotate it into any desired plane.

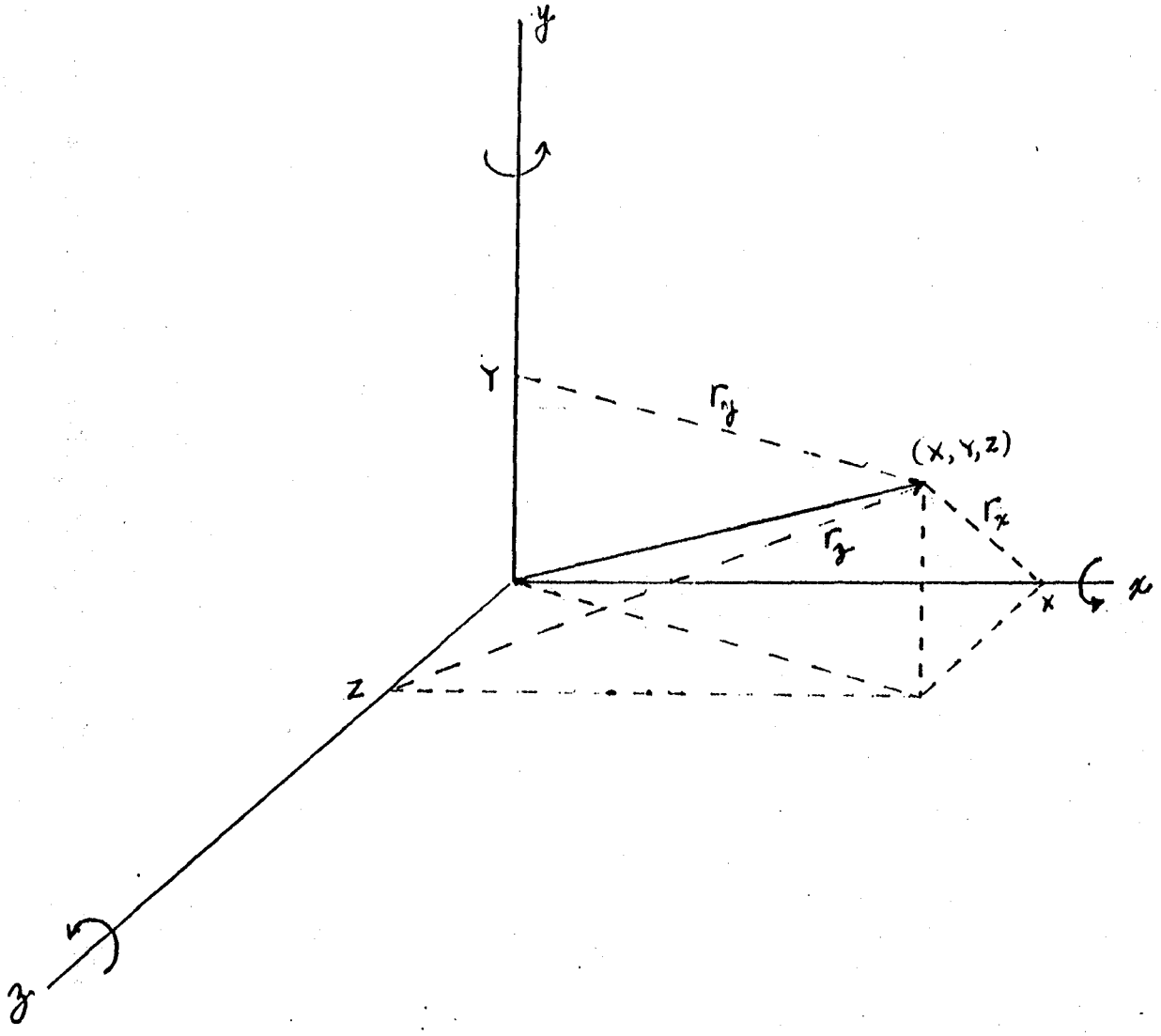

Figure 3-4 Vector In 3 Space With Positive Angular Rotation

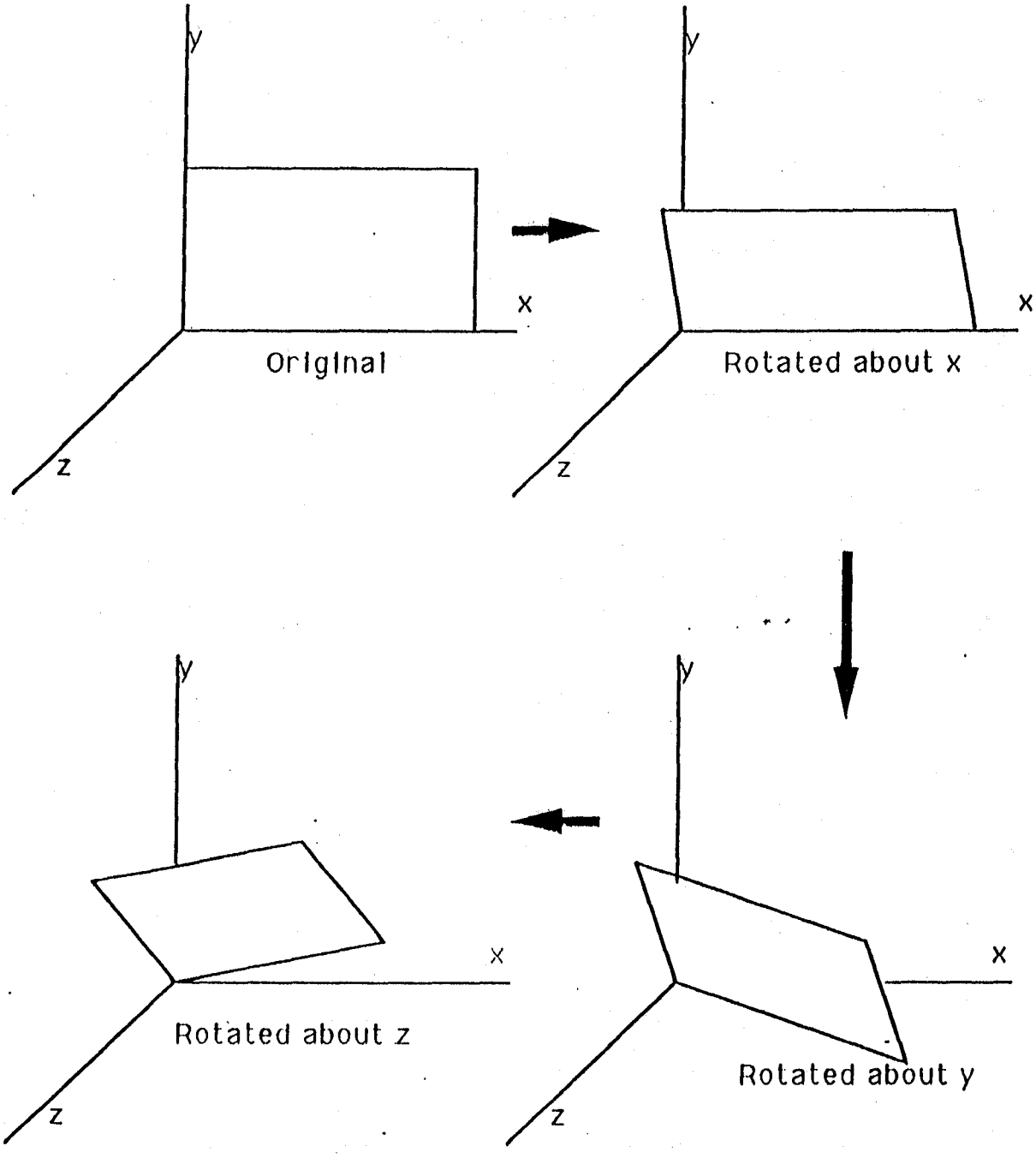

Figure 3-5 Rotation of a Surface In Space

IV. CONCLUSIONS

It was the purpose of this study to evaluate a method which was under consideration for use in compensating for rotation, translation and warp. The findings were that the method could not satisfy the stringent requirements. It therefore was necessary to develop a more reliable, accurate method.

Given information about the position and warp of the radiator panels, the ARID system would be able to make adjustments for inexact parking attitude, door opening angle and warpage. This information was to be used to allow the ARID system to compensate for these inaccuracies and to locate the desired inspection points. The method described in the report proved to be easy to implement and accurate to within a fraction of a degree and small fraction of an inch. The procedure is based on a linear warp model.

The method is also applicable to higher order warp. The procedure needs accurate measurements of only four fiducial points and knowledge of their ideal placement for the linear warp model. It is possible to simplify the complex trigonometry needed to solve this problem by the fact that the actual rotation angles and warpage are small. The small angle approximations were evaluated for the expected angles. It was found that small angle approximations could often be used. This replaces the computing of trigonometric functions with simple numbers. This will greatly reduce the computational demands on the computer.

The measurement of the four fiducial points is sufficient data to allow the method to compute the displacement in the three axes, the rotations about the three axes and the amount of linear warp. When the ARID system needs to inspect a point whose coordinates are in its memory it must be able to make the adjustments from ideal to actual. The inspection point is read from memory then compensated for the warp, rotation and translation. The ARID system then has the exact location of the desired inspection point. It should be mentioned that the application of this procedure with the ARID system may require some changes in the radiator panels alignment procedure.

APPENDIX A

THE BOEING FRAME SHIFT/WARP COMPENSATION METHOD

The procedure devised by Boeing, was intended to automatically deal with both the problem of frame shift and warp at the same time. The method will be described in conjunction with Figure A-1. Given the ARID system has its origin at x,y,z = 0,0,0. In this system there are four Fiducial points labeled F1, F2, F3 and F4. No three of these points may be colinear.

Two coordinate systems are constructed at dimetrically opposed fiducials, i.e. F1 and F3. The origin of the u1,u2,u3 coordinate system is at F1. u1 is defined as the unit vector pointing from F1 to F2. u2 is defined as the unit vector perpendicular to u1 in the plane defined by u1 and fiducial F4. u2 is arbitrarily selected to point in the general direction of F4. u3 is defined as the cross product of u1 and u2 using the right hand rule. v1, v2 and v3 are similarly defined using fiducials F3, F2 and F4. Every inspection point Pi is defined in the two coordinate systems. Pi is vector u when seen from u1, u2, u3, and v if seen from the v1, v2, v3 coordinate system. When the surface is displaced, rotated and warped every point Pi becomes some Pi'.

To find this point, the ARID system must, based on the new fiducial points F1', F2' F3' and F4', construct the new u and v coordinate systems. Since all fiducials are known to ARID, the origins of the two coordinate systems is known. Using the old (pre warp) values for vector u, within the new coordinate system some point in space is identified. This does not coincide with Pi' because of warp. Repeating the process, this time with vector v again fails to locate Pi'. It was hoped that the average or weighted average of these two vectors would be close to the true value of Pi'. The evaluation of the procedure was done by applying it to a rectangualr planar surface like that in Figure 3-2 and determine what error values resulted.

Applying a linear warp approximation to a rectangular surface with one corner lifted by some small value W resulted in errors of magnitude W/2. Since it is known that W may be in the order of inches while tolerances are in the order of 0.125 inches the method was discarded. It was also concluded that attempts to weight the

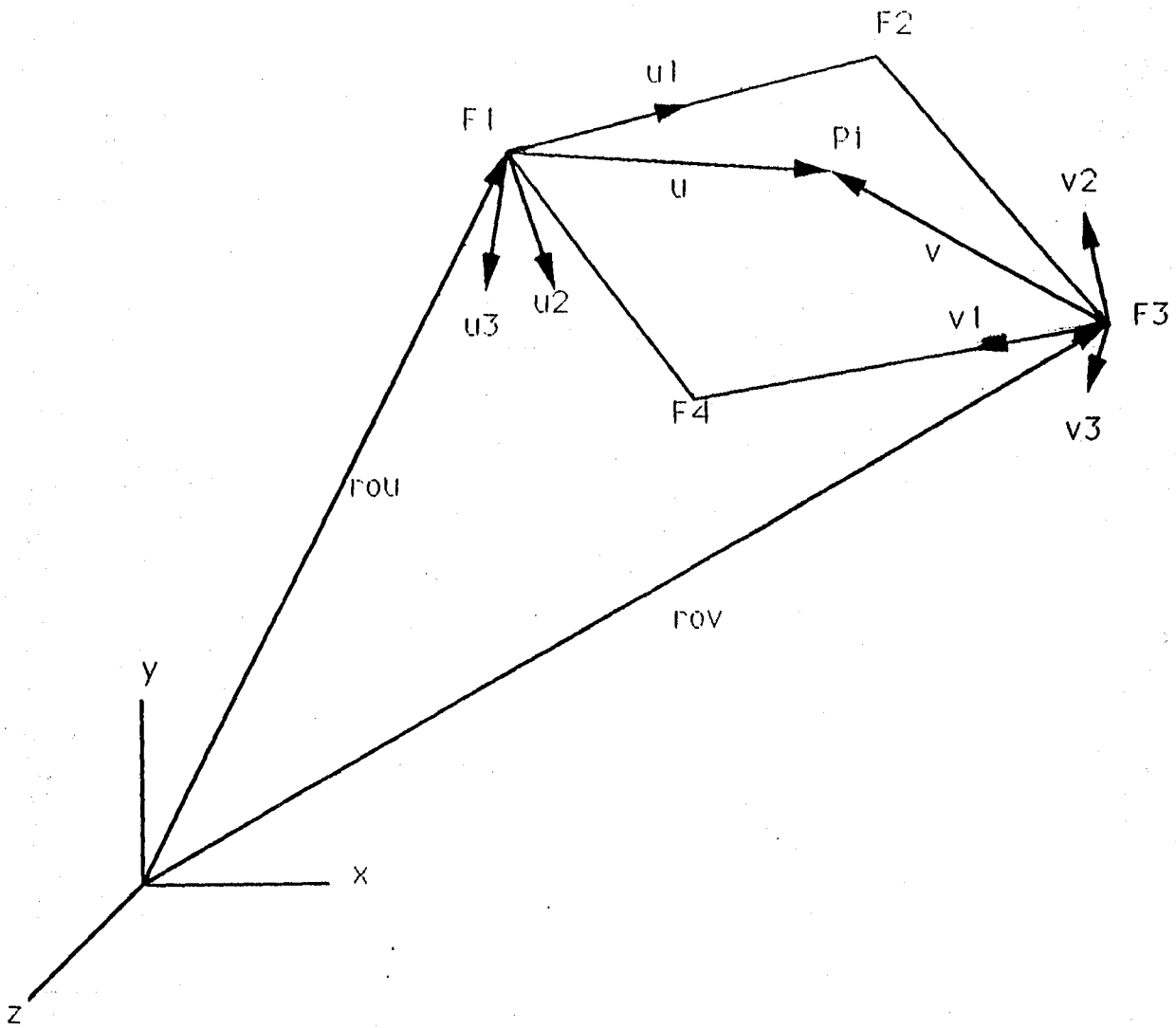

Figure A-1 The Boeing Method of Frame Shift/ Warp Compensation

two vectors were doomed to failure since, for this example at least, all errors were of the same sign.

APPENDIX B

SOFTWARE

Some brief programs were written in Turbo C++ during the course of this project. The first one, called WARP1.C, was used to generate synthetic data for the evaluation of the Boeing Frame Shift/Warp Compensation method. This program was based on the vertical displacement approximation. It applied the method to a rectangular plane which was "lifted" at one corner to simulate a linear warp of the surface. The exact vertical displacement of the surface at each xy location can be calculated given the linear warp assumption. The program also located the exact displacements as calculated by the two separate coordinate systems. The results showed that the error was one half the maximum warp displacement. The method is also dependent on which fiducials are selectd as the two coordinate origins. It was based on these findings that the method was rejected as a viable alternative.

CARL1.C is a program which takes four points in space, rotates and translates them to locate the new points. This computes the "exact" positions of the translated surface.

The third program, FRAMESHI.C, uses two sets of points, the original and shifted ones. Based on this data the warpage is approximated by the linearized approach developed in the report.

```
/*      Program Name: ### WARP1 ###  June 18, 1991 update 7/3/91      */
/*      This program computes the vertical displacements from a fixed */
/* plane to the corresponding point on a warped surface.  The actual  */
/* displacement is calculated then compared to the value obtained by  */
/* the method suggested by Alex Ladd.                                 */
/*      The program writes the data into a file named trash.dat.  To  */
/* view the data exit to the DOS shell and do a TYPE trash.dat.  For  */
/* a hard copy, redirect the output to the printer.                   */
/*                                                                    */

#include <stdio.h>
#include <conio.h>

int main()

{
        FILE *fp;
        int X,Y,DZ;
        float x1,y1,za,vd,ud,avg;
        fp= fopen( "trash.dat","wt" );
        DZ=2;        /*  Displacement of corner (X,Y) in inches */
        fprintf(fp, "\n Disp.(in inches) of corner (X,Y) is %4d ",DZ);
        fprintf(fp, "\n Xdisp Ydisp Actual DispV DispU AvgUV Error \n");
        X=16*12;     /*  Size of panel in inches X dimension */
        Y=12*12;     /*  Size of panel in inches Y dimension */
        for (y1 = 0; y1 <= Y; y1 = y1 + 24)
         {
         for (x1 = 0; x1 <= X; x1 = x1+24)
           {
            za=(x1/X)*(y1/Y)*DZ;
            vd=(y1/Y)*DZ;
            ud=(x1/X)*DZ;
            avg=(vd+ud)/2;
            fprintf(fp, "\n %3.0f %3.0f      %3.3f %3.3f %3.3f ",x1,y1,za,vd,ud,
            fprintf(fp, "%3.3f %3.3f ",avg,za-avg);
            }
         }
         fprintf(fp, "\n ");
        fclose( fp );
}
```

```
/*      Program name  ###    CARL1    ###  July 3,1991      11:24 A.M.     */
/*                                                                          */
/*      In this program uses four original points.  It rotates and          */
/* shifs them into four new points.  Each of the four point systems use     */
/* three points to define a plane and the fourth to define warp.            */
/*      The two planes are defined by taking the cross product of two       */
/* vectors (which are defined by the three points).  The output is the      */
/* x, y and z components of the resultant vector as well as the square      */
/* of the magnitude of the cross product vector.                            */
/*                                                                          */
/*      This program converts four 3 X 1 vectors (iv[3][4]), in the xyz     */
/* coordinate system into four that are rotated in the three axes then      */
/* translated to become zz[3][4].                                           */
/*      The rotation is first about the x axis, the y axis the z axis       */
/* and finally translated by a vector.                                      */
/*      To run this program, it must be edited to define angles thx,        */
/* thy, thz and vector xyz.                                                 */
/*      To reverse this effect, the operations must be taken in reverse     */
/* order.  The vector must be the negative of the original vector and       */
/* the rotation angles the negative of the original angles).                */

#include <stdio.h>
#include <conio.h>
#include <math.h>

/*      Rotation angles about the three coordinate axes                     */

#define thx 90*3.141592654/180  /* Theta is in radians i.e. 5 deg   */
#define thy 0*3.141592654/180   /* Theta y in radians  or 10 degrees */
#define thz 0*3.141592654/180   /* Theta z in radians  or 15 degrees */

int main()
{
        int N,x,y,k;
        double rotx[3][3]={
        {1, 0, 0},
        {0, 1, 0},
        {0, 0, 1}
        };
        double roty[3][3]={
        {1, 0, 0},
        {0, 1, 0},
        {0, 0, 1}
        };
        double rotz[3][3]={
        {1, 0, 0},
        {0, 1, 0},
        {0, 0, 1}
        };

/*      Input vectors are called iv[][].  output vectors zz[][].            */

        double v[3],w[3],xx[3],yy[3],zz[3][4],I,J,K,LSQ;
        double iv[3][4]={
        {0, 10, 10, 0},
        {0,  0,  5, 5},
        {0,  0,  0, 0}
        };
```

```
/*    The displacement vector                          */
        double xyz[3] = {1, 11, 3};

        rotx[1][1]=cos(thx);
        rotx[1][2]=-sin(thx);
        rotx[2][1]=sin(thx);
        rotx[2][2]=cos(thx);

        roty[0][0]=cos(thy);
        roty[0][2]=sin(thy);
        roty[2][0]=-sin(thy);
        roty[2][2]=cos(thy);

        rotz[0][0]=cos(thz);
        rotz[0][1]=-sin(thz);
        rotz[1][0]=sin(thz);
        rotz[1][1]=cos(thz);

/*      the four vectors are already defined     */

       for (k=0;k<4;k++)
        {


/*      Rotate about x axis      */
/*      printf("\n The vector rotated about the x axis is:\n");*/

        for (x=0;x<3;x++)
          { v[x] = 0;
            for (y=0;y<3;y++)
              {
              v[x]=v[x] + rotx[x][y] * iv[y][k];
              }

          }

/*      rotate about y axis                          */
/*      printf("\n The vector rotated about the y axis is:\n");*/


        for (x=0;x<3;x++)
          { w[x] = 0;
            for (y=0;y<3;y++)
              {
              w[x]=w[x] + roty[x][y] * v[y];
              }
          }

/*      rotate about z axis                          */

        for (x=0;x<3;x++)
          { xx[x] = 0;
            for (y=0;y<3;y++)
              {
              xx[x]=xx[x] + rotz[x][y] * w[y];
              }
          }

/*      Translate in xyz coordinates                 */
        printf(" The translated vector is:\n");
```

```
        for (x=0;x<3;x++)
              {
              yy[x]=xx[x] + xyz[x];
              zz[x][k]=yy[x];
              printf("%8.8e\n",zz[x][k]);
              }
    }

/*  Get the xyz components of the two input vectors that will be used in the
  cross product calculation.  v[0] is the x component, v[1], the y component
  and v[2] the z component ov vector v.  Similarly for vector w.          */

        for (x=0;x<3;x++)
          {
          v[x]=iv[x][1]-iv[x][0];
          w[x]=iv[x][3]-iv[x][0];
          printf("\n v[x] w[x] %8.8f %8.8f",v[x],w[x]);
          }
  /*  This portion takes the two vectors v and w and computes their cross
    product.  I is the x component of resulting vector, J the y component
    and K the z component.                                                */

          I=v[1]*w[2]-v[2]*w[1];
          J=-(v[0]*w[2]-v[2]*w[0]);
          K=v[0]*w[1]-v[1]*w[0];

        LSQ=I*I+J*J+K*K;          /* LENGTH SQUARED */
        printf("\n Plane defined by the input vectors");
        printf("\n I J K LSQ %8.8f %8.8f %8.8f %8.8f \n",I, J, K, LSQ);

        for(x=0;x<3;x++)
          {
          for(y=0;y<4;y++)
            {
            printf("  %3.3f %3.3f ",iv[x][y],zz[x][y]);
            }
            printf("\n");
          }

/*  Get the xyz components of the two output vectors that will be used in the
  cross product calculation.  v[0] is the x component, v[1], the y component
  and v[2] the z component ov vector v.  Similarly for vector w.          */

        for (x=0;x<3;x++)
          {
          v[x]=zz[x][1]-zz[x][0];
          w[x]=zz[x][3]-zz[x][0];
          printf("\n v[x] w[x] %8.8f %8.8f",v[x],w[x]);
          }
  /*  This portion takes the two vectors v and w and computes their cross
    product.  I is the x component of resulting vector, J the y component
    and K the z component.                                                */

          I=v[1]*w[2]-v[2]*w[1];
          J=-(v[0]*w[2]-v[2]*w[0]);
          K=v[0]*w[1]-v[1]*w[0];
```

```
LSQ=I*I+J*J+K*K;          /* LENGTH SQUARED */
printf("\n Plane defined by the rotated vectors");
printf("\n I J K LSQ %8.8f %8.8f %8.8f %8.8f \n",I, J, K, LSQ);

for(x=0;x<3;x++)
  {
  for(y=0;y<4;y++)
    {
    printf("  %3.3f %3.3f ",iv[x][y],zz[x][y]);
    }
    printf("\n");
  }
```

```
/*      Program name  ###    FRAMESHI(FT).C   ###  July 10,1991 4:50 P.M. */
/*      In this program uses four original points.  The rotated and     */
/* shifted points are also known.  Each of the four point systems use */
/* three points to define a plane and the fourth to define warp.        */

#include <stdio.h>
#include <conio.h>
#include <math.h>

int main()
{
        int x,y;

/* tv[3][4] is temporary vectors, dsp[3] is displacement vector          */
/* tx is x displacement, ty and tz are y and z displacements             */

        double tv[3][4],dsp[3],tx,ty,tz,W;

/* ov[3][4] is original vectors (or points), dv[3][4] is displaced vect.*/
/* ov[x,y,z][vect.#-1].  i.e.  ov[1][3] is the y comp. of vector 4       */

        double ov[3][4]={
        {0, 180, 180,   0},
        {0,  0,  144, 144},
        {0,  0,    0,   0}
        };
/*  The following assumes that X=180,Y=144,tx=.01,ty=.015,tz=.02
        W=4, dx=1, dy=3 and dz=5                                        */

        double dv[3][4]={
        {1, 181, 181,   2.12},
        {3,  6.6,  147, 149},
        {5,  7.7,    7.74,  6.44}
        };

/*  P1=(0,0,0)  PD1=(dx,dy,dz)
    P2=(X,0,0)  PD2=(X+dx,X*tz+dy,-X*ty+dz)
    P3=(X,Y,0)  PD3=(X+dx,Y+dy,Y*tx-X*ty+dz+W)
    P4=(0,Y,0)  PD4=(-Y*tz+dx,Y+dy,Y*tx+dz)
    where dx, dy and dz are linear displacements in the x, y and z dir.
    tx, ty and tz are angular rotations about the x, y and z axes using
    the right hand rule.  W is the warp value.
*/

/* Update each point by the displacement (dx,dy,dz)     */

       for (y=0;y<4;y++)
        {
          for (x=0;x<3;x++)
            {
              tv[x][y]=dv[x][y]-dv[x][0];
              printf ("\n x, y, tv[x][y] %3d %3d %3.8f",x,y,tv[x][y]);
            }
           printf ("\n");
        }

/*  Calculate theta z (tz) [ PD2y-P2y = X*tz]           */
        tz=(tv[1][1]-ov[1][1])/ov[0][1];
        printf ("\n Theta z in radians is = %3.6f",tz);
```

```
/* Calculate theta y (ty) -[PD2z-P2z = X*ty]                    */
        ty=(tv[2][1]-ov[2][1])/ov[0][1];
        printf ("\n Theta y in radians is = %3.6f",ty);

/* Calculate theta x (tx) -[PD4z-P4z = Y*tx]                    */
        tx=(tv[2][3]-ov[2][3])/ov[1][3];
        printf ("\n Theta x in radians is = %3.6f",tx);

/*  Calculate the warp W.  Y*tx-X*ty+W = PD3z                   */
        W=(tv[2][2]-tv[2][3]+tv[0][1]*ty);
        printf ("\n The warp value W is = %3.6f",W);

}
```

REFERENCES

[1] Paul, Richard P. "Robot Manipulators", The MIT Press, Cambridge, Massachussets, 1982

[2] Koren, Yoram "Robotics for Engineers", McGraw-Hill, 1985

[3] Swokowski, Earl W. "Calculus With Analytic Geometry," second edition, Prindle Weber and Schmidt, 1979

1991 NASA/ASEE SUMMER FACULTY FELLOWSHIP PROGRAM

JOHN F. KENNEDY SPACE CENTER
UNIVERSITY OF CENTRAL FLORIDA

INVESTIGATION OF THE FINITE ELEMENT SOFTWARE PACKAGES AT KSC

PREPARED BY:	Dr. Chu-Ho Lu
ACADEMIC RANK:	Assistant Professor
UNIVERSITY AND DEPARTMENT:	Memphis State University Department of Mechanical Engineering
NASA/KSC	
DIVISION:	Data Systems
BRANCH:	CAD/CAE
NASA COLLEAGUE:	Mr. Hank Perkins Mr. Eddie Bertot
DATE:	August 9, 1991
CONTRACT NUMBER:	University of Central Florida NASA-NGT-60002 Supplement: 6

ACKNOWLEDGMENTS

I would like to thank Eddie Bertot and Hank Perkins of DL-DSD-22 for their support in obtaining the necessary resources to do this research, Dave Paton of MDSSC and Karl Meyer of LSOC for suggesting NASTRAN test cases, Mark Sorger, Shawn Riley and Richard Neely of EG&G for fixing VAX workstation and Intergraph workstation and providing the documentation of MSC/NASTRAN and SDRC/I-DEAS.

Additionally, I would like to thank the administrative support of Dr. E. Ramon Hosler and Mrs. Kari Stiles, University of Central Florida, and Dr. Mark Beymer and Mr. Dennis Armstrong, the director of the summer faculty fellowship program at NASA/KSC.

ABSTRACT

This research report concerns a discussion of the useful and powerful features of NASTRAN and documents three real world problems for the testing of the capabilities of different NASTRAN versions. The test problems involve direct transient analysis, nonlinear analysis and static analysis. The experiences in using highly graphics software packages are also discussed. It is found that (1) MSC/XL can be more useful if it can be improved to generate picture files of the analysis results and to extend its capabilities to support finite element codes other than MSC/NASTRAN, (2) the current version of SDRC/I-DEAS (version VI) may have bugs in the module "Data Loader".

TABLE OF CONTENTS

LIST OF ILLUSTRATIONS

I. INTRODUCTION

The finite element method has been established as a powerful and popular numerical procedure for analyzing structures and continua governed by differential equations. The technique, in general, discretizes the domain of the problem under consideration into a number of geometrically simple regions (elements). The governing equations of the problem are then approximated over each element by continuous functions to formulate so-called element equations. By doing this, a continuous model with infinite degrees of freedom is converted into a discrete model having finite degree of freedom, and a mathematical model including differential equations is generally converted into a mathematical model involving algebraic equations. After these algebraic equations are assembled and the constraints are introduced, the solution and the derived variables can be obtained with the aid of computers.

Instead of writing a finite element program to analyze a specific problem, the modern engineering analysts will turn to commercial finite element packages. In fact, hundreds of commercial finite element programs are available, from small to large. The most well known large general-purpose analysis software packages are NASTRAN, ANSYS and ABAQUS. They provide many different element types, so that almost any conceivable structure, loads and boundary conditions can be treated. Linear problems of statics and dynamics are certainly included. Several nonlinear capabilities are also provided. At John F. Kennedy Space Center (KSC), such computer packages are MSC/NASTRAN (provided by The MacNeal-Schwendler Corporation), SDRC/I-DEAS (provided by Structural Dynamics Research Corporation) and I/FEM (provided by Intergraph Corporation).

Using the commercially available finite element programs to solve problems, one does not begin with differential equations. Instead, there are three basic phases which can be identified (i.e., preprocessing, analysis modeling and solution, and postprocessing). In the preprocessing phase, a continuous media is discretized, element types are selected, loads and constraints are provided, and material and physical properties of the problem are specified. Then the problem is solved in the analysis phase. The derived variables are also computed. The results are finally analyzed and managed in the form of reports or plots in the postprocessing phase. The process is repeated if mesh refinement is necessary.

Although the large general-purpose finite element software packages offer an extremely versatile capability, engineers typically consume more than 65% of their time in the pre- and post-processing processes. It is clear that the effort in these processes can be reduced if other softwares having highly interactive graphics capability can be interfaced. Three such computer software packages are currently available at KSC, i.e., I-DEAS/FEM, I/FEM and MSC/XL. The interfaces between the former two computer packages and MSC/NASTRAN were investigated [1] in which four different combinations of the three software packages were studied in designing a solid rocket booster fixture.

Different from I-DEAS/FEM and I/FEM, which provide linear analysis capability and

can also be interfaced with COSMIC/NASTRAN, ANSYS, ABAQUS for nonlinear analysis, MSC/XL (introduced by MSC during 1990) is a pure pre- and post-processing software package and only supports MSC/NASTRAN. Although the combination of MSC/XL and MSC/NASTRAN provides powerful finite element modeling, analysis and results processing, the cost in using these software packages seems expensive. It would be interesting to know the possibility of replacing MSC/NASTRAN by different general-purpose finite element packages. Because the finite element users at KSC have been familiar with the features of NASTRAN, the computer packages suggested are different versions of NASTRAN.

Due to the complicate nature of the program, it is impossible to have a comprehensive study to all aspects of NASTRAN in a short period of time. In this research report several problems which employ some useful features of MSC/NASTRAN, suggested by engineering analysts at KSC, will be examined. The purpose of this work is to document test cases so that the capabilities of other versions of NASTRAN can be investigated. In the following sections the development history of NASTRAN and its functions will first be briefly described. Then the test problems will be illustrated. The last section contains discussions and conclusions.

II. NASTRAN DEVELOPMENT AND ITS FUNCTIONS

2.1 Introduction

Different from the current general purpose finite element software packages developed by individual companies and universities, NASTRAN (NASA STRucture ANalysis) was developed under NASA's sponsorship in 1964-1969. During that period NASA had a NASTRAN project management office which administered the software development, released and updated periodically the voluminous documentation, and reported any systematic error and correction procedure. The responsibility was shifted in 1969 to the Computer Software Management and Information Center (COSMIC) at the University of Georgia.

In using COSMIC/NASTRAN people often found that it was very difficult to make any correction when they realized some bugs in the program. Instead of trying to debug the program they reported the problems to the COSMIC which in turn gave subcontracts to individuals to solve the problems. The solutions to the problems might not be available until the release of the next version of COSMIC/NASTRAN.

Although only media costs were required in using COSMIC/NASTRAN, the ineffective software management and the lack of hot-line user's service made a number of finite element users shift to commercial software packages in early seventies. The most popular one inside (and/or outside) the United States is MSC/NASTRAN which was described in the previous section. The other versions are UAI/NASTRAN (offered by Universal Analytics Incorporation), CSA/NASTRAN (offered by Computerized Structural Analysis and Research Corporation.), PM/NASTRAN (offered by MARC Analysis Research Corporation), etc. In this section the general features of NASTRAN will be briefly discussed.

2.2 Program Architecture

The original NASTRAN was designed to meet certain criteria [2,3,4], such as: the ease of input, the minimization of user's intervention during the execution of the program, the independence of functions in solution modules, the restart capability, etc. Based on these goals NASTRAN is operated in the batch mode and is divided into four components which are given in order as follows [5]:

NASTRAN Card. This card is designed for changing the default values of certain operational parameters such as buffer size (keyword: BUFFSIZE), working space (keyword: HICORE), the amount of real memory available (keyword: REAL) and the numbers of lines printed per page (keyword: NLINES), etc. To get a solution of a large problem the first three parameters may need to be modified.

The Executive Control Deck. This deck is the heart of NASTRAN. It defines the type of solution and the general conditions to be performed, the allowed maximum execution

time, the types of system diagnostics required, the execution of DMAP alter library and the restart conditions. The general concept in designing this deck is the reliability and efficiency. Few changes were anticipated in the Executive system as NASTRAN grew. This leads to the result that the executive system is a sophisticated, but difficult to modify system.

The Case Control Deck. The function of this deck is to provide the selections of the data from the Bulk Data Deck, the subcase structure, the boundary conditions and loading cases, and the output requests for printing, punching and /or plotting.

Finally, the Bulk Data Deck provides all the data necessary to define the geometry of the structural model, the constraint and the loading conditions. It is the major portion of the input data for NASTRAN. The various pools of data which are selected by Case Control Cards will be used at execution time. For example, constraint conditions, loading conditions and thermal conditions may be specified to sets identified by number, but only those sets which are selected for a particular subcase in the Case Control Deck will be used in the solution.

2.3 Rigid Formats

A rigid format is an established sequence of DMAP instructions stored in the Executive system to perform some standardized analysis. It is usually identified with an integer number and an analysis approach. In COSMIC/NASTRAN there are 22 rigid formats [6] in which 16 rigid formats (1 to 16) in the displacement approach, 3 rigid formats (1, 3 and 9) in the heat transfer approach, and 3 rigid formats (9, 10, 11) in the aerodynamic approach. On the other hand there are more than 45 solution sequences in MSC/NASTRAN [7]. The rigid formats provide users with a very large range of analysis options. Section 3.1 of Reference 7 contains excellent tables which summarizes the various modeling options offered versus rigid body format number. For some particular problems, the user can also modify the rigid formats by DMAP alters.

2.4 Direct Matrix Abstraction Program (DMAP)

DMAP is a unique feature of NASTRAN and is one of the most powerful matrix manipulation tool offered in any code. The use of DMAP alters in rigid formats provides users with new analysis capability and increased efficiency. The DMAP is a program language of NASTRAN, which contains macro instructions of matrix operations. A DMAP has the following form:

(Module Name) (Input Data Block)/(Output Data Block)/(Parameter)$

where a slash is a delimiter between data blocks and a dollar sign terminates the DMAP instruction. The sequence shown below gives as example [4].

To compute [C] = [A] + [B] and [D] = [A][C], the DMAP sequence is,

```
BEGIN$          Start DMAP
ADD  A,B/C/$    Adds [A] to [B]
```

```
MATPRN  C//$        Print  [C]
MPYAD   A,C/D/$     Compute [D]
MATPRN  D//$        Print  [D]
END$                Terminate
```

To relieve users in preparation of matrix manipulation, NASTRAN provides in each new version a library of useful predefined DMAP alters which are called RFALTERS. The user has to insert these alters into the Executive Control Deck by using a machine-dependent operation system utility for merging files.

2.5 Checkpoint/Restart Capability

NASTRAN offers a sophisticated checkpoint/restart capability. The advantages of this feature are: (1) continuation of an execution of a job which terminated due to data errors or time limitation; (2) requesting additional information output for a job already completed; (3) restarting to run additional load cases in static analysis; and (4) extracting real eigenvalue for additional frequency ranges in normal mode analysis. In using this capability the NASTRAN card "CHKPNT YES" in the Executive Control Deck must be provided. This card makes the system save information on a file called NPTP (New Problem Tape) which will be renamed as OPTP (Old Problem Tape) in the future run.

2.6 Nonlinear Capabilities

Nonlinear analysis should be performed whenever problems involve nonlinear materials and finite deformation. The nonlinear capabilities are different among the various versions of NASTRAN and are all primitive when compared with those offered by current nonlinear codes such as ANSYS and ABAQUS. There are two types of static nonlinearities offered in COSMIC/NASTRAN, i.e., the differential stiffness of rigid format 4 and the material plasticity of rigid format 6.

Nonlinear capabilities have been improved in the latest version (66) of MSC/NASTRAN [7]. The static nonlinear solution methods, SOLs 64 and 66, provide for modeling inelastic effects such as material plasticity and creep, "gaps" in the structure which open, close, and slide (if the friction force is smaller than the product of the normal force and the friction coefficient), and nonlinear elastic material properties. Furthermore the rigid format 99 offers transient dynamic solutions for material nonlinearity and large deformation. The nonlinear capabilities in the UAI/NASTRAN is said to be comparable to those offered in MSC/NASTRAN. This argument can not be judged because of unsuccessful access of the UAI/NASTRAN User's Manual.

2.7 Superelement

A structure is divided into pieces called substructures or superelements. The automated multi-stage substructuring system for NASTRAN [8], developed by Universal Analytics, Inc., is very useful and user oriented. The reasons for subdividing a structure into superelements are that: (1) the reduction in the computational cost when design changes

are of localized nature because the design changes for single substructure may not affect matrices of all other substructures; (2) the simplification in data generation and in checkout; (3) the efficiency in computation to form the condensed stiffness matrix of the typical substructure because those internal degree of freedom need to be processed only once; and (4) the different design groups can study different substructures simultaneously.

In using this feature the user should keep in mind that the boundaries of substructures must be small, so that the ratio of masters (the retained degree of freedom) to slaves (the condensed degree of freedom) is small and the overall stiffness matrix can be kept in manageable size. Accordingly, a long cylinder can be more efficiently substructured than a sphere [9]. An excellent discussion of superelements can be found in Reference 10.

2.8 Cyclic Symmetry

For a structure which can be generated through rotation of a superelement (fundamental region), its circumstance is called cyclic symmetry. A structure such as an propeller in a centrifugal pump is a good example. The analytical model required for cyclic symmetry analysis, in general, is substantially smaller. In fact, the cyclic symmetry analysis can be treated as a special form of superelement analysis. The difference between these two techniques are that the cyclic symmetry analysis deals with problems having all identical superelements while the superelement analysis involves the subdivision of a structure into superelements of arbitrary shapes. The cyclic symmetry analysis offered in NASTRAN can automatically impose boundary conditions and also deals with the applied loads which may act at arbitrary locations throughout the entire structure.

III. TEST PROBLEMS

3.1 Introduction

Even with a noncomprehensive discussion of the features offered in NASTRAN, as shown in the previous section, one will be very impressed with the complexity of a problem which can be handled by NASTRAN. In this section three real world problems, which have been solved by MSC/NASTRAN and verified by experiments, will serve as test cases for other versions of NASTRAN. The problems are selected so that a number of different type elements, the medium-to-large size of problems, and transient or nonlinear analysis may be included. Since the documentation and source codes of the other NASTRAN versions are not available at KSC, the capabilities of those software packages in handling the three problems are not studied. Due to the lengthy output of the results, the solution printout to these problems won't be shown in this report, however it can be found from the VAX/VMS computer at KSC.

Before we start to discuss test cases, it may be interesting to know some problems encountered on the interface between the latest versions of pre- (post-) processing softwares and NASTRAN. Here, we will briefly discuss two interactive engineering modeling and results interpretation tools: MSC/XL (version 1A) and SDRC/I-DEAS (version 6).

MSC/XL runs on DEC VAX/VMS processors with Tektronix (4111, 4129 and 42xx) or X windows version 11 from the VAX workstation. MSC/XL has made MSC/NASTRAN be more powerful and attractive, however the current version of MSC/XL cannot generate picture files. Therefore the quality of hard-copy plots can be very poor, nor be in color if the Tektronix or VAX workstation are used. The color plots for displacements and stress fields are the important means for clearly presenting analysis results. Its discrepancy can be overcome if one uses Intergraph workstation as a graphic device.

On the other hand the use of SDRC/I-DEAS is more involved than that of MSC/XL. Once a model is developed in I-DEAS, the command sequence shown in any task: Mange_Model, Write, MSC/NASTRAN, can generate Case Control Deck and Bulk Data Deck. To have the computational results be able to transfer back to I-DEAS, the user need to use functional module OUTPUT2 in the Executive Control Deck to stole all the data blocks. In using MSC/NASTRAN version 65, those data blocks must be specified and then written into a FORTRAN unit which in turn assigned to a file [1]. This procedure has been improved in version 66 which contains certain RFALTERS supporting rigid formats 3, 5, 24, 26, 27, 47, 48, 61, 63 and 66. As an example, the Executive Control Deck for nonlinear material analysis [12] is shown below:

```
ASSIGN OUTPUT2=out.OP2,NEW,UNIT=12,UNFORMATTED
ID MATERIAL NONLINEAR
SOL 66
TIME 20
COMPILE SOL66, SOLIN=MSCSOU
RFALTER RF66D66
CEND
```

This deck together with an additional "Param, Post, -2" card in the Bulk Data Deck will make all the resulting data block be stored in out.OP2 which can be accessed by I-DEAS through the command "Data Loader" in the post-processing.

Although I-DEAS version VI has been claimed to be much better than its previous versions, the functional module, Data Loader, in the current version does not work well. In one of the three test problems - Rolling Beam Umbilical System, both geometry data and analysis data can be loaded to I-DEAS when version V is used, however none of the data can be processed if version VI is used.

3.2 Rolling Beam Umbilical System

A rolling beam retract mechanism in the primary disconnect of the liquid hydrogen (LH_2) umbilical carrier plate was modeled by means of MSC/NASTRAN [12]. The dynamic response was perform through the direct transient analysis (SOL 27). Figure 1 shows the isometric view of the structure. The model includes 786 one-dimensional elements, 237 two-dimensional elements, 8 one-dimensional elbow elements, 121 spring elements and one general element. The rolling beam motion is initiated by firing a pyro bolt. The dead-load, time dependent forcing function was applied to the rolling beam in vertical direction (Z_R), while the time dependent displacement function was applied to the LH_2 umbilical carrier plate in the vertical direction (X_0) and horizontal direction (Y_0). The MSC/NASTRAN input deck and output files for this problem can be accessed from the filename "Roll" of the directory [LU] in KSCDL1. The typical displacement, velocity and acceleration histories are respectively shown in Figures 2, 3 and 4.

3.3 KSC SRB Hold-down Post

The location of the solid rocket booster (SRB) hold-down post on the launch pad is shown in Figure 5. During the shuttle launch the ignition of the main engine starts at t=-7 seconds, while that of the SRB starts at t=0. There will be some forces built up on the SRB hold-down post due to the small oscillation of the whole system. The maximum values of the loading applied to the bearing of the hold-down post were given as 1457 kip in compression and 500 kip in shear. Nonlinear analysis sequence (SOL 66) have been used in the study. The structure model is shown in Figure 5 containing 3449 nodes, 319 GAP elements. 1633 HEXA elements and 3264 TETRA elements. Figure 6 shows the deformed shape of the SRB hold-down post (in solid line) superimposed with the undeformed configuration. The displacement and the stress fields are respectively shown in Figures 7 and 8. The details of the input deck and outputs can be found from the file "SRBHP" of the directory [LU] in KSCDL1.

3.4 Single Pallet Rotation Device Cover Rivet Analysis

A single pallet rotation device (SPRD) panel lifting lug with extra rivets was studied. The finite element model which includes 349 BAR elements, 319 BEAM elements, 1008 HEXA elements, 1153 QUAD4 elements and 27 TRIA3 elements. The total number of the nodes is 3944. Static analysis (SOL 101) was performed and the results for the deformed shapes and stress fields are shown in Figures 9, 10 and 11. The MSC/NASTRAN input deck and output for this problem are stored in the files "SPRD" of the directory of [LU] of KSCDL1.

IV. DISCUSSIONS AND CONCLUSIONS

Although NASTRAN has been reported too costly for running small to medium-size problems, it is generally accepted that NASTRAN solves medium to large structures as well or better than most general purpose program [4]. For the usage of finite element codes, NASTRAN has been reported to be the most widely used in the world and may have the most complete documentation.

In this report some of the important features of NASTRAN have been summarize and three cases were documented for the testing of the different versions of NASTRAN. The test problems, including direct transient analysis, nonlinear analysis and static analysis, were modeled by means of MSC/NASTRAN. Due to unsuccessful access the software package of the other commercial versions of NASTRAN, their capabilities are not studied.

For the use of the highly graphics software packages in the pre- and post- processing phases, it has been found that MSC/XL cannot generate picture files for producing good quality plots nor support the finite element codes other than MSC/NASTRAN. On the other hand, SDRC/I-DEAS provides more capabilities to interface a number of finite element packages and can produce high quality plots. However, there may exits errors in the functional module "Data Loader" of the current version (VI).

In the course of surveying finite element users at KSC, one has commented good capabilities of UAI/NASTRAN in handling direct transient problems such as the first test case. It would be beneficial to KSC to have future study to investigate the capabilities of the other latest general purpose finite element packages as long as the reduced cost in the replacement versus the cost of MSC/NASTRAN is substantial.

REFERENCES

1. Lu, C.H., "Study of The Available Finite Element Software Packages at KSC," Research Report for 1990 NASA/ASEE Summer Faculty Fellowship Program at Kennedy Space Center, Contract Number NASA-NGT-6002 Supplement:4.

2. Mueller, G.E., "The Future of Data Processing in Aerospace," Aeronautical Journal, April 1979, PP 149-158.

3. "Trends in Computing: Applications for the 80's," Fortune, May 19, 1980, pp. 29-70.

4. Jones, J.W., Fong, H.H. and Blehm, D.A., "Evaluation of NASTRAN General Purpose computer Program," Final Report to The Office of Naval Research, Code 474, August, 1980.

5. MSC/NASTRAN Handbook for Linear Analysis, MSC/NASTRAN Version 64, The MacNeal-Schwendler Corporation, August, 1985.

6. COSMIC/NASTRAN User's Manual Updates, Section 5.5-43, 1987-1990.

7. MSC/NASTRAN User's Manual, Version 66, The MacNeal-Schwendler Corporation, November, 1989.

8. Field, E.I., Herting, D.N., Herendeen, D.L. and Hoesly, R.L., "The Automater Multi-stage Substructuring System for NASTRAN," NASTRAN: User's Experiences, NASA TM X-3278, Fouth NASTRAN User's Colloquium, NASA Langley Research Center, 9-11 September, 1975.

9. Cook, R.D., Malkus, D.S. and Plesha, M.E., Concepts and Applications of Finite Element Analysis, Third Edition, John Wiley & Sons, 1989.

10. MSC/NASTRAN Handbook for Superelement Analysis, MSC/NASTRAN Version 61, The MacNeal-Schwendler Corporation, April, 1982.

11. SDRC/I-DEAS Finite Element Modeling User's Guide, Level VI, SDRC, 1990.

12. Meyer, K., "Dynamic Response and stress analyses of the STS/Centaur Rolling Beam Umbilical System Rolling Beam," KSC-DD-803-TR, John F. Kennedy Space Center, NASA, June 1985

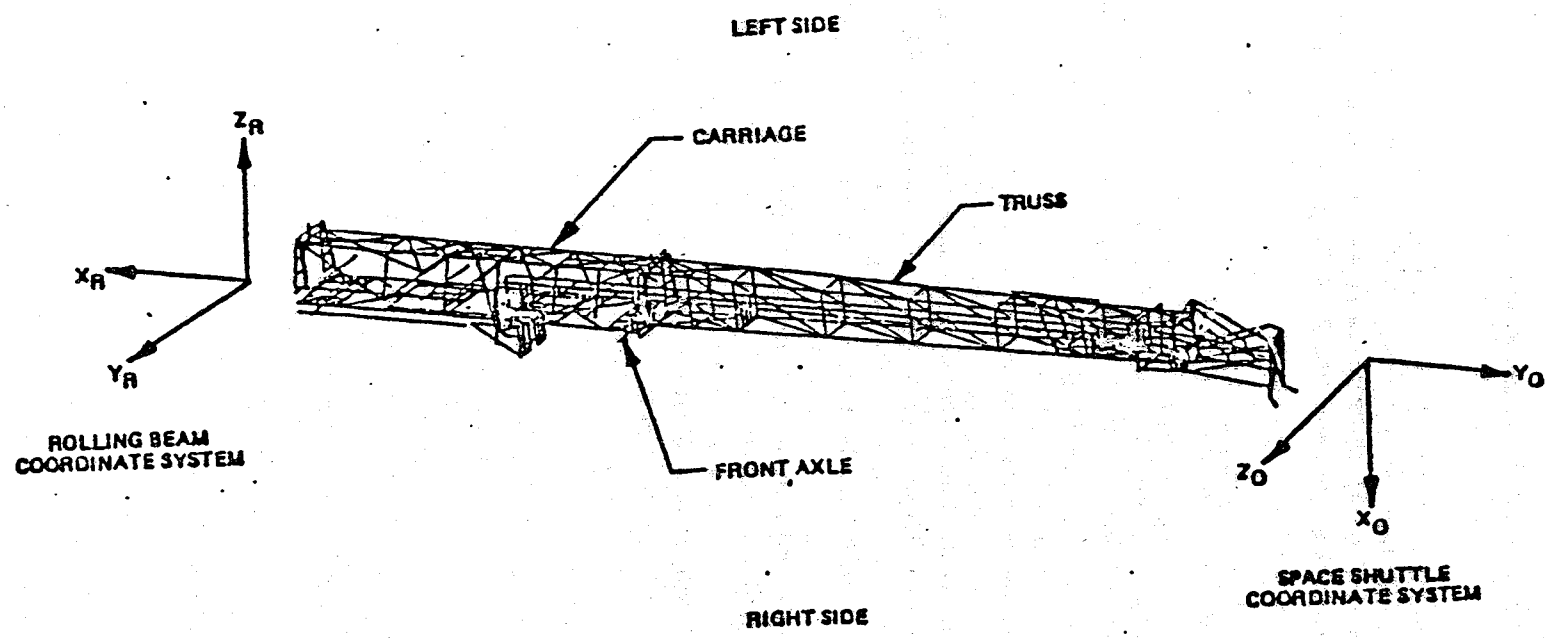

Figure 1 An Isometric View of Rolling Beam Umbilical System

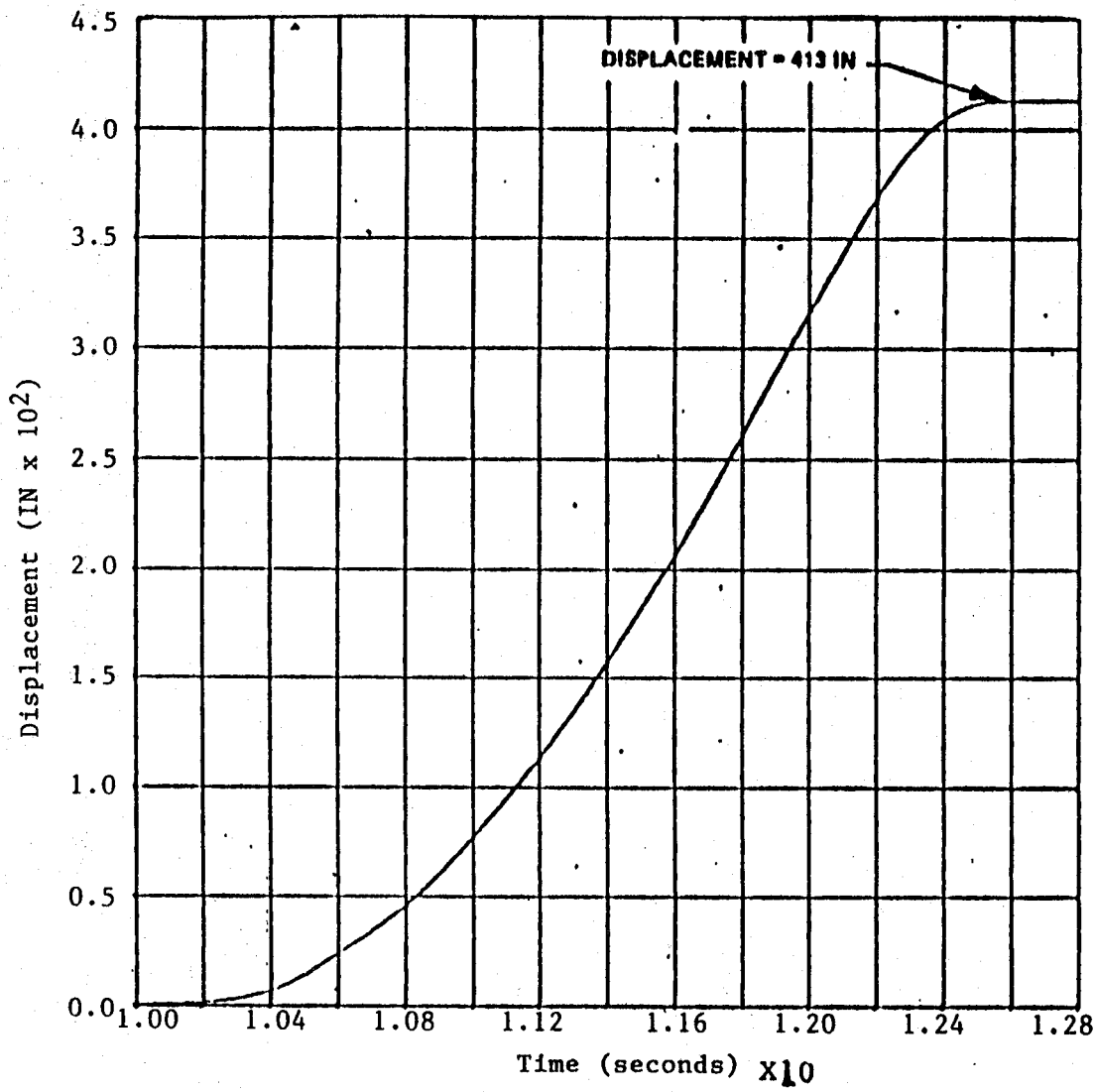

Figure 2. X_R Displacement History at Carriage/Truss Interface

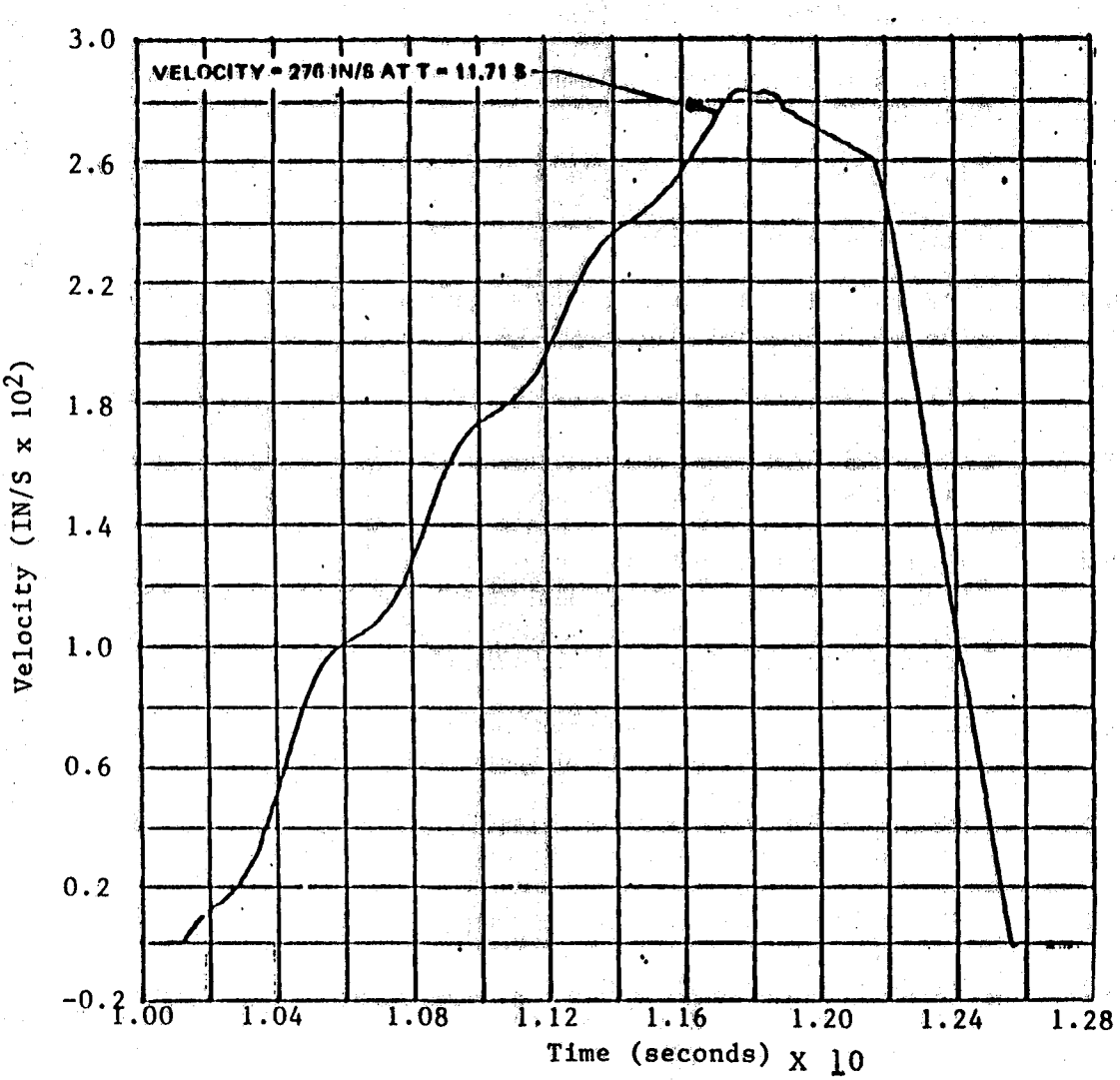

Figure 3. X_R Velocity History at Carriage/Truss Interface

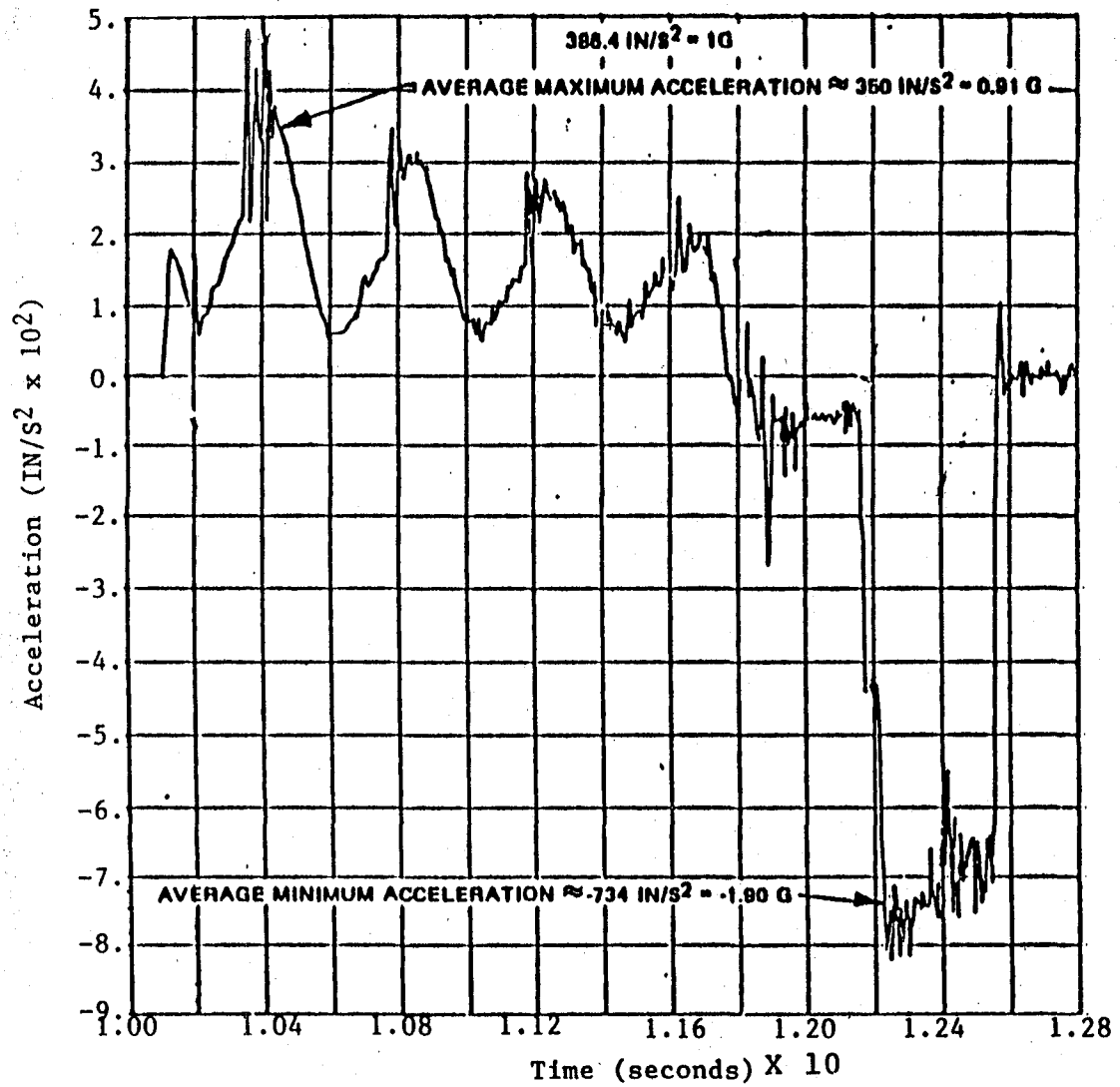

Figure 4. X_R Acceleration History at Carriage/Truss Interface

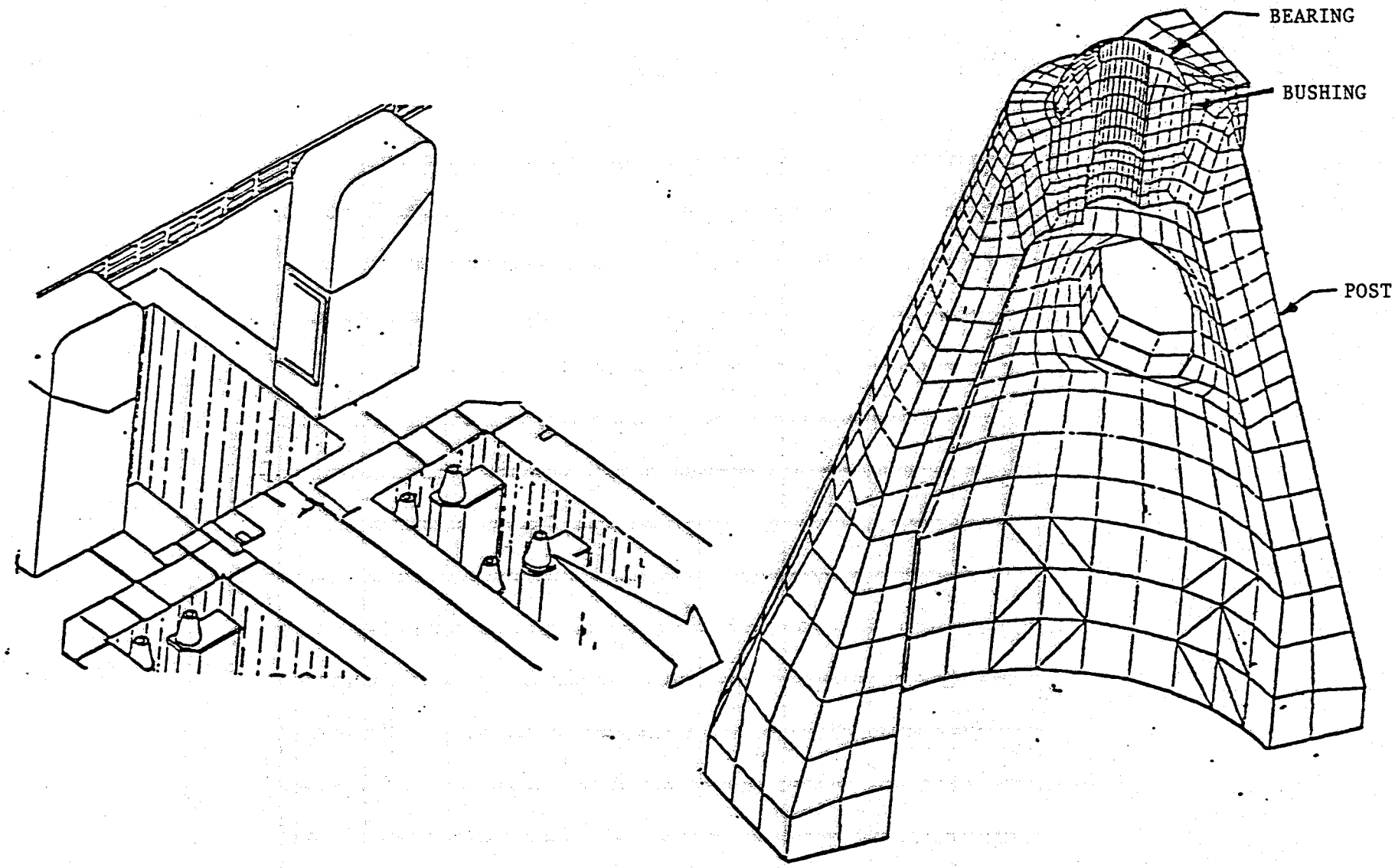

Figure 5. The Location and Finite Element Model of SRB Hold-down Post

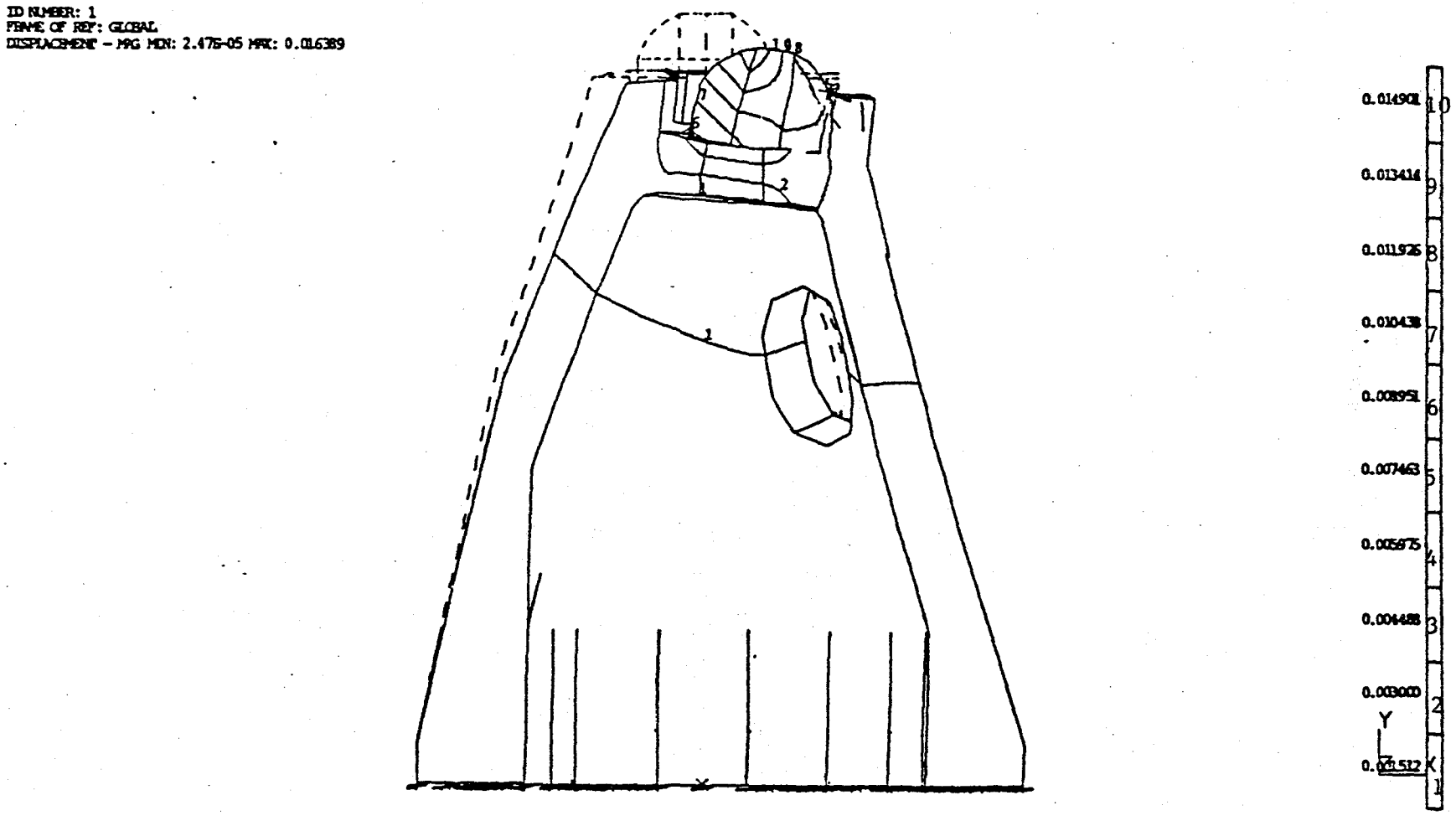

Figure 6. The Deformed Configuration of SRB Hold-down Post

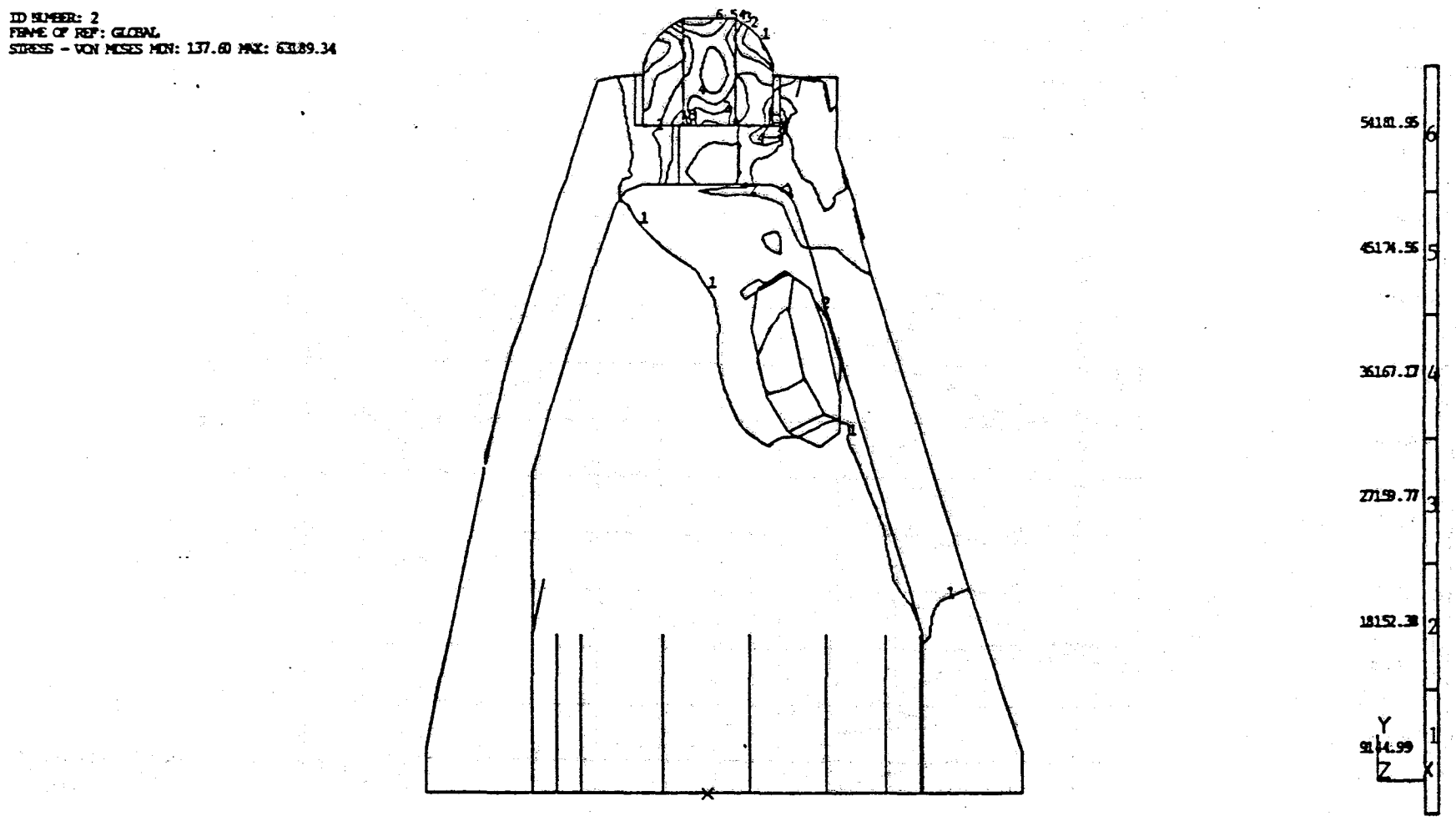

Figure 7. The Stress Field of The SRB Hold-down Post

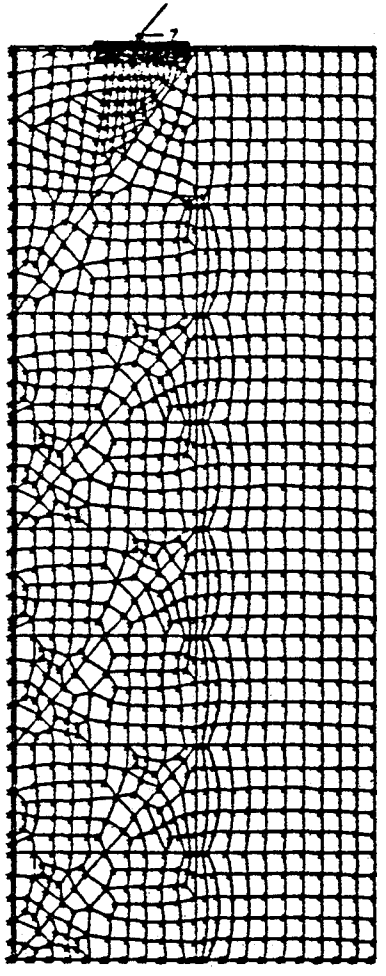

Figure 8. The Finite Element Model of A Single Pallet Rotation Device

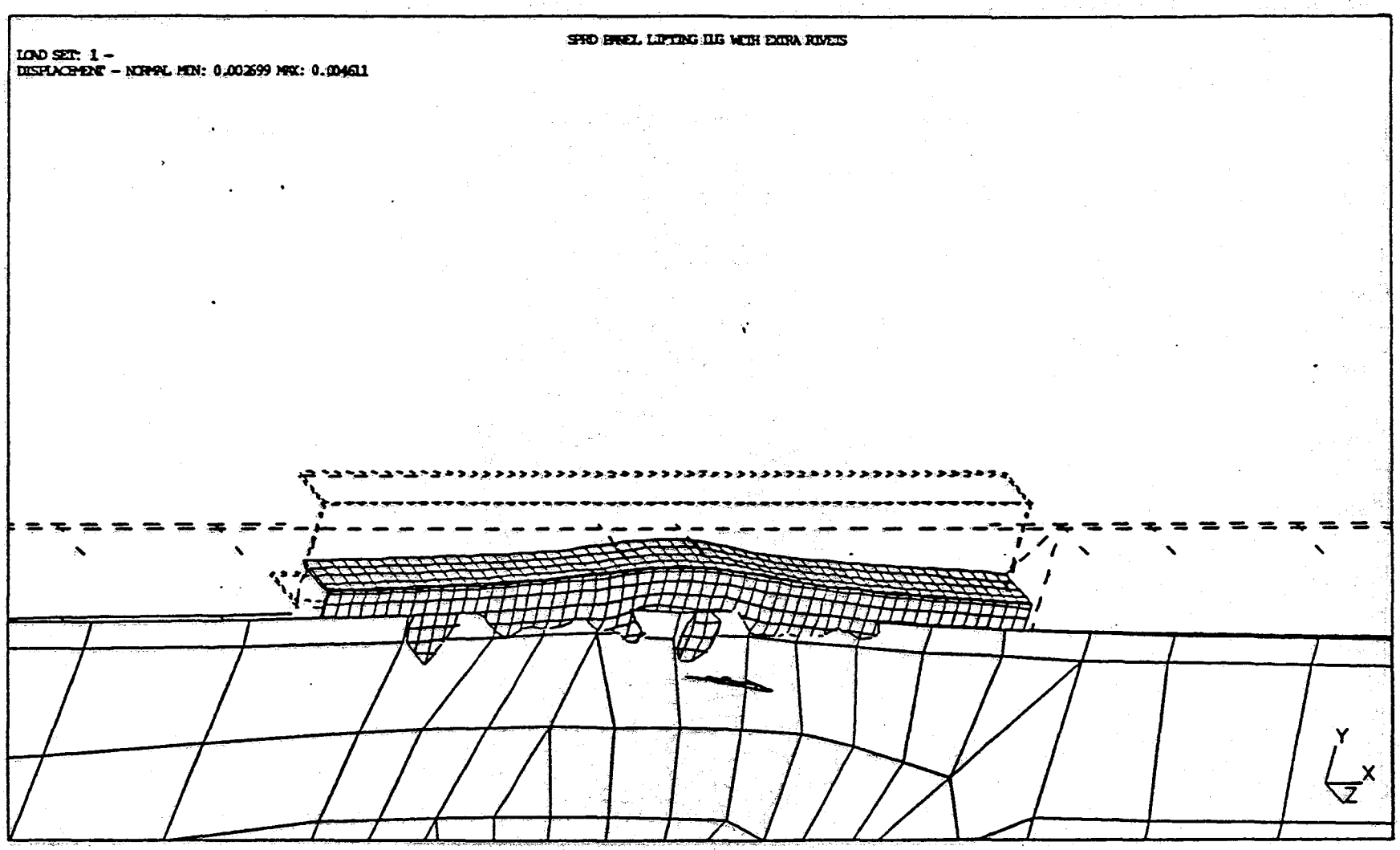

Figure 9. The Deformed Shape of The Single Pallet Rotation Device

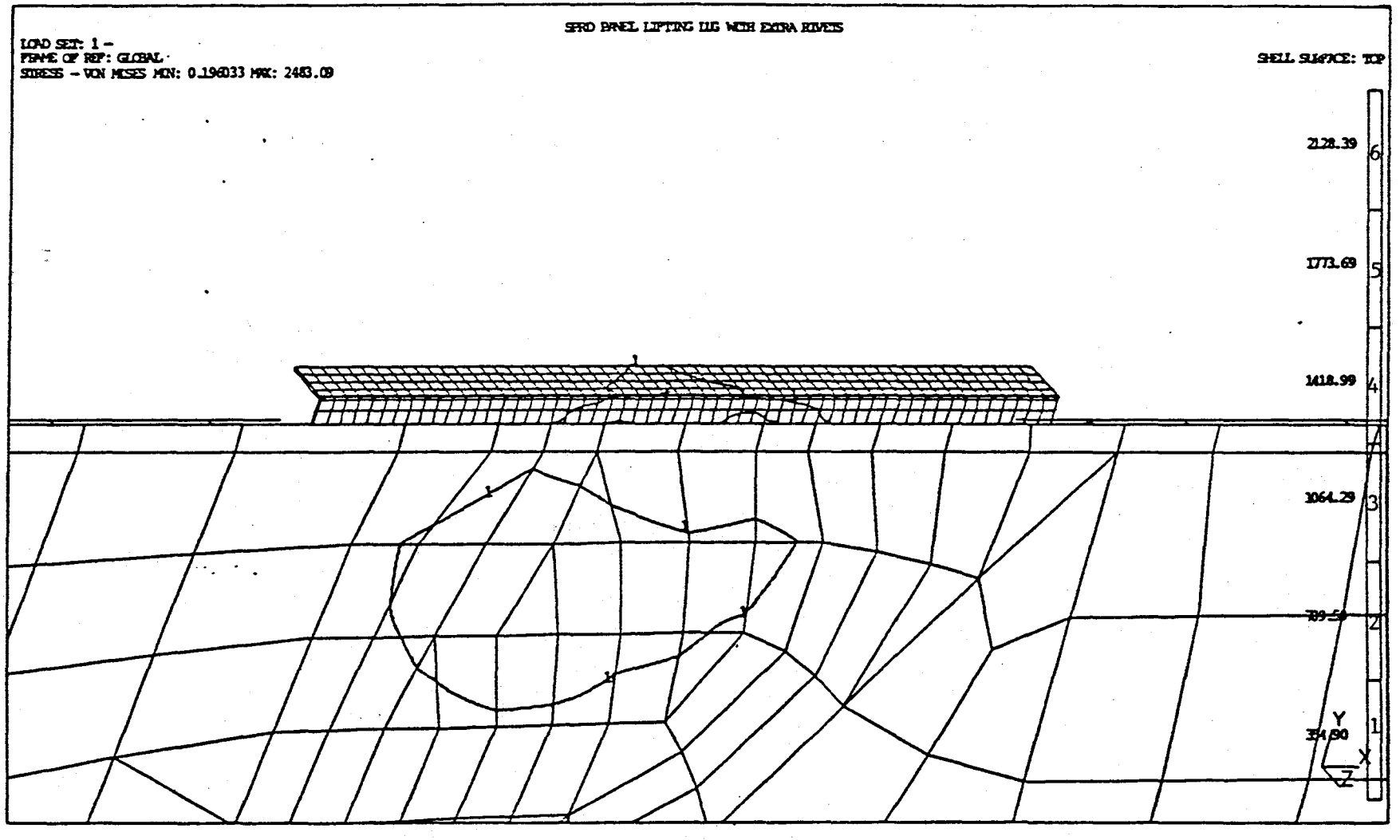

Figure 10. The Stress Field of The Single Pallet Rotation Device

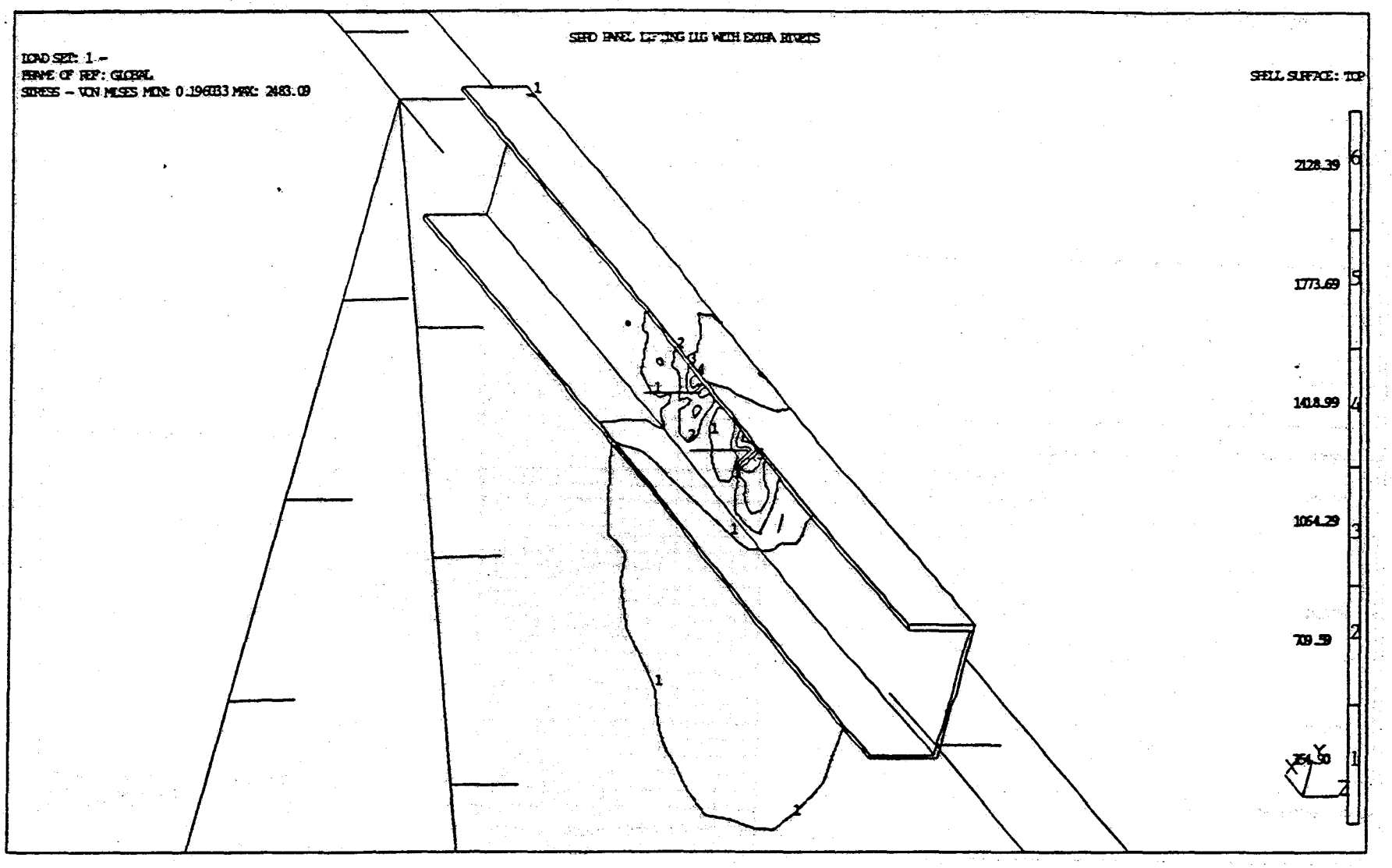

Figure 11. A Different Angle View for The Stress Field of The Single Pallet Rotation Device

1991 NASA/ASEE SUMMER FACULTY FELLOWSHIP PROGRAM

JOHN F. KENNEDY SPACE CENTER
UNIVERSITY OF CENTRAL FLORIDA

MULTISPECTRAL IMAGE PROCESSING FOR PLANTS

PREPARED BY:	Gaines E. Miles
ACADEMIC RANK:	Professor
UNIVERSITY AND DEPARTMENT:	Purdue University Agricultural Engineering
NASA/KSC	
DIVISION:	Biomedical Operations and Research
BRANCH:	Biological Research and Life Support
NASA COLLEAGUE:	John C. Sager
DATE:	August 1, 1991
CONTRACT NUMBER:	University of Central Florida NASA-NGT-60002 Supplement: 6

Acknowledgements

Without the able assistance of many Bionetics and NASA personnel in the Biological Research and Life Sciences Office, this work would not have been possible. Mark Provancha loaned a 1.2 Gigabyte Fujitsu disk drive that made it possible to install *sunvision* and store the images. Ray Wheeler collected the LICOR spectral radiometer data. Peggy Heeb and Larry Gross visited from Agave Analytics and worked overtime to collect the data. Mike Koller and Joe Parker have been great sources of information on computer hardware and helped get *coastal* up on the network. Peter Chetirkin and Glenn Markwell taught me how to use *grafit* to perform regression analysis. To all who answered a myriad of questions, many, many thanks.

To Bill Knott, John Sager, and Ralph Prince who were instrumental in providing this most enjoyable opportunity, I express my deepest appreciation. These two summers have been too short, but they have been fun. Thank you.

Abstract

The development of a machine vision system to monitor plant growth and health is one of three essential steps towards establishing an intelligent system capable of accurately assessing the state of a controlled, ecological life support system for long-term space travel. Besides a network of sensors, simulators are needed to predict plant features, and artificial intelligence algorithms are needed to determine the state of a plant based life support system. Multispectral machine vision and image processing can be used to sense plant features, including health and nutritional status.

Summary

Low-pass, spectral filters added to a CCD camera and digital image processing were used to sense the multispectral reflectance from potato leaves and measurements were compared to laboratory standard reflectors and to a multispectral sensor. The techniques developed for multispectral imaging satisfactorily measure leaf reflectance. The results for black and white images were well correlated to the multispectral sensor for bright surfaces, but not so well for dark ones. Full, 24-bit color images with spectral filters could be used to further explore the application of machine vision to sense plant health and nutrition status.

TABLE OF CONTENTS

LIST OF ILLUSTRATIONS

INTRODUCTION

1.1 Plants

Plants grown for food are necessary components of life support systems for long-term, manned space voyages. Current research on controlled, ecological life support systems (CELSS) has shown that plants grown in liquid cultures may rapidly develop health or nutrient problems which degrade the performance of a CELSS. If this situation were to occur on a long term voyage, it would pose a serious threat to the crew's food supply and life support system.

1.2 Sensors

Sensors which monitor plant features could be used to provide feedback to environmental controls and to the nutrient delivery system. Alarms could be activated when plant features exceed predetermined limits. Active monitoring of the plants provides positive feedback for control systems. Sensors which monitor environmental conditions (carbon dioxide, oxygen, ethylene, etc.) or nutrient concentrations are indirectly monitoring the plants and the data may be difficult to interpret. For instance, does an increase in carbon dioxide level mean the plants are fixing less carbon from the atmosphere, or that plant respiration has increased? or that respiration has increased in a bioreactor digesting inedible plant materials?

Many features of plants are sensible. Plants grow in size and change shape with age, leaves move in response to light, stems and leaves shrink and swell with water content. Root tips of healthy plants grow approximately 3 microns per minute. Plant nutrient deficiencies (Al-Abbas, *et al.*, 1974) and molds (Ruiz and Chen, 1982) have been sensed by measuring the spectral reflection of light from leaves. Stutte, Bors and Stutte, 1989, measured decreases in reflectance between 710 to 1100 nanometers 7 days before symptoms of nitrogen deficiency were visible in laboratory grown plants. Miles, 1989, used machine vision to quantify iron, nitrogen, and potassium deficiencies and water stress in wheat seedlings.

1.3 Information

The data from sensors, including machine vision, must be processed to extract desired features and to resolve conflicts between sensors. This processing provides knowledge of conditions such as severity of moisture stress and stage of growth. Miles, 1989, used a Sobel operator to detect edges of leaves, then compared the absolute and relative amounts of green in the image to determine nutrient stresses. Additional algorithms could perform operations

such as edge following to detect features such as marginal necrosis which is a symptom of potassium deficiency in wheat.

1.4 Intelligence

The ultimate use of a sensor is to provide the basis for determining the state of a CELSS: **Good**, **Bad**, or **Ugly**. When the life support system is on course, that is, conditions are **good**, nothing needs to be done. When the life support system is off course, but knows what has happened and is correcting back to course, conditions are **bad**. When the life support system has failed, or failing, that is, it is lost, then conditions are **ugly**. Classifying the CELSS into one of these states requires not only the basic data and information, but the intelligence to know where the life support system should be. This requires algorithms to distinguish features well enough to identify the source of the problem. For example, lower levels of green in a leaf image may be due to nitrogen deficiency; but is that caused by a lack of an essential nutrient in the solution feeding the plant roots, or is it due to a deficiency of oxygen to the roots (such as occurs when field crops "drown" with excess water).

Intelligence also requires a system of differential equations relating plant growth and development to environmental conditions, *ie*, a model. Such a model must be able to predict the magnitude of sensible features, thereby providing a targeted course for comparison.

One form of intelligence is an expert system such as the muskmelon disorder diagnostic system written in CLIPS, a C-based development shell (Latin, *et al.*, 1989). In such a system, rules are built in the form: IF...THEN...ELSE. When the if conditions are met, then the action is taken. The action could be to fulfil the conditions of another if statement. Ultimately the rules seemingly provide the intellect process of an expert when confronted with the same set of conditions.

1.5 Solution

Determining whether the state of a CELSS is **good**, **bad**, or **ugly** requires a three pronged effort. The first is to develop an integrated network of sensors monitoring the plants and environmental conditions. This will include but not be limited to machine vision systems. The second effort must be the development of models which predict the occurrence and magnitude of features such as leaf area, flowering, and so forth. Equations in the models may well predict other, internal (not sensible without destructive sampling) parameters, but the essential output is detectible features. The third effort is to develop an intelligent

program capable of interpreting information from the sensor network, comparing it to model predictions and assessing the state of the system. The program could be a combination of numerical simulation, expert systems, neural networks and other artificial intelligence algorithms.

This work will focus on the development of a sensor to monitor the growth, health, and nutritional status of plants.

1.6 Objectives

The objectives of this project are:

1. Develop techniques to capture and process spectral images using machine vision, and

2. Determine the relationship between the machine vision sensor and a multispectral sensor.

PROCEDURES

2.1 Plants

Norwood potatoes were grown in Chamber 5, Hanger L, at elevated levels of carbon dioxide (10000 ppm). Normal chamber lighting was provided by a combination of Vita-Lite and Daylight fluorescent bulbs. The spectrum of the incident light (Figure 1) was measured with a LICOR spectral radiometer. For half the images, an Halogen lamp was used to illuminate the potato leaf.

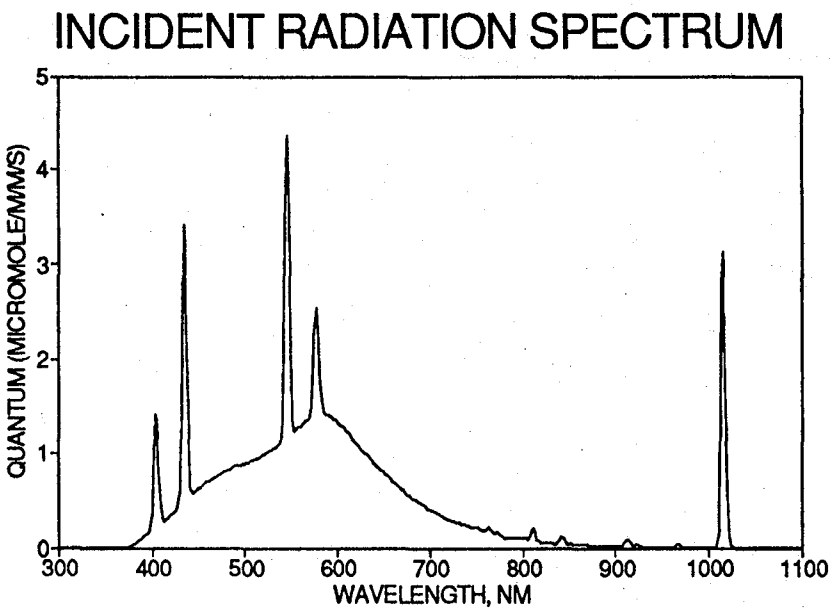

Figure 1. Incident Radiation Spectrum in Chamber Produced by Vita-Lite and Daylight Fluorescent Lights.

2.2 Machine Vision

Images of a Norwood potato leaf (Figure 2) were sensed by a Panasonic CCD camera. The VHS output of the camera was digitized by a Videopix frame grabber installed in a Sun Microsystems Sparc 2 workstation. Software supplied with the Videopix card, **vfctool**, was used to capture and store the image as an 8 bit black and

white, **tiff** file. Melles Griot 40 nanometer wide band-pass filters (450, 550 and 650 nanometers) were secured in a modified step ring and attached to the front of the camera lens to provide the filtered images. An 850 nanometer filter was tried, but the resultant image was too dark to distinguish any of the plant features, so it was not processed.

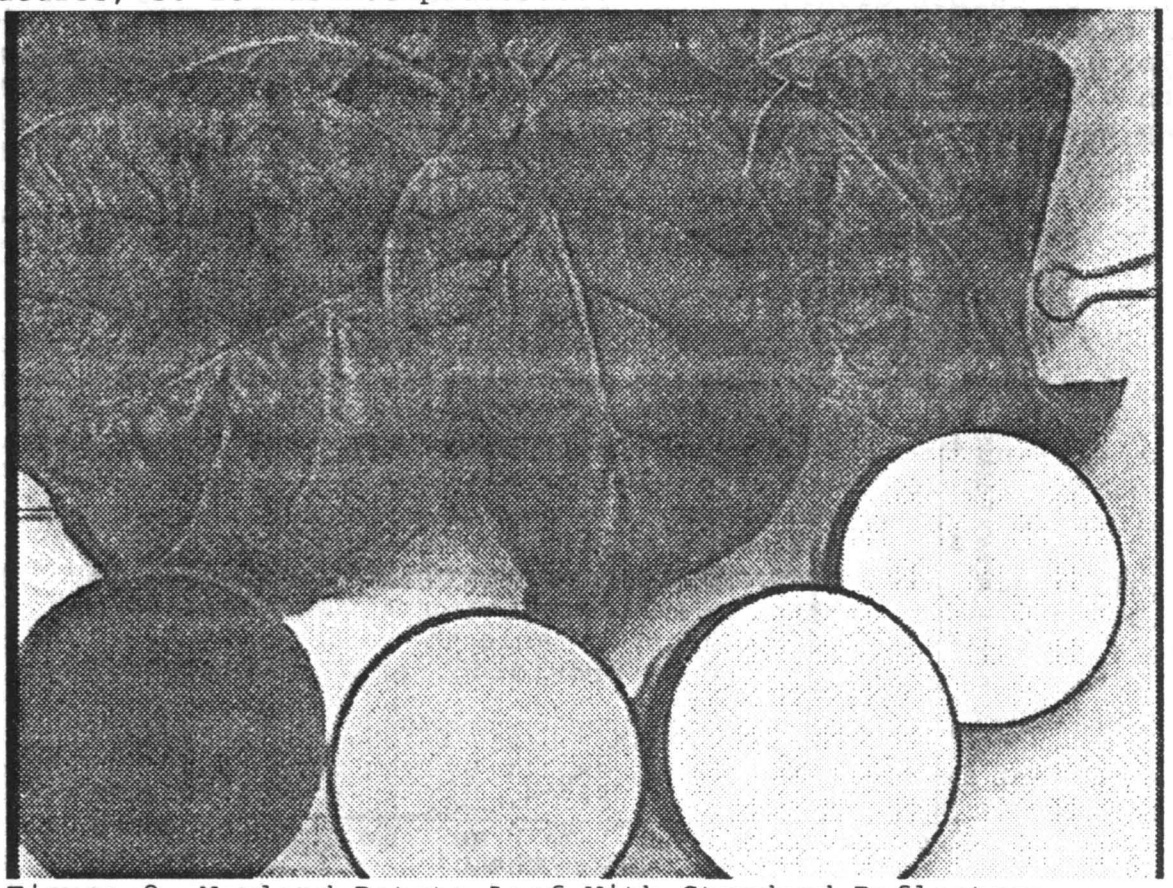

Figure 2. Norland Potato Leaf With Standard Reflectors.

Laboratory standard reflectors were placed around the leaf to provide calibration data. In Figure 2, the standards are from left to right, 2%, 25%, 75% and 100%.

After the images were captured and stored on disk, **sunvision** was used to position a window 50 x 50 pixels over each standard reflector and over the right, middle and left sections of the center potato leaf. The menu-driven **ip** software contained in **sunvision** was used to compute the maximum, minimum, median, mean and standard deviation of the gray level values in each window. Because only the 8-bit black and white image was saved (a 24-bit color image from the Videopix card requires over 900 K bytes of storage), the maximum gray level value is 255. Statistics for the left, middle and right windows of the leaf were summed and divided

by three to compute an average.

2.3 Agave Multispectral Sensor

Just before and after the machine vision data were captured, personnel from Agave Analytics used a multispectral sensor (a Spectron Model CE 390 wideband camera) to record the entire spectra of light reflected from the potato leaf and each of the standards. The results reported are the weighted average of the reflectance spectrum of the leaf over the wavelength range of the corresponding filter. The product of the reflectance of the leaf and that of the filter was summed over the wavelength ranges 401 to 501, 502 to 604, and 605 to 700 nanometers for the 450, 550, and 650 nm filters, respectively. The reflectance of the filter is actually a transmittance spectra obtained by ratioing the spectrum for the 100% standard with the filter, to the 100% standard without the filter. The *no filter* data were calculated by summing the reflectance for the leaf over the interval 401 to 700 nm with a weight factor of one, then dividing by the number of channels (102) to average.

RESULTS AND DISCUSSION

3.1 Machine Vision

Figures 3 and 4 illustrate the relationship between the average gray level values obtained by the machine vision system and the laboratory standard reflectors for the normal chamber lighting and the added Halogen light treatment. The *no filter* gray level values are universally greater than any of the filtered curves. Between 25% and 100% reflectance, the relationship appears to be linear, but the 2% reflectance values deviate considerably from the straight line model. The addition of the Halogen lamp did not increase the gray level values; in fact they decreased, for some unknown reason. The barcharts in Figures 5, 6, 7 and 8 compare the filter performance for each reflectance standard. In general, the longer wavelength filter apparently reduces the gray scale values, with the exception of the 550 filter where the values are slightly higher than the 450 and 650 ones. The filters do have a significant affect on the gray levels recorded by the machine vision system. The reflectance standard also has a significant affect on the gray scale values. The machine vision system appears to be very sensitive to the low reflectance, that is the *dark* standards. Most of the change in gray level values occur between 2% and 25% reflectance.

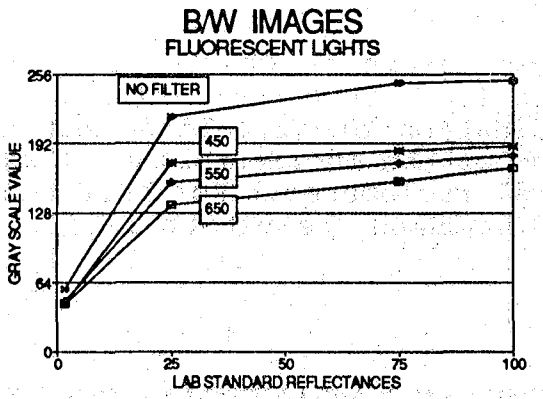

Figure 3. Machine Vision Measurement of Standard Reflectors with Fluorescent Lights.

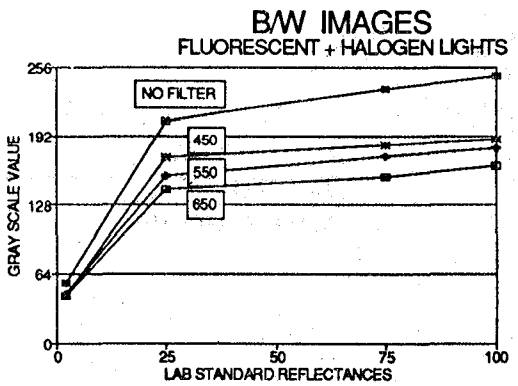

Figure 4. Machine Vision Measurement of Standard Reflectors with Fluorescent and Halogen Lights.

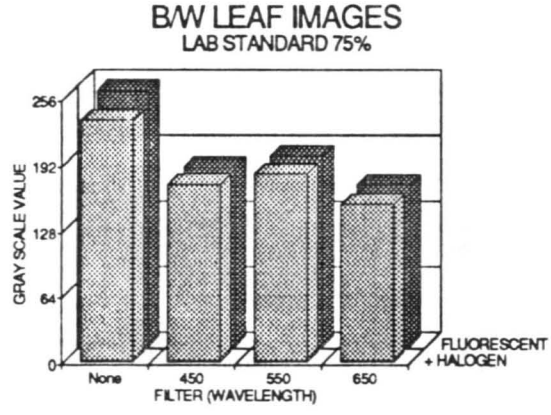

Figure 5. Machine Vision Measurement of 75% Reflector.

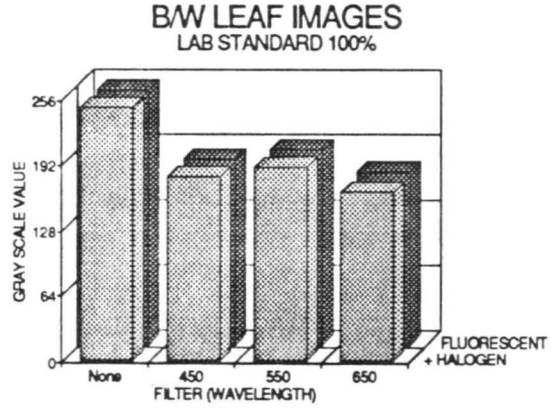

Figure 6. Machine Vision Measurements of 100% Reflector.

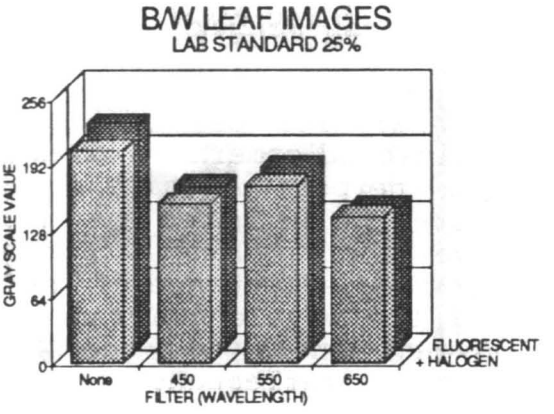

Figure 7. Machine Vision Measurement of 25% Reflector.

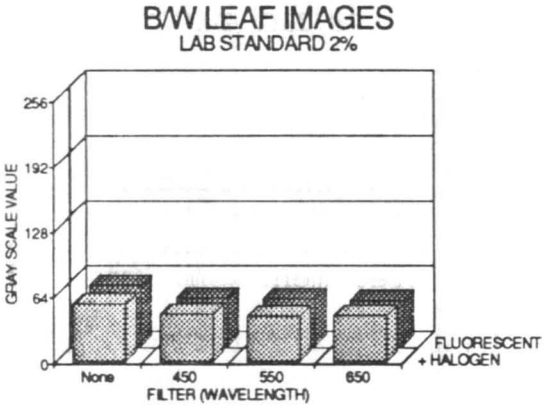

Figure 8. Machine Vision Measurement of 2% Reflector.

Figures 9 and 10 present the gray scale reflectors for the potato leaf. In general, the values are much less than the standards, and indicate the leaf reflects approximately 25% as much as the *white* reflectance. The middle window of the leaf has slightly higher gray scale values than the left or right windows, possibly because it contains the midrib. When Halogen light is added, the difference between the middle and sides is even greater. This may mean that differences in the reflectance of light in the near infrared region may be a means of identifying the midrib feature in machine vision images of potato leaves. For the purposes of this study, the differences were considered small, and an overall leaf average used in the remaining comparisons. Figure 11 compares all the reflectance standards to the leaf for the *no filter* treatment. From this figure it is apparent that leaf reflectance is between the 2% and 25% standards.

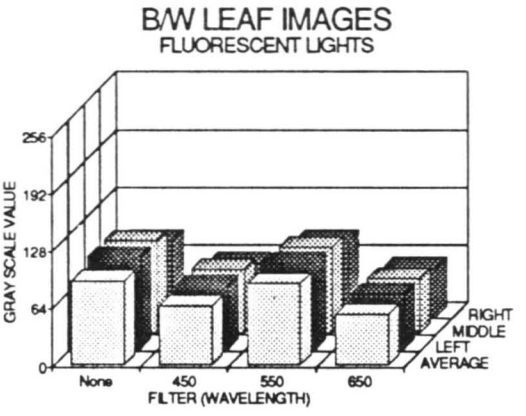

Figure 9. Machine Vision Measurement of Potato Leaf with Fluorescent Lights.

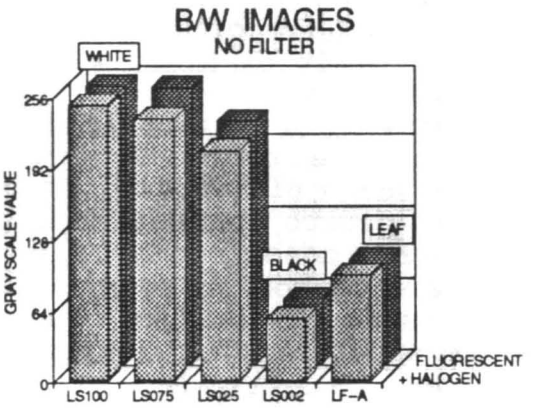

Figure 10. Summary of Machine Vision Measurements without a Filter.

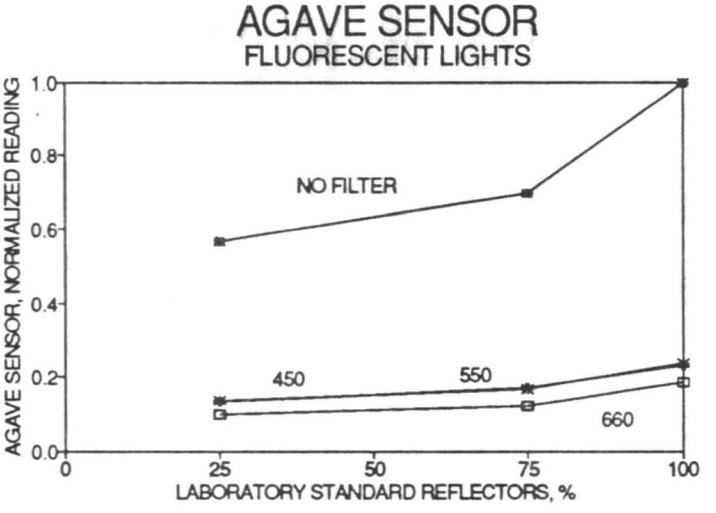

Figure 11. AGAVE Multispectral Sensor Measurement of Standard Reflectors with Fluorescent Lights.

3.2 Agave Multispectral Sensor

Figures 12 and 13 contain the results for the Agave multispectral sensor measurements of the standard reflectance surfaces. The *no filter* readings are significantly higher than the filtered treatment readings. The 450 and 550 nm readings are practically identical to each other. The Halogen light did not add much to the readings. From 25% to 100% reflectance, the multispectral readings increase, but in a nonlinear fashion.

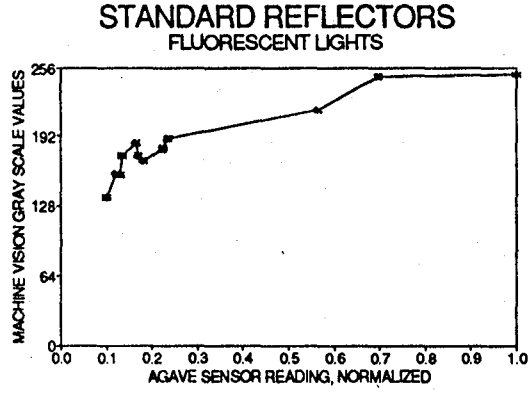

Figure 12. Machine Vision versus Multispectral Sensor Measurement of Standard Reflectors with Fluorescent Lights.

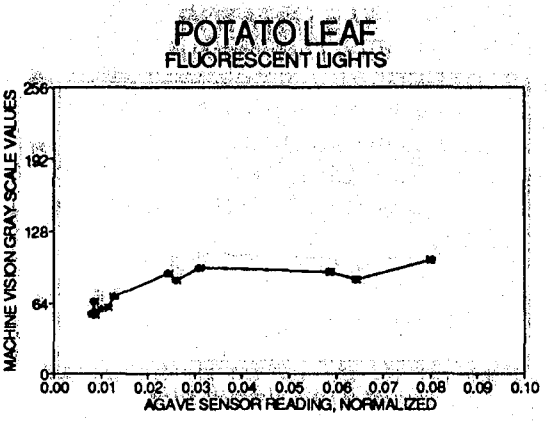

Figure 13. Machine Vision versus Multispectral Sensor Measurement of Norland Potato Leaf with Fluorescent Light.

3.3 Machine Vision versus Multispectral Sensor

Figures 14 and 15 compare the machine vision gray scale values to the readings obtained from the multispectral sensor for the standard reflectors. For multispectral readings above .3, there appears to be a strong, positive correlation. However, below that point, there are some disturbing variations. Equations 1 and 2 have R^2 values greater than 0.92, but most of the variance is at the low readings of the multispectral sensor.

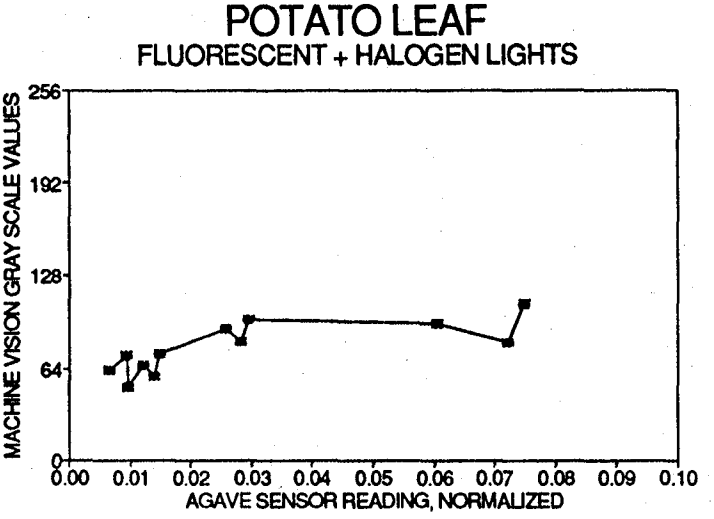

Figure 14. Machine Vision versus Multispectral Sensor Measurement of Norland Potato Leaf with Fluorescent and Halogen Lights.

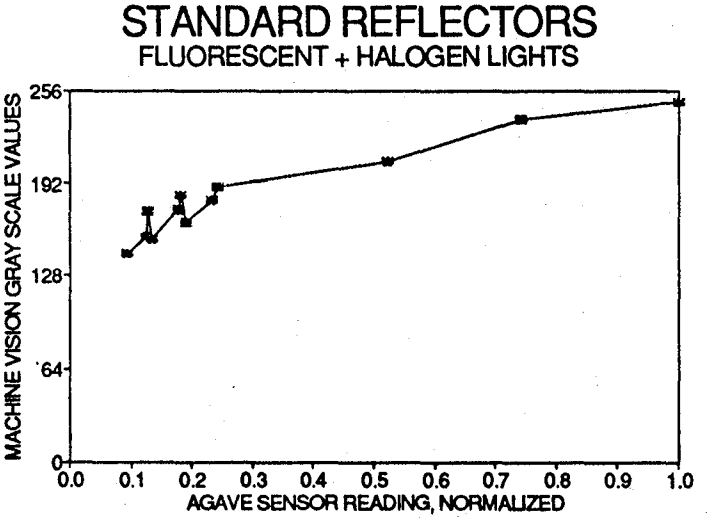

Figure 15. Machine Vision versus Multispectral Sensor Measurement of Standard Reflectors with Fluorescent and Halogen Lights.

$$Y=-135.51X^2+253.16X+130.94, R^2=0.92$$

$$Y=-87.13X^2+196.21X+137.15, R^2=0.93$$

That's the range of leaf readings, as seen in Figures 16 and 17. The scales of these two figures have been changed to illuminate any relationship. It does not appear that the relationship between the machine vision sensor and the multispectral sensor is strongly correlated for leaf reflectors. Equations 3 and 4 have R^2 values of .8 or less.

$$Y=-0.0001753X^2+0.001942X+46.51, R^2=0.70$$

$$Y=-0.0001558X^2+0.001827X+45.5, R^2=0.80$$

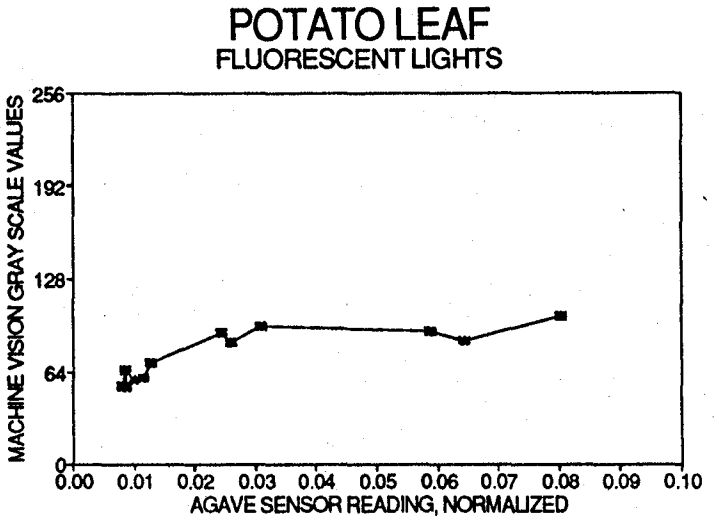

Figure 16. Machine Vision versus Multispectral Sensor Measurement of Norland Potato Leaf with Fluorescent Light.

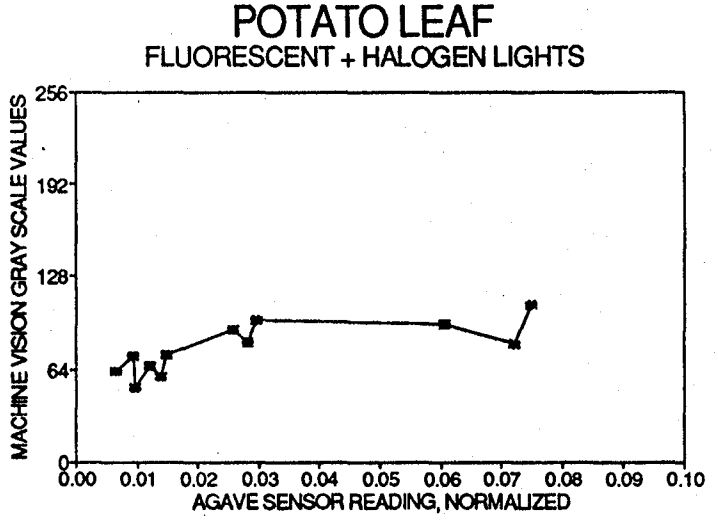

Figure 17. Machine Vision versus Multispectral Sensor Measurement of Norland Potato Leaf with Fluorescent and Halogen Lights.

CONCLUSIONS

The process of digitizing images with a Videopix card, then windowing and analyzing portions of the image using *sunvision* appears to satisfy the first objective. The C callable image processing library available with *sunvision* makes it attractive for use with CLIPS or other C-based expert system shell. Using narrow, band-pass optical filters proved successful for wavelengths less than 850 nanometers.

The machine vision gray scale values and the Agave multispectral sensor appear to correlate well for highly reflective surfaces, but not so well for lower reflectors, which include leaves. The differences in these sensors must be resolved before proceeding with the development of a machine vision sensor for monitoring the health and nutritional status of plants. Factors which may have contributed to differences included the lack of precise control over field of view and view angle for both sensors, and the fact that the multispectral sensor reading for each wavelength was computed for a band of approximately 50 nanometers either side of the central wavelength. The optical, bandpass filters used for the machine vision system have significant attentuation beyond 20 nanometers either side of the center wavelength. The difference caused by the angle of view can be seen in the potato leaves shown in Figure 2. This indicates that a laser or other structured light source will be required to determine the three-dimensional leaf surface, and thereby enable the sensor to be positioned normal to the surface. Further studies are necessary to quantify the differences due to view angle and to devise means of controlling view angle.

The results reported here were based on black and white images. There is considerable merit in exploring the use of the red, green, and blue planes of a color image. The videopix image digitizer, the Panasonic CCD camera, and *sunvision* software are capable of color image processing and further research with this system is urged.

REFERENCES

1. Al-Abbas, A. H., R. Barr, J. D. Hall, F. L. Crane, and M. F. Baumgardner. Spectra of Normal and Nutrient-Deficient Maize Leaves. Agronomy Journal. Vol. 66. Jan-Feb pp 16-20.

2. Ruiz, Margarita and Pictiaw Chen. Use of the First Derivative of Spectral Reflectance to Detect Mold on Tomatoes. Transactions of the ASAE. 1982. Vol 25 No 3 pp 759-762.

3. Stutte, G. W., R. Bors, and C. A. Stutte. Quantification of Nutrient Stress from Video Images. Horticultural Science. 1989. Vol 24. p. 75.

4. Miles, Gaines E. Plant Features Measurements for Robotics. NASA/ASEE Summer Faculty Fellowship Program. Kennedy Space Center Florida. 1989. 22p.

5. Latin, R. X., G. E. Miles, J. C. Rettinger, and J. R. Mitchell. An Expert System for Diagnosing Muskmelon Disorders. Plant Disease. 1990. Vol 74. No 1. pp 83-87.

1991 NASA/ASEE SUMMER FACULTY FELLOWSHIP PROGRAM

JOHN F. KENNEDY SPACE CENTER
UNIVERSITY OF CENTRAL FLORIDA

KATE'S MODEL VERIFICATION TOOLS

PREPARED BY:	Steve Morgan, Ph.D., P.E.
ACADEMIC RANK:	Associate Professor
UNIVERSITY AND DEPARTMENT:	Baylor University Department of Engineering and Computer Science
NASA/KSC	
DIVISION:	Engineering Development Laboratories
BRANCH:	Artificial Intelligence Laboratory
NASA COLLEAGUE:	Carrie Parrish, Ph.D.
DATE:	August 9, 1991
CONTRACT NUMBER:	University of Central Florida NASA-NGT-60002 Supplement: 6

Acknowledgements

Thank you, Carrie Parrish, for helping define and execute the Model Verification Tools project this summer. Thanks especially to four of KATE's modelers, Charlie, Goodrich, Bob Merchant, Steve Beltz, and Scott Budzowski, for telling how models evolve, what tools they use, and what tools they need. Thanks to NASA's Mark Beymer and Dennis Armstrong, and to UCF's Ray Hosler for making the NASA/ASEE Summer Faculty Fellowship Program possible.

Abstract

Kennedy Space Center's Knowledge-based Autonomous Test Engineer (KATE) is capable of monitoring electromechanical systems, diagnosing their errors, and even repairing them when they crash. A survey of KATE's developer/modelers revealed that they were already using a sophisticated set of productivity enhancing tools. They did request five more, however, and those make up the body of this report. Inside is the tested code of their new: 1) transfer function curve fitter and 2) Fortran-Lisp translator. 3) To aid in syntax checking their modeled device frames, three existing structural consistency checkers are also documented here. 4) An automated procedure for calibrating knowledge base admittances is designed here to protect KATE's hardware mockups from inadvertent hand valve twiddling. 5) And three alternatives are described for the "pseudo object," a programming patch that currently apprises KATE's modeled devices of their operational environments.

Summary

When KATE's modelers revealed their need of five new productivity aids this summer, I set about the task of creating them. They now have a new Lisp program that fits straight lines or exponential curves to random time functions, and another that translates transfer functions written in Fortran into Lisp's stilted prefix format. When I started to streamline their favorite syntax checker, I discovered that some modelers already had what others needed, so I ended up documenting three existing checkers instead. Guided by a modeler whose hardware mockup keeps changing, I designed a control procedure by which KATE automatically recalibrates admittances in his knowledge base. An essential programming patch that the modelers call a "pseudo object" hasn't fit neatly into either KATE's knowledge bases or her shell. Three alternatives are offered here. Solving modeled fluid dynamics equations off-line could provide KATE the necessary flow time functions when she needs them. If these complicated equations must be reconfigured and solved on-line, a signal processing analog computer model offers a fast way of doing it. Modeling KATE's devices as Thevenin's equivalent two-port networks could enable each object to reveal its remote environment (much as a transformer reflects its load resistance to its input) without the need of extra pseudo objects or equation solving. KATE is about to get a much needed pass through the Software Development Life Cycle as part of her forthcoming translation to the C language.

Table of Contents

LIST OF ILLUSTRATIONS

LIST OF TABLES

I
INTRODUCTION

1.1 KATE

Kennedy Space Center's Knowledge-based Autonomous Test Engineer (KATE) mimics human engineers as they test and repair electromechanical systems. Working in KSC's Artificial Intelligence Laboratory, KATE's modelers painstakingly create software simulations of the hardware that KATE monitors. (KATE's models typically take on an appearance like that shown in Figure 1-1.) KATE later delivers the same inputs to this software model that the hardware sees, and she compares their outputs. Showing complete confidence in her software, she blames the hardware for any deviations in modeled and actual outputs. Her diagnoser then experimentally fails selected software "devices" in an effort to duplicate the deviant hardware outputs. Thus KATE is able to isolate the one failed device that is responsible for the errors. She may then advise her user to bring up a redundant device, or she may make the repair herself, if the user has seen fit to give her that much control ahead of time. Lately, users have not seen fit to give her that much control in her only production application, the shuttle's liquid oxygen tanking operation. In fact, firing room personnel are unwilling to hear KATE's advice when real problems arise. NASA is conservative. Systems must log hundreds of hours of trouble-free service or show some sort of quality assurance pedigree before being placed in a critical position. KATE is not there yet.

1.2 KATE'S MODEL VERIFICATION TOOLS

Like all Knowledge Base Engineers, KATE's model builders have difficulty mixing human-like reasoning with computer speed and thoroughness in their software product. My job this summer has been make those modelers more productive, so that KATE's models may go forth and multiply throughout KSC. I became intimately acquainted with KATE by observing her modelers and streamlining their tools. I coded two new tools for them from scratch in Symbolics ZMACS Lisp. Also intending to enhance the code of an existing syntax checker, I ended up documenting three modelers' favorite checkers for use by all. I also designed an automated calibration procedure for one of KATE's knowledge bases, and I offered three design alternatives to KATE's philosophically awkward "pseudo object." Though not immediately executable, these designs helped train me for next summer's project, and they may well provide proposal content for some productivity enhancing projects this fall.

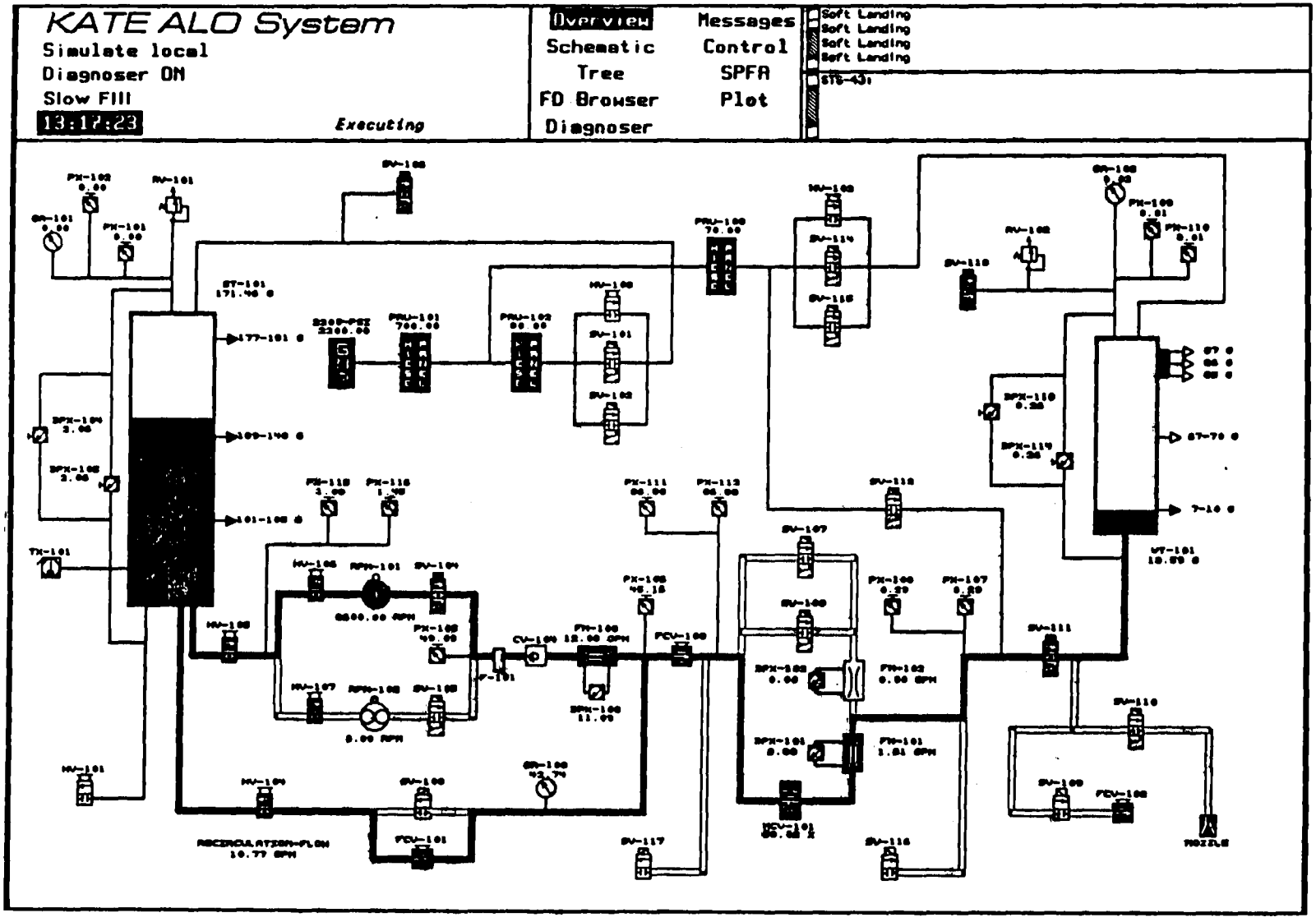

Figure 1-1. KATE's Overview Screen (ALO Model).

II
BUILDING KATE'S MODELS

2.1 KATE'S CURRENT APPLICATIONS

KATE's most visible application today is LOX, her shuttle liquid oxygen tanking advisor. (KATE does not actually advise firing room personnel, but she is tested as if she were advising them on every shuttle launch.) With 1000 to 1500 device frames in her knowledge base and 50- to 75-thousand lines of Lisp code in her shell, KATE's LOX model is as complicated as her models will likely ever get. Figure 1-1 shows LOX (actually this is a schematic overview of another very similar KATE model) to be essentially a cryogenic fluid dynamics model, with a large number of sensors and actuators. Because the oxygen tanking equipment is critical to any launch, failed devices in it can be replaced quickly by bringing up standby pumps, valves, and sensors along redundant pathways.

A variety of KATE's earlier feasibility demonstrations can be found around KSC. An air purge system with redundant air compressors and power supplies introduced the new-born KATE to KSC about eight years ago. A mockup of the Space Station's Environmental Control System (fully equipped with heaters, blowers, and temperature sensors) is attached to KATE's ECS model. A Launch Processing System mockup (called "LPS" and "The Little Red Wagon," because it is mounted on a heavy red cart) is attached to a TI Lisp machine version of KATE. KATE has been translated into ADA, Common Lisp for the IBM PC, a generic version for quickly prototyping new models, and it will soon be translated into C for the IBM PC (more on KATE's future later).

KATE's Autonomous Launch Operations (ALO) application suggests her intended future. Created to supervise unmanned Air Force launches, the ALO model features goal-directed control and unsupervised repair. A hardware mockup at KSC's Launch Equipment Test Facility has demonstrated KATE's ability to complete all 12 LOX tanking procedure steps typically pursued by shuttle firing room personnel, even when devices fail. Water in the hardware mockup will be replaced with liquid nitrogen in a forthcoming demonstration. (Liquid oxygen is not used for obvious safety reasons.) The ALO-H20 model now includes some 472 frames, and the number grows with each requirement for greater modeling precision.

2.2 THE MODEL BUILDING PROCESS

Developing a new application consists of building a software model of the hardware that KATE is to monitor, and then improving it until it works. The model builder usually gets started by studying a ten-pound stack of printed schematic diagrams (see Figure 2-1). He draws fault trees of the devices he sees there to appreciate the impact of every device failure upon the whole model. Finally he types a Lisp frame into the Symbolics ZMACS editor for every device that can fail, every input, and every measurement. The frames look like database records, in which named slots describe every aspect of the part and its connections to other parts [1]. Coding a device transfer function can be as

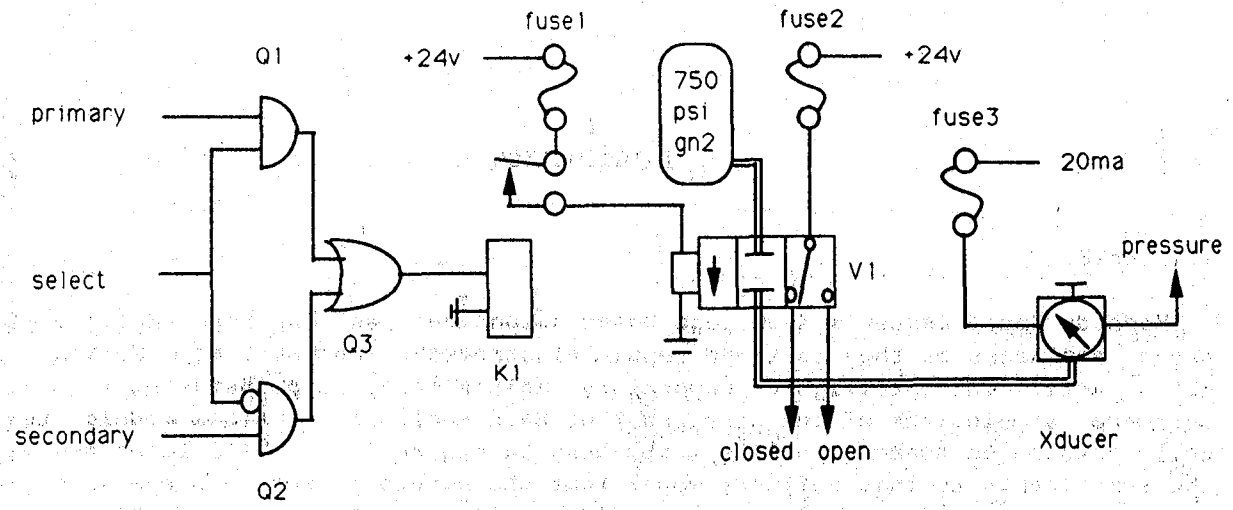

(a)

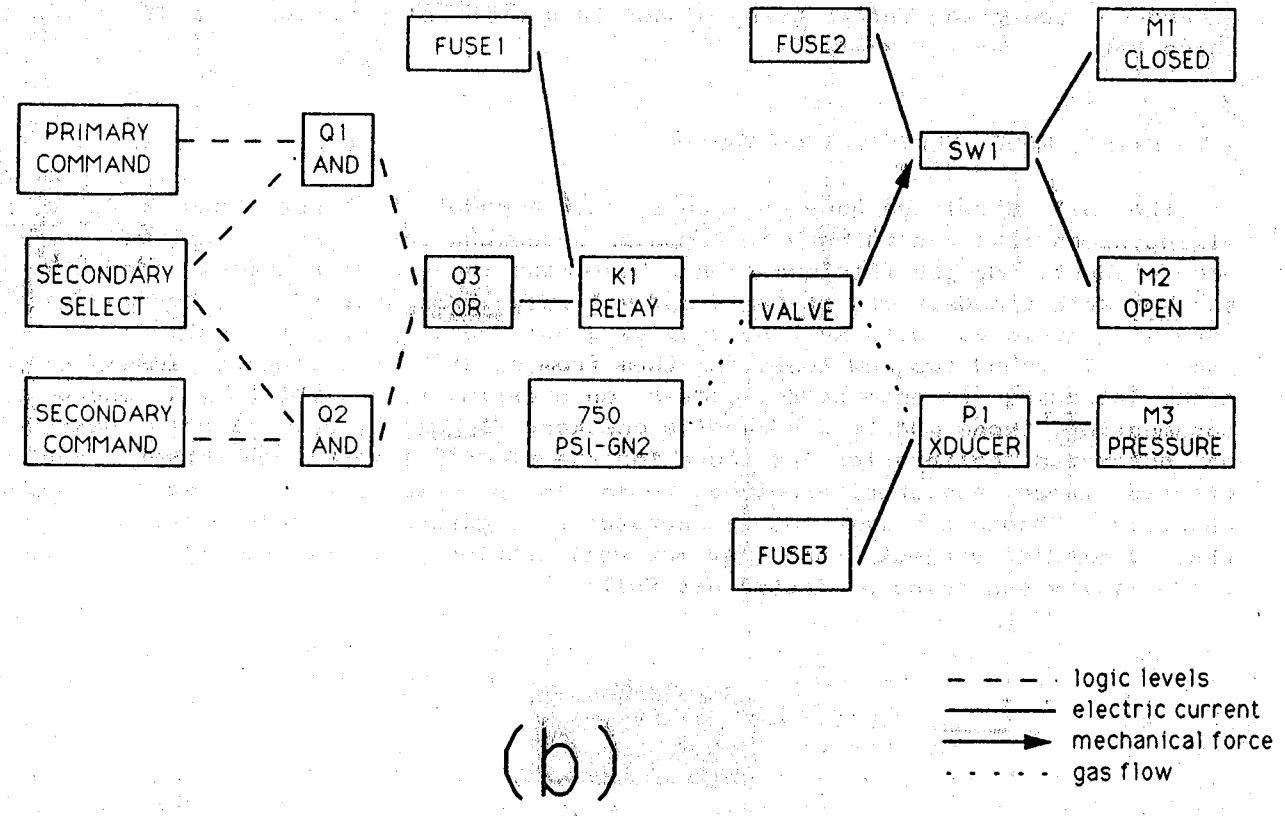

(b)

Figure 2-1. KATE's model building process.

simple as transcribing a pressure/flow curve off a printed pump specification or very complicated indeed. Its original electronic designer may have drawn a hardware controller as a tangled feedback network of filters and amplifiers. Ten years later, the KATE modeler is compelled to Lisp-code the simplest possible transfer function for the controller, considered as a single line-replaceable unit.

Before KATE executes a model the first time, the modeler tries to remove frame errors that are obvious by inspection (white box testing) but would be very hard to isolate during execution (black box testing). Automated structural consistency checkers find or repair simple frame syntax errors (e.g., frame A outputs to frame B, but B does not input from A). They may also identify frames that have not been coded yet. Subtle semantic errors (e.g., relays do not accept input from water pipes) generally are obvious in a visual inspection of KATE-generated schematics.

When the frames all look pretty, verification testing begins. The first time KATE runs a new model, actual (hardware) measurements often deviate from modeled values, and KATE blames innocent hardware devices for errors in the model. KATE's diagnoser thus functions as a system-level model verification tester. Taking a closer look at the offending measurement, the modeler often finds a variety of transfer function errors. He may have assumed the wrong time constant in an exponential decay. Perhaps he failed to consider the affect of ullage (the air above the fluid) pressure that impedes flow into a tank. In his zeal to model very accurately, he may have modeled quantizing error that appeared on a prior launch data broadcast. (It has happened!) In the latter stages of knowledge base development, subtle timing errors sometimes occupy the modeler. For example, KATE must guess when firing room personnel transition from stage to stage in the LOX filling procedure (e.g., nobody tells KATE when fast fill ceases and slow fill begins), and her ways of dealing with these ambiguities can be obscure.

2.3 MODEL BUILDERS' PROBLEMS

KATE's developer/modelers face problems that range from clerical to very sophisticated. (See modelers' testimonies in Appendix A.) Typing frames into the LISP machine ZMACS editor is tedious, compared with using an interactive-graphics Computer-Aided Design terminal. It is difficult to write the equations of lines that approximate random time functions. It is just as difficult to recode Fortran transfer functions in Lisp without a few errors, even for bilingual programmers. Thousand-frame knowledge bases often start out full of syntax errors. The structural consistency checkers used to find these errors never find them all. Modelers that use hardware mockups need to recalibrate admittances in their knowledge bases each time valves on the mockup change. When computing input pressure of a device, a modeler sometimes needs more information than the device model can provide (e.g., upstream driving pressure and downstream back pressure in its external environment). That may lead him to create a "pseudo object," having no structural relationship with modeled devices and no relationship with generic objects in KATE's shell either (because it is application-specific). KATE's modelers have invented "soft landing," which

wiggles all modeled measurements to ease the pain of errors that the modeler considers tolerable, and "external influence," which accounts for measurement trends arising outside the declared model domain. With each shuttle launch KATE shows her developers a few new errors, and her design or code changes a little to accommodate an unforeseen operational condition.

III
KATE'S MODEL VERIFICATION TOOLS

3.1 MODEL VERIFICATION PERSPECTIVE

Someday, KATE's very graphical Knowledge Base Editor will make creating frames easy even for the novice end user. Like a CAD terminal, the editor provides a library of device icons that can be picked and placed, moved and interconnected without ever touching the keyboard. Most knowledge about a device will be supplied by the editor. If desired, the user can modify default transfer functions, time delays, units, etc. at the keyboard via a database-like fill-in-the-blanks editor interface. KATE's Model Verification Tools are that part of her Knowledge Base Editor that helps find errors in completed knowledge bases.

Today, KATE's Model Verification Tools already are used to find errors in completed knowledge base frames that are typed in manually using Symbolics' ZMACS editor. (See Appendix A for the details.) Structural consistency checkers find simple frame syntax errors. A family of interactive plotters clarify troublesome deviations in actual and modeled time functions. KATE's overview, schematic, and fault tree graphic displays clarify frame mismatch errors.

Cleverly conceived as KATE's Model Verification Tools are, her modelers agree that a few good tools are missing. More insightful frame syntax checkers are always needed. Coding transfer functions would be much easier if a curve fitter could recite the equations of straight line and exponential plotted data. And careless errors could be prevented if a program could convert transfer functions from familiar algebraic (infix) notation into Lisp's stilted prefix notation. Tedious calibration of KATE's ALO-H2O knowledge base admittances (which happens frequently) should be automated. Clever as KATE's pseudo objects may be, they do not fit well into either her application-specific knowledge bases nor her generic shell. Solutions are offered for all of these model verification tool problems below. They range from executable code to proposal-ready design to white papers on a better pseudo object.

3.2 LEAST-SQUARES CURVE FITTER

Modelers frequently need a transfer function equation that mimics a plotted measurement time function. Though random variables, the time functions generally are approximately straight lines or exponentials that rise or fall toward some asymptote. Symbolics' Genera 8.1 operating system fits least-squares straight lines to plotted random variables, but it does not reveal their equations. KATE's modelers need a least-squares curve fitter with an optional capability of taking the log of its time coordinates.

Such a program appears in Appendix B [2]. Given two lists of x and y coordinates, it returns three parameters: the slope, the y-axis intercept, and the sample correlation coefficient of the given points. First the program computes means, variances, and covariances of all of the x and y coordinates:

$$Xmean = (x1 + \ldots + xn) / n,$$

$$Xvar = (x1^2 + \ldots + xn^2) / n,$$

$$XYcovar = (x1 * y1 + \ldots + xn * yn) / n.$$

The equation of the least-squares line, $y = a + b\,x$, is then defined by the slope,

$$b = \frac{XYcovar - Xmean * Ymean}{Xvar - Xmean^2},$$

the y-axis intercept,

$$a = Ymean - b * Xmean.$$

The sample correlation coefficient,

$$r = \frac{XYcovar - Xmean * Ymean}{SQRT(Xvar - Xmean^2) * SQRT(Yvar - Ymean^2)},$$

approaches 100% when the straight line fits the data well or falls below 80% when it fits poorly.

No design diagram is attached to this program, which is obviously crafted to be more readable than efficient. Abelson and Sussman [3] contend that Lisp is so powerful that it may be used as a design language to describe Lisp code. Especially in cases like this one, where control flow is obvious, carefully crafted Lisp can be almost English-like. To the simple test cases for this curve fitter, its modeler-customer (Scott Budzowski) added a graphical output. He composed this enhancement at the keyboard, testing each module as he completed it, in about 10 minutes -- it was a lot of fun to watch.

3.3 FORTRAN-TO-LISP TRANSFER FUNCTION TRANSLATOR

Most good Lispers can translate a device transfer function from ordinary algebraic (infix) notation,

```
p_out = pump_coef * rpm ^ 2 / max_rpms_squared,
```

into Lisp's prefix notation,

```
(setq p_out (* pump_coef (/ (square rpm) max_rpms_squared))),
```

with very few careless errors. But KATE's targeted end users are not Lispers. They are ordinary Electrical Engineering graduates whose first computer language is Fortran. Both KATE's AI Lab developers and her end users can benefit from a

tool that translates functions from infix (algebraic, Fortran) to prefix (Lisp) notation.

Such a translator appears in Appendix C. The simple first version insists that binary operators be in the middle of three-item lists. (It also accepts unary operators in two-item lists.) This list length constraint frees it from having to handle operator precedence (e.g., multiplying before adding in w + x * y), but it forces the user to add a lot of parentheses to a valid Fortran function. The modeler that requested this program thought this burden too great.

The more complicated second translator in Appendix C handles operator precedence very nicely, allowing the user to string any number of operations together in each parenthetical expression. Taken from Winston and Horn's LISP textbook [4], this more complicated version does not handle unary operators gracefully. They must be made to look like binary operators by adding a nil to their lists before translation, and removing the nil after translation.

A Warnier-Orr Data Structured System Design Diagram precedes the second program's Lisp code as documentation. The design shows in plain English that the translator is fiercely recursive; in fact, it hard to follow without a design. Designing code makes it readable to its coder and other code auditors, such as module test engineers, and thus makes code more error free and reliable. The several test cases attached to the translator complete its documentation package, further enhancing its reliability by demonstrating its capabilities and limitations. Sound configuration management requires that design and test data be attached to every coded module in a production software system.

3.4 A BETTER STRUCTURAL CONSISTENCY CHECKER

Perhaps the reader can tell from the survey in Appendix A that a structural consistency (i.e., frame syntax) checker means several different things to several different modelers. Bob prefers to repair his errors one category at a time, so he needs a syntax checker that can be modified to check one frame slot at a time. Charlie's syntax checker keeps him apprised of what frames remain to be coded in his evolving knowledge base, so he doesn't care which slot it checks. Steve wants to be told about as many kinds of syntax errors as possible in his complete and almost perfect knowledge base, with a minimum of user interaction. Mark wants his Mondo syntax checker to quietly fix the errors it finds.

Initially, I understood that KATE's consistency checking file contained just two programs. Mondo-Consistency-Checker repairs five kinds of syntax errors (see Table 3-1), and wimpy but modifiable Check-KB points out all syntax errors of one kind. Most modelers wanted the greater power of Mondo, but without its repair feature, which tended to add unpredictable errors to their already fragile knowledge bases. Intent upon defanging Mondo to satisfy the needs of all, I first drew a module hierarchy chart to document its performance (see Figure 3-1). As I drew, I discovered a third program, Check-All-Frames, which is much more powerful (see Table 3-1 again) than the other two but dusty from disuse. I ended up documenting all three of KATE's unmodified syntax checkers to better serve the diverse needs of KATE's several modelers.

TABLE 3-1. What KATE's Structural Consistency Checkers Test.

CHECK-KB tests only instance-level frames for input/output reciprocity (now):

instance-level frame A	<===>	instance-level frame B
inputs slot: B	<===>	outputs slot: A

MONDO-CONSISTENCY-CHECKER repairs 4 kinds of reciprocal frame references:

top-level frame D	<===>	mid-level frame C
kinds slot: C	<===>	ako slot: D
mid-level frame B	<===>	instance-level frame B
instances slot: A	<===>	aio slot: B
mid-level frame F	<===>	instance-level frame E
parts slot: E	<===>	apo slot: F
instance-level frame G	<===>	instance-level frame H
draw-connects slot: H	<===>	draw-connects slot: G

CHECK-ALL-FRAMES tests frames for the following (optionally interactively):

Top-level Frames:
1. Does a parts, apo, instances, or aio slot accidentally appear here?

Mid-level Frames:
2. Wrong type of input or icon name (e.g., numeric)?
3. Is outputs, output-functions, or units slot missing?
4. Is any of these missing its value?
5. Is an output referred to in an output-functions, units, tolerance, or delay slot not defined in this frame's outputs slot?

Instance Frames:
6. Wrong type of input or output name?
7. Icon plotting coordinates missing or not in (system x y) form?

All Frames:
8. Is it not a frame?
9. No slots?
10. Is a slot empty?
11. Is nomenclature missing?
12. Slots of an unknown type?

Does that frame referred to in a slot of the type below not refer back?

13.	top-level kinds slot	<===>	mid-level ako slot
14.	mid-level instances slot	<===>	instance-level aio slot
15.	mid/instance-level input slot	<===>	mid/instance-level output slot
16.	instance-level parts slot	<===>	instance-level apo slot
17.	instance-level draw-connects	<===>	instance-level draw-connects

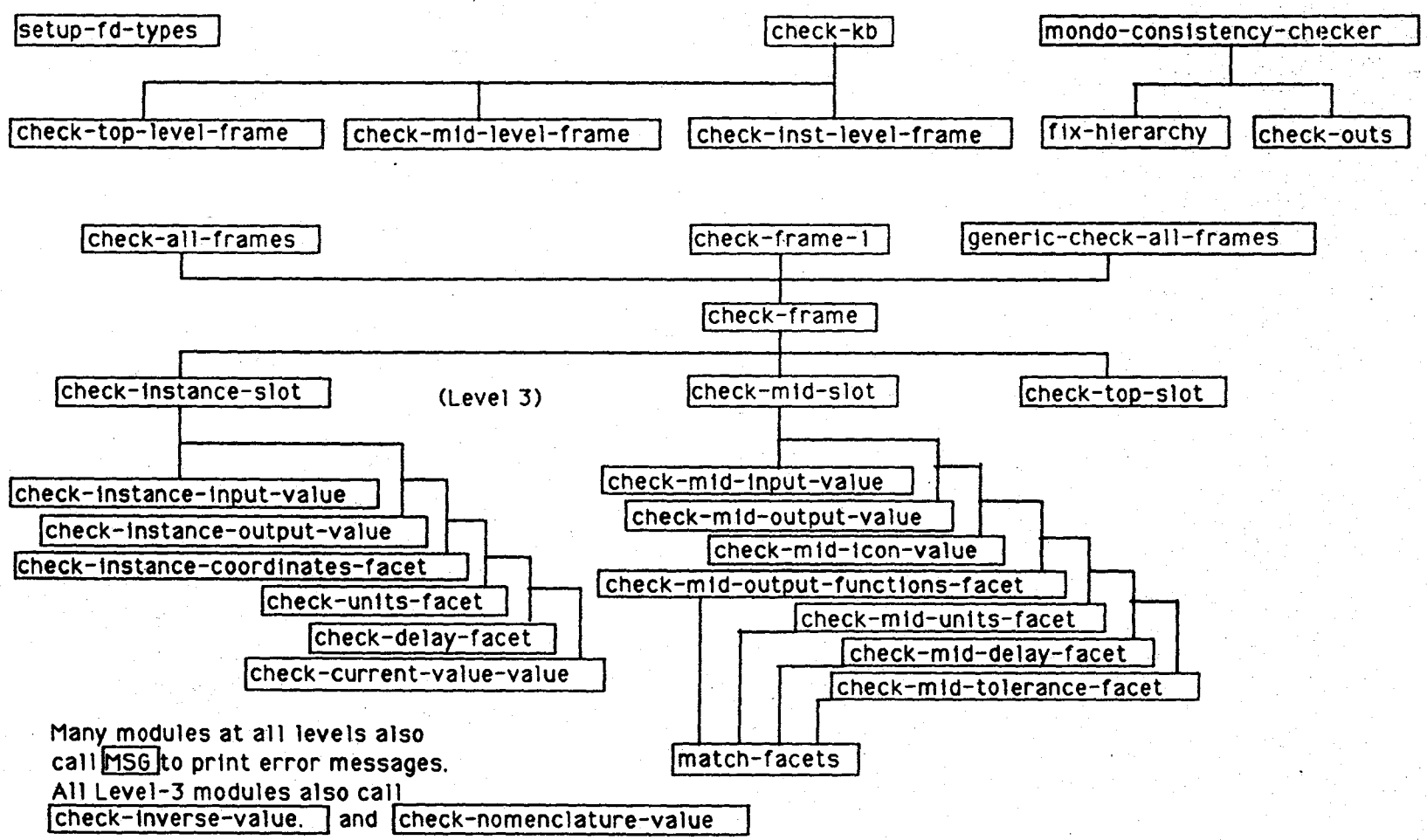

Figure 3-1. Consistency Checking file hierarchy chart.

Mondo's typical printout appears in Figure 3-2a. It counts five kinds of errors (printing the tallies on the terminal screen), and repairs them, but does not point them out to the user. As such, it is less of a tester more of a compiler, accepting a mere skeleton of the intended frames and producing a working knowledge base. Changes Mondo makes in the knowledge base are not permanent, and the original knowledge base can be reloaded over the repaired one if desired.

Check-KB's typical printout appears in Figure 3-2b. It points out syntax errors so that the user can correct them himself (and learn not to make the same mistakes next time). Changing just a line or two of code in Check-KB redirects its attention to any slot of interest in the frames being tested. Check-KB's printout is often lengthy, so it is written to file KB-LISTING instead of the user's screen. Its input nominally comes from file ALO-KB>ALO-H20. Both file names can be readily changed, of course, by modifying its Lisp code.

Written in 1988 for an earlier version of KATE, Check-All-Frames apparently doesn't work at all now. But its ability to point out 32 different kinds of frame syntax errors piques many modelers' interests. (See Table 3-1 and Parrish' dissertation [5] for more detailed documentation.) Upgrading Check-All-Frames to work with today's KATE would really pay premiums in modelers' productivity, and it should be considered in any future KATE contract negotiations. When it is ready, the test plan of Appendix D will verify its performance. KATE's configuration managers should keep a closer eye on such powerful modeling tools in the future and prevent their obsolescence.

3.5 AUTOMATED ADMITTANCE MEASUREMENT

Workmen frequently upset KATE's ALO-H20 model by adjusting hand valves in its hardware mockup. When actual admittances disagree with modeled admittances in her knowledge base, KATE's simulated pressures and flows differ from those in the real world, and she blames a hardware device failure. Minor admittance differences can lead KATE to make subtle reasoning errors that cost her modeler significant debugging effort. After discovering the source of these obscure errors, he still has to manual remeasure valve admittances and edit them into the knowledge base. KATE's ALO-H20 modeler needs a way of automatically calibrating these frame admittances before every demonstration.

KATE's control facility can set up the solenoid valves in the ALO-H20 hardware mockup in configurations that enable measuring key flows and pressures. Then KATE can use these pressures and flows to calculate all admittances in the knowledge base automatically.

The test procedure in Appendix E enables KATE to discover all 22 admittances (see Table 3-2 and Figure 3-3 for their definitions) that appear in the ALO-H20 knowledge base frames. It can be executed as a control procedure (see similar examples in the knowledge base file G:>KATE>ALO-KB>CONTROL-PROCEDURES) before each run of the model. The admittances Gm, Gn, and Gp must be updated for every procedure during model execution, since they depend upon valve positions. Pump

```
Placing ITERATE-IT into an inversion slot!
Placing ITERATE-IT into an inversion slot!
Placing ITERATE-IT into an inversion slot!
Placing ITERATE-IT into an inversion slot!
Placing ITERATE-IT into an inversion slot!
Placing ITERATE-IT into an inversion slot!
Placing ITERATE-IT into an inversion slot!
Placing ITERATE-IT into an inversion slot!
Placing ITERATE-IT into an inversion slot!
Placing ITERATE-IT into an inversion slot!
Placing ITERATE-IT into an inversion slot!
Placing ITERATE-IT into an inversion slot!
Placing ITERATE-IT into an inversion slot!
AIO errors: 27
INSTANCES errors: 133
AKO errors: 12
KINDS errors: 45
APO errors: 1
PARTS errors: 4
OTHERS errors: Ø
CONNECTION errors: 42

AIO errors: Ø
INSTANCES errors: Ø
AKO errors: Ø
KINDS errors: Ø
APO errors: Ø
PARTS errors: Ø
OTHERS errors: Ø
CONNECTION errors: Ø
```

(a)

```
Frame RV1Ø2's input P-IN doesn't jibe with frame NIL's output NIL.

Frame CV1Ø4's input P-IN doesn't jibe with frame NIL's output NIL.

Frame TX1Ø1's input TEMP-IN doesn't jibe with frame NIL's output NIL.

Frame RV1Ø1's input P-IN doesn't jibe with frame NIL's output NIL.
```

(b)

Figure 3-2. Consistency Checkers' printouts: a) Mondo's, b) Check-KB's.

TABLE 3-2.
ADMITTANCE DEFINITIONS

Fig.	Name[1]	Definition[1]	ALO-H2O[2]	FlowRatePres[3]
Tank pressurization circuits....				
A1	st_vent_admit	storage tank ullage vent admittance	p.7	-
A2	st_up_admit	" " " pressurization network "	p.9	-
A3	vt_vent_admit	vehicle tank ullage vent admittance	p.24	-
A4	vt_up_admit	" " " pressurization network "	p.25	-
Pump circuits....				
A5	pump_circuit_admit	From ST to PX1Ø6, used by SV1Ø4.	p.11,12	p.2
A6	pumps_admit	Nonlinear flow change with pressure.	p.11,12	-
A7	pump_to_4_way_admit	From pump1(or 2) to PX1Ø5.	-	p.1
A8	suction_line_admit	From ST to PX115.	-	p.6
A9	recirculation_admit	from PX1Ø6 to ST.	p.13	p.2
Aa	recirc_line_admit	From P1 to GA1Ø3.	-	p.6
Ab	No name.	= A9 - Aa, from above.	-	-
As	No name.	= A6 + A7, from above.	-	-
Ar	No name.	From PX1Ø5 to PX1Ø6.	-	-
Vehicle tank fill circuits....				
Ac	transfer_line_admit	Long piping & FCV1Ø3.	p.14	p.6
Ad	fast_fill_circuit_admit	SV1Ø7(8) and FM1Ø2.	p.16	p.4
Ae	final_fill_circuit_admit	MCV1Ø1 @ 33% and FM1Ø1.	p.19	p.4
Af	replenish_circuit_admit	Ditto, adjust % to hold VT level.	p.17	p.4
Vehicle tank drain circuits....				
Ag	tsm_drain_assist_admit	From PRU1Ø3 thru SV112 & SV116 to atmos	p.2Ø	-
Ah	drain_admit	From PX1Ø8 thru SV116 to atmosphere	p.18	-
Ai	No name.	Negligible wrt H2O-carrying drain.	-	-
Aj	nozzle_admit	" " " SV11Ø " " (= 2.5)	p.2Ø,21	-
Ak	bleed_admit	" " " SV1Ø9 " "	p.21	-
(NOTE: "tsm" = tail service mast.)				
Miscellany....				
--	rv_admit_max	= 1Ø (not a measurement)	p.24	-
Am	tank_fill_admit	PX1Ø6 to VT or drain, whichever open	p.2,4	-
An	upper_fill_circuit_admit	PX111 to VT or drain, "	-	p.6
Ap	skid_admit	From PX1Ø8 to PX111.	-	-
(NOTE: tank_fill, upper_fill, and skid admittances vary with procedure.)				

NOTE: Comments in the following listings provided these definitions:
1. G:>KATE>ALO-KB>CONTROL-PROCEDURES
2. G:>KATE>ALO-KB>ALO-H2O
3. G:>KATE>ALO-KB>FLOW-RATE-PRESSURES

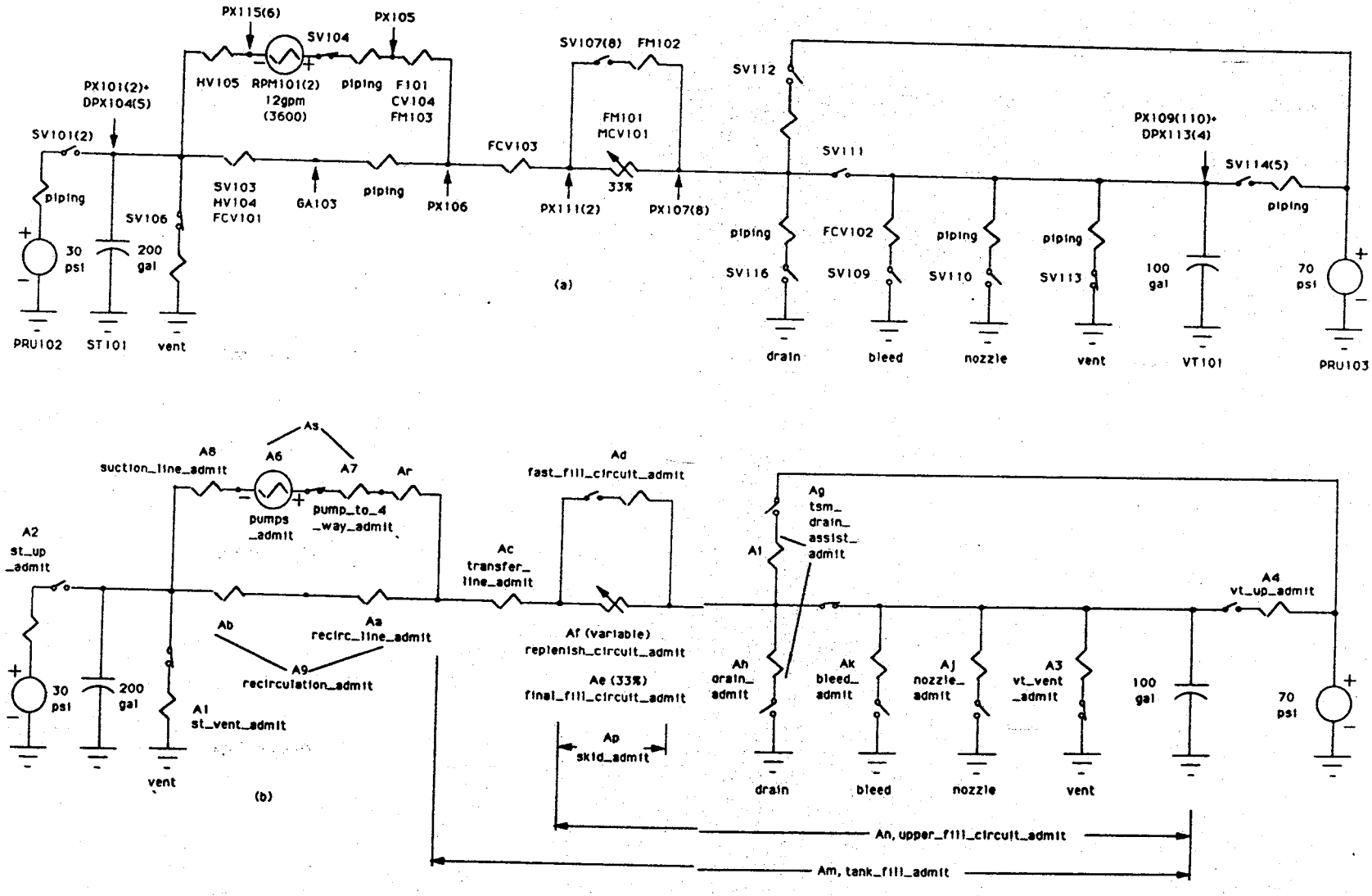

Figure 3-3. The ALO model's admittances: a) perspective (compare with Figure 1-1), b) admittances labeled as they appear in ALO's knowledge base frames.

admittances must be measured in isolation or gleaned from pump specifications before the admittance measuring procedure begins. This test procedure should be coded in Lisp and added to the procedures file above to enhance the ALO-H2O model and modeler productivity.

By the way, the admittance measurement procedure was designed earlier to measure only the admittances of the nine hand valves. This design was abandoned when the modeler realized upon inspection that it would not help him calibrate his 22 knowledge base admittances. Am I glad I completed a design before coding! The aborted design succeeded in pointing out a serious error, and thus served a very useful purpose. The design we abandoned also mistakenly assumed that pipe admittances are negligible compared with valve admittances. Laboratory researchers at Marshall Space Flight Center apparently still think that is true [6].

3.6 BETTER PSEUDO OBJECTS

KATE's modelers invented pseudo objects to apprise ordinary objects of remote pressures and flows in a complicated fluid flow circuit. The fluid flow output of a valve, for example, depends not only upon that valve itself but also upon the backpressure of its downstream load and the driving pressure of its upstream fluid supply. In KATE's ALO-H2O model, PX-1Ø6 is called the "all knowing" pressure. The rather complicated frame of this pseudo object evidences influence of far ranging pump flows and admittances. All other pressures and flows in the circuit can be readily computed from the keystone pressure PX-1Ø6, without the necessity of solving multiple simultaneous differential equations. Equation solving takes too much time, and it would interfere with KATE's failure diagnosis process. [6]

A pseudo object typically starts out looking like any ordinary object (i.e., a frame-modeled device), but then it starts growing like a cancer. Initially the flow through a device may be specified as a function of only local pressures. When modeled flows or pressures deviate from actuals, the modeler searches for any measurable time function which correlates well with actual flow, and then "mixes it in" with his original transfer function. These incremental improvements continue until the pseudo object's transfer function becomes a sort of multiple regression equation, combining the weighted contributions of many remote flow and pressure measurements throughout the circuit. A part of the specific application's knowledge base, the pseudo object describes the functioning of only one fluid flow circuit. But it is distinctly different from those true objects in the knowledge base which define the structure of the circuit. Stepchildren of the modeling process, pseudo objects do not fit well into either KATE's knowledge bases nor her shell. Furthermore, a single keystone pressure cannot be found in circuits that have multiple flow loops.

I resolved to find some alternatives to pseudo objects that would not run aground of the limitations imposed by on-line equation solving. Three alternatives are advanced below as proposal-ready philosophical white papers. The modelers' evaluations follow each description.

3.6.1 OFF-LINE EQUATION SOLVER ALTERNATIVE

If KATE needs an equation solver, but the equations aren't soluble in real time, why not solve all the equations KATE will need off-line and feed their analytic solutions to KATE as she needs them? A different solved equation is placed into the modeled knowledge base for every configuration of valves (e.g., every subprocedure in the LOX tanking procedure). Mathematica easily solves these simultaneous differential equations for all modeled flows and pressures as functions of time.

Consider the application of this technique to KATE's ALO-H2O model. During this model's slow fill subprocedure, only 12 of the 26 valves are open, producing the rather simple two-loop circuit of Figure 3-4. The modeler writes the two flow equations:

$$f1^2\,(1/aHV105^2+1/aHV107^2+1/aSV105^2+1/aF101^2+1/aCV104^2+1/aFM103^2) + (f1-f2)^2\,(1/aFCV101^2+1/aHV104^2) = k * RPM102, \quad (1)$$

$$\int f2\,dt \,/\, aVT101 = (f2-f1)^2\,(1/aHV104^2+1/aFV101) + f2^2\,(1/aFCV103^2+1/aFM101^2+1/aSV111^2+1/aSV113^2). \quad (2)$$

Off-line, Mathematica solves these for the time functions, f1 and f2, in terms of the circuit constants. The modeler codes f1 and f2 as pseudo object transfer functions for KATE to use throughout the slow fill procedure. Other objects in the knowledge base may refer to these flows in computing their own output pressures:

$$poutSV105 = pinSV105 - f1^2 \,/\, aSV105^2,$$

or even these time functions can be computed off-line.

Solving systems of simultaneous differential equations off-line moves the complexity out of KATE's shell that Whitlow found she couldn't bear [8]. This technique handles multiple loop flow models well. Constraining the valve closures of a particular modeled procedure also simplifies off-line equation solving. A small fraction of the original complexity (i.e., the flow time functions) moves into the knowledge base, where the modeler can handle it more cleverly than KATE could in her shell. Steve laments, however, that KATE's diagnoser would have to been modified to accommodate this procedure. The diagnoser currently twiddles valves, in an effort to duplicate erred hardware measurements, thus invalidating the simplified model and its off-line solution. Apparently these equations must be solved on-line.

3.6.2 ANALOG COMPUTER ALTERNATIVE

Is there a novel way to solve these equations on-line very rapidly? Yes, Abelson and Sussman suggest that the equations be solved by a signal processing analog computer [3]. Including the tank pressurization circuits, the ALO-H2O

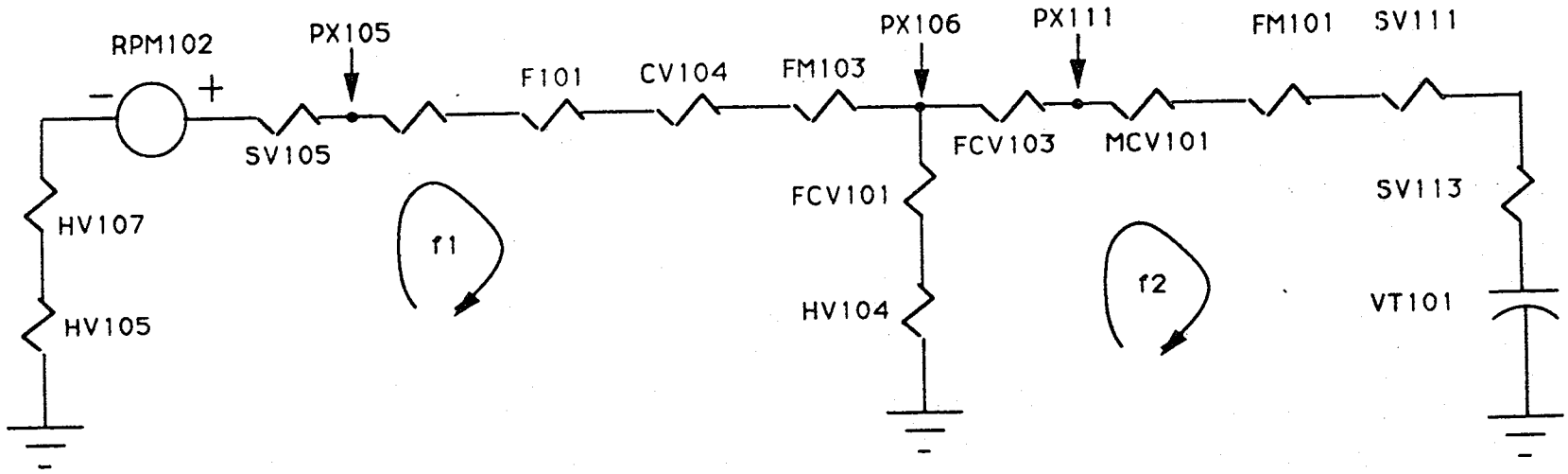

Figure 3-4. The simplified slow fill model.

model in slow fill includes four flow loops. Kirchoff's Law states that the sum of all the pressures around a loop must be zero. Four simultaneous equations state these sums in terms of the four flow rates around the loops of Figure 3-5.

$$\int f1\ dt\ /\ Cst = f1\hat{}2\ /\ A1\hat{}2, \tag{1}$$

$$k * RPM1\emptyset1 = (f2\hat{}2)(1/A8\hat{}2+1/A6\hat{}21/A7\hat{}2+1/Ar\hat{}2) + (f2-f3)\hat{}2\ (1/Aa\hat{}2+1/Ab\hat{}2), \tag{2}$$

$$(f3-f2)\hat{}2\ (1/A1\hat{}2+1/Ab\hat{}2+1/Aa\hat{}2) + f3\hat{}2\ (1/Ac\hat{}2+1/Ae\hat{}2) + (f3-f4)\hat{}2/A3\hat{}2 = \emptyset, \tag{3}$$

$$(f4-f3)\hat{}2\ /\ A3\hat{}2 = \int f4\ dt\ /\ Cvt. \tag{4}$$

After these equations are differentiated, a fast signal processing analog computer can solve them simultaneously.

$$df1/dt = A1\ /\ 2\ Cst. \tag{1}$$

$$\frac{df2}{dt} = \frac{df3}{dt}\ \frac{(f2-f3)\ (1/Aa\hat{}2+1/Ab\hat{}2)}{f2\ (1/A8\hat{}2+1/A6\hat{}2+1/A7\hat{}2+1/Ar\hat{}2) + (f2-f3)\ (1/Aa\hat{}2+1/Ab\hat{}2)} \tag{2}$$

$$\frac{df3}{dt} = \left[\frac{df1}{dt}\ \frac{f3-f1}{A1\hat{}2} + \frac{df2}{dt}\ (f3-f2)\ (1/Ab\hat{}2+1/Aa\hat{}2) + \frac{df4}{dt}\ (f3-f4)/A3\hat{}2\right] \times$$

$$[(f3-f1)(1/A1\hat{}2+1/Ab\hat{}2+1/Aa\hat{}2)+ f3(1/Ac\hat{}2+1/Ae\hat{}2)+ (f3-f4)/A3\hat{}2]\hat{}-1, \tag{3}$$

$$df4/dt = 2\ df3/dt + (A3\hat{}2\ /\ Cvt) * f4\ /\ (f4 - f3) \tag{4}$$

Figure 3-6 renders these equations graphically as an analog computer block diagram. Abelson and Sussman tell how to code signal processors that have troublesome feedback loops like these. Essentially they recommend that the fedback input be a global, given some initial value. That value is used to compute an output, and the output thus provides a new fedback value for the next sampling period.

The simple multiply-accumulate operations inherent in these signal processor difference equations run much faster than a general purpose simultaneous equation solver. Thus KATE's diagnoser can freely reconfigure valves on-line and can expect to harvest accurate flows and pressure values in real time. Integrators in the analog computer are inherently stable, thus combatting the convergence problem Whitlow encountered with his flow solver [8]. Experiments with Gensym's G2 program, however, indicate that any equation solver obscures device failures to some extent [6]. Is there a compromise between equation solving and our current pseudo objects?

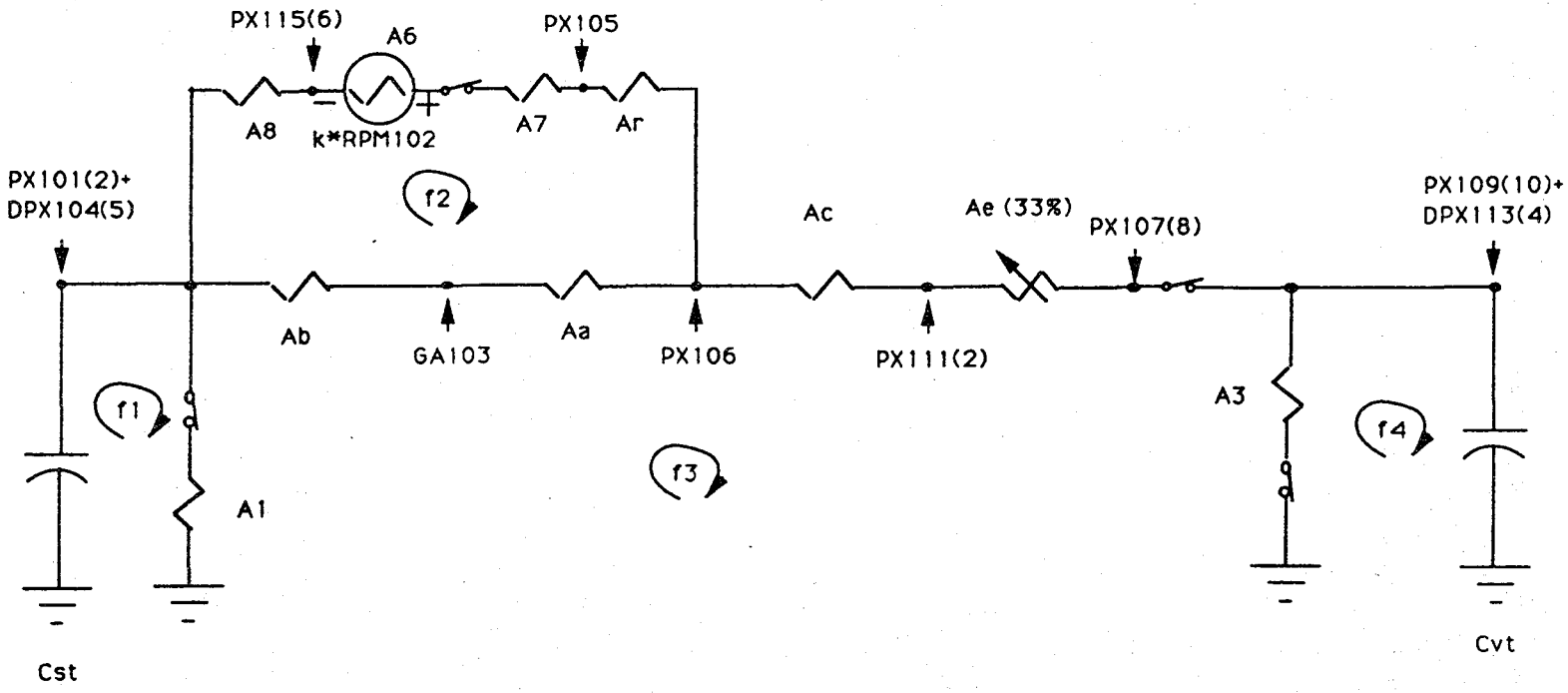

Figure 3-5. Four flow loops in ALO during slow fill.

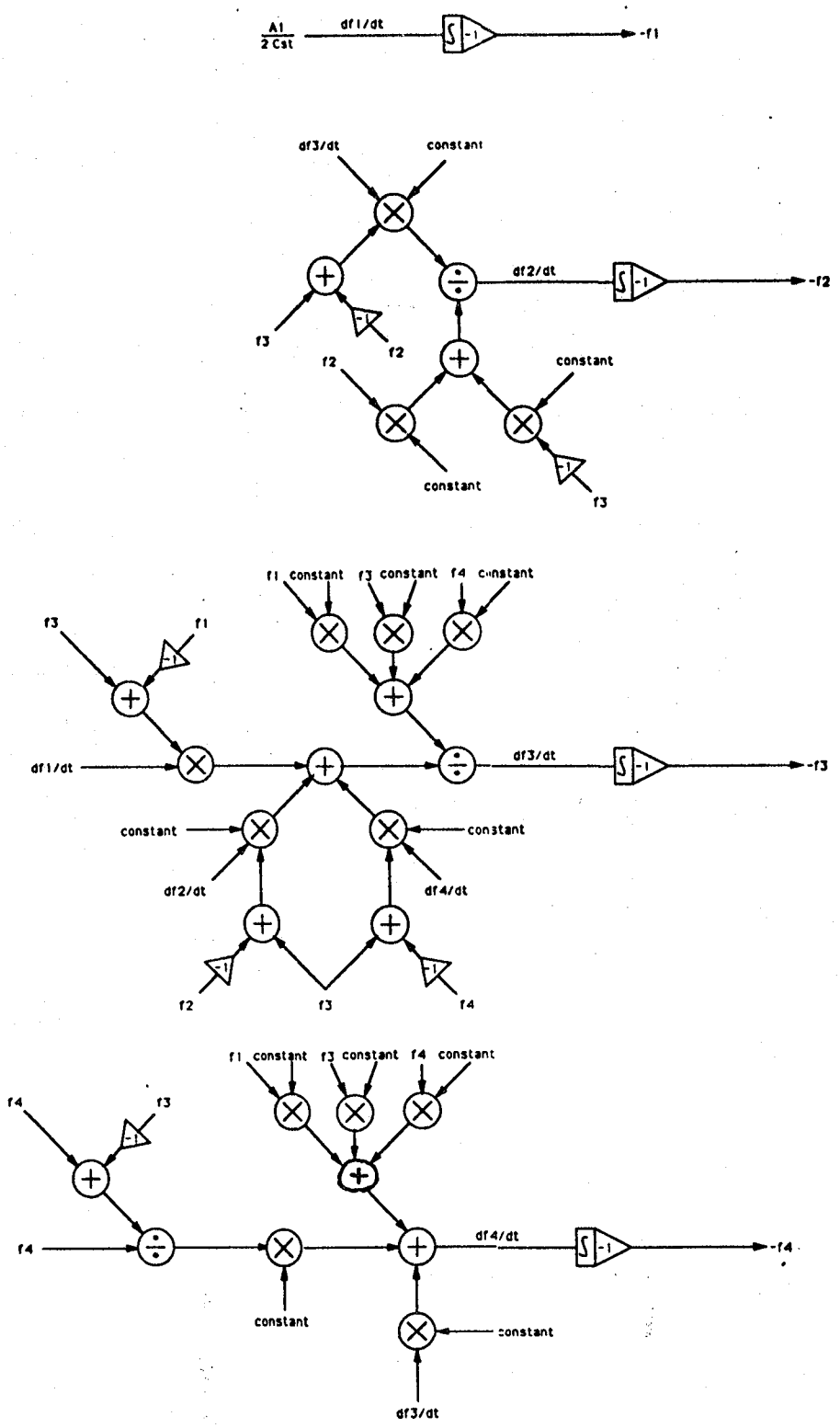

Figure 3-6. An analog computer designed to solve ALO's equations.

3.6.2 TWO-PORT ALTERNATIVE

The final alternative strives to distribute the complexity of KATE's pseudo objects over all the trueobjects, without requiring equation solving. The frame of every object describes the device itself, as well as all downstream (upstream) objects viewed through its input (output) port. Modeled objects are like a series of dirty windows, through which a viewer sees both the nearest window and other windows beyond. We obtain a Thevenin's equivalent circuit (to embody both local and remote devices) for each viewing port of every modeled device. Just the equivalent circuits of the two devices on either side of it are sufficient for computing any modeled pressure.

Thevenin's Law reduces a hydraulic network of any complexity to a single pressure source and a series admittance. It states that the equivalent pressure is the pressure that can be measured at the network's output. Furthermore, the equivalent admittance is that measured at the output when all network pressure and flow sources set to zero. (The admittance of a pressure source alone is zero.)

Figures 3-7 and 3-8 show how Thevenin's Law is applied to two-terminal devices and pipe tees in a hydraulic circuit. Looking into the input port of a two-port device in Figure 3-7a reveals the admittance itself and the equivalent circuit of all devices connected to its output. Furthermore, its internal admittance and the equivalent circuit of all devices connected to its input are visible at its output port. Thus, the device may be rendered as the equivalent circuit in Figure 3-7b, in which its input and output admittances and pressures may be computed.

$$Ain = An + Ao,\ Aout = An + Ai,$$

$$Pin = Po,\ Pout = Pi.$$

Similarly, the equivalent circuit of a pipe tee connected to the three devices shown in Figure 3-8a can be redrawn as the equivalent circuit of Figure 3-8b with the following parameter definitions.

$$Ain = 1 / (1/Ao + 1/Ab),$$

$$Aout = 1 / (1/Ai + 1/Ab),$$

$$Aby = 1 / (1/Ai + 1/Ao),$$

$$Pin = Po + (Pb - Po) * (Ao + Ab)^2 / Ao^2,$$

$$Pout = Pb + (Pi - Pb) * (Ab + Ai)^2 / Ab^2,$$

$$Pby = Pi + (Po - Pi) * (Ai + Ao)^2 / Ai^2.$$

With these definitions, we can model pressures and flows anywhere in a hydraulic circuit simply by referring to their adjacent devices. The affects of all remote devices are handled recursively by equivalent circuit formulas in the

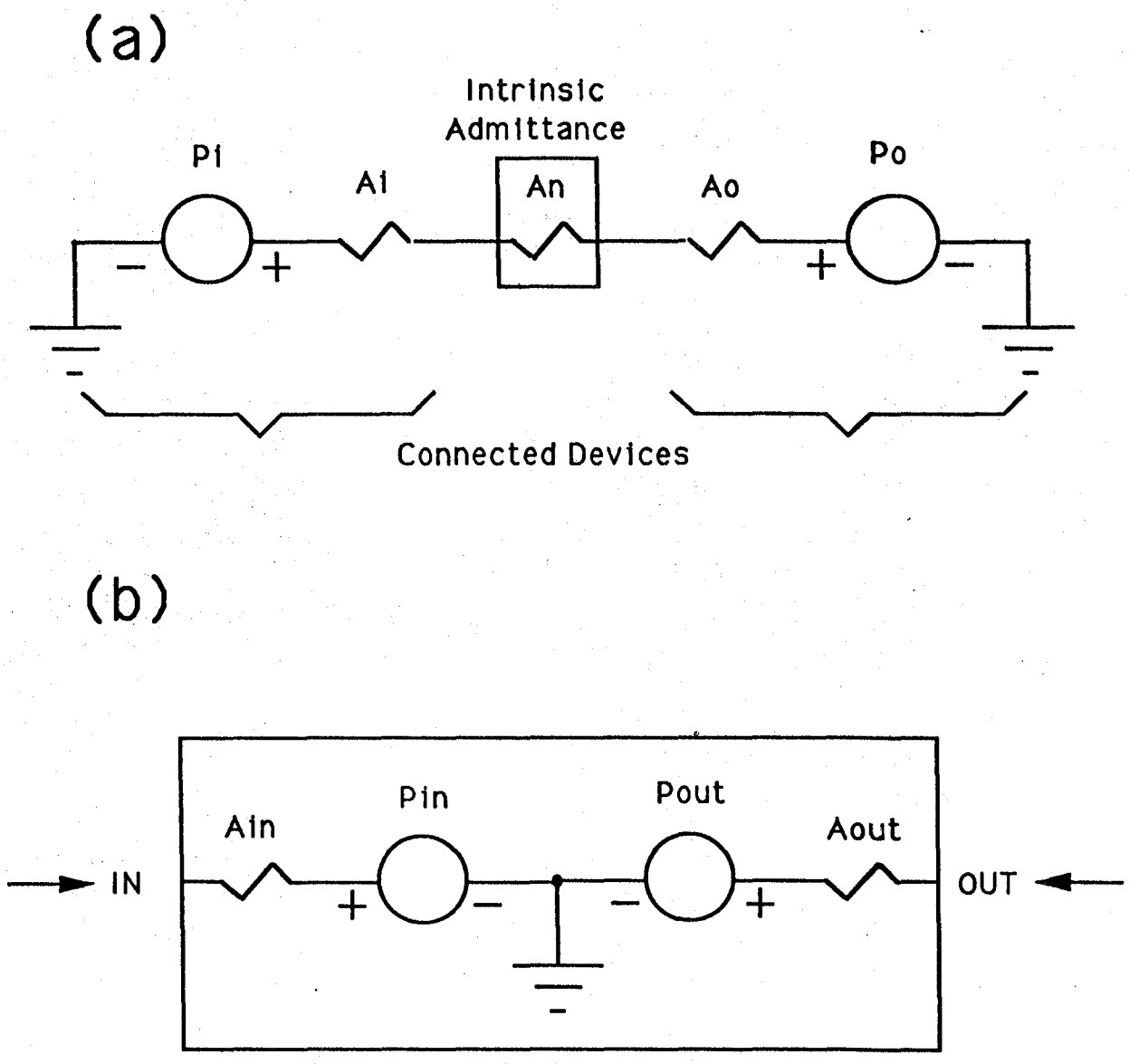

Figure 3-7. Thevenin's equivalent of a two-port device: a) device environment, b) equivalent device model.

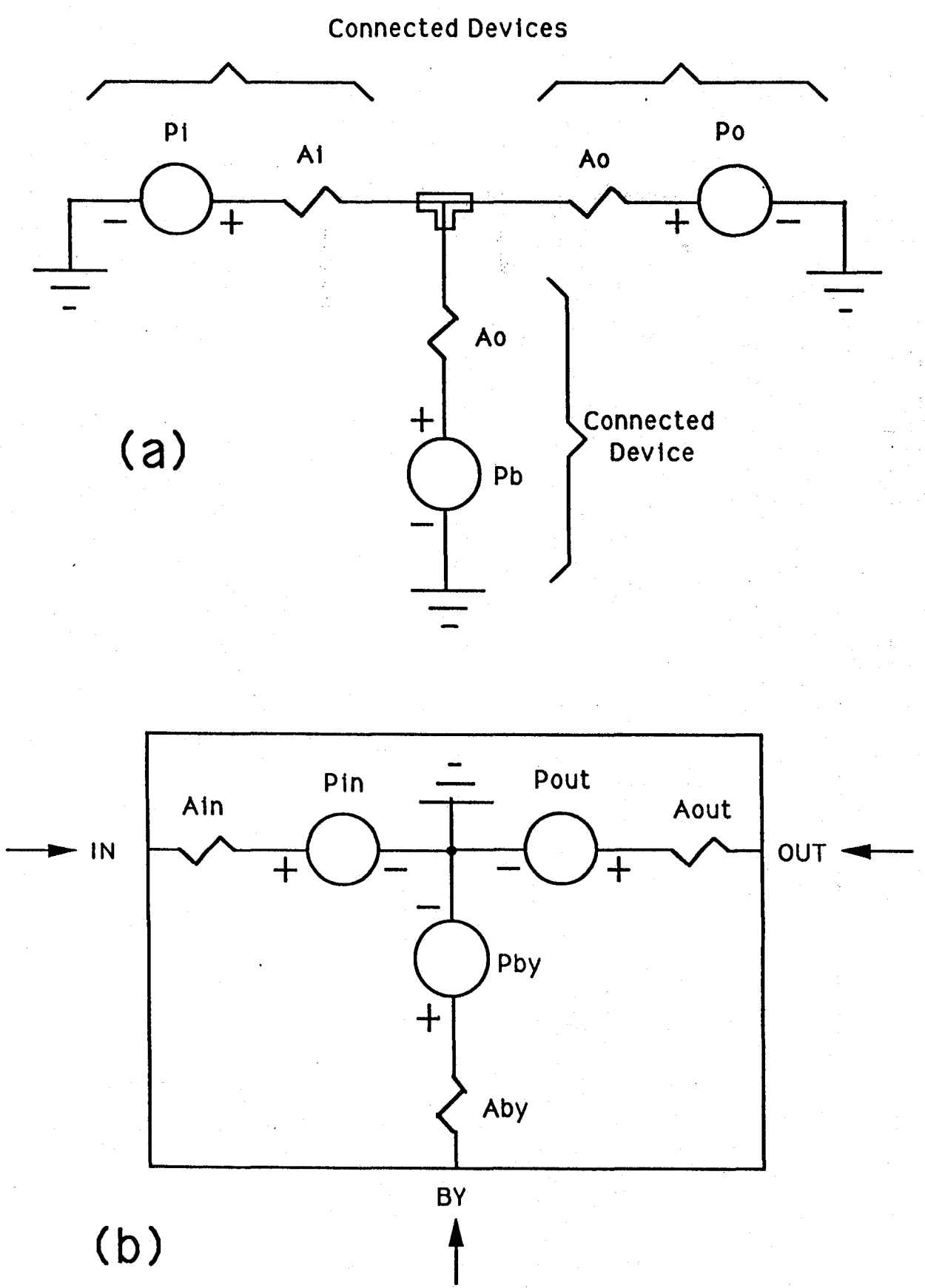

Figure 3-8. Thevenin's equivalent of a pipe tee: a) device environment, b) equivalent device model.

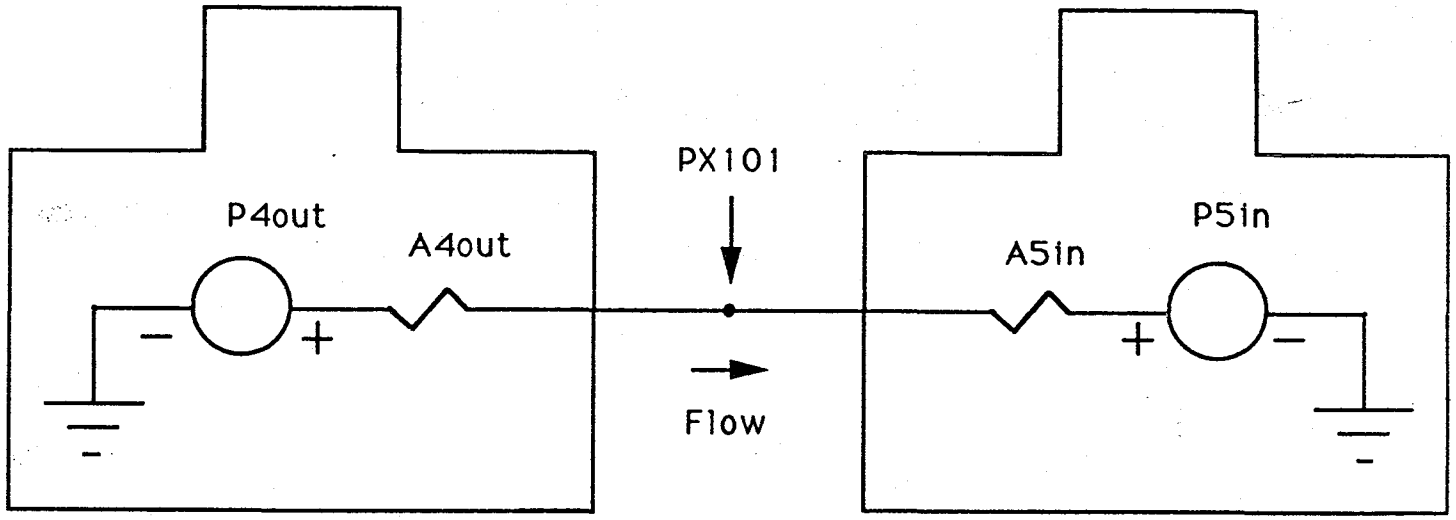

Figure 3-9. Two-port modeling an AL0-H20 pressure.

connected frames. For example, fluid flowing from tee 4 to tee 5 in a section of KATE's ALO-H2O model (see Figures 3-9 and 1-1),

$$Flow = SQRT(P4out - P5in) * (A4out + A5in).$$

And the pressure PX1Ø1 at that node,

$$PX1Ø1 = P4out + (Flow / A4out)^2.$$

Can the two-port object model flows and pressures in multiple loop circuits, or do infinite recursions result? No problem. Every remote device is viewed in the same direction as the local device for which an equivalent circuit is sought. Shown in Figure 3-1Ø is the former example in which we viewed tee 4's output port. Looking into tee 4's output port, we see the output ports of SV1Ø2 and tee 3. Looking into tee 3's output port reveals the output ports of SV1Ø1 and HV1Ø3. Viewing HV1Ø3, SV1Ø1, and SV1Ø2's output ports reveals the output ports of tee 2 and tee 1 and the bypass port of tee 2. Finally, looking into the bypass and output ports of tee 1 reveals the output port of PRU1Ø2, which is defined. No viewing step reflects back upon the viewer; no infinite recursion occurs in the equivalent circuit modeling process. A coding suggestion appears in Appendix F.

The two-port alternative is attractive because it is so similar to the original pseudo object idea. Thus it would be the easiest alternative to implement under KATE's current architecture. It offers more precision than the ALO-H2O model's all-knowing P1, because it exactly reflects the affects of remote devices (it is not the trial-and-error result of "mixing in" correlated measurements). A two-port object truly is an "object," retaining the devices' structural position in the circuit. Yet in its greater complexity, it accounts for the modeled device's environment, without need to resort to all-function pseudo objects. Like a neural network, each device is aware of its only nearest neighbors, yet that is enough to model the whole circuit, as viewed in one direction from a single point. This alternative does not obscure the affects of failed devices as an equation solver does; thus it is more compatible with KATE's diagnoser. It is hard to say in detail just how diagnosis might be affected by implementing the two-port pseudo object alternative.

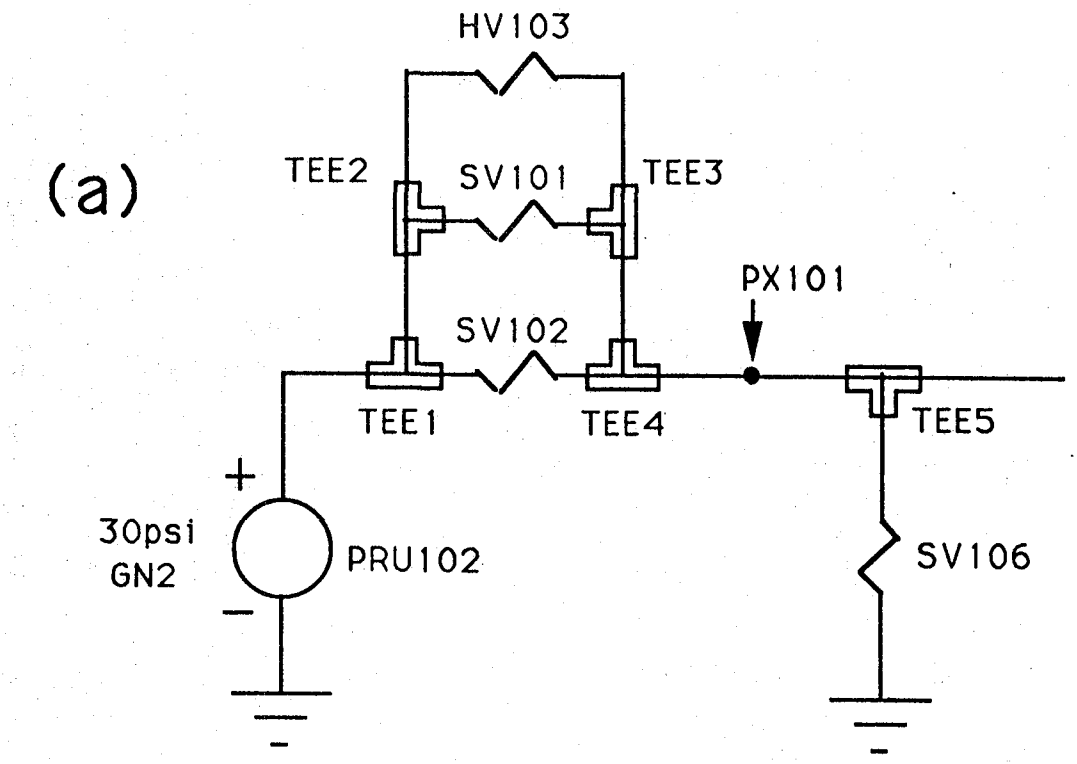

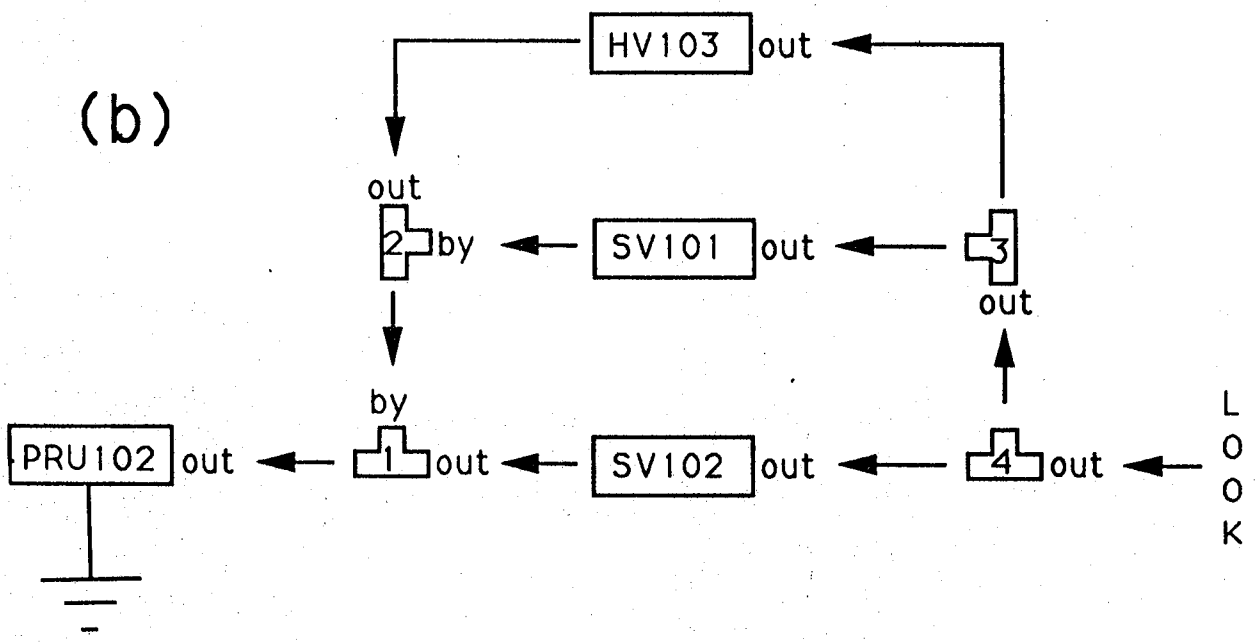

Figure 3-1Ø. No infinite recursions in multiple loops: a) ALO circuit segment, b) views always leftward.

IV
RESULTS AND DISCUSSION

4.1 MY MODEL VERIFICATION TOOLS

I added five useful tools to KATE's Model Verification Toolkit this summer. The already coded transfer function curve fitter and translator will make building new models easier, starting immediately. Documentation of KATE's three structural consistency checkers makes two of them available right away to all modelers, and the more powerful third will be useful as soon as it can be enhanced to match KATE's new knowledge bases. Bob has already decided to code the my automated admittance calibrator design in his spare time, with or without funding. Evidently he expects it to boost his productivity. Several stimulating discussions of the three pseudo object alternative white papers revealed some useful ideas in the first two, even if they are not altogether workable. The third alternative may enable KATE to embrace multiple flow applications that previously could not be modeled.

4.2 KATE'S FUTURE

How else can we make KATE's modelers more productive? There are two answers to that question. Traditional computer-automation aids, such as Computer Aided Design terminals, serve the end user. Mostly clerical, this modeler's task can be described in a series of very predictable steps for which KATE's responses are (hopefully) well known. KATE's end user needs a highly interactive graphical Knowledge Base Editor for creating frames, a Check-All-Frames syntax checker that doesn't miss a thing, and more refined on-line plotting facilities for debugging transfer functions. But KATE's end user hasn't shown up for work yet. And it's a good thing, because his Knowledge Base Editor isn't ready. KATE's developer/modelers have more difficult productivity problems. Redesign and recoding efforts (e.g., softlanding and external influences) spring up regularly in response to modeling problems that are currently beyond KATE's grasp. Weekly reports of these incremental changes in KATE provide evidence that she is a prototype, not a production program.

Production programs always pass through a Software Development Life Cycle (see Figure 4-1) before their release to end users. The development steps along the left of this "waterfall" chart start with a proposal phase, and proceed to a rapid prototyping sessions with the new customer if the proposal is successful. The rapid prototype uses powerful computers (like Symbolics) and powerful languages (like Lisp) to quickly define required system performance and user interactions before design begins. Design occurs in three top-down phases: system design to allocate jobs to subsystems, preliminary design to find the best path to module implementation, and detailed design to specify the performance of every software module. Coding follows. According to plans written during the design phases, testing proceeds from the bottom-up along the right side of the waterfall chart. Module testers diligently seek errors in modules, so that coders can remove them and increase product quality. Errors repaired here are

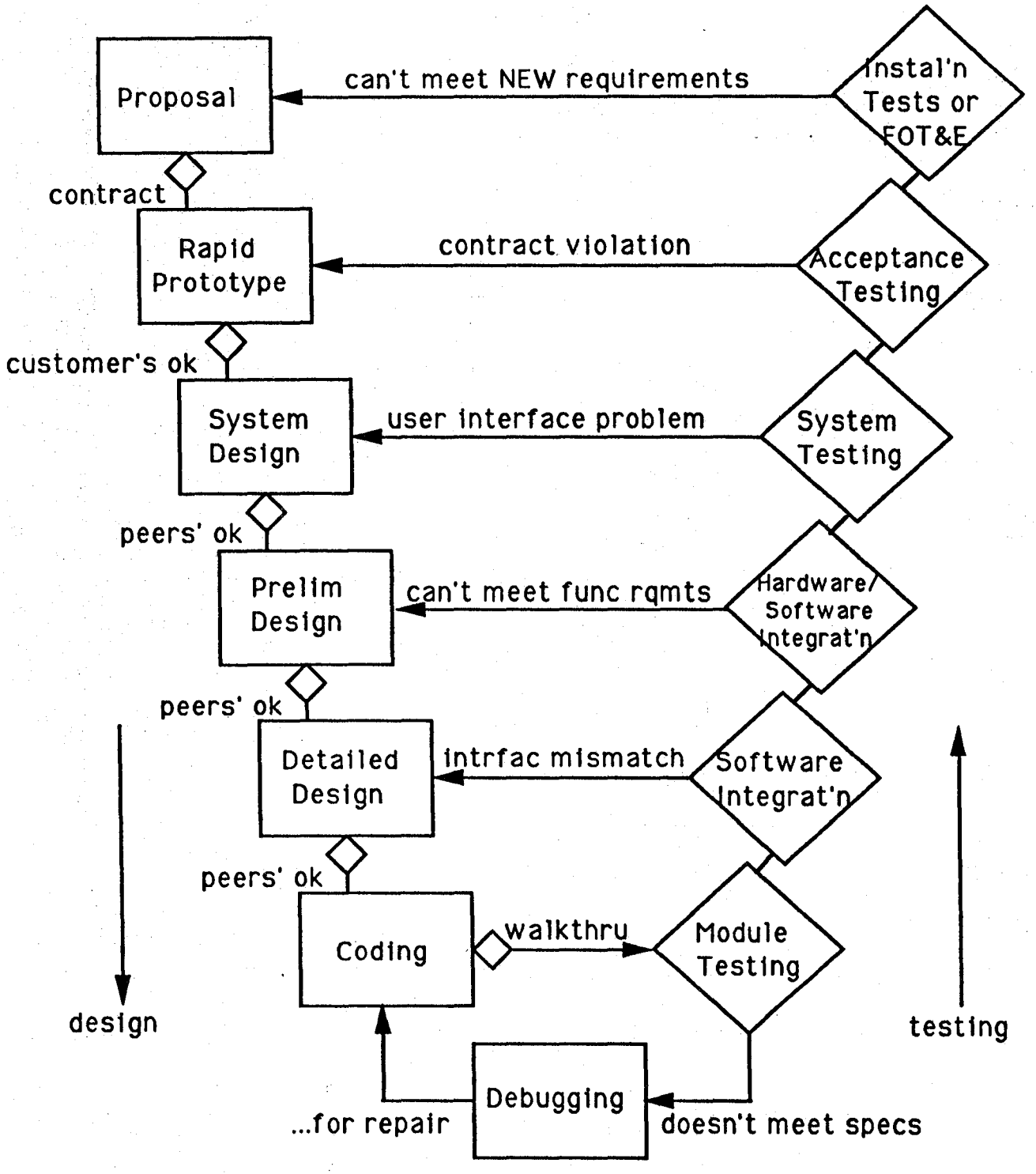

Figure 4-1. The Software Development Life Cycle.

27Ø times cheaper to fix than those found during production use. [7] In the software integration phase, modules are added to the evolving system, one at a time from the bottom-up, as module interface errors are discovered and eliminated. The hardware/software integration phase sees working subsystems being joined together with a similar testing goal. The system testing phase scrutinizes the complete system's responses to user commands, looking for errors the system engineer inadvertently designed in. Acceptance tests convince the customer that the system is ready for production use. Installation tests qualify each copy of the system for work at the user's site, or... they may provide content for a new proposal. Thus begins another trip through the Software Development Life Cycle.

For the past several years, KATE has been stuck in one proposal and rapid prototyping cycle after another. Her errors have been costly to fix, but her conceptual design has gradually matured to the point of convincing some that she will be able to handle critical tasks at KSC someday. Soon KATE will win her long-awaited ride through the Software Development Life Cycle. Folks here refer to the event as "recoding KATE in the C language for higher speed and lower cost," but you and I realize that Symbolics' Lisp machines are for prototyping and that C-programmed PCs are KATE's logical target system. Given an alert Computer Scientist as Configuration Manager, KATE will soon be as error free and incredibly reliable as KSC's other launch equipment. She will have the pedigree that she needs to win positions of responsibility and respect around KSC.

IV
CONCLUSIONS

KATE had some wonderful Model Verification Tools before I came, and now she has a few more (transfer function curve fitter, translator, and three documented syntax checkers). She has the prospect of some even more powerful ones in the foreseeable future (automated admittance calibrator and better pseudo objects). Her forthcoming "recoding in C" promises a error-purging turn through the Software Development Life Cycle.

With NASA and Boeing's able leadership, I have trained myself for KATE development work next summer by:

1. Surveying KATE's modelers.
2. Coding two new Model Verification Tools.
3. Enhancing some existing tools.
4. Designing a new tool.
5. Writing white papers on a better modeling technique.

I'm already looking forward to next summer.

KATE is an incredibly clever artificially intelligent computer program whose time has come. It is thrilling to be counted part of her development team just as she begins to turn a profit.

APPENDIX A

MODEL VERIFICATION TOOLS SURVEY

This list of desirable Knowledge Base Editor features came from conversations with Charlie Goodrich, Scott Budzowski, Bob Merchant, and Steve Beltz. It reflects their needs as bonifide KATE model builders, not my own.

Charlie's four-channel time-function plotter (defmacro plot, plotq, and its calls) is already heavily used in comparing actual measurements with their modeled values. It can be invoked from KATE's Command window as a LISP evaluation [Charlie, 10 June 1991] or by mouse-selecting a device on KATE's Overview screen and choosing "plot" on the menu. Bob is adding low-pass noise filtering and manual scaling to his plotq now. [Bob, 18 June 1991]

Scott's KATE Data Plotting Facility plots any number of time functions in real-time or from archived data, scrolling horizontally in time or vertically among functions. Scott mouse-selects every function to plot first by category and then from a reduced menu. As he chooses a mixture of analog and digital measurements, KATE's knowledge base automatically fills in all type-dependent plotting options. Actual measurements and their models may be overlaid on the same graph for easy comparison. Mousing to any plot and time position displays the numeric value of the point plotted there. A TCP/IP networking feature even allows KATE to plot measurements on remote terminals. This tool is especially useful in figuring out how to model complicated pseudo objects, such as heat flux arising from a combination of heater element, controller, and thermal load. [Scott, 12 June 1991]

Our existing Structural Consistency Checker should identify mismatched frames better than its current "flat file" output allows. A "hot key" could attach a mouseable handle to the next loose-end frame's name, so that it would not be necessary to type the name (lengthy alphabet soup) again. [Charlie, 10 June 1991] A graphical output format could be even friendlier; e.g., frame A's output to B without frame B's input from A would appear as a half-connection on an evolving Schematic screen. The Editor could find semantic inconsistencies too; e.g., relays usually go with transducers, power lines seldom connect to cryogenic flow lines. [Scott, 12 June 1991] Check-KB's input/output slot con consistency check is good enough for Bob. Simple enough to modify, Check-KB could even be called "configurable.") It might be nice to check for ALL errors and even correct them (Mark's "Mondo" does, see the "consistency-checking" LISP file), but such a checker would be too "destructive." [Bob, 18 June 1991] A checker may tell the modeler which frames should be modeled next (i.e., his knowledge base loose ends) during a knowledge base building process [Charlie, 10 June 1991], or it may be used to find all the frame mismatch errors in a complete knowledge base [Steve, 19 June 1991].

Charlie's Symbolics screen should be adjusted so that the bezel doesn't cut off his top line of text. [Charlie, 10 June 1991]

The Firing Room Operator's Console Log explains transients that appear on

plots of KATE's input measurements. Compare the Zulu (Greenwich Mean) time in the log with the HHMMSS.SSS time code broadcast along with KATE's measurements by the Command, Control, and Measurement System (CCMS) to identify those transient events that KATE must model. Every measurement is broadcast with 8-bit precision every 1.7 seconds, if it has changed (a few percent for analog measurements). [Charlie, 10 June 1991]

Charlie's 10-pound D-size paper schematic diagram file is KATE's present CAD input interface. The ultimate source of device frame data, these hand-drawn schematics identify device part numbers, show their connections, suggest device behavior (e.g., switches and lamps go T and nil), and occasionally reveal control system transfer functions (e.g., Charlie's proportional-integral-derivative nose cone heater controller). Oscillation frequencies, rise times, etc. in CCMS-broadcast data also help define transfer functions. [Charlie, 10 June 1991]

KSC's CAD systems are producing Component Data lists (brief device specifications) and To-From lists (device connections) for new system designs. This information will go a long way toward completing the frames of KATE's new applications. (Only actual operational ranges, initial values, failed values, update periods, delayed response times, etc., and pseudo objects remain to be added.) A rather simple program (compared with University of Central Florida's Automatic Knowledge-base Generator) could be attached to KSC's CAD terminals to gather the rest. Until now, KATE has modeled only old hand-designed systems, and modeler productivity has suffered. [Frank, 13 June 1991]

The ZMACS Editor Command box is a convenient LISP calculator for prototyping new LISP transfer functions, finding useful constants, etc. [Charlie, 10 June 1991]

Typing GOALs into the ZMACS Editor Command box asserts new values of switches, etc., while KATE is operational. (KATE actually takes about 2 seconds to implement these changes.) A few seconds later, the effects of the assertions can be verified in the model. [Charlie, 10 June 1991]

The FD (Function Designator) Browser on KATE's Overview screen offers a variety of database queries to modelers with broad interests (e.g., show all switch positions, show all 320 measurements). [Charlie, 10 June 1991]

KATE's Control menu item on the Overview screen prompts her to take over the system she is modeling to achieve a top-level Goal, like "fill tank." If essential measurements go out of specified limits, KATE calls up Diagnoser, which figures out which device failed. (KATE can handle just one device failure per two-second measurement cycle.) Automatic repair ensues, in which KATE figures out some other way of achieving her top-level goal, and brings up whatever redundant device is available. (Carrie's air-purge system demonstrates this most dramatically.) KATE is unable to foresee any possibly adverse effects of these logical repairs, such as the start-up arcing of a dc motor drenched with spilled liquid hydrogen and LOX. [Bob, 18 June 1991]

All of KATE's out-of-tolerance measurements initially turn purple on Bob's

color screen. When the failed device is diagnosed, its measurement turns red and others return to neutral. [Bob, 18 June 1991]

KATE's new Fortran-fluent end-users need an Infix-to-Postfix Translator to rewrite algebraic transfer functions in LISP's reverse Polish notation; e.g., Temperature_Change = 237 * Heat_Flux / Flow_Rate becomes (* 237 (/ Heat-Flux Flow-Rate)). [Charlie, 10 June 1991]

A Transfer Function Curve Fitter is needed to accept device history plots and deliver cubic-spline polynomials or least-squares-fit linear regression equations. [Scott, 11 June 1991]

Bob needs a tool that adjusts admittances in all of his device frames after workmen adjust the hardware they model. A KATE-controlled test procedure would make inducing a flow through every device its Goal. KATE would (at all times?) gather available flow rates and pressures, deduce others using Kirchoff's current law, calculate the admittances using Ohm's law, and edit them into their frames. Could this procedure be generalized to fit any model configuration (i.e., fit into KATE's shell)? No, Bob thinks we would have to custom-build a new test procedure for every KATE model (i.e., put one into every knowledge base). No sweat, Bob.... [Bob, 18 June 1991]

Someday end-users will create models almost entirely on their accustomed CAD terminals. They will interconnect graphic icons to create instance-level frames, and "fill in some blanks" with expected application-specific device data. To a device that optionally accepts a command (e.g., set valve to 33%, set pump speed to 2400 rpm) or produces a measurement (e.g., pressure is 15 psi, flow is 14 gpm) they will add another instance-level icon. When KATE matures, her mid- and top-level device definitions will be complete. Occasionally, abstract concepts (e.g., total back pressure of the external tank piping network, aggregate gravity and pump flows from a supply tank) will be edited directly into frames. Occupying no particular position in the graphical structure, these intangible PSEUDO OBJECTS nonetheless play essential functional roles in most models. [Steve, 19 June 1991]

While debugging KATE's typical applications, modelers easily isolate sources of big measurement deviations, and ignore little ones by opening up their tolerance specifications; but little errors that accumulate in objects with state can be troublesome. Editing "SOFTLANDING" directly into the frame of such a device can save the day. When accumulating error causes the Diagnoser to mark that device "failed," KATE repeatedly evaluates "global pain" of the model (i.e., the sum of the squares of all measurement deviations) and adjusts modeled measurements until pain is minimized. Thus the failed device moves back into its tolerance limits, and correct model performance resumes. [Steve, 19 June 1991]

KATE's Tolerance Graph is more useful than measuring global pain in most knowledge base debugging. This avionic-like needle-ball display pin-points most device related measurement errors quickly without the run time burden of Soft-landing. [Steve, 19 June 1991]

The KB Editor is splitting along a line variously described as:

nonLISP System Engineer end-user vs. LISP-fluent developer
object modeler vs. pseudo object modeler
KATE instantiation producer vs. KATE mid-level standard object producer

The KB Editor's new graphical editing tools are primarily intended for the end-user, whose needs for tangible objects are simple and predictable. Traditional KATE editing will continue to be at the frame level, where unusual (even invisible) pseudo object behavior is more readily modeled. (AI Lab personnel get clerk typists to do their simple editing for them.) [Charlie, 10 June 1991]

KATE's Knowledge Base Editor and Model Verification Tools (MVTs) are closely related but separate entities. From the end-user's point of view, MVTs are seamlessly integrated into the KB Editor to ease their use. On the other hand, KATE's developers know that editing is typically done with KATE off-line, but MVTs are used while KATE is operational. (Used to find loose ends during off-line frame editing, the Structural Consistency Checker MVT is an exception to this general rule.) [Scott, 11 June 1991]

KATE appears to be getting heavy. After the Structural Consistency Checker revealed 220 frame mismatch errors among the nose cone anti-icer's new frames, Charlie remarked, "You make a little correction, and that causes a lot of problems for you because all of a sudden a lot of things aren't there." Some of KATE's frames are in their 200th or more version; i.e., almost 40 accumulated hours of revisions. [Charlie, 10 June 1991] Stanford University's MYCIN sank under the weight of 6000 disease-diagnostic rules, when every incremental "improvement" caused more errors than it fixed. MYCIN's little children, like ONCONCIN, live on. Moral: Keep KATE's applications small and autonomous.

Given a choice, KATE's modelers should prefer KSC's new CAD-designed applications. Creating device frames automatically from flat CAD data files would make the modeler's job a lot easier. Unfortunately, KATE's current shuttle tanking applications involve old hardware that dates back to the preCAD era. [Carrie, 13 June 1991]

Multiple-flow modeling looms as a problem on KATE's horizon. ALO and the Little Red Wagon have a single pressure ("P1") at their cores, from which KATE can compute all other pressures and flows. Whitlow's generalized multiple-flow model tried to consider all possible topologies of main-stream and bleed flows, and failed. We dropped it after Clay Johnson's in-depth literature search revealed that nobody has a handle on this thorny problem. A straight-forward simultaneous equation solver, like a SPICE circuit simulation, apparently isn't useful because KATE needs to be aware of fault-tree connectivity among its modeled devices too. Ethan Scarl at Boeing-Seattle is currently pursuing the problem further on somebody else's nickel. Maybe Johan de Kleer and Randall Davis, model-based reasoning experts at MIT's AI Lab, could shed some light on it. [Bob, 18 June 1991]

The "pedigree" of any reliable software system is its design documentation. The evolving product of many prototyping demonstrations, KATE apparently has not been designed yet. Consisting entirely of 50,000 lines of commented LISP code and 15 published papers [Tom, 19 June 1991], KATE could die instantly if Henry, Chuck, Charlie, Steve, Bob, Mark, or Scott were hit by a truck. It isn't too

late to design KATE. Of the many design methodologies described by contemporary Software Engineering texts, perhaps the graphical Warnier-Orr Data Structured System Design technique is the most understandable to seasoned System Engineers (see example in Appendix C). Completing KATE's design would pave the way for her comprehensive testing, also essential to any reliable software product. KATE's impending translation to C may be just what she has needed to get designed and tested, as she moves from the laboratory into production use.

APPENDIX B

LEAST-SQUARES CURVE FITTER

```
;;; -*- Mode: LISP; Syntax: Common-lisp; Package: COMMON-LISP-USER; Base: 10 -*-


(defflavor graph-pane (mxx mnx mxy mny scale)
           (tv::window)
  :settable-instance-variables
  :readable-instance-variables)

(defvar *graph-pane* nil)

(setq *graph-pane*
      (tv::make-window 'graph-pane
                       :size '(500 500)
                       :blinker-p nil
                       :save-bits t
                       :label nil))

(defmethod (scale graph-pane)(xl yl)
  (setq mxx (apply #'max xl)
        mnx (apply #'min xl)
        mxy (apply #'max yl)
        mny (apply #'min yl))
  (cond ((> (- mxx mnx)(- mxy mny))
         (setq scale (/ 450 (- mxx mnx))))
        (t (setq scale (/ 450 (- mxy mny))))))

(defmethod (plot graph-pane)(xl yl)
  (do* ((xw xl (cdr xw))
        (yw yl (cdr yw))
        (x (car xw)(car xw))
        (y (car yw)(car yw)))
       ((null x))
    (graphics::draw-circle (+ 25 (round (* (- x mnx) scale)))
                           (- 475 (round (* (- y mny) scale)))
                           4
                           :stream self)))

(defmethod (draw-fit graph-pane)(xl yl)
  (let* ((a-b (regres xl yl))
         (a (car a-b))
         (b (cadr a-b))
         (pt1-y (+ a (* b mnx)))
         (pt2-y (+ a (* b mxx))))
    (graphics::draw-line (+ 25)
                         (- 475 (round (* (- pt1-y mny) scale)))
                         (+ 25 (round (* (- mxx mnx) scale)))
                         (- 475 (round (* (- pt2-y mny) scale)))
                         :thickness 2
                         :stream self)))

(defun test-fit (x y)
  (send *graph-pane* :expose)
  (send *graph-pane* :clear-window)
  (scale *graph-pane* x y)
  (plot *graph-pane* x y)
  (draw-fit *graph-pane* x y))

;;; Least-squares curve fitter: prints y = a + b x, r = __.
;;; (Steve Morgan, 8 July 1991)

;;;  Test Case: y = -3.93 + 1.10 x, r = 0.96...
(defun test1 ()
  (regres (print '(4.7 4.8 4.9 5.0 5.1))
          (print '(1.2 1.4 1.5 1.5 1.7))))

;;;  Test Case: y = 21.69 + 3.471 x, r = 0.976...
(defun test2 ()
  (regres (print '( 4  9 10 14  4  7 12 22  1 17))
          (print '(31 58 65 73 37 44 60 91 21 84))))

;;;  Test Case: y = -1.27 + 1.17 x, r = 0.936...
(defun test3 ()
  (regres (print '(8.2 9.6 7.0 9.4 10.9 7.1 9.0 6.6 8.4 10.5))
          (print '(8.7 9.6 6.9 8.5 11.3 7.6 9.2 6.3 8.4 12.3))))

;;;  Log Test Case: y = x, r = 1.00...
```

```
(defun test4 ()
  (regres (logem (print '(2.7 7.4 20.1 54.6)))
          (print '(1 2 3 4))))

;;;  Optionally change to log (base e) or log-log graph...
(defun logem (x)
  (mapcar 'log x))

;;;  Regression line: y = a + b x, r = ___...
(defun regres (x y)
  (list '(y=__*x+__&r=__)
        (slope  (length x) (sum x) (sum y) (sumsqr x) (sumxy x y))
        (y-intcpt (length x) (sum x) (sum y)
                  (slope (length x) (sum x) (sum y) (sumsqr x) (sumxy x y)))
        (correl (length x) (sum x) (sum y) (sumsqr x) (sumsqr y) (sumxy x y))))

;;;  Slope, b = (n * sumxy - sumx * sumy) / (n * sumxsqr - sumx * sumx)...
(defun slope (n sx sy sx2 sxy)
  (/ (- (* n sxy) (* sx sy))
     (- (* n sx2) (* sx sx))))

;;;  Y-intercept, a = (sumy - b * sumx) / n...
(defun y-intcpt (n sx sy b)
  (/ (- sy (* b sx))
     n))

;;;  Correlation, r = (n * sumxy - sumx * sumy) / sqrt[(n  * sumxsqr - sumx * sumx) ( n * sumysqr - sumy
* sumy)]...
(defun correl (n sx sy sx2 sy2 sxy)
  (/ (- (* n sxy) (* sx sy))
     (sqrt (* (- (* n sx2) (* sx sx))
              (- (* n sy2) (* sy sy))))))

;;;  Mean...
(defun sum (x)
  (cond ((null x) 0.0)
        ((atom x) x)
        (t (apply '+ (mapcar 'sum x)))))

;;;  Variance...
(defun sumsqr (x)
  (cond ((null x) 0.0)
        ((atom x) (* x x))
        (t (apply '+ (mapcar 'sumsqr x)))))

;;;  Covariance...
(defun sumxy (x y)
  (cond ((null x) 0.0)
        ((atom x) (* x y))
        (t (apply '+ (mapcar 'sumxy x y)))))

;;;  Reference:  JE Freund & RE Walpole: Mathematical Statistics, 3rd Ed., P-H, 1972.
```

```
(defun test4 ()
  (regres (logem (print '(2.7 7.4 20.1 54.6)))
          (print '(1 2 3 4))))

;;;  Optionally change to log (base e) or log-log graph...
(defun logem (x)
  (mapcar 'log x))

;;;  Regression line: y = a + b x, r = ___...
(defun regres (x y)
  (list '(y=__*x+__&r=__)
        (slope  (length x) (sum x) (sum y) (sumsqr x) (sumxy x y))
        (y-intcpt (length x) (sum x) (sum y)
                  (slope (length x) (sum x) (sum y) (sumsqr x) (sumxy x y)))
        (correl (length x) (sum x) (sum y) (sumsqr x) (sumsqr y) (sumxy x y))))

;;;  Slope, b = (n * sumxy - sumx * sumy) / (n * sumxsqr - sumx * sumx)...
(defun slope (n sx sy sx2 sxy)
  (/ (- (* n sxy) (* sx sy))
     (- (* n sx2) (* sx sx))))

;;;  Y-intercept, a = (sumy - b * sumx) / n...
(defun y-intcpt (n sx sy b)
  (/ (- sy (* b sx))
     n))

;;;  Correlation, r = (n * sumxy - sumx * sumy) / sqrt[(n  * sumxsqr - sumx * sumx) ( n * sumysqr - sumy
* sumy)]...
(defun correl (n sx sy sx2 sy2 sxy)
  (/ (- (* n sxy) (* sx sy))
     (sqrt (* (- (* n sx2) (* sx sx))
              (- (* n sy2) (* sy sy))))))

;;;  Mean...
(defun sum (x)
  (cond ((null x) 0.0)
        ((atom x) x)
        (t (apply '+ (mapcar 'sum x)))))

;;;  Variance...
(defun sumsqr (x)
  (cond ((null x) 0.0)
        ((atom x) (* x x))
        (t (apply '+ (mapcar 'sumsqr x)))))

;;;  Covariance...
(defun sumxy (x y)
  (cond ((null x) 0.0)
        ((atom x) (* x y))
        (t (apply '+ (mapcar 'sumxy x y)))))

;;;  Reference:  JE Freund & RE Walpole; Mathematical Statistics, 3rd Ed., P-H, 1972.
```

APPENDIX C

FORTRAN-TO-LISP TRANSFER FUNCTION TRANSLATOR

```
;;;  Fortran-to-Lisp Translator....
;;;  Steve Morgan, 15 July 1991
;;;  Ref: PH Winston & BKP Horn's "LISP," 2nd Ed., Addison-Wesley, 1984, Chapter 12.
;;;
;;;            (Print arithmetic expression.
;;;            (arithmetic expression
;;;  Translate (consists of just an operand       (Return it unchanged.
;;;  infix-to  (          +
;;;  prefix.   (arithmetic expression consists of (Parse arithmetic expression with
;;;            (lists of operators and operands   (empty operator & operand stacks.
;;;
;;;             (Print arithmetic expression, operators, and operands (indented).
;;;  Parse      (Translate infix-to-prefix just the first arithmetic expression element.
;;;  arithmetic (Push the result onto the operands stack.
;;;  expression.(Iterate through the rest of the arithmetic expression list.
;;;
;;;             (Print arithmetic expression, operators, and operands (indented twice).
;;;             (                    (no more operators
;;;  Iterate    (no more arithmetic  (remain             (Return the first operand.
;;;  through    (expression remains  (    +
;;;  arithmetic (                    (more operators    (Build  (Operands: (A B C) <- ((x B A) C),
;;;  expression.(                    (remain            (output ( operators: (x y z) <- (y z),
;;;             (       +                               (tree.  ( arithmetic expression unchanged.
;;;             (                                               (Iterate thru arithmetic expression.
;;;             (
;;;              (more arithmetic    (no more operators (Save     (Push operator onto its stack.
;;;              (expression remains (remain            (operator.(Parse the rest of arith. expr.
;;;                                  (    +
;;;                                  (more operators    (arithmetic expression's
;;;                                  (remain            (operator is heavier than (Save
;;;                                                     (operator at top of stack (operator.
;;;                                                     (         +
;;;                                                     (arithmetic expression's  (Build
;;;                                                     (operator is lighter or   (output
;;;                                                     (same as top of stack     (tree.
;;;
;;;  Iterate's Operator Precedence Decision Table:
;;;
;;;    Arithmetic Expression Operator
;;;                    *
;;;       nil  =  +  rem  ^  unary
;;;               -   /       opr
;;;                          _____ unary opr
;;;    pop operand, pop ____/      ^            Top
;;;   operator, &   ___/           * rem /      of
;;;  build output__/    push       + -          Operator
;;;    _________/     operator     =            Stack
;;;     return/                    nil
;;;     first /
;;;    operand/

;;;  Test Case: (A + B * C)
(defun test1 ()
  (print (setq ftrn '(A + B * C)))
  (lsp ftrn))

;;;  Test Case: (setq total (* principal (expt (+ 1.0 interest) years)))
(defun test2 ()
  (print (setq ftrn '(total = principle * (1.0 + interest) ^ years)))
  (lsp ftrn))

;;;  The Opposite Test Case:
(defun test3 ()
  (print (setq lsp '(setq total (* principal (expt (+ 1.0 interest) years)))))
  (ftrn lsp))

;;;  Unary Operator Test Case: (sin (x))
(defun test4 ()
  (print (setq ftrn '(nil sin (x))))
  (lsp ftrn))

;;;  Harder Unary Operator Test Case: (setq y (sqrt (- (cos (x) (* (j sin (x)))))))
(defun test5 ()
```

```
  (print (setq ftrn '(y = nil sqrt (nil cos (x) - j * nil sin (x)))))
  (lsp ftrn))

(defun lsp (arithexpr)
  (progn (terpri) (prinl arithexpr))
  (cond ((atom arithexpr) arithexpr)                    ;Easy case first,
        (t (parse arithexpr nil nil))))                 ; else stacks start empty.

(defun parse (arithexpr operators operands)
  (progn (terpri) (sp) (prinl arithexpr) (sp) (prinl operators) (sp) (prinl operands))
  (iterate (cdr arithexpr)                              ;Work on CDR after
           operators
           (cons (lsp (car arithexpr)) operands)))      ; recursion on CAR.

(defun iterate (arithexpr operators operands)
  (progn (terpri) (sp) (sp) (prinl arithexpr) (sp) (prinl operators) (sp) (prinl operands))
  (cond ((and (null arithexpr) (null operators))        ;Finished?
         (car operands))
        ((and (not (null arithexpr))
              (or (null operators)
                  (> (weight (car arithexpr))           ;Compare weights of
                     (weight (car operators)))))        ; operator & list head.
         (parse (cdr arithexpr)
                (cons (car arithexpr) operators)        ; Push operator
                operands))                              ; and continue.
        (t (iterate arithexpr
                    (cdr operators)                     ;Pop operator,
                    (cons (list (opcode (car operators))
                                (cadr operands)         ; construct sublist,
                                (car operands))
                          (cddr operands))))))          ; and pop operands.

(defun weight (operator)                                ;Determine weight of operator.
  (cond ((equal operator '=) 0)
        ((equal operator '+) 1)
        ((equal operator '-) 1)
        ((equal operator '*) 2)
        ((equal operator '/) 2)
        ((equal operator '\\) 2)
        ((equal operator '^) 3)
        ((equal operator 'SQRT) 4)
        ((equal operator 'SIN) 4)
        ((equal operator 'COS) 4)
        (t 5)))

(defun opcode (operator)                                ;Get appropriate LISP primitive.
  (cond ((equal operator '=) 'SETQ)
        ((equal operator '+) '+)
        ((equal operator '-) '-)
        ((equal operator '*) '*)
        ((equal operator '/) '/)
        ((equal operator '\\) 'REM)
        ((equal operator '^) 'EXP)
        ((equal operator 'SQRT) 'SQRT)
        ((equal operator 'SIN) 'SIN)
        ((equal operator 'COS) 'COS)
        (t (print '(,operator not an operator)) operator)))

(defun ftrn (lsp)
  (recurse lsp -1))

(defun recurse (lsp win)
  (cond ((null lsp) lsp)                                        ;Easy case.
        ((atom lsp) (list lsp))                                 ;Easy case.
        (t (let ((wout (precedence (car lsp))))                 ;get weight of new.
             (cond ((< wout win)                                ;Compare weights.
                    (list (append (recurse (cadr lsp) wout)
                                  (list (opsymbol (car lsp)))   ;Need parens.
                                  (recurse (caddr lsp) wout))))
                   (t (append (recurse (cadr lsp) wout)
                              (list (opsymbol (car lsp)))       ;No parens.
                              (recurse (caddr lsp) wout)))))))))

(defun precedence (x)           ;Find weight
  (cond ((equal x 'SETQ) 0)         ; given LISP procedure.
        ((equal x '+) 1)
```

```
        ((equal x '-) 1)
        ((equal x '*) 2)
        ((equal x '/) 3)
        ((equal x 'REM) 3)
        ((equal x 'EXPT) 4)
        (t 5)))

(defun opsymbol (x)                ;Get symbol
  (cond ((equal x 'SETQ) '=)           ; given LISP primitive.
        ((equal x '+) '+)
        ((equal x '-) '-)
        ((equal x '*) '*)
        ((equal x '/) '/)
        ((equal x 'REM) '\\)
        ((equal x 'EXPT) '^)
        (t x)))

(defun sp ()
  (princ '| |))
```

APPENDIX D

Errors Put Into The ALO-H20 Knowledge Base To Test CHECK-ALL-FRAMES.

Test Page *** Errors Inserted Into G:>morgan>kate-top.lisp.2 ***

```
1  1    (deframe PIPE-JOINT
            ...(parts ST-1Ø1)...
1  1    (deframe COMMAND
            ...(apo ALO-DIS)...
1  1    (deframe MEASUREMENT
            ...(aio INST-LEVEL-ANALOG-PSEUDO-OBJECT)...
1  1    (deframe EDGE
            ...(instances ST-1Ø1)...
8  1    (deflame-misspelled NOT-A-FRAME)
9  1    (deframe UNSLOTTED-FRAME)
1Ø 1    (deframe EMPTY-SLOT-FRAME
            (nomenclature "empty-slot-frame")
            ( ))
11 1    (deframe NO_NOMENCLATURE-FRAME
            (outputs (status))
12 1    (deframe UNKNOWN-SLOT-FRAME
            (nomenclature "unknown-slot-frame")
            (blivit 6))
13 1    (deframe DISCRETE-OBJECT
            ... (ako STUFF)...
13 1    (deframe EXTERNAL-INFLUENCE
            ... (kinds DISCRETE-MEASUREMENT) ...

        *** Errors Inserted Into G:>morgan>kate-mid.lisp.2 ***

2  6    (deframe CAMERA-FEEDBACK-MEASUREMENT
            ...(inputs 2)...
2  6    (deframe ANALOG-TEMPERATURE-MEASUREMENT
            ...(outputs 4)...
2  6    (deframe ANALOG-PRESSURE-MEASUREMENT
            ...(icon 6)...
3  6    (deframe ANALOG-DIFFERENTIAL-PRESSURE-MEASUREMENT
            ...delete (outputs meas-out)...
3  6    (deframe ANALOG-DIFFERENTIAL-PRESSURE-VENTURI-27Ø-MEASUREMENT
            ...delete (output-functions (meas-out in))...
3  9    (deframe TANK-GAS-VOLUME
            ... delete (units (volume "scf"))
4  11   (deframe GAS-FLOW
            ...(units )...
4  11   (deframe TANK-ULLAGE-PRESSURE
            ...(outputs )...
4  11   (deframe TANK-TOTAL-PRESSURE
            ... (output-functions )...
```

```
5  12   (deframe FLOW-CONTROL-VALVE
            ... (output-functions (admit init-pos))...
5  14   (deframe TEMPERATURE-TRANSDUCER
            ... (units (temp-in "F"))
5  7    (deframe ANALOG-DIFFERENTIAL-PRESSURE-VENTURI-MEASUREMENT
            ... (tolerances (second-meas-out 2.Ø))...
5  1    (deframe DELAY-SLOT-FRAME
            (nomenclature "delay-slot-frame")
                          TABLE 3-2.  continued...

            (outputs right-out)
            (delay (wrong-out 3Ø)))
8  1    (deflame-misspelled NOT-A-FRAME)
9  1    (deframe UNSLOTTED-FRAME)
1Ø 1    (deframe EMPTY-SLOT-FRAME
            (nomenclature "empty slot frame")
            ( ))
11 1    (deframe NO_NOMENCLATURE-FRAME
            (outputs (status))
12 1    (deframe UNKNOWN-SLOT-FRAME
            (nomenclature "unknown-slot-frame")
            (blivit 6))
13 2    (deframe CAMERA
            ... (ako ANALOG-OBJECT) ...
14 3    (deframe OPTO-BOARD
            ...delete OPTO-4A1 from instances...
15 4    (deframe POWER-SUPPLY
            ... (inputs elec-out) ...
15 4    (deframe RELAY
            ... (outputs cmd-in) ...

        *** Errors Inserted Into G:>morgan>alo-h2o.lisp.2 ***

6  3    (deframe KSC-POWER
            ... (outputs 6)...
6  3    (deframe 12ØVAC
            ... (inputs 2) ...
6  1Ø   (deframe HV-1Ø1
            ... (cam-coords 227.Ø ) ...
8  1    (deflame NOT-A-FRAME)
9  1    (deframe UNSLOTTED-FRAME)
1Ø 1    (deframe EMPTY-SLOT-FRAME
            (nomenclature "empty slot frame")
            ( ))
11 1    (deframe NO_NOMENCLATURE-FRAME
            (outputs (status))
12 1    (deframe UNKNOWN-SLOT-FRAME
            (nomenclature "unknown-slot-frame")
            (blivit 6))
14 14   (deframe SV-117-CMD
            ... (aio RELAY)...
```

```
15 14   (deframe SV-117
             ... (inputs (elec-in (RELAY-124 cmd-in))) ...
15 14   (deframe PX-105
             ... (outputs (pout PX-106-M in)))
16 14   (deframe PX-106-M
             ... (apo ALO-H20)
16 1    (deframe ALO-DIS
             ... delete VT-101 from parts slot ...
17 1    (deframe DISCONNECTED-FRAME
             (nomenclature "disconnected-frame")
             (icon LEVEL-SENSOR-ICON)
             (draw-connects (LEVEL-SENSOR-ICON frame-connected-to PUMP-ICON)))
```

APPENDIX E

KATE'S AUTOMATED ADMITTANCE INITIALIZATION PROCEDURE

Commands	Measurements
Consult pump specifications.	A6, pumps_admit = flow as function of pump pressure.
Vent tanks, close valves, etc., as in INITIALIZE-LAUNCH-SYSTEM procedure (see 1st reference below).	Patm = (avg PX1Ø1 PX1Ø2).
Open pilot valve SV1Ø4 & recirculation valve SV1Ø3, & run pump RPM1Ø1 @ 36ØØrpm.	f=FM1Ø3, P1=PX1Ø6, DPst=(avg DPX1Ø4 DPX1Ø5), A5[1], pump_circuit_admit =f/SQRT(P1 - Patm - DPst), A9[flow], recirculation_admit =f/SQRT(P1-Patm-DPst), Aa, recirc_line_admit = f / SQRT(P1 - GA1Ø3 - Patm), Ab = A9 - Aa, As = f / SQRT(PX1Ø5 - Patm - DPst), A7, pump_to_4_way = As - A6, DPsuc = (avg PX115 PX116), A8, suction_line_admit = f / SQRT(Patm+DPst-DPsuc), Ar = A5 - A8 - As.
Close SV1Ø4, open pilot valve SV1Ø5, stop RPM1Ø1, run pump RMP1Ø2 @ 36ØØrpm.	f = FM1Ø3, P1 = PX1Ø6, DPst = (avg DPX1Ø4 DPX1Ø5), A5[2], pump_circuit_admit = f / SQRT(P1-Patm-DPst),
Close SV1Ø3.	f = FM1Ø3, P1 = PX1Ø6, DPst = (avg DPX1Ø4 DPX1Ø5), A9[choke], recirculation_admit=f/SQRT(P1-Patm-DPst).
Open primary fast-fill valve SV1Ø7 & drain valve SV116.	f = FM1Ø1 + FM1Ø2, Ptsm = (avg PX1Ø7 PX1Ø8), Ah, drain_admit = f / SQRT(Ptsm - Patm). Ag, tsm_drain_asist_admit = Ah (approximately).
Close SV116 & open engine bleed valve SV1Ø9 & vehicle isolation valve SV111.	f = FM1Ø1 + FM1Ø2, Ptsm = (avg PX1Ø7 PX1Ø8), Ak, bleed_admit = f / SQRT(Ptsm - Patm).
Close SV1Ø9 & open nozzle valve SV11Ø.	f = FM1Ø1 + FM1Ø2, Ptsm = (avg PX1Ø7 PX1Ø8), Aj, nozzle_admit = f / SQRT(Ptsm - Patm).
Close SV11Ø.	f=FM1Ø1+FM1Ø2, P1=PX1Ø6, Pskid=(avg PX111 PX112), Ac, transfer_line_admit = f / SQRT(P1 - Pskid), f = FM1Ø2, Ptsm = (avg PX1Ø7 PX1Ø8), Ad, fast_fill_circuit_admit[pri]=f/SQRT(Pskid-Ptsm), Ap = Ad, DPvt = (avg DPX113 DPX114), Am, tank_fill_admit[vt] = f / SQRT(P1-Patm-DPvt), An, upper_fill_circuit_admit = Am - Ac.

Close SV1Ø7 & open second fast fill valve SV1Ø8.	f = FM1Ø2, Pskid = (avg PX111 PX112), Ptsm = (avg PX1Ø7 PX1Ø8), Ad, fast_fill_circuit_admit[sec]=f/SQRT(Pskid-Ptsm).
Close SV1Ø8 and scan replenish valve MCV1Ø1 from fully closed to 35% open.	For i = Ø to 35, fi = FM1Ø1, Pskid = (avg PX111 PX112), Ptsm = (avg PX1Ø7 PX1Ø8), Af[i], replenish_circuit_admit=fi/SQRT(Pskid-Ptsm). Ae, final_fill_circuit_admit = Af[33].

Continue pumping till the 2ØØ-gallon supply tank's 157-gallon level sensor LS1Ø5 = nil or the 1ØØ-gallon vehicle tank's 1Ø-gallon level sensor LS1Ø3 = t....

When LS1Ø5 = nil (157gal H2Ø & 43gal ullage), stop pump, close SV1Ø6, & open SV1Ø1. Pressurize ST1Ø1 to 27psi.	tau = elapsed time till (avg PX1Ø1 PX1Ø2) = 27psi, Pfinal = 27psi, Pasymptote = 3Øpsi, C = 43gal, R = -tau / (C * ln(1 - Pfinal / Pasymptote)), A2, st_up_admit = R.
Close SV1Ø1 & open SV1Ø6. Depressurize to 2.7psi.	tau = elapsed time till (avg PX1Ø1 PX1Ø2) = 2.7psi. Pinitial = 27psi, Pfinal = 2.7psi, C = 43gal, R = -tau / (C * ln(Pfinal / Pinitial)), A1, st_vent_admit = R.
When LS1Ø3 = t (1Øgal H2Ø & 9Øgal ullage), stop pump, close SV11Ø, & open SV114. Pressurize VT1Ø1 to 63psi.	tau = elapsed time till (avg PX1Ø9 PX11Ø) = 63psi, Pfinal = 63psi, Pasymptote = 7Øpsi, C = 9Øgal, R = -tau / (C * ln(1 - Pfinal / Pasymptote)), A4, vt_up_admit = R.
Close SV114 & open SV11Ø. Depressurize to 6.3psi.	tau = elapsed time till (avg PX1Ø9 PX11Ø) = 6.3psi. Pinitial = 63psi, Pfinal = 6.3psi, C = 9Ø gal, R = -tau / (C * ln(Pfinal / Pinitial)), A3, vt_vent_admit = R.

Continue pumping till the supply tank's 12Øgal level sensor LS1Ø6 = nil, and repeat the supply tank pressurization/depressurization cycle above, substituting an 8Øgal ullage in the st_vent_admit and st_up_admit formulas. Actual values of st_vent_admit and st_up_admit are averages of their original and new measurements.

Continue pumping till the vehicle tank's 8Øgal level sensor LS1Ø2 = t, repeat the vehicle tank pressurization/depressurization cycle above, substituting an 2Øgal ullage in the vt_vent_admit and vt_up_admit formulas. Actual values of vt_vent_admit and vt_up_admit are averages of their original and new measurements.

Unmeasureable.	Ai, admittance of the GN2-carrying supply line that assists in tsm drainage, probably is negligible compared with the attached H2O-carrying drain line admittance, Ah.

APPENDIX F

TWO-PORT PSEUDO OBJECT ALTERNATIVE CODING SUGGESTION

```
;;;   Two-Port Pseudo Object Alternative
;;;   Steve Morgan, 2 August 1991.

;;;   Test a particular ALO-H2O modeled pressure.
(defun PX101 ()
  (pressure-between T4 T5))

;;;   Pressure at a node between two devices.
(defun pressure-between (left right)
  (+ (P left 'out) (* (R left 'out) (/ (- (P right 'in) (P left 'out))
                                       (+ (R left 'out) (R right 'in))))))

;;;   First listed parameter for this port is its Thevenin equivalent pressure.
(defun P (object port)
  (CAR (object port)))

;;;   First listed parameter for this port is its Thevenin equivalent resistance.
(defun R (object port)
  (CADR (object port)))

;;;   Third listed parameter for this port is its Thevenin equivalent admittance.
(defun G (object port)
  (CADDR (object port)))

;;;  The instance-level devices and their connections.

(defun T4 (port)
  (tee port (SV102 'out) (T5 'in) (T3 'out)))

(defun T5 (port)
  (tee port (T4 'out) (T6 'in) (SV106 'out)))

(defun T1 (port)
  (tee port (PRU102 'out) (SV102 'in) (T2 'in)))

(defun T2 (port)
  (tee port (T1 'by) (HV103 'in) (SV101 'in)))

(defun T3 (port)
  (tee port (HV103 'out) (T4 'by) (SV101 'out)))

(defun SV101 (port this-admittance in out)
  (admit port 1 (T2 'by) (T3 'by)))

(defun SV102 (port)
  (admit port 2 (T1 'out) (T4 'in)))

(defun HV103 (port)
  (admit port 3 (T2 'out) (T3 in)))

(defun PRU102 (port)
  (COND (EQ port 'out) (LIST 30 0 'bignum)))

(defun SV106 (port)
  (COND (EQ port 'out) (LIST 0 (invert 6) 6)))

(defun T6 (port)
  (COND (EQ port 'in) (LIST 0 (invert 101) 101))) ;;this is a stub...

;;;  P,R,G of this port, given devices connected to tee's in, out, and by ports.
(defun tee (port in out by)
       (COND ((EQ port 'in)  (LIST (Pt in out by) (Rt in out by) (Gt in out by)))
             ((EQ port 'out) (LIST (Pt out in by) (Rt out in by) (Gt out in by)))
             ((EQ port 'by)  (LIST (Pt by in out) (Rt by in out) (Gt by in out)))
             (t (PRINT '(No such tee port)))))

;;;  Pressure seen in this port, given devices connected to tee's other and 3rd ports.
(defun Pt (this-port other-port third-port)
  (+ (P other-port) (* (R other-port) (/ (- (P third-port) (P other-port))
                                         (+ (R other-port) (R third-port))))))

(defun Gt (this-port other-port third-port)
  (+ (G other-port) (G third-port)))

(defun Rt (this-port other-port third-port)
  (invert (Gt this-port)))
```

```
;;;   P,R,G for this port, given inside admittance & devices connected to it.
(defun admit (port thisG inG outG)
       (COND ((EQ port 'in)  (LIST (P out) (sumR thisG outG)
                                   (invert (sumR thisG outG))))
             ((EQ port 'out) (LIST (P in)  (sumR thisG inG)
                                   (invert (sumR thisG inG))))
             (t (PRINT '(No such admit port)))))

(defun sumR (G1 G2)
  (+ (invert G1) (invert G2)))

(defun invert (thing)
  (/ 1. thing))
```

REFERENCES

1. Tom Gould: "KATE Knowledge Base Generation Guide." Boeing Artificial Intelligence Lab, NASA Kennedy Space Center, 4 September 1990.

2. J.E. Freund & R.E. Walpole: "Mathematical Statistics." 3rd Ed., Prentice-Hall, 1972.

3. H. Abelson & G.J. Sussman: "Structure and Interpretation of Computer Programs." Cambridge, MIT Press (McGraw-Hill), 1986.

4. P.H. Winston & B.K.P Horn, "LISP." 2nd Ed., Reading, MA, Addison-Wesley, 1984, Chapter 12.

5. C.L. Belton: "Verification and Continual Adaptation of Model-Based Representations of Engineering Systems Through Learning." PhD Dissertation, University of London, June 1990.

6. Boeing Computer Services' Artificial Intelligence Center: "Environmental Control and Life Support System Advanced Automation Project -- 1990 Annual Report." Prepared for NASA's Marshall Space Flight Center under Contract No. NASA 8-37200, 30 November 1990.

7. T.J. McCabe: "McCabe Complexity Measurement Seminar," NASA Kennedy Space Center, 22 July 1991.

8. J.E. Whitlow: "Modeling of Flow Systems for Implementation Under KATE." 1990 Research Reports, L.A. Anderson & M.A. Beyner, Eds., NASA/ASEE Summer Faculty Fellowship Program, NASA Contractor Report No. CR-187638, September 1990, pp. 488 ff.

1991 NASA/ASEE SUMMER FACULTY FELLOWSHIP PROGRAM

JOHN F. KENNEDY SPACE CENTER
UNIVERSITY OF CENTRAL FLORIDA

EVALUATION OF SURLYN 8920 AS PHE VISOR MATERIAL AND EVALUATIONS OF NEW ADHESIVES FOR IMPROVING BONDING BETWEEN TEFLON AND STAINLESS STEEL AT CRYOGENIC TEMPERATURE

PREPARED BY:	Dr. Asit K. Ray
ACADEMIC RANK:	Associate Professor
UNIVERSITY AND DEPARTMENT:	Christian Brothers University Department of Chemical Engineering
NASA/KSC	
DIVISION:	Materials Science Laboratory
BRANCH:	Failure Analysis and Materials Evaluation Branch
NASA COLLEAGUE:	Mr. Coleman Bryan
DATE:	August 16, 1991
CONTRACT NUMBER:	University of Central Florida NASA-NGT-60002 Supplement: 6

ACKNOWLEDGMENT

I am grateful to NASA/ASEE Summer Faculty Program, to Dr. E. R. Hosler of the University of Central Florida and Dr. Mark Beymer of the Kennedy Space Center (KSC) for providing me the opportunity of spending an enjoyable, productive and rewarding summer. Many thanks to Dr. Hosler for his kind and efficient overseeing of the Fellows and to Mrs. Kari Stiles for her administrative help. Thanks are due to Mr. Charles Hoppesch and Mr. Irby Moore of the Materials Science Division for their help and cooperation.

Special thanks are extended to my KSC colleague, Mr. Coleman Bryan for suggesting the projects and for his guidance and encouragement in all phases of these projects. Special thanks are also due to Mr. Mark Davis, a Summer Co-op student from the University of California, Santa Barbara, for helping me in all the phases of these projects. Special appreciations are due to Mrs. Karen Thompson and Mr. Peter Marciniak for generous help and interesting discussions and to Mr. Napoleon Salvail, Mr. Dean Lewis and Ms. Devon Sorrell for coordinating and running the tensile test on the Instron. Ms. Judy Blocker and Ms. Sharon Drake deserve special appreciation for typing the two-part report under constraint of time. Finally, thanks are due to all of the professionals working in the Failure Analysis and Materials Evaluation Branch who made me feel welcome and for the helps and pleasant interactions we all had while working in the different laboratories.

EVALUATION OF SURLYN 8920 AS PHE VISOR MATERIAL

TABLE OF CONTENTS

ABSTRACT

Surlyn 8920 (an ionic and amorphous low density polyethylene made by Dupont) was evaluated as a possible replacement of Plexyglass G as PHE visor material. Four formulations of the polymer were made by adding different amounts of UV stabilizer, energy quencher, and antioxident in a Brabender plasticorder. The formulated polymers were molded in the form of sheets in a compression molder. Cut samples from the molded sheets were exposed in a weatherometer and tested on Instron Tensile Tester for strength and elongation. Specially molded samples of the formulated polymers were subjected to Charpy Impact test.

Data from the Instron Tensile test of samples showed some loss in strength and ductility of the formulated Surlyn polymers at 500 and 1000 hours of exposure in the weatherometer. The unformulated polymer had greater loss in strength and complete loss of ductility at 1000 hours of exposure. The plexyglass samples gave higher tensile strength but zero ductility (% elongation) at zero exposure.

Charpy impact tests of specially molded samples show Surlyn 8920 to have impact strength 30 - 40 times higher than Plexyglass G (current PHE visor material) and an order of magnitude higher than Lexan (polycarbonate made by G.E.). Formulated Surlyn gave 50% higher impact strength than unformulated Surlyn.

The formulated polymer giving the best balance of tensile and impact resistant properties was them molded in the form resembling a visor. These curved, molded samples successfully passed the ANSI Weight Drop Impact Test.

Based on the Instron and Impact test data, Surlyn 8920 indicated superior ductility and impact strength with adequate tensile strength compared to Plexyglass G, the current PHE visor material. On the basis of these results, it is recommended that Surlyn 8920 replace Plexyglass G as PHE visor material.

1.0 INTRODUCTION

1.1 Background Information

Current material used for making Propellant Handlers Ensembles (PHE) visor, Plexyglass G, has poor impact and scratch resistance. Because of its brittle nature the plexyglass PHE visor can be easily damaged during the process of handling solid propellants and endanger the health and life of a handler due to exposure to highly toxic hypergolic chemicals.

Surlyn 8920, an ionic and amorphous polyethylene made by Dupont Co. was chosen by Coleman Bryan because of its excellent mechanical and optical properties and resistances to toxic chemicals including the hypergols. This polymer should possess excellent impact resistance because of its ethenic and noncrystalline nature. Low cost of the polymer ($1.60/lb.) is an additional bonus.

Resistance to UV and oxidation degradation were to be improved by adding optimum quantities of UV stabilizer, energy quencher, and antioxidants.

2.1 Scope of the Project

This project involves evaluation of the formulated polymer encompassing the following four steps:

a. Formulation of the polymer.

b. Molding of the formulated polymer to make samples (exposed or unexposed in the weatherometer) for testing on the Instron Tensile Testing machine.

c. Molding of formulated polymers to make special samples for Charpy impact testing.

d. Evaluation of the tensile and impact properties of these samples.

e. Molding of the polymer formulation giving the best balance of tensile and impact resistant properties in the form of visor and subject these to ANSI Weight Drop Impact Test.

f. Make final recommendation regarding suitability of Surlyn 8920 as a replacement for current PHE visor material.

2.0 MATERIALS AND METHODS

2.1 Formulation of Polymer

Four formulations of Surlyn 8920 were made in a Brabender Plasticorder by adding different amounts of UV stabilizer (Tinuvin 328, 0.7%), energy quencher (Tinuvin 770, 0.5 or 1.0%), antioxidant (Irganox, 0.1 or .3%) and color masking agent (Monastal Blue, 2-10 ppm). The plasticorder was run at 165°C with mixing time of 10 minutes at 120 RPM with 1 minute of melting time for the polymer. The hygroscopic polymer was stored in a dessicant and dried periodically by pulling vacuum. Weight of each batch was 40 gms of dry polymer plus the ingredients listed above. Presence of moisture in the polymer necessitates the use of higher temperature in the plasticorder (145°C vs 165°C). The plasticorder was fitted with Branbury mixer containing sigma type mixing blades.

2.2 Molding of the Formulated Polymer

The formulated and unformulated polymer batches (38 gms) were then molded into 6-inch x 6-inch x 0.07-inch sheets in a Dake Compression molder at 270°F (132°C) at a force of 30,000 pounds (833 psi) using Mylar film on both sides as mold releasing agent. A molding cycle of five minutes was used. The sheets had some defects caused by air bubbles formed during thermoforming. No further experimentation was made to solve this problem because of the shortness of this summer program. The 6-inch x 6-inch molded sheets were molded to 10-inch x 10-inch sheets to improve product uniformity. Dogbone shaped samples were cut according to ASTM D 638-86 (Type V) specifications taking care to exclude molding defects. These were then mounted in the ATLAS Weather-meter at 50°C, energy density = 0.35 Watt/m^2 at 340 nm, humidity = 30% for 500, 1000, and 1500 hours exposures. A total of 60 samples were mounted for four formulated polymers and unformulated polymer (3 samples per polymer type per type of exposure). The samples exposed and unexposed were tested on the Instron Tensile Testing machine for strength and elongation (ductility).

2.3 Charpy Impact Test

Notched samples (ASTM D 256-84) of the formulated and unformulated polymers were molded using the Dake Compression molder (temperature 130°C, cycle time 5 minutes, force 10,000 pounds (600 psi) using a special mold fabricated by the Prototype Shop. The samples molded had defects caused by air bubbles formed during the thermoforming. No further effort was made to

correct this. Similar samples of dexan (polycarbonate) and Plexyglass G were also made from flat sheets of materials made industrially. These samples were tested on the Charpy Impact tester for plastics according to ASTM method.

2.4 Instron Tensile Test

The tensile tests of the polymer samples (Surlyn 8920 and Plexyglass G) were completed using an Instron Tensile Testing Machine (Model 1125) at a pulling speed of 20 inch/min. and having a computerized data handling facility. The testing procedures followed specification according to ASTM standard (D412).

2.5 ANSI Weight Drop Impact Test

The polymer formulation giving the best balance of tensile and impact resistant properties were then molded into the form of visor (duplicating its curved surface) using a mold designed by Coleman Bryan and fabricated by the Prototype Shop. These samples were tested for impact strength using ANSI Weight Drop Test (Z87.1). Where 2.5 ounce, one inch diameter weight steel ball was dropped from a height of 50 inches on the curved sample.

3.0 RESULTS

3.1 Charpy Impact Test

The results of the Charpy Impact tests on unformulated, formulated Surlyn 8920, Plexyglass G, and Lexan (polycarbonate) are shown on Table 1. All the Surlyn 9020 samples had 30 to 40 times higher impact strength than that of Plexyglass G and one order of magnitude higher impact strength than Lexan (Polycarbonate made by G.E.). The unformulated samples gave lower impact strength compared with those of the formulated ones. The formulated polymer M_3 gave slightly lower impact strength than the other three formulated polymers (M_1, M_2, and M_4) and this can be ascribed to higher defect level of the samples caused during the compression molding process.

3.2 Instron Tensile Test

The results of the tensile tests are given in Table 2 for Surlyn 8920 at zero, 500, and 1000 hours of exposure in the Atlas Weatherometer and for Plexyglass G at zero hour exposure. Also, the literature data of Surlyn 8920 and Plexyglass G are presented. The formulated polymer samples show some loss of strength and ductility at 500 hours of exposure. The unformulated polymer samples

show greater loss in strength and ductility. At 1000 hours exposure the formulated polymer samples showed no further loss in tensile properties. But the unformulated polymer samples showed further loss in strength and total loss in ductility (percent elongation). At 1000 hours of exposure, samples of polymer M_4 show an increase in strength and ductility over these values at zero or 500 hours of exposure, which is unexpected. One explanation is that the samples, used for the 1000 hours of exposure were of better quality, having a lower defect level. The Plexyglass G samples at zero exposure gave higher strength but zero percent elongation. The Surlyn (formulated and unformulated) samples gave higher strength and about equal elongation compared to data supplied by Dupont Co. Exposures up to 1500 hours of the Surlyn 8920 samples and up to 500 hours for Plexyglass G samples are under way.

3.3 ANSI Weight Drop Impact Test

The polymer formulations M_1 and M_2 gave the best balance of tensile and impact resistance properties. Curved samples made using these polymers successfully passed the ANSI Impact test where a steel ball weighing 2.5 ounce was dropped from the height of 50 inches.

4.0 CONCLUSIONS

4.1 The Brabender Plasticorder with mixing head proved adequate mixing of the Surlyn 8920 polymer beads with UV stabilizer, energy quencher, antioxidant, and color masking agent. The Dake Compression Molder gave adequate samples; however, some defects that occurred during molding operation caused variations in the tensile and impact strength data.

4.2 The formulated Surlyn polymer samples successfully withstood (some loss in strength and ductility) the exposure to UV light and moisture at 1000 hours of exposure in the Weatherometer. Where as the unformulated polymer samples did not. The unexposed plexyglass samples having UV stabilizer gave higher strength but zero percent elongation (ductility).

4.3 Formulated Surlyn samples gave 30 to 40 times higher Charpy Impact strength than Plexyglass G samples and greater than 10 times higher impact strength than Lexan (polycarbonate). Formulation of Surlyn by addition of ingredients mentioned in Section 4.1 improved its impact strength by 50% over the unformulated polymer, an unexpected bonus.

4.4 Special molded samples made from the best formulated polymer (based on tensile and impact test data) easily passed the ANSI Weight Drop Impact Test.

5.0 RECOMMENDATIONS

Based on the tensile and impact test data, formulated Surlyn 8920 samples show strength comparable to that of Plexyglass G at zero exposure in the Weatherometer; however, ductility was far superior (350% to 0% elongation). These formulated polymer samples maintained most of its optical clarity, strength, and ductility at 1000 hours of exposure in the Weatherometer.

Based on these results, it is recommended that Surlyn 8920, modified according to formulation M_1 or superior, replace Plexyglass G, the current materials for PHE visor.

TABLE 1

CHARPY IMPACT TEST DATA OF SURLYN 8920
LEXAN AND PLEXYGLASS

		IMPACT STRENGTH (INCH-POUND)					
POLYMER	TYPE	SAMPLE #1	SAMPLE #2	SAMPLE #3	SAMPLE #4	SAMPLE #5	AVERAGE
SURLYN (M_1)	FORMULATED	164	146	150	144	168	154.4
SURLYN (M_2)	FORMULATED	128	150	164	168	156	153.2
SURLYN (M_3)	FORMULATED	130	122	130	128	162	134.4
SURLYN (M_4)	FORMULATED	160	144	148	140	152	148.8
SURLYN (P)	UNFORMULATED	110	106	90	90	80	95.2
*SURLYN (P)	UNFORMULATED	88	100	94	100	-	95.5
PLEXYGLASS	UNFORMULATED	4.5	4.0	4.0	4.5	4.0	4.2
LEXAN (POLYCARBONATE)	UNFORMULATED	14	14	12	12	14	13.2

*REPLICATED

TABLE 2

STRENGTH AND DUCTILITY DATA OF SURLYN 8920 FORMULATED POLYMER

SAMPLE	TYPE	TENSILE STRENGTH (PSI)	ELONGATION (PER CENT)
P_0	FORMULATED AND UNEXPOSED	3492	315
M_{10}	FORMULATED AND UNEXPOSED	3262	340
M_{20}	FORMULATED AND UNEXPOSED	3249	345
M_{30}	FORMULATED AND UNEXPOSED	3445	343
M_{40}	FORMULATED AND UNEXPOSED	3111	283
PX_0 (PLEXYGLASS)	FORMULATED AND UNEXPOSED	7052	0
P_1	UNFORMULATED BUT EXPOSED 500 HOURS	2966	285
M_{11}	FORMULATED AND EXPOSED 500 HOURS	3047	300
M_{21}	FORMULATED AND EXPOSED 500 HOURS	3181	280
M_{31}	FORMULATED AND EXPOSED 500 HOURS	3250	243
M_{41}	FORMULATED AND EXPOSED 500 HOURS	3183	220
SURLYN 8920	VENDOR DATA	2200	350
PLEXYGLASS G	LITERATURE DATA	5500	35

M_1	ANTIOXIDANT	0.3%	M_2	ANTIOXIDANT	0.1%
	ENERGY QUENCHER	1.0%		ENERGY QUENCHER	1.0%
M_3	ANTIOXIDANT	0.3%	M_4	ANTIOXIDANT	0.1%
	ENERGY QUENCHER	0.5%		ENERGY QUENCHER	0.5%

ALL FORMULATIONS HAD 0.7% UV STABILIZER AND 2 - 10 PPM MONASTAL

BLUE AS COLOR MASKING AGENT.

TABLE 2

STRENGTH AND DUCTILITY DATA OF SURLYN 8920 FORMULATED POLYMER

SAMPLE	TYPE	TENSILE STRENGTH (PSI)	ELONGATION (PER CENT)
M_{12}	FORMULATED AND EXPOSED 1000 HOURS	3179	350
M_{22}	FORMULATED AND EXPOSED 1000 HOURS	3180	353
M_{32}	FORMULATED AND EXPOSED 1000 HOURS	3146	323
M_{42}	FORMULATED AND EXPOSED 1000 HOURS	3285	367
P_2	UNFORMULATED AND EXPOSED 1000 HOURS	2765	0
*M_{13}	FORMULATED AND EXPOSED 1500 HOURS	--	--
*M_{23}	FORMULATED AND EXPOSED 1500 HOURS	--	--
*M_{33}	FORMULATED AND EXPOSED 1500 HOURS	--	--
*M_{43}	FORMULATED AND EXPOSED 1500 HOURS	--	--
*PLEXYGLASS G	FORMULATED AND EXPOSED 500 HOURS	--	--

*UNDERGOING EXPOSURE IN THE WEATHEROMETER

BRABENDER PLASTICORDER WITH BRANBURY MIXER
EQUIPPED WITH SIGMA TYPE MIXING BLADE.

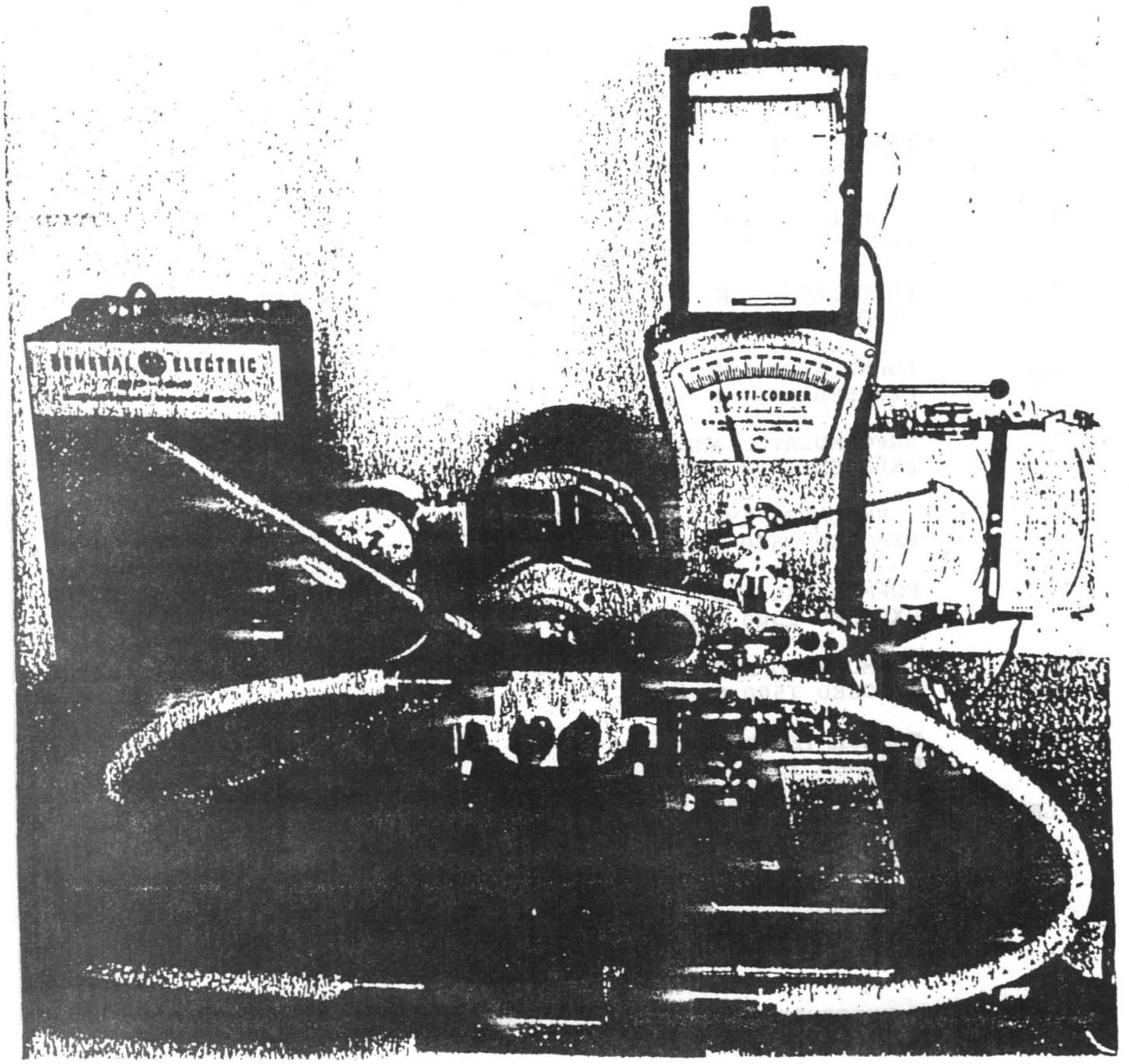

SHOWN IS THE LATEST HIGH TORQUE
STEPLESS VARIABLE SPEED MODEL PL-V150
WITH SCR CONTROL

EVALUATION ON NEW ADHESIVES FOR IMPROVING BONDING OF TEFLON AND STAINLESS STEEL AT CRYOGENIC TEMPERATURE

TABLE OF CONTENTS

ABSTRACT

Preliminary evaluations of adhesives for improvement of bonding between Teflon and stainless steel (SS) were done. Kapton, a high temperature polyimide made by Dupont Co., and a rubber based adhesive made by Potter Paint Co. of Indiana, were evaluated against industrial quality epoxy, the current material used to bond Teflon and SS. The degreased surfaces of the Teflon discs were etched chemically. The surfaces of the SS discs were etched mechanically, with a few of these etched chemically. The surfaces of the SS discs were etched mechanically, with a few of these etched chemically. Bonding strengths were evaluated using lap shear test on the Instron Tensile tester for the samples bonded by Kapton and industrial quality epoxy. Bond strengths were also evaluated using pull test on the Instron for the samples bonded by Potter adhesive (CWL-152) and industrial quality epoxy. Based on limited lap shear data, Kapton gave bond strength favorable compared to that of industrial epoxy. Based on limited pull test data, Kapton bonded and CWL-152 bonded samples showed poor strength compared to epoxy bonded sample.

1.0 INTRODUCTION

Teflon-clad stainless steel (SS) pipes and valves are used for transporting liquid oxygen from storage tank to the external tank used with the Orbiter. The adhesive (epoxy) used to bond the SS with Teflon is adequate at room or lower temperature. However, at liquid nitrogen temperature, the bonding material becomes brittle leading to debonding and delamination. Hence, there is the necessity of finding an adhesive that will be able to maintain adequate bonding at liquid oxygen or nitrogen temperature.

Two materials were selected as possible replacement of epoxy as the bonding agent. Kapton, made by Dupont Co. and CWL-152, made by Potter Paint Co. of Indiana. The former was selected by Coleman Bryan, the colleague of the author on telephone inquiry to Dupont Co. The second one was recommended to the author by Mr. Charles Olie Pike, one of the consultant accessed through TelTech Inc.

This project was to learn to use and evaluate these two materials as possible adhesive for bonding SS with Teflon at liquid nitrogen temperature.

2.0 MATERIALS AND METHODS

2.1 Adhesives

Kapton (RK-692) is a high temperature aromatic polyimide developed by Dupont Co. to be used as varnish film for electrical wire and film. It has excellent thermal, electrical, and mechanical properties at high temperature. Low temperature property data are not available.

CWL-152 is a waterborne lacquer developed by Mr. Charles Olie Pike for Potter Paint Co. of Indiana for low temperature application meant for automotive industry. The epoxy used in a general purpose epoxy Stycast 2651 made by Emerson & Cumming Co., to be used with a suitable catalyst.

2.2 Stainless Steel and Telfon

The materials for bonding test were in the form of discs (3/4 inch x 1/2 inch) cut from sheet of Teflon with one side etched chemically by the vendor. The SS discs (3/4 inch x 1/2 inch) were fabricated at the Prototype Shop.

2.3 Surface Preparation

The Teflon and SS discs were degreased in a Sonblaster vapor degreaser using Freon-113 as solvent, air dried, and stored in brand new or cleaned glass petri dishes with covers. The SS disc surfaces were further roughened by rubbing with #180 sandpaper and cleaned with MEK. The surface of Teflon (one side already etched) discs were etched using Tetra-Etch and procedures recommended by W. L. Gore & Associates, Inc. The surfaces of aluminium coupons used for the lap shear test for evaluation of bond strength were cleaned by sulfuric acid Pasajell-105, washed with deionized water, abraded using #180 sandpaper, washed with deionized water and air-dried. A few of the SS discs were chemically etched by treating these with acetic acid, nitric acid, and hydrochloric acid in proportions of 2:2:7 for a half-hour with frequent stirring.

2.4 Bonding and Curing

2.4.1 Kapton

The SS discs were bonded with Teflon discs (industrially etched side) using two step bonding and curing process developed after several experimental runs.

Step 1- Apply the Kapton (refrigerated) with an eye dropper to both discs. Heat it in a forced convection oven (BLUE M) at 265°F (~130°C) for eight to ten minutes. The Kapton should have the consistency semi-solid at this point. Pull these out of the oven and bond these with hand pressure to squeeze out excess glues and wipe it off making sure not to contaminate the outside surfaces and then clamping with small clip-binders.

Step 2- Heat the bonded discs in the oven at 440°F (~230°C) for one hour.

The first step is essentially a solvent removal, and the second step is the conversion of the polymer to its final insoluble, infusible form. Use of forced convection oven facilitates proper removal of solvent.

2.4.2 CWL-152

Step 1- Apply the adhesive to the SS disc. Heat the SS disc and Teflon disc (without adhesive) in

the forced convection oven at 150°F for at least ten minutes. Bond these together by hand pressure, removing and wiping off excess adhesive and ensuring no contamination of the outside surfaces and clamp using small clip-binders.

Step 2- Heat the bonded materials at 265°F (130°C) for one hour to improve bonding.

Step 3- Cure for 72 hours at room temperature.

2.4.3 Epoxy - Stycast 2651

Step 1- The epoxy is mixed with #9 catalyst (6-7% by weight) allowing about 30 minutes for this to reach consistency of semi-solid. Apply the epoxy on both or either of the Teflon and SS discs, bond by hand pressure, remove excess adhesive, and clamp with small clip binders.

Step 2- Cure in oven at temperature of 160-170°F (71-77°C) for one hour.

3.0 MAKING SAMPLES FOR BOND STRENGTH TEST

Two types of samples were made for two types of test: lap shear and pull test, both on the Instron Tensile Tester. For the pull test, aluminium rods (surface degreased, cleaned, and roughened using sandpaper) were bonded to the outer Teflon and stainless surfaces using epoxy as described in section 2.4.3. For the lap shear test, four aluminium coupons were bonded to the SS surfaces first using epoxy. Four aluminium coupons were bonded to the Teflon surfaces making sure to provide proper weight on this aluminium coupon in order to keep the bonds in place.

4.0 RESULTS - BOND STRENGTH

4.1 Kapton and Epoxy

Initially Kapton was evaluated against Epoxy (Stycast 2651) as adhesive. Results of the lap-shear test are given: Epoxy-300 psi, Kapton-180 and 150 psi.

Examination of the surfaces of the Instron-broken samples showed good bonding on the Teflon side and poor bonding on the SS side (mechanically etched) hence the SS discs needs more effective surface preparation. The pulling tests were not done on the Instron because the Kapton samples broke by slight pressure applied by fingers.

4.2 Kapton, CWL-152 and Epoxy

Samples were made for pull test using chemically etched (hoping to improve bonding) SS discs for Kapton, CWL-12 and mechanically roughened SS discs for CWL-152 and epoxy. The Teflon discs were chemically etched, one side industrially, the other side by the author. Results of pull tests are given: Epoxy = 505 psi, CWL-152 = 11.5 psi.

5.0 CONCLUSIONS

Based on this preliminary evaluation of bonding ability of the three adhesives, Kapton, CWL-152, and epoxy (Stycast 2651 and #9 catalyst), the following conclusions are made:

a. Kapton can bond Teflon with SS and, with proper processing, can give bond strength comparable to epoxy, based on lap shear tests. The bond strength of Kapton bonded SS and Teflon is poor compared to that of epoxy bonded SS and Teflon, based on pull tests.

b. Teflon bonded with SS by CWL-152 gave poor bond strength compared to those bonded by epoxy, based on pull tests.

c. Bonds between SS and Teflon made by all the three adhesives fell apart at liquid nitrogen temperature most probably due to different degree of contractions of the Telfon, SS, and the bonds in between.

6.0 RECOMMENDATIONS

A more detailed study based on fundamentals of adhesion theory and technology is recommended. This should include:

a. Searching and/or formulation of adhesives specially designed for cryogenic temperature.

b. Evaluation of surfaces of Teflon and SS using state of the art spectroscopic methods (ESCA, SIM, etc.) and optimize these to improve bonding at that will overcome the stress caused due to unequal contractions of the bond and bonded materials at cryogenic temperature.

APPENDIX

NASA
DIRECTOR OF ENGINEERING DEVELOPMENT
DIRECTOR, MECHANICAL ENGINEERING
MATERIALS SCIENCE LABORATORY
FAILURE ANALYSIS AND MATERIALS EVALUATION BRANCH
PHYSICAL TESTING SECTION
DM-MSL-24, ROOM 1218, O&C BUILDING
KENNEDY SPACE CENTER, FLORIDA 32899

JULY 23, 1991

REPORT NUMBER 91-4873

SUBJECT: EXPERIMENTAL PLASTICS

REQUESTOR: ASIT K. RAY
MAIL CODE: DM-MSL-22
PHONE: 867-3400

TEST METHOD: PER ASTM

SPECIMEN	LOAD (LBS)	AREA (SQ. IN)	ULTIMATE TENSILE STRENGTH (PSI)
P_0	75.093	0.0228	3492.07*
P_1	66.293	0.0232	2966.00*
M_{10}	66.733	0.0204	3262.00
M_{20}	67.467	0.0228	3249.00*
M_{30}	76.267	0.0222	3445.00
M_{40}	75.167	0.0241	3111.27
M_{11}	60.647	0.0207	2946.28
M_{21}	73.260	0.0230	3181.37
M_{31}	69.667	0.0215	3249.60
M_{41}	74.067	0.0233	3183.47

SPECIMEN	YIELD (LBS)	ELONGATION %
P_0	54.67	315*
P_1	63.00	285*
M_{10}	44.73	340
M_{20}	48.40	345*
M_{30}	49.13	343
M_{40}	49.87	283
M_{11}	48.40	243
M_{21}	52.80	280
M_{31}	47.67	243
M_{41}	47.67	220

*BASED ON TWO OF THE THREE DATA POINTS. THE THIRD DATA POINT WAS DISCARDED BECAUSE OF A POOR SAMPLE.

INVESTIGATOR: N. Sarrell
for D. SORRELL

APPROVAL: N. Sarrell
N. SALVAIL, CHIEF

NASA
DIRECTOR OF ENGINEERING DEVELOPMENT
DIRECTOR, MECHANICAL ENGINEERING
MATERIALS SCIENCE LABORATORY
FAILURE ANALYSIS AND MATERIAL EVALUATION BRANCH
PHYSICAL TESTING SECTION
DM-MSL-24, ROOM 1218, O&C BUILDING
KENNEDY SPACE CENTER, FLORIDA 32899

91-4940

SUBJECT: POLYMER SAMPLES

REQUESTOR: ASIT K. RAY
MAIL CODE: DM-MSL-22
PHONE # : 867-3400

TEST METHOD: PER ASTM SPECIFICATIONS.

SPECIMEN (#)	MAX. LOAD (LBS)	STRESS AREA (IN2)	ULTIMATE TENSILE STRENGTH (PSI)	ELONGATION (%)
M12-1	73.81	0.022	3355	360
M12-2	67.43	0.0224	3010	330
M12-3	74.58	0.0235	3173	360
AVERAGE	71.94	0.0226	3179	350
M22-1	77.88	0.0233	3342	370
M22-2	70.18	0.0227	3091	340
M22-3	69.30	0.0223	3107	350
AVERAGE	72.45	0.0227	3180	353
M32-1	58.30	0.0214	2724	210
M32-2	75.24	0.0225	3344	380
M32-3	72.38	0.0215	3366	380
AVERAGE	68.64	0.0218	3144	323
M42-1	80.30	0.0221	3633	420
M42-2	65.12	0.022	2960	320
M42-3	78.21	0.024	3258	360
AVERAGE	74.54	0.0227	3283	366
P2-1	68.20	0.0239	2853	N/A
P2-2	67.10	0.0242	2772	N/A
P2-3	63.80	0.0239	2669	N/A
AVERAGE	66.36	0.024	2764	N/A
PXo-1	103.18	0.0133	7757	N/A
PXo-2	92.73	0.0135	6868	N/A
PXo-3	83.60	0.0128	6531	N/A
AVERAGE	93.17	0.0132	7052	N/A

CWL-152-1	4.4	0.441	9.97	N/A
CWL-152-2	5.72	0.441	12.97	N/A
AVERAGE	5.06	0.441	11.47	N/A
EPOXY-1E	220	0.441	498.87	N/A
EPOXY-1E	225.28	0.441	510.84	N/A
AVERAGE	222.64	0.441	504.85	N/A

COMPLETED ON: 14 AUGUST 1991

INVESTIGATOR: Dean C. Lewis
D. LEWIS, DM-MSL-24/NASA

APPROVAL: N. Salvail
N. SALVAIL, CHIEF, DM-MSL-24/NASA

1991 NASA/ASEE SUMMER FACULTY FELLOWSHIP PROGRAM

JOHN F. KENNEDY SPACE CENTER
UNIVERSITY OF CENTRAL FLORIDA

TRANSIENT STUDY OF A CRYOGENIC HYDROGEN FILLING SYSTEM

PREPARED BY:	Dr. John T. Rompala
ACADEMIC RANK:	Assistant Professor
UNIVERSITY AND DEPARTMENT:	University of Wisconsin - Stout Physics Department
NASA/KSC	
DIVISION:	Electronic Systems
BRANCH:	Atmospheric Science
NASA COLLEAGUE:	William Jafferis
DATE:	August 14, 1991
CONTRACT NUMBER:	University of Central Florida NASA-NGT-60002 Supplement: 6

ACKNOWLEDGEMENTS

This participant in the NASA/ASEE Summer Faculty Fellowship Program extends his thanks to all those associated with the program for this opportunity for creativity and education. In particular, he wishes to thank Dr. M. Beymer, Dr. E. Hosler, and their assistant, Ms. K. Stiles for organizing excellent activities and procedures.

The support, advice, direction, and encouragement given to the participant by his colleague, Mr. W. Jafferis, is greatly appreciated.

Much is owed to many others for their contributions to this summer's effort. A partial list includes: Mr. D.Conover, another colleague, for providing insight and perspective; Mr. N. Schultz, for providing hardware and data support; Mr. R. Wojtasinski, for offering historical insight; and Mr. R. Neely and Ms. B. Atkins, for offering information on computer support and solutions. A special thanks goes to Mr. O. Varosi for timely advice and assistance in bringing this work to a successful conclusion.

JTR

ABSTRACT

A flexible and functional analytical tool is developed for the study of electric fields during adverse weather conditions. This tool is designed for use by members of the Atmospheric Science Group as part of their overall effort to appraise environmental conditions during these situations. It is also used to illustrate approaches open to those interested in the study of the physics of ambient electric field phenomena.

Computer resources of the Kennedy Space Center are coordinated with original software to produce contour interpretations of electric field data available from a grid of field mills spanning the region. Three model algorithms are presented and examples given illustrating the systems design, flexibility and utility.

SUMMARY

The Kennedy Space Center and Cape Canaveral Air Force Station support an irregular grid of ground level electric field mills which monitor the vertical components of the electric field generated by ambient charge. Data from these mills, on line and archived, represents a wealth of information on electric fields during adverse weather conditions. Presenting that data in an intelligible and informative manner increases its utility in meeting both operational and investigative goals.

One form of presenting electric field data is in a contour format in which those geographic locations experiencing a common electric field are connected. Due to their value as an analytical, investigative tool and the importance placed on these contours as an operational tool, the current work was directed toward making that tool available to members of the Atmospheric Science Group and other interested investigators.

Original software was developed and coordinated with resources at KSC to provide the group with an analytical utility which will allow the members to produce contours based on field mill data and present those contours on an outline of the KSC/CCAFS region.

Three programs were developed in order illustrate the use of the system, its flexibility, and the link between data, model and contour. Each program represents a choice of a mathematical model of the physical situation and each provides a mechanism for the determination of the parameters associated with that distribution based on available data. The electric field based on the model along with determined parameters are then used in producing a contouring graphic.

In the first program, a model once used by the group is reformulated for use with currently available hardware and software. The second program represents an original formulation using a single point charge model. This model finds limited application but is found to have utility in the development of more complex models. The third program is an original formulation based on the second and assumes the presence of two point charges. An iterative technique is used to determine these charges and their location. An illustration of this model is given resulting in physically acceptable results.

TABLE OF CONTENTS

INTRODUCTION

1.1 AMBIENT GROUND LEVEL ELECTRIC FIELDS

The John F. Kennedy Space Center and Cape Canaveral Air Force Station are spanned by an irregular grid of thirty-four electric field mills. That system provides data on the vertical component of the ambient electric fields at ground level due to atmospheric electric charge. The field and its associated charge distribution are of interest to investigators and operations personnel during adverse weather conditions. The data from these field mills provides a mechanism for monitoring the potential for ligthning strikes and for understanding the physics of these situations. It is a matter of great importance that this data be interpreted and presented in a concise and reliable fashion.

1.1.1 UTILIZATION OF FIELD MILL DATA BY THE ATMOSPHERIC SCIENCE GROUP. Information on electric field conditions, along with other meteorological information, is used by the members of the Atmospheric Science Group and guest investigators in gauging the potential for natural occuring and for rocket triggered lightning. Data on electric fields is an integral part of the group's analysis of environmental conditions associated with adverse weather conditions (1).

1.1.2 UTILIZATION OF FIELD MILL DATA BY OPERATIONS PERSONNEL. Field mill data is monitored by those overseeing operations at KSC in appraising the treat of lightning associated with adverse weather conditions. Their analysis of that data and judgements based on that analysis are critical in maintaining employee safety and in protecting the integrity of KSC facilities and equipment especially during launch preparations. Their analysis of data is used in developing standards for safety (2).

1.1.2 UTILIZATION OF FIELD MILL DATA BY INVESTIGATORS. Field mill data also plays an important role in the analysis of the physics of thunderstorm activity (3,4,5,6,7). It provides information on static or slowly evolving situations during the development and passing of a storm. It also provides information on the dynamics of lightning strikes. The unique location and expanse of the field mill grid makes it a valuable tool for this purpose. Data from these mills has been gathered consistently over several years and constitutes a wealth of archived information.

1.2 FIELD MILL DATA FORMATS

Data from field mills in the vacinity of the Atmospheric Science Field Station are directed to host and guest investigators there during operations. Data from all mills is directed to those involved with operations and to the KSC's VAX/VMS main-frame computer for processing and storage. Historic data is currently being archived on

optical disk. Processing by the computer management team involves digitalizing the original pulse modulated signal and, correlating the data with time and with meteorological data. Hard copies of the readings are supplied to users for subsequent analysis.

1.2.1 STRIP CHART FORMAT OF DATA. The strip chart format is the most direct format for presenting readings from any individual mill. This format shows the electric field values at an individual mill location as a function of time. It is suggested that this format be use in the development of an artificial intelligence, expert system of pattern recognition to be used in appraising the hazard associated with various conditions (8).

1.2.2 CONTOUR FORMAT OF DATA. An alternate mode of presenting data is by means of contours. In this format readings from all mills at a particular time, or time average, are used to estimate the electric field at locations within the grid and to present lines connecting locations experiencing the same intensity electric field. Here electric fields at a time are presented as a function of position along the ground.

1.3 ATTRIBUTES OF CONTOUR FORMAT

The graphical character of the contour mode of presentation of data is a favorable format for a variety of uses in analysis. Patterns are more easily recognized in a graphical format and a large amount of data is discernible at a glance. Time development is easily included and the pattern of change is more easily analyzed. This heavy dependence on patterns in contours can be misleading to the observer. The observer must recall that the entire map is generated using data from a finite set of grid points and that the interpolation relies on some specific algorithm. Thus any reliance placed on interpreting these contours is dependent on the validity of this algorithm. The validity of the algorithm, in turn, depends on its agreement with the physical situation. The nature of the model used is an essential aspect to be considered by operations personnel and investigators.

1.4 THE ROLE OF THE ATMOSPHERIC SCIENCE GROUP IN THE DEVELOPMENT OF THE CURRENT CONTOUR ALGORITHM

Historically the original contour algorithm was developed by H. W. Kasemir with improvements introduced by E. Magazinner and D. Crandall of the Atmospheric Science Group. The original system was developed to utilize the computer facilities of the time. The mathematical model employed is linear and leads to a closed solution. That system was transferred to the new operations personnel and remains part of their evaluation system.

1.5 MOTIVATION FOR THE DEVELOPMENT OF NEW CONTOUR ALGORITHMS

The investigation, as presented in this paper, represents an effort to reintroduce contour analysis as part of the Atmospheric Science Group's analytical tools. This work is also designed to provide an investigative tool for those in the scientific community interested in determining the physics of adverse weather situations. The work also introduces a new algorithm which could serve as the basis for further investigation.

The development of valid electric field algorithms offer advantages in several areas. The development of a currect algorithm relies on a clear understanding of the physics of the situation and an understanding of the charge distirbution in particular. With an understanding of the charge distribution and its time evolution, prospects for formulating a more reliable evaluation of the potential for the occurance of lightning are enhanced.

With the development of artificial intelligence systems to monitor and appraise data, it will become increasingly important that the expert systems employed be truly expert, with the ability to formulate reactions based on credible models. It is anticipated that the combined information from field mills and wind convergence will lead to a better predictions.

The major goal of this investigation is to give members of the Atmospheric Science Group and other interested investigators the tools to carry out such studies.

DEVELOPMENT OF ALGORITHMS FOR GENERATING ELECTRIC FIELD CONTOURS

2.1 GENERAL THEORY

A charge distribution is a function of time and position $\rho(X,Y,H,t)$. In this investigation the static situation was considered. The effects of this source charge on object charges can be appraised by means of an intermediary environmental electric field produced by the source charge and experienced by the object charges.

In the systems considered here, the source charge resides in cloud cover and the resulting electric field is investigated at ground level. It was assumed that the ground is a regular surface and acts as a perfect conductor. It was also assumed that no surface charges mask the source charge. The sign convention used is the one commonly used by investigators in the field: a positive vertical field component is associated with a positive charge overhead.

Under these assumptions, the electric field at the surface is perpendicular to the surface and can be expressed analytically by employing an additional charge distribution which mirrors the source charge distribution. This mirror charge is of equal size but opposite sign and altitude compared to the source. The situation and corresponding equation are given in figure 1 for the point charge case. For more complex cases the cumulative effect is the sum [or integral] of influences from individual charges [or differential charge elements] (9,10).

In the most common type of electrostatic problem the potential is known over a given boundary as well a the charge distribution. In this boundary value type problem, the field within the boundary is to be determined. Techniques for investigating these situations are well known (11).

In the current study, however, the electric field is known over only a limited region of space and, from that information, the possible charge distributions producing the general electric field is to be discerned. Techniques available for addressing this type of problem are limited.

Due to the limited set of electric field values, there need not be a unique solution for the charge distribution producing the data set (9). Analysis can be guided, however, by additional information on cloud expanse and wind convergence (12,13). Constraints such as these can be introduced to limit the solutions which conform to the physical situation.

The development used here exhibits the following pattern. Field mill data is used in conjuntion with a model of the presumed charge distribution to determine the parameters associated with that model. Once the charge distribution is determined an expression can be written for the field produced at all points in the environment including ground level locations intermediate to field mill grid points. The loci of points on the ground experiencing the same field values can then be determined and contours representing incremental increases in field values can be constructed.

2.2 MODEL_A

The original model used by the Atmospheric Science Group for generating electric field contours was developed by H. W.Kasemir and revised by E. Magazinner and D. Crandall. This model was employed by researchers and members of the group in analyzing adverse weather situations. These contours were generated by programs written in Fortran for the Raytheon system once used at the Kennedy Space Center.

These capabilities have been transfered to the the Air Force as part of their operations responsibilities (2).

This investigation represents an effort to provide the Atomspheric Science Group direct access to a flexible, updated analytical tool for formulating contours. The first phase of that work involved the reformulation of this original model. In this phase of the study, the reformulation of the original model, here called MODEL_A, was used as a mechanism for assembling and coordinating the resources available at KSC. This was done in a away which incorporates flexibility of design for expanded application of the mechanism to new models.

2.3 MATHEMATICAL STUCTURE OF MODEL_A

The original algorithm employed relied on some restricting assumptions on the character of the charge distribution. Since, as described earlier, there is latitude in choosing a functional charge distribution to match data, a distribution was considered which lent itself to a linear analysis.

MODEL_A takes, as input information, the data from N field mills. Each of these mill generates a value E_i, i=1...N, at the various locations (X_i,Y_i), i=1...N. An equal number of point charges, Q_i, i=1...N, are assumed to have a fixed altitude, H. A single charge resides above a corrsponding mill location. In the test case studied the altitude used is 7000.0 meters.

The information is placed in matrix notation:

$$E = D\,Q,$$

where elements of matrix D are given by

$$D_{i,j} = (2*H*K)/((X_i-X_j)^2+(Y_i-Y_j)^2+H^2)^{1.5},$$

and where K is 9.0 X 10^9 N*m^2/$Coul^2$. Each of these elements can be determined numerically. The charges can then be determined using direct matrix manipulation (11).

$$Q = D^{-1}\,E.$$

With the charges thus determined the generating expression for the electric field at any surface location (X,Y) becomes,

$$E(X,Y) = \sum_{i=1}^{N} (2*H*K*Q_i)/((X_i-X)^2+(Y_i-Y)^2+H^2)^{1.5}.$$

This function can then be used to determine the electric field on a rectangular grid spanning the region of concern and the contour constructed by connecting points on the grid of a common value. The resolution of the grid becomes a concern and the method for analyzing region undergoing sharp changes was treated by E. Magazinner.

2.4 SOFTWARE RE-FORMULATION OF MODEL_A

In the current investigation this mathematical formulation was translated into Fortran programming language (14,15). This language is widely use by those interested in application as well as researchers. It provides the intelligibility and flexibility need for this project.

Fortran is supported by the center's VAX/VMS main-frame system thereby giving the programs possible direct access to data stored in the system (16). This software/hardware combination provides the opportunity of developing mathematically sophisticated models and provides a link to computer systems throughout the country. This access to software and data should encourage other interested investigators apart from the center to participate in Atmospheric Science Group activities.

A major factor in facilitating the current projects was the ability to access software in the computer's support library. In particular elements in the IMSL/Library of Fortran subroutines was of particular value. The mathematical applications portion of that library was used in carrying out the matrix inversion associated with MODEL_A. The recently acquired graphics portion of that library, IMSL *exponent graphics*, was used extensively in producing contours based on functions or grids generated by a model as well as in presenting the map of the region. A wide variety of mathematical tools and graphicing formats are available to Fortran programmers. Two of these tools fit the need of this investigation well and others suggest imaginative extensions of the mechanism.

The program developed for MODEL_A are presented in Appendix A. This program was tested using set of data, #1, entered as part of the program along with field mill coordinates. The resulting contour is presented in figure 4. The data set and the contour generated by the original software are presented in figure 2a. A comparison shows that the correct interpretaion of the original work has been employed in the current effort.

2.5 KSC/CCAFS REGIONAL MAP

The development of a contour finds its utility in offering a correlation between electric field values and geographic locations. Establishing this correlation is essential if the contour is to serve as an operational tool. For this reason the formulation of a background reference map of the KSC/CCAFS region was considered an integral part of this effort. This map would show the general, but accurate, outline of major land forms and the location of field mills. The scaling of contours and geography must agree.

The development of data files compatible with the software being formulated and referenced proved to be a formidable project. Exact maps showing landforms and mill locations were readily available from Master Planning. Also available are raster and vector formats of the region. These files were deemed inapproopriate for the present investigation on two counts. [1] They contained far more information than necessary for the current purposes. Reducing the file to a the level of information needed would require an unreasonable effort. [2] These files were produced on independent systems for unique functions and did not have the level of flexibility commensurate with other aspects of the project.

In therefore became necessary to construct a map for use in this system. Data for this map was obtained by using a hand tracing of the regional survey map in conjunction with a NAC Film Motion Analyzer. With this system and the MOVIAS software accompaning it, it was possible to obtain a set of scaled data points representing the outline of the major land forms in the region. This data and field mill coordinates were then transferred to Fortran files referred to by the GEOMP and MILLCR prefixes. This process proved to be tedious but worthwhile, for the resulting files permit the utilation of the same IMSL graphing software used in presenting the contours. The Fortran program for presenting this graphic is referred to as MAP and is presented in Appendix D. This program is used as a subroutine supporting the display of each of the models developed. The process then maintained the streamline character of the overall program and insured the compatibility of the geographical and contour components. The resulting map is presented in figure 3.

2.6 MODEL_B

Having gathered the resources to structure and present the results of a model, work was begun on development of alternate approaches. The most direct model was chosen as a starting point, a monople with a charge, Q, located above coordinates, X and Y, at an altitude, H. This model, with four degrees of freedom, does not lend itself to the linear approach used in the previous model. It is possible, however, to obtain solutions using analytical techniques with the knowledge of the field at four non-coaxial locations. The validity of this approach was verified using MathCad software in the analysis of a hypothetical situation. The cooresponding Fortran program for the scheme was then written and is presented in the Appendix B. The function which generates the contours is similar to the function used in the previous model. Only one source charge is present, N=1. The altitude, H, now appears as a variable along with ground position, (X,Y). The test field values are given in the program presented in the appendix. The determined charge of 40 Coulombs at coordinates X=994m, Y=2000m and H=6000m agree very well with the test charge and location. The contour for this situation is also presented as a figure 5.

This model finds limited direct application for it assumes that charge of only one type is located in the region. This is not a expected situation in adverse weather situations. The model is useful, however, as the bases of a more practical model.

2.7 MODEL_C

This model assumes that the charge distribution consisting of two point charges, Q_1 and Q_2, at coordinates (X_1,Y_1,H_1) and (X_2,Y_2,H_2). It is assumed that one of these charges dominates the field by virtue of its size or location and the influence of the second is a perturbation.

This model agrees more favorably with the charge distributions associated with lightning strikes. In the model tested by Krider the charge distribution consists of three charge (1). The commonly accepted system consists of a large charge at a low altitude, a nearby small charge of opposite polarity and a third charge of comparable size to the first but of opposite polarity at a higher altitude. Model_C approaches this distribution and is designed as a demonstration of the flexibility of the system.

For this model an iterative approach is employed since a linear or direct analytical analysis are no longer possible (17). The dominate charge, Q_1, is taken as producing a field, E_1, which is taken as initially being equal to the full field E.

$$E_1 \sim E .$$

An approximation to charge Q_1 and its position are found using the analytical techniques of MODEL_B and the four dominate, non-coaxial field values.

The field produced at mill sites from this first approximation of charge Q_1 is then determined and that field is removed from the total field values. The residual influence, E_2, is then attributed to charge Q_2 of undertermine polarity relative to Q_1.

$$E - E_1 \sim E_2.$$

The software again searches for the dominate four field sites. These may not necessarily be the original four sites. The residual field at these sites is used to determine a first approximation to charge, Q_2, and its position.

These approximate values are used to determine their approximate contribution, E_2, to the field at mill sites. The cycle is repeated; this time assuming that the residual field is given by,

$$E - E_2 \sim E_1$$

The iteration continues if the system converges to a fixed pair of charge values, of opposite polarity, and locations.

A test case was chosen to demonstrate the utility of this model. The data set, #2, is stored in a Fortran file prefixed by MILLVAL. The contour generated by the original model based on that data is presented in figure 2b.

Data set #2 was interpreted by MODEL_C are resulting from a charges: Q_1 of +70.0 Coulombs located at an altitude of 12.6 km above coordinates X_1= 189 km, and Y_1= 469 km; and Q_2 of -30.5 Coulombs located at an altitude of 8.1 km above coordinates X_2= 195 km, and Y_2= 459 km. These results seem reasonable in terms of expected sizes and altitudes.

The resulting contour generated by MODEL_C for this data set is presented in figure 6.

CONCLUDING REMARKS

Two algorithms are now available to members of the Atmospheric Science Group and other investigator for presenting field mill data in contour format. The first is a familiar operational mechanism reformulated with the introduction of additional flexibility. The second is a new mechanism which is designed primarily as an investigative tool. The systems are complimentary and can be used for comparative analysis and evaluation.

In both systems the software is structured to permit the incorporation of variations in the models and extensions of their structure. By virtue of the support software employed, the mathematical and contouring innovations that can be used for these purposes is extensive. The support software offers several modes of presenting contour results. That software is currently requiring too much time to generate contours, but this situation can be corrected by increasing the memory available for software initiated calculations.

The systems are currently designed for use on the VAX/VMS which gives investigators the potential to use either on-line or archived data.

The potential of immediate and future use of the system is extensive.

```
C       ************** MODEL A ************************
C       ELECTRIC FIELD CONTOUR USING AN OLD ALGORITHM
C
C       CONSTANTS RELATED TO EVALUATION OF CHARGE AND FIELD
C
C       SET COMMON VARIABLES AND DIMENSION ARRAYS
C
        DIMENSION FLDS(34),FLDX(34),FLDY(34),CRG(34),CVAL(2),
     &            DIS(25,25),DISIN(25,25)
C
        COMMON /FLDCR/FLDX,FLDY/CRGZ/CRG/FLDST/FLDS/
     &          INIT/E,CN,R,NV,ZR
C
C       ESTABLISH EXTERNALS
C
        EXTERNAL ELF,FNCTR,EGSGL,LINRG,EPSPLT,MAP
C
C       SET PARAMETERS
C
        PARAMETER (NCV=11,NX=10,NY=10)
        AX=1.6500E+05
        AY=4.4958E+05
        BX=2.0200E+05
        BY=4.8768E+05
        IUNIT=0
        IOPT=1+4+8
        DATA CVAL/-5000.0,5000.0/

C
C       ELIMINATE READINGS FROM INOPERATIVE MILLS
C
        DO 90 I=1,34
                IF(FLDS(I).EQ.ZR) THEN
                R=R+1
                ELSE
                FLDX(I-R)=FLDX(I)
                FLDY(I-R)=FLDY(I)
                FLDS(I-R)=FLDS(I)
                END IF
90      CONTINUE
C
C       CREATE INVERSE SQUARE MATRIX
C
        DO 100 I=1,25
        BLXI=FLDX(I)
        BLYI=FLDY(I)
                DO 110 J=1,25
                BLXJ=FLDX(J)
                BLYJ=FLDY(J)
                BLD=((BLXI-BLXJ)**2.0+
     &               (BLYI-BLYJ)**2.0+
     &                R**2)**1.5
                DIS(I,J)=1.0/BLD
                DIS(I,J)=2.0*E*CN*DIS(I,J)
                DIS(J,I)=DIS(I,J)
110             CONTINUE
100     CONTINUE
C
C
C       CALL IMSL TO INVERSE THE MATRIX
C
        CALL LINRG(25,DIS,25,DISIN,25)
C
C       DETERMINE THE CHARGE
C
        DO 120 I=1,25
                DO 118 J=1,25
                CRG(I)=CRG(I)+FLDS(J)*DISIN(I,J)
118             CONTINUE
120     CONTINUE
C
        CALL MAP

C
C       CALL IMSL TO PLOT CONTOUR USING THE FUNCTION ELF
C
        CALL FNCTR(ELF,NX,NY,AX,BX,AY,BY,IOPT,NCV,CVAL)

C
        CALL EGSGL('!CONTOUR_PLOT.PLOT-TITLE title$',
     &                   'MODEL_A CONTOUR, DATA SET 61$')
C
        CALL EGSGL('!CONTOUR_AXIS.X.AXIS-TITLE title$',
     &                                   'meters$')
        CALL EGSGL('!CONTOUR_PLOT.LEGEND title$','volts/meter$')
C       PRINT GRAPH
C
        CALL EPSPLT(IUNIT,' ')
C
        STOP
        END
C
C       SUBROUTINES
C
        BLOCK DATA FLDCR
C       FIELD MILL COORDINATES IN METERS
        DIMENSION FLDX(34),FLDY(34)
        COMMON/FLDCR/FLDX,FLDY
                DATA FLDX/0.1847597E+06,0.1797880E+06,0.1766515E+06,
     &                    0.1876875E+06,0.1817664E+06,0.1849935E+06,
     &                    0.1770530E+06,0.1893371E+06,0.1907119E+06,
     &                    0.1821315E+06,0.1842724E+06,0.1874933E+06,
     &                    0.1925358E+06,0.1906694E+06,0.1872805E+06,
     &                    0.1941248E+06,0.1846632E+06,0.1815265E+06,
     &                    0.1895227E+06,0.1871755E+06,0.1893639E+06,
     &                    0.1823736E+06,0.1862367E+06,0.1846248E+06,
     &                    0.1853178E+06,0.1947760E+06,0.1956620E+06,
     &                    0.1987060E+06,0.1931880E+06,0.1956450E+06,
     &                    0.0          ,0.1935360E+06,0.1910250E+06,
     &                    0.1951570E+06/,
     &                FLDY/0.4841795E+06,0.4823839E+06,0.4817947E+06,
     &                    0.4798339E+06,0.4791357E+06,0.4775659E+06,
     &                    0.4773711E+06,0.4770553E+06,0.4750857E+06,
     &                    0.4744568E+06,0.4733297E+06,0.4729585E+06,
     &                    0.4729460E+06,0.4703309E+06,0.4701347E+06,
     &                    0.4699786E+06,0.4684616E+06,0.4677181E+06,
     &                    0.4671083E+06,0.4662378E+06,0.4644784E+06,
     &                    0.4623739E+06,0.4576360E+06,0.4575546E+06,
     &                    0.4532707E+06,0.4671770E+06,0.4620490E+06,
     &                    0.4573120E+06,0.4575490E+06,0.4589490E+06,
     &                    0.0          ,0.4547040E+06,0.4523050E+06,
     &                    0.4561440E+06/
        END

        BLOCK DATA CRGZ
        DIMENSION CRG(34)
        COMMON/CRGZ/CRG
        DATA CRG/34*0.0/
        END
C
        BLOCK DATA FLDST
C       FIELD MILL VALUES IN VOLTS/M ENTERED AS A BLOCK
        DIMENSION FLDS(34)
        COMMON/FLDST/FLDS
```


APPENDIX A

```
      DATA FLDS/2046.0,  15.0,   0.0,2138.0, 169.0,2046.0,
     &          -170.0,1461.0,3861.0,1153.0,3307.0,4569.0,
     &          4138.0,5678.0,4046.0,5461.0,5984.0,4569.0,
     &          4907.0,0.0,-16.0,1615.0,2907.0,0.0,0.0,0.0,0.0,
     &          -3954.0,0.0,-2539.0,-5493,0.0,0.0,0.0,-7308.0/
      END
C
      FUNCTION ELF(X,Y)
C     FUNCTION TO GENERATE CONTOUR
C     ELECTRIC FIELD FROM COULOMB
C
      DIMENSION CRG(34),FLDX(34),FLDY(34)
      COMMON/CRG2/CRG/FLDCR/FLDX,FLDY/INIT/H,CN,R,NV,ZR
            ELF=0
            DO 140 I=1,25
                  TMPX=FLDX(I)
                  TMPY=FLDY(I)
                  TMP=(((X-TMPX)**2)+((Y-TMPY)**2)+
     &                  (H**2))**3
                  TMP=SQRT(TMP)
                  ELF=ELF+((CRG(I)*2.0*H*CN)/TMP)
140         CONTINUE
      RETURN
      END
C
      BLOCK DATA INIT
C
C     H IS THE ALTITUDE
C     CN IS COULOMB'S CONSTANT
C     NV IS THE NUMBER OF MILLS
C     R IS THE NUMBER OF INACTIVE MILLS
C     OTHER CONSTANTS ARE FOR THE IMLS GRAPHING
C
      COMMON/INIT/H,CN,R,NV,ZR
      DATA H/7.0E+03/,CN/9.0E+09/,R/0/,NV/25/,ZR/0.0/
      END


      SUBROUTINE MAP
C
C     START OF A RSC/CCAPS MAP USING IMSL/EXP
C
      EXTERNAL SCATR,EFSPLT,EGSGL
C
      DIMENSION XCR(350),YCR(350),XPL1(287),YPL1(287)
      DIMENSION XPL2(2),YPL2(2),XPL3(2),YPL3(2),XPL4(2),YPL4(2)
      DIMENSION XPL5(2),YPL5(5),XPL6(37),YPL6(37)
      DIMENSION XTL(2),YTL(2),XBL(2),YBL(2)
      DIMENSION XFLD(34),YFLD(34)
C
      NPL1=287
      NPL2=2
      NPL3=2
      NPL4=2
      NPL5=2
      NPL6=37
      NFLD=33
      DATA XTL/0.165E+06,0.2025E+06/
      DATA YTL/0.4876838E+06,0.4876838E+06/
      DATA XBL/0.165E+06,0.2025E+06/
      DATA YBL/0.4496525E+06,0.4496525E+06/
C
C     GET GEOGRAPHICAL PTS FROM FILE
C
      OPEN(UNIT=7,NAME='GEOMP1.DAT;1',TYPE='OLD')
C
```

```
C       ************** MODEL B ************************************
C       MONOPOLE MODEL FOR STATIC FIELD
C       AND CONTOUR PLOT
C
C       DEFINE AND FILL DATA HOLDING AREAS
C
        DIMENSION CRG(10),CRGX(10),CRGY(10),CRGB(10),RR(10)
        DIMENSION COEFF(4),COEFA(4),COEFB(4),COEFR(4)
        DIMENSION HLDS(24)
        DIMENSION IRNK(24),IGR(20,4)
        DIMENSION FLDX(34),FLDY(34),FLDS(34)
        DIMENSION CVAL(2)
        COMMON /FLDCR/FLDX,FLDY/FLDST/FLDS/INIT/E,Q,XX,YY,R,STDE,STDQ,STDX,
     &                STDY,STDR,CN,NV,ZR
C
        EXTERNAL ELF,FNCTP,EPSPLT,EGSGL
        NX=10
        NY=10
        IOPT=1+4+8
        CVAL(1)=1.5E+4
        CVAL(2)=2.5E+4
        IUNIT=0
        NCV=10
        AX=100
        BX=3000
        AY=100
        BY=3000
C
C       ESTABLISH A HOLDING FILE FOR DATA
C
        DO 10 I=1,NV
                HLDS(I)=FLDS(I)
10      CONTINUE
C
C       USE THE HOLDING AREA TO BUBBLE (RANK) FIELD VALUES
C
        DO 12 I=1,NV
                IRNK(I)=I
12      CONTINUE
C
        DO 40 I=1,(NV-1)
        K=(NV-1)
                DO 30 J=1,K
                        IF (HLDS(J).GT.HLDS(J+1)) THEN
                        TEMP1=HLDS(J)
                        HLDS(J)=HLDS(J+1)
                        HLDS(J+1)=TEMP1
                        TEMP2=IRNK(J)
                        IRNK(J)=IRNK(J+1)
                        IRNK(J+1)=TEMP2
                        END IF
30              CONTINUE
40      CONTINUE
C
C       DETERMINE THE NUMBER OF OPERABLE MILLS
C
        NV=NV
        DO 50 I=1,NV
                IF (FLDS(I).EQ.ZR) THEN
                NV=NV-1
                END IF
50      CONTINUE
C
C       PUT MILLS INTO GROUPS OF FOUR
C
        IFRG=(NV/4)
        FRG=IFRG
C
        DO 60 I=1,IFRG
                DO 70 J=1,4
                        IGR(I,J)=IRNK((IFRG*(J-1))+I+NV-NV)
70              CONTINUE
60      CONTINUE
C
C       DEFINE COEFFICIENTS
C
        DO 80 I=1,IFRG
                DO 90 J=1,4
                        COEFF(J)=FLDS(IGR(I,J))**(2.0/3.0)
90              CONTINUE
C
                DO 100 J=2,4
                COEFA(J)=(COEFF(1)*FLDX(IGR(I,1))-COEFF(J)*FLDX(IGR(I,J)))/
     &                  (COEFF(1)-COEFF(J))
                COEFB(J)=(COEFF(1)*FLDY(IGR(I,1))-COEFF(J)*FLDY(IGR(I,J)))/
     &                  (COEFF(1)-COEFF(J))
                COEFR(J)=(COEFF(1)*COEFF(J)/(COEFF(1)-COEFF(J))**2)*
     &                  ((FLDX(IGR(I,1))-FLDX(IGR(I,J)))**2+
     &                   (FLDY(IGR(I,1))-FLDY(IGR(I,J)))**2)
100             CONTINUE
C
                BD2=2.0*(COEFB(2)-COEFB(3))
                BD4=2.0*(COEFB(2)-COEFB(4))
                AD3=2.0*(COEFA(2)-COEFA(3))
                AD4=2.0*(COEFA(2)-COEFA(4))
C
C               DETERMINE THE X COORDINATE OF CHARGE
C
                CRGX(I)=(((COEFR(3)-COEFR(2))/BD3)-
     &                  ((COEFR(4)-COEFR(2))/BD4)-
     &                  ((COEFB(3)**2-COEFB(2)**2)/BD3)+
     &                  ((COEFB(4)**2-COEFB(2)**2)/BD4)-
     &                  ((COEFA(3)**2-COEFA(2)**2)/BD3)+
     &                  ((COEFA(4)**2-COEFA(2)**2)/BD4))/
     &                 ((2.0*(COEFA(2)-COEFA(3))/BD3)-
     &                  (2.0*(COEFA(2)-COEFA(4))/BD4))
C
C               DETERMINE THE Y COORDINATE OF CHARGE
C
                CRGY(I)=(((COEFR(3)-COEFR(2))/AD3)-
     &                  ((COEFR(4)-COEFR(2))/AD4)-
     &                  ((COEFB(3)**2-COEFB(2)**2)/AD3)+
     &                  ((COEFB(4)**2-COEFB(2)**2)/AD4)-
     &                  ((COEFA(3)**2-COEFA(2)**2)/AD3)+
     &                  ((COEFA(4)**2-COEFA(2)**2)/AD4))/
     &                 ((2.0*(COEFB(2)-COEFB(3))/AD3)-
     &                  (2.0*(COEFB(2)-COEFB(4))/AD4))
C
C               DETERMINE THE AVERAGE CHARGE AND ALT FOR THIS GROUP
C
                CRG(I)=ZR
                CRGB(I)=ZR
                        DO 130 J=2,4
                        CRGB(I)=CRGB(I)+(COEFR(J)-((CRGX(I)-COEFA(J))**2-
     &                                          (CRGY(I)-COEFB(J))**2)**(0.5
C
130                     CONTINUE
                CRGB(I)=CRGB(I)/3.0
C
                        DO 140 J=1,4
                        CRG(I)=CRG(I)+((FLDS(IGR(I,J)))/(2.0*CN*CRGB(I)))*
     &                                  ((CRGX(I)-FLDX(IGR(I,J)))**2+
```


APPENDIX B

```
     &                                  (CRGY(I)-FLDY(IGR(I,J)))**2+
     &                                  CRGR(I)**2)**(1.5)
140                  CONTINUE
           CRG(I)=CRG(I)/4.0
C
80      CONTINUE
C
C       DETERMINE AVERAGES AND STD DEVIATIONS
C
        DO 150 I=1,IFRG
                R=CRGR(I)+R
                XX=CRGX(I)+XX
                YY=CRGY(I)+YY
                Q=CRG(I)+Q
                RR(I)=(CRGX(I)**2+CRGY(I)**2)**(0.5)
                P=RR(I)+R
150     CONTINUE
                R=R/FRG
                XX=XX/FRG
                YY=YY/FRG
                Q=Q/FRG
                P=R/FRG
C
        DO 160 I=1,IFRG
                STDQ=STDQ+(CRG(I)-Q)**2
                STDR=STDR+(CRGR(I)-R)**2
                STDR=STDR+(RR(I)-R)**2
                STDY=STDY+(CRGY(I)-YY)**2
                STDX=STDX+(CRGX(I)-XX)**2
160     CONTINUE
        DO 170 I=1,IFRG
                STDQ=(STDQ/FRG)**(0.5)
                STDR=(STDR/FRG)**(0.5)
                STDR=(STDR/FRG)**(0.5)
                STDX=(STDX/FRG)**(0.5)
                STDY=(STDY/FRG)**(0.5)
170     CONTINUE
C
C       PLOT CONTOUR USING FUNCTION ELF
C
        CALL FNCTR(ELF,NX,NY,AX,BX,AY,BY,IOPT,NCV,CVAL)
C
        CALL EGSGL('!CONTOUR_PLOT.PLOT-TITLE title$','MODEL_B, TEST$')
C
        CALL EGSGL('!CONTOUR_AXIS.X.AXIS-TITLE title$','meters$')
C
        CALL EGSGL('!CONTOUR_PLOT.LEGEND title$','volts/meter$')
C
        CALL EPSPLT(IUNIT,' ')

        STOP
        END
C
C       BLOCKS
C
        BLOCK DATA FLDST
        DIMENSION FLDS(34)
        COMMON/FLDST/FLDS
        DATA FLDS/1.959E04,1.808E04,1.915E04,1.722E04,1.765E04,
     &          1.965E04,0.0,1.97E04,1.951E04,1.957E04,24*0.0/
        END
C
        BLOCK DATA FLDCR
        DIMENSION FLDX(34),FLDY(34)
        COMMON/FLDCR/FLDX,FLDY
        DATA FLDX/1.500E03,2.500E03,.750E03,2.666E03,1.750E03,
     &          1.250E03,.250E03,.400E03,.800E03,.800E03,24*0.0/,
     &      FLDY/1.500E03,2.500E03,3.00E03,1.000E03,.400E03,
     &          2.600E03,.750E03,2.000E03,1.250E03,2.700E03,24*0.0/
        END
C
        BLOCK DATA INIT
        COMMON/INIT/R,Q,XX,YY,R,STDR,STDQ,STDX,STDY,STDR,CN,WV,ZR
        DATA R/0.0/,Q/0.0/,XX/0.0/,YY/0.0/,R/0.0/,STDR/0.0/,STDQ/0.0/
     &      ,STDX/0.0/,STDY/0.0/,STDR/0.0/,CN/9.0E+09/,WV/10/,ZR/0.0/

        END
C
        FUNCTION ELF(X,Y)
        COMMON/INIT/R,Q,XX,YY,R,STDR,STDQ,STDX,STDY,STDR,CN,WV,ZR
C
        ELF=2.0*CN*R*Q
        ELF=ELF/((((X-XX)**2.0)+((Y-YY)**2.0)+(R**2.0))**(1.5))
C
        RETURN
        END
```

```
C       ******************MODEL_C.FOR******************
C       DIPOLE MODEL FOR STATIC FIELD USING ITERATION
C       AND PRODUCTION OF A CONTOUR PLOT
C
C       DEFINE DATA HOLDING AREAS
C
        DIMENSION CRG(-10:+10),CRGX(-10:+10),CRGY(-10:+10),
     &            CRGH(-10:+10)
        DIMENSION COEFF(4),COEFX(4),COEFY(4),COEFH(4)
        DIMENSION HLDV(34),FLDV(34,-11:+11),TMPV(34)
        DIMENSION CVAL(2)
        DIMENSION IRNK(34),SAMPV(4),ISAMP(4)
        DIMENSION FLDX(34),FLDY(34)
        COMMON /INIT/CN,ZR/CRGH/CRG,CRGH,CRGX,CRGY
C
CC      ESTABLISH EXTERNALS
C
        EXTERNAL ELP,PNCTR,EGSGL,LINRG,EPSPLT,MAP
C
C       DEFINE CONSTANTS USED IN PLOTING
C
        PARAMETER(MCV=11,NX=10,NY=10)
        AX=0.16500E+06
        AY=0.44958E+06
        BX=0.20200E+06
        BY=0.48768E+06
        IUNIT=0
        IOPT=1+4+8
        DATA (CVAL(I),I=1,2)/-5000.0,5000.0/
C
CC      ENTER FIELD MILL VALUES FROM A PARTICULAR FILE
C
        OPEN(UNIT=7,NAME='MILLVAL.DAT;2',TYPE='OLD')
C
10      FORMAT(I,E)
                DO 20 I=1,34
                READ(7,10) ITMP,VTMP
                FLDV(I,0)=VTMP
20              CONTINUE
        CLOSE(UNIT=7,STATUS='KEEP')
C
C       ENTER FIELD MILL COORDINATES
C
        OPEN(UNIT=7,NAME='MILLCR.DAT;1',TYPE='OLD')
C
30      FORMAT(I,E,E)
                DO 40 I=1,34
                READ(7,30) ITMP,XTMP,YTMP
                FLDX(I)=XTMP
                FLDY(I)=YTMP
40              CONTINUE
        CLOSE(UNIT=7,STATUS='KEEP')
C
C       OPEN FILE TO HOLD DATA
C
        OPEN(UNIT=7,NAME='MODEL_C.DAT',TYPE='NEW')
600     FORMAT(I,E,E,E,E)
C
C       REGISTERS FOR COUNTING THE NUMBER OF +,0,- VALUES
C       ZERO VALUES DESIGNATE INACTIVE MILLS
C
        NP=0
        NZ=0
        NN=0
C
C       FILL FIELD VALUE MATRIX WITH ZEROS
C
                DO 50 I=-10,-1
                        DO 60 J=1,34
                        FLDV(J,I)=ZR
60                      CONTINUE
50              CONTINUE
                DO 70 I=1,10
                        DO 80 J=1,34
                        FLDV(J,I)=ZR
80                      CONTINUE
70              CONTINUE
C
C       DETERMINE NUMBER OF POS,NEG, AND ZERO FIELD VALUES
C       AND FILL BOLDING AREAS-THESE AREAS ARE USED TO BUBBLE
C       MILL VALUES AND ESTABLISH THEIR RANK ACCORDINGLY
C
                DO 90 I=1,34
                        IF(FLDV(I,0).EQ.ZR)NZ=NZ+1
                        IF(FLDV(I,0).GT.ZR)NP=NP+1
                        IF(FLDV(I,0).LT.ZR)NN=NN+1
                        HLDV(I)=FLDV(I,0)
                        IRNK(I)=I
                        FLDV(I,1)=FLDV(I,0)
90              CONTINUE
C
C       START ITERATION CALCULATIONS
C
        DO 1000 ITER=1,10
        I=ITER
400     CONTINUE
C
        DO 100 L=1,33
        K=34-L
                DO 110 J=1,K
                        IF (HLDV(J).GT.HLDV(J+1)) THEN
                        TEMP1=HLDV(J)
                        HLDV(J)=HLDV(J+1)
                        HLDV(J+1)=TEMP1
                        TEMP2=IRNK(J)
                        IRNK(J)=IRNK(J+1)
                        IRNK(J+1)=TEMP2
                        END IF
110             CONTINUE
100     CONTINUE
C
C       DETERMINE IF THE DOMINATE INFLUENCE COMES FROM POS OR
C       NEG TERMS
C
        IF(NN-NP)120,120,130
120     IBAS=34
        ITOG=-1
        GOTO 140
130     IBAS=1
        ITOG=+1
C
140     ISAMP(1)=IRNK(IBAS)
        SAMPV(1)=HLDV(IBAS)
        K=1
C
C       FIND FOUR NON-EQUAL, DOMINATE FIELD MILL VALUES
C
        DO 160 J=2,4
150     IF(HLDV(IBAS+(ITOG)*(K+J-2)).EQ.HLDV(IBAS+(ITOG)*(K+J-3)))THEN
                K=K+1
                GOTO 150
                END IF
```


APPENDIX C

```
            ISAMP(J)=IRNR(IBAS+(ITOG)*(R+J-2))
            SAMPV(J)=BLDV(IBAS+(ITOG)*(R+J-2))
160     CONTINUE
C
C       DEFINE COEFFICIENTS AS ESTABLISHED IN MODEL B TO DETERMINE
C       THE CHARGE AND ITS LOCATION BASED ON THE FIELD VALUES CHOSEN
C       ABOVE
C
            DO 170 J=1,4
                COEFF(J)=(ABS(FLDV(ISAMP(J),I)))**(2.0/3.0)
170         CONTINUE
C
            DO 180 J=2,4
            COEFX(J)=(COEFF(1)*FLDX(ISAMP(1))-
     &              COEFF(J)*FLDX(ISAMP(J)))/
     &             (COEFF(1)-COEFF(J))
            COEFY(J)=(COEFF(1)*FLDY(ISAMP(1))-
     &              COEFF(J)*FLDY(ISAMP(J)))/
     &             (COEFF(1)-COEFF(J))
            COEFR(J)=((COEFF(1)*COEFF(J))/
     &              (COEFF(1)-COEFF(J))**2)*
     &             ((FLDX(ISAMP(1))-FLDX(ISAMP(J)))**2+
     &              (FLDY(ISAMP(1))-FLDY(ISAMP(J)))**2)
180         CONTINUE
C
            BD3=2.0*(COEFY(2)-COEFY(3))
            BD4=2.0*(COEFY(2)-COEFY(4))
            AD3=2.0*(COEFX(2)-COEFX(3))
            AD4=2.0*(COEFX(2)-COEFX(4))
C
C           DETERMINE THE X COORDINATE OF CHARGE
C
            CRGX(I)=(((COEFR(3)-COEFR(2))/BD3)-
     &              ((COEFR(4)-COEFR(2))/BD4)-
     &              ((COEFY(3)**2-COEFY(2)**2)/BD3)+
     &              ((COEFY(4)**2-COEFY(2)**2)/BD4)-
     &              ((COEFR(3)**2-COEFX(2)**2)/BD3)+
     &              ((COEFX(4)**2-COEFX(2)**2)/BD4))/
     &             ((2.0*(COEFX(2)-COEFX(3))/BD3)-
     &              (2.0*(COEFX(2)-COEFX(4))/BD4))
C
C           DETERMINE THE Y COORDINATE OF CHARGE
C
            CRGY(I)=(((COEFR(3)-COEFR(2))/AD3)-
     &              ((COEFR(4)-COEFR(2))/AD4)-
     &              ((COEFY(3)**2-COEFY(2)**2)/AD3)+
     &              ((COEFY(4)**2-COEFY(2)**2)/AD4)-
     &              ((COEFX(3)**2-COEFX(2)**2)/AD3)+
     &              ((COEFX(4)**2-COEFX(2)**2)/AD4))/
     &             ((2.0*(COEFY(2)-COEFY(3))/AD3)-
     &              (2.0*(COEFY(2)-COEFY(4))/AD4))
C
C           DETERMINE THE AVERAGE CHARGE AND ALT FOR THIS GROUP
C           AND IGNORING ANY COMBINATION WHICH RESULTS IN A
C           NON-PHYSICAL SOLUTION
C
            CRG(I)=ZR
            CRGB(I)=ZR
            IR=3
                DO 190 J=2,4
                CR=(COEFR(J)-(CRGX(I)-COEFX(J))**2-
     &              (CRGY(I)-COEFY(J))**2)
                IF(CR.LT.ZR)THEN
                IR=IR-1
                GOTO 190
                END IF
                CRGB(I)=CRGB(I)+SQRT(CR)
C
190             CONTINUE
            ZIR=IR
            CRGB(I)=CRGB(I)/ZIR
C
                DO 200 J=1,4
                CRG(I)=CRG(I)+((FLDV(ISAMP(J),I))
     &                      /(2.0*CN*CRGB(I)))*
     &                     ((CRGX(I)-FLDX(ISAMP(J)))**2+
     &                      (CRGY(I)-FLDY(ISAMP(J)))**2+
     &                      CRGB(I)**2)**(1.5)
200             CONTINUE
            CRG(I)=CRG(I)/4.0
C
C       WRITE TO THE FILE TO BE USED IN CHECKING ON CONVERGENCE
C
        WRITE(7,600)I,CRG(I),CRGB(I),CRGX(I),CRGY(I)
C
C       DETERMINE THE FIELD DUE TO THIS CHARGE
C
            DO 210 J=1,34
            THPV(J)=(2.0*CRG(I)*CRGB(I)*CN)/
     &              SQRT(((FLDX(J)-CRGX(I))**2+
     &                    (FLDY(J)-CRGY(I))**2+
     &                     CRGB(I)**2)**3)
210     CONTINUE
C
C       RETAIN INACTIVE MILL READINGS AS INACTIVE
C
            DO 220 J=1,34
                IF(FLDV(J,0).EQ.ZR)THPV(J)=ZR
220         CONTINUE
C
C       DETERMINE IF THE (+I,-I) LOOP IS COMPLETED
C
        IF(FLDV(1,-I).NE.ZR.AND.FLDV(34,-I).NE.ZR)THEN
        GOTO 500
        END IF
C
C       FINISH THE LOOP
C
        NZ=0
        NP=0
        NN=0
            DO 230 J=1,34
            FLDV(J,-I)=FLDV(J,0)-THPV(J)
            BLDV(J)=FLDV(J,-I)
            IF(FLDV(J,-I).EQ.ZR)NZ=NZ+1
            IF(FLDV(J,-I).GT.ZR)NP=NP+1
            IF(FLDV(J,-I).LT.ZR)NN=NN+1
            IRNR(J)=J
230         CONTINUE
        I=-I
        GOTO 400
C
C       FILL BOLDING AREAS WITH INFO FOR THE NEXT ITERATION
C
500     NZ=0
        NP=0
        NN=0
C
C       MAKE SURE THE CORRECT SIDE (+,-) OF THE FIELD MATRIX
C       IS FILLED
C
```

```
      IF(I.LT.0)L=-(I-1)
      IF(I.GT.0)L=(I+1)
C
            DO 240 J=1,34
            FLDV(J,L)=FLDV(J,0)-THPV(J)
            HLDV(J)=FLDV(J,L)
            IRNK(J)=J
            IF(FLDV(J,L).EQ.0)NZ=NZ+1
            IF(FLDV(J,L).GT.0)NP=NP+1
            IF(FLDV(J,L).LT.0)NN=NN+1
240         CONTINUE
1000  CONTINUE
C
      CLOSE(UNIT=7,STATUS='KEEP')
C
C     CALL IMSL GET MAP INFO AND SET UP PLOTS
C
      CALL MAP
C
C     CALL IMSL TO SET UP PLOT CONTOUR USING THE FUNCTION ELF
C
      CALL FNCTR(ELF,NX,NY,AX,BX,AY,BY,IOPT,NCV,CVAL)
C
      CALL EGSGL('!CONTOUR_PLOT.PLOT-TITLE title$',
     &           'MODEL_E CONTOUR - DATA SET #2$')
C
      CALL EGSGL('!CONTOUR_AXIS.X.AXIS-TITLE title$',
     &           'meters$')
C
      CALL EGSGL('!CONTOUR_PLOT.LEGEND title$','volts/meter$')
C
C     CALL IMSL TO PRESENT CONTOUR IN INTERACTIVE FORMAT
C
      CALL EPSPLT(IUNIT,' ')
C
      STOP
      END
C
      FUNCTION ELF(X,Y)
C     ELECTRIC FIELD DUE TO THE CHARGES DETERMINED AT THE END
C     OF THE ITERATION
C
      DIMENSION CRG(-10:+10),CRGH(-10:+10),CRGX(-10:+10),CRGY(-10:+10)
C
      COMMON/INIT/CN,ZR/CRGH/CRG,CRGH,CRGX,CRGY
C
      ELF=((2.0*CN*CRG(+10)*CRGH(+10))/
     &     (((X-CRGX(+10))**2+(Y-CRGY(+10))**2+
     &       (CRGH(+10))**2)**(1.5)))+
     &     ((2.0*CN*CRG(-10)*CRGH(-10))/
     &     (((X-CRGX(-10))**2+(Y-CRGY(-10))**2+
     &       (CRGH(-10))**2)**(1.5)))
C
      RETURN
      END
C
      BLOCK DATA INIT
      COMMON/INIT/CN,ZR
      DATA CN/9.0E+09/,ZR/0.0/
      END
C
      SUBROUTINE MAP
      EXTERNAL SCATR,EPSPLT,EGSGL,ERSET
C
      DIMENSION XCR(350),YCR(350),XPL1(287),YPL1(287)
      DIMENSION XPL2(2),YPL2(2),XPL3(2),YPL3(2),XPL4(2),YPL4(2)
```

```
C       ********** A RSC/CCAPS MAP USING IMSL/EXP ****************
C
        EXTERNAL SCATR,EPTITL,EPSPLT,EGSGL,ERSET
C
        DIMENSION XCR(350),YCR(350),XPL1(287),YPL1(287)
        DIMENSION XPL2(2),YPL2(2),XPL3(2),YPL3(2),XPL4(2),YPL4(2)
        DIMENSION XPL5(2),YPL5(5),XPL6(37),YPL6(37)
        DIMENSION XTL(2),YTL(2),XBL(2),YBL(2)
        DIMENSION XFLD(34),YFLD(34)
C
        NPL1=287
        NPL2=2
        NPL3=2
        NPL4=2
        NPL5=2
        NPL6=37
        NFLD=33
        IUNIT=0
        DATA XTL/0.165E+06,0.2025E+06/
        DATA YTL/0.4876838E-06,0.4876838E+06/
        DATA XBL/0.165E+06,0.2025E+06/
        DATA YBL/0.4496525E+06,0.4496525E+06/
C
C       GET GEOGRAPHICAL PTS FROM FILE
C
        OPEN(UNIT=7,NAME='GEOMP1.DAT;1',TYPE='OLD')
C
200     FORMAT(I,E,E)
        DO 100 I=1,100
                READ(7,200) ICNT,XTMP,YTMP
                XCR(I)=XTMP
                YCR(I)=YTMP
100     CONTINUE
                XCR(101)=0.1905E+06
                YCR(101)=0.4743E+06
        DO 150 I=1,2
                READ(7,200) ICNT,XTMP,YTMP
                XCR(I+101)=XTMP
                YCR(I+101)=YTMP
150     CONTINUE
C
        CLOSE(UNIT=7,STATUS='KEEP')
C
        OPEN(UNIT=7,NAME='GEOMP2.DAT;1',TYPE='OLD')
C
        DO 300 I=104,205
                READ(7,200) ICNT,XTMP,YTMP
                XCR(I)=XTMP
                YCR(I)=YTMP
300     CONTINUE
C
        CLOSE(UNIT=7,STATUS='KEEP')
C
        OPEN(UNIT=7,NAME='GEOMP3.DAT;1',TYPE='OLD')
C
        DO 400 I=206,307
                READ(7,200) ICNT,XTMP,YTMP
                XCR(I)=XTMP
                YCR(I)=YTMP
400     CONTINUE
C
        CLOSE(UNIT=7,STATUS='KEEP')
C
        OPEN(UNIT=7,NAME='GEOMP4.DAT;1',TYPE='OLD')
C
        DO 450 I=308,338
                READ(7,200) ICNT,XTMP,YTMP
                XCR(I)=XTMP
                YCR(I)=YTMP
450     CONTINUE
C
        CLOSE(UNIT=7,STATUS='KEEP')
C
C       ENTER FIELD MILL COORDINATES
C
        OPEN(UNIT=7,NAME='MILLCR.DAT;1',TYPE='OLD')
C
        DO 475 I=1,30
                READ(7,200) ICNT,XTMP,YTMP
                XFLD(I)=XTMP
                YFLD(I)=YTMP
475     CONTINUE
                READ(7,200) ICNT,XTMP,YTMP
        DO 480 I=31,33
                READ(7,200) ICNT,XTMP,YTMP
                XFLD(I)=XTMP
                YFLD(I)=YTMP
480     CONTINUE
C
        CLOSE(UNIT=7,STATUS='KEEP')
C
C       DIVIDE DATA INTO SEGMENTS
C
        DO 500 I=1,287
                XPL1(I)=XCR(I)
                YPL1(I)=YCR(I)
500     CONTINUE
C
        DO 600 I=1,2
                XPL2(I)=XCR(I+287)
                YPL2(I)=YCR(I+287)
600     CONTINUE
C
        DO 700 I=1,2
                XPL3(I)=XCR(I+289)
                YPL3(I)=YCR(I+289)
700     CONTINUE
C
        DO 750 I=1,2
                XPL4(I)=XCR(I+291)
                YPL4(I)=YCR(I+291)
750     CONTINUE
C
        DO 800 I=1,2
                XPL5(I)=XCR(I+293)
                YPL5(I)=YCR(I+293)
800     CONTINUE
C
        DO 850 I=1,37
                XPL6(I)=XCR(I+301)
                YPL6(I)=YCR(I+301)
850     CONTINUE
C
C       SEND DATA TO IMSL/EXP
C
        CALL ERSET(3,0,0)
C
        CALL SCATR(NPL1,XPL1,YPL1)
C
        CALL SCATR(NPL2,XPL2,YPL2)
C
        CALL SCATR(NPL3,XPL3,YPL3)
```

APPENDIX D

```
C
      CALL SCATR(NPL4,XPL4,YPL4)
C
      CALL SCATR(NPL5,XPL5,YPL5)
C
      CALL SCATR(NPL6,XPL6,YPL6)
C
      CALL SCATR(2,XTL,YTL)
C
      CALL SCATR(2,XBL,YBL)
C
      CALL SCATR(NPLD,XPLD,YPLD)
C
C     CONNECT DATA POINTS BY LINES
C
      CALL EGSGL('.1.AXIS.1.DATA.1 flag$',1)
C
      CALL EGSGL('.1.AXIS.1.DATA.2 flag$',1)
C
      CALL EGSGL('.1.AXIS.1.DATA.3 flag$',1)
C
      CALL EGSGL('.1.AXIS.1.DATA.4 flag$',1)
C
      CALL EGSGL('.1.AXIS.1.DATA.5 flag$',1)
C
      CALL EGSGL('.1.AXIS.1.DATA.6 flag$',1)
C
      CALL EGSGL('.1.AXIS.1.DATA.7 flag$',1)
C
      CALL EGSGL('.1.AXIS.1.DATA.8 flag$',1)
C
      CALL EGSGL('.1.AXIS.1.DATA.9 flag$',2)
C
C     ADD TITLES
C
      CALL EPTITL('RSC and CCAPS REGION','meters',' ')
C
C     CARRY OUT PLOT
C
      CALL EPSPLT(IUNIT,' ')
C
      STOP
      END
```

REFERENCES

1. Krider, E. P., A Study of Thunderstorm Electric Field Changes and Associated Meteorological Conditions at the Kennedy Space Center; Progress Report to NASA under contract NAS10-8518, October, 1976.

2. Weems, J., N. Wyse, J. Madura, M. Seerist, and C. Pinder; Assessment and Forecasting of Lightning Potential and its Effects on Launch Operations at Cape Canaveral Air Force Station and John F. Kennedy Space Center; International Aerospace and Ground Conference on Lightning and Static Electricity, vol II; NASA Conference Publication 10058, 1991.

3. Uman, Martin A.; Lightning; McGraw-Hill, 1969.

4. Golde, R. H., editor; Lightning-Physics of Lightning; vol 1; Academc Press; 1977.

5. Soula, S., and S. Chauzy; The Detection of the Electric Field, Vertical Distribution Underneath Thundercloud, Principle and Applications: International Aerospace and Ground Conference on Lightning and Static Electricity, vol I; NASA Conference Publication 10058, 1991.

6. Jacobson, E. A., and E. P. Krider; Electrostatic Field Charges Produced by Florida Lightning; *Journal of Atmospheric Science*, vol. 33, no. 1, pp 103-117; January, 1976.

7. Maier, L., and E. P. Krider; The Charges That Are Deposited by Cloud-to-Ground Lightning in Florida; *Journal of Geophysical Research*, vol. 91, no. D12, pp 13275-13289; November, 1986.

8. Marcotte, R. A., and A. M. Mulvehill; Detecting and Interpreting Signatures within Electric Field Mill Sensor Data; report to NASA under a contract of Mitre Corp.; February, 1991.

9. Jackson, John D.; Classical Electrodynamics; Wiley; 1969.

10. Sadiku, Matthew N.; Elements of Electromagnetics; Holt, Rinehart and Winston; 1989.

11. Boas, Mary L.; Mathematical Methods in the Physical Sciences, 2nd ed.; Wiley; 1983.

12. Watson, A. I., R. L. Holle, and R. E. Lopez; Surface Wind Convergence as a Short-term Predictior of Cloud-to-Ground Lightning at Kennedy Space Center, A Four Year Summary and Evaluation; International Aerospace and Ground Conference on Lightning and Static Electricity, vol II; NASA Conference Publication 10058, 1991.

13. Glori, K. L., and J. E. Nanevicz; Airborne Observations of Electric Fields Around Growing and Decaying Cumulus Clouds; International Aerospace and Ground Conference on Lightning and Static Electricity, vol I; NASA Conference Publication 10058, 1991.

14. Chirlian Paul M.; Introduction to Structured Fortran; Matrix Publishers Inc.; Portland, Oregon; 1979.

15. McCracken, Daniel D.; A Guide to Fortran Programming; Wiley; 1961.

16. Shannon, Terry C.; Introduction to VAX/VMS; Professional Press Inc.; Spring House, Pennsylvania; 1986.

17. Morrison, Foster; The Art of Modeling Dynamic Systems; Wiley; 1991.

$$E_i = \frac{9.0X10^9 X 2Q X H}{([X-x_i]^2+[Y-y_i]^2+H^2)^{1.5}} \text{ volts/meter}$$

vertical component of the Electric Field

distance in meters
charge in coulombs

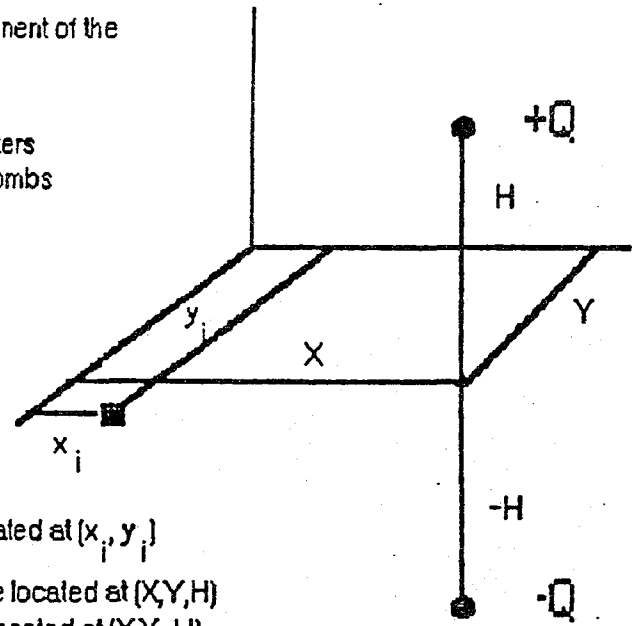

Field Mill (i) located at (x_i, y_i)

Primary Charge located at (X,Y,H)
Mirror Charge located at (X,Y,-H)

Figure 1
Field Due to a Source Charge and Its Image

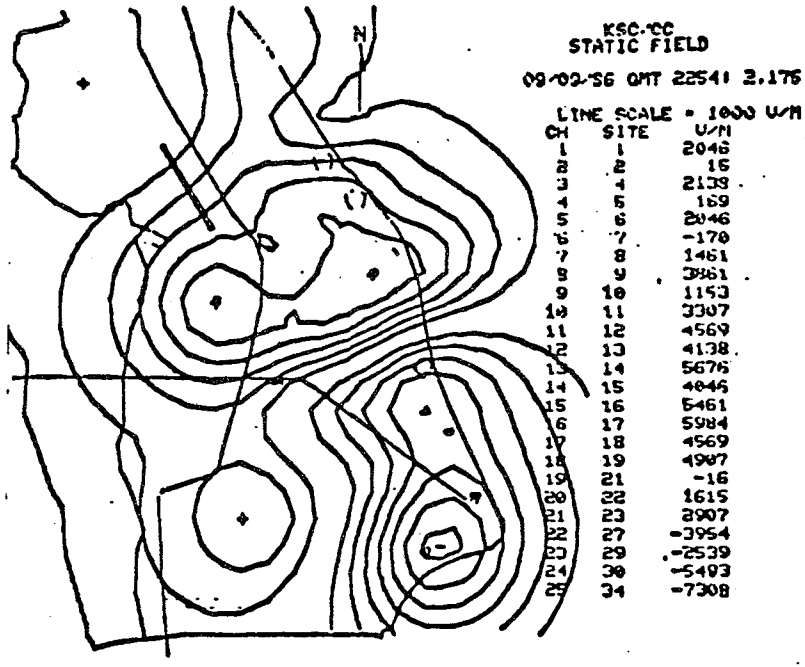

Figure 2a
Application of Original Model to Data Set #1

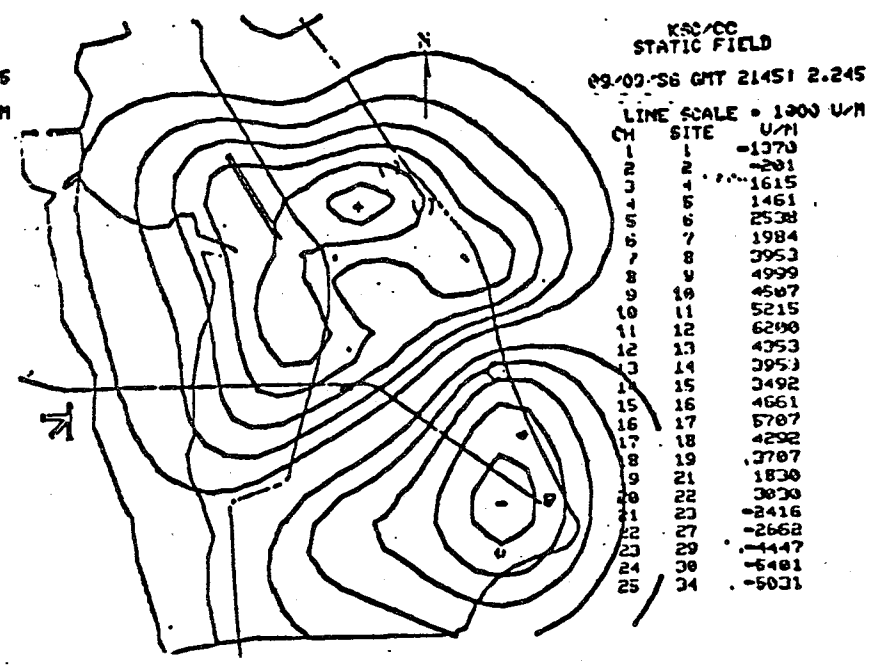

Figure 2b
Application of Original Model to Data Set #2

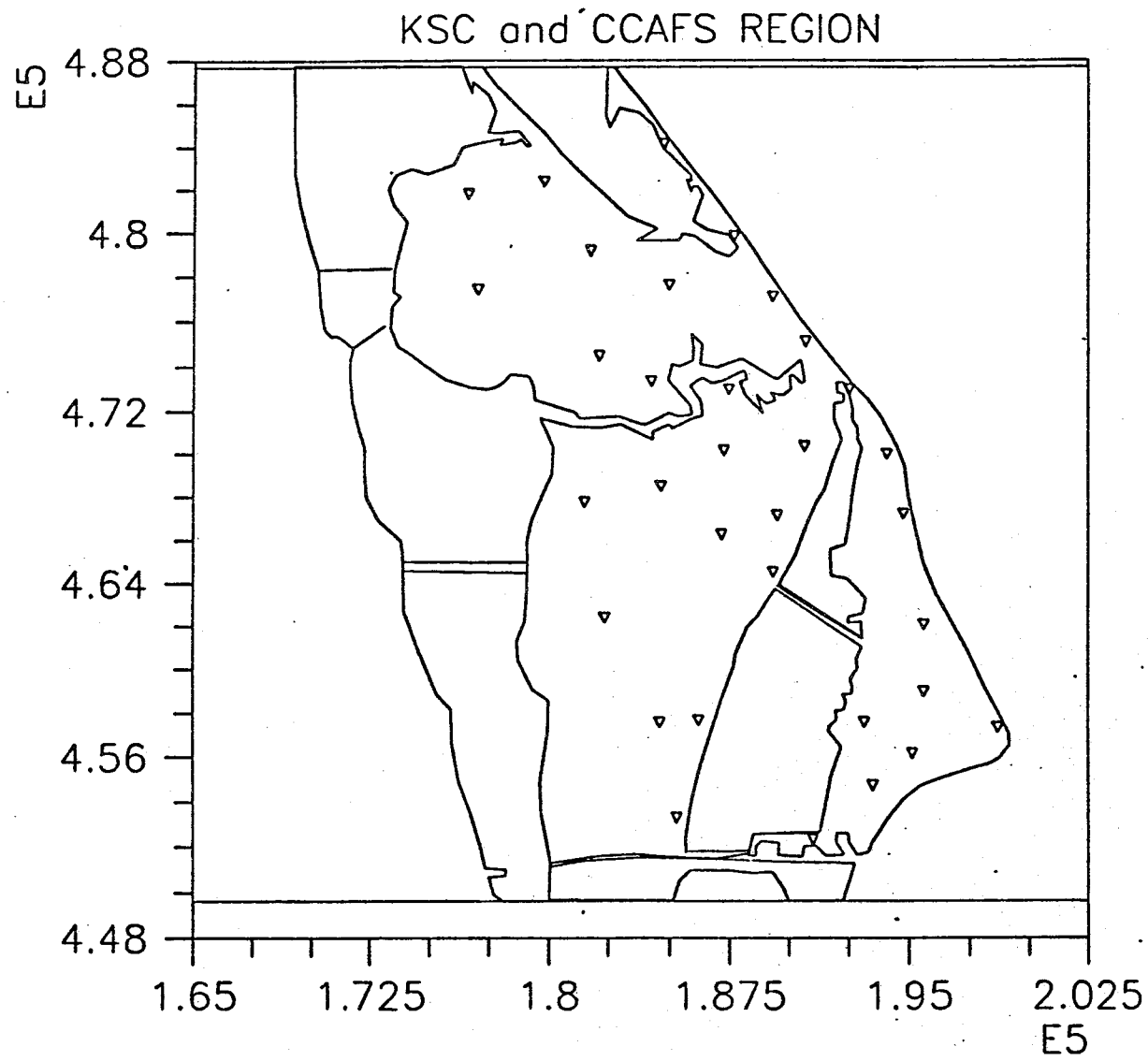

Figure 3
Contour Background Map

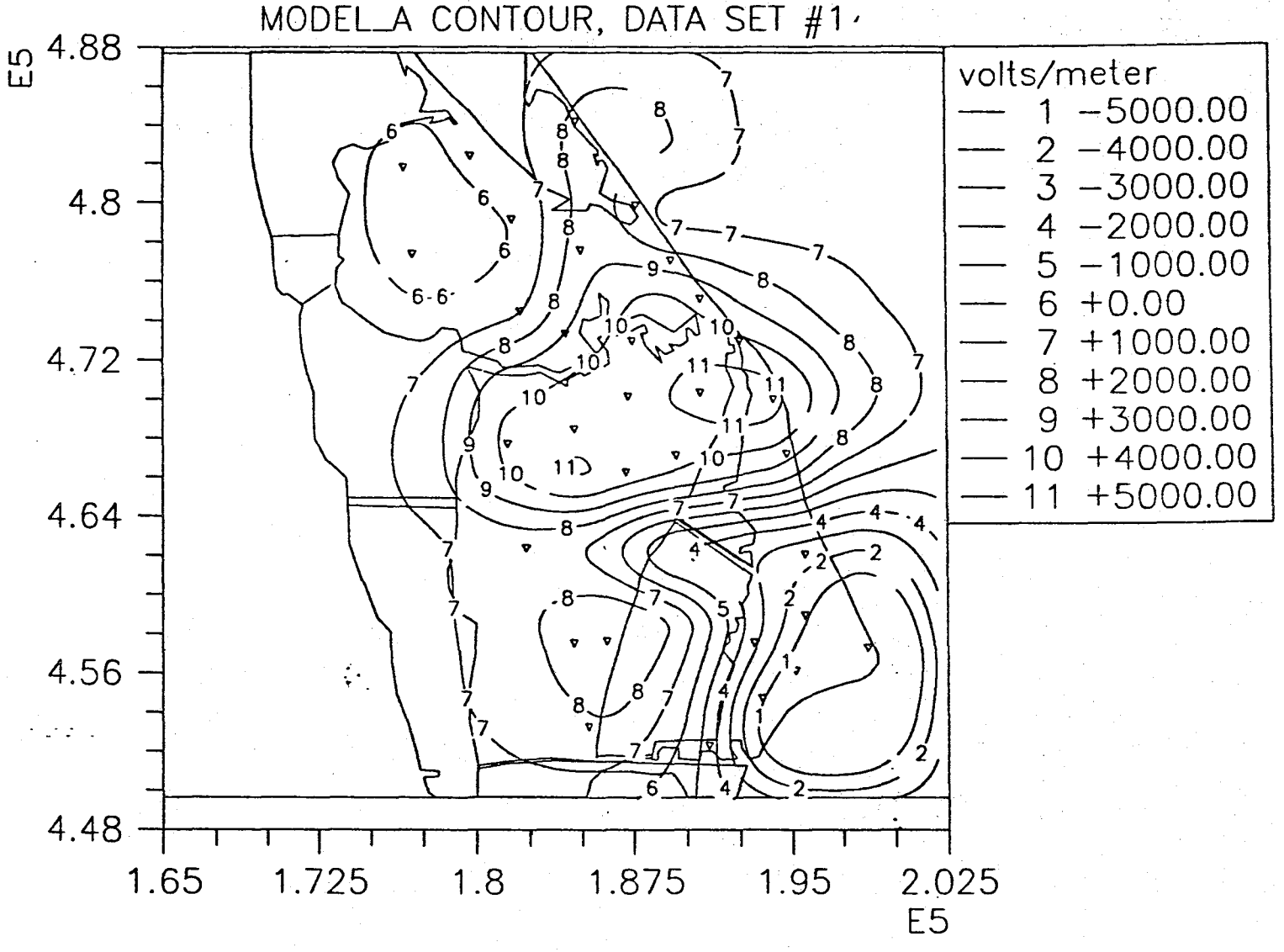

Figure 4
Application of Model_A to Data Set #1

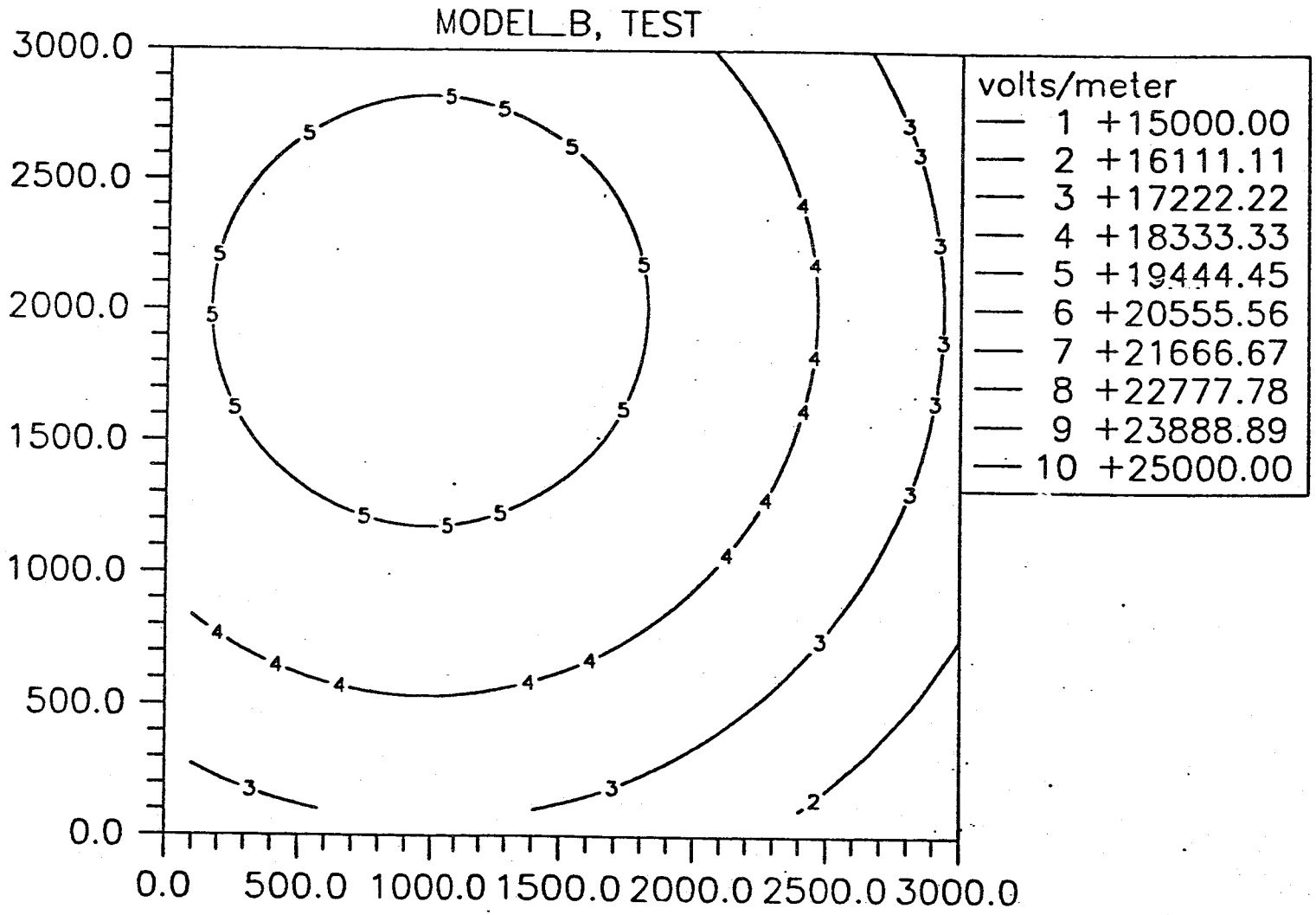

Figure 5
Application of Model_B to Test Data Set

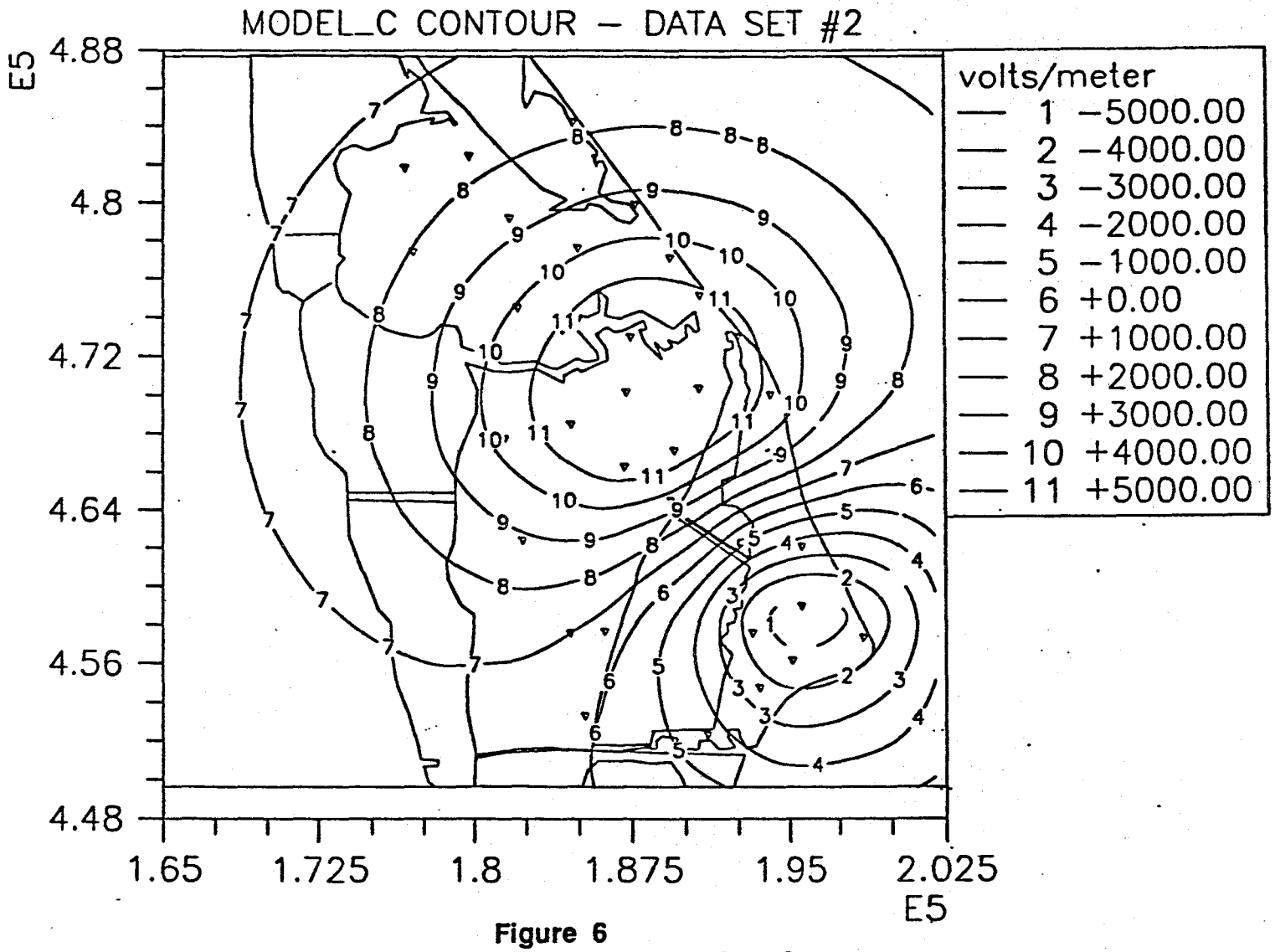

Figure 6
Application of Model_C to Data Set #2

1991 NASA/ASEE SUMMER FACULTY FELLOWSHIP PROGRAM

JOHN F. KENNEDY SPACE CENTER
UNIVERSITY OF CENTRAL FLORIDA

TRANSIENT STUDY OF A CRYOGENIC HYDROGEN FILLING SYSTEM

PREPARED BY:	Mr. Howard Schleier
ACADEMIC RANK:	Associate Professor
UNIVERSITY AND DEPARTMENT:	Norwalk State Technical College Mathematics/Science Department
NASA/KSC	
DIVISION:	Mechanical Engineering
BRANCH:	Special Projects
NASA COLLEAGUE:	Gary Lin Eric Thaxton
DATE:	August 21, 1991
CONTRACT NUMBER:	University of Central Florida NASA-NGT-60002 Supplement: 6

I

ACKNOWLEDGEMENTS

The author would like to thank his colleagues Gary Lin and Eric Thaxton for their leadership, guidance, and inspiration. It was their efforts that made this project possible. Sincere appreciation is also given Dr. E. Ramon Hosler and Ms. Kari Stiles, whose charismatic personalities insured the success of this project. The staff at DM MED at KSC, who were friendly and thoughtful, who accepted the author as one of them, and who never hesitated to attend to my needs are certainly worthy of the author's gratitude. Acknowledgement is also given to the staff at VAX Operations, and the librarians at KSC who were always ready to render first class service at the drop of a hat. Finally, mention is given to the remaining staff at KSC for their part in making this summer a memorable experience.

ABSTRACT

2.1 PREPARATION. An investigation was made as to producing a workable model for the transient analysis of a cryogenic hydrogen filling system. A series of programs and subprograms defining: the momentum, mass, and energy balances, the physical properties, the transport properties, and their interactions were devised.

2.2 TEST. The program was modified for a simple theoretical test fluid. Exhaustive runs and modifications were made and at this point no stability has been achieved except in trivial cases.

III

SUMMARY

3.1 SCOPE AND PURPOSE. This investigation was of a theoretical nature. A pressure driven, flow controlled cryogenic filing system was modeled to accept time dependent input. The system consists of an upstream tank (feedtank), upstream piping, a control element, downstream piping,and a downstream tank (external tank). The piping configuration is contained in block data, while certain initial conditions, ambient temperature, run time, and time interval, are entered as input.

3.2 RANGE OF VARIABLES. Though the algorithm is not limited in its variable range, some practical restrictions do exist. No inconsistency with the fundamental scientific constraints should be entered. Piping should be of order 1km, diameters 0.2m to 0.5m, and node lengths 1m to 10m. The time interval should be chosen such that it is no more than 10% of the residence time of the smallest node, however it should be long enough to avoid computational error. Pressures range from 1E5Pa to 5E5Pa, while temperatures between 20K and 300K are considered. Mass flows of course should be consistent with the 10% of the residence time restriction.

3.3 RESULTS. The transport and physical property routines used previously were reprogrammed. Most of them worked fairly well while others did not work at all. Several were improved upon. A transient cryogenic hydrogen filling process was programmed and tested with a fictitious fluid. Except in trivial cases, the program failed to reach convergence as of this date.

TABLE OF CONTENTS

Abbreviations and Acronyms List

VARIABLE	TYPE	DEFINITION	UNITS
CP	INTEGER*2	NODE # OF CONTROL POINT	LESS
ET	"	" " " EXTERNAL TANK	"
FRAME	"	TIME INTERVAL #	"
K	"	FITTING TYPE	"
NODE	"	NODE #	"
PUMP	"	NODE # OF PUMP	"
D	REAL*8	INSIDE DIAMETER	M
DELTAT	"	TIME INTERVAL	S
DO	"	OUTSIDE DIAMETER	M
E	"	U+V**2/2+G*Z	M**2/S**2
EPS	"	PIPE ROUGHNESS	M
H	"	ENTHALPY	M**2/S**2
H0	"	H+V**2/2+G*Z	M**2/S**2
H	"	HEAT TRANSFER COEFFICIENT	KG/S**3/K
F	"	FANNING FRICTION FACTOR	LESS
K	"	THERMAL CONDUCTIVITY	KG*M/S**3/K
KCO	"	TOTAL DISCHARGE COEFFICIENT	LESS
KELVIN	"	BULK TEMPERATURE	K
KELWAL	"	WALL TEMPERATURE	K
M	"	MASS OF NODE	M
MDOT	"	MASS FLOW	KG/S
MU	"	VISCOSITY	KG/M/S
P	"	PRESSURE	KG/M/S**2
PF	"	FRICTIONAL PRESSURE DROP	KG/M/S**2
PET	"	EXTERNAL TANK PRESSURE	KG/M/S**2
PFT	"	FEED TANK PRESSURE	KG/M/S**2
Q	"	HEAT FLUX	KG/S**3
QEXT	"	EXTERNAL HEAT FLUX	KG/S**3
QMAX	"	MAXIMUM HEAT FLUX	KG/S**3
REY	"	REYNOLDS NUMBER	LESS
RHO	"	DENSITY	KG/M**3
U	"	INTERNAL ENERGY	M**2/S**2
TAMB	"	AMBIENT TEMPERATURE	K
TIME	"	ELAPSED TIME	S
TFINAL	"	TOTAL ELAPSED TIME	S
V	"	VELOCITY	M/S
VET	"	EXTERNAL TANK VOLUME	M**3
X	"	QUALITY	LESS
Z	"	ELEVATION	M

VI

BODY OF TEXT

6.1 INTRODUCTION

6.1.1 SUBJECT. The subject of this project is the transient study of a cryogenic line. The intricate procedure involved in the filling of the external tank on the shuttle, coupled the large capacity of a long filling system, suggests a complicated transient. Predicting the nature of this transient might enable NASA to develop a more efficient filling procedure.

6.1.2 STATUS OF THE PROBLEM. NASA had developed some software to analyse transient flow of cryogenic fluids. However, all but one of these programs, fail to include the effects of heat transfer and two-phase flow. The program that includes these effects the TCTP(1) or "transient cryogenic transfer program". TCTP has reasonable success analyzing LOX systems, but is not as reliable for LH2-H2 modeling. TCTP is not well structured and is very poorly documented. after careful analysis, it was decided to start anew rather than modify TCTP.

6.1.3 SIGNIFICANCE OF WORK DONE. "H2FILL", a highly structured and rigidly documented FORTRAN code was developed to solve the problem. In the course of attempting to modify TCTP a set of subprograms defining the properties of hydrogen were developed. "H2FILL" is still being analyzed for run time stability at this point.

6.2 MAIN TEXT-DESCRIPTIVE INFORMATION

6.2.1 BACKGROUND. In the process of trying to decide whether to modify TCTP or start anew, the author investigated the possibility of locating software that might flowsheet the TCTP program and thereby facilitate the possibility of deciphering it. The "TAMU" code was located (2). It was available for $3500. After weighing the trade-offs between modification and initiation,it was decided to go with the latter.

6.2.2 CONFIGURATION. The configuration consists of the feedtank, the upstream piping, the control point (control valve), the downstream piping, and the external tank.

The parameters of this configuration are described in the BLOCK DATA statement "H2BLOCK". The time sensitive parameters are read in from an input list "H2LIS,LIS'.

6.2.3 PROGRAM. Program "H2FILL" the mainline program calls in four subroutines in sequence. These subroutines are: 1)"H2INPUT", 2)"H2INIT", 3)"H2MOMNRG", AND 4)"H2OUTPUT". The data between the subroutines is transferred by an unlabeled COMMON.

6.2.3.1 Input. Subprogram "H2INPUT" reads in the initial inventories in the tanks, the ambient temperature, and the initial pressures in the tanks. Then, the time of the the run and the time interval are read. The remaining data read in are the tank pressures and the mass flow at each non-zero time interval.

6.2.3.2 Initiation. Subprogram "H2INIT" initializes the conditions in the nodes. "H2INIT" also establishes the initial properties through "H2LSAT", "PROPHP",and "PROPPTGS".In addition it returns elevation from the inventory through "FEEDTANK" and "EXTANK".

6.2.3.3 Processing. "H2MOMNRG" simultaneously solves the momentum, continuity, and energy equations; the properties and flows at each node are updated. "TRANS" updates the transport coefficients and the wall temperature at each node from the properties and the design data.

6.2.3.4 Output. "H2OUTPUT" creates a file "H2DAT.DAT" on which it prints the data in spreadsheets. The first set is a node scan of each time. The second set is a time scan of each node.

6.3 MATHEMATICAL PRESENTATION

6.3.1 MOMENTUM From Newton's second law (1)
F=d(M*V)/dTIME+(MDOT*V)out-(MDOT*V)in
where F is the net force.

The parameters of this configuration are described in the
and

```
M=RHO*PI/4*D**2*L                                                    (2)
```

for a cylinder.Also note that

```
dF=-PI/4*D**2*(dP+dPF+RHO*G*dZ)                                      (3)
```

and

```
MDOT=RHO*V*PI/4*V*D**2                                               (4)
```

combining (1), (2) (3), and (4) and integrating we get

```
(P(NODE,FRAME-1)-P(NODE-1,FRAME-1)+
(RHO(NODE,FRAME-1)*V(NODE-1,FRAME-1)**2-
RHO(NODE-1,FRAME-1)*V(NODE-1,FRAME-1)**2)+
PF(NODE,FRAME-1)+G*(Z(NODE)-Z(NODE-1))=L(NODE)/DELTAT*
                    (RHO(NODE,FRAME-1)*(V(NODE,FRAME-1)-
                    RHO(NODE,FRAME)*V(NODE,FRAME))           (5)
```

Substituting (4) in (5) and rearranging the following appears:

```
MDOT(NODE,FRAME)=MDOT(NODE,FRAME-1)-
                 PI/4*D(NODE)**2*DELTAT/L(NODE)*
                 (P(NODE,FRAME-1)-P(NODE-1,FRAME-1)+
                 RHO(NODE,FRAME-1)*V(NODE,FRAME-1)**2-
                 RHO(NODE-1,FRAME-1)*V(NODE-1,FRAME-1)**2
                 +PF(NODE,FRAME-1)+RHO(NODE,FRAME-1)*
                 G*(Z(N0DE)-Z(NODE-1)))                          (6)
```

which updates the mass flow.

6.3.2 CONTINUITY. For mass conversation one sees that

```
dM/dTIME=MDOTin-MDOTout                                              (7)
```

integrating we get

```
M(NODE,FRAME)=M(NODE,FRAME-1)+DELTAT*
              MDOT(NODE-1,FRAME)-MDOT(NODE,FRAME))                   (8)
```

and

```
RHO(NODE,FRAME)=M(NODE,FRAME)/
                (PI/4*D(NODE)**2*L(NODE))                            (9)
```

also

```
V(NODE,FRAME)=MDOT(NODE,FRAME)/
              (RHO(NODE,FRAME)*PI/4*D(NODE,FRAME)**2)                (10)
```

hence the momentum and mass conservation laws has allowed us to update MDOT, M, RHO, and V. However, in in order to ascertain the state of the system we need another independent variable. Energy conservation will satisfy this requirement.

6.3.3 ENERGY. For the energy conservation (1) through (8)

```
d(MDOT*E)/dTIME=(MDOT*(U+V**2/2+G*Z))in
                -MDOT*(U+V**2/2+G*Z))out
                +(heat)in-(work)out,(7)                              (11)
where (work)out=(MDOT*P/RHO)out-(MDOT*P/RHO)in,(1)                   (12)
and (heat)in=HC*PI*D*L*(KELWAL-KELVIN),(1)                           (13)
```

combining (11), (12), and (13) and noting the definition of H0 we obtain:

```
d(M*E)/dTIME=(MDOT*H0)in-(MDOT*H0)out+
             HC*PI*D*L*(KELWAL-KELVIN),(7).                (14)
```

Integrating and solving for the update of E gives

```
E(NODE,FRAME)=(((MDOT(NODE-1,FRAME-1)*H0(NODE-1,FRAME-1)-
                MDOT(NODE,FRAME)*H0(NODE,FRAME)+
                HC(NODE,FRAME-1)*PI*D(NODE)*L(N0DE)*
                (KELWAL(NODE,FRAME)-KELVIN(NODE,FRAME)))*
                DELTAT+M(NODE,FRAME-1)*E(NODE,FRAME-1)/
                M(NODE,FRAME)                              (15)
```

then we update U

```
U(NODE,FRAME)=E(NODE,FRAME)-V(NODE,FRAME)**2/2-G*Z(NODE)(16)
```

With U and RHO determined the state of the system is also determined.Therefore P, H, KELVIN, MU, K and X can all be updated. A combination of physical properties an the flow conditions then can produce F, HC, and eventually KELWAL, PF, and H0. Hence the update would be complete, and the next iteration can proceed.

6.4 DISCUSSION

6.4.1 HISTORY. NASA has several programs that simulate the cryogenic fueling systems at the Kennedy Space Center. However, only one of those algorithms accounts for both heat transfer and two-phase flow. The program with both of these attributes is the TCTP code. TCTP seems to be satisfactory for oxygen, but fails in describing hydrogen fueling. The authors' suspicion is that the hydrogen properties are "stiff", and are not converging with the numerical techniques used in TCTP.

6.4.2 AGENDA. In order to produce a program that would successfully model the hydrogen fueling system, the question of whether to modify the existing TCTP, or to start anew had to be contemplated. Ordinarily, the easier path would seem to be to attempt modification of the existing code. However, TCTP turned out to be very poorly structured, and hardly documented at all. Due to the above, and the fact that something might be gained from a new approach, it was decided that a new approach would be the way to go.

6.4.3 PROJECT. A highly structured intricately documented FORTRAN code was started and developed for numerically solving the momentum, continuity, and energy equations.

VII

CONCLUDING SECTION

7.1 CONCLUDING REMARKS

7.1.1 PHYSICAL PROPERTIES. A battery of subprograms describing the properties of cryogenic hydrogen were developed. The mode was made compatible to the SI system of units. Most of the data agreed reasonably well with NBS data, while did not agree well at all. On several points the author improved on the existing algorithms. Extensive documentation and perfect structure was used at all times.

7.1.2 TRANSPORT PROPERTIES. An improved algorithm was produced for flow conditions and the thermal equations were rewritten.

7.1.3 TRANSIENT CRYOGENIC FLOW ALGORITHM. A highly structured, extensively documented program was written. A ficticious fluid was introduced and at this point convergence to reasonable numbers has not as yet been achieved.

7.1.4 RECOMMENDATIONS. The author that some minor revision would stabilize the run time condition of H2FILL. The author also believes that when actual cryogenic hydrogen properties are evaluated the previous troubles experienced with TCTP will reappear. A more novel method of presenting the equation of state, might alleviate the problem. Differential techniques with smoothing might provide the answer. Other alternatives in the numerical analysis of the equation of state might also be tried. One might also note that proper adjustment of the input parameters can also bring about convergence.

VIII

APPENDIX

8.8 APPENDIX A

8.8.1 TIME SCAN OF NODES

FEED TANK AT NODE = 0
CONTROL POINT AT NODE = 4
EXTERNAL TANK AT NODE = 35
NODE # = 3

TIME	QUALITY	PRESSURE	TEMPERATURE	WALL TEMP.	DENSITY	VELOCITY	MASS	MASS FLOW
0.000000D+00	0.000000D+00	0.499421D+06	0.203967D+02	0.203900D+02	0.589015D+01	0.000000D+00	0.185044D+01	0.000000D+00
0.150000D-01	0.000000D+00	0.499421D+06	0.203967D+02	0.203900D+02	0.589015D+01	0.540411D-11	0.185044D+01	0.100000D-11
0.300000D-01	0.000000D+00	0.499421D+06	0.203967D+02	0.203900D+02	0.589015D+01	0.540411D-11	0.185044D+01	0.100000D-11
0.450000D-01	0.000000D+00	0.499421D+06	0.203967D+02	0.203900D+02	0.589015D+01	0.540411D-11	0.185044D+01	0.100000D-11
0.600000D-01	0.000000D+00	0.499421D+06	0.203967D+02	0.203900D+02	0.589015D+01	0.540411D-11	0.185044D+01	0.100000D-11
0.750000D-01	0.000000D+00	0.499421D+06	0.203967D+02	0.203900D+02	0.589015D+01	0.540411D-11	0.185044D+01	0.100000D-11
0.900000D-01	0.000000D+00	0.499421D+06	0.203967D+02	0.203900D+02	0.589015D+01	0.540411D-11	0.185044D+01	0.100000D-11
0.105000D+00	0.000000D+00	0.499421D+06	0.203967D+02	0.203900D+02	0.589015D+01	0.540411D-11	0.185044D+01	0.100000D-11
0.120000D+00	0.000000D+00	0.499421D+06	0.203967D+02	0.203900D+02	0.589015D+01	0.540411D-11	0.185044D+01	0.100000D-11
0.135000D+00	0.000000D+00	0.499421D+06	0.203967D+02	0.203900D+02	0.589015D+01	0.540411D-11	0.185044D+01	0.100000D-11
0.150000D+00	0.000000D+00	0.499421D+06	0.203967D+02	0.203900D+02	0.589015D+01	0.540411D-11	0.185044D+01	0.100000D-11
0.165000D+00	0.000000D+00	0.499417D+06	0.203966D+02	0.203900D+02	0.589015D+01	0.540411D-11	0.185044D+01	0.100000D-11
0.180000D+00	0.000000D+00	0.499426D+06	0.203969D+02	0.203900D+02	0.589015D+01	0.540411D-11	0.185044D+01	0.100000D-11
0.195000D+00	0.000000D+00	0.499696D+06	0.204078D+02	0.203900D+02	0.589018D+01	0.540407D-11	0.185046D+01	0.100000D-11
0.210000D+00	0.000000D+00	0.499607D+06	0.204042D+02	0.203900D+02	0.589017D+01	0.540408D-11	0.185045D+01	0.100000D-11
0.225000D+00	0.000000D+00	0.482641D+06	0.197145D+02	0.203900D+02	0.586803D+01	0.540605D-11	0.184978D+01	0.100000D-11
0.240000D+00	0.000000D+00	0.453474D+06	0.185376D+02	0.203900D+02	0.582462D+01	0.540918D-11	0.184671D+01	0.100000D-11
0.255000D+00	0.000000D+00	0.168173D+07	0.672791D+02	0.203900D+02	0.601307D+01	0.529363D-11	0.188906D+01	0.100000D-11
0.270000D+00	0.000000D+00	-0.126012D+08	-0.467474D+03	0.203900D+02	0.648448D+01	0.490880D-11	0.203716D+01	0.100000D-11
0.285000D+00	0.000000D+00	0.239541D+10	-0.461194D+06	0.203900D+02	-0.871501D+00	-0.365243D-10	-0.273790D+00	0.100000D-11
0.300000D+00	0.000000D+00	-0.794325D+11	0.432888D+07	0.203900D+02	-0.441410D+01	-0.721121D-11	-0.138673D+01	0.100000D-11

8.8.2 NODE SCAN OF TIME

FEED TANK AT NODE = 0
CONTROL POINT AT NODE = 4
EXTERNAL TANK AT NODE = 35
ELAPSED TIME = 0.0000000D+00

NODE	QUALITY	PRESSURE	TEMPERATURE	WALL TEMP.	DENSITY	VELOCITY	MASS	MASS FLOW
0	0.000000D+00	0.500000D+06	0.203900D+02	0.000000D+00	0.518483D+01	0.000000D+00	0.100000D+03	0.000000D+00
1	0.000000D+00	0.489421D+06	0.203967D+02	0.203967D+02	0.518015D+01	0.000000D+00	0.100000D+03	0.000000D+00
2	0.000000D+00	0.489421D+06	0.203967D+02	0.203900D+02	0.518015D+01	0.000000E+00	0.185044D+01	0.000000D+00
3	0.000000D+00	0.489421D+06	0.203967D+02	0.203900D+02	0.518015D+01	0.000000D+00	0.185044D+01	0.000000D+00
4	0.000000D+00	0.200047D+06	0.100020D+03	0.100020D+03	0.166399D+00	0.000000D+00	0.000000D+00	0.181060D-11
5	0.000000D+00	0.200047D+06	0.100020E+03	0.100020D+03	0.160399D+00	0.000000D+00	0.125977D+01	0.000000D+00
6	0.000000D+00	0.200047D+06	0.100020D+03	0.100020D+03	0.160399D+00	0.000000D+00	0.125977D+01	0.000000D+00
7	0.000000E+00	0.200047D+06	0.100020D+03	0.100020D+03	0.160399D+00	0.000000D+00	0.125977D+01	0.000000D+00
8	0.000000D+00	0.200047D+06	0.100020D+03	0.100020D+03	0.160399D+00	0.000000D+00	0.125977D+01	0.000000D+00
9	0.000000D+00	0.200047D+06	0.100020D+03	0.100020D+03	0.160399D+00	0.000000D+00	0.125977D+01	0.000000D+00
10	0.000000D+00	0.200047D+06	0.100020D+03	0.100020D+03	0.160399D+00	0.000000D+00	0.125977D+01	0.000000D+00
11	0.000000D+00	0.200047D+06	0.100020D+03	0.100020D+03	0.160399D+00	0.000000D+00	0.125977D+01	0.000000D+00
12	0.000000D+00	0.200047D+06	0.100020D+03	0.100020D+03	0.160399D+00	0.000000D+00	0.125977D+01	0.000000D+00
13	0.000000D+00	0.200047D+06	0.100020D+03	0.100020D+03	0.160399D+00	0.000000D+00	0.125977D+01	0.000000D+00
14	0.000000D+00	0.200047D+06	0.100020D+03	0.100020D+03	0.160399D+00	0.000000D+00	0.125977D+01	0.000000D+00
15	0.000000D+00	0.200047D+06	0.100020D+03	0.100020D+03	0.160399D+00	0.000000D+00	0.125977D+01	0.000000D+00
16	0.000000D+00	0.200047D+06	0.100020D+03	0.100020D+03	0.160399D+00	0.000000D+00	0.125977D+01	0.000000D+00
17	0.000000D+00	0.200047E+06	0.100020E+03	0.100020D+03	0.160399D+00	0.000000D+00	0.125977D+01	0.000000D+00
18	0.000000D+00	0.200047D+06	0.100020D+03	0.100020D+03	0.160399D+00	0.000000D+00	0.125977D+01	0.000000D+00
19	0.000000D+00	0.200047D+06	0.100020D+03	0.100020D+03	0.160399D+00	0.000000D+00	0.125977D+01	0.000000D+00
20	0.000000D+00	0.200047D+06	0.100020D+03	0.100020D+03	0.160399D+00	0.000000D+00	0.125977D+01	0.000000D+00
21	0.000000D+00	0.200047D+06	0.100020D+03	0.100020D+03	0.160399D+00	0.000000D+00	0.125977D+01	0.000000D+00
22	0.000000D+00	0.200047D+06	0.100020D+03	0.100020D+03	0.160399D+00	0.000000E+00	0.125977D+01	0.000000D+00
23	0.000000D+00	0.200047D+06	0.100020D+03	0.100020D+03	0.160399D+00	0.000000D+00	0.125977D+01	0.000000D+00
24	0.000000D+00	0.200047D+06	0.100020D+03	0.100020D+03	0.160399D+00	0.000000D+00	0.125977D+01	0.000000D+00
25	0.000000D+00	0.200047D+06	0.100020D+03	0.100020D+03	0.160399D+00	0.000000D+00	0.125977D+01	0.000000D+00
26	0.000000E+00	0.200047D+06	0.100020E+01	0.100020D+03	0.160399D+00	0.000000D+00	0.125977D+01	0.000000E+00
27	0.000000D+00	0.200047D+06	0.100020D+03	0.100020D+03	0.160399D+00	0.000000D+00	0.125977D+01	0.000000D+00
28	0.000000D+00	0.200047D+06	0.100020D+03	0.100020D+03	0.160399D+00	0.000000D+00	0.125977D+01	0.000000D+00
29	0.000000D+00	0.200047D+06	0.100020D+03	0.100020D+03	0.160399D+00	0.000000D+00	0.125977D+01	0.000000D+00
30	0.000000D+00	0.200047D+06	0.100020D+01	0.100020D+03	0.160399D+00	0.000000D+00	0.125977D+01	0.000000D+00
31	0.000000D+00	0.200047D+06	0.100020D+03	0.100020D+03	0.160399D+00	0.000000D+00	0.125977D+01	0.000000D+00
32	0.000000D+00	0.200047D+06	0.100020D+03	0.100020D+03	0.160399D+00	0.000000D+00	0.125977D+01	0.000000D+00
33	0.000000D+00	0.200047D+06	0.100020D+03	0.100020D+03	0.160399D+00	0.000000D+00	0.125977D+01	0.000000D+00
34	0.000000D+00	0.200047D+06	0.100020D+03	0.100020D+03	0.160399D+00	0.000000D+00	0.125977D+01	0.000000D+00
35	0.000000D+00	0.200000D+06	0.100000D+03	0.000000D+00	0.160372D+00	0.000000D+00	0.100000E+03	0.000000D+00

8.9 APPENDIX B

8.9.1 FORTRAN PROGRAM H2FILL

```
      program h2fill
     integer*2 cp,et,frame,kc(5,0:99),node,pump
     real*8 cpr(0:99,0:99),cvo(0:99,0:99),
    &       d(0:99),deltat,do(0:99),e(0:99,0:99),eps(0:99),
    &       h(0:99,0:99),hc(0:99,0:99),
    &       h0(0:99,0:99),f(0:99,0:99),k(0:99,0:99),
    &       kco(0:99,0:99),kelvin(0:99,0:99),kelwal(0:99,
    &       0:99),l(0:99),m(0:99,0:99),mdot(0:99,0:99),
    &       mu(0:99,0:99),p(0:99,0:99),pf(0:99,0:99),
    &       pet(0:99),pft(0:99),q(0:99,0:99),
    &       qext(0:99,0:99),
    &       qmax(0:99),rey(0:99,0:99),
    &       rho(0:99,0:99),tamb,tfinal,time(0:99),
    &       u(0:99,0:99),v(0:99,0:99),
    &       vet,x(0:99,0:99),z(0:99)
      common
    &       cp,et,frame,kc,node,pump,
    &       cpr,cvo,
    &       d,deltat,do,e,eps,
    &       h,hc,h0,f,k,
    &       kco,kelvin,kelwal,
    &       l,m,mdot,
    &       mu,p,pf,pet,
    &       pft,q,qext,qmax,
    &       rey,rho,tamb,tfinal,
    &       time,u,
    &       v,vet,x,z
C*********************************************************************
C     H2FILL CALCULATES THE TRANSIENT OF A PRESSURE DRIVEN H2 FILL  *
C     SYSTEM. THE PROGRAM REQUIRES THAT INITIAL CONDITION IN THE    *
C     TWO TANKS,THE MASS FLOW AT THE CONTROL POINT,AND THE AMBIENT  *
C     TEMPERATURE BE GIVEN. TIME INDEPENDENT DATA ARE INCLUDED IN A *
C     BLOCK DATA STATEMENT. A SINGLE UNLABLED COMMON IS USED IN ALL *
C     SUBPROGRAMS FOR TRANSFER OF CONTROL. BOUNDARY CONDITIONS RE-  *
C     QUIRED ARE THE PRESSURES AT THE TOP OF THE TANKS,AND THE MASS *
C     FLOW AT EACH TIME INTERVAL.                                   *
C*********************************************************************
C*********************************************************************
C     ALL DIMENSIONED VARIABLES ARE IN THE SI SYSTEM INTERNALLY.    *
C     ON I/O NON-SI DATA ARE CONVERTED TO/FROM SI DATA AT THE  I/O  *
C     OR BLOCK DATA INTERFACE.                                      *
C*********************************************************************
C
C*********************************************************************
C     VARIABLE    TYPE          DEFINITION              UNITS       *
C     -------- --------- -------------------------   ----------    *
C     CP       INTEGER*2  NODE # OF CONTROL POINT      LESS        *
C     ET          "          "  "  "  EXTERNAL TANK      "         *
C     FRAME       "       TIME INTERVAL #               "         *
C     KC          "       FITTING TYPE                  "         *
C     NODE        "       NODE #                        "         *
C     PUMP        "       NODE # OF PUMP                "         *
C     D        REAL*8     INSIDE DIAMETER             M           *
C     DELTAT      "       TIME INTERVAL               S           *
C     DO          "       OUTSIDE DIAMETER            M           *
C     E           "       U+V**2/2+G*Z                M**2/S**2   *
C     EPS         "       PIPE ROUGHNESS              M           *
C     H           "       ENTHALPY                    M**2/S**2   *
C     H0          "       H+V**2/2+G*Z                M**2/S**2   *
C     HC          "       HEAT TRANSFER COEFFICIENT   KG/S**3/K   *
C     F           "       FANNING FRICTION FACTOR     LESS        *
C     K           "       THERMAL CONDUCTIVITY        KG*M/S**3/K *
```

```
C     KCO          "       TOTAL DISCHARGE COEFFICIENT  LESS          *
C     KELVIN       "       BULK TEMPERATURE             K             *
C     KELWAL       "       WALL  TEMPERATURE            K             *
C     M            "       MASS OF NODE                 M             *
C     MDOT         "       MASS FLOW                    KG/S          *
C     MU           "       VISCOSITY                    KG/M/S        *
C     P            "       PRESSURE                     KG/M/S**2     *
C     PF           "       FRICTIONAL PRESSURE DROP     KG/M/S**2     *
C     PET          "       EXTERNAL TANK PRESSURE       KG/M/S**2     *
C     PFT          "       FEED TANK PRESSURE           KG/M/S**2     *
C     Q            "       HEAT FLUX                    KG/S**3       *
C     QEXT         "       EXTERNAL HEAT FLUX           KG/S**3       *
C     QMAX         "       MAXIMUM HEAT FLUX            KG/S**3       *
C     REY          "       REYNOLDS NUMBER              LESS          *
C     RHO          "       DENSITY                      KG/M**3       *
C     U            "       INTERNAL ENERGY              M**2/S**2     *
C     TAMB         "       AMBIENT TEMPERATURE          K             *
C     TIME         "       ELAPSED TIME                 S             *
C     TFINAL       "       TOTAL ELAPSED TIME           S             *
C     V            "       VELOCITY                     M/S           *
C     VET          "       EXTERNAL TANK VOLUME         M**3          *
C     X            "       QUALITY                      LESS          *
C     Z            "       ELEVATION                    M             *
C*************************************************************************
C
C*************************************************************************
C     INPUT REQUIRED:                                                   *
C                              H2LIS.LIS                                *
C     OUTPUT GENERATED:                                                 *
C                              H2DAT.DAT                                *
C     SUBROUTINES CALLED:                                               *
C                              H2INPUT                                  *
C                              H2INIT                                   *
C                              h2MOMNRG                                 *
C                              H2OUTPUT                                 *
C*************************************************************************
C
C*************************************************************************
C     INFORMATION CONCERNING THE PIPING CONFIGURATION IS CONTAINED      *
C     IN THE BLOCK DATA STATEMENT "H2BLOCK.BLK".THE INITIAL AND         *
C     BOUNDARY CONDITIONS ARE READ IN ON DEVICE #20 FROM FILE           *
C     "H2LIST.LIS".                                                     *
C*************************************************************************
C
C*************************************************************************
C     H2INPUT IS THE INPUT SUBROUTINE.                                  *
C*************************************************************************
      call h2input
C*************************************************************************
C     H2INIT IS THE INITIALIZATION SUBROUTINE                           *
C*************************************************************************
      call h2init
C*************************************************************************
C     h2MOMNRG IS THE PROCESSING SUBROUTINE                             *
C*************************************************************************
      call h2momnrg
C*************************************************************************
C     H2OUTPUT IS THE OUTPUT SUBROUTINE                                 *
C*************************************************************************
      call h2output
C*************************************************************************
C     H2OUTPUT CREATES A REPORT ON A NEW FILE "H2DAT.DAT" ON DE-        *
```

```
C     VICE #21.                                                         *
C***********************************************************************
C
C***********************************************************************
C     THEN                                                              *
C***********************************************************************
      stop
C***********************************************************************
C     AND                                                               *
C***********************************************************************
      end
      subroutine h2input
C***********************************************************************
C     H2INPUT READS "H2LIS.LIS". THE FIRST RECORD CONSISTS OF THE       *
C     MASS IN THE FEED TANK, THE AMBIENT TEMPERATURE,THE INITIAL        *
C     PRESSURE IN THE FEED TANK, AND THE INITIAL PRESSURE IN THE        *
C     EXTERNAL TANK. THE SECOND RECORD CONTAINS THE TIME INTERVAL       *
C     AND THE THE TOTAL TIME OF THE RUN. ALL OF THE                     *
C     REMAINING RECORDS CONSIST OF THE PRESSURE AT THE FEED TANK        *
C     THE MASS FLOW AT THE CONTROL POINT, AND THE PRESSURE AT THE       *
C     EXTERNAL TANK AT ALL TIMES. THE THE RECORDS CONSIST OF THREE      *
C     FLOATING POINT NUMBERS EACH SEPERATED BY A COMMA. THE             *
C     INITIAL MASS FLOW WILL BE SET TO 0.0. DURING INITIATION.          *
C***********************************************************************
      integer*2 cp,et,frame,kc(5,0:99),node,pump
      real*8 cpr(0:99,0:99),cvo(0:99,0:99),
     &       d(0:99),deltat,do(0:99),e(0:99,0:99),eps(0:99),
     &       h(0:99,0:99),hc(0:99,0:99),
     &       h0(0:99,0:99),f(0:99,0:99),k(0:99,0:99),
     &       kco(0:99,0:99),kelvin(0:99,0:99),kelwal(0:99,
     &       0:99),l(0:99),m(0:99,0:99),mdot(0:99,0:99),
     &       mu(0:99,0:99),p(0:99,0:99),pf(0:99,0:99),
     &       pet(0:99),pft(0:99),q(0:99,0:99),
     &       qext(0:99,0:99),
     &       qmax(0:99),rey(0:99,0:99),
     &       rho(0:99,0:99),tamb,tfinal,time(0:99),
     &       u(0:99,0:99),v(0:99,0:99),
     &       vet,x(0:99,0:99),z(0:99)
      common
     &       cp,et,frame,kc,node,pump,
     &       cpr,cvo,
     &       d,deltat,do,e,eps,
     &       h,hc,h0,f,k,
     &       kco,kelvin,kelwal,
     &       l,m,mdot,
     &       mu,p,pf,pet,
     &       pft,q,qext,qmax,
     &       rey,rho,tamb,tfinal,
     &       time,u,
     &       v,vet,x,z
C***********************************************************************
C     OPEN "H2LIS.LIS" AND CONNECT TO DEVICE # 20                       *
C***********************************************************************
      open (file='h2lis.lis', unit=20, status='old')
C***********************************************************************
C     READ THE FIRST RECORD (INITIAL CONDITIONS)                        *
C***********************************************************************
      read(20,*)m(1,0),tamb,pft(0),pet(0)
C***********************************************************************
C     READ THE SECOND RECORD (TIME PARAMETERS)                          *
C***********************************************************************
      read(20,*)deltat,tfinal
```

```
C*********************************************************************
C     READ THE REMAINING RECORDS (BOUNDARY CONDITIONS)                *
C*********************************************************************
      read(20,*)(pft(frame),mdot(cp,frame),
     &          pet(frame),
     &          frame=1,tfinal/deltat)
C*********************************************************************
C     DISCONNECT AND CLOSE THE FILE                                   *
C*********************************************************************
      close(unit=20,status='keep')
C*********************************************************************
C     THEN                                                            *
C*********************************************************************
      return
C*********************************************************************
C     AND                                                             *
C*********************************************************************
      end
      subroutine h2init
C*********************************************************************
C     SUBROUTINE "H2INIT.FOR" SETS THE INITIAL CONDITIONS FOR         *
C     H2FILL. THE INITIAL CONDITION IS CONSIDERED TO BE STATIC.       *
C     THE PRESSURE IS DETERMINED HYDROSTATICALLY, TAKING INTO         *
C     CONSIDERATION THAT H0 IS CONSERVED IN THIS INSTANCE, H IS       *
C     DETERMINED, FORCING THE DETERMINATION OF THE OTHER PROP-        *
C     ERTIES AT THE NODE. THE FEED TANK IS CONSIDERED TO BE           *
C     PARTIALLY FILLED WITH SATURATED LIQUID, WHILE THE EXTERNAL      *
C     TANK IS GAS AT AMBIENT TEMPERATURE.                             *
C*********************************************************************
C
C*********************************************************************
C     SUBROUTINES CALLED:                                             *
C                         FEEDTANK                                    *
C                         H2LSAT                                      *
C                         PROPHP                                      *
C                         PROPPTGS                                    *
C*********************************************************************
      integer*2 cp,et,frame,kc(5,0:99),node,pump
      real*8 cpr(0:99,0:99),cvo(0:99,0:99),
     &       d(0:99),deltat,do(0:99),e(0:99,0:99),eps(0:99),
     &       h(0:99,0:99),hc(0:99,0:99),
     &       h0(0:99,0:99),f(0:99,0:99),k(0:99,0:99),
     &       kco(0:99,0:99),kelvin(0:99,0:99),kelwal(0:99,
     &       0:99),l(0:99),m(0:99,0:99),mdot(0:99,0:99),
     &       mu(0:99,0:99),p(0:99,0:99),pf(0:99,0:99),
     &       pet(0:99),pft(0:99),q(0:99,0:99),
     &       qext(0:99,0:99),
     &       qmax(0:99),rey(0:99,0:99),
     &       rho(0:99,0:99),tamb,tfinal,time(0:99),
     &       u(0:99,0:99),v(0:99,0:99),
     &       vet,x(0:99,0:99),z(0:99)
      common
     &       cp,et,frame,kc,node,pump,
     &       cpr,cvo,
     &       d,deltat,do,e,eps,
     &       h,hc,h0,f,k,
     &       kco,kelvin,kelwal,
     &       l,m,mdot,
     &       mu,p,pf,pet,
     &       pft,q,qext,qmax,
     &       rey,rho,tamb,tfinal,
     &       time,u,
```

```
     &       v,vet,x,z
C*********************************************************************
C     SIX VARIABLES ARE INITIALIZED                                  *
C*********************************************************************
      p(0,0)=pft(0)
      p(et,0)=pet(0)
      kelvin(0,0)=20.39d0
      kelvin(et,0)=tamb
      time(0)=0.
      m(0,0)=m(1,0)
      frame=0
      node=0
C*********************************************************************
C     "H2LSAT" RETURNS THE PROPERTIES OF THE SATURATED LIQUID        *
C*********************************************************************
      call h2lsat
C*********************************************************************
C     "FEEDTANK" RETURNS THE ELEVATION OF THE LIQUID LEVEL           *
C*********************************************************************
      call feedtank
C*********************************************************************
C     FOR THE INITIAL CONDITION H0 IS INVARIENT AND IT IS            *
C     CALCULATED FOR THE TOP OF THE LIQUID LEVEL.                    *
C*********************************************************************
      h0(0,0)=h(0,0)+9.81d0*z(0)
C*********************************************************************
C     FROM THE OUTLET OF THE FEED TANK TO THE INLET OF THE           *
C     CONTROL POINT INITIAL PROPERTIES ARE CALCULATED.               *
C*********************************************************************
      do node=1,cp-1
C*********************************************************************
C     THE PRESSURE IS CALCULATED HYDROSTATICALLY.                    *
C*********************************************************************
       p(node,0)=rho(node-1,0)
     &           *9.81d0*(z(node)-z(node-1))
     &           +p(node-1,0)
C*********************************************************************
C     H IS DETERMINED FROM H0.                                       *
C*********************************************************************
       h0(node,0)=h0(0,0)
       h(node,0)=h0(node,0)-9.81d0*z(node)
C*********************************************************************
C     "PROPHP" DETERMINES THE PROPERTIES FROM H AND P                *
C*********************************************************************
       call prophp
C*********************************************************************
C     FIVE MORE VARIABLES ARE INITIALIZED                            *
C*********************************************************************
       mdot(node,0)=0.
       e(node,0)=h0(node,0)-p(node,0)/rho(node,0)
       hc(node,0)=0.
       pf(node,0)=0.
       kelwal(node,0)=kelvin(node,0)
      end do
C*********************************************************************
C     THE REMAINING MASSES OF THE UPSTREAM NODES ARE ESTABLISHED.    *
C*********************************************************************
      do node=2,cp-1
       m(node,0)=rho(node,0)*datan(1.d0)
     &           *d(node)**2*l(node)
      end do
C*********************************************************************
```

```
C     THE INITIAL CONDITION IS NOW ESTABLISHED FROM THE CONTROL   *
C     POINT TO THE EXTERNAL TANK.                                 *
C*************************************************************************
      node=et
C*************************************************************************
C     "PROPPTGS" RETURNS THE PROPERTIES OF A GAS GIVEN PRESSURE   *
C     TEMPERATURE INPUT.                                          *
C*************************************************************************
      kelvin(node,0)=tamb
      call h2lsat
C*************************************************************************
C     THE MASS AND H0 FOR THE EXTERNAL TANK ARE ESTABLISHED.      *
C*************************************************************************
      m(et,0)=rho(et,0)*vet
C*************************************************************************
C     FOR THE INITIAL CONDITION H0 IS INVARIENT AND IT IS         *
C     CALCULATED FOR THE TOP OF THE EXTERNAL TANK.                *
C*************************************************************************
      h0(et,0)=h(et,0)+9.81d0*z(et)
C*************************************************************************
C     FROM THE INLET OF THE EXTERNAL TANK TO THE OUTLET OF THE    *
C     CONTROL POINT THE INITIAL PROPERTIES ARE CALCULATED.        *
C*************************************************************************
      do node=et-1,cp,-1
C*************************************************************************
C     THE PRESSURE IS CALCULATED HYDROSTATICALLY.                 *
C*************************************************************************
       p(node,0)=rho(node+1,0)
     &           *9.81d0*(z(node+1)-z(node))
     &           +p(node+1,0)
C*************************************************************************
C     H IS DETERMINED FROM H0.                                    *
C*************************************************************************
       h0(node,0)=h0(et,0)
       h(node,0)=h0(node,0)-9.81d0*z(node)
C*************************************************************************
C     "PROPHP" DETERMINES THE PROPERTIES FROM H AND P             *
C*************************************************************************
       call prophp
C*************************************************************************
C     FIVE MORE VARIABLES ARE INITIALIZED                         *
C*************************************************************************
       mdot(node,0)=0.
       e(node,0)=h0(node,0)-p(node,0)/rho(node,0)
       hc(node,0)=0.
       pf(node,0)=0.
       kelwal(node,0)=kelvin(node,0)
      end do
C*************************************************************************
C     THE REMAINING MASSES OF THE DOWNSTREAM NODES ARE            *
C     ESTABLISHED.                                                *
C*************************************************************************
      do node=cp+1,et-1
       m(node,0)=rho(node,0)*4.d0*datan(1.d0)
     &           *d(node)*l(node)
      end do
      do frame=1,tfinal/deltat
       p(0,frame)=pft(frame)
       node=0
       call h2lsat
       p(et,frame)=pet(frame)
       node=et
```

```
       call h2lsat
      end do
      do node=0,et
       mdot(node,0)=mdot(node,1)
      end do
C*********************************************************************
C     THEN                                                           *
C*********************************************************************
      return
C*********************************************************************
C     AND                                                            *
C*********************************************************************
      end
      subroutine h2momnrg
C*********************************************************************
C     "H2MOMNRG" BASICALLY SOLVES THE TRANSIENT MOMENTUM AND         *
C     ENERGY EQUATIONS IN ORDER TO UPDATE M, MDOT, RHO, V, E, U,     *
C     AND THEN THE PHYSICAL PROPERTIES. AFTER THE ABOVE HAS          *
C     BEEN ESTABLISHED, THE TRANSPORT COEFFICIENTS HC, F, AND KCO    *
C     ARE DETERMINED.                                                *
C*********************************************************************
C
C*********************************************************************
C     SUBROUTINES CALLED:                                            *
C                           EXTANK                                   *
C                           FEEDTANK                                 *
C                           PROPURHO                                 *
C                           TRANS                                    *
C*********************************************************************
      integer*2 cp,et,frame,kc(5,0:99),node,pump
      real*8 cpr(0:99,0:99),cvo(0:99,0:99),
     &       d(0:99),deltat,do(0:99),e(0:99,0:99),eps(0:99),
     &       h(0:99,0:99),hc(0:99,0:99),
     &       h0(0:99,0:99),f(0:99,0:99),k(0:99,0:99),
     &       kco(0:99,0:99),kelvin(0:99,0:99),kelwal(0:99,
     &       0:99),l(0:99),m(0:99,0:99),mdot(0:99,0:99),
     &       mu(0:99,0:99),p(0:99,0:99),pf(0:99,0:99),
     &       pet(0:99),pft(0:99),q(0:99,0:99),
     &       qext(0:99,0:99),
     &       qmax(0:99),rey(0:99,0:99),
     &       rho(0:99,0:99),tamb,tfinal,time(0:99),
     &       u(0:99,0:99),v(0:99,0:99),
     &       vet,x(0:99,0:99),z(0:99)
      common
     &       cp,et,frame,kc,node,pump,
     &       cpr,cvo,
     &       d,deltat,do,e,eps,
     &       h,hc,h0,f,k,
     &       kco,kelvin,kelwal,
     &       l,m,mdot,
     &       mu,p,pf,pet,
     &       pft,q,qext,qmax,
     &       rey,rho,tamb,tfinal,
     &       time,u,
     &       v,vet,x,z
C*********************************************************************
C     START THE CLOCK.                                               *
C*********************************************************************
      do frame=1,tfinal/deltat
C*********************************************************************
C     RECORD THE TIME.                                               *
C*********************************************************************
```

```
       time(frame)=frame*deltat
C*********************************************************************
C     NO ACCUMULATION OCCURS WITHIN THE CONTROL POINT NODE.          *
C*********************************************************************
       mdot(cp-1,frame)=mdot(cp,frame)
C*********************************************************************
C     THE FEED TANK PRESSURE IS ZEROED IN ORDER TO ENTER THE DO      *
C     LOOP. IT IS LATER UPDATED TO WITHIN 1% OF PFT IN AN            *
C     ITERATIVE PROCESS.                                             *
C*********************************************************************
       p(cp-1,frame)=p(0,frame)*9.d-1
C        do while
C     &           ((abs(p(cp-1,frame)/p(cp-1,frame-1))
C     &            .lt. .99d0) .or.
C     &           (abs(p(cp-1,frame)/p(cp-1,frame-1))
C     &            .gt. 1.01d0))
C*********************************************************************
C     FOR THE INTERMEDIATE PIPING UPSTREAM OF THE CONTROL POINT.     *
C*********************************************************************
         do node=cp-2,1,-1
C*********************************************************************
C     CALCULATE THE CROSS SECTIONAL AREA.                            *
C*********************************************************************
          s=datan(1.d0)*d(node+1)**2
C*********************************************************************
C     UPDATE MDOT                                                    *
C*********************************************************************
          mdot(node,frame)=mdot(node,frame-1)-s*deltat/l(node+1)*
     &                     (p(node+1,frame-1)-p(node,frame-1)+
     &                     v(node+1,frame-1)**2*
     &                     rho(node+1,frame-1)-
     &                     v(node,frame-1)**2*rho(node,
     &                     frame-1)+rho(node+1,frame-1)
     &                     *9.81d0*(z(node+1)-z(node))+pf(
     &                     node+1,frame-1))
C*********************************************************************
C     UPDATE M, RHO, AND V                                           *
C*********************************************************************
         end do
         do node=cp-1,2,-1
          s=datan(1.d0)*d(node)**2
          m(node,frame)=(mdot(node-1,frame-1)-mdot(node,frame-1))
     &                  *deltat+m(node,frame-1)
          rho(node,frame)=m(node,frame)/s/l(node)
          v(node,frame)=mdot(node,frame)/s/rho(node,frame)
         end do
C*********************************************************************
C     UPDATE MDOT FOR THE FEED TANK                                  *
C*********************************************************************
         mdot(0,frame)=mdot(1,frame)
         m(0,frame)=m(0,frame-1)-mdot(0,frame-1)*deltat
C*********************************************************************
C     UPDATE M, RHO, AND V FOR THE TERMINAL UPSTREAM NODES           *
C*********************************************************************
         m(1,frame)=m(0,frame)
C.... THIS IS A COURSE APPROXIMATION FOR AN IDEAL GAS ONLY
C.... A BARAMETRIC SUBROUTINE WOULD BE DEVELOPED FOR THE
C.... GENERAL CASE
         rho(1,frame)=rho(2,frame)
         v(1,frame)=v(2,frame)
C*********************************************************************
C      UPDATE E,U,H,H0, AND PF FOR ALL THE UPSTREAM PIPE NODES        *
```

```
C*********************************************************************
        do node=cp-1,1,-1
         if (node .ne. 1)then
          e(node,frame)=((mdot(node-1,frame-1)*h0(node-1,
     &                  frame-1)-mdot(node,frame-1)*h0
     &                  (node,frame-1))+hc(node,frame-1)
     &                  *(4.d0*datan(1.d0)*d(node)*l(node))*
     &                  (kelwal(node,frame-1)-kelvin(node,
     &                  frame-1))*deltat+m(node,frame-1)*
     &                  e(node,frame-1))/m(node,frame)
         else
          e(node,frame)=-mdot(node,frame-1)*h0(node,frame-1)
     &                 +e(node,frame-1)*m(node,frame-1)/
     &                  m(node,frame)
         endif
         u(node,frame)=e(node,frame)
     &                -v(node,frame)**2/2-9.81d0*z(node)
C*********************************************************************
C        "PROPURHO" RETURNS THE PHYSICAL PROPERTIES FROM AN         *
C        INPUT OF U AND RHO.                                        *
C*********************************************************************
          call propurho
          h0(node,frame)=h(node,frame)+v(node,frame)**2/2
     &                  +9.81d0*z(node)
C*********************************************************************
C         "TRANS" RETURNS THE TRANSPORT PROPERTIES F,KCO,AND HC      *
C         FROM THE PHYSICAL PROPERTIES AND CERTAIN FLOW              *
C         PARAMETERS THAT HAVE ALREADY BEEN ESTABLISHED. TW IS       *
C         ALSO RETURNED.                                             *
C*********************************************************************
           if(node .ne. 1)then
            call trans
            pf(node,frame)=(4.d0*f(node,frame)+kco(node,frame))*
     &                     rho(node,frame)*
     &                     v(node,frame)**2/2*
     &                     l(node)/d(node)
         endif
        end do
C*********************************************************************
C     "FEEDTANK" RETURNS THE ELEVATION OF THE LIQUID LEVEL IN THE    *
C     FEED TANK FROM THE FEED TANK MASS.                             *
C*********************************************************************
        call feedtank
C*********************************************************************
C     UPDATE E,H,AND H0 FOR THE TOP OF THE FEED TANK                 *
C*********************************************************************
        e(0,frame)=(-mdot(1,frame-1)*h0(1,frame-1)*
     &              deltat+m(1,frame-1)*e(0,frame-1))
     &              /m(1,frame)
        u(0,frame)=e(0,frame)-
     &             9.81d0*z(0)
        node=0
        call propurho
        h0(0,frame)=h(0,frame)+
     &              9.81d0*z(0)
C*********************************************************************
C     THIS IS THE THROTTLING CONDITION.                             *
C*********************************************************************
       h0(cp,frame)=h0(cp-1,frame)
C*********************************************************************
C     INITALIZE P INORDER TO ENTER LOOP. AN ITERATIVE PROCESS WILL*
C     THEN BRING UPDATE IT TO WITHIN 1% OF PET.                     *
```

```
C*********************************************************************
        p(et,frame)=0.
        do while
     &          (abs(pet(frame)-p(et,frame))
     &          .gt. 0.01d0*pet(frame))
C*********************************************************************
C     EVALUATE MDOT, RHO, V, M, E, H0, U, H, PLUS THE PHYSICAL     *
C     AND TRANSP0RT PROPERTIES FOR THE INTERMEDIATE NODES. NOTE    *
C     THAT TW IS ALSO RETURNED.                                    *
C*********************************************************************
         do node=et-1,cp+1,-1
          s=datan(1.d0)*d(node)**2
          mdot(node,frame)=mdot(node,frame-1)-s*deltat/l(node)*
     &                    (p(node,frame-1)-p(node-1,frame-1)+
     &                    v(node,frame-1)**2*
     &                    rho(node,frame-1)-
     &                    v(node-1,frame-1)**2*rho(node-1,
     &                    frame-1)+rho(node-1,frame-1)
     &                   *9.81d0*(z(node)-z(node-1))+pf(
     &                    node,frame-1))
          m(node,frame)=(mdot(node-1,frame-1)-mdot(node,frame-1))*deltat
     &                  +m(node,frame-1)
          rho(node,frame)=m(node,frame)/s/l(node)
          v(node,frame)=mdot(node,frame)/s/rho(node,frame)
          e(node,frame)=((mdot(node-1,frame-1)*h0(node-1,
     &                   frame-1)-mdot(node,frame-1)*h0
     &                   (node,frame-1))+hc(node,frame-1)
     &                   *(4.d0*datan(1.d0)*d(node)*l(node))*
     &                   (kelwal(node,frame-1)-kelvin(node,
     &                   frame-1))*deltat+m(node,frame-1)*
     &                   e(node,frame-1))/m(node,frame)
          u(node,frame)=e(node,frame)
     &                 -v(node,frame)**2/2-9.81d0*z(node)
          call propurho
          h(node,frame)=u(node,frame)+p(node,frame)
     &                  /rho(node,frame)
          h0(node,frame)=h(node,frame)+v(node,frame)**2/2
     &                   +9.81d0*z(node)
          call trans
          pf(node,frame)=(4.d0*f(node,frame)+kco(node,frame))*
     &                   rho(node,frame)*
     &                   v(node,frame)**2/2*
     &                   l(node)/d(node)
         end do
C*********************************************************************
C     UPDATE THE DOWNSTREAM PROPERTIES FOR THE CONTROL ELEMENT     *
C     AND THE TOP OF THE EXTERNAL TANK.                            *
C*********************************************************************
        rho(cp,frame)=rho(cp+1,frame)
        v(cp,frame)=mdot(cp,frame)/rho(cp,frame)
     &              /datan(1.d0)/d(node)**2
        h(cp,frame)=h0(cp,frame)
     &             -v(cp,frame)**2/2
     &             -9.81d0*z(frame)
        node=cp
C*********************************************************************
C       "PROPHRHO" RETURNS THE PHYSICAL PROPERTIES FROM AN          *
C       INPUT OF H AND RHO.                                         *
C*********************************************************************
        call prophrho
        e(cp,frame)=h0(cp,frame)-
     &              p(cp,frame)/
```

```
     &              rho(cp,frame)
        u(cp,frame)=h(cp,frame)-
     &              p(cp,frame)/
     &              rho(cp,frame)
C*********************************************************************
C     "EXTANK" RETURNS THE ELEVATION OF THE FLUID LEVEL FROM THE    *
C     MASS AND QUALITY IN THE EXTERNAL TANK.                        *
C*********************************************************************
        call extank
        e(et,frame)=mdot(et-1,frame-1)*h0(et,frame-1)
     &              *deltat+m(et,frame-1)*e(et,frame-1)
     &              /m(et,frame)
        u(et,frame)=e(et,frame)-
     &              9.81d0*z(et)
        node=et
        call propurho
        h0(et,frame)=e(et,frame)+
     &               p(et,frame)/
     &               rho(et,frame)
        h(et,frame)=u(et,frame)+
     &              p(et,frame)/
     &              rho(et,frame)
       end do
C*********************************************************************
C     RESET THE CLOCK                                               *
C*********************************************************************
      end do
C*********************************************************************
C     THEN                                                          *
C*********************************************************************
      return
C*********************************************************************
C     AND                                                           *
C*********************************************************************
      end
      subroutine h2output
C*********************************************************************
C     "H2OUTPUT" CREATES THE FILE "H2DAT.DAT" ON DEVICE # 21. IT    *
C     THEN PRINTS A TABULAR OUTPUT OF THE TIME AT VARIOUS NODES,    *
C     FOLLOWED BY A REARRANGEMENT OF THE DATA FOR THE NODES AT      *
C     VARIOUS TIMES.                                                *
C*********************************************************************
      integer*2 cp,et,frame,kc(5,0:99),node,pump
      real*8 cpr(0:99,0:99),cvo(0:99,0:99),
     &       d(0:99),deltat,do(0:99),e(0:99,0:99),eps(0:99),
     &       h(0:99,0:99),hc(0:99,0:99),
     &       h0(0:99,0:99),f(0:99,0:99),k(0:99,0:99),
     &       kco(0:99,0:99),kelvin(0:99,0:99),kelwal(0:99,
     &       0:99),l(0:99),m(0:99,0:99),mdot(0:99,0:99),
     &       mu(0:99,0:99),p(0:99,0:99),pf(0:99,0:99),
     &       pet(0:99),pft(0:99),q(0:99,0:99),
     &       qext(0:99,0:99),
     &       qmax(0:99),rey(0:99,0:99),
     &       rho(0:99,0:99),tamb,tfinal,time(0:99),
     &       u(0:99,0:99),v(0:99,0:99),
     &       vet,x(0:99,0:99),z(0:99)
      common
     &       cp,et,frame,kc,node,pump,
     &       cpr,cvo,
     &       d,deltat,do,e,eps,
     &       h,hc,h0,f,k,
     &       kco,kelvin,kelwal,
```

```
     &        l,m,mdot,
     &        mu,p,pf,pet,
     &        pft,q,qext,qmax,
     &        rey,rho,tamb,tfinal,
     &        time,u,
     &        v,vet,x,z
C*********************************************************************
C     CREATE OUTPUT FILE "H2DAT.DAT" AND CONNECT TO DEVICE # 21.    *
C*********************************************************************
      open (file='h2dat.dat', unit=21, status='new')
C*********************************************************************
C     START THE CLOCK.                                              *
C*********************************************************************
      do frame=0,tfinal/deltat
C*********************************************************************
C     PRINT THE HEADING.                                            *
C*********************************************************************
       write(21,100) cp,et,time(frame)
 100   format(1x,'FEED TANK AT NODE =  0',/,
     &        1x,'CONTROL POINT AT NODE = ',i2,/,
     &        1x,'EXTERNAL TANK AT NODE = ',i2,/,
     &        1x,'ELAPSED TIME = ',d13.6,/)
       write(21,101)
 101   format(1x,5x,'NODE',5x,
     &           4x,'QUALITY'3x,
     &           3x,'PRESSURE',3x,
     &           2x,'TEMPERATURE',1x,
     &           2x,'WALL TEMP.',2x,
     &           4x,'DENSITY',3x,
     &           3x,'VELOCITY',3x,
     &           5x,'MASS',5x,
     &           3x,'MASS FLOW',/)
C*********************************************************************
C      SCAN THE NODES.                                              *
C*********************************************************************
       do node=0,et
        write(21,102)node,x(node,frame),p(node,frame),
     &               kelvin(node,frame),kelwal(node,frame),
     &               rho(node,frame),v(node,frame),
     &               m(node,frame),mdot(node,frame)
 102   format(1x,6x,i2,6x,8(1x,d13.6))
C*********************************************************************
C     NEXT NODE                                                     *
C*********************************************************************
       end do
C*********************************************************************
C     RESET THE CLOCK                                               *
C*********************************************************************
      end do
C*********************************************************************
C     TOP OF THE PAGE FOR THE TIME SCAN OF THE NODES.               *
C*********************************************************************
      write(21,103)
 103   format('1')
C*********************************************************************
C     SCAN THE NODES.                                               *
C*********************************************************************
      do node=0,et
C*********************************************************************
C     PRINT A HEADING.                                              *
C*********************************************************************
       write(21,104) cp,et,node
```

```
 104  format(1x,'FEED TANK AT NODE =  0',/,
     &       1x,'CONTROL POINT AT NODE = ',i2,/,
     &       1x,'EXTERNAL TANK AT NODE = ',i2,/,
     &       1x,'NODE #  = ',i2,/)
       write(21,105)
 105  format(1x,5x,'TIME',5x,
     &          4x,'QUALITY'3x,
     &          3x,'PRESSURE',3x,
     &          2x,'TEMPERATURE',1x,
     &          2x,'WALL TEMP.',2x,
     &          4x,'DENSITY',3x,
     &          3x,'VELOCITY',3x,
     &          5x,'MASS',5x,
     &          3x,'MASS FLOW',/)
C*********************************************************************
C      START THE CLOCK                                               *
C*********************************************************************
       do frame=0,tfinal/deltat
C*********************************************************************
C      PRINT THE DATA.                                               *
C*********************************************************************
        write(21,106)time(frame),x(node,frame),p(node,frame),
     &               kelvin(node,frame),kelwal(node,frame),
     &               rho(node,frame),v(node,frame),
     &               m(node,frame),mdot(node,frame)
 106  format(1x,9(1x,d13.6))
C*********************************************************************
C     RESET THE CLOCK.                                               *
C*********************************************************************
       end do
C*********************************************************************
C     NEXT NODE.                                                     *
C*********************************************************************
      end do
C*********************************************************************
C     CLOSE AND DISCONNECT FILE "H2DAT.DAT".                         *
C*********************************************************************
      close(unit=21)
C*********************************************************************
C     THEN                                                           *
C*********************************************************************
      return
C*********************************************************************
C     AND                                                            *
C*********************************************************************
      end
      subroutine h2lsat
      integer*2 cp,et,frame,kc(5,0:99),node,pump
      real*8 cpr(0:99,0:99),cvo(0:99,0:99),
     &       d(0:99),deltat,do(0:99),e(0:99,0:99),eps(0:99),
     &       h(0:99,0:99),hc(0:99,0:99),
     &       h0(0:99,0:99),f(0:99,0:99),k(0:99,0:99),
     &       kco(0:99,0:99),kelvin(0:99,0:99),kelwal(0:99,
     &       0:99),l(0:99),m(0:99,0:99),mdot(0:99,0:99),
     &       mu(0:99,0:99),p(0:99,0:99),pf(0:99,0:99),
     &       pet(0:99),pft(0:99),q(0:99,0:99),
     &       qext(0:99,0:99),
     &       qmax(0:99),rey(0:99,0:99),
     &       rho(0:99,0:99),tamb,tfinal,time(0:99),
     &       u(0:99,0:99),v(0:99,0:99),
     &       vet,x(0:99,0:99),z(0:99)
      common
```

```
&       cp,et,frame,kc,node,pump,
&       cpr,cvo,
&       d,deltat,do,e,eps,
&       h,hc,h0,f,k,
&       kco,kelvin,kelwal,
&       l,m,mdot,
&       mu,p,pf,pet,
&       pft,q,qext,qmax,
&       rey,rho,tamb,tfinal,
&       time,u,
&       v,vet,x,z
 call propptgs
 return
 end
 subroutine prophrho
 integer*2 cp,et,frame,kc(5,0:99),node,pump
 real*8 cpr(0:99,0:99),cvo(0:99,0:99),
&       d(0:99),deltat,do(0:99),e(0:99,0:99),eps(0:99),
&       h(0:99,0:99),hc(0:99,0:99),
&       h0(0:99,0:99),f(0:99,0:99),k(0:99,0:99),
&       kco(0:99,0:99),kelvin(0:99,0:99),kelwal(0:99,
&       0:99),l(0:99),m(0:99,0:99),mdot(0:99,0:99),
&       mu(0:99,0:99),p(0:99,0:99),pf(0:99,0:99),
&       pet(0:99),pft(0:99),q(0:99,0:99),
&       qext(0:99,0:99),
&       qmax(0:99),rey(0:99,0:99),
&       rho(0:99,0:99),tamb,tfinal,time(0:99),
&       u(0:99,0:99),v(0:99,0:99),
&       vet,x(0:99,0:99),z(0:99)
 common
&       cp,et,frame,kc,node,pump,
&       cpr,cvo,
&       d;deltat,do,e,eps,
&       h,hc,h0,f,k,
&       kco,kelvin,kelwal,
&       l,m,mdot,
&       mu,p,pf,pet,
&       pft,q,qext,qmax,
&       rey,rho,tamb,tfinal,
&       time,u,
&       v,vet,x,z
 u(node,frame)=h(node,frame)/1.4d0
 call propurho
 return
 end
 subroutine propptgs
 integer*2 cp,et,frame,kc(5,0:99),node,pump
 real*8 cpr(0:99,0:99),cvo(0:99,0:99),
&       d(0:99),deltat,do(0:99),e(0:99,0:99),eps(0:99),
&       h(0:99,0:99),hc(0:99,0:99),
&       h0(0:99,0:99),f(0:99,0:99),k(0:99,0:99),
&       kco(0:99,0:99),kelvin(0:99,0:99),kelwal(0:99,
&       0:99),l(0:99),m(0:99,0:99),mdot(0:99,0:99),
&       mu(0:99,0:99),p(0:99,0:99),pf(0:99,0:99),
&       pet(0:99),pft(0:99),q(0:99,0:99),
&       qext(0:99,0:99),
&       qmax(0:99),rey(0:99,0:99),
&       rho(0:99,0:99),tamb,tfinal,time(0:99),
&       u(0:99,0:99),v(0:99,0:99),
&       vet,x(0:99,0:99),z(0:99)
 common
&       cp,et,frame,kc,node,pump,
```

```
&       cpr,cvo,
&       d,deltat,do,e,eps,
&       h,hc,h0,f,k,
&       kco,kelvin,kelwal,
&       l,m,mdot,
&       mu,p,pf,pet,
&       pft,q,qext,qmax,
&       rey,rho,tamb,tfinal,
&       time,u,
&       v,vet,x,z
 if((frame .eq. 0) .or.
&   (node .eq. 0) .or.
&   (node .eq. et)) then
  if(node .lt. cp)kelvin(node,frame)=20.39d0
  if(node .ge. cp)kelvin(node,frame)=tamb
 endif
 rho(node,frame)=p(node,frame)/
&                4157.d0/kelvin(node,frame)
 u(node,frame)=2.5d0*4157.d0*kelvin(node,frame)
 call propurho
 return
 end
 subroutine propurho
 integer*2 cp,et,frame,kc(5,0:99),node,pump
 real*8 cpr(0:99,0:99),cvo(0:99,0:99),
&       d(0:99),deltat,do(0:99),e(0:99,0:99),eps(0:99),
&       h(0:99,0:99),hc(0:99,0:99),
&       h0(0:99,0:99),f(0:99,0:99),k(0:99,0:99),
&       kco(0:99,0:99),kelvin(0:99,0:99),kelwal(0:99,
&       0:99),l(0:99),m(0:99,0:99),mdot(0:99,0:99),
&       mu(0:99,0:99),p(0:99,0:99),pf(0:99,0:99),
&       pet(0:99),pft(0:99),q(0:99,0:99),
&       qext(0:99,0:99),
&       qmax(0:99),rey(0:99,0:99),
&       rho(0:99,0:99),tamb,tfinal,time(0:99),
&       u(0:99,0:99),v(0:99,0:99),
&       vet,x(0:99,0:99),z(0:99)
 common
&       cp,et,frame,kc,node,pump,
&       cpr,cvo,
&       d,deltat,do,e,eps,
&       h,hc,h0,f,k,
&       kco,kelvin,kelwal,
&       l,m,mdot,
&       mu,p,pf,pet,
&       pft,q,qext,qmax,
&       rey,rho,tamb,tfinal,
&       time,u,
&       v,vet,x,z
 kelvin(node,frame)=u(node,frame)/2.5d0/4157.d0
 p(node,frame)=rho(node,frame)*4157.d0*
&              kelvin(node,frame)
 h(node,frame)=1.4d0*u(node,frame)
 mu(node,frame)=2.d-6
 k(node,frame)=0.05d0
 return
 end
 block data h2block
 integer*2 cp,et,frame,kc(5,0:99),node,pump
 real*8 cpr(0:99,0:99),cvo(0:99,0:99),
&       d(0:99),deltat,do(0:99),e(0:99,0:99),eps(0:99),
&       h(0:99,0:99),hc(0:99,0:99),
```

```
&       h0(0:99,0:99),f(0:99,0:99),k(0:99,0:99),
&       kco(0:99,0:99),kelvin(0:99,0:99),kelwal(0:99,
&       0:99),l(0:99),m(0:99,0:99),mdot(0:99,0:99),
&       mu(0:99,0:99),p(0:99,0:99),pf(0:99,0:99),
&       pet(0:99),pft(0:99),q(0:99,0:99),
&       qext(0:99,0:99),
&       qmax(0:99),rey(0:99,0:99),
&       rho(0:99,0:99),tamb,tfinal,time(0:99),
&       u(0:99,0:99),v(0:99,0:99),
&       vet,x(0:99,0:99),z(0:99)
 common
&       cp,et,frame,kc,node,pump,
&       cpr,cvo,
&       d,deltat,do,e,eps,
&       h,hc,h0,f,k,
&       kco,kelvin,kelwal,
&       l,m,mdot,
&       mu,p,pf,pet,
&       pft,q,qext,qmax,
&       rey,rho,tamb,tfinal,
&       time,u,
&       v,vet,x,z
 data cp,et/4,35/
 data d/
&       4*0.2d0,32*0.25d0,64*0.d0/
 data do/
&       4*0.22d0,32*0.27d0,64*0.d0/
 data eps/
&        100*0.0d0/
 data l/
&      100*10.d0/
 data qmax/
&        '100*1500.d0/
 data z/
&      10.d0,34*0.d0,30.d0,64*0.d0/
 end


 subroutine trans
 integer*2 cp,et,frame,kc(5,0:99),node,pump
 real*8 cpr(0:99,0:99),cvo(0:99,0:99),
&       d(0:99),deltat,do(0:99),e(0:99,0:99),eps(0:99),
&       h(0:99,0:99),hc(0:99,0:99),
&       h0(0:99,0:99),f(0:99,0:99),k(0:99,0:99),
&       kco(0:99,0:99),kelvin(0:99,0:99),kelwal(0:99,
&       0:99),l(0:99),m(0:99,0:99),mdot(0:99,0:99),
&       mu(0:99,0:99),p(0:99,0:99),pf(0:99,0:99),
&       pet(0:99),pft(0:99),q(0:99,0:99),
&       qext(0:99,0:99),
&       qmax(0:99),rey(0:99,0:99),
&       rho(0:99,0:99),tamb,tfinal,time(0:99),
&       u(0:99,0:99),v(0:99,0:99),
&       vet,x(0:99,0:99),z(0:99)
 common
&       cp,et,frame,kc,node,pump,
&       cpr,cvo,
&       d,deltat,do,e,eps,
&       h,hc,h0,f,k,
&       kco,kelvin,kelwal,
&       l,m,mdot,
&       mu,p,pf,pet,
&       pft,q,qext,qmax,
```

```
&       rey,rho,tamb,tfinal,
&       time,u,
&       v,vet,x,z
 f(node,frame)=0.002d0
 hc(node,0)=0.d0
 hc(node,frame)=1360.d0
 if(node .lt. cp)kelwal(node,0)=20.39d0
 if(node .ge. cp)kelwal(node,0)=tamb
 qext(node,frame)=qmax(node)
&                 *(tamb-kelwal(node,frame-1))
&                 /(tamb-20.39d0)
 kelwal(node,frame)=kelwal(node,frame-1)
&                  +qext(node,frame-1)
&                  /419/7800/datan(1.d0)
&                  /(do(node)**2
&                  -d(node)**2)/l(node)
&                  *deltat-hc(node,frame-1)
&                  *4.d0*datan(1.d0)*d(node)*l(node)
&                  *(kelwal(node,frame-1)
&                  -kelvin(node,frame-1))
&                  *deltat
&                  /419.d0/7800.d0/datan(1.d0)
&                  /(do(node)**2
&                  -d(node)**2)/l(node)
 return
 end
 subroutine prophp
 integer*2 cp,et,frame,kc(5,0:99),node,pump
 real*8 cpr(0:99,0:99),cvo(0:99,0:99),
&       d(0:99),deltat,do(0:99),e(0:99,0:99),eps(0:99),
&       h(0:99,0:99),hc(0:99,0:99),
&       h0(0:99,0:99),f(0:99,0:99),k(0:99,0:99),
&       kco(0:99,0:99),kelvin(0:99,0:99),kelwal(0:99,
&       0:99),l(0:99),m(0:99,0:99),mdot(0:99,0:99),
&       mu(0:99,0:99),p(0:99,0:99),pf(0:99,0:99),
&       pet(0:99),pft(0:99),q(0:99,0:99),
&       qext(0:99,0:99),
&       qmax(0:99),rey(0:99,0:99),
&       rho(0:99,0:99),tamb,tfinal,time(0:99),
&       u(0:99,0:99),v(0:99,0:99),
&       vet,x(0:99,0:99),z(0:99)
 common
&       cp,et,frame,kc,node,pump,
&       cpr,cvo,
&       d,deltat,do,e,eps,
&       h,hc,h0,f,k,
&       kco,kelvin,kelwal,
&       l,m,mdot,
&       mu,p,pf,pet,
&       pft,q,qext,qmax,
&       rey,rho,tamb,tfinal,
&       time,u,
&       v,vet,x,z
 u(node,frame)=h(node,frame)/1.4d0
 rho(node,frame)=p(node,frame)/(h(node,frame)
&                -u(node,frame))
 call propurho
 return
 end
 subroutine feedtank
 integer*2 cp,et,frame,kc(5,0:99),node,pump
 real*8 cpr(0:99,0:99),cvo(0:99,0:99),
```

```
&       d(0:99),deltat,do(0:99),e(0:99,0:99),eps(0:99),
&       h(0:99,0:99),hc(0:99,0:99),
&       h0(0:99,0:99),f(0:99,0:99),k(0:99,0:99),
&       kco(0:99,0:99),kelvin(0:99,0:99),kelwal(0:99,
&       0:99),l(0:99),m(0:99,0:99),mdot(0:99,0:99),
&       mu(0:99,0:99),p(0:99,0:99),pf(0:99,0:99),
&       pet(0:99),pft(0:99),q(0:99,0:99),
&       qext(0:99,0:99),
&       qmax(0:99),rey(0:99,0:99),
&       rho(0:99,0:99),tamb,tfinal,time(0:99),
&       u(0:99,0:99),v(0:99,0:99),
&       vet,x(0:99,0:99),z(0:99)
 common
&       cp,et,frame,kc,node,pump,
&       cpr,cvo,
&       d,deltat,do,e,eps,
&       h,hc,h0,f,k,
&       kco,kelvin,kelwal,
&       l,m,mdot,
&       mu,p,pf,pet,
&       pft,q,qext,qmax,
&       rey,rho,tamb,tfinal,
&       time,u,
&       v,vet,x,z
        z(0)=z(0)
        return
        end
 subroutine extank
 integer*2 cp,et,frame,kc(5,0:99),node,pump
 real*8 cpr(0:99,0:99),cvo(0:99,0:99),
&       d(0:99),deltat,do(0:99),e(0:99,0:99),eps(0:99),
&       h(0:99,0:99),hc(0:99,0:99),
&       h0(0:99,0:99),f(0:99,0:99),k(0:99,0:99),
&       kco(0:99,0:99),kelvin(0:99,0:99),kelwal(0:99,
&       0:99),l(0:99),m(0:99,0:99),mdot(0:99,0:99),
&       mu(0:99,0:99),p(0:99,0:99),pf(0:99,0:99),
&       pet(0:99),pft(0:99),q(0:99,0:99),
&       qext(0:99,0:99),
&       qmax(0:99),rey(0:99,0:99),
&       rho(0:99,0:99),tamb,tfinal,time(0:99),
&       u(0:99,0:99),v(0:99,0:99),
&       vet,x(0:99,0:99),z(0:99)
 common
&       cp,et,frame,kc,node,pump,
&       cpr,cvo,
&       d,deltat,do,e,eps,
&       h,hc,h0,f,k,
&       kco,kelvin,kelwal,
&       l,m,mdot,
&       mu,p,pf,pet,
&       pft,q,qext,qmax,
&       rey,rho,tamb,tfinal,
&       time,u,
&       v,vet,x,z
        z(et)=z(et)
        return
        end
```

REFERENCES

1.Lin, T.Y.

Technical summary and user's guide for the transient cryogenic transfer program.

KSC-DD-988 (1984)

2.Coulter Jr., B.M.

Superflow.

Fluid Research Publishing, Melbourne,FL (1987)

3.Cosmic software catalogue

NASA-CR-187366 (1991)

4.Perry, R.H.

Perry's chemical engineer's handbook

6th edition

McGraw-Hill (1984)

5.Scott, R.B.

Cryogenic engineering

1963 edition

Met-Chem Research Inc., Boulder,CO (1988)

6.McCarty, R.D.
Selected properties of hydrogen
U.S. G.P.O. (1981)

7.Bejan, A.
Advanced engineering thermodynamics
Wiley (1988)

8.Bejan, A.
Convective heat transfer
Wiley (1984)

1991 NASA/ASEE SUMMER FACULTY FELLOWSHIP PROGRAM

JOHN F. KENNEDY SPACE CENTER
UNIVERSITY OF CENTRAL FLORIDA

DEVELOPMENT OF A COMMON USER INTERFACE FOR THE LAUNCH DECISION SUPPORT SYSTEM

PREPARED BY:	Dr. Jean C. Scholtz
ACADEMIC RANK:	Assistant Professor
UNIVERSITY AND DEPARTMENT:	Portland State University Computer Science Department
NASA/KSC	
DIVISION:	Data Systems
BRANCH:	Technical and Information Systems
NASA COLLEAGUE:	Arthur E. Beller
DATE:	August 23, 1991
CONTRACT NUMBER:	University of Central Florida NASA-NGT-60002 Supplement: 6

ACKNOWWLEDGEMENTS

I would like to thank Dr. Raymond Hosler of the University of Central Florida, Dr. Mark Beymer and Mr. Dennis Armstrong of the Kennedy Space Center for their efforts in making the NASA/ASEE Summer Faculty Fellowship Program an enjoyable and educational summer. Many thanks to Ms. Kari Stiles for answering so many questions prior to starting the summer program and for her efforts in making the program run so smoothly.

Special thanks to Art Beller,Greg Hadaller, Mark Ricci,and Mike Richardson for all their help with hardware and software issues. Their input throughout the summer was most valuable. Their efforts at making me feel welcome in the group were very much appreciated.

Thanks to Frank Merlino and members of the NTD staff for their assistance. Their input on suggested revisions was extremely helpful.

ABSTRACT

The Launch Decision Support System (LDSS) is software to be used by the NASA Test Director (NTD) in the firing room during countdown. This software is designed to assist the NTD with time management, that is, when to resume from a hold condition. This software will assist the NTD is making and evaluating alternate plans and will keep him advised of the existing situation. As such, the interface to this software must be designed to provide the maximum amount of information in the clearest fashion and in a timely manner. This research involves applying user interface guidelines to a mature prototype of LDSS and developing displays that will enable the users to easily and efficiently obtain information from the LDSS displays. This research also extends previous work on organizing and prioritizing human-computer interaction knowledge.

SUMMARY

The Launch Decision Support System (LDSS) is being developed as an aid to the NASA Test Director (NTD) during countdown activities. This report presents suggested revisions of many LDSS displays. The revisions were developed by applying human-computer interaction guidelines to the original interface. Data collected from potential users was also considered in developing the revisions. This data was collected via a think aloud protocol, numerous interviews, and a questionnaire. This data verified that users found the color coding of the revisions sufficient, that they could correctly interpret information coded into one window rather than three, and that reducing the time labels was acceptable. The emphasis in developing the revisions was on presenting the information so that it could be interpreted quickly, easily and unambiguously by casual users in a critical, real-time environment.

The task of applying Human-Computer Interaction knowledge is difficult because research done in this area is often difficult to translate into practical guidelines. A means of organizing human-computer interaction knowledge into a generic framework is discussed. However this method alone is not sufficient to be able to use HCI knowledge. Other problems still exist. For example, during the revision process many trade-offs were made when deciding which guidelines to apply. A method was used to prioritize guidelines by examining different characteristics of tasks and users. For various characteristics the criteria of primary importance are proposed. Using task and user characteristics of LDSS and applying this prioritizing method resulted in the following primary criteria: consistency, guidance, workload, and significance of code.

TABLE OF CONTENTS

LIST OF ILLUSTRATIONS

LIST OF ABBREVIATIONS AND ACRONYMS

ANTD	Assistant NASA Test Director
APU	Auxiliary Power Unit
CDT	Count Down Time
COBT	Crew on Back Time
COLA	Collision Avoidance
GLS	Ground Launch Sequencer
HCI	Human-Computer Interaction
LCC	Launch Commit Criteria
LDBT	LOX (Liquid Oxygen) Drain Back Time
LDSS	Launch Decision Support System
LOX	Liquid Oxygen
LOX DB	Liquid Oxygen Drain Back
LW	Launch Window
NTD	NASA Test Director
OIS	Operations Information System
OMI	Operations and Maintenance Instructions
TMID	Time Management Integrated Display
UT	Universal Time

I. INTRODUCTION

1.1 Organization of the Paper

This paper documents the application of Human-Computer Interaction knowledge to the interface for the LDSS software for use in the KSC firing room. The first section discusses the role of the NASA Test Director (NTD) who is seen as the principle user of LDSS. The functionality of LDSS is explained in this section. Section II presents redesigned displays and discusses the rationale behind the redesign. Also included in Section II are the results of data collection on usage of the displays. A discussion of complexity measures in original and revised displays is also presented. Section III discusses how human factors knowledge can be organized and applied to interface designs. A method of addressing the trade offs involved in interface design is presented. Section IV presents Interface Guidelines for future firing room software. Additional suggestions are included for a proposed windows version of such software. Section V contains concluding remarks.

1.2. The Role of the NTD

The NASA Test Director functions as the coordinator of information during a launch countdown. He receives information from several diverse sources: firing room clocks located on the wall in front of him and to his left, procedural information in hard copy from the OMI (Operations and Maintenance Instructions) and status information received over the OIS (Operations Information System). The current firing room clocks are universal time (UT), local time(local), countdown time (shuttle), window remaining, post LOX drain back elapsed, APU hold time remaining, time to T-0, and hold time remaining. Specific information about each launch, such as projected time of lift-off, launch window end,etc., is contained in a launch document for that particular mission. He also has access to closed circuit television which is directed at operations occurring around the launch pad. One of the many responsibilities of the NTD is that of time management. That is, given that a hold has occurred in the countdown, The NTD must decide upon the time to resume the count so that lift off will not occur within a COLA or with little contingency time. In making decisions concerning time management, the NTD has to carry out some arithmetic operations and base his decision on those calculations plus his knowledge of specific launch information. In addition, he uses knowledge of approaches used in previous launches.

The LDSS consists of several parts: the time management integrated display, the what-if capability, the

situation assessment capability, and anomoly management. The time management subsystem presents an integrated display. That is, all firing room clocks are duplicated on this display. Additionally, some clocks that perform arithmetic are displayed. The launch window is shown along with any COLAS (collision avoidance). These represent periods in the launch window such that a lift-off during this period could results in a collision with another orbiting vehicle. Contingency times are shown in the launch window as these also affect resumption from a hold. The time management display (shown in figure 1) calculates the advisability of resumming from a hold and displays this information in its resume window. A now bar displays the current position in the countdown and a projected T-0 bar is consistently updated to reflect where lift off will occur. The LOX DB is the contingency time currently deemed to be the most constraining.

1.3 The Need for Human-Computer Interaction Knowledge

LDSS is designed to assist an NTD during countdown activities. Activities such as these are performed on the order of every two weeks. This includes simulations and actual launch activities. The NTDs alternate with one NTD and one ANTD assigned to every launch team. Therefore, these are casual users. The activity they perform, launching a manned shuttle, is a critical operation. The countdown activity is a cognitively demanding activity that must be carried out in a real-time situation. This means that any tools designed to assist the NTD and ANTD need to present the needed information in such a fashion that it can be easily comprehended and used. This project reports on a suggested redesign of the user interface for the LDSS. Accomplishing this redesign led to many tradeoff decisions. This study also proposes a method for prioritizing guidelines in order to make consistent decisions about trade-offs.

II. LDSS Revised Displays and Data Collection Results

2.1 TMID Revised Display

Figure 1 shows the original TMID screen and Figures 2,3 and 4 show the revised display. The largest change was using one "window" on the display for information concerning the launch window. The original display contained a launch window which showed COLAS, a resume window which showed the advisability of resuming from a hold, and a LOX drain back window which showed the LOX contingency time remaining. In addition, the display contained a "now bar" and a projected T-0 bar, to show where the countdown currently was and where this meant that T-0 would occur. Interviews with members of the NTD staff indicated that there was confusion with using three different windows, especially the launch window and the resume window. Therefore, the display was reworked using only one window - the launch window - and incorporating the information about COLAS, contingency time and advisability of resumming in this window and elsewhere on the display. The revised display uses the stop light coloring coding on the launch window. Green indicates that the window is open at this point. Yelllow indicates contingency times and is seen prior to COLAS (indicated in red) and prior to the end of the launch window. The end of the launch window is labeled as such and nothing is displayed after this point. The "now bar" is coded to indicate the advisability of resumming at this point in time. Green indicates that resumption is safe (or that the countdown is not currently in a hold). Yellow indicates that a resumption at this time would not have the full contingency time. Red indicates that resumming from a hold at this time would place T-0 in a COLA. There are two methods of finding out how long the period for resumming exists. One is by looking at the launch window to see the amount of green, yellow or red (also labeled) displayed below the projected T-0 bar. At the beginning of the T-20 hold this information would have to be obtained by scrolling the launch window. Additionally, this information is contained in a new clock "Time to No Start". This will provide exact times that indicate how long the current condition exists.

The time labels were also changed. The original display labeled all times, universal time and countdown time. The revised display only labels significant times. That is, only the minutes in which a GLS event or a COLA or a contingency time appears will be labeled with the univeral and countdown time. Countdown times are only labeled for times prior to T-0. Positive countdown times make little sense for COLAS and contingency labels. The "now bar" always reflects the current time correct to the second.

Using a reduced amount of time labels will make those that are significant stand out and reduce the overall complexity of the display. More will be said about this in Section III.

The original TMID screen contained a scroll bar on the left side of the display which was used to indicate which portion of the display was being viewed. The revised TMID screen had more room so that the scroll bar could be moved to the right hand side of the display in keeping with an OSF/Motif presentation. The scroll bar was designed so that it resembles that of OSF/Motif. Recommended movement with the display window should be via the scroll bar or by using the up arrows and page keys. Either motion results in the slider of the scroll bar being changed to relfect what portion of the display one is viewing. In a direct manipulation version, the user should also be able to position the slider to cause movement.

Color coding on the revised TMID screen is consistent. Graphic information is color coded using the green (safe), yellow (cautionary), and red (warning) traffic light metaphor. However, the graphic data has also been labeled so that color coding is redundant and therefore, can be used by a visually impaired person. Text information uses cyan for labels and place holder values. White indicates information that needs to be input. Values in green are relevant; that is, data that has occurred. Yellow labels and values depict information concerning a hold. Red values are values that indicate a warning situation exists. One color change that was made to the original TMID screen is that recommendation of using cyan as the color for data that is not yet relevant. Previously non-relevant data had been displayed in white. White should be reserved for very important data. Data that is not yet relevant is not invalid, but merely serves as a placeholder. Therefore, using the same color as labels (cyan) is recommended for such data. In general, no more than four colors should be used for alphanumeric information. The revised TMID screen (and other screens in LDSS) use cyan, green, yellow and red. As red is used very sparingly and only in the case of warning situations, the use of the three colors to display text, plus the background color of black, closely adheres to this guideline.

The clocks in the original TMID screen were rearranged and "chunked" together according to function. For example, **time in hold** and **hold time remaining** were located together. This reduces the complexity for the user by presenting a few chunks of information rather than a large number of information pieces. In addition, the clocks were arranged in order from top to bottom with those on the top being the highest priority. This arrangement was based on interviews with the NTD staff. This rearrangement allowed enough room on the display to include the maximum hold time remaining and the latest resume time. For time values that are not currently in use the recommendation is

to use a default value of HHMM/SS or DDD:HHMM/SS as a prompt to the user of the format of the clocks. This is due to the lack of room for labels on the clock values. A graphic depiction of where the projected T-0 falls in the launch window was also incorporated into the clock display. This was purposely designed NOT to look like a scroll bar as it CANNOT be manipulated and is used to quickly show the NTD how close to the end of the launch window, the projected T-0 is.

2.2 Finer grain TMID Screen

Feedback from the users indicated that as T-0 neared, the minute resolution on the TMID screen was too coarse to follow. A finer grain of time, namely a 10 second resolution, is recommended. Figure 5 presents this new display. The same format as the TMID screen is used. The time bars in the launch window now become 10 second bars so that one rectangular box per line is used. Time labels are indicated on whole minute entries. This display should be included in the menu and the user could select to view this display when a certain point in the countdown is reached.

2.3 Overview Display

Another new display that was developed during this period of time is the overview display. The concept is that this display would present the entire launch window picture to the NTD. The display, shown in Figure 6, could be derived from the mission parameters that are input prior to bringing up LDSS. The entire window is displayed with COLAs, COBT, and built-in holds at T-20 and T-09. This display could be used in a static fashion. That is, hard copies of it could be printed and used by the NTD to get an overall picture of the launch window. Figure 7 shows that the same display might also be used in a dynamic fashion with the addition of a now bar and a projected T-0 bar.

2.4 Test Parameters Display

Figures 8 and 9 present the original and revised Test Parameters display. The original display listed the built-in holds by time. Normally, searching would be done according to the time of the hold. Therefore, these columns were rearranged to facilitate that search. As LDSS currently is designed to function from T-20, only those built-in holds at T-20 and T-9 need to be displayed. The original display contained only the start and end time of the launch window (unlabeled). The revised display contains the start, end and length of the launch window, COLAS, and COBT. In addition, the point of no recycle is now included on this display rather than on the TMID screen.

This same display could be used for input about each specific mission. The input display looks very much

like the mission parameters display but contains information on how to input new values. The data fields are displayed in white, indicating that these fields are to be filled in by the user. The fields indicate the number of positions that are to be filled in and the format of that data. For example, a length field in countdown time format would look like HHMM/SS. A universal time format would be coded as DDD:HHMM/SS. In entering data, the user should not have to enter the fixed delimiters, e.g., : and /. These delimiters are shown in cyan to indicate that they do not have to be typed in. Movement through the display should automatically position the user at the next number to be filled in, skipping over any fixed field delimiters.

An alternative suggestion is to retain values from a previous mission in these positions. This is feasible if many values do not change from launch to launch. Such items as LOX drain back and APU hold times and build-in hold times do not vary between launches. Therefore, some time could be saved when entering these parameters. With this method of entering data, the user should be able to retype only those positions within a field that need to be changed. For example, changing 0004/00 to 0007/00 should necessitate positioning the cursor on the 4 and retyping a 7. Deciding on the method to use depends on the ability to support the correct interaction method and on the amount of data entry that the user could be spared. This method should be used only if the above interaction can be implemented and if the users feel comfortable using cursor positioning and retyping data. If this is not the case, then the first method should be used.

2.5 What If Display

The What If display allows the user to do some calculation on various times that are adjustable. The end result is to determine the maximum hold time remaining and the latest possible resume time. These calculations are based on COLA and contingency information in the launch window and the current countdown time and universal time. A possibility that exists within these calculations is resuming the count and holding for a certain amount of time later in the countdown. Figure 10 is the current version of the display. As the what if portion of the program is now implemented, three displays are used. Each display presents a different default plan. One display reflects the situation where no intermediate hold is used. The second display uses this intermediate hold situation. The thought behind revising these displays was to create one generic template that would encompass both scenarios as well as other scenarios. Two possible revisions were developed. The first is a textual display and the other a graphic version.

Figure 11 presents the textual display. The times in the original display were presented in three columns,

universal time, countdown time, and interval time. The thought in revising the display was that the universal time and time intervals were most frequently used. Therefore, the countdown column was eliminated and the times were put into a middle column. The labels were put into two columns, one for events and the second for intervals. An up/down arrow beside of selected items indicates that the user may change the value of that item. The display allows for the user to choose the countdown time of the intermediate hold. The thought here is that by clicking on the selection arrows the times displayed would be the prescribed hold times, e.g., T-4M, T-2/55M, T-31S. The display includes start/end times for COLAS, but this information does not necessarily have to be included. As with the original display the events are ordered by time.

The graphical version (Figure 12) lends itself to full direct manipulation but could function in the same manner as the textual display thus allowing implementation to proceed in stages. In a full direct manipulation mode the user could position events by dragging them to a position on the time line. The time value would be shown as the item is being moved. This allows a finer grain of control than the user has by dragging. The user could also click on the up/down arrows and the item would be positioned on the time line relative to the value selected for it. Repositioning would only take place after the user has pressed "enter" to indicate he has selected the desired value. A first implementation involving selection of values in this manner is advocated before implementing the direct manipulation interface. The benefit of this type of interface is that it allows the user to easily accomplish such tasks as "position T-0 close to the end of the window". Figure 13 shows how the user could be notified of constraints.

In addition, a suggestion is to allow the user to setup several default plans, such as going to T-5M and holding for 5 minutes, prior to countdown and then selecting those plans by selecting the label. Input of these plans could be done via an input display that resembles the what if display. Figure 14 presents a prototype of an input display for default plans. These plans would be setup after the mission parameters have been input so that values for contingency time and launch window end would be obtained from there. These values could then be changed in the default plan. For example, the NTD could construct a default plan that would necessitate asking for an extra five minutes on the end of the launch window. These plans could then be filed and later retrieved and applied to the current situation.

Both the graphic and textual displays could be made available to the user and he could choose to display whichever is more appropriate to his style of decision making.

2.6 The Situation Assessment Display

The situation assessment display contains information about the hold, the end of launch window, projected T-0 and other information and makes a recommendation to resume or not based upon this information. This recommendation also includes the rationale for the decision. This module is still being developed and hence the information that will be displayed is not yet fully specified. Recommendations for a display are shown in Figures 15 and 16. A template of information should be developed and those labels should always be displayed. Information that is not relevant to the present situation should not be filled in. Furthermore, information should be color coded so as to convey to the user the values in the template that are contributing to the seriousness of the situation. For example, if the projected T-0 is within a cola, that text would be displayed in red. The assessment information would display information about resumming in red. This would allow the user to quickly assess that it is unadvisable to pick up by using the red indicators in the resume field. If he wishes to read the text to obtain more information, he may do so. But he would be able to obtain initial information via position and color. Further work is being done on this module. Using this initial display will help in defining a set of variables that should be examined in any given situation.

2.7 Data Collection

The revisions that were made to the displays are based upon guidelines and theories (Dumas, 1988; Galitz, 1989; Gilmore, Gertman, and Blackman, 1989; Helander, 1988; NASA, 1980; Smith and Mosier, 1986; Tullis, 1981) and upon data collected from the users. User data collection was difficult due to the workload on the NTD staff. Several launches were carried out during this research period and the NTDs were engaged in those as well as the simulation runs prior to each launch. However, the following procedure was carried out. The current system was used by an NTD during a simulation, his verbalizations were recorded on audio tape and notes were made about situations. The following items were noted during this process. Included is the resolution of each item.

1. Qualitative information on window remaining should be easily accessable.

Resolution: a graphical representation of projected T-0 within the window was incorporated into the clock section.

2. COLA information is used for picking up at T-9M.

Resolution: this information is shown in launch window but consideration should be given to including the exact times on the labels.

3. The point of no recycle should be included on the test parameter screen but does not need to be included with clock information.

Resolution: this has been incorporated in the revised TMID and test paramater display.

4. The major benefit of the what if display was envisioned to be taking the launch window end and working backwards from this. The time between launch window end and projected T-0 was seen to be dependent upon contingency time but not entirely.

Resolution: The textual version of the revised what if display breaks this time interval into two parts: contingency time plus an additional time. Both should be capable of being changed to give a resulting interval.

5. The clocks that are used differ in importance depending on the countdown time of the hold. At T-20M, the hold time remaining is most important. At T-9M the window remaining is important. At T-5M and under the hold time remaining (which increments at this point) is important.

Resolution: consideration should be given to incorporating code to highlight the appropriate clocks at these times in order to direct the user's attention.

6. When scrolling through the launch window it was easy for the user to loose his orientation.

Resolution: moving the scroll bar to the right hand side of the display and making it more visible is important. The user can use this information to judge which portion of the display he is viewing. This has been incorporated into the revised TMID screen.

7. A method of intially putting in parameters for each launch and for changing them during countdown should be provided.

Resolution: A display has been prototyped for this purpose. This feature is currently on the list of items to incorporate into LDSS.

The second method of data collection involved an initial series of displays, namely the TMID screen, which were revised based upon informal comments and guidelines. Several situations were setup in order to obtain information about interpretations of specific decision making processes. These were shown to an NTD and discussed. Based upon this information, further revisions were made and again shown to the same NTD. This set of displays was distributed to other members of the NTD staff along with a questionnaire. This data yielded the following information:

1. The clocks provided are sufficient.
2. The LOX drain back clock in the firing room has been changed. This change will soon be incorporated into LDSS.

3. Make sure that users understand which values in the clock section are static (Launch Window End) and which are computed. This needs further discussion with more members of the NTD staff. A color code could possibly be used here or the positioning could be changed.

4. Reduced time marks are suficient.

5. A finer grain of time (second resolution) was suggested. This is provided in two ways. First, when the LDSS runs the time shown is dynamic and updated on a second by second basis. Secondly, a new display has been developed which the user could switch to close to lift off which provides a ten second resolution.

6. The color coding of the graphic display was deemed useful and clear.

7. Color coding for the data values and time was questioned. The explanation of the color coding should be separated when presented to the user. For graphics, green represents safe, yellow cautionary and red represents a warning. For data values, cyan represents not yet relevant, green represents a valid, relevant data item, yellow represents a hold condition. Therefore, all clock values should appear either as cyan or green. The only exception is time to T-0 which should appear in yellow when there is a hold in the countdown. On the timeline of the TMID screen, the countdown times will be displayed in yellow when there is a hold. UT, CDT and event labels that have happened should change from cyan to green.

8. GLS milestones should be labeled to refect times accurate to seconds. This has been incorporated on the revised TMID screen.

9. Displaying latest resume time on TMID screen is useful. This was used in the decision making process. Therefore having this time available on the TMID screen will reduce movement between displays.

10. A suggestion was made that it would be useful to have more information on time crital actions such as *start recorders, APU Fuel ISO's,* etc. This information will be displayed on a planned configuration management display.

2.8 Complexity Issues

In predicting a user's ability to easily obtain information from a display several items must be taken into account (Tullis, 1981). The number of items in a group and the average size of the group is one determining factor in lowering search times. Results by Tullis suggest that the optimum range for alphanumeric displays is 40 groups averaging 4.9 degrees in size. Local density, how tightly packed a screen is, and layout complexity (the alignment) of the display also affects performance. Also important, these two issues affect subjective ratings by users. These issues were examined in the displays that are suggested for revision. The grouping of items and the size of the groups was considered somewhat in the revisions. This was mostly

in the clock information. Rather than keeping each clock as a separate entity, information was grouped according to functionality. The size of the groups was determined by the information presented and therefore, other rearrangements were limited.

Complexity was analyzed for an original TMID and a revised TMID screen. As the information presented on these displays changes, various complexity measures will be obtained. For this analysis, two displays were chosen that represent one of the more complex displays. Using a easier calculation than the original Tullis calculation from information theory (Galitz, 1989) the following are summed: the number of data fields, the number of horizontal alignments (columns) and the number of vertical alignments (rows). For the original TMID screen shown in Figure 17 this produces a complexity score of 177. For the revised TMID screen, the complexity score is 153. This revision is a 13.6% reduction from the original.

Density of a display is the proportion of characters displayed on the screen as opposed to the amount of blank screen. For density calculations, the screen was considered without its border. Dimensions were 70 by 28 resulting in 1960 positions. For the original TMID screen, the density was calculated to be 52 percent. The density calculation for the revised screen was 40 percent. Although, this revision is still higher than the overall recommended level of 25 to 30 percent the fact that a portion of it is graphical should still result in a usable display. Further reduction is impossible as a principle adhered to in redesign was to reduce the amount of movement between displays. Therefore, this trade-off of higher density versus time to switch displays was made.

III. Trade-offs in Organizing Human-Computer Interaction Knowledge

3.1. Introduction

Currently, a large body of human-computer interaction knowledge exists. Most of this exists in the form of recommendations and guidelines. One of the difficulties in interface design is transferring this information to interface designers in such a manner that it can be incorporated into the design. Scapin (1991) examined the problems encountered when trying to implement human-computer interaction knowledge into the design. Scapin developed a framework for organizing this knowledge. This section discusses this framework, the problems that arise in using this framework, and a method for resolving one of the problems, namely, that of weighing trade-offs.

3.2 Organization of HCI Data

Scapin collected HCI data with the intent of organizing it into a database accessible by attributes. Attributes that were used for characterizing HCI recommendations were: criterion or criteria describing the rationale, the level (conceptual, semantic, syntactic, lexical) that describes the outcome and rationale, and the type of interface object to which the recommendation applies. Several conclusions were drawn by Scapin during this process. He found that a recommendation in the literature could lead to more than one recommendation in terms of implementation. Many recommentations were too vague and needed elaboration in order to be useful in implmentation. Additionally, different authors used different wording for the same recommendations necessitating translation to a stable vocabulary.

Scapin proposed a generic deciphering framework of the form:

if (a premise)...(using **Criteria**)... **then** (a **Conclusion**)

Premises are defined to be of four types:

- type/characteristics of user
- type of user task
- design activity of the interface for which the knowledge is being used.
- context or the particular state of the user interface.

The criteria used are:

Compatability with past habits and skills of the user, between input and output, between noncomputerized support and software, and with interface standards.

Consistency in location, format, syntax and naming conventions.

User Workload with respect to minimizing mental and physical effort required.

Adaptability or the capability of the interface to adapt to various user actions.

User Explicit Control allows the user to control the dialogue and to explicitly enter information.

Significance of codes or use of labels, codes, and abbreviations that are meaningful to the user.

Guidance so that the user can identify what he can do next. This includes feedback and clarity in display.

Error Managment is the attempt to prevent or avoid errors and to give meaningful feedback when errors do occur.

Conclusions can be of two types: design activity which represents a conclusion or specific activity or an action item which is the type of activity required to apply a rule.

Scapin notes intrinsic and usage problems involved in applying human factors knowledge. Intrinsic problems consist of recommendations that are incomplete, recommendations that are too general to be useful and recommendations that lack robustness (apply only in limited contexts). Usage problems are accessing recommendations, making trade-offs in deciding which recommendations to apply, and the varying degree of detail of the recommendations.

3.3 A Method for Prioritizing Trade-offs

Recommendations do not come organized in a hierarchy. Therefore, the designer will often be faced with several approaches, each giving priority to different recommendations and resulting in different solutions. In order to balance trade-off decisions, several issues arise. The first is what factors should be used to determine weights for guidelines. The second issue is how to ensure that these trade-off decisions are made consistently. The method presented here builds on Scapin's work. As discussed in section 3.2, Scapin presented eight criteria and suggested the types of guidelines that pertain to each. In order to prioritize decision making, these criteria are used and weighted according to some known user and task information. During the evaluation of LDSS, the following information was used to prioritize guidelines: type of user, attention time, timing of task, critical aspect of task, and critical aspect of software. Each of these categories can have several different values which would dictate prioritizing different criteria and hence, guidelines. The following discussion is a suggested set of values and emphasized criteria.

Type of user refers to the novice, casual, expert classification. For a novice user the primary criteria

would be guidance. Error management, compatability with past habits, significance in codes, consistency workload and explicit control would be secondary criteria. A casual user would dictate the same criteria but consistency and workload would become primary criteria along with guidance, error management, and compatability. Expert users would be more concerned with adaptability than any of the other criteria.

The attention time of the user is also an important factor in determining trade-offs. What else competes for the user's attention while dealing with the software? Suggested values range from undivided attention to moderate attention to little attention. In the case of little attention, where the user is attending to many other tasks and using the software primarily for support, issues of consistency, guidance, workload and significance of code become the primary criteria. Compatability becomes a secondary concern. In the case of moderate attention the same criteria are important but could be considered secondary concerns rather than primary concerns. If the user has undivided attention to devote to the software then adaptability could be classified as a primary concern. The user has time to discover various aspects of the system and is able to choose a method of performing a task that is more suited to his individual style.

Task considerations should include whether the task is a real-time or nonreal-time task. That is, is the software supporting a shuttle launch or is the software an income tax spreadsheet? This consideration is similar to the attention of the user consideration in that the primary criteria for real-time tasks should be the same as for limited attention: workload, guidance and consistency. Nonreal-time tasks place adaptability as a primary concern. The critical issue of the task involves the importance of the software to the task. That is, can the task be completed without use of the software? Critical software would dictate that error management be a prime concern with guidance as a secondary concern. A second concern is the nature of the task. Software that aids in landing aircraft would be deemed more critical than software for producing slides. Criteria important for this type of critical software would be: significance of codes, guidance, and consistency. The emphasis is placed on the ability to correctly interpret information presented.

The method for prioritizing criteria and hence, guidelines, involves collecting this information concerning users and tasks. Then individual criterion is given two points for each time it appears as a primary concern and one point each time it appears as a secondary concern. The criteria with the highest scores should then be used as the deciding factor in trade-off decisions. Guidelines that support those high scoring criteria should be utilized over guidelines supporting criteria receiving lower scores.

The method used here needs further refinement to ensure that it correctly addresses all values for suggested

categories. Nonetheless, this method was used quite successfully in making consistent trade-off decisions during revision of the LDSS interface. In this case, the users were casual, the attention of the users limited, the task was real-time, and critical but the software is not critical for success of the task. Using this scheme an interface was produced in which priority was given to guidelines which enhance the users' ability to discern information from the screen and to minimize the amount of interaction required by the user. Consistency and guidance were the highest ranking criteria followed by work load and significance of codes. Little effort was put into making the system flexible. As the amount of interaction was limited, little effort was put into error management. In order to further refine this method and to determine its robustness, it will be necessary to evaluate more interfaces which have different tasks and users. A successful method would be capable of producing usable interfaces for a wide range of user and task characteristics.

IV. CONCLUSIONS

Suggested revisions for the LDSS interface have been developed using a combination of empirical information and application of human-computer interaction knowledge. The process of developing these revisions was tracked and led to a method for prioritizing criteria for use in trade-off decisions. As LDSS will now be field tested in the KSC firing room, the actual usability of the interface can be assessed. Due to the nature of the ANTD/NTD job, information concerning the use of the interface will have to be collected in a nonintrusive fashion. As the use of LDSS is optional and will require a change in the ANTD/NTD procedures during countdown, the initial and sustained use of LDSS will be a major indication of the usability of the system. Additionally, information must be collected after use of the system. This information should discriminated between missing information, misinterpreted information and mistrusted information. Audio tapes of countdown activities, especially S0044 simulations, along with observations by the LDSS staff can be used to obtain this information. In addition, post countdown interviews with the ANTD and NTD are very valuable. Any changes that are made to LDSS as a result of these observations and interviews should be documented in the form of guidelines. New software development will benefit in the form of time savings and monetary savings from use of these guidelines. Utimately, the users of these software tools will benefit from the increased usability of newly developed tools.

REFERENCES

Dumas, J.,*Designing User Interfaces for Software,* Prentice Hall, 1988.

Helander, M., *Handbook of Human-Computer Interaction,* North Holland: The Netherlands, 1990.

Galitz, W., *Handbook of Screen Format Design,* QED Information Sciences, Inc. Wellesley, MA, 1989.

Gilmore, W., Gertman, D., and Blackman, H., *User-Computer Interface in Process Control,* Academic Press, 1989.

Scapin, D., Organizing Human Factors Knowledge, *International Journal of Human-Computer Interaction,* Vol. 2, No. 3, 203-229.

Smith, S. and Mosier, J., Guidelines for Designing User Interface Software, ESD-TR-86-278.

Spacelab Display Design and Command Usage Guidelines, NASA, MSFC-Proc-711A, April, 1990.

Tullis, T., The formatting of alphanumeric displays: A review and analysis. *Human Facotrs,* 25, 1983, 657-682.

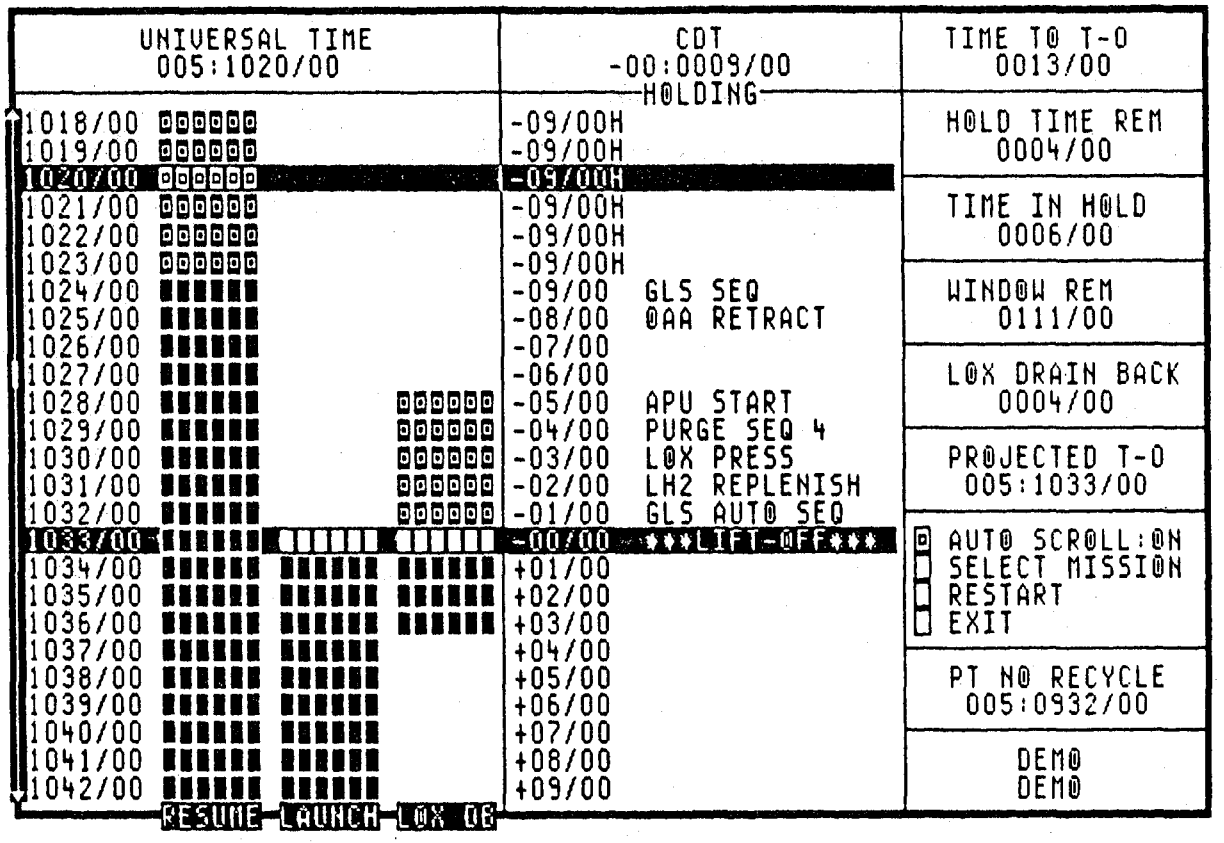

Figure 1: Original TMID

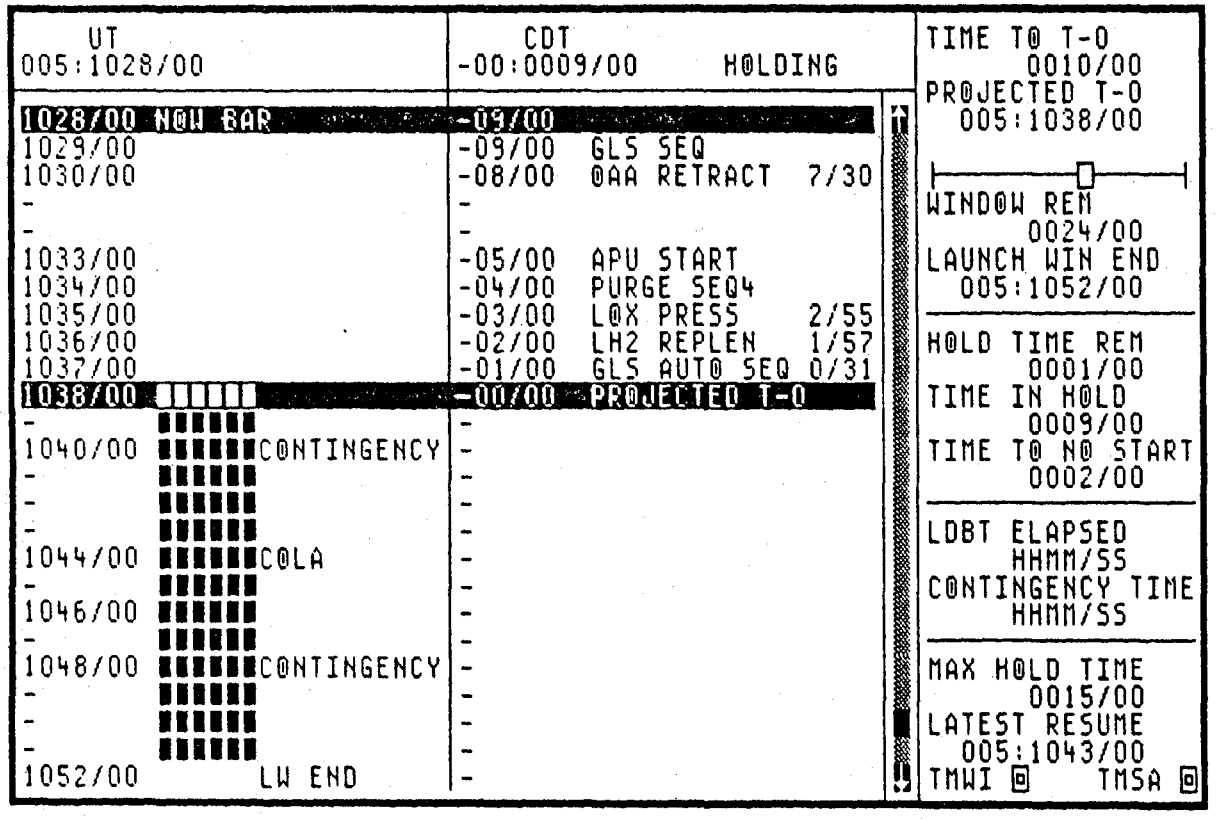

Figure 2: Revised TMID

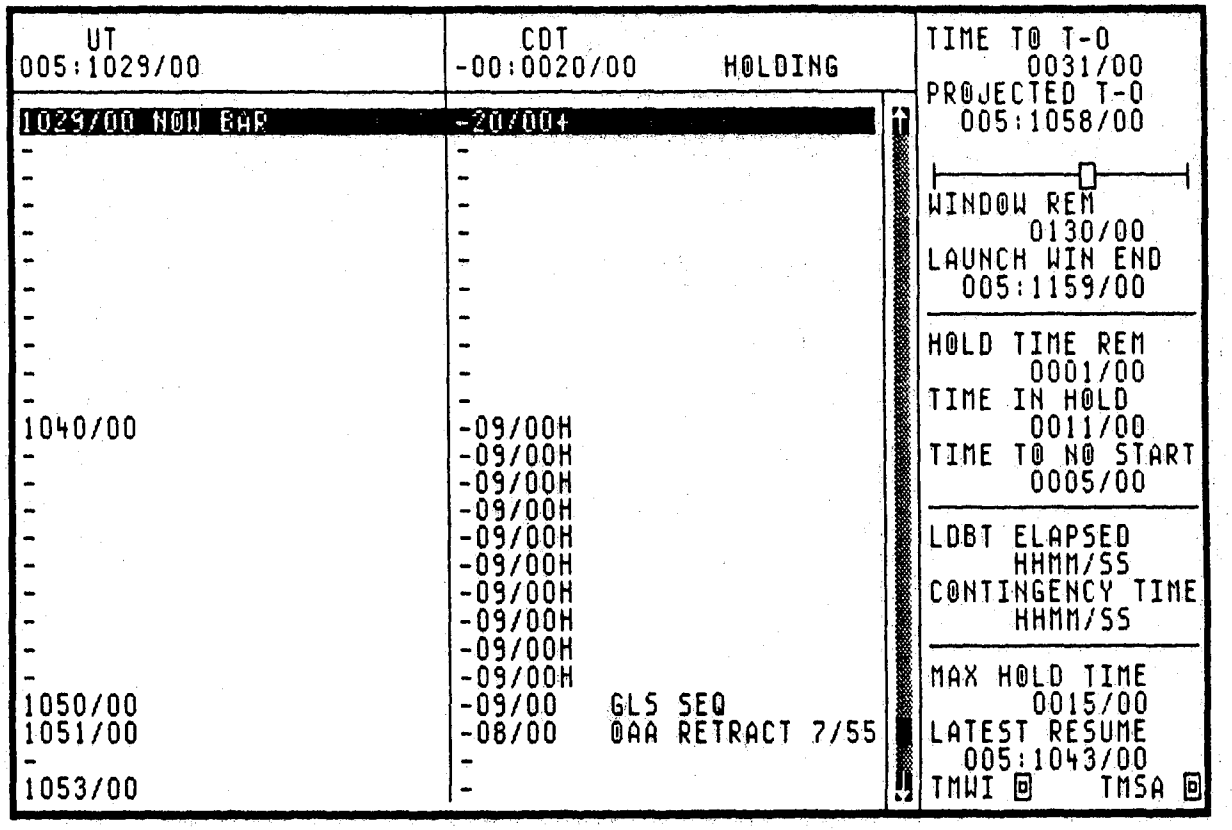

Figure 3: Revised TMID, T-20M

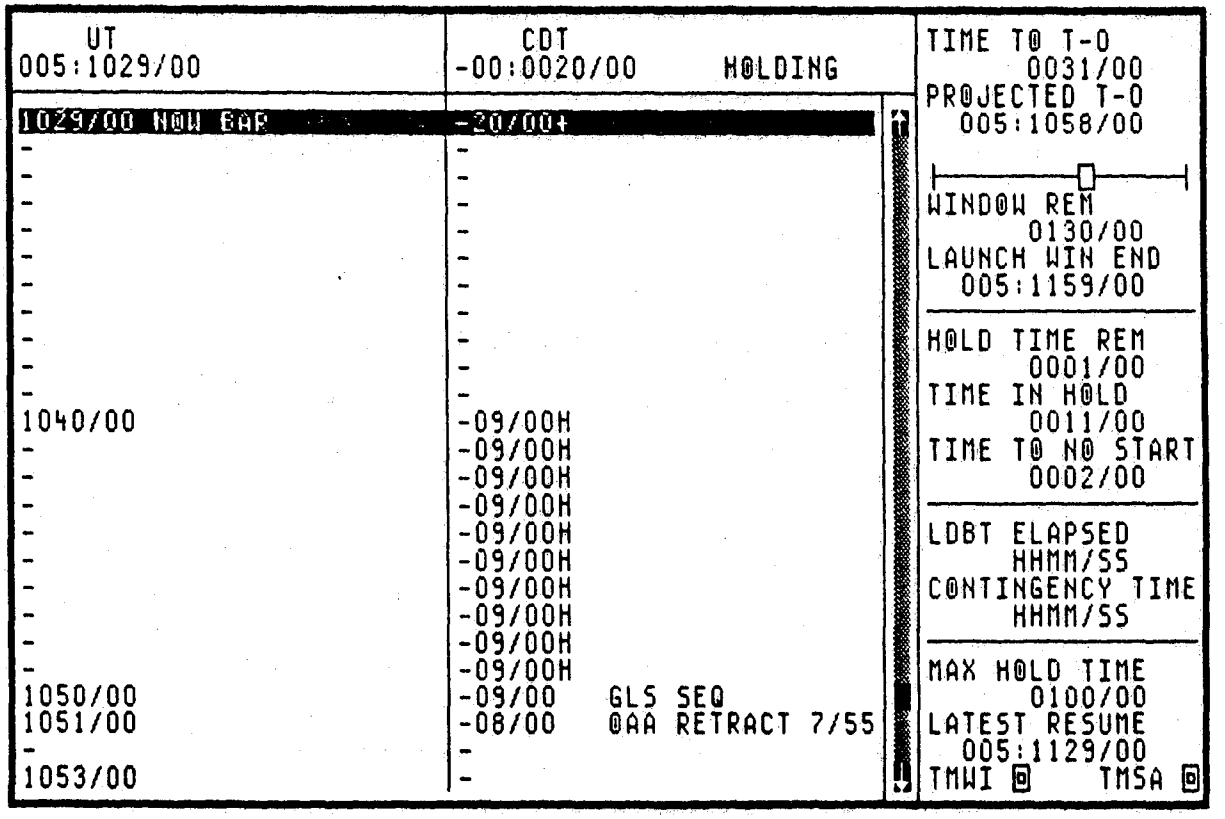

Figure 4: Revised TMID, T-20M, Unable to Resume

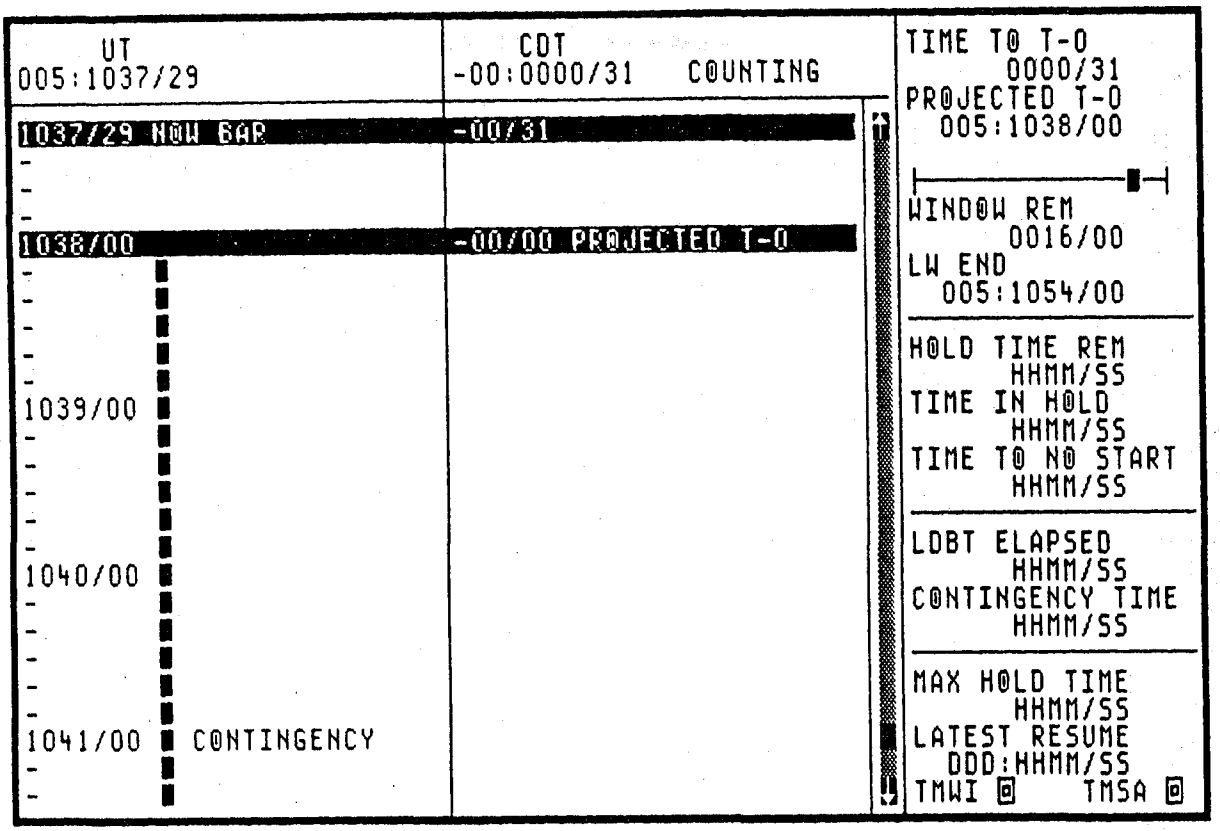

Figure 5: TMID with fine grain resolution

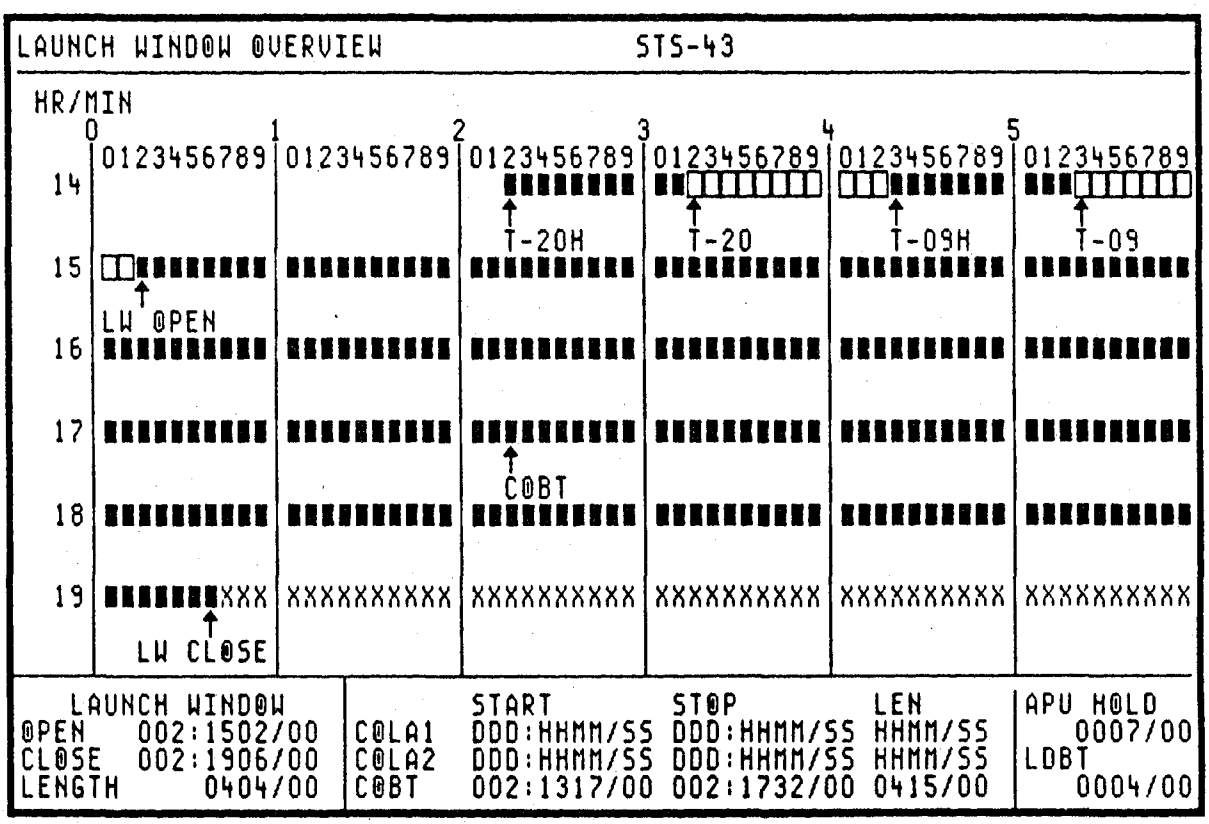

Figure 6: Overview Display

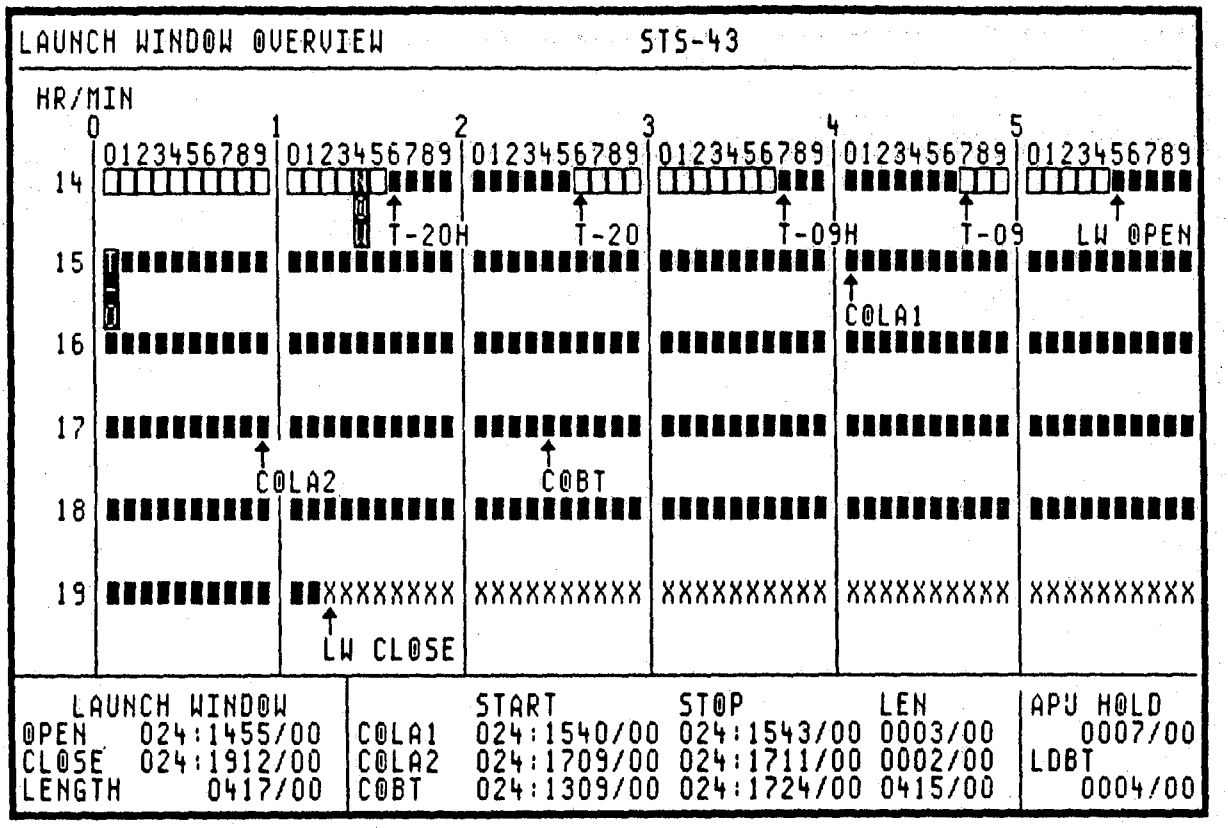

Figure 7: Dynamic Overview Display

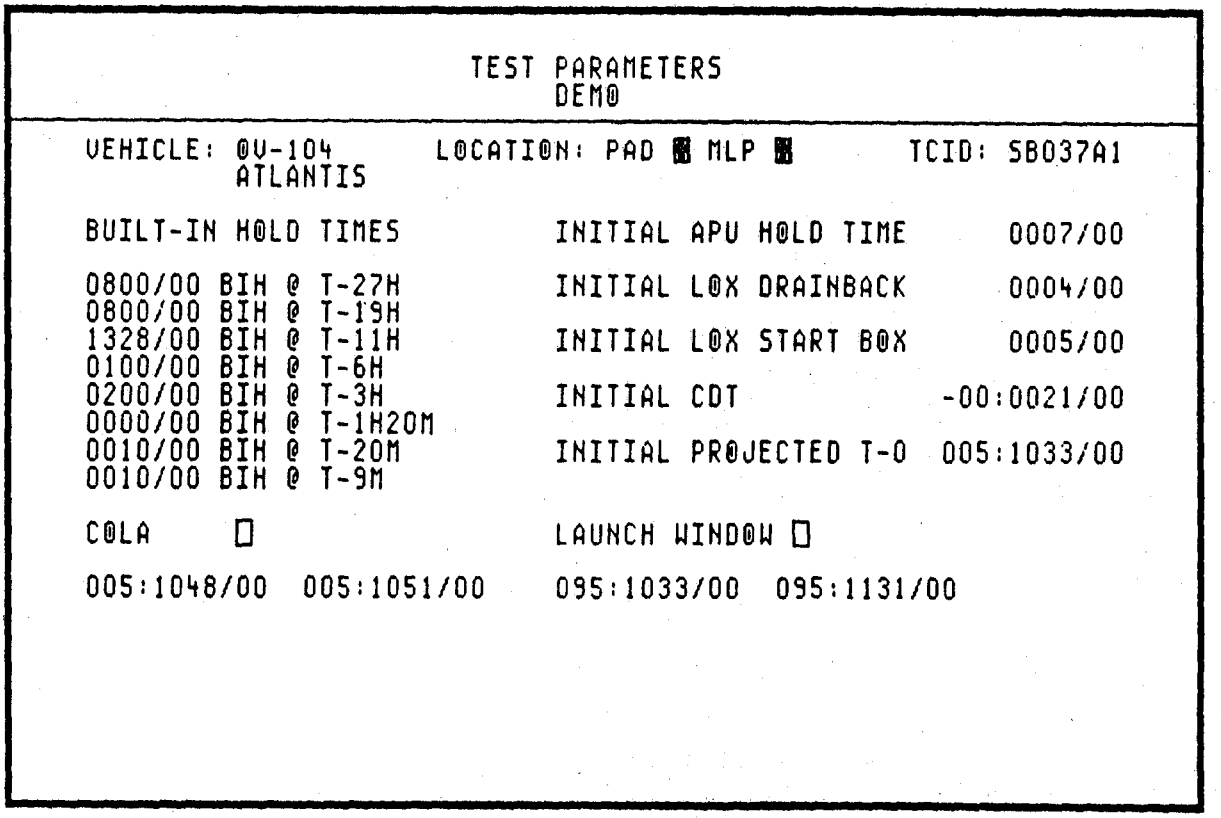

Figure 8: Original Test Parameters Screen

```
                              MISSION   STS48

VEHICLE: OV-XXX        LOCATION: PAD X MLP X          TCID: XXXXXXX

BIH          LENGTH                  APU HOLD TIME        0007/00
                                     LDBT                 0004/00
T-20M        0010/00                 LOX START BOX        0000/00
T-9M         0010/00                 PROJECTED T-0   000:0000/00
                                     PT NO RECYCLE   000:0000/00


                     START           END             LENGTH
LAUNCH WINDOW        000:0000/00     000:0000/00     0000/00

COLA1                000:0000/00     000:0000/00     0000/00
COLA2                000:0000/00     000:0000/00     0000/00
COLA3                000:0000/00     000:0000/00     0000/00

COBT                 000:0000/00     000:0000/00     0000/00
```

Figure 9: Revised Test Parameters Screen

```
UNIVERSAL TIME          CDT                    TIME TO T-0
  005:1017/00       -00:0009/00                  0016/00
                       HOLDING                 HOLD TIME REM
                                                  0007/00
 WHAT
   MAX HOLD TIME REM                  0056/00   TIME IN HOLD
   LATEST RESUME TIME   1113/00                   0003/00

 CDT      DESCRIPTION          UTC      INTERVAL  WINDOW REM
                                                   0114/00
 IF                                                CONTING TIME
                                                   0004/00
 -09/00  HOLD START TIME      1014/00
         TIME IN HOLD                    0003/00   PROJECTED T-0
         NOW                  1017/00              005:1033/00
         MAX HOLD TIME REM               0056/00
         LATEST RESUME TIME   1113/00

 □ -05/00 HOLD START TIME     1117/00
         TIME IN HOLD                  □ 0005/00
         RESUME TIME          1122/00

 -00/00  DESIRED GMT OF T-0   1127/00              PT NO RECYCLE
         CONTINGENCY TIME              □ 0004/00    005:0932/00
         LAUNCH WINDOW END  □ 1131/00
                                                      DEMO
```

Figure 10: Original What If Display

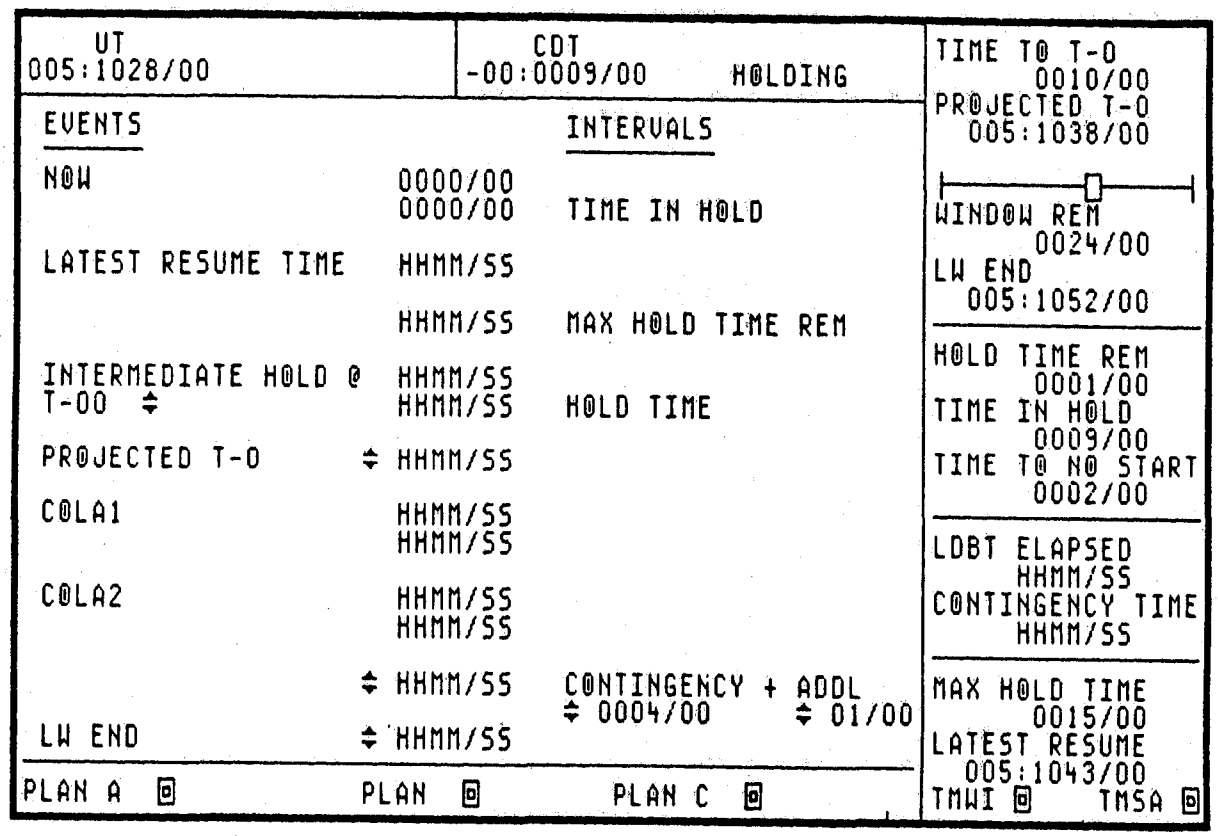

Figure 11: Revised What If Display, Textual Version

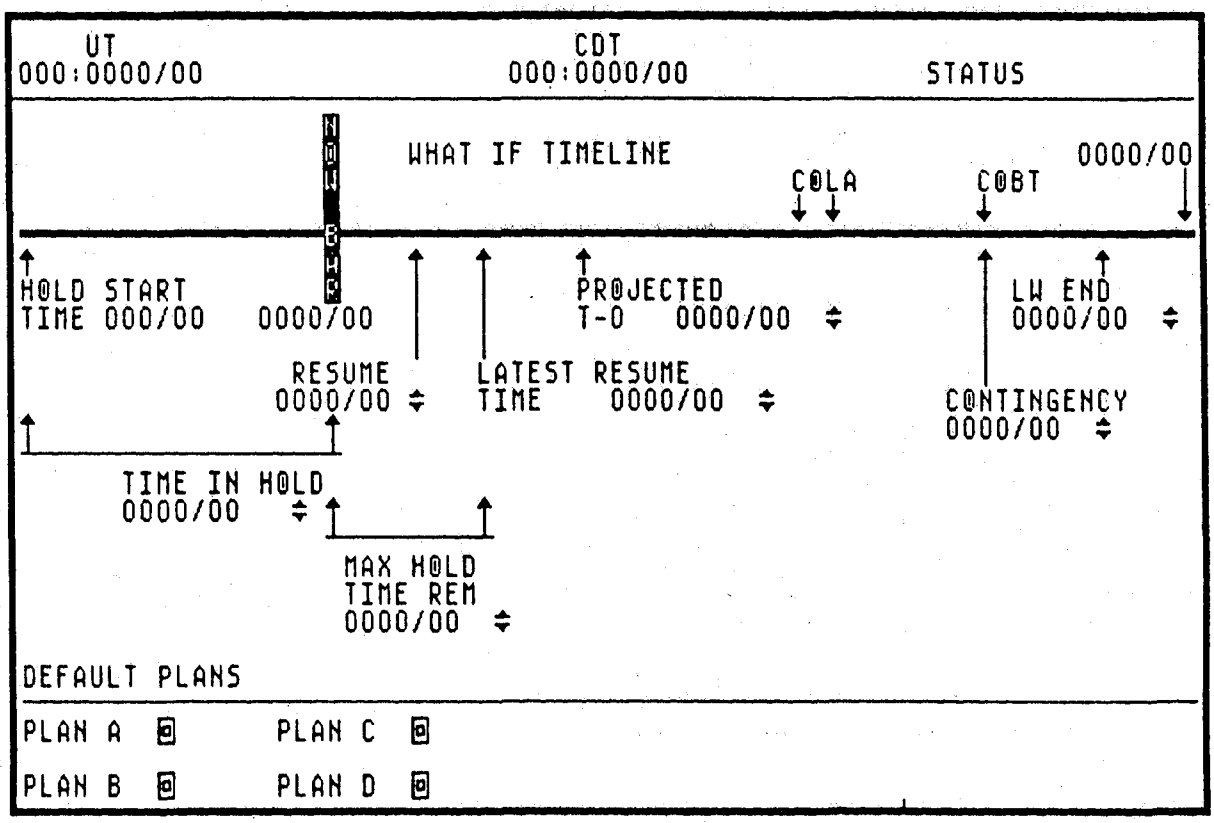

Figure 12: Revised What If Display, Graphical Version

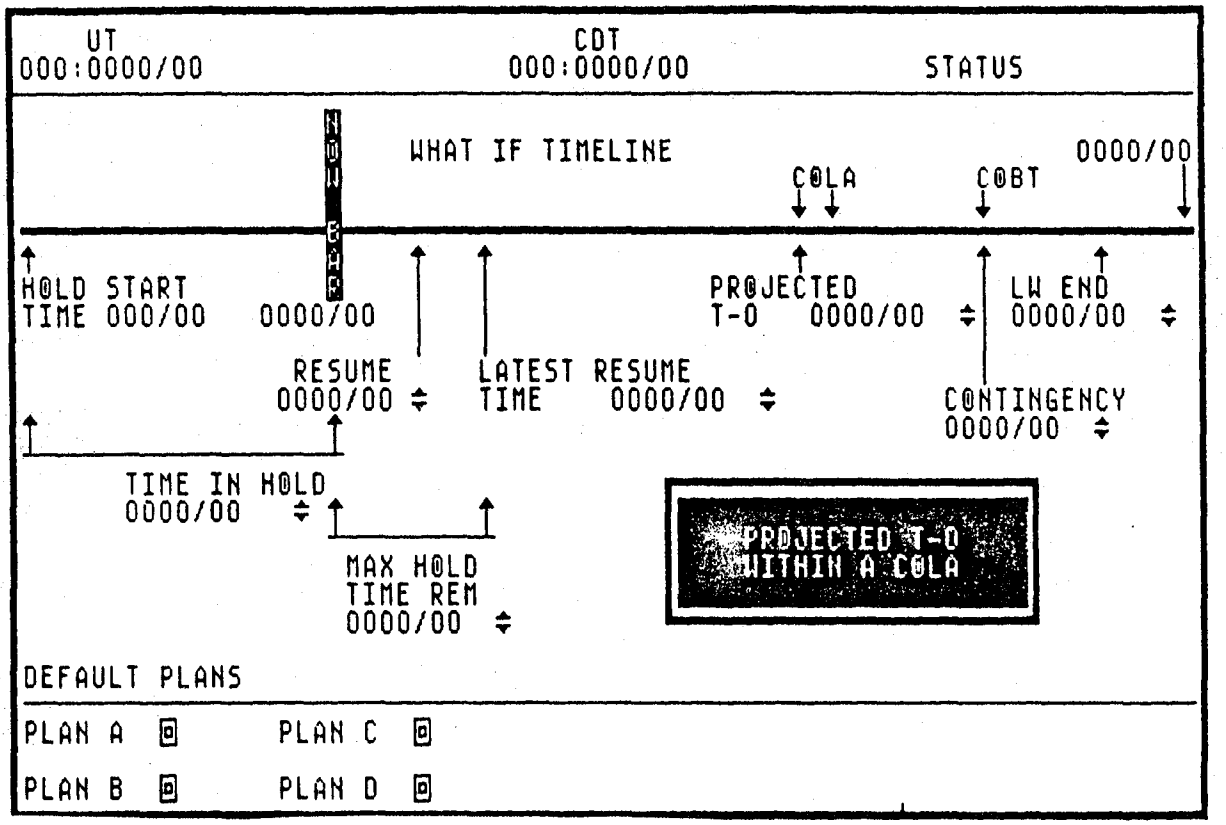

Figure 13: Revised What If Display, Graphical showing Constraints

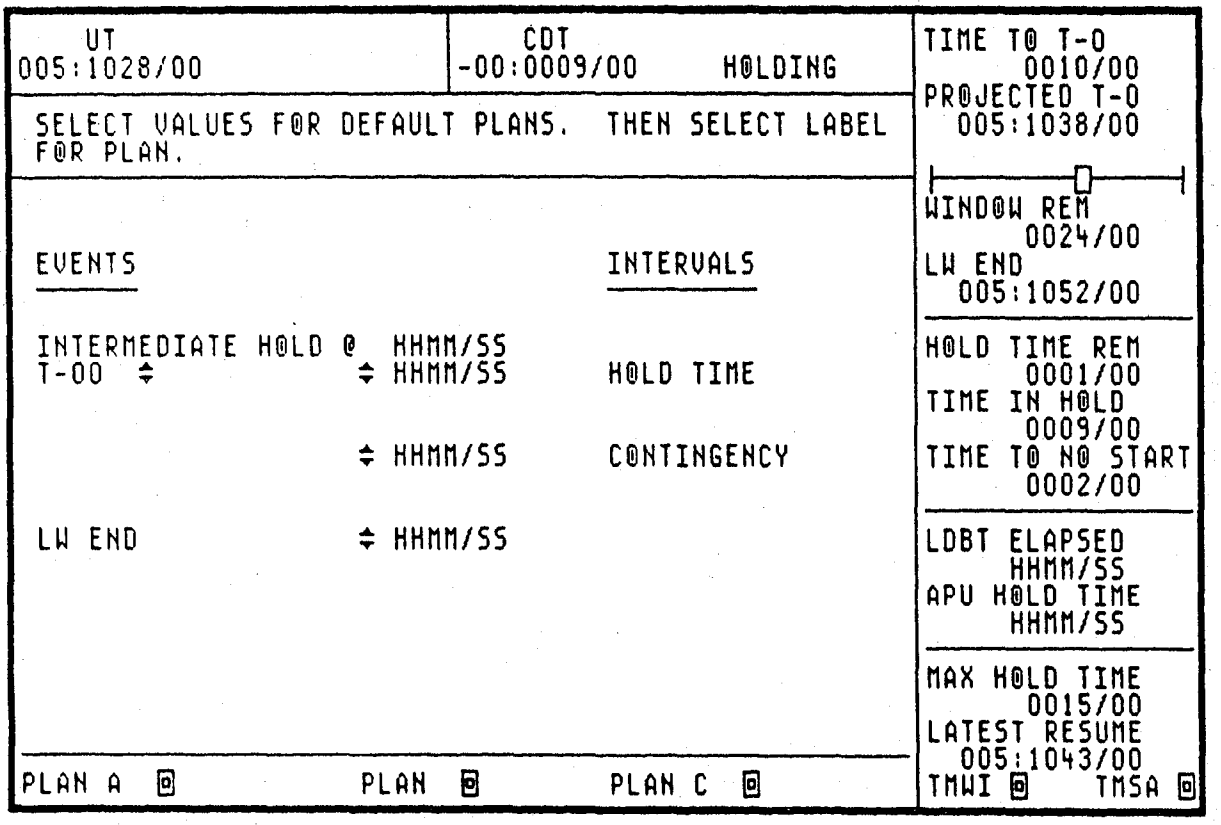

Figure 14: What If Default Input

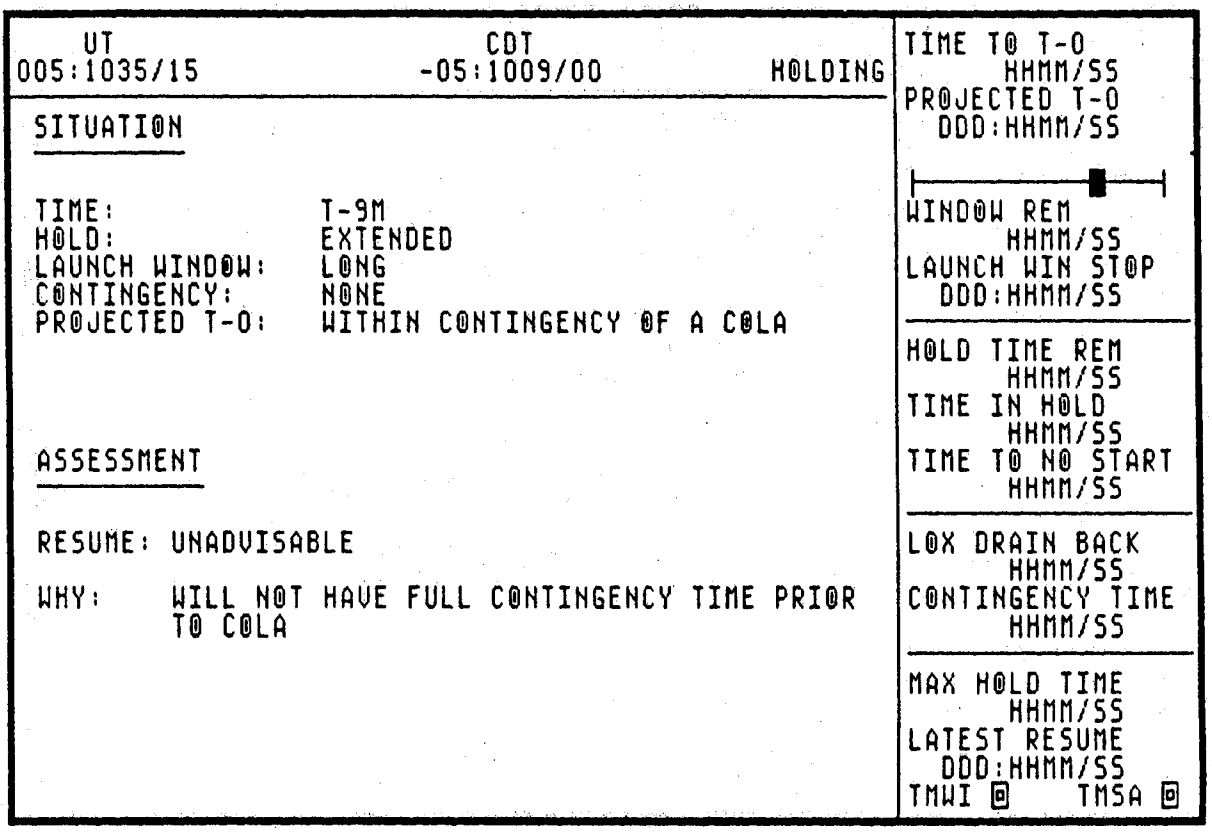

Figure 15: Revised Situation Assessment

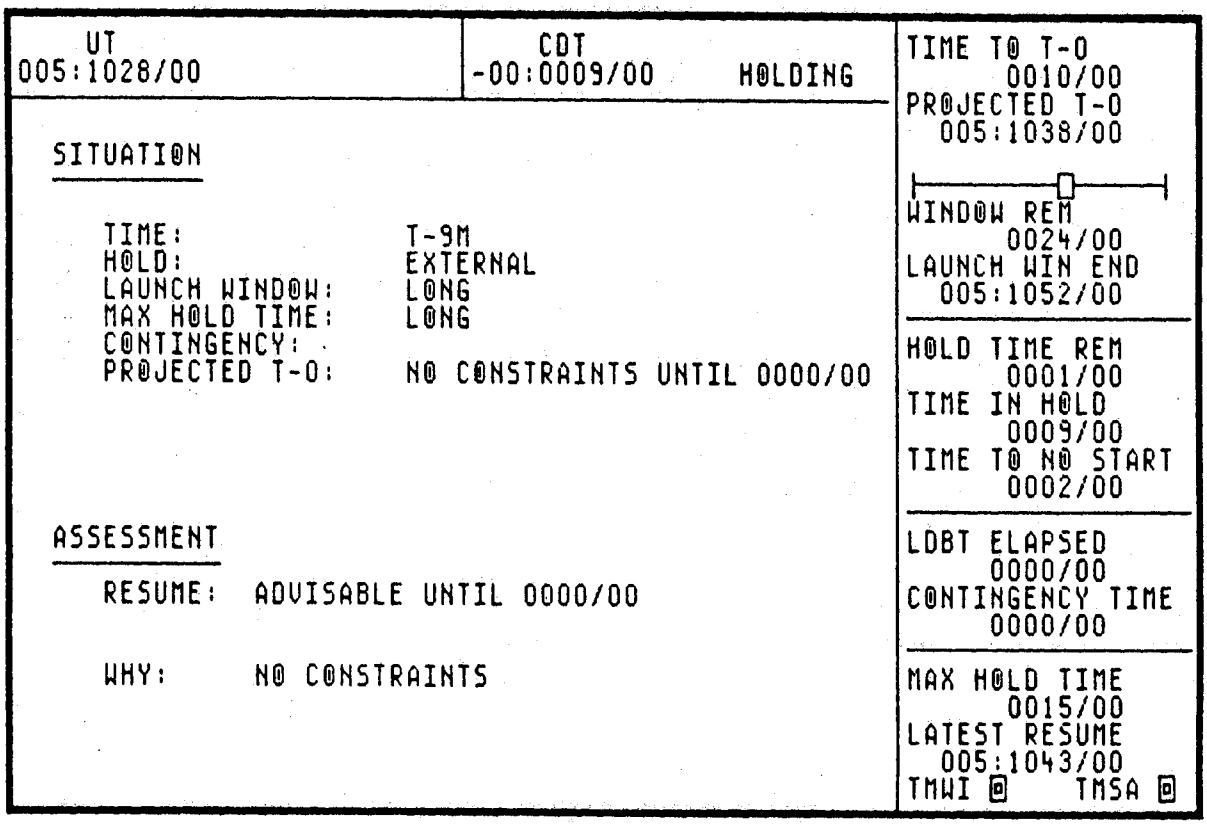

Figure 16: Revised Situation Assessment, Display 2

1991 NASA/ASEE SUMMER FACULTY FELLOWSHIP PROGRAM

JOHN F. KENNEDY SPACE CENTER
UNIVERSITY OF CENTRAL FLORIDA

PRECISION CLEANING VERIFICATION OF NONVOLATILE RESIDUES BY USING WATER, ULTRASONICS AND TURBIDITY ANALYSES

PREPARED BY:	Dr. S. Balloû Skinner
ACADEMIC RANK:	Professor
UNIVERSITY AND DEPARTMENT:	The University of South Carolina Coastal Carolina College Physics Department
NASA/KSC	
DIVISION:	Materials Science Laboratory
BRANCH:	
NASA COLLEAGUE:	Mr. Charles W. Hoppesch
DATE:	July 19, 1991
CONTRACT NUMBER:	University of Central Florida NASA-NGT-60002 Supplement: 6

ACKNOWLEDGMENT

I am grateful to the NASA/ASEE Summer Faculty Fellowship Program and to Mr. Charles W. Hoppesch, Chief of the Materials Science Laboratory of the Engineering Development Directorate at the Kennedy Space Center (KSC), for the opportunity of spending an enjoyable, productive and rewarding summer verifying precision cleaning of nonvolatile residues by using water, ultrasonics and turbidity analyses.

There are many people who assisted me in the research project. First and foremost was Mr. Charlie Hoppesch whose consultation, guidance and advice was most valuable. I greatly valued the helpfulness of Mr. Ed Dumas for the preparation of graphs and figures. I am also grateful to Mr. Billy Dearing for his assistance and advice throughout the project.

I further acknowledge the generous assistance provided by Mr. Jim Jones, Chief of the Microchemical Analysis Branch, Messrs. Lee Underhill and Charlie Bassett and Ms. Martha Williams.

Also, appreciation goes to Mr. Mitchell Buckely for his help in sample preparation and testing and Ms. Gayle Krisingha for typing this paper.

The expertise and kindness of the program director, Dr. Ray Hosler, is also gladly acknowledged.

ABSTRACT

Chlorofluorocarbons (CFC's) in the atmosphere are believed to present a major environmental problem because they are able to interact with and deplete the ozone layer. NASA has been mandated to replace chlorinated solvents in precision cleaning, cleanliness verification and degreasing of aerospace fluid systems hardware and ground support equipment. The Kennedy Space Center has a CFC phase-out plan which provides for the elimination of over 90% of the CFC and halon use by 1995.

The Materials Science Laboratory at the Kennedy Space Center is evaluating four analytical methods for the determination of nonvolatile residues removal by water: (1) Infrared analyses using an Attenuated Total Reflectance, (2) Surface Tension analyses, (3) Total Organic Content analyses, and (4) Turbidity analyses.

This research project examined the ultrasonic-turbidity responses for 22 hydrocarbons in an effort to determine (1) if ultrasonics in heated water (70°C) will clean hydrocarbons (oils, greases, gels and fluids) from aerospace hardware, (2) if the cleaning process by ultrasonics will simultaneously emulsify the removed hydrocarbons in the water, and (3) if a turbidimeter can be used successfully as an analytical instrument for quantifying the removal of the hydrocarbons.

Sixteen of the 22 hydrocarbons tested showed that ultrasonics would remove at least 90% of the contaminated hydrocarbon from the hardware in 10 minutes or less giving a good ultrasonic-turbidity response. Six hydrocarbons had a lower percentage removal, a slower removal rate and a marginal ultrasonic-turbidity response.

TABLE OF CONTENTS

List of Illustrations

List of Tables

I. Introduction

1.1 Background Information

Chlorofluorocarbons (CFC's) in the atmosphere are believed to present a major environmental problem because they are able to interact with and deplete the ozone layer. As the ozone layer deteriorates, more ultraviolet radiation reaches the Earth's surface, causing skin cancer, eye cataracts and immune deficiencies in people, reducing crop yields and wreaking havoc on other life forms.

In accordance with the NASA Headquarters policy letter on the use of CFC and halon compounds (dated June 26, 1990), Kennedy Space Center (KSC) has developed a CFC and halon phase-out plan to comply with the established requirements. Annual KSC use of CFC and halons was 450,000 lbs. in 1989. About 70% of this usage was for solvent and cleaning operations. Approximately 25% was refrigerant make-up for facility and ground support equipment in heating, ventilation, air conditioning and refrigerant operations. The phase-out plan provides for the elimination of over 90% of the CFC and halon use at KSC by 1995.

At KSC, the Wiltech cleaning facility is responsible for precision cleaning, cleanliness verification and degreasing of fluid systems hardware and ground support equipment used in the Space Shuttle launch operations. The KSC precision cleaning specifications require a cleanliness inspection in which 1,1,2-trichlorotrifluoroethane (CFC-113) is used as the verification fluid for gravimetric nonvolatile residue (NVR) analysis. The cleaned parts/components are rinsed with the verification fluid and NVR is defined as the nonvolatile material remaining after the filtration and evaporation of a volatile solvent (verification fluid, CFC-113).

1.2 Purpose of the Research

In an effort to convert from a CFC system (pre-clean and cleanroom) to a totally aqueous system, water is being evaluated as a precision cleaning verification fluid.

There are four analytical methods being evaluated in the Materials Science Laboratory at KSC for the determination of nonvolatile residues removal by water: (1) Infrared analyses using an Attenuated Total Reflectance (ATR), (2) Surface Tension analyses, (3) Total Organic Content (TOC) analyses, and (4) Turbidity analyses.

My research employed the turbidity analyses. The research design addressed the following questions:

1. Will ultrasonics in heated water (70°C) clean hydrocarbons (oils, greases, gels and fluids) from aerospace hardware?

2. Will the cleaning process by ultrasonics simultaneously emulsify the removed hydrocarbons in the water?

3. Can the turbidimeter be used successfully as an analytical instrument for quantifying the removal of the nonvolatile residues (hydrocarbons) from the hardware in the heated water via ultrasonic cleaning?

II. Instrumentation

2.1 Ultrasonic Cleaning with Water

The ultrasonic cleaner used in this research to remove hydrocarbons from aerospace hardware is a Branson 521 ultrasonic cleaner (Figure 1). The tank size is 12"L X 10.5"W X 8"D. It has four bottom mount piezoelectric transducers which operate at a frequency of 40 kilohertz and 200 watts power. Seventy degree centigrade (70°C) demineralized water is used as the liquid cleaning solution.

A 3/8 inch fitting (Figure 2) is the hardware on which the hydrocarbon contaminant is deposited. The fitting is placed in a 1000 ml beaker holding 500 ml of water. The beaker is suspended in a 70°C water bath for ultrasonic cleaning.

2.2 Turbidimetric Analyses

The turbidimeter used in this research is a DRT-100B (H.F. Scientific, Inc.) (Figure 3). It is a direct reading Nephelometric Instrument which measures scattered light from colloidal suspensions (or from particles in suspension) and direct light passing through a liquid. The ratioed optical signal which results is stabilized and amplified to energize a meter. The turbidimeter provides a linear display of turbidity in nephelometric turbidity units (NTU's).

Turbidity is an expression of the optical properties that cause light to be scattered or absorbed through a liquid sample and is largely a function of the refractive index, the size and shape of the particles suspended in the solution. As a result, turbidimeters do not produce an "absolute" measurement, but one that is "relative" to the optical nature of the solids suspended in a solution. Formazin polymer is accepted as the turbidity standard because when carefully prepared, it is uniform in number, size and shape of its particles.

III. Criteria for Acceptance Standards

The standard for precision cleaning at Wiltech states that if more than one milligram of the nonvolatile residue (in 500 milliliters of a verification fluid) is removed from one square foot of hardware, the cleanliness of the hardware is considered nonacceptable and must be recycled in the precision cleaning process.

IV. Design of the Experiment

Over 120 tests were conducted in order to answer the following questions regarding hydrocarbon response to ultrasonic cleaning-turbidity reading:

1. Which is the better remover of hydrocarbons from the fittings: the ultrasonic cleaner or the sonic dismembrator (Figure 4)?

2. Which is the better remover of hydrocarbons from the fittings: ambient water (25°C) or hot water (70°C)?

3. Will ultrasonics emulsify the hydrocarbons in water or will a virtis emulsifier or hand mixer (Figure 5) be needed?

4. Will ultrasonics remove the hydrocarbons no matter how or where they are located on the fitting?

5. Will ultrasonics remove the hydrocarbons from the fittings (percentage removed) and how long does it take for this removal (removal rate)? In other words, is ultrasonic cleaning effective on all hydrocarbons? Will we see a good ultrasonic-turbidity response for all the hydrocarbons?

V. Results and Analysis

Test results from the questions proposed in Part IV are discussed below:

1. The analysis of 10 tests revealed that the ultrasonic cleaner was better than the sonic dismembrator at removing the hydrocarbon from the fittings. Therefore, all tests were conducted with the ultrasonic cleaner. The testing procedure called for placing a fitting contaminated with a hydrocarbon into 500 ml of water in a 1000 ml polyethylene beaker and ultrasounding for 2 minute intervals up to 10 minutes. If less than 75% of the hydrocarbon has been removed after 10 minutes, the fitting is further ultrasounded for 5 minute intervals up to 40 minutes or until more than 75% of the hydrocarbon is removed. Turbidity readings in NTU's are displayed by a turbidimeter and recorded at the end of each time interval (Figure 10).

2. The analysis of 8 tests showed that hot water (70°C) on an average would give a three-fold increase in removal rate of hydrocarbons from the fittings compared to ambient water (25°C). This research convinced me that it is crucial to keep the water in the beaker and the water in the ultrasonic bath at 70°C throughout the testing for optimum cleaning.

3. The research indicated that the ultrasonics in the heated water (70°C) were successful in emulsifying the removed hydrocarbons. Further testing revealed that the use of a hand mixer or a virtis emulsifier added very little to the total emulsification as shown by the turbidity responses.

4. A limited number of tests showed that ultrasonics were successful in removing the hydrocarbons no matter where or how they were located on the fitting, i.e., on the top, down in the hole, on the threads, in a glob, or spread out uniformly. However, more tests probably need to be run to substantiate this claim.

5. A list of 22 hydrocarbons tested (Figure 6) with their generic name, chemistry, percent and time for ultrasonic removal of one milligram and ultrasonic turbidity (NTU) is given in Table 1.

Table 1 shows that Krytox 240AC (77% removal, 40 min., 0.6 turbidity), DS-FS-1265 (75% removal, 30 min., 0.7 turbidity), Titan-Lube (68% removal, 40 min., 0.8 turbidity), Halovac 100 (100% removal, 35 min., 0.5 turbidity), DC-200 (100% removal, 25 min., 1.0 turbidity) and Dri-Tube (85% removal, 40 min., 0.9 turbidity) are the hydrocarbons with marginal ultrasonic-turbidity response at the 1 mg level. Additional tests using 5 mg and 10 mg samples for 10 minute ultrasonics will be run in the future to determine if an acceptable ultrasonic-turbidity response can be seen for these marginal hydrocarbons at these higher contamination levels.

Tables 2 and 3 depict each of the 22 hydrocarbons with the weight of the hydrocarbon removed from the fitting via ultrasonics along with corresponding turbidity readings. The data in Tables 2 and 3 is displayed in graphical form in Figures 7, 8 and 9.

Figures 7, 8 and 9 show that there is a direct relationship between turbidity and the hydrocarbon emulsified in the 500 ml of water for all 22 hydrocarbons. There is a linear relationship between ultrasonic removal of hydrocarbon and turbidity response at the 1/2 mg, 1 mg and 2 mg levels for all 22 hydrocarbons. It further shows clearly that six hydrocarbons (Krytox 240AC, DS-FS-1265, Titan-Tube, Halovac 100, DC-200 and Dri-Lube) have marginal ultrasonic-turbidity responses while 16 other hydrocarbons have good responses.

The slope of the lines in Figures 7, 8 and 9 is an indicator of the emulsion taking place and the capability of the hydrocarbon to remain in emulsion. The lines which are almost parallel (near "zero" slope) and close to the X-axis are those hydrocarbons which give marginal ultrasonic-turbidity responses. These are the problem hydrocarbons. The lines which are high above the X-axis and have large slopes are those hydrocarbons which have good ultrasonic-turbidity responses. These hydrocarbons present no problems in the verification of precision cleaning.

VI. Conclusions and Recommendations

Approximately three quarter of the 22 hydrocarbons tested showed that ultrasonics would remove at least 90% of the contaminant from the fitting in 10 minutes or less. The hydrocarbons giving low percentage removal over long times of ultrasonics with low turbidity readings were two silicones, a fluorosilicone, a fluorinated polyether, a PCTFE and an Isobutylene.

This research project shows that hot water (70°C), ultrasonics and turbidity analyses can be used for precision cleaning verification of most nonvolatile residues. For the marginal ultrasonic-turbidity response hydrocarbons, better cleaning methods for removing hydrocarbons need to be found and other analytical methods may be needed in conjunction with the ultrasonics-turbidity analyses (e.g., infrared analyses using an attenuated total reflectance, surface tension analyses, total organic carbon analyses, fluorescence/scatter analyses, or some method to be determined) to completely solve the problem of quantifying the removal of nonvolatile residues by water.

VII . References

1. "Encyclopedia of Chemical Technology", Vol. 8, 1978, New York, John Wiley and Sons, 900-930.

2. "Encyclopedia of Chemical Technology", Vol. 22, 1978, New York, John Wiley and Sons, 332-347.

3. Halbut, Jim, "Ultrasonic Cleaning with Water, Sonic Report No. SR1641", Delta Sonic, Inc., 1987.

4. Instruction Manual, DRT-100B and DRT-100B Research Turbidimeters, July 1990, Published by H.F. Scientific, Inc., Fort Myers, Florida.

5. Kashkoush, I. and Busnaina, A., "Submicron Particle Removal from Surfaces Using Acoustic Streaming", 1991 Proceedings, Institute of Environmental Sciences, 861-867.

6. Law, R. J., "Analytical Methods and Their Problems in the Analysis of Oil in Water", 1990 Seminar Proceedings, Ministry of Agriculture, Fisheries and Food, Buraham-on-Cronch, UK.

7. Sherman, Alan and Sherman, Sharon J., "Chemistry and Our Changing World", Second Edition, 1989, McGraw-Hill Publishing Company, New York, NY, 462-471.

HYDROCARBON	GENERIC	CHEMISTRY	ULTRASONIC REMOVAL (1MG) PERCENT TIME	ULTRASONIC TURBIDITY (NTV)
DC-200	FLUID	SILICONE	100 (25M)	1.0
HOUGHTON SAFE 1055	FLUID	PHOSPHATE ESTER BASED HYROCARBON	98 (10M)	2.9
MOBIL JET II	FLUID	ESTER BASED HYDROCARBON	100 (10M)	2.5
AMOCO - RYKON #2	GREASE	HYDROCARBON	100 (16M)	2.8
MOBIL - MOBILUX 2	GREASE	HYDROCARBON	100 (6M)	2.8
CHEVRON SRI	GREASE	HYDROCARBON	100 (8M)	3.0
SHELL TELLUS - 32	FLUID	HYDROCARBON	100 (8M)	2.4
MIL-G-8188C	FLUID	ESTER BASED HYDROCARBON	100 (4M)	2.0
MIL-G-5606	FLUID	HYDROCARBON	100 (6M)	1.7
CASTROL MOTOR OIL	FLUID	HYDROCARBON	100 (10M)	2.1
DC-55M	GREASE	SILICONE	100 (10M)	1.3
DRILUBE - TYPE 822	GREASE	SILICONE	85 (40M)	0.9
MIL-H-83282	FLUID	ESTER BASED HYDROCARBON	100 (10M)	2.3
MIL-G-3545C	GREASE	HYDROCARBON, SOAP ADDITIVE	90 (10M)	2.4
DC-44	GREASE	SILICONE	91 (10M)	2.8
KRYTOX 240AC	GREASE	FLUORINATED POLYETHER	77 (40M)	0.6
DC-33	GREASE	SILICONE	90 (8M)	1.1
HALOVAC 100 SB	FLUID	PCTFE	100 (35M)	0.5
DC FS-1265	FLUID	FLUOROSILICONE	75 (30M)	0.7
MIL-G-23549C	GREASE	HYDROCARBON GREASE CONTAINING MOLYB-DENUM DISULFIDE	54 (35M)	1.6
MINERAL OIL	FLUID	HYDROCARBON	91 (10M)	1.2
TITAN LUBE	FLUID	ISOBUTYLENE	68 (40M)	0.8

TABLE 1 - LIST OF HYDROCARBONS TESTED

HYDROCARBON	WEIGHT OF HYDROCARBON REMOVED FROM FITTING (Mg)	TURBIDITY (NTU)
DC-200	0.52	0.4
	0.83	0.7
	0.94	1.0
	1.68	1.3
HOUGHTON-SAFE 1055	0.26	0.8
	1.08	2.9
	2.06	3.5
MOBIL JET II	0.34	1.1
	0.93	2.5
	1.50	2.8
AMOCO-RYKON #2	0.45	0.9
	0.80	1.5
	0.96	2.8
MOBIL-MOBILUX 2	0.51	1.9
	1.06	2.8
	2.09	4.8
CHEVRON SRI	0.48	0.9
	1.00	3.0
	1.96	6.2
SHELL TELLUS-32	0.60	1.4
	1.04	2.4
	1.95	4.8
MIL-G-8188C	0.47	1.1
	0.96	2.0
	2.18	3.8
MIL-G-5606	0.55	1.0
	1.09	1.7
	2.22	3.7
TITAN LUBE	0.35	0.6
	0.67	0.8
	1.36	0.9
CASTROL MOTOR OIL	0.62	1.3
	0.97	2.1
	2.09	4.4

TABLE 2 - TURBIDITY RESPONSE TO WEIGHT REMOVED

HYDROCARBON	WEIGHT OF HYDROCARBON REMOVED FROM FITTING (Mg)	TURBIDITY (NTU)
DC-55M	0.48	0.7
	0.92	1.3
	2.00	2.4
DRILUBE-TYPE 822	0.38	0.3
	0.94	0.9
	1.29	1.3
MIL-H-83282	0.55	1.3
	1.29	2.3
	2.18	4.0
MIL-G-3545C	0.46	1.8
	0.94	2.4
	2.08	5.5
DC-44	0.52	0.9
	0.99	2.8
	1.30	3.4
KRYTOX 240 AC	0.32	0.2
	0.73	0.5
	0.77	0.6
DC-33	0.43	0.3
	0.94	1.1
	2.00	2.0
HALOVAC 100 SB	0.56	0.3
	0.97	0.5
	0.98	0.5
DC-FS-1265	0.22	0.5
	0.66	0.7
	0.88	0.7
MIL-G-23549C	0.31	1.2
	0.77	1.6
	1.17	2.2
MINERAL OIL	0.49	0.6
	0.95	1.2
	1.52	1.7

TABLE 3 - TURBIDITY RESPONSE TO WEIGHT REMOVED

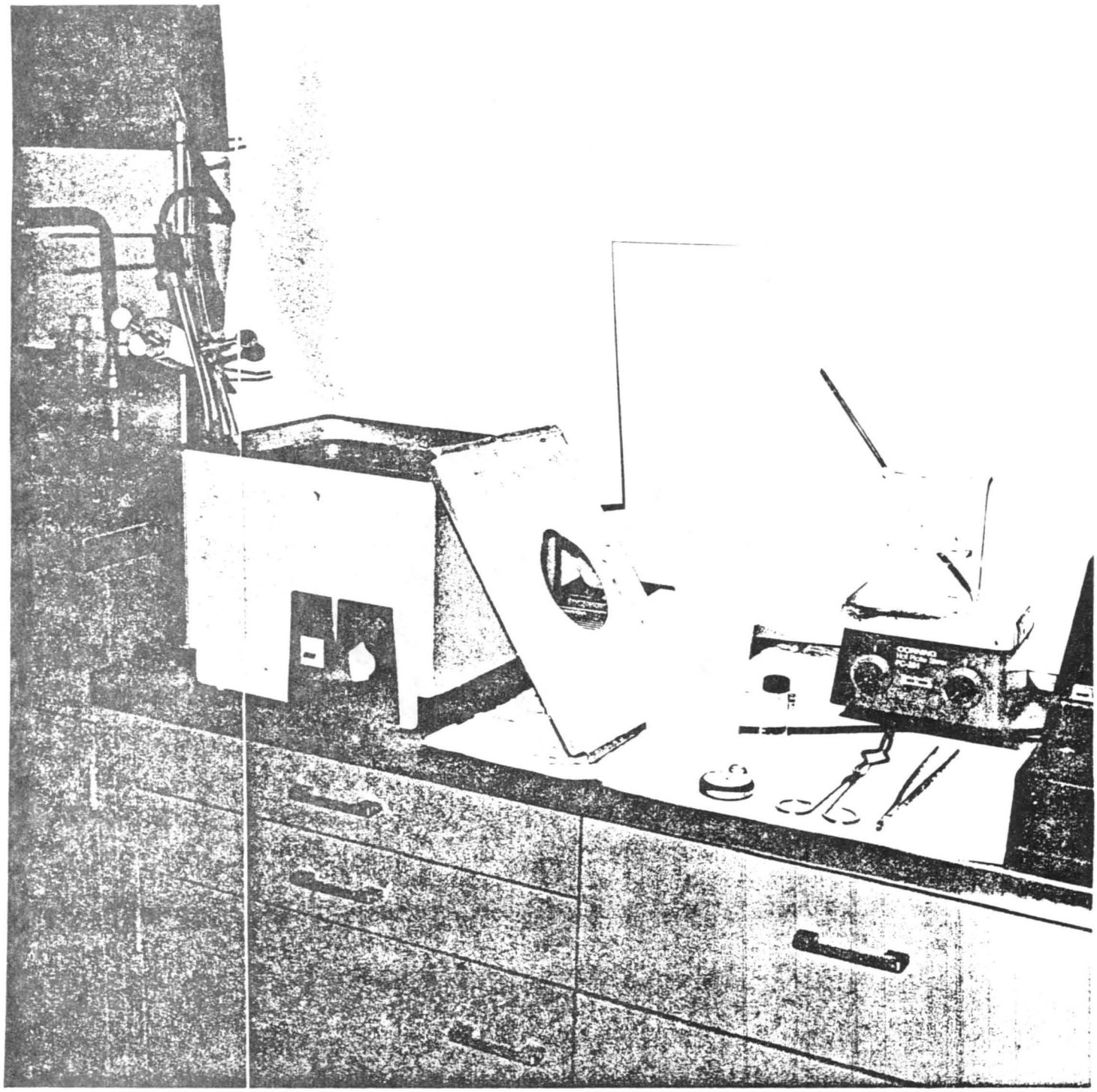

Figure 1. Ultrasonic Cleaner

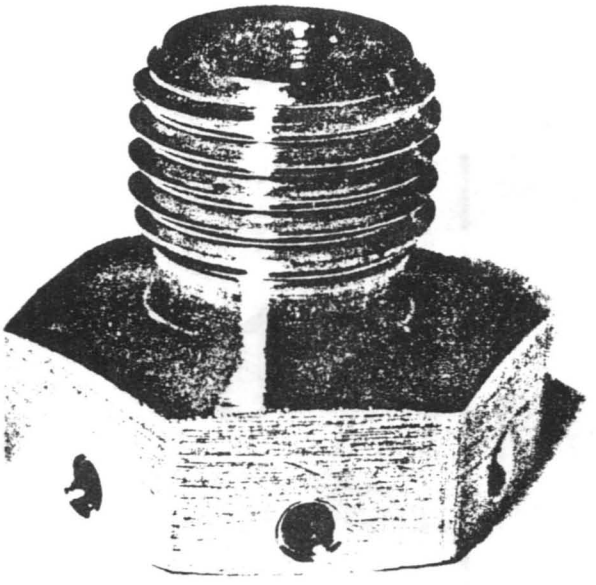

Figure 2. Fitting

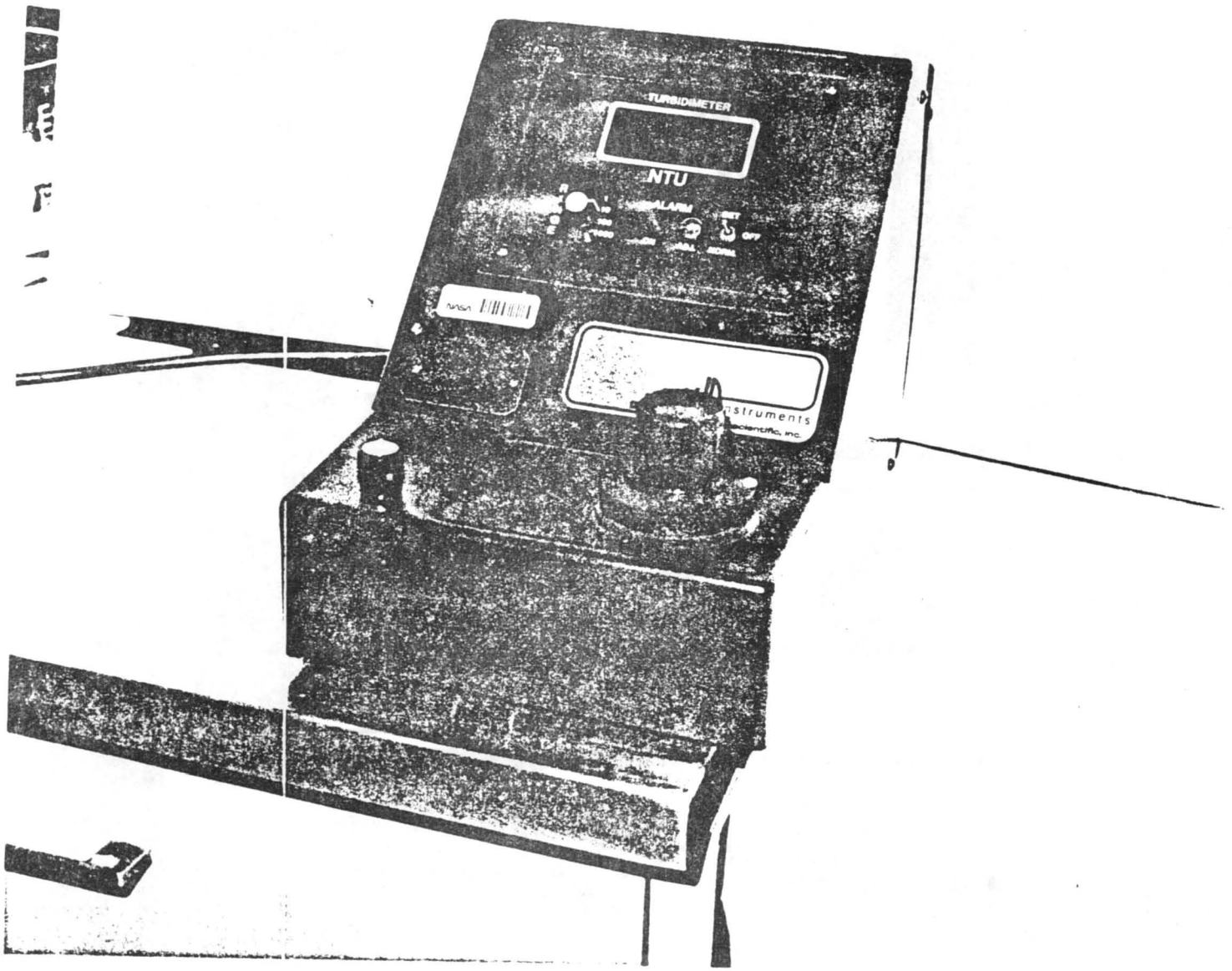

Figure 3. Turbidimeter

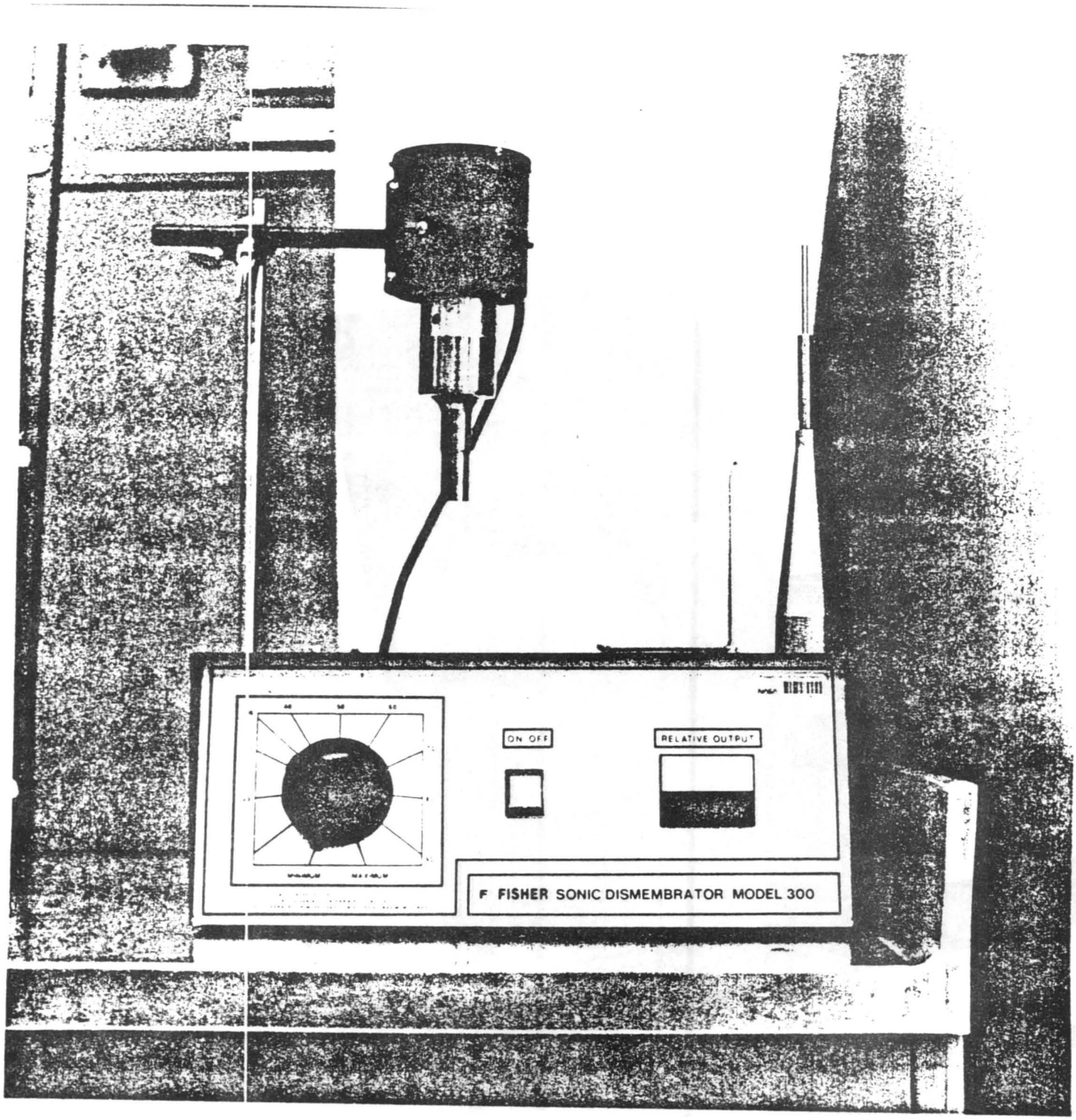

Figure 4. Sonic Dismembrator

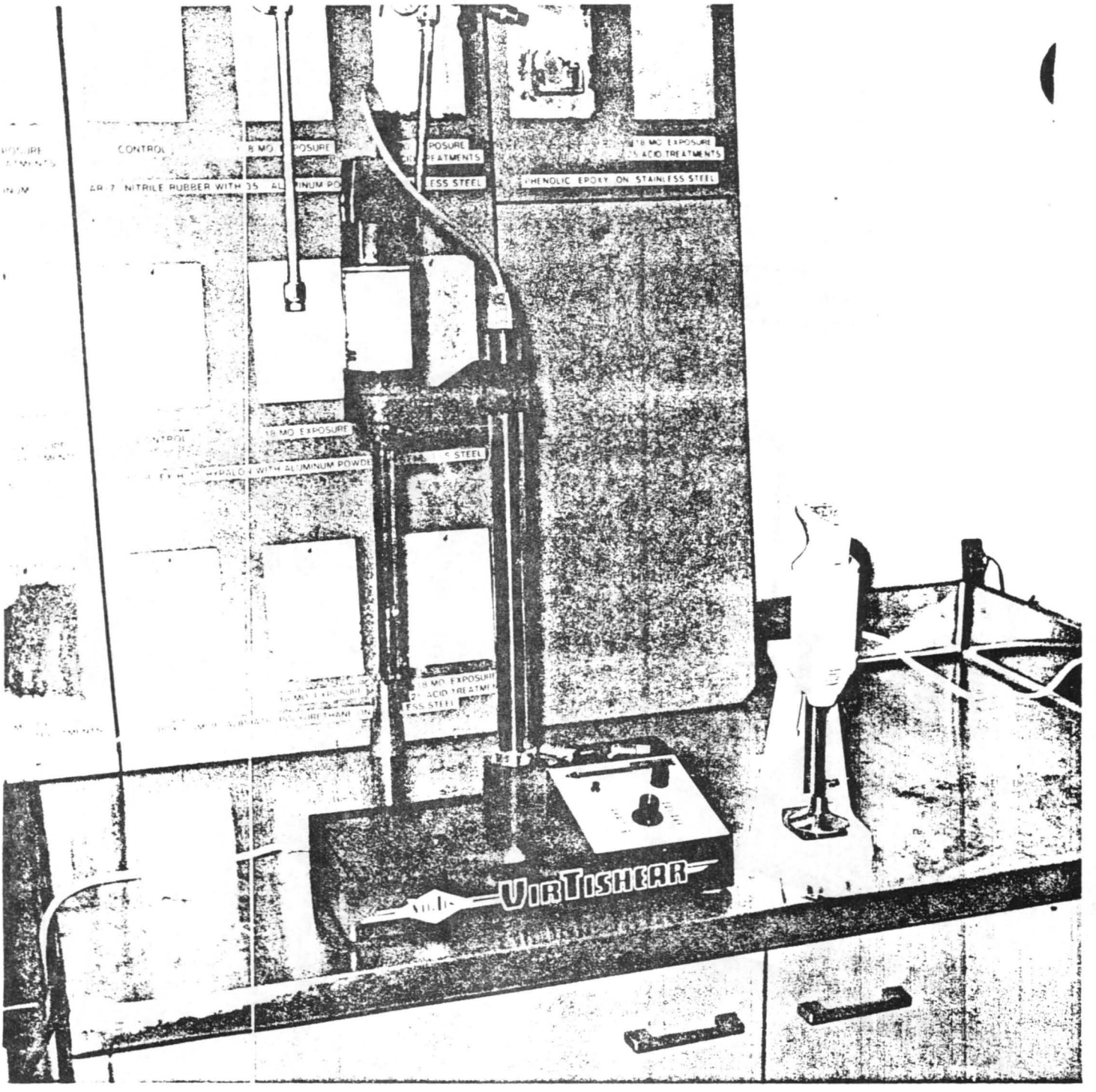

Figure 5. Virtis Emulsifier And Hand Mixer

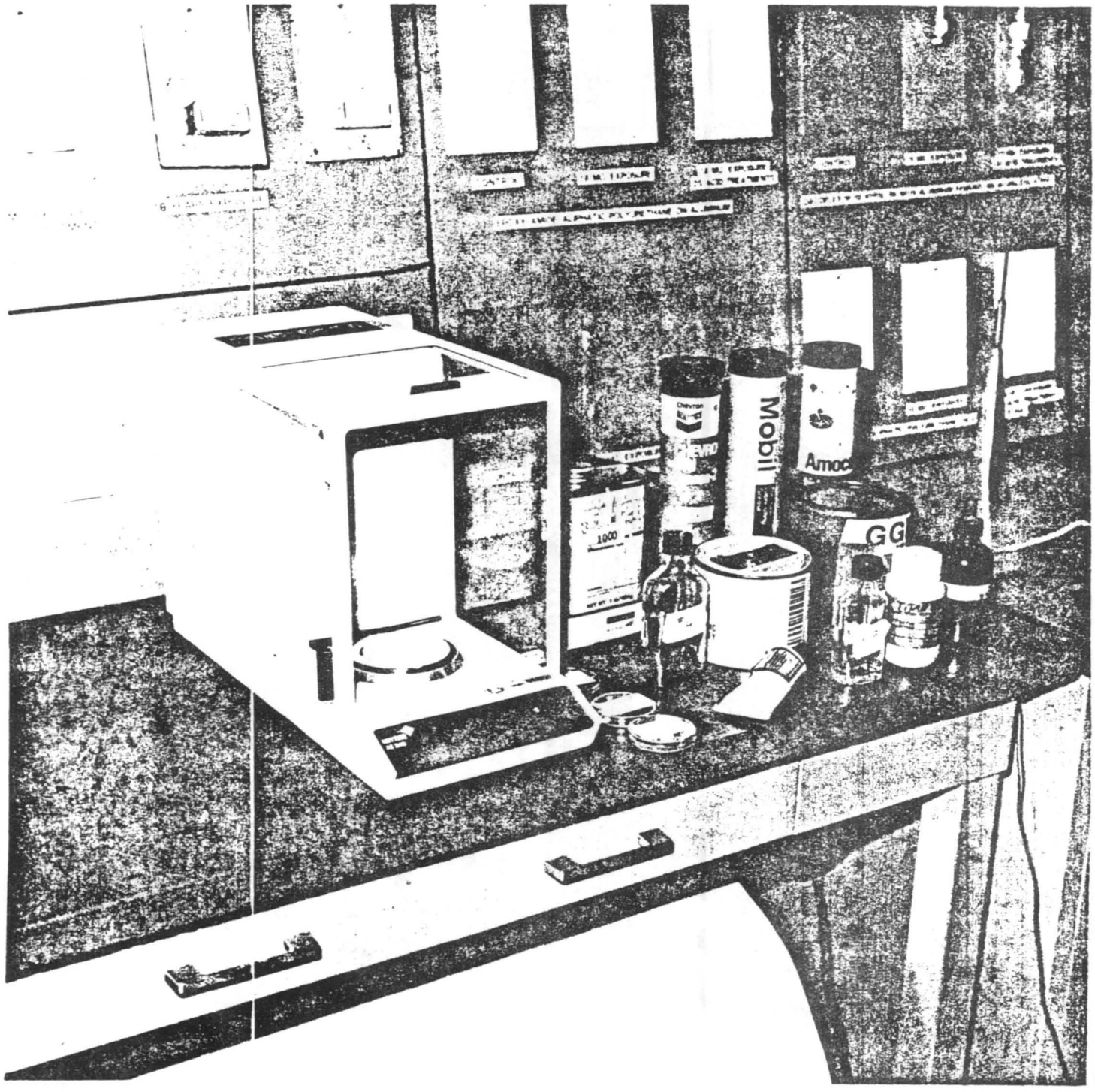

Figure 6. Hydrocarbons Tested

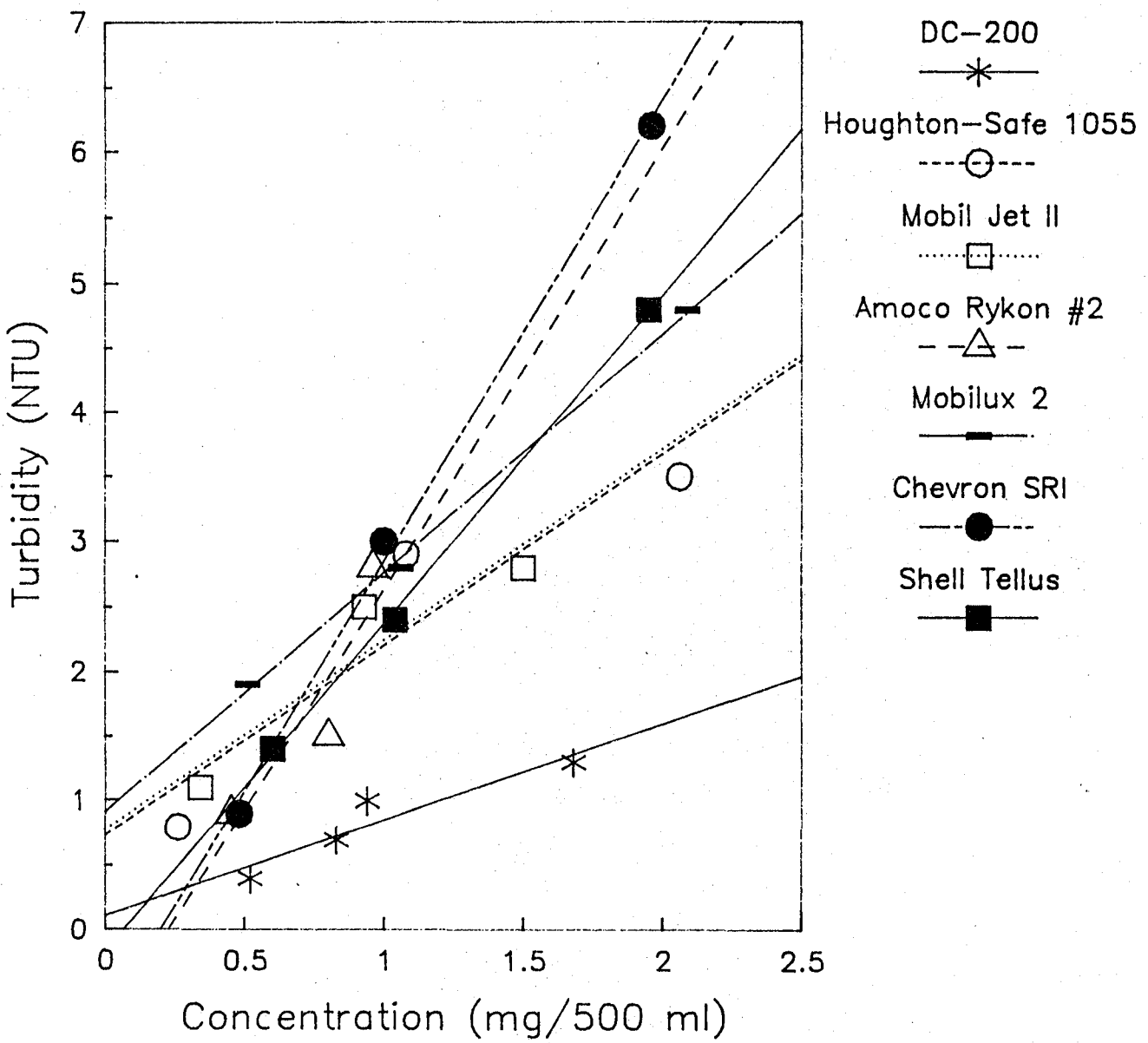

Figure 7. Ultrasonic – Turbidity Response

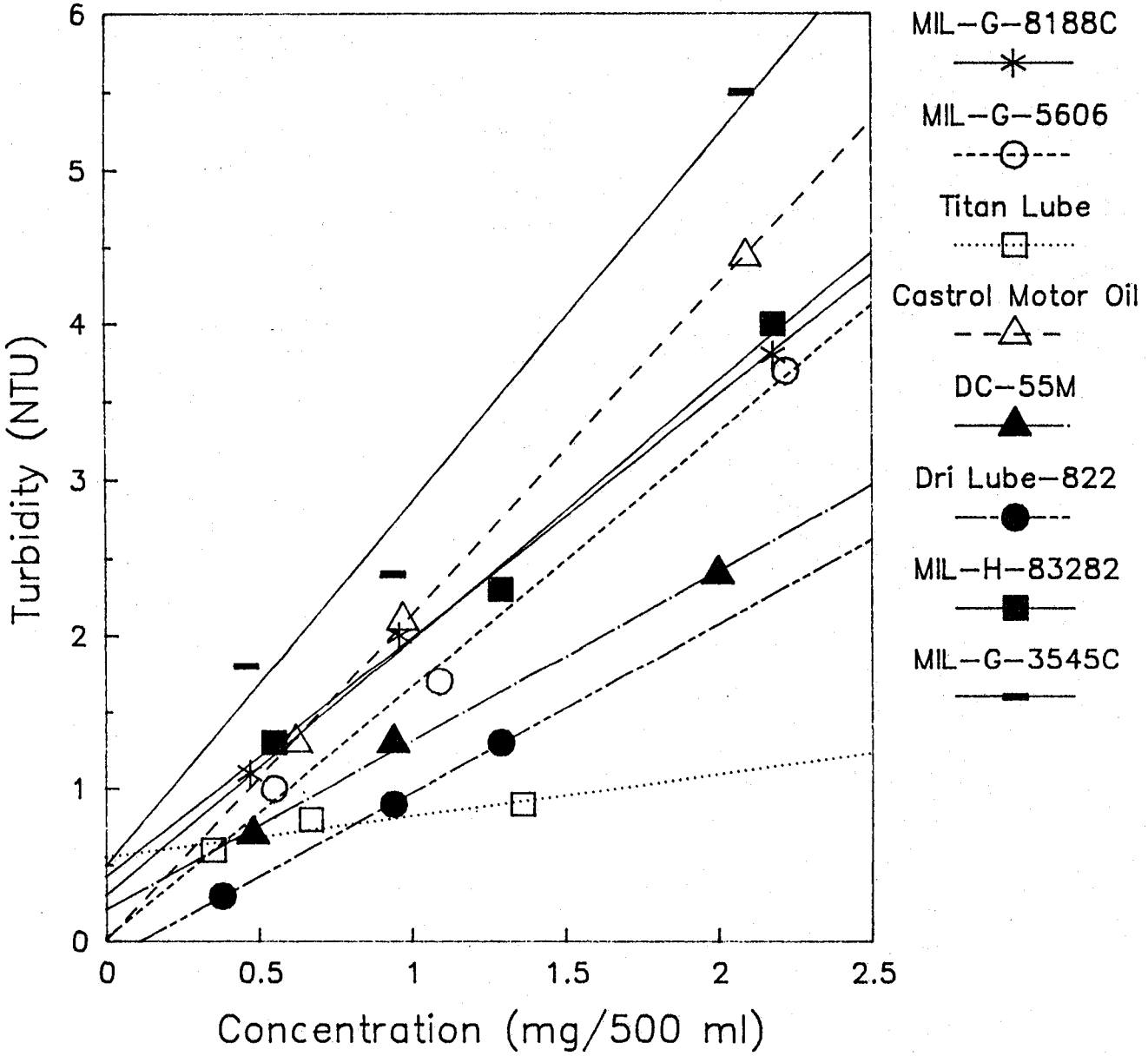

Figure 8. Ultrasonic – Turbidity Response

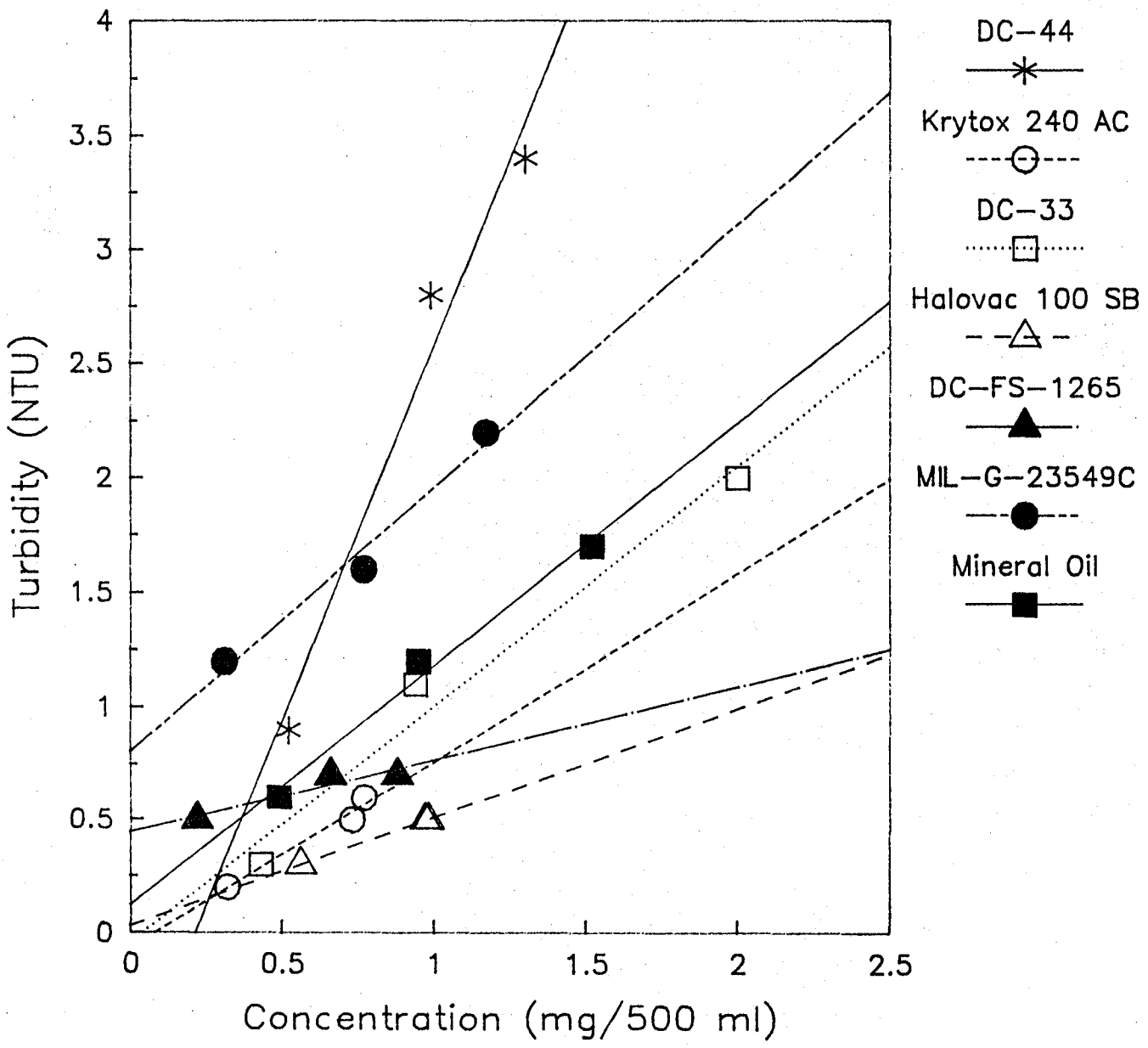

Figure 9. Ultrasonic – Turbidity Response

RESEARCHER:
DATE:

TEST #:
DESCRIPTION:

CLEAN BEAKER
CLEAN FITTING

WEIGHT OF FITTING & CONTAMINANT: _____

WEIGHT OF FITTING: _____

WEIGHT OF CONTAMINANT: _____

TIME (MIN)	0	2	4	6	8	10	15	20	25	30	35	40
TURBIDITY READING												

EMULSIFY

WEIGHT OF FITTING & CONTAMINANT BEFORE US _____

WEIGHT OF FITTING & CONTAMINANT AFTER US _____

WEIGHT OF CONTAMINANT REMOVED _____

% REMOVAL = [%]

FIGURE 10 - DATA SHEET

1991 NASA/ASEE SUMMER FACULTY FELLOWSHIP PROGRAM

JOHN F. KENNEDY SPACE CENTER
UNIVERSITY OF CENTRAL FLORIDA

GENERIC TECHNIQUES FOR THE CALIBRATION OF ROBOTS WITH APPLICATION OF THE 3-D FIXTURES AND STATISTICAL TECHNIQUE ON THE PUMA 500 AND ARID ROBOTS

PREPARED BY:	Dr. Hazem Tawfik
ACADEMIC RANK:	Professor
UNIVERSITY AND DEPARTMENT:	State University of New York - Farmingdale Mechanical Engineering
NASA/KSC	
DIVISION:	Mechanical Engineering
BRANCH:	Special Projects (RADL)
NASA COLLEAGUE:	Mr. V. Leon Davis
DATE:	August 9, 1991
CONTRACT NUMBER:	University of Central Florida NASA-NGT-60002 Supplement: 6

ACKNOWLEDGEMENTS

I would like to thank my KSC colleague Mr. Leon Davis for giving me such a wonderful opportunity to participate in the interesting activities taking place in the robotics section at KSC for a second year. Also, thanks should be extended to the whole robotics engineering team for their cooperation; especially Mr. Chau Le.

I am also grateful to the UCF program director Dr. E. Ramon Hosler for making the summer program as much fun as it was a challenge. Ms. Kari Stiles's enthusiasm and helpfulness was very much appreciated.

Many thanks to the NASA/KSC summer program directors Dr. Mark Beymer and Mr. Dennis Armstrong for their friendliness.

ABSTRACT

The main objective of this project is two fold: first, to provide the reader with a brief literature survey of the advanced robotics calibration techniques and indicate the advantages, disadvantages, and the suitability of each technique to KSC/RADL's current and future robotics applications. Secondly, to introduce RADL to a relatively simple, inexpensive, and generic technique that could be used in both laboratories and some operation site environments.

In addition, this report gives detailed explanation of the set up procedure, data collection and analysis using this new technique that was developed at the State University of New York at Farmingdale. The technique was used to evaluate the repeatability, accuracy, and overshoot of Unimate Industrial Robot, PUMA 500. The obtained data was statistically analyzed to provide an insight into the performance of the various robotics systems and components. Also, the same technique was used to check the forward kinematics against the inverse kinematics of RADL's PUMA robot.

Recommendations were made for RADL to use this technique for laboratory calibration of the currently existing robots such as the ASEA, high speed controller, Automated Radiator Inspection Device (ARID) etc. Also, recommendations were made to develop and establish other calibration techniques that will be more suitable for site calibration environment and robot certification.

SUMMARY

Industrial robots are known to facilitate and expedite many maintenance processes, reduce tedious manual tasks, enhance quality and improve accuracy of various engineering applications. Accordingly, the Robotics Applications and Development Laboratory (RADL) at NASA/KSC is currently developing numerous robotics systems to support Shuttle launch operations and preparations.

However, due to various sources of error in the design, manufacturing, and assembly of robotics systems, they experience a lack of accuracy in the positioning of their end effectors. Generally, industrial robots exhibit better repeatability than accuracy. In many cases, current industrial robots show excellent positioning repeatability but relatively poor absolute positioning accuracy. For on-line programming applications where positions are taught and encoder readings are recorded and replayed this will not present a serious accuracy problem as long as the robot control system is capable of repositioning the tool center point within acceptable range . On the other hand, in cases of off-line applications where robots are commanded to locate their end effectors at certain points within the work envelope, robot calibration would play an increasingly important role because most sources of errors will cumulatively influence the robot's accuracy. Therefore, a calibration procedure that is classified as both time-efficient and cost-effective is deemed necessary for RADL/KSC.

Accordingly, this report surveys the available techniques in the literature and examines its suitability for the current and future robotics applications and certification at Kennedy Space Center for both laboratory and on site calibrations. Two systems were recommended for this purpose: the first, is a modified theodolite (Optical telescope) equipped with a laser or ultrasonic generation device and the second is a vision system with a charge couple device (CCD) camera and calibration target. Although these systems provide excellent flexibility and accuracy in an actual robotics operational environment, they are relatively costly.

A simple, inexpensive and straight forward calibration technique that was developed at the State University of New York - Farmingdale is used to establish calibration procedure for RADL. The technique was used to evaluate the accuracy, repeatability, and overshoot of a PUMA 500 robot. Moreover, the report provides step by step statistical analysis that could lead to the source of a problem in a robotics system and help its troubleshooting scheme. RADL can follow the exact similar calibration procedure to calibrate and/or troubleshoot other robots such as ASEA, High speed controller, and the ARID.

TABLE OF CONTENTS

LIST OF ABBREVIATIONS AND ACRONYMS

RADEL - Robotics Applications And Development Laboratory

GTE - Gear Transmission Error

OPF - Orbit Process Facility

KSC - Kennedy Space Center

ARID - Automatic Radiator Inspection Device

TRE - Total Repeatability Error

USL - Upper Spec Limit

LSL - Lower Spec Limit

UCL - Upper Control Limit

LCL - Lower Control Limit

LIST OF ILLUSTRATIONS

I INTRODUCTION

1.1 OVERVIEW OF A ROBOT'S PRECISION

Most of the robotics applications require a considerable degree of positioning accuracy to be maintained by the manipulator's end effectors for a successful continuous operation of the robot. However, the precision and performance of most industrial robots were jeopardized due to inevitable design, manufacturing, environment, and operation cumulative sources of errors that are introduced to the robot's operation. Accordingly, many researchers have addressed the issue of robotic calibration that is mainly conducted using different devices and techniques to close the loop between the robot's tool center point (TCP) and its base coordinate origin point and accurately evaluate this vector. The pose of the end effector with respect to the robot base coordinate system is described in six parameters (three for location and three for orientation).

In general, robotic calibration could be summarized in four steps: measurement data, analysis, identification of key sources of errors, and elimination or compensation for these errors.

1.2 SOURCES OF ERRORS IN ROBOTICS SYSTEMS

(A) Design:

Encoder Resolution, Control System, Flexibility of links and joints

(B) Manufacturing:

Tolerances, Electronic and Mechanical Zeros not Coinciding

(C) Environmental:

Temperature Variation

(D) Operation:

Target Shift (Frame Shift)

In many cases, the sources of error are classified as geometric; affecting the dynamic parameters such as manufacturing tolerances on joints and links etc. and non-geometric; such as, the flexibility of joints and links, gear transmission error etc.

1.3 LITERATURE SURVEY

Robot calibration is a process that mainly aims at the improvement of a robot's accuracy by modifying the robot positioning software rather than changing or altering the design of the robot or its control system. Calibration assumes that a nominal relationship between the end-effector position and joint transducer readings is known but that this relationship is not necessarily accurate due to the previously indicated sources of errors.

Calibration procedures vary widely in their complexity and approach. For example, some robot calibration procedures only consider the joint transducer information while others may involve changes in the kinematic and/or dynamic model of the robot [1]. Accordingly, Roth et al. [1] classified calibration in three levels:

Level 1: To ensure that the reading from a joint sensor yields the correct joint displacement

This procedure is usually done as a part of the construction of the robot, and the user may perform such calibration if damage has occurred or if the joint has been disassembled for maintenance. At this level a 3D fixture could be used as indicated later in this report. Also, a different approach [2] involves the use of a polygonal mirror and a theodolite to determine the joints angles accurately Figure (1-1). In this method the operator looks through the theodolite and the joint is rotated until the operator sees his own reflection centered in the theodolite. When this occurs, the mirror surface is almost perfectly normal to the axis of the theodolite Figure (1-2). The particular measurement technique chosen at this level is a trade-off between precision and cost.

In robot calibration the essential issue is not the method but rather the ability to obtain a large number of measurements over a wide area of robot locations [2]. For this technique to be valid it is important to know the location of the theodolite in robot base coordinates which could be laborious and time consuming for the ARID application if not permanently fixed to its base.

Level 2: To improve the accuracy of the kinematic model of the manipulator

A number of different approaches have based on the most popular procedure that was established by Denavit and Hartenberg [3] for developing the kinematic model of a robot manipulator. For example Haung et al [4] of the Florida Atlantic University used the idea of a closed-loop mechanism to measure the actual positions of the manipulator end effector. The measuring device consisted of a passive instrumented mechanical linkage, with its one end fixed to the ground whereas the other end connected to the manipulator end effector through an extension bar

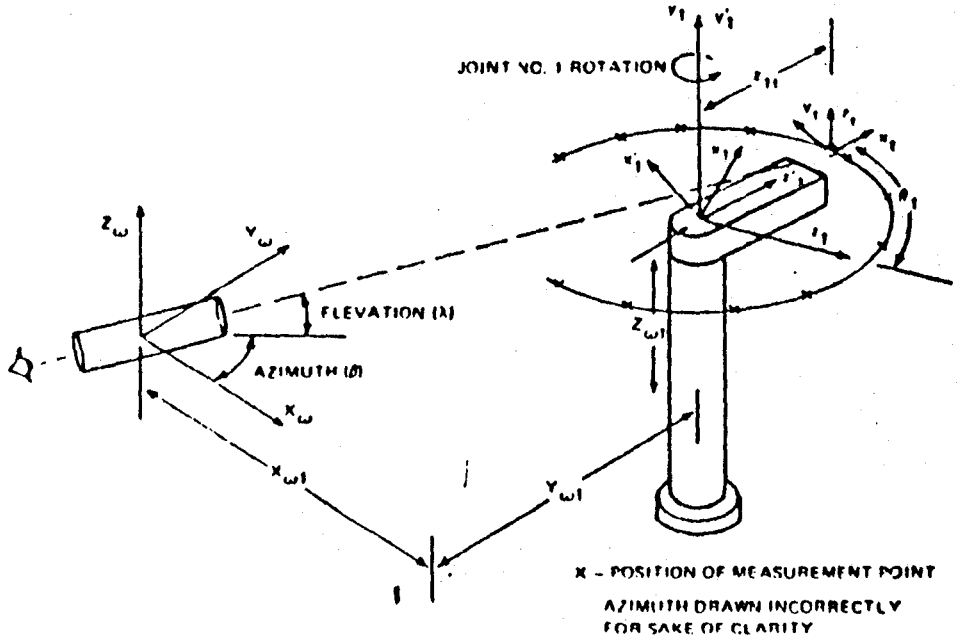

Fig.(1-1) One-degree-of-freedom calibration

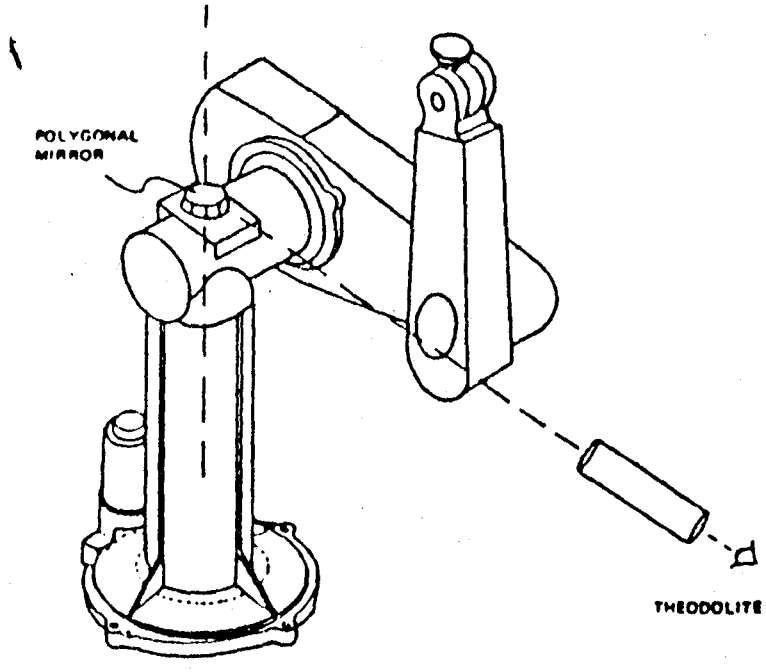

Fig.(1-2) Measuring the gear transmission error in joint 1

Fig(1-3). The ground end of the sensing linkage consists of a universal joint instrumented with position feedback devices and a linear scale type axis attached to it. Although this linkage seems inaccurate to be used as a calibration reference, also it is limited to the identification of the manipulator kinematic parameters caused by the geometric errors inherent to the arm. This method assumes rigid joints and links and does not account for their flexibility or the arm non-geometric inherent errors such as links deflection, joint flexibility, gear transmission error (GTE), clearance, backlash,etc. Also, this technique will not be suitable for application in the Orbit Process Facility (OPF) at KSC or with large and heavy arm such as the ARID.

Level 3: "Non-kinematic" (non-geometric) calibration

Non-kinematic errors in positioning of the end effector of a robot are due to effects, such as joint and link compliance, friction, and clearance. Also, if the robot is under dynamic (rather than kinematic) control, then correction for changes in the dynamic model of the robot constitutes a level 3 calibration.

A vision system technique Figure (1-4) is a promising level 3 robotic calibration technique but is not completely developed yet and its accuracy is still questionable particularly in the z-axis perpendicular to the camera lens. However, with a relatively small lens distortion and rather accurate calibration and evaluation of the camera intrinsic and extrinsic parameters, much better accuracy could be achieved and the vision system could be used to its full potential. It is a trade off between precision and cost. The calibration of the vision system consists of camera (eye) calibration, eye-to-hand calibration, and hand calibration see Fig(1-5). The calibration of such system is briefly outlined in the following [5]:

- Camera (eye) calibration

Camera calibration is the problem of determining the elements that govern the relationship or transformation between the 2D image that the camera perceives and the 3D information of the object. There are two kinds of parameters that define this 2D/3D relationship, namely, the intrinsic and extrinsic parameters. The intrinsic parameters are those that characterize the inherent properties of the camera and optics, such as the focal length, lens distortion, scale factor (relationship of the computer image coordinate to the true image coordinate), and image center(point where the optical axis intersects with the image plane). The extrinsic parameters are those defining the position and orientation of the camera with respect to the world coordinate system. There are six of them: three for rotation, and three for translation.

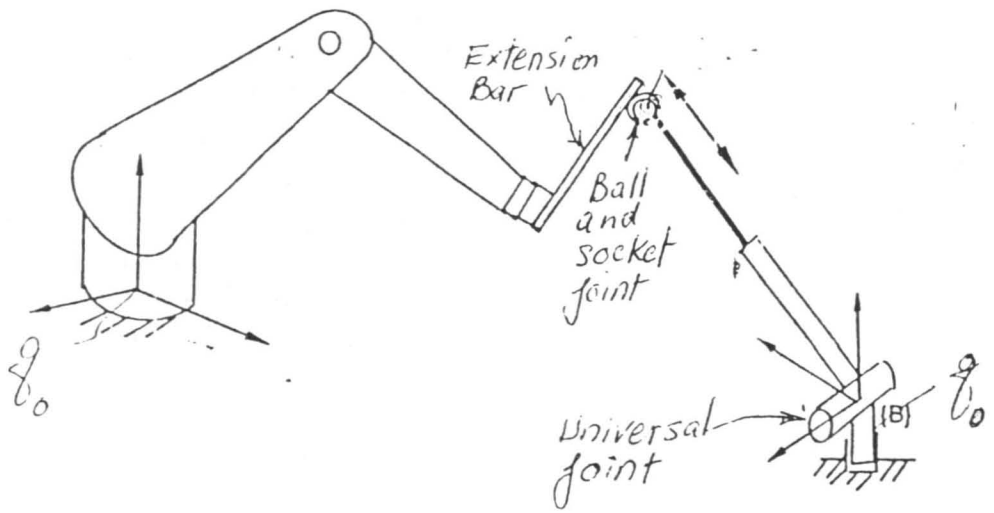

Figure (1-3) System configuration of the passive instrumented Mech. Linkage

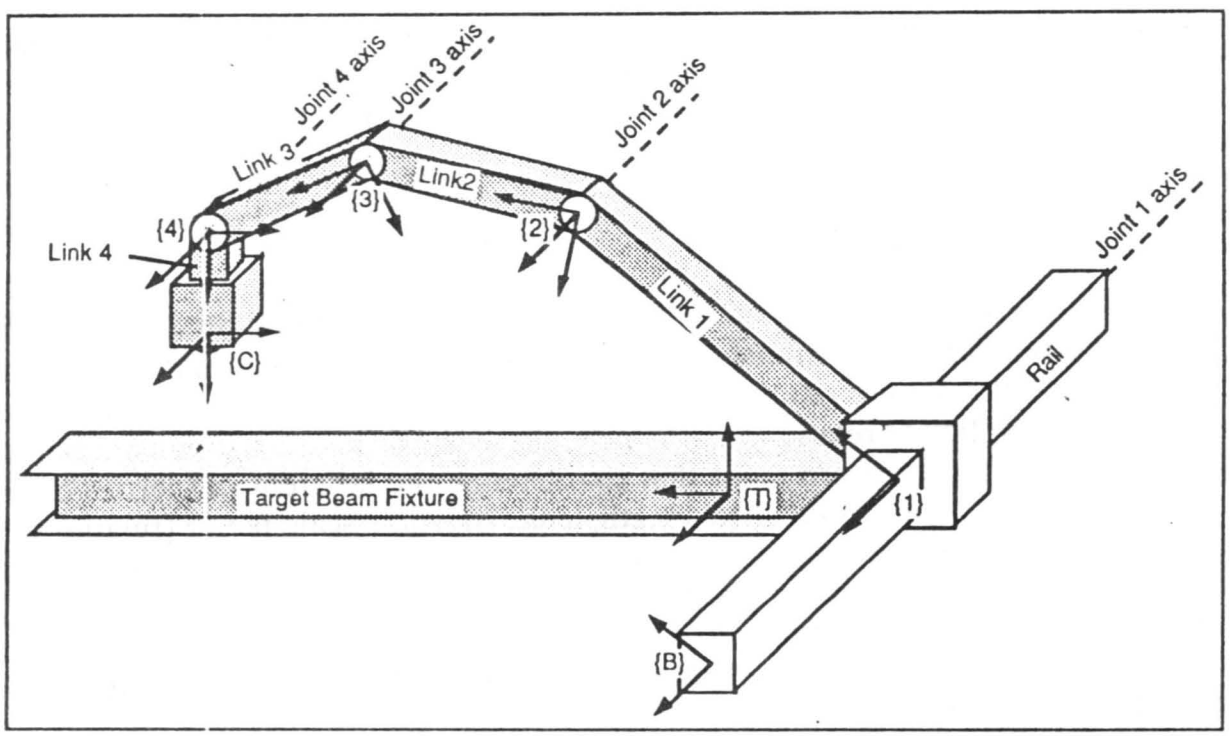

Figure (1-4) Naming conventions and coordinate frames for the ARID robot.

- Robot Eye-to-Hand Calibration

3D robotics hand/eye calibration is the task of computing the relative 3D position and orientation between the camera and the robot gripper in an eye-on-hand configuration, meaning that the camera is rigidly connected to the robot gripper. The camera is either grasped by the gripper, or just fastened to it. More specifically, this is the task of computing the relative rotation and translation (homogeneous transformation) between two coordinate frames, one centered at the camera lens center, and the other at the robot gripper. The gripper co-ordinate frame is centered on the last link of the robot manipulator. All 3D measurements made using TV cameras refer to measurement relative to the camera. In order to relate the 3D measurement information to the robot world frame, it is necessary to know the transformation between the robot hand and eye. This is crucial for any robotic vision system.

Whitney et al [2] also generated a model for joint compliance and link bending, the apparatus is shown in Fig.(1-6). Forces were applied to the robot arm first at F_1 and F_2. Deflections were measured at X_i (i=1,7). The resulting data fit a model of rigid links connected by compliant joints that act as torsional springs. The stiffness at the joints could be evaluated and used to calculate the deflection under any payload. Inaddition, backlash was evaluated for a horizontal arm where gravity loading forces the backlash to one extreme. A vertical force was applied at F_2. Displacement is measured at X_4. When the applied torque is less than the torque due to the arm's weight, the arm's weight keeps the backlash loaded. The arm acts as rigid links on torsional springs. As the applied force increases, the arm is lifted. The arm passes through the backlash dead zone, and is forced against the opposite extreme. Again the arm acts like a linear spring. The backlash dead zone shows up in the force deflection curves drawn in Figure(1-7).

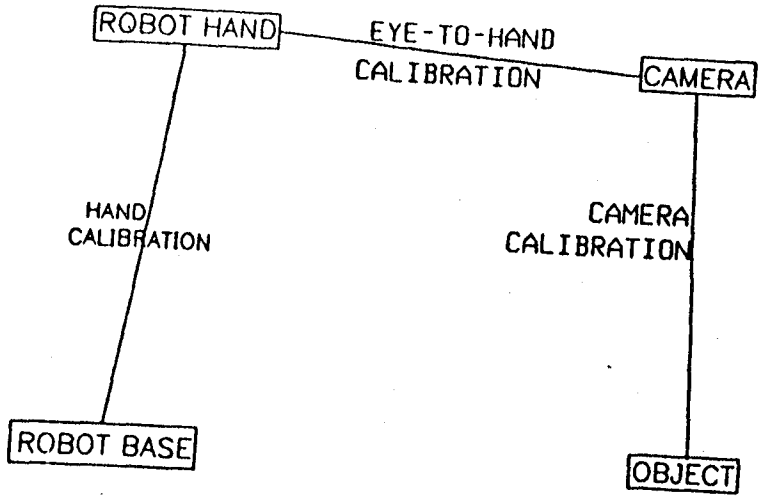

Figure(1.5) To obtain the 3D position and orientation of an object relative to the robot world base, it is necessary to do three calibrations, namely robot hand, eye-to-hand and eye (camera) calibration

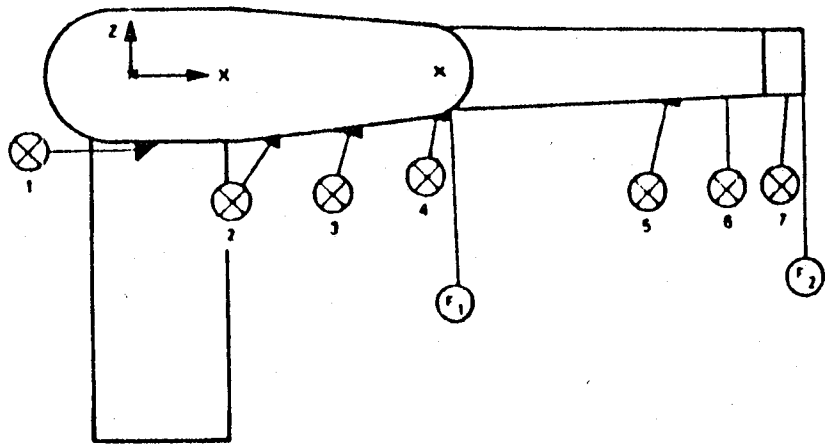

F REPRESENTS FORCE MEASUREMENT
⊗ REPRESENTS POSITION MEASUREMENTS

Fig. (1-6) Measurement points for force deflection curves

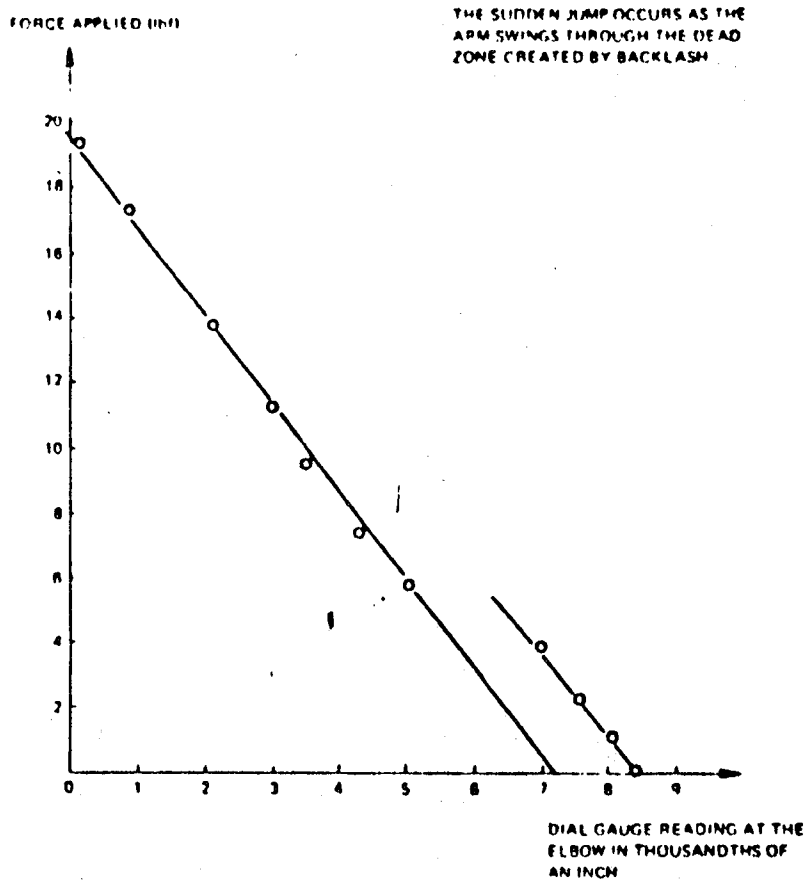

Fig. (1-7) Backlash in joint 2

II MEASUREMENT OF ACCURACY AND REPEATABILITY OF UNIMATE INDUSTRIAL ROBOT PUMA 500

2.1 OBJECTIVES

The objectives of this task are first: to develop a simple, inexpensive, and straightforward robotic calibration technique to be used for the certification of the high speed controller and the calibration of the ARID. Second: to demonstrate to NASA/KSC robotics group the use of the 3D fixtures and the method of evaluation of the repeatability, overshoot, relative and absolute accuracy of any robot. Third: To provide statistical techniques for the evaluation of these parameters, reduction of noise in the processed data, and the analysis of measured data to examine the performance of a robot. This statistical technique could also be helpful in the troubleshooting of various sources of errors. In addition this technique will have direct application in the certification of the High Speed Controller as well as the calibration procedure of the ARID robot.

2.2 EVALUATION OF THE PUMA 500 REPEATABILITY:

2.2.1 SET UP AND PROCEDURE:

The 3D fixture Figure (2-1) fitted with dial indicators in the X,Y, and Z direction was used in the evaluation of the PUMA's repeatability. The fixture was leveled, clamped to the calibration table, and positioned within the work envelope of the PUMA robot. A square cross-section calibration bar 1.5"X1.5"X6" Figure (2-1A) was fitted to the adaptor plate at the end effector of the arm. Each face of the calibration bar is aligned with an axis of the fixture. The alignment was checked by moving the bar in the direction of an axis and no variations were observed in the other two axes. However, if the orientation was of concern to the researcher, a fixture shown in Figure (2-2) will measure the position and orientation of the calibration bar and give necessary information of the end effector pose.

The fixture in Figure (2-1) was used and the robot arm was moved using the teach pendant to bring the calibration bar between the indicators and depress each one 0.250" approximately. At this setting the indicators were zeroed off and this position was " taught" to the robot i.e. all the encoders readings at this position were saved in the computer memory and remembered by the robot as point "A" Figure (2-1). The robot arm and the calibration bar were moved to various locations within the work envelope and the zone of operation, such as points "B","C","D" etc. Move the TCP back to the previously taught point "A". Make sure that the indicator spindles are detracted so they will not be damaged by the returning calibration bar to point "A". Gently return the indicators to touch the calibration bar and record the three

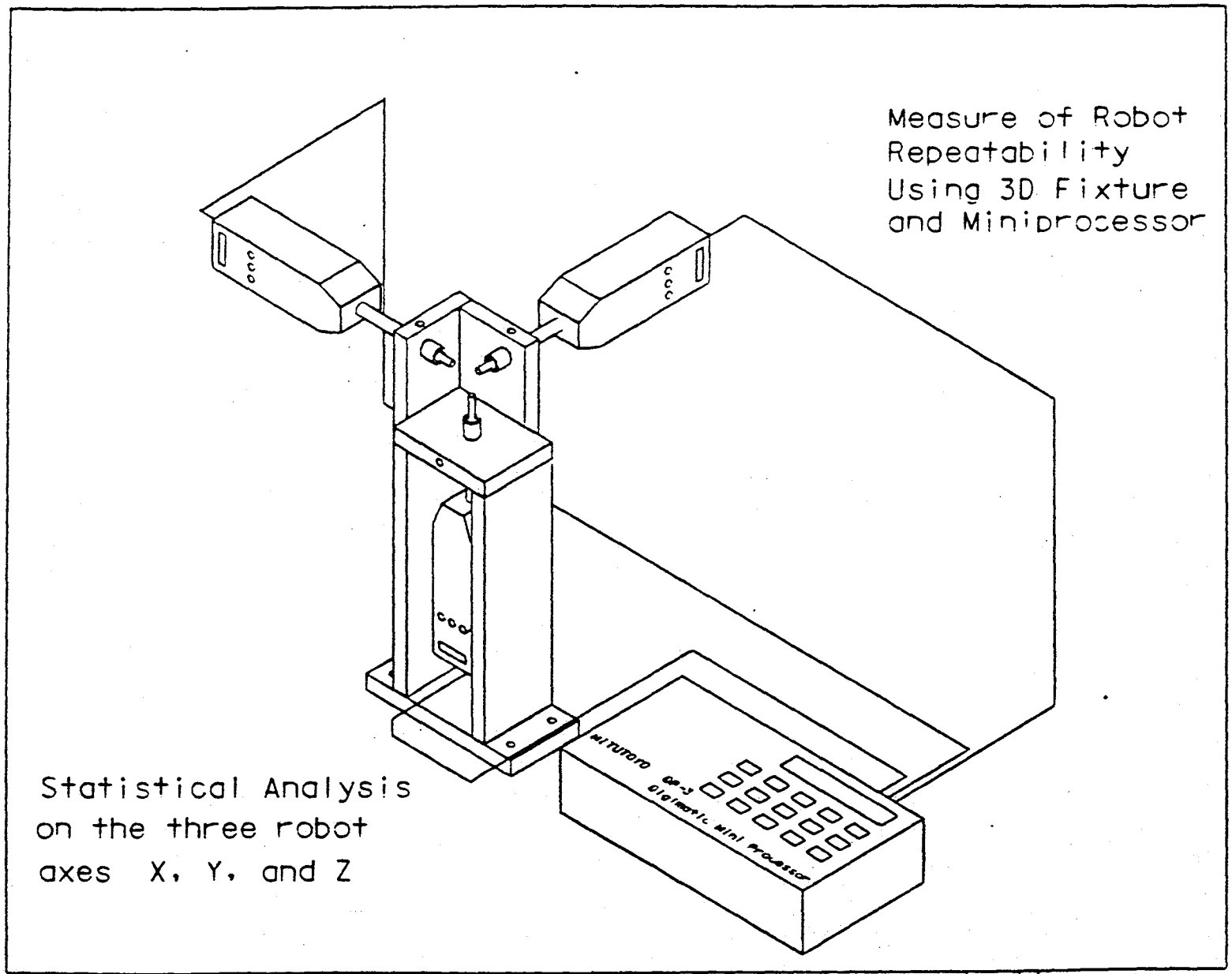

Figure (2-1) 3D Fixture For measuring repeatability

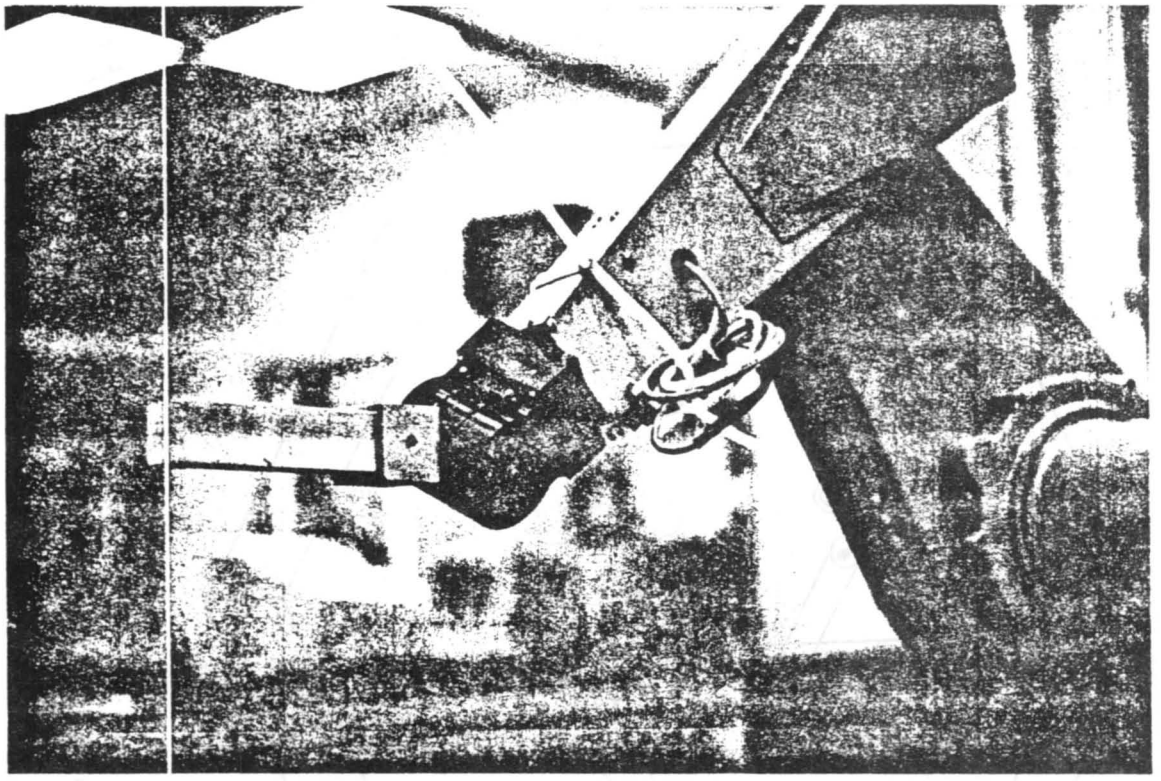

Figure (2-1A) Calibration Bar (1.5"x1.5"x6")

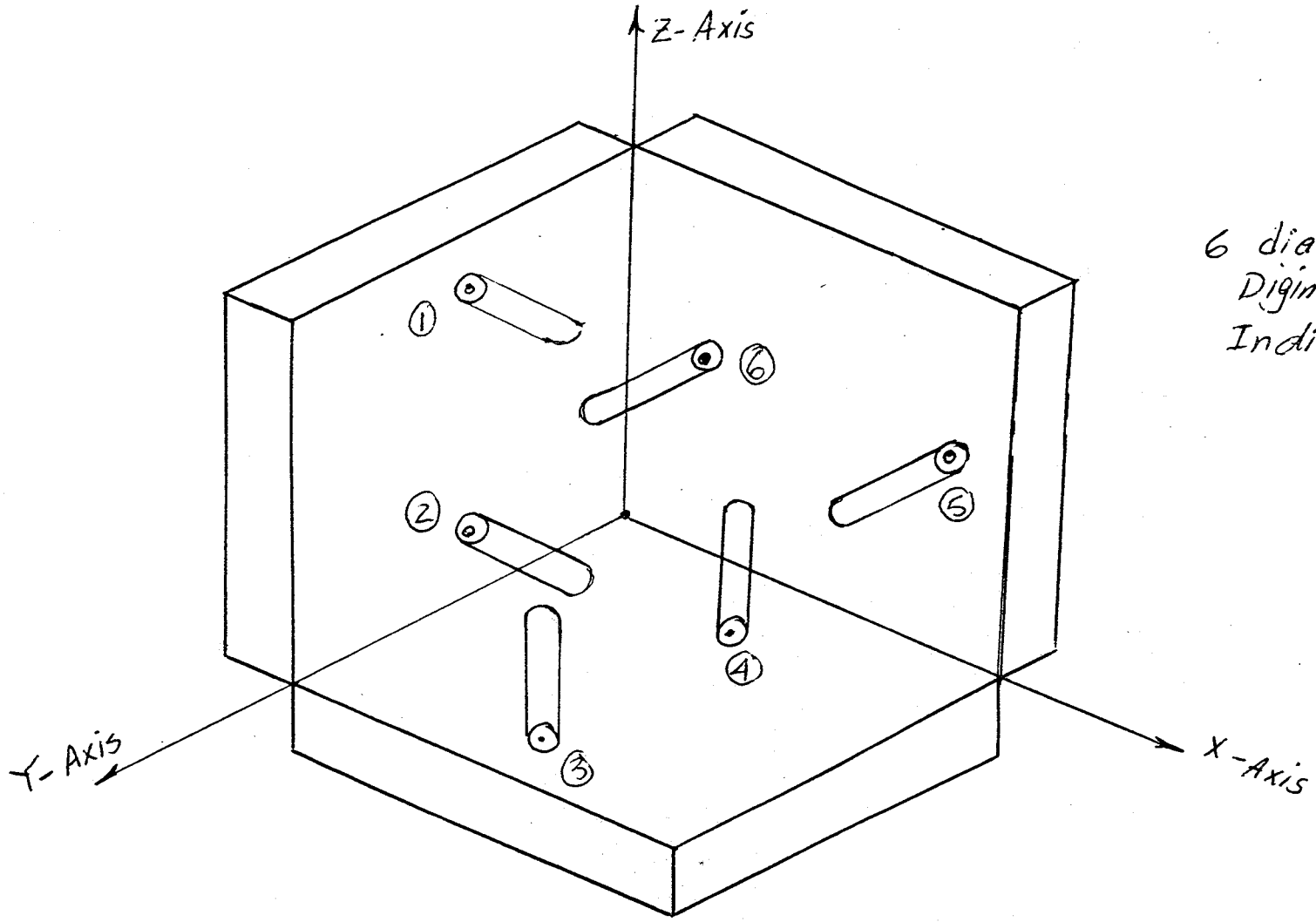

6 dials or Digimatic Indicators

Figure (2-2) 3-D Fixture Provides measurements of the position and orientation errors

components X, Y, and Z of the repeatability error vector for this run. Repeat the same procedure for ten to fifteen times or more. In the current work twelve runs were conducted for the evaluation of the PUMA repeatability and the results were recorded in table (1).

Table (1) X, Y, and Z Components of the Repeatability Error Measurement

RUN No.	X - Axis inch	Y - Axis inch	Z - Axis inch
1	-0.003	+0.001	-0.008
2	+0.001	+0.001	-0.002
3	+0.003	+0.000	-0.003
4	+0.003	-0.003	+0.002
5	+0.004	-0.002	+0.002
6	+0.002	+0.000	+0.000
7	+0.003	+0.000	+0.000
8	+0.003	-0.001	+0.000
9	-0.003	+0.001	+0.001
10	-0.001	-0.001	+0.000
11	-0.001	+0.000	-0.001
12	+0.004	-0.002	-0.003

2.2.2 RESULTS AND STATISTICAL ANALYSES:

The plots of the repeatability errors for each axis are shown in Figures (2-3), (2-4), and (2-5). The Mean and the Standard Deviation of each axis positional errors were calculated and the corresponding Histograms were constructed as shown in Figures (2-6), (2-7), and (2-8). In the present analysis it was assumed that the PUMA has to meet positioning requirement of $\pm$ 0.010 inch as a tolerance limits.

The study of these figures will give clear indication of the performance and capability of the robot that was tested. When the points in Figures (2-3), (2-4), and (2-5) appear very close to the control limits or beyond, this will be sufficient sign that calls for the immediate maintenance of the robot.

$$\text{The mean positional error} = \frac{1}{N} \sum_{i=1}^{N} d_i$$

$$\text{The standard deviation } (\sigma) = \sqrt{\frac{\sum_{i=1}^{N} (d_i - \text{mean})^2}{N-1}}$$

Accordingly, the components average of the positioning error vector for the repeatability of the PUMA could be obtained from the following table:

Table (2) Average Values of The Positioning Error Vector Components

X - Axis	Y - Axis	Z - Axis
0.0012"	-0.0005"	0.001"

The positioning error vector for the repeatability of the PUMA 500 in the RADL at KSC now reads the following:

.0012 i + -0.0005 j + 0.001 k

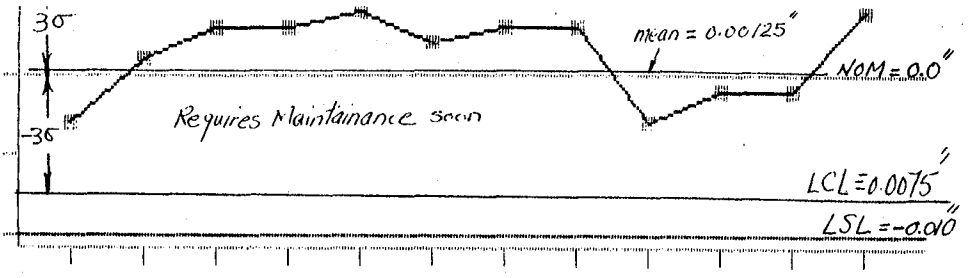

MAX:	+0.00400	USL:	+0.01000
XBAR:	+0.00125	NOM:	+0.00000
MIN:	-0.00300	LSL:	-0.01000
SIG:	+0.00249	RNG:	0.00700
n: 12	NUSL: 0	NLSL:	0

Figure (2-3) Plot of Repeatability Errors X-Axis

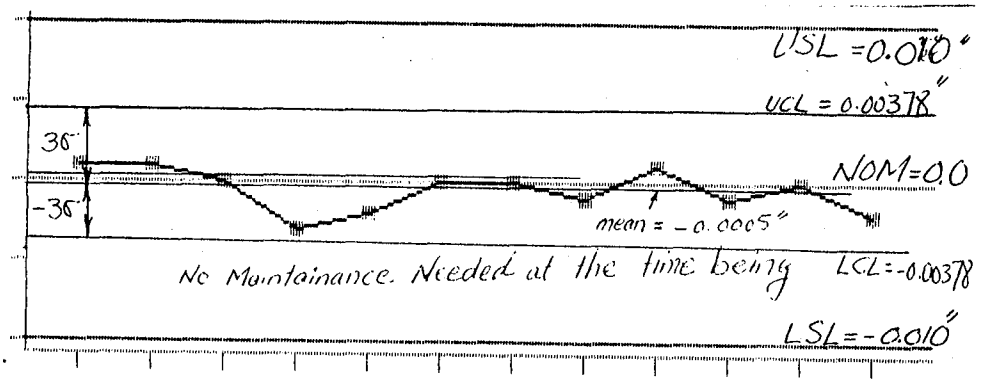

MAX:	+0.00100	USL:	+0.01000
XBAR:	-0.00050	NOM:	+0.00000
MIN:	-0.00300	LSL:	-0.01000
SIG:	+0.00126	RNG:	0.00400
n: 12	NUSL: 0	NLSL:	0

Figure (2-4) Plot of Repeatability Errors Y-Axis

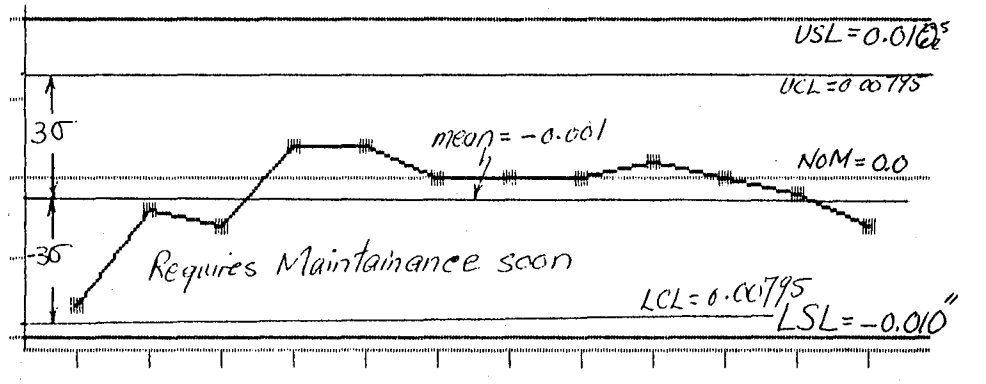

MAX:	+0.00200	USL:	+0.01000
XBAR:	-0.00100	NOM:	+0.00000
MIN:	-0.00800	LSL:	-0.01000
SIG:	+0.00265	RNG:	0.01000
n: 12	NUSL: 0	NLSL:	0

Figure (2-5) Plot of Repeatability Errors Z-Axis

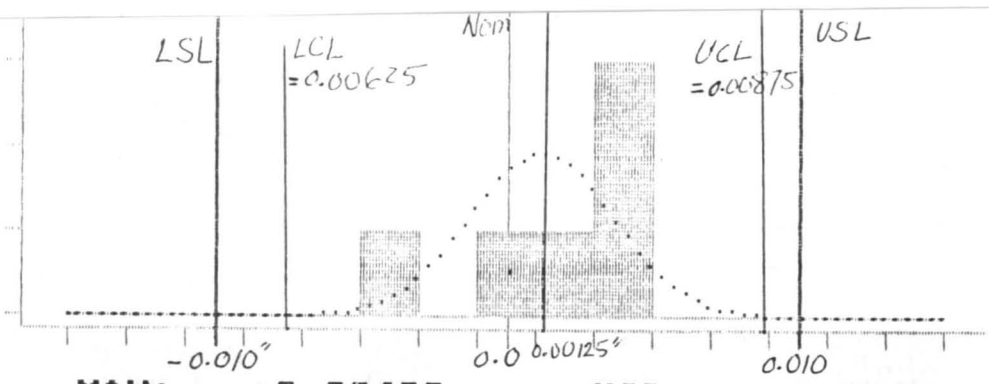

MAX:	+0.00400	USL:	+0.01000
XBAR:	+0.00125	NOM:	+0.00000
MIN:	-0.00300	LSL:	-0.01000
SIG:	+0.00249	RNG:	0.00700
MODE:	+0.00400	INTERVAL:	+0.00200

Figure (2-6) Histogram for Repeatability Errors X-Axis

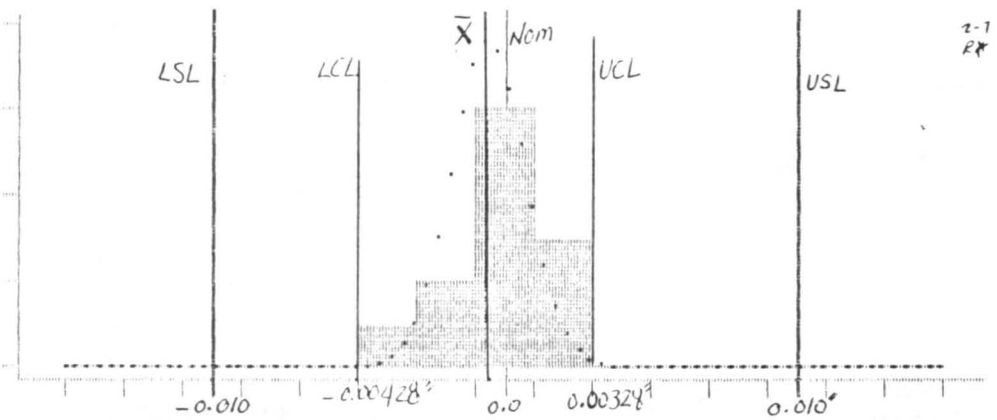

MAX:	+0.00100	USL:	+0.01000
XBAR:	-0.00050	NOM:	+0.00000
MIN:	-0.00300	LSL:	-0.01000
SIG:	+0.00126	RNG:	0.00400
MODE:	+0.00000	INTERVAL:	+0.00200

Figure (2-7) Histogram for Repeatability Errors Y-Axis

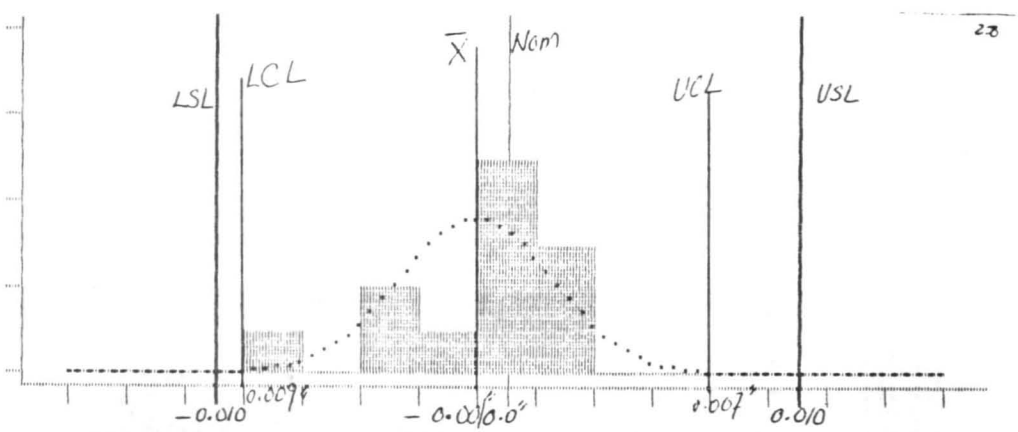

MAX:	+0.00200	USL:	+0.01000
XBAR:	-0.00100	NOM:	+0.00000
MIN:	-0.00800	LSL:	-0.01000
SIG:	+0.00265	RNG:	0.01000
MODE:	+0.00000	INTERVAL:	+0.00200

Figure (2-8) Histogram for Repeatability Errors Z-Axis

The above error vector should be compensated for, only, in the forward Kinematics software. After the introduction of this correction model in the software, the calibration procedure should be repeated once more to evaluate the degree of improvement in the robot repeatability that could be measured using the following parameters.

The Total Repeatability Error (TRE):

$$TRE = \sqrt{(\text{Ave. Error}_x)^2 + (\text{Ave. Error}_y)^2 + (\text{Ave. Error}_z)^2}$$

The PUMA's (TRE) could easily be calculated as follows:

$$\sqrt{\{(0.00125)^2 + (-0.0005)^2 + (0.001)^2\}} = 0.00167 \text{ INCH}$$

The (TRE) represents the magnitude of the repeatability error vector as well as the radius of the repeatability error sphere.

2.2.3 IMPORTANT PARAMETERS IN ROBOTICS CALIBRATION

There are important statistical parameters that should be evaluated and used as guide lines to examine the robot's capability of meeting the positioning requirements (upper and lower specification limits) of its end effector to perform a certain task. These parameters are described and evaluated for the PUMA robot as shown in the following:

(A) Process (Robot) Capability Index C_p:

The robot capability is evaluated by this parameter C_p (see reference [6] for more details) that is defined as

follows:

$$C_p = \frac{\text{Upper Spec Limit - Lower Spec Limit}}{6*\text{Standard Deviation}} = \frac{UCL - LCL}{6*\sigma}$$

(B) The Shift or The Off Set Parameter C_{pk}:

It is an important parameter to identify if the error measurement is experiencing any major off set or shift from the zero error line. This parameter is defined as follows:

$$C_{pk} = \text{Minimum of } \left\{ \frac{(\text{Average Error - Lower Spec Limit})}{3 * \text{Standard Deviation}} \right\} \text{ or } \left\{ \frac{(\text{Upper Spec limit - Average Error})}{3 * \text{Standard Deviation}} \right\}$$

A robot is classified as capable of performing a task that requires certain tolerance limits and specifications on the positioning of its end effector, if the repeatability error data of this robot exhibit C_p and C_{pk} values ≥ 1. However, the higher the values of C_p , and C_{pk} are, the better the suitability and capability of the robot to perform that task.

In particular, the C_{pk} parameter lends itself very well to the evaluation for the degree of improvement in a robot's accuracy and repeatability after calibration. The comparison of C_{pk} values before and after the robot calibration and error compensation will give a good indication of the degree of improvement in a robot's performance.

The previously described statistical parameters were evaluated based on the PUMA repeatability error measurement given in tables (1) and (2) for each axis. The values for σ , C_p , and C_{pk} were calculated based on an assumed allowable positioning tolerance for the PUMA of $\pm$ 0.010". The obtained results were tabulated in table (3) below:

Table (3) Statistical Parameters

Parameter	X - Axis	Y - Axis	Z - Axis
σ	0.00249	0.00126	0.00265
Cp	1.338	2.645	1.258
Cpk	1.17	2.513	1.132

The study of the obtained statistical parameters in table (3) indicates that the PUMA robot is classified as capable of positioning its TCP at a previously recorded point repeatedly within the acceptable tolerance zone of ± 0.010" . The probability that the PUMA will fail to meet this tolerance requirement could be calculated as follows:

Area under the curve of the Standard Normal Distribution bounded by the Lower Spec Limit (LSL) and (-∞):

Find the value of A_1 for $\frac{\text{LSL - Average Error}}{\text{Standard Deviation } (\sigma)}$ use tables in Appendix

Find the value of A_2 for $\frac{\text{USL - Average Error}}{\text{Standard Deviation } (\sigma)}$ use tables in Appendix

Probability of failure = $A_1 + A_2$

The study of table (3) indicated that the most susceptible axis for failure is the PUMA's Z - Axis. Therefore, applying the probability of failure study on that axis shows the following:

$$\frac{\text{LSL - Average Error}}{\text{Standard Deviation } (\sigma)} = \frac{-0.01 - 0.001}{0.00265} = -4.15$$

From table (1) in the appendix the probability corresponding to - 4.15 is Zero i.e. $A_1 = 0.0$

$$\frac{\text{USL - Average Error}}{\text{Standard Deviation } (\sigma)} = \frac{0.01 - 0.001}{0.00265} = 3.39$$

From table (2) in the appendix the probability corresponding to 3.39 is 0.0003 i.e. $A_2 = 0.0003$

The Probability = $A_1 + A_2 = .0003$ i.e 0.03%

Briefly, using this calibration technique on the PUMA 500 at the RADL indicates that the robot is capable of repeating the recorded position of its TCP within ± 0.010" with probability of failure of 0.03%.

2.3 MEASUREMENT OF A ROBOT'S RELATIVE ACCURACY (i.e. FORWARD KINEMATICS VERSUS THE INVERSE KINEMATICS)

In most robots the forward kinematic model is usually a closed form accurate mathematical model. The inverse kinematic model however usually has intrinsic inaccuracy due to the linear approximation of the Jacobian matrix that results in accumulation of errors in that model. Thus the relative calibration of the inverse kinematics against the forward kinematics is a useful approach in many six degrees of freedom manipulators. In the ARID both the inverse and forward kinematic models are as accurate because both are closed form solutions.

The calibration of a Robot and the measurements of its relative accuracy requires two 3D fixtures as shown in Figure(2-9).

2.3.1 SET UP PROCEDURE:

Place the two fixtures at a reasonable distance from each other within the work envelope of the robot. Align the X,Y, and Z axis of each fixture with respect to the robot axis and with respect to each other following the same technique previously explained in section 2.2. Level the fixtures and clamp them to the calibration table. Move the robot arm with the teach pendent to place the calibration bar between the indicators of the first fixture. Align the fixture coordinates with the robot base or world coordinates such that each indicator is depressed about 0.250".

Zero off all three indicators and record this point as "origin 1" see Figure (2-9). Establish a frame "frame 1" or a coordinate system with its origin at this point "origin 1" for the first fixture. Repeat the same with the other fixture to establish "frame 2" with "origin 2" at the second fixture. Make sure that "origin 1" and "origin 2" are also recorded with respect to the other frame under different name i.e. "origin 1" should be recorded with respect to "frame 2" under a different name such as "origin 3" and do the same for "origin 2" record this point with respect to "frame 1" under a different name such as "origin 4". Display the pose at "origin 1" or "origin 3" in relation to "frame 2" and copy three values for the position and three angles for the orientation on a separate sheet. Note that the 6 values specifying a recorded pose at a certain point such as "origin 1,2,3, or 4" are calculated by the forward kinematics model. Once more, display the pose at "origin 2" and "origin 4" in relation to "frame 1". Make sure that both poses compare very closely before proceeding to the next step.

Locate the calibration bar end at "origin 1" and zero off all the indicators. Do the same for "origin 2". Command the robot to move from "origin 2" to reach "origin 1" by entering the pose six values copied earlier on a separate sheet. Note that the

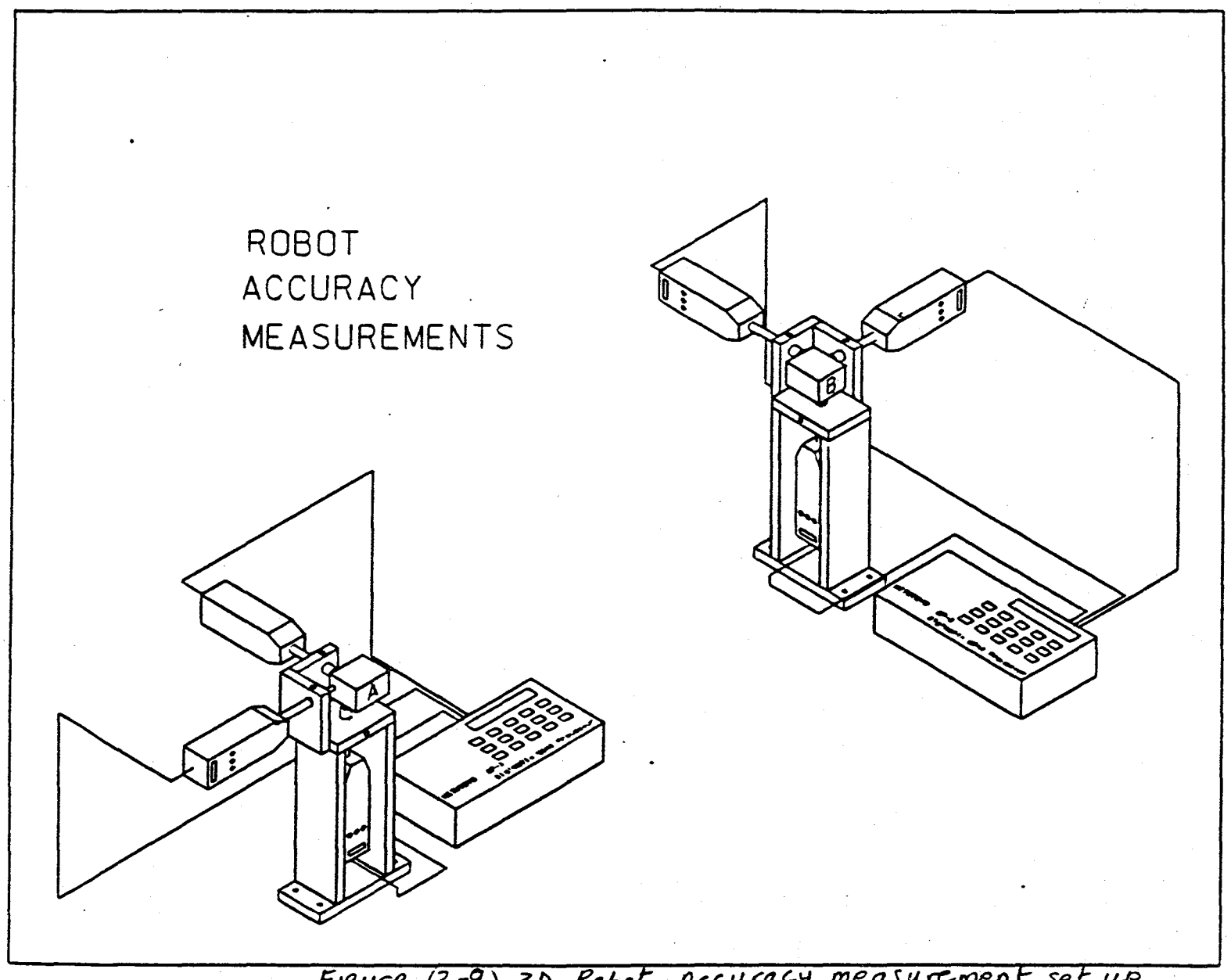

Figure (2-9) 3D Robot Accuracy measurement set up

inverse kinematic model will receive the pose information and calculate the joints angle required to position the robot at that commanded point. Write down the readings of the three indicators. These three readings represent the error vector in the inverse kinematic model relative to the forward kinematic model in that run. Move the robot to the recorded "origin 1" and again zero off the indicators. Repeat the process of shuttling the robot between the two fixtures ten to twenty times and record the error vector for each run.

In the current work ten runs were conducted on the PUMA 500 and the results are given in table (4):

Table (4) Error Vectors of The Inverse Kinematics Relative to the Forward Kinematic Model of the PUMA 500.

RUN No.	X - Axis	Y - Axis	Z - Axis
1	-0.007	-0.001	0.001
2	0.000	-0.005	0.009
3	-0.002	-0.002	0.002
4	-0.003	-0.001	0.004
5	-0.004	-0.001	0.003
6	-0.003	-0.002	0.004
7	0.001	-0.002	0.003
8	0.002	-0.002	0.002
9	-0.004	-0.001	0.004
10	0.001	-0.004	0.003

2.3.2 RESULTS AND ANALYSIS

The obtained results for the relative accuracy of the PUMA were analyzed in a similar fashion as the repeatability data were analyzed. The average X, Y, and Z components of the relative error vector are given in the following:

Table (4) The average component of the relative error vector

X - Axis	Y - Axis	Z - Axis
-0.0019"	-0.0021"	0.0035"

Accordingly, the relative error vector of the PUMA 500 in the RADL at KSC now reads the following:

$$-0.0019\,i - 0.0021\,j + 0.001\,k$$

The previous relative error vector should be compensated for in the inverse kinematics model. After compensation for that error vector the relative calibration procedure should be conducted once more to examine the degree of improvement in the robot performance. The improvement is measured by the following parameters:

The magnitude of the error vector is evaluated using the following formula:

$$= \sqrt{\{(\text{Ave. Error}_x)^2 + (\text{Ave. Error}_y)^2 + (\text{Ave. Error}_z)^2\}}$$

$$= 0.0045 \text{ inches}$$

The comparison of the total repeatability error (0.00167") with the total relative error (0.0045") indicated what always had been expected with industrial robots, they are more repeatable than accurate with an order of magnitude of almost 3. It is expected the ARID robot will not exhibit such discrepancy between its total repeatability error and relative accuracy error because both the ARID's forward and inverse kinematic models are closed form solutions. However it is expected that the ARID's total absolute accuracy will be some orders of magnitudes higher than its (TRE) mainly because of its joints and links flexibility. Therefore, the proposed calibration scheme for the ARID in section 3 is based on the expected high

repeatability of the ARID. This will preclude the need for rigorous calibration techniques for the ARID's absolute accuracy.

The comparison of the values of C_p, C_{pk} in tables (3) and (5) emphasizes the fact that the PUMA's relative accuracy and repeatability errors did not disqualify it from being capable of meeting the specs. The probability that the PUMA will fail to meet the specs is approximately 1%.

Table (5) Statistical Parameters For Relative Accuracy Errors

Parameter	X - Axis	Y - Axis	Z - Axis
σ	0.0027	0.0013	0.00206
Cp	1.234	2.564	1.618
Cpk	0.999	2.025	1.052

2.4 OVERSHOOT MEASUREMENTS OF THE PUMA

The overshoot is well described in Figure (2-10). The 3D fixtures are also used to measure the overshoot of the PUMA at three different speeds. The measurements shown in table (6) indicated that as the speed increases the overshoot is also increased. Note that the overshoot of the ARID could be evaluated by using the same 3D fixture technique applied to the PUMA.

Table (6) Overshoot for Puma 500

PERCENT. SPEED	OVERSHOOT
SPEED 5	0.0000"
SPEED 50	0.0040"
SPEED 100	0.0090"

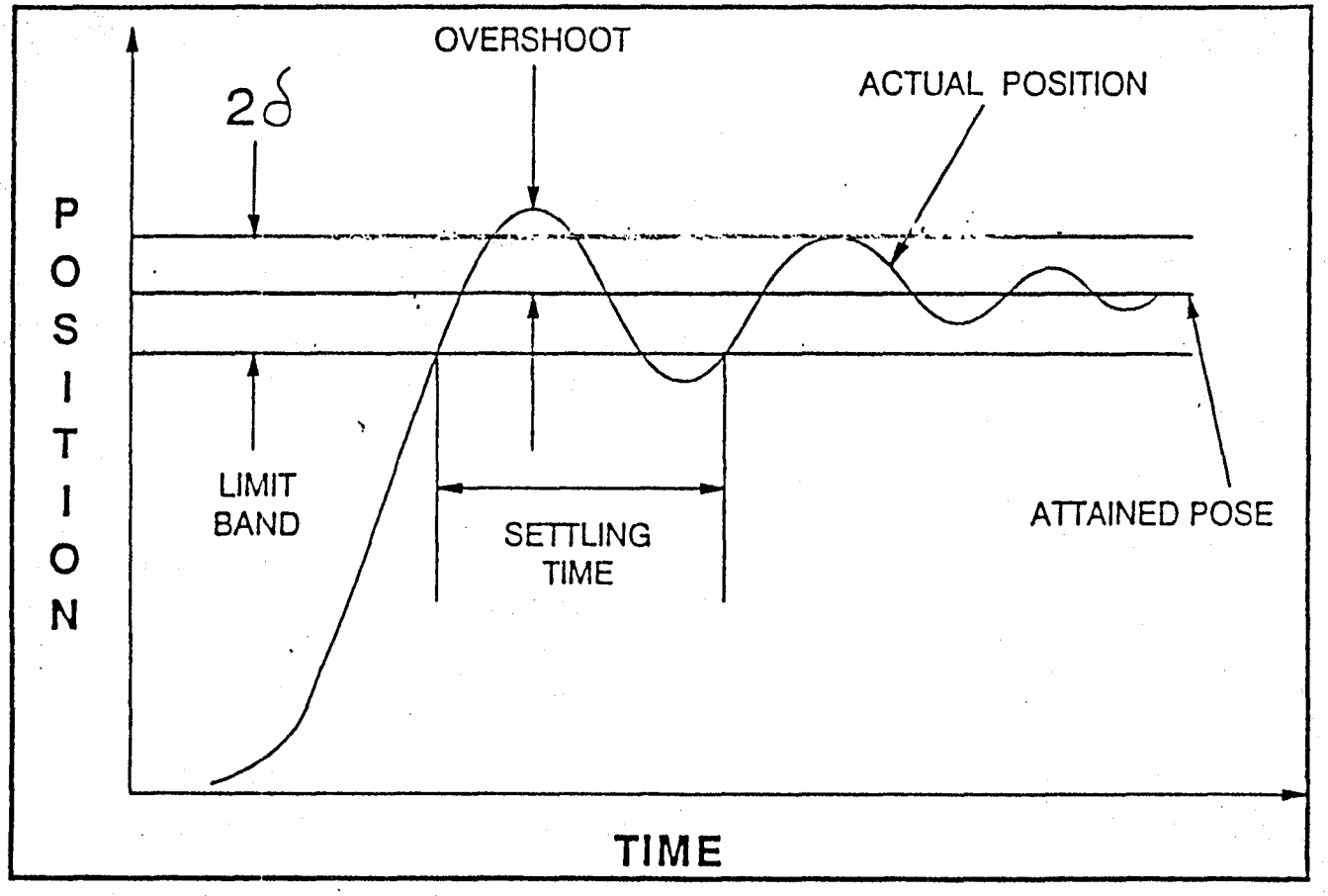

Figure (2-16) **Overshoot and Settling Time Concepts**

III CALIBRATION AND TROUBLE SHOOTING PROCEDURES OF THE ARID ROBOT

As mentioned earlier in this report, robot calibration is a process by which robot accuracy can be improved by modifying the robot positioning software rather than changing the design of the robot hardware or its control system. In the literature various procedures and techniques were used to modify the forward and inverse kinematics parameters through an error correction model. Most of these techniques are expensive, labor intensive, and time consuming.

Accordingly, a simple, inexpensive, and straight forward statistical technique and procedures were developed to evaluate and correct for the repeatability and relative accuracy error vectors of the ARID using 3D fixtures. The current design of these fixtures only allows for the calibration of the positioning error. However, if the orientation calibration is also needed the fixture should be modified as shown in Figure (2-2) and a mathematical algorithm should be developed to process the indicators readings and evaluate the pose (position, and orientation).

Because ARID is a dedicated robot to perform an on line inspection, its calibration technique only relays on the manipulator's repeatability and relative accuracy as well as the frame shift of the radiator. Therefore there is no need for the evaluation of the ARID's absolute accuracy and using any of the literature calibration techniques that are expensive, laborious and time consuming. The evaluation of the absolute accuracy is only needed for off line programming which is not the case in the ARID; as ARID only uses on line programing. Thus a tailored calibration technique for the ARID project is proposed to include the radiator frame shift compensation as a part of the calibration package and is described as follows:

3.1 CALIBRATION PROCEDURE FOR THE (ARID) ROBOT AT KSC:

The calibration and troubleshooting procedure using this statistical technique is explained in the following steps:

STEP 1: EVALUATION OF ROBOT REPEATABILITY

Evaluate the repeatability of the ARID robot at several points selected randomly within a zone that encompasses the radiator surface where the 4x4 photo frames are expected to cover. Note that the control system was designed to control the free end of a two feet long imaginary fourth link. This was considered to simulate the camera and the length of its axis at the point of intersection with the radiator surface. Therefore, it is recommended to use a calibration bar with a length of 24 inches + the length of the camera. Note that the bar material should be selected such that the weight of the bar will approximately match the weight of the camera. Evaluate the

repeatability error vector as previously described in section 2 of this report and correct for it in the ARID kinematic model (if necessary).

STEP 2: EVALUATION OF ARID's STATISTICAL CAPABILITY PARAMETERS

If correction is performed in step 1, recollect a few error measurements or use the same error measurement in Step 1 and calculate the statistical parameters C_p, C_{pk} - base the calculation on Upper Spec Limit = 0.125 in, and Lower Spec limit = -0.125 in. If both parameters are in the acceptable range i.e. both are greater than unity (at least) then proceed to the next step. If the value(s) of one or both parameter(s) is (are) not in the acceptable zone i.e. less than unity conduct the trouble shooting procedure described later in this section.

STEP 3: EVALUATION OF THE ARID RELATIVE ACCURACY

Evaluate the relative accuracy error vector as described earlier in section 2.3 of this report. Compensate for the error vector in the inverse kinematic model if needed. Recollect a few error measurements or use the same data obtained before correction to evaluate the C_p, C_{pk} for this mode of calibration. If both parameters have values greater than one proceed to the next step. If one parameter or both are less than one conduct the troubleshooting procedure (1) described later in this section.

STEP 4: CAMERA SET UP AND ADJUSTMENT

Replace the calibration bar by the camera. Consider that the radiator has four or six fiducial points. Move the camera to the first fiducial point and locate the cross hair to the center of the fiducial point image. This could be achieved by coinciding the circular image with a circle drawn on the camera screen that has its center right on the cross hair. Also, this could be achieved by image processing and the evaluation of the number of picture cells need for the camera to be moved to get the image exactly in the center of the screen. After centering the image in the exact middle of the screen, use the sonar to set the camera perpendicular to the radiator and at two feet away from it. Re-center the image to the middle of screen that may have be shifted during the adjustment of the camera's perpendicularity and distance relative to the radiator. Keep on refining these three parameters, namely, perpendicularity, centering, and distance (24") with respect to the radiator until acceptable positioning accuracy is achieved. Record this position i.e the readings of the encoders and the corresponding values of the tool center point X,Y, and Z coordinates in the memory of the computer under "fiducial 1" for example.

STEP 5: FORMATION OF A REFERENCE DATA BASE OF ARID'S JOINT READINGS

Repeat step 4 for all the fiducial points and all the inspection points and generate a permanently stored reference data base that contains reference joints readings end tool center point location coordinates for all these fiducial and inspection points. Now the ARID will be ready to inspect any radiator using this data bank as a reference.

STEP 6: ACTUAL INSPECTION PROCESS

For the ARID to inspect any radiator the reference data base has to be corrected by the amount of frame shift between the radiator under inspection and the reference data. The correction model for the frame shift will be based on comparison between the fiducial points of the radiator under inspection and the reference points. The frame shift model should correct for the TCP location and the perpendicularity to the radiator for each inspection point. The corrected inspection points will specify the scanning path for ARID to follow. It is strongly recommended that ARID scans on the fly to avoid possible and harmful vibration.

3.2 ARID TROUBLESHOOTING PROCEDURE USING THIS STATISTICAL TECHNIQUE

3.2.1 TROUBLESHOOTING PROCEDURE (1); REPEATABILITY ERROR:

If repeatability error data in any of the axes showed a value less than unity for the C_p parameter; examine the repeatability error of each joint one at a time and evaluate the C_p parameters for each. The joint that experiences less than unity value for C_p should be examined for hardware damage and/or encoder or resolver problem(s)

If all joints consistently exhibited repeatability errors that give less than unity for the statistical parameter Cp; the control system design has to be rechecked.

3.2.2 TROUBLESHOOTING PROCEDURE (2), RELATIVE ACCURACY CHECK

Examine the inverse kinematics model and software

IV CONCLUSIONS

(1) THE LITERATURE SURVEY EXHIBITED THE RECENT DEVELOPMENT OF ROBOTICS CALIBRATION TECHNIQUES; MOST OF WHICH CAN NOT BE CLASSIFIED AS TIME-EFFICIENT AND/OR COST EFFECTIVE.

(2) THE 3D FIXTURE IS A SIMPLE, INEXPENSIVE, AND STRAIGHTFORWARD TECHNIQUE THAT COULD BE USED TO CALIBRATE AND TROUBLESHOOT ANY ROBOT SUCH AS THE ARID, ASEA, HIGH SPEED CONTROLLER etc.

(3) THE 3D FIXTURE AND THE STATISTICAL TECHNIQUE WERE USED TO MEASURE THE PUMA 500 REPEATABILITY AND RELATIVE ACCURACY ERROR VECTORS; THEY READ:
.0012 I - 0.0005 J + 0.001 K
AND -0.0019 I - 0.0021 J + 0.001 K
RESPECTIVELY

(4) PUMA SHOWED TOTAL REPEATABILITY AND RELATIVE ACCURACY ERROR OF 0.00167" AND 0.0045" RESPECTIVELY

(5) ARID'S REPEATABILITY, RELATIVE ACCURACY, AND FRAME SHIFT ARE THE MAIN ASPECTS IN THE RECOMMENDED STEP BY STEP CALIBRATION PROCEDURE FOR THE ARID

(6) THE 3D FIXTURE AND THE STATISTICAL TECHNIQUE ARE RECOMMENDED FOR THE ARID CALIBRATION AND TO EVALUATE ITS REPEATABILITY AND RELATIVE ACCURACY AS WELL AS TROUBLESHOOTING ITS SOURCES OF ERRORS

(7) IT IS RECOMMENDED THAT THE SAME TECHNIQUE BE USED FOR THE CERTIFICATION OF ASEA'S HIGH SPEED CONTROLLER

REFERENCES

[1] Z.R.Roth, B.W. Mooring, and B. Ravani," An Overview of Robot Calibration", IEEE Journal of Robotics And Automation, Vol. RA-3, No.5, October 1987

[2] D.E.Whitney, C.A.Lozinski, J.M.Rourke," Industrial Robot Forward Calibration Method And Results", Journal of Dynamic Systems, Measurement, and Control, March 1986,Vol.108/1

[3] J.Denavit, R.S.Hartenberg,"A Kinematic Notation for Lower-Pair Mechanisms Based on Matrices", Transactions of The American Society of Mechanical Engineers, June 1955, Vol.22, No.2

[4] M.Z.Huang, O.Masory" Design Simulation of A Flexible Three DOF Device For Robot Calibration", Proc. of the Fourth Conf. on Recent Advances in Robotics, Boca Raton, May 16-17, 1991, (pp.181 - 189)

[5] R.Y. Tsai and R.K.Lenz, "Overview of a Unified Calibration Trio for Robot Eye, Eye-to-Hand, and Hand Calibration using 3D Machine Vision", SPIE Vol.1003 Sensor Fusion: Spatial Reasoning and Scene Interpretation, 1988.

[6] H.H.Tawfik, "Some Aspects of Robotics Calibration, Design, and Control", 1990 NASA/ASEE Summer Faculty Fellowship Program, John F Kennedy Space Center/ University of Center Florida.

V APPENDIX

Appendix

TABLE 1. Values of the Standard Normal Distribution Function*

$$\Phi(z) = \int_{-\infty}^{z} \frac{1}{\sqrt{2\pi}} e^{-u^2/2}\, du = P(Z \leq z)$$

z	0	1	2	3	4	5	6	7	8	9
−3.0	0.0013	0.0010	0.0007	0.0005	0.0003	0.0002	0.0002	0.0001	0.0001	0.0000
−2.9	0.0019	0.0018	0.0017	0.0017	0.0016	0.0016	0.0015	0.0015	0.0014	0.0014
−2.8	0.0026	0.0025	0.0024	0.0023	0.0023	0.0022	0.0021	0.0021	0.0020	0.0019
−2.7	0.0035	0.0034	0.0033	0.0032	0.0031	0.0030	0.0029	0.0028	0.0027	0.0026
−2.6	0.0047	0.0045	0.0044	0.0043	0.0041	0.0040	0.0039	0.0038	0.0037	0.0036
−2.5	0.0062	0.0060	0.0059	0.0057	0.0055	0.0054	0.0052	0.0051	0.0049	0.0048
−2.4	0.0082	0.0080	0.0078	0.0075	0.0073	0.0071	0.0069	0.0068	0.0066	0.0064
−2.3	0.0107	0.0104	0.0102	0.0099	0.0096	0.0094	0.0091	0.0089	0.0087	0.0084
−2.2	0.0139	0.0136	0.0132	0.0129	0.0126	0.0122	0.0119	0.0116	0.0113	0.0110
−2.1	0.0179	0.0174	0.0170	0.0166	0.0162	0.0158	0.0154	0.0150	0.0146	0.0143
−2.0	0.0228	0.0222	0.0217	0.0212	0.0207	0.0202	0.0197	0.0192	0.0188	0.0183
−1.9	0.0287	0.0281	0.0274	0.0268	0.0262	0.0256	0.0250	0.0244	0.0238	0.0233
−1.8	0.0359	0.0352	0.0344	0.0336	0.0329	0.0322	0.0314	0.0307	0.0300	0.0294
−1.7	0.0446	0.0436	0.0427	0.0418	0.0409	0.0401	0.0392	0.0384	0.0375	0.0367
−1.6	0.0548	0.0537	0.0526	0.0516	0.0505	0.0495	0.0485	0.0475	0.0465	0.0455
−1.5	0.0668	0.0655	0.0643	0.0630	0.0618	0.0606	0.0594	0.0582	0.0570	0.0559
−1.4	0.0808	0.0793	0.0778	0.0764	0.0749	0.0735	0.0722	0.0708	0.0694	0.0681
−1.3	0.0968	0.0951	0.0934	0.0918	0.0901	0.0885	0.0869	0.0853	0.0838	0.0823
−1.2	0.1151	0.1131	0.1112	0.1093	0.1075	0.1056	0.1038	0.1020	0.1003	0.0985
−1.1	0.1357	0.1335	0.1314	0.1292	0.1271	0.1251	0.1230	0.1210	0.1190	0.1170
−1.0	0.1587	0.1562	0.1539	0.1515	0.1492	0.1469	0.1446	0.1423	0.1401	0.1379
−0.9	0.1841	0.1814	0.1788	0.1762	0.1736	0.1711	0.1685	0.1660	0.1635	0.1611
−0.8	0.2119	0.2090	0.2061	0.2033	0.2005	0.1977	0.1949	0.1922	0.1894	0.1867
−0.7	0.2420	0.2389	0.2358	0.2327	0.2297	0.2266	0.2236	0.2206	0.2177	0.2148
−0.6	0.2743	0.2709	0.2676	0.2643	0.2611	0.2578	0.2546	0.2514	0.2483	0.2451
−0.5	0.3085	0.3050	0.3015	0.2981	0.2946	0.2912	0.2877	0.2843	0.2810	0.2776
−0.4	0.3446	0.3409	0.3372	0.3336	0.3300	0.3264	0.3228	0.3192	0.3156	0.3121
−0.3	0.3821	0.3783	0.3745	0.3707	0.3669	0.3632	0.3594	0.3557	0.3520	0.3483
−0.2	0.4207	0.4168	0.4129	0.4090	0.4052	0.4013	0.3974	0.3936	0.3897	0.3859
−0.1	0.4602	0.4562	0.4522	0.4483	0.4443	0.4404	0.4364	0.4325	0.4286	0.4247
−0.0	0.5000	0.4960	0.4920	0.4880	0.4840	0.4801	0.4761	0.4721	0.4681	0.4641

*B. W. Lindgren, *Statistical Theory*, The Macmillan Company, 1960.

TABLE 1 (*Continued*)

$$\Phi(z) = \int_{-\infty}^{z} \frac{1}{\sqrt{2\pi}} e^{-u^2/2}\, du = P(Z \leq z)$$

z	0	1	2	3	4	5	6	7	8	9
0.0	0.5000	0.5040	0.5080	0.5120	0.5160	0.5199	0.5239	0.5279	0.5319	0.5359
0.1	0.5398	0.5438	0.5478	0.5517	0.5557	0.5596	0.5636	0.5675	0.5714	0.5753
0.2	0.5793	0.5832	0.5871	0.5910	0.5948	0.5987	0.6026	0.6064	0.6103	0.6141
0.3	0.6179	0.6217	0.6255	0.6293	0.6331	0.6368	0.6406	0.6443	0.6480	0.6517
0.4	0.6554	0.6591	0.6628	0.6664	0.6700	0.6736	0.6772	0.6808	0.6844	0.6879
0.5	0.6915	0.6950	0.6985	0.7019	0.7054	0.7088	0.7123	0.7157	0.7190	0.7224
0.6	0.7257	0.7291	0.7324	0.7357	0.7389	0.7422	0.7454	0.7486	0.7517	0.7549
0.7	0.7580	0.7611	0.7642	0.7673	0.7703	0.7734	0.7764	0.7794	0.7823	0.7852
0.8	0.7881	0.7910	0.7939	0.7967	0.7995	0.8023	0.8051	0.8078	0.8106	0.8133
0.9	0.8159	0.8186	0.8212	0.8238	0.8264	0.8289	0.8315	0.8340	0.8365	0.8389
1.0	0.8413	0.8438	0.8461	0.8485	0.8508	0.8531	0.8554	0.8577	0.8599	0.8621
1.1	0.8643	0.8665	0.8686	0.8708	0.8729	0.8749	0.8770	0.8790	0.8810	0.8830
1.2	0.8849	0.8869	0.8888	0.8907	0.8925	0.8944	0.8962	0.8980	0.8997	0.9015
1.3	0.9032	0.9049	0.9066	0.9082	0.9099	0.9115	0.9131	0.9147	0.9162	0.9177
1.4	0.9192	0.9207	0.9222	0.9236	0.9251	0.9265	0.9278	0.9292	0.9306	0.9319
1.5	0.9332	0.9345	0.9357	0.9370	0.9382	0.9394	0.9406	0.9418	0.9430	0.9441
1.6	0.9452	0.9463	0.9474	0.9484	0.9495	0.9505	0.9515	0.9525	0.9535	0.9545
1.7	0.9554	0.9564	0.9573	0.9582	0.9591	0.9599	0.9608	0.9616	0.9625	0.9633
1.8	0.9641	0.9648	0.9656	0.9664	0.9671	0.9678	0.9686	0.9693	0.9700	0.9706
1.9	0.9713	0.9719	0.9726	0.9732	0.9738	0.9744	0.9750	0.9756	0.9762	0.9767
2.0	0.9772	0.9778	0.9783	0.9788	0.9793	0.9798	0.9803	0.9808	0.9812	0.9817
2.1	0.9821	0.9826	0.9830	0.9834	0.9838	0.9842	0.9846	0.9850	0.9854	0.9857
2.2	0.9861	0.9864	0.9868	0.9871	0.9874	0.9878	0.9881	0.9884	0.9887	0.9890
2.3	0.9893	0.9896	0.9898	0.9901	0.9904	0.9906	0.9909	0.9911	0.9913	0.9916
2.4	0.9918	0.9920	0.9922	0.9925	0.9927	0.9929	0.9931	0.9932	0.9934	0.9936
2.5	0.9938	0.9940	0.9941	0.9943	0.9945	0.9946	0.9948	0.9949	0.9951	0.9952
2.6	0.9953	0.9955	0.9956	0.9957	0.9959	0.9960	0.9961	0.9962	0.9963	0.9964
2.7	0.9965	0.9966	0.9967	0.9968	0.9969	0.9970	0.9971	0.9972	0.9973	0.9974
2.8	0.9974	0.9975	0.9976	0.9977	0.9977	0.9978	0.9979	0.9979	0.9980	0.9981
2.9	0.9981	0.9982	0.9982	0.9983	0.9984	0.9984	0.9985	0.9985	0.9986	0.9986
3.0	0.9987	0.9990	0.9993	0.9995	0.9997	0.9998	0.9998	0.9999	0.9999	1.0000

1991 NASA/ASEE SUMMER FACULTY FELLOWSHIP PROGRAM

JOHN F. KENNEDY SPACE CENTER
UNIVERSITY OF CENTRAL FLORIDA

LOW FLOW VORTEX SHEDDING FLOW METER FOR HYPERGOLICS/ALL MEDIA

PREPARED BY:	Dr. Ngo Dinh Thinh
ACADEMIC RANK:	Professor
UNIVERSITY AND DEPARTMENT:	California State University - Sacramento Mechanical Engineering Department
NASA/KSC	
DIVISION:	Electronic Systems Support
BRANCH:	Instrumentation-Transducers Section
NASA COLLEAGUE:	Mr. R.H. Howard and Mr. W. Larson
DATE:	August 2, 1991
CONTRACT NUMBER:	University of Central Florida NASA-NGT-60002 Supplement: 6

SUMMARY

Current turbine flow meters have been used to measure the loading of hypergols into the Space Shuttle Orbiter. Because of the problems associated with the refurbishment of these meters after each launch, NASA has considered the development of a vortex shedding flow meter which would have no internal moving parts. The objective of the current project was to develop a family of vortex shedding flow meters with outside diameters varying from 1/2" to 2" for a low flow environment.

To test the meters with the flow of water and Freon 113 which has fluid properties similar to hypergols, two flow test loops were designed and built. One loop was for the 1/2" model using Freon 113 as operating fluid. Another loop consisted of a pump system was designed for the larger models of 3/4", 1", 1.5" and 2" O.D. using water as operating fluid. A family of flow meter models consisted of 13 different configurations were designed and fabricated. Test runs were conducted successfully on the 1/2" models with Freon 113 and the others with water.

Results showed that the linearity between the frequency of the vortices and the flow rate of Freon 113 and water for all flow meters with a rectangular shedder bar was very close to that of the turbine type. It is concluded that the vortex shedding flow meter is a possible replacement for the turbine flow meter being used on the space shuttle.

ACKNOWLEDGEMENTS

I would like to thank all members of the **Transducers Section** for their help during my tenure at Kennedy Space Center. I am grateful to **Bob Howard** for his encourage words which brought me to this interesting project and his strong support toward my research endeavour. Special thanks should be extended to **Bill Larson** for his support and assistance that make my work less painful. I also would like to thank **Jerry Mason, Jim Hillis, Drew Schmidt** and **Steve Stout** for their assistance, without their help I would not be able to complete successfully this experimental study. Finally, I would like to thank **Dr. E. Ramon Hosler** and **Dr. Mark A. Beymer,** Directors of the NASA/ASEE Summer Faculty Fellowship Program, and **Mrs. Kari L. Stiles**, Administrative Assistant, for their assistance and hospitality which make my days at KSC very educational and enjoyable.

Abstract

The purpose of this summer project was to develop a family of vortex shedding flow meters for flow measurements of hypergols that requires a long term operation without removal from system lines. A family of vortex shedding flow meters without moving parts was designed and fabricated. The test loops to evaluate the meters for water flow as well as Freon -113 flow which simulates the hypergolic fluids, have been modified and constructed to utilize a pump system which has an output capacity of 200 gpm.

Test runs were conducted on the small 1/2" model with Freon 113 and on the larger size models with water. Results showed that the linearity between the frequency of the vortices and the flow rate of the fluids was very close to that of the turbine flow meter. It is suggested that the vortex shedding flow meter is a possible replacement for the existing turbine type.

TABLE OF CONTENTS

LIST OF ILLUSTRATIONS

LIST OF TABLES

I. INTRODUCTION

1.1 STATEMENT OF PROJECT NEEDS.

During the loading of hypergolic fuels and oxidizers, flow meters are used to measure the amount of fluid. The current method of metering these fluids involves turbine type meters and shuttle-ball type vortex shedding meters. One of the problems that occurs with these meters is that after each launch the meters have to be taken apart and refurbished then recalibrated. The reason for this process is that there are moving parts of the meters in contact with the flowing fluid. The bushings and bearings of these meters are susceptible to wear, especially during the purge phase of fuel loading process when severe over-speeds of the rotor occur due to gas flow through the lines. The process of refurbishment of the meters is costly due to the techniques required to handle the very toxic hypergols. It is estimated that a saving of about $1000 per flow meter per launch can be made if the meters do not require this maintenance. There are about 6000 flow meters of all sorts being used.

1.2 OBJECTIVE OF THE PROJECT.

The objective of this project is to develop a family of vortex shedding flow meter for applications that require long term operation without removal from system lines. This family of vortex shedding flow meters would have no moving parts. The linearity between the frequency of the vortices and the flow rate of the fluid would be as close as that of the turbine type. The flow meters would be installed permanently after the initial calibration and only the signal conditioner would be removed for calibration. This procedure would not affect the total calibration accuracy of the meters.

II. VORTEX SHEDDING FLOW METER

2.1 BACKGROUND OF VORTEX SHEDDING PHENOMENA.

The phenomenon of vortices being shed from a surface in a flowing fluid is not new, and the application of the vortex shedding to the measurement of flow rate is well established. For an uniform flow past a circular past a circular cylinder, vortices are formed at the two separation points and shed off regularly in an alternating fashion, as shown in figure 2.0. These vortices move downstream in a regular pattern.

The vortices move downstream with a velocity which is less than the mainstream velocity . The alternating shedding of vortices from the separation points on the surface of a circular cylinder produces transverse forces on the cylinder and causes the cylinder to oscillate. Such effects were first studied in the laboratory about 1878 by Strouhal, who showed that the vibrations would cause the pressure pulses to transverse to the fluid. He also showed that the frequency f of the vibration was related to the AIR speed U and the cylinder diameter d by the approximate equation:

$$f = U/(6*d) \qquad (1)$$

The vortex shedding flow meter works on the principle that the mass flow rate of the fluid is proportional to the frequency of the vortex shedding behind a bluff body as shown in Figure 2.1.

The proportionality constant or the relationship between the vortex shedding frequency and velocity of the uniform flow is called the **Strouhal number** which is related to the vortex shedding frequency in the following equation:

$$f = St*U/d*(1 - 20/Re) \qquad (2)$$

where:

f	Vortex shedding frequency, Hz
St	Strouhal number
U	Fluid flow velocity, ft/sec
d	Characteristic dimension of bluff body, ft
Re	Reynolds number of pipe flow

2.2 DESIGN OF THE PROTOTYPES

Figure 2.2 shows the design for a family of vortex shedding flow meter with a shedder bar. Table 2.1 shows all dimensions in inches. The geometry of the shedder bar may determines the characteristic of the frequency of vortices. Three shapes for the shedder bar were selected for this study. They are circular, rectangular, and reversed wedge as shown in following figure 2.3. Table 2.2 shows the dimensions of the flow meter diameters and the shedder bar.

III. EXPERIMENTAL STUDY

3.1 INTRODUCTION

The test runs in this study were conducted on the family of vortex shedding flow meters using Freon 113 and water as operating fluids. A Labview software was used to acquire and analyse the pressure signals. The Least Squared Estimation method was used to curvefit the data points and to determine the linearity of the flow rate and the vortex shedding frequency.

3.2 FLOW BENCH DESIGN

Two flow benches were designed and built for the testing of the flow meters. Figures 3.1 and 3.2 show the flow loop for the study of the 1/2" models using Freon as an operating fluid. Two 50-gallon dewars were used as containers for the Freon fluid. Dewar #1 was located inside the laboratory and was placed on a load platform used to measure the mass flow rate of Freon 113. Dewar #2 was located outside of the laboratory window and was connected to the flow loop through the window. By proper adjustments of the valve system, Freon 113 could flow through the loop from either dewar. High pressurized air was used to vent Freon from one dewar through the test section into the other dewar. The quantities measured in the loop include the output signals from the turbine flow meter used as a reference, from the vortex shedding flow meter under test, from the pressure transducer and the thermocouple in the test loop, and from the load cell transducers installed under dewar #1. The vortex flow meter output signals were detected by a Kistler transducer (model 206). The Kistler transducer was a piezoelectric type of device and came with a Kistler signal coupler (model 5116) which could produce an AC coupled millivolts output proportional to the pressure fluctuations. The Labview data acquisition was used to analyze the output signals. The frequency of the vortices as well as the mass flow rate of the fluids were also obtained. Figure 3.3 and 3.4 show the flow bench designed for the larger size models. The flow bench consists of two 250-gallon tanks acting as a source and a sink, a pumping system, and a test section. Similar to the previous flow loop, the vortex flow meter output signals were also detected by a Kistler transducer (model 206) and amplified by by a Kistler signal coupler (model 5116). The Labview software was also used for the test runs with this flow bench.

3.3 TEST RUNS AND DATA COLLECTIONS

The goal for this summer project was to study experimentally a family of vortex

shedding flow meter using the turbine type as a reference. The pump speed or the valve system was adjusted to vary the flow rate. Steady flow was indicated by a steady output reading from the calibrated turbine meter in series with the vortex meter. The turbine meter output consists of a voltage from the signal conditioner which is linearly proportional to the flow rate.

The output from the vortex shedding flow meter was analyzed using the Labview data acquisition software. The output signal from the Kistler transducer was clearly picked up on the Labview oscilloscope and the primary frequency results were obtained easily from the FFT (Fast Fourier Transform) operation. The measurement of pressure, temperature, and turbine flow rate were also conducted simultaneously. Figure 3.5 shows a sample output consisted of a raw signal waveform, a low frequency filtered waveform, FFT calculation, and related information.

3.4 RESULTS AND EVALUATIONS

Figures 3.7 to 3.11 represent the relationship between the frequency of the vortices and the flow rate of the fluid for all the flow meters designed. The goal for this study is to determine the linearity of the flow meter frequency curves. Figures 3.7a to 3.11a show the straight line equations for the test data obtained on the models with a rectangular shedder bar. Figures 3.7b to 3.11b and Figures 3.7c to 3.9c show the same results for the cylindrical and reversed wedge bars respectively.

It is noted that the rectangular and reversed wedge shedder bars produced a clear separation flow which in term provided a good waveform for the pressure pulses. The frequency was also easier to be calculated by hands or with the FFT operation. To determine the validity of the linearity for the flow rate vs frequency curves, the Multiple Correlation Coefficient Squared named "R^2" was used. For a straight line curve R^2 was calculated to be 100%. Figures 3.7 to 3.11 showed that the MCCS or R^2 for the rectangular and reversed wedge bars was about 99.2% and for the cylindrical shedder bar the MCCS was about 95%.

IV. CONCLUSION AND RECOMMENDATION

Test results on the designed family of vortex shedding flow meters suggested that the vortex shedding flow meter is a **possible replacement** for the turbine flow meter which has been used to measure the loading of hypergols into the space shuttle.

The rectangular and reversed wedge shedder bars generate stable vortices; therefore, the frequency count is easily obtained. From the manufacturing point of view the rectangular bar may be simpler to be fabricated.

It is suggested that a production prototype (Fig. 3.12) be developed for qualification tests and specification requirements.

Further studies can be made on the existing models such as the experimental study of a vortex shedding flow meter for gases (air, nitrogen...) and for a two-phase flow (gas + liquid, ...).

Because of the symmetrical aspect of the design, a bi-directional vortex shedding flow meter can be easily developed.

LIST OF REFERENCES

1. Birkhoff, G. and Zarantonello, E.H., Jets, Wakes, and Cavities, Academic Press Inc., New York, 1957.

2. Pao, R. , Fluid Dynamics, Charles E. Merrill, Inc. Columbus, Ohio, 1967.

3. Siegwarth, J.D., "Vortex Shedding Flowmeters for Space Shuttle Main Engines", National Bureau of Standards Tech. No. X89-10227, Boulder, Colorado.

4. Faber, E.A. and Hansen, E.C., "Vortex Shedder Flowmeter", Final Report for NASA Contract Number NAS 10-11230, December 31, 1986.

5. Hansen, E.C. and Restrepo, J.A., "Development of a Small Vortex Shedding Flowmeter for Hypergolic Propellants", AIAA, ASME, SIAM, and APS First National Fluid Dynamics Congress, Cincinnati, OH, July 25-28, 1988, AIAA Paper 88-3602, p. 1500-1504.

6. Baird, R.S., "Flowmeter Evaluation for On-Orbit Operations. NASA Technical Memorandum 100465, August 1988.

7. Thinh, N.D. and Howard, R.H., "Experimental Study of a Vortex Shedding Flow Meter", 32nd Heat Transfer and Fluid Mechanics Institute, California State University, Sacramento, California, June 1991.

8. Daniel, C. and Wood, F., Fitting Equations to Data", John Wiley & Sons, New York, 1980.

TABLE 2.1

VORTEX SHEDDING FLOW METER
DIMENSIONS IN INCHES

FLOW METER (O.D.)	1/2"	3/4"	1"	1 1/2"	2"
a	2.500	3.000	3.500	4.000	4.500
b	0.435	0.570	0.587	0.685	0.850
c	0.815	0.930	1.163	1.315	1.400
d	0.815	0.930	1.163	1.315	1.400
e	0.435	0.570	0.587	0.685	0.850
f	1.250	1.5625	2.1875	2.750	3.375
g	1.000	1.000	1.000	1.000	1.000
h	0.500	0.6563	0.8435	1.125	1.4375
i	0.447	0.398	0.328	0.281	0.205
j	0.394	0.609	0.844	1.312	1.780
k	1.000	1.3125	1.6875	2.250	2.875
l	0.4375	0.4375	0.4375	0.4375	0.4375
m	0.625	0.625	0.625	0.625	0.625
n	0.125	0.125	0.125	0.125	0.125
o	1.000	1.3125	1.6875	2.250	2.875
p	0.125	0.125	0.250	0.250	0.250
q	0.303	0.3515	0.422	0.469	0.5475
r	0.394	0.609	0.844	1.312	1.780
s	0.303	0.3515	0.422	0.469	0.5475
t	0.125	0.125	0.250	0.250	0.250
u	0.375	0.375	0.500	0.625	0.750
v	0.250	0.250	0.375	0.500	0.625

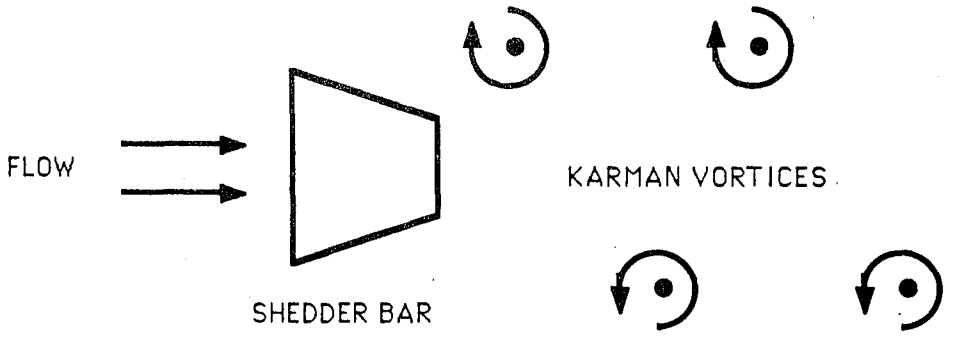

FIG. 2.0 VORTEX SHEDDING PHENOMENON

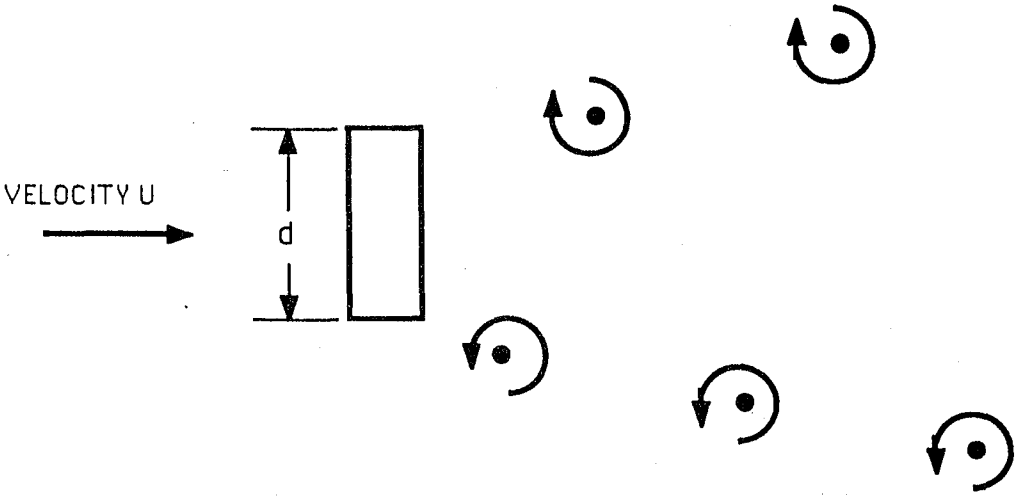

FIG. 2.1 VORTEX SHEDDING BEHIND A BLUFF BODY

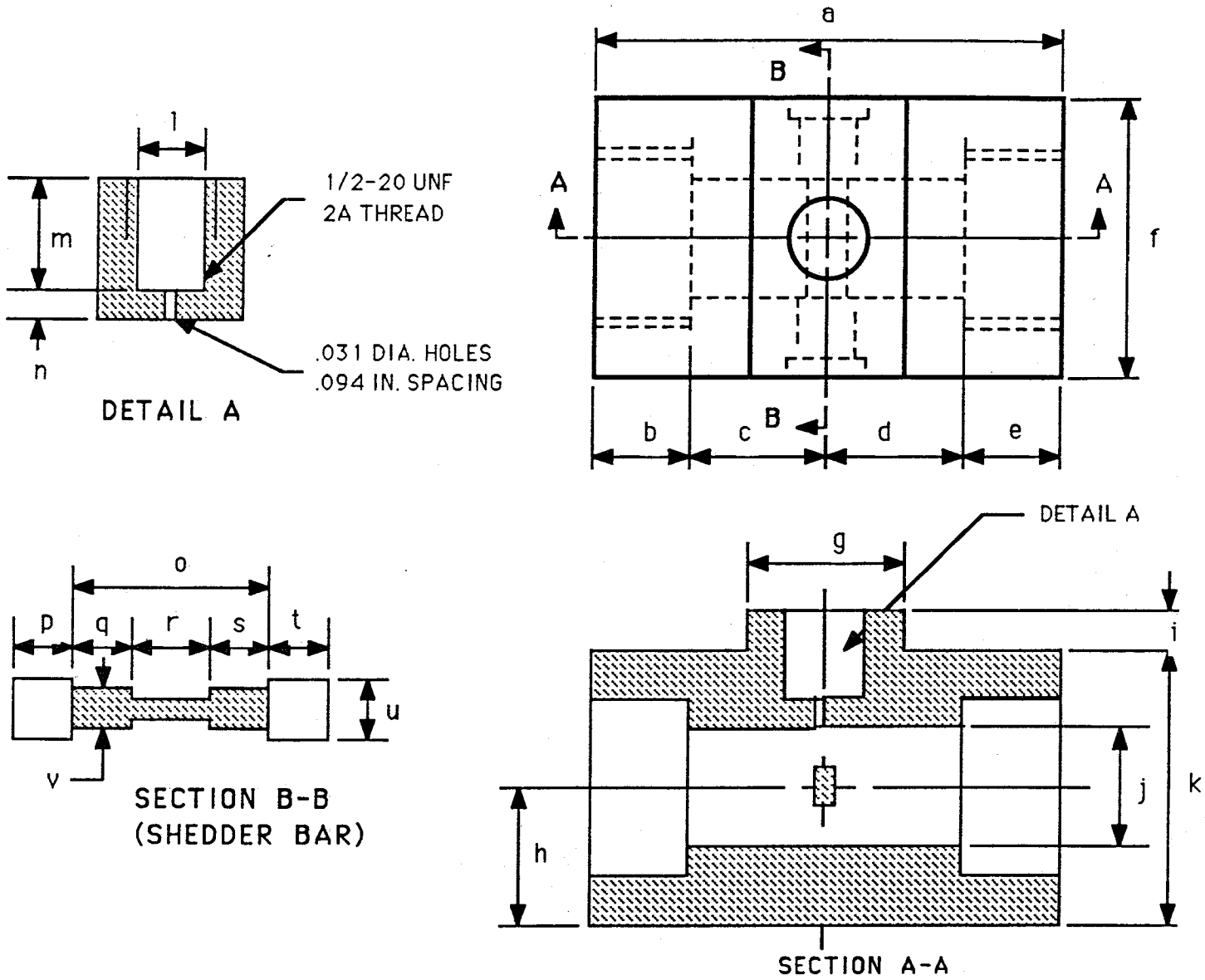

FIG. 2.2 VORTEX SHEDDING FLOWMETER PROTOTYPE

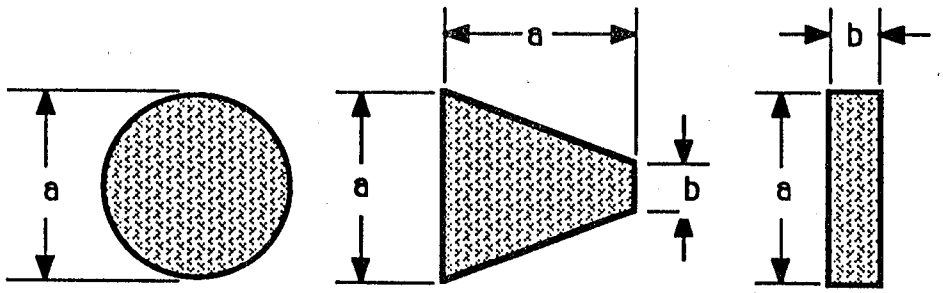

FIG. 2.3 SHEDDER BAR GEOMETRY

TABLE 2.2

SHEDDER BAR DIMENSIONS

FLOW METER (O.D)	1/2"	3/4"	1"	1 1/2"	
I.D. (in.)	.410	.609	.844	1.312	1.781
a (in.)	.110	.170	.235	.367	.500
b (in.)	.075	.115	.155	.245	.335

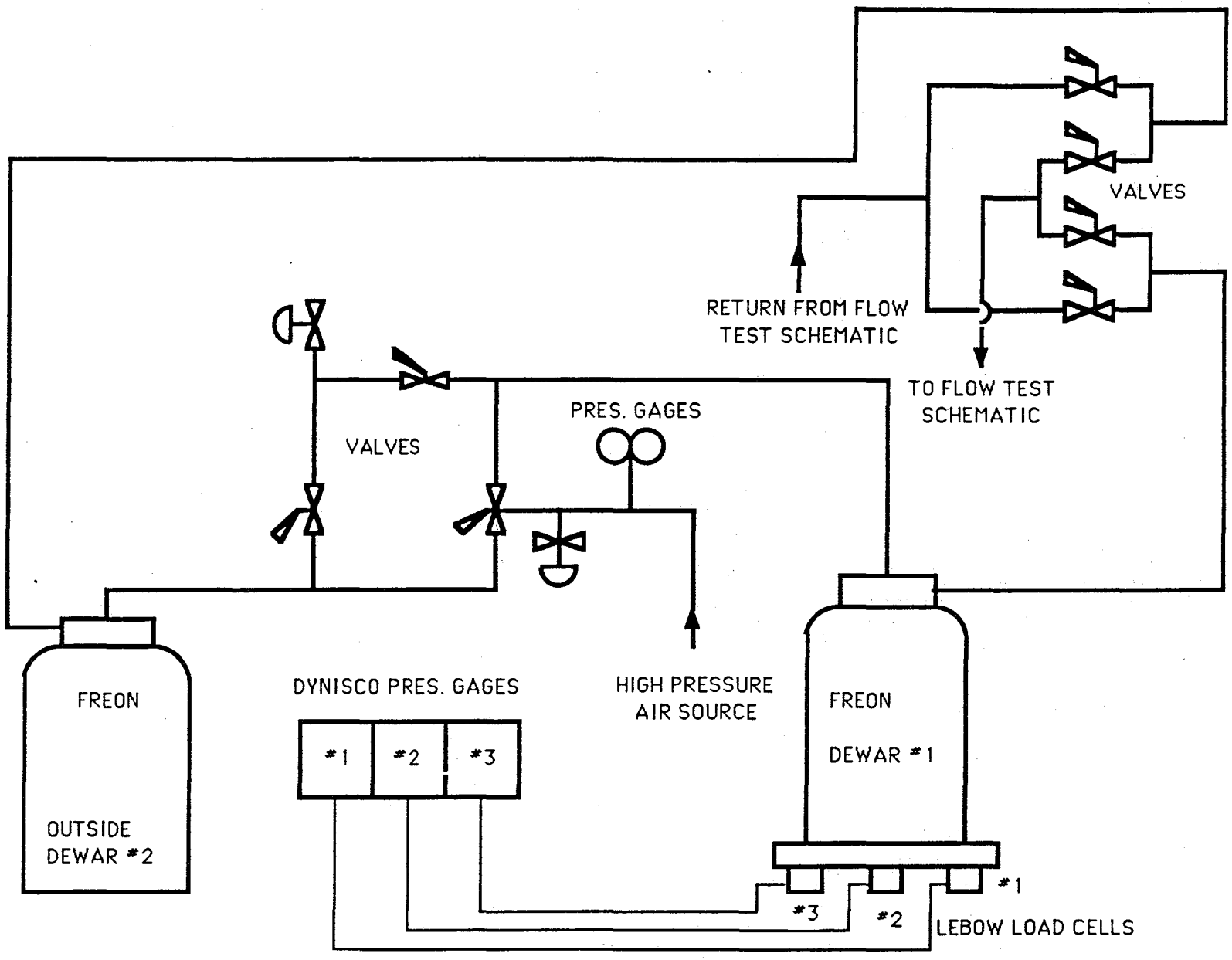

FIGURE 3.1 FLOW TANK SET UP

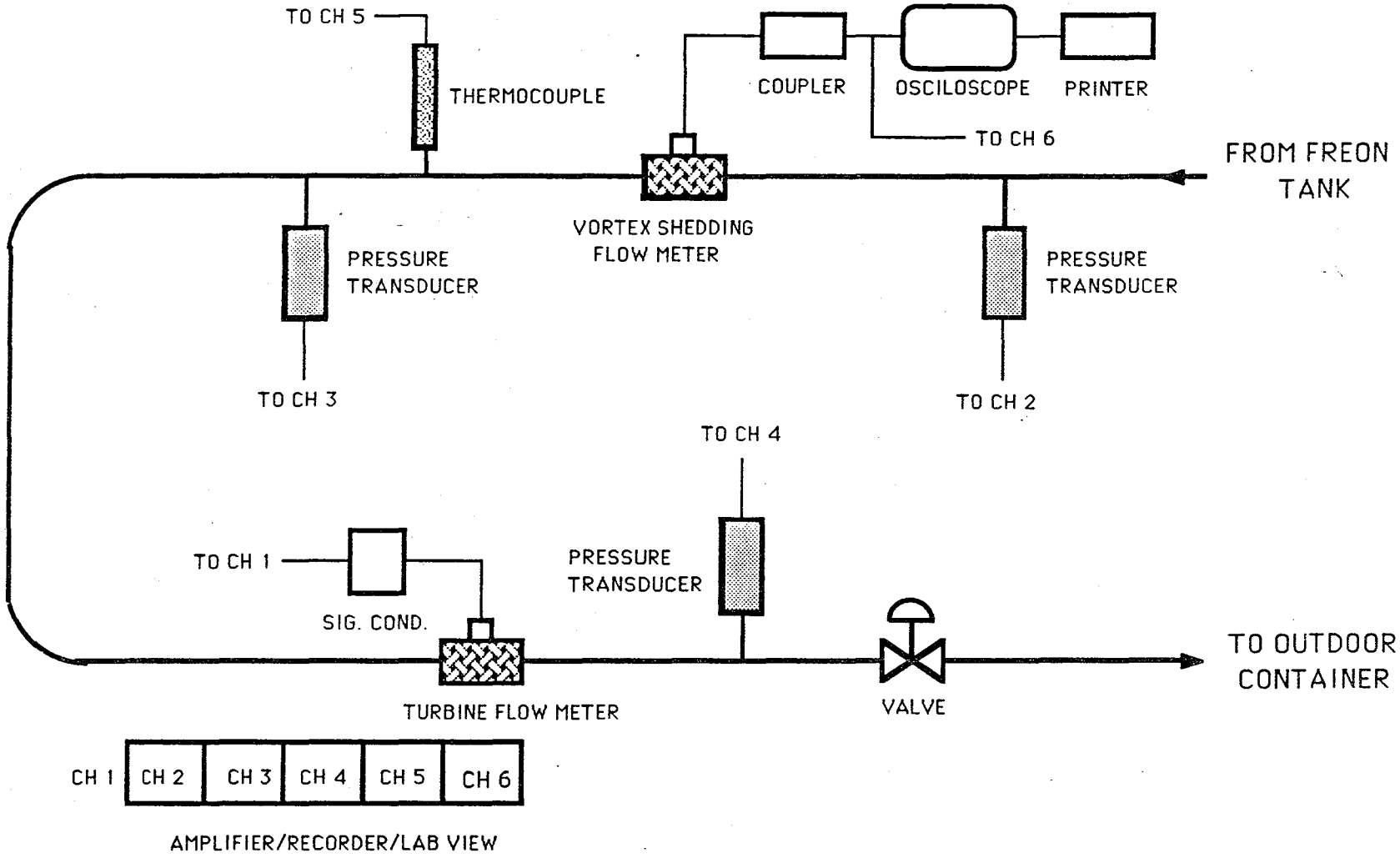

FIGURE 3.2 FLOW TEST SCHEMATIC

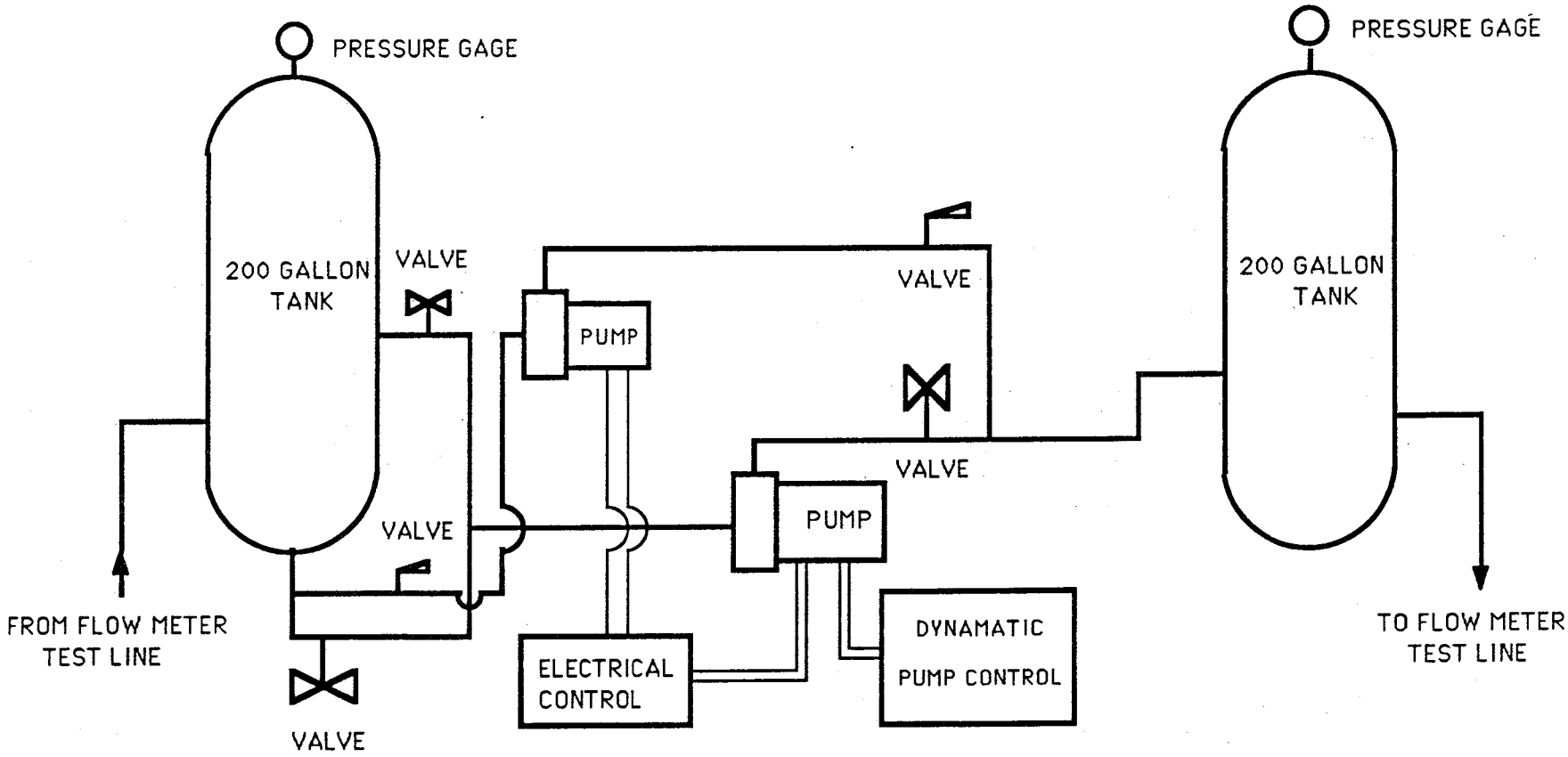

FIGURE 3.3 FLOW BENCH SCHEMATIC

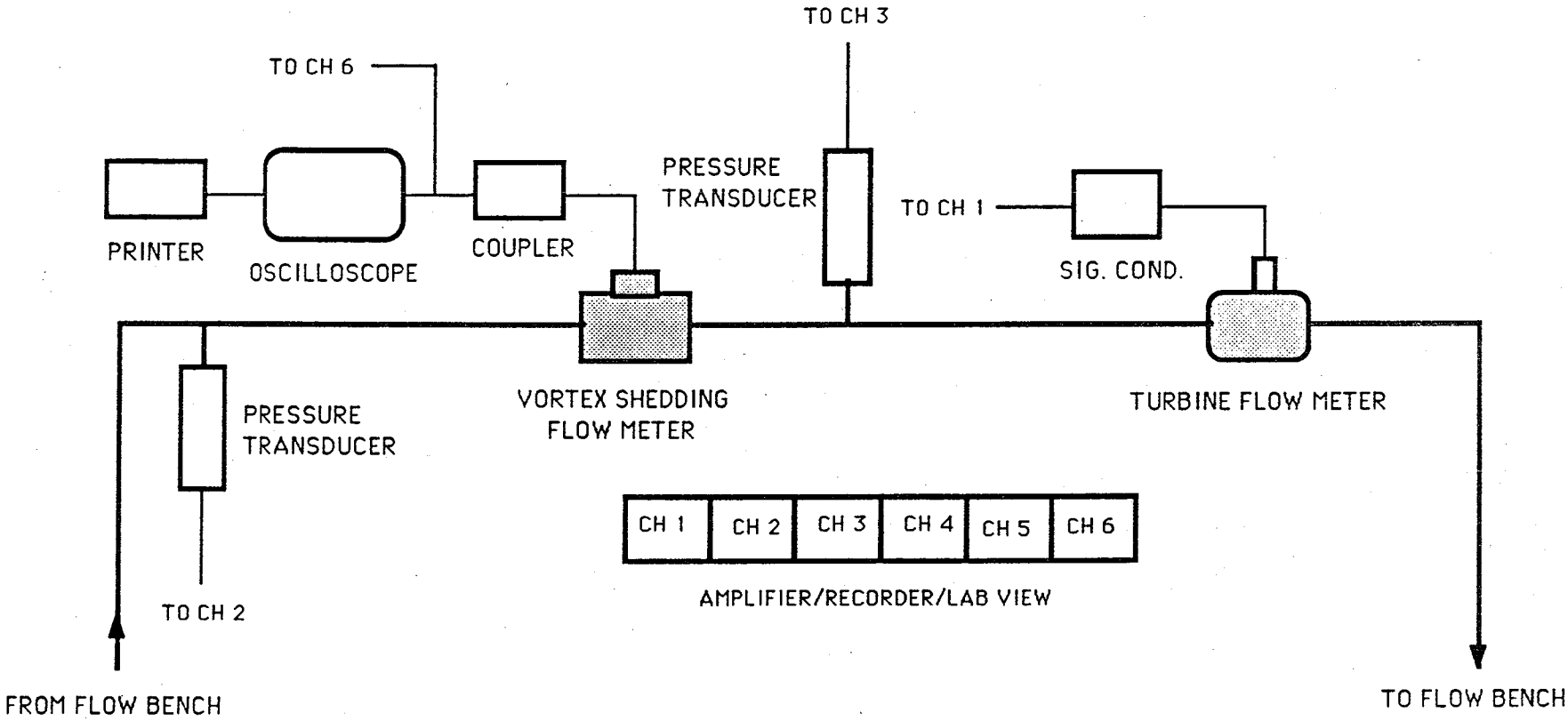

FIGURE 3.4 FLOW METER TEST LINE

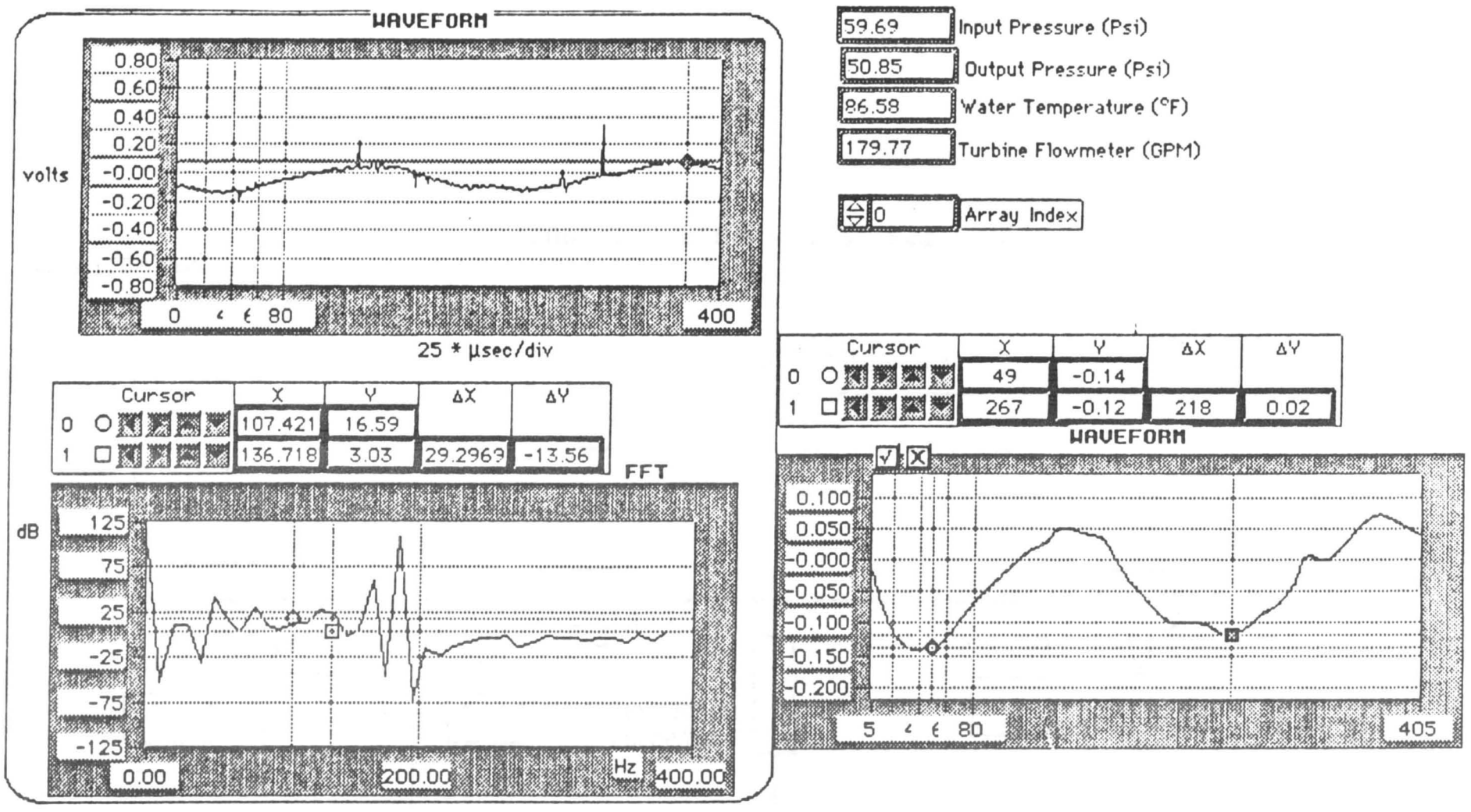

FIGURE 3.5 LABVIEW OUTPUT SAMPLE

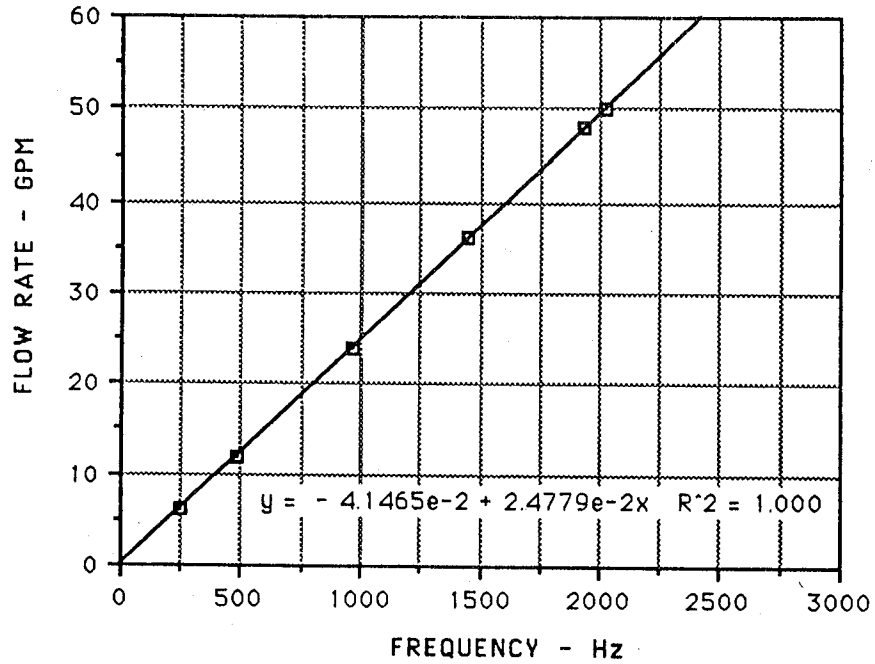

FIG. 3.6 LEAST SQUARED ESTIMATION

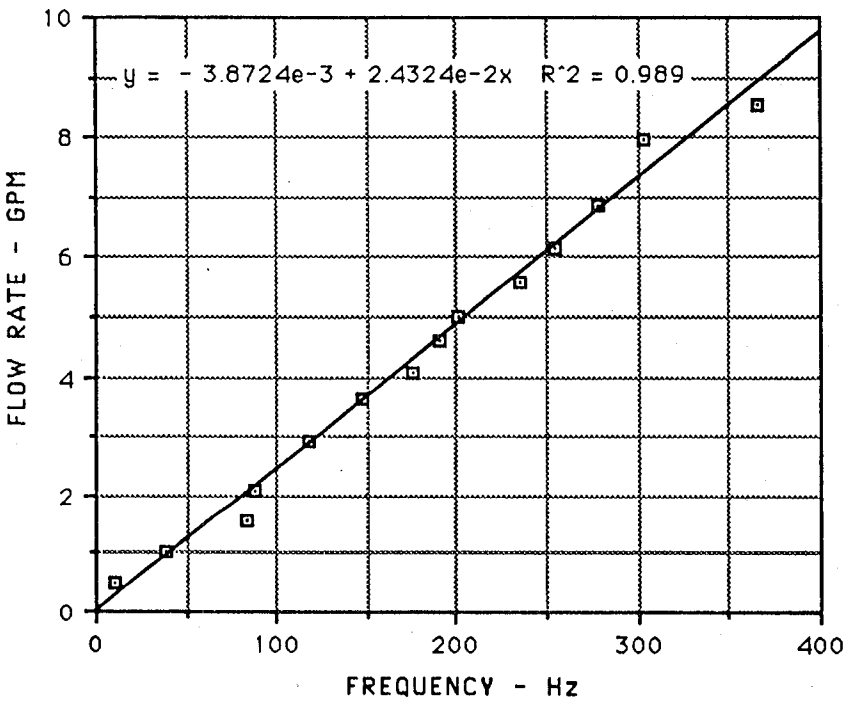

FIG. 3.7a 0.5" MODEL -RECT. BAR - FREON

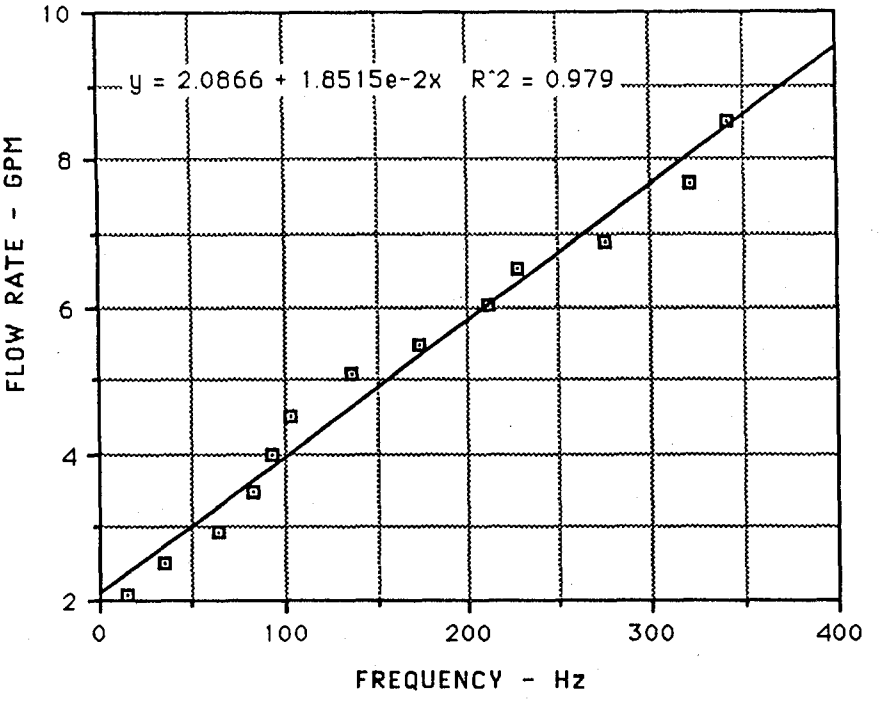

FIG. 3.7b 0.5" MODEL - CYL. BAR - FREON

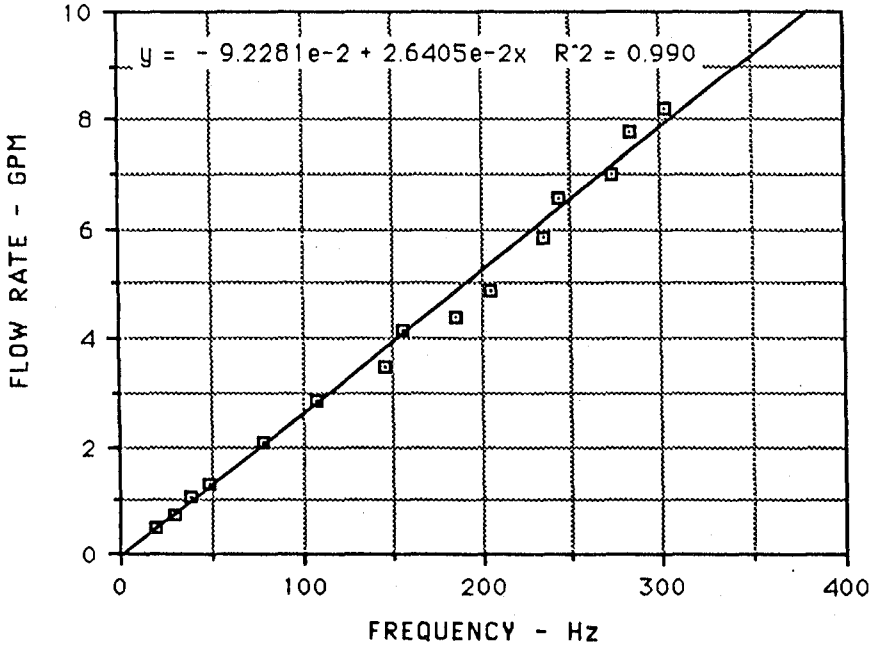

FIG. 3.7c 0.5" MODEL -REVERSED WEDGE BAR - FREON

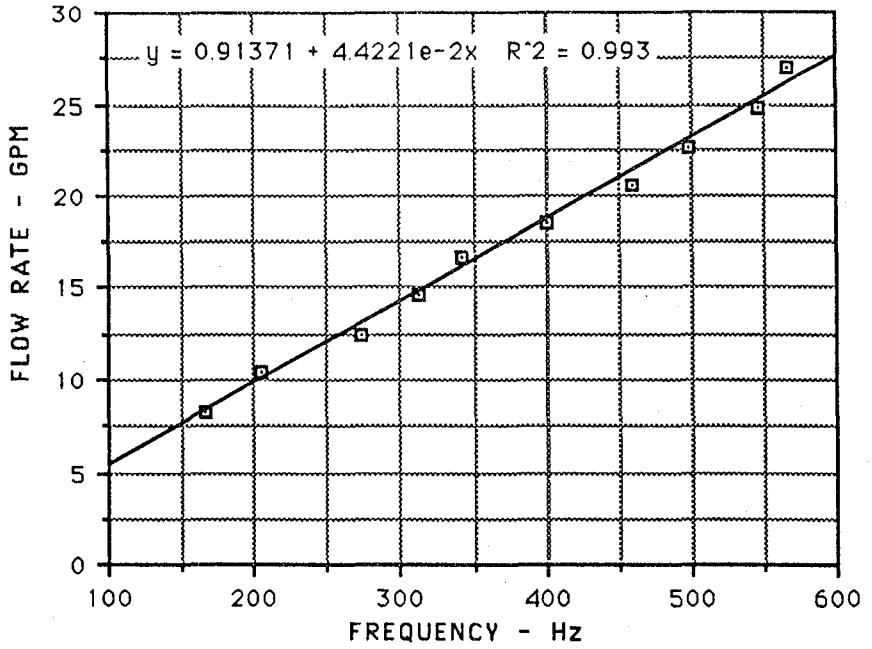

FIG. 3.8a .75" MODEL - RECT. BAR - WATER

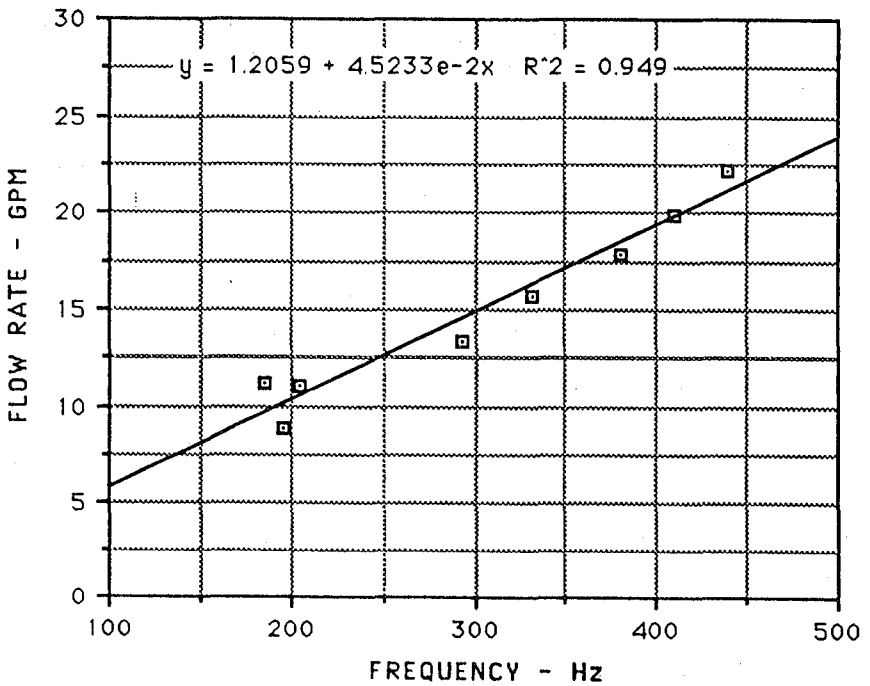

FIG. 3.8b .75" MODEL - CYL. BAR - WATER

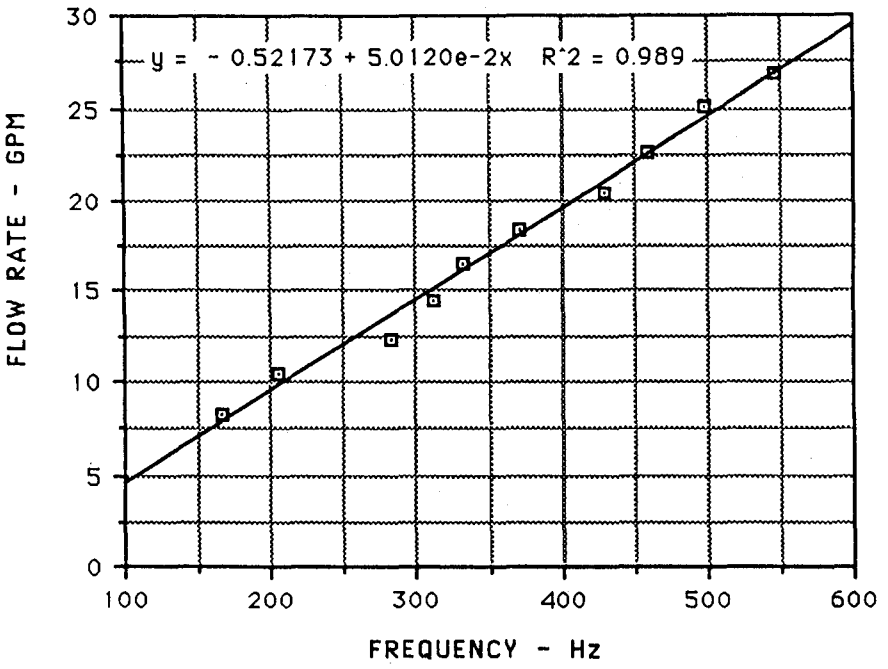

FIG. 3.8c .75" MODEL - REVERSED WEDGE BAR - WATER

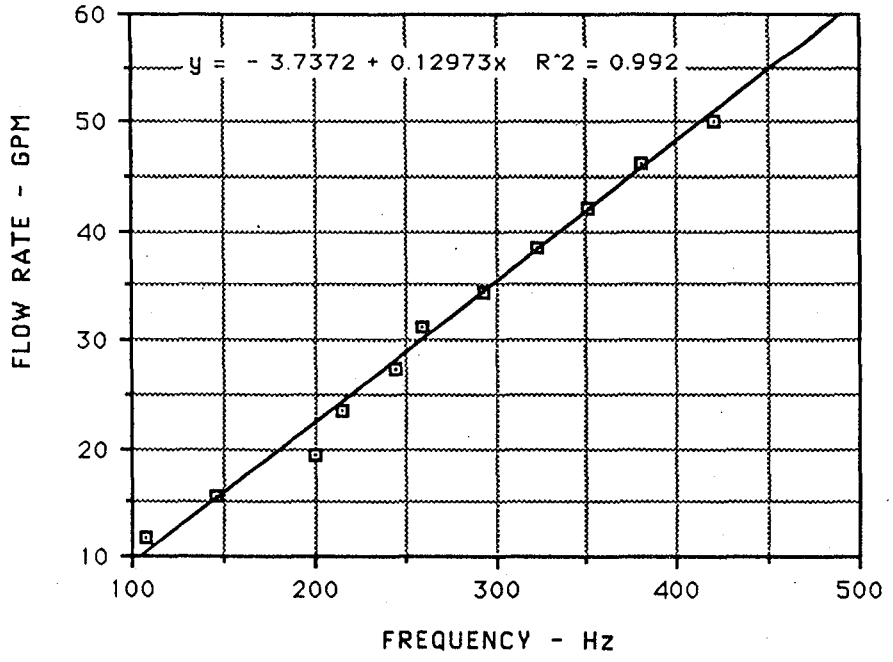

FIG. 3.9a 1" MODEL -RECT. BAR - WATER

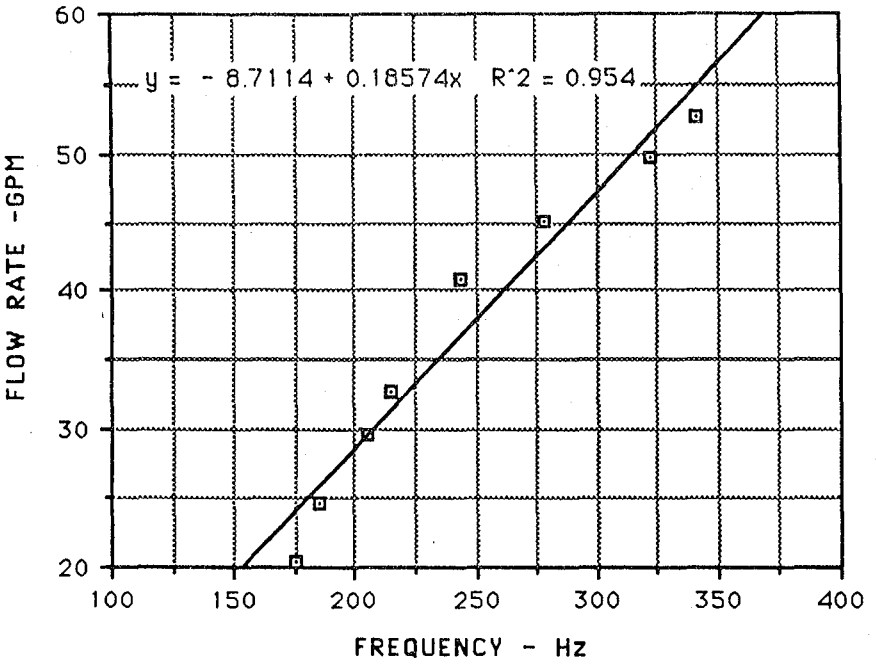

FIG. 3.9b 1" MODEL - CYL. BAR - WATER

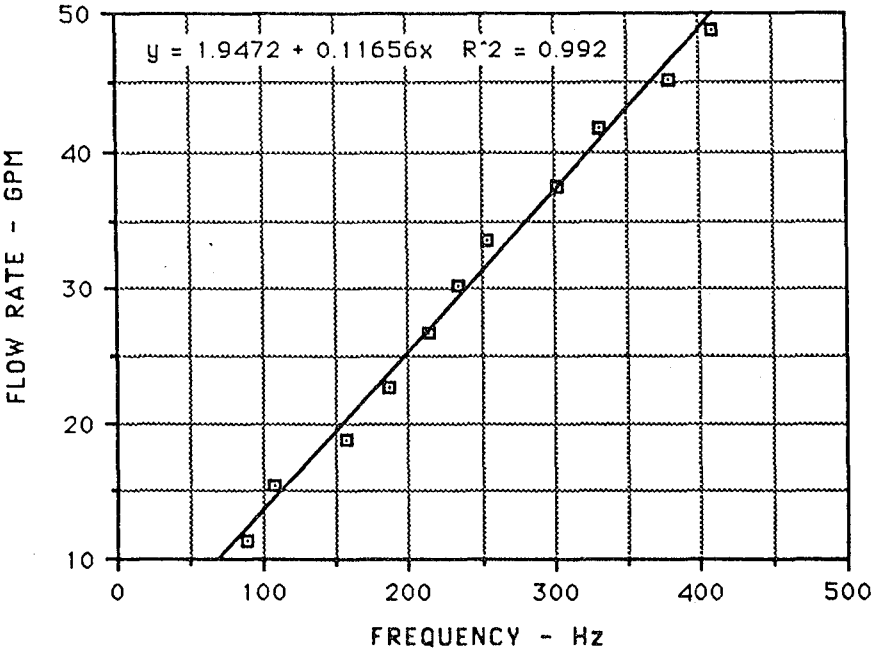

FIG. 3.9c 1" MODEL - REVERSED WEDGE BAR - WATER

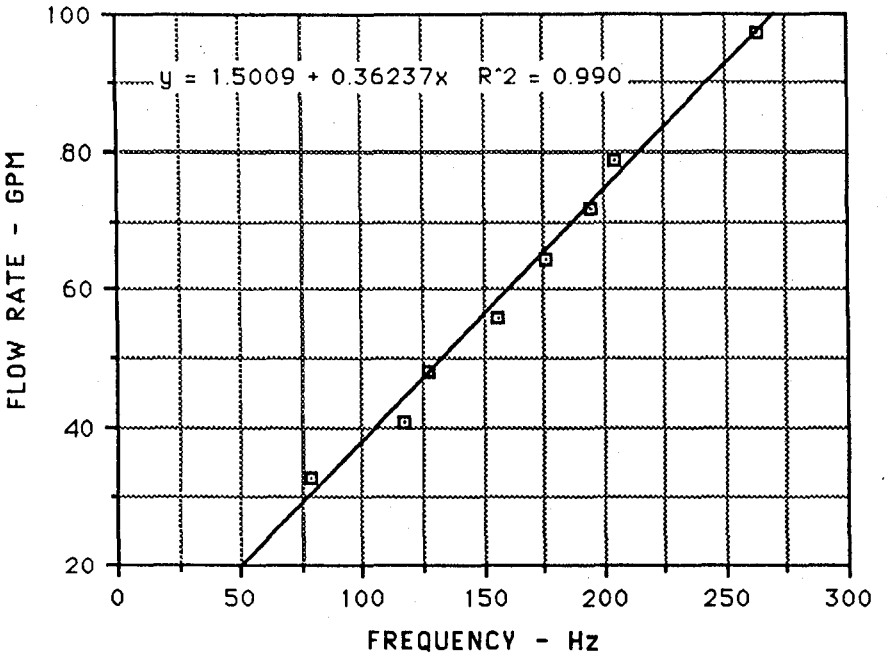

FIG. 3.10a 1.5" MODEL - RECT. BAR - WATER

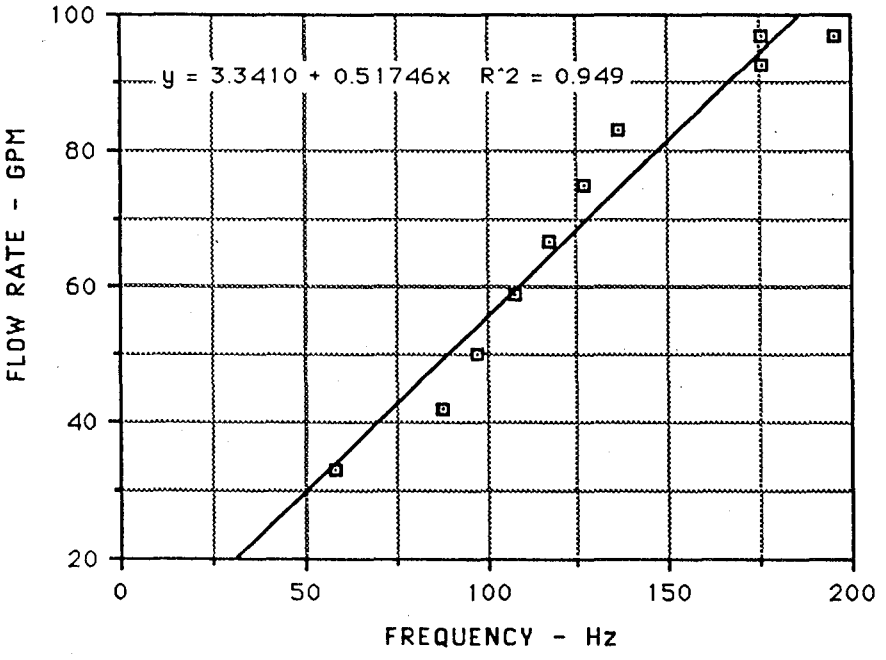

FIG. 3.10b 1.5" MODEL - CYL. BAR - WATER

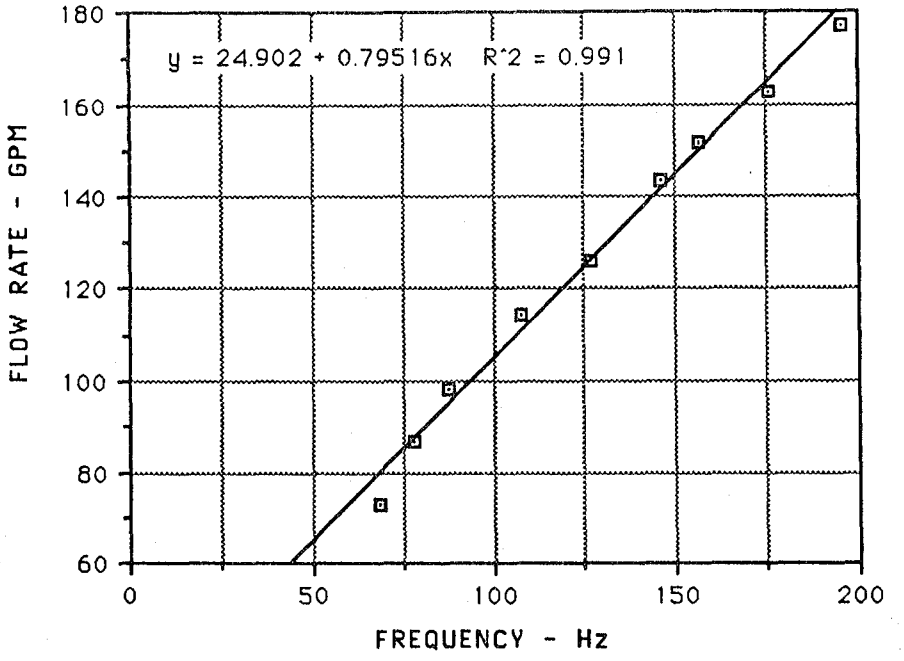

FIG. 3.11a 2" MODEL - RECT. BAR - WATER

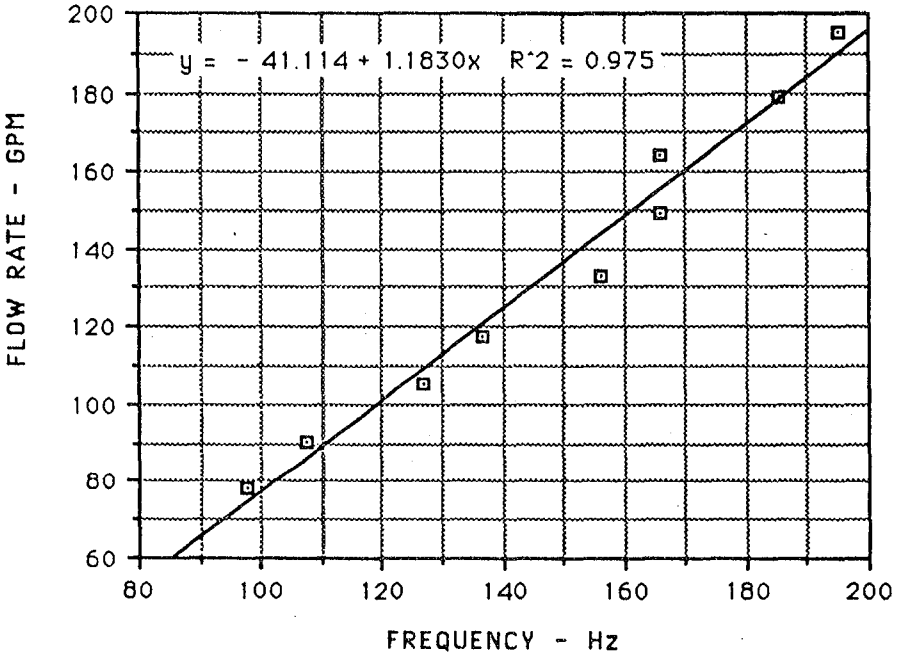

FIG. 3.11b 2" MODEL - CYL. BAR - WATER

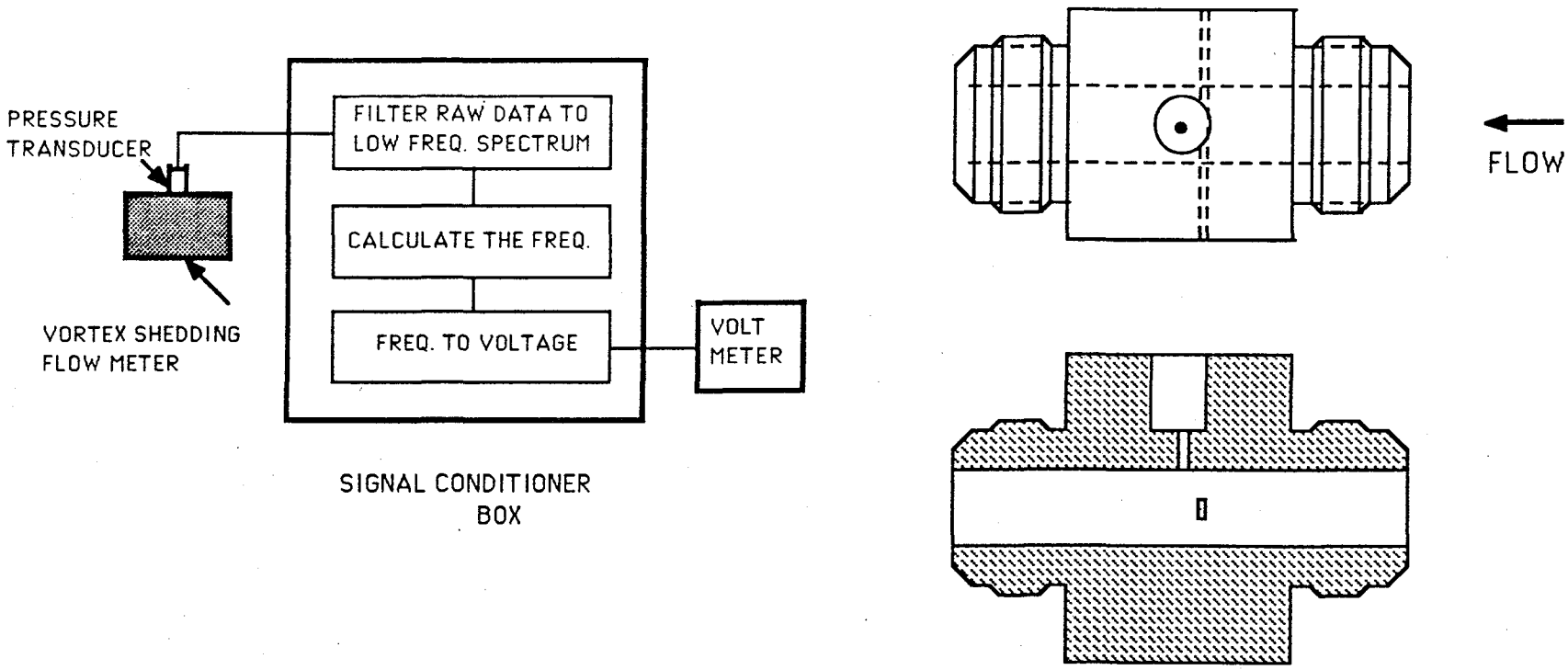

FIG. 3.12 PROTOTYPE FOR QUALIFICATION TEST AND SPEC. REQUIREMENTS

1991 NASA/ASEE SUMMER FACULTY FELLOWSHIP PROGRAM

JOHN F. KENNEDY SPACE CENTER
UNIVERSITY OF CENTRAL FLORIDA

STUDY AND DEVELOPMENT OF AN AIR CONDITIONING SYSTEM OPERATING ON A MAGNETIC HEAT PUMP CYCLE

PREPARED BY:	Mr. Pao-lien Wang
ACADEMIC RANK:	Associate Professor
UNIVERSITY AND DEPARTMENT:	University of North Carolina - Charlotte Department of Engineering Technology
NASA/KSC	
DIVISION:	Mechanical Engineering
BRANCH:	Cryogenics and Propellants
NASA COLLEAGUE:	Mr. Frank Howard
DATE:	August 19, 1991
CONTRACT NUMBER:	University of Central Florida NASA-NGT-60002 Supplement: 6

TABLE OF CONTENTS

LIST OF ILLUSTRATIONS

ACKNOWLEDGMENTS

I would like to thank NASA/ASEE Summer Faculty Fellowship Program, to Dr. E. Ramon Hosler of the University of Central Florida, to Dr. Gary Lin and Mr. willis Crumpler of the Kennedy Space Center for providing me with the opportunity to work on this challenging and rewarding project.

Ms. Kari Baird's enthusiasm and helpfulness was very much appriciated.

Special thanks are extended to my KSC colleague Mr. Frank Howard for his generous help, guidance, and encouragement throughout the project.

ABSTRACT

This report describes the design of a laboratory scale demonstration prototype of an air conditioning system operating on a magnetic heat pump cycle.

Design paramters were selected through studies perfromed by using a KSC System Simulation Computer Model.

The heat pump consists of a rotor turning through four magnetic field area created by permanent magnets. Gadolinium was selected as the working material for this demonstration prototype. Rotor was designed to be constructed of flat parallel disks of gadolinium with very small space in between. The rotor rotates in an aluminum housing. The laboratory scale demonstration prototype are designed to provide theoretically an efficiency of 62% of Carnot cycle and a Coefficient of Performance of 16.55.

SUMMARY

The objectives of the project are: (a) to complete the design of a laboratory scale demonstration magnetic heat pump prototype utilizing a KSC System Simulation Computer Model, (b) to provide engineering drawing of the prototype, and (c) to evaluate the design and begain fabrication of the demonstration prototype.

The heat pump consists of a rotor turning through four magnetic field area created by permanent magnets. Permanent magnets are selected for its considerably less expensive than with superconducting magnets for demonstration purposes. Rotor was designed to be constructed of flat parallel disks of gadolinium with very small spaces in between. Gadolinium was selected as the working material for its convenient room temperature Curie point of 293K. Parallel flat plates provide good heat transfer and maximize the ratio of heat transfer coefficient to pressure drops. The rotor rotates in an aluminum housing. Aluminum is nonmagnetic. The laboratory scale demonstration prototype was designed to provide theoretically an efficiency of 62% of Carnot cycle and a Coefficient of Performance of 16.55.

I. INTRODUCTION

The use of Freon gas-cycle to provide refrigeration and space heating has broad application in industry and for domesticluse in this country. Research has shown that the release of Freon into the atmosphere will deteriorate the ozone layer in the earth's atmosphere. As a result, research has begun to try to limit or eliminate the use of Freon for refrigeration purposes. One alternative to consider is the magnetic heat pump.

NASA Kennedy Space Center has initiated the development of an air conditioning system operating on a magnetic heat pump cycle. The project is being managed by Mr. Frand S. Howard of DM-MDE-11. The preliminary study of a laboratory scale demonstration prototype has been completed. The design and fabrication of this prototype is proposed to be continued during the 1991 NASA/ASEE Summer Faculty Fellowship Program.

1.1 Concept Description

Many configurations of magnetic heat pump have been studied; they are rotory, reciprocating, and those in which working material is stationary and the magnetic field is switched on and off. Studies have shown rotary recuperative devices to have significant advantage over the others.

The rotory magnetic heat pump consists of a rotor of magnetic working matrial with flow passages to allow heat transfer fluid to move through the rotor in thermal contact with the magnetic material. The rotor moves in a housing with ports for fluid to enter and exit the system as shown in Fig, I. The cycle executed as follows:

(1) Fluid is pumped into the housing at point 1. Fluid flow through rotor to point 2 and 4 with most fluid flows to 2.

(2) Fluid entering at 3 flows to 4 and 2 with most fluid flows to 4.

(3) Between 1 and 2 rotor becomes magnetized and heats up. Fluid flowing between 1 and 2 with the rotor removes most of the heat of magnetization of the working material and transferred to the load.

(4) In the constant magnetic field region from 2 to 3 working material is cooled against colder fluid entering at 3.

(5) From 3 to 4 working material demagnetizes while absorbing heat from the fluid.

(6) The rotor traveling from 4 to 1 is heated by fluid flowing from 1 to 4.

(7) Recuperative heating of the working material from 4 to 1 and recuperative cooling

from 2 to 3 are essential for obtaining large temperature lifts with an efficient magnetic cycle.

A KSC System Simulation Computer Model and other documentations and data were utilized to the design of the laboratory prototype.

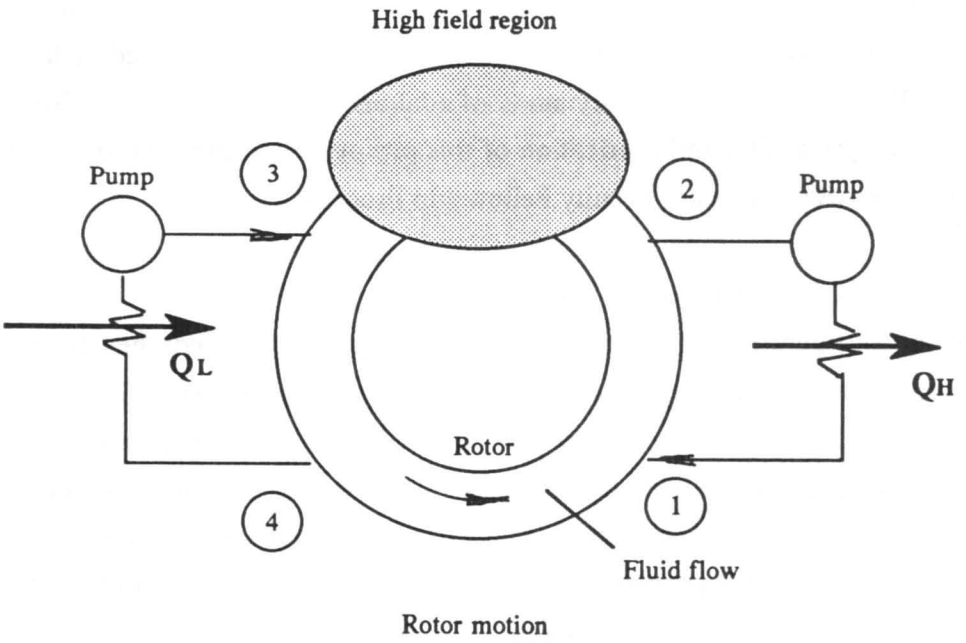

Fig. 1 Flow Schematic

II THE DESIGN OF HEAT PUMP PROTOTYPE

The design of the magnetic heat pump laboratory demonstration prototype configurations are basically done by utilyzing a KSC system simulation computer model.

2.1 The KSC System Simulation Computer Model

Structured programming

Forty separate subroutines for the following functions:

- Refrigerant entropy calculation and table building
- Refrigerant entropy from calcualated table
- Recuperator fluid data
- Heat transfer correlations
- presure drop correlations
- Adiabatic temperature rise
- Data impuit and output
- Plotting and iteration control

2.2 Use of the System Simulation Computer Model

This model is an interactive computer progaram to simulate the performance of a rotor recuperative magnetic heat pump. The computer prompts for data to define the heat pump configuration. After all data values are entered, the program prompts for the name of file containing entropy data. This file contains entropy data for various working materials and MAPS of magetic field profiles to allow simulation of heat pump with any circumferential field variation. The program also prompts for the name of a file containing recuperator fluid data. The current file contains data for several recuperator fluids. The program will print out a summary of heat pump configuration and performance. The computer will then ask for increment rotation time. This is useful for comparing one heat pump to another since each may have optimum performance at different speeds. If rotation time increment are given, a plot file will be created and an efficiency versus power density will be plotted. After runs for speeds entered are completed other variables can be changed until desirable configurations of the magnetic refrigerator found by computer iterations.

2.3 Data Input and Results of Design

Data Input:

Core Material: GDTC293
Recuperator Material: Water
Core Type: Plate
Rotor OD: 0.1524m
Rotor ID: 0.1379m
Core Hight: 0.0254m
Plate Thickness: 0.762D-04
Plate Spacing: 0.127D-03
Source Temperature: 282K
Delivery Temperature: 293K
High Field: 1
Low Field: 0
Rotation Time: 8 Sec.
Cycle/Revolution: 4

Anticipated Results:

COP W/0 Cryocooler: 16.55
Efficiency: 62.15 %Carnot
Power Density: 354.16 W/Kg
Fluid Flow Rate: 0.46701E-01 Kg/s

2.4 The Design

The laboratory scale demonstration prototype is intended to demonstratrate high efficiency greater than 50% of Carnot cycle, and to verify that the design concept is physically operable.

2.4.1 Design Parameters

Design parameters were selected by using the KSC system simulation computer model. The working material is gadolinium. Gadolinium is used because its room temperature Curie point of 293 K is convenient and because gadolinium is malleable and well characterized thermodynamically. The heat pump consists of a rotor turning through four permanent magnets. Working material executes four complete thermodynamic cycles each revolution instead of one as illustrated in Fig. I. Permanent magnets are used because demonstration of the heat pump with permanent magnets is considerably less expensive than with superconducting magnets. Peak fields

are about 1.0 T. The rotor is constructed of flat disks of gadolinium with very small gaps in between. Actual disk and gap thickness were selected by using the computer model. Rotor disks are parallel to the plane of rotation because they are simpler to manufacture and assemble. The magnetic field is applied parallel to plates to minimize the demagnetization field of the magnetic working material. The width of the rotor is designed to be only 1/4 inch to minimize the permanent flux gap. The stacked hight of gadolinium disks is one inch. Rotor turns in an aluminum housing that provids bearing races and flow ports. Aluminum is used because it is nonmagnetic and easy to machine.

The sketch of magnetic heat pump, pictorial sketch of magnetic heat pump housing, prototype assembly sketch, and selected drawings are shown in the list of illustrations section.

III CONCLUSION

This design is intended to demonstrate anticipated efficiency of the laboratory scale prototype and to verify the design is physicslly operable. It is not a device designed for practical services. Permanent magnets (peak field strength are about 1 Tesla) are selected for its less expensive than superconducting magnets (peak field strength are about 7-9 Tesla) for demonstration purposes.

The laboratory scale demonstration prototype will be fabricated and tested at Kennedy Space Center. Analysis of test results are not available at the present time.

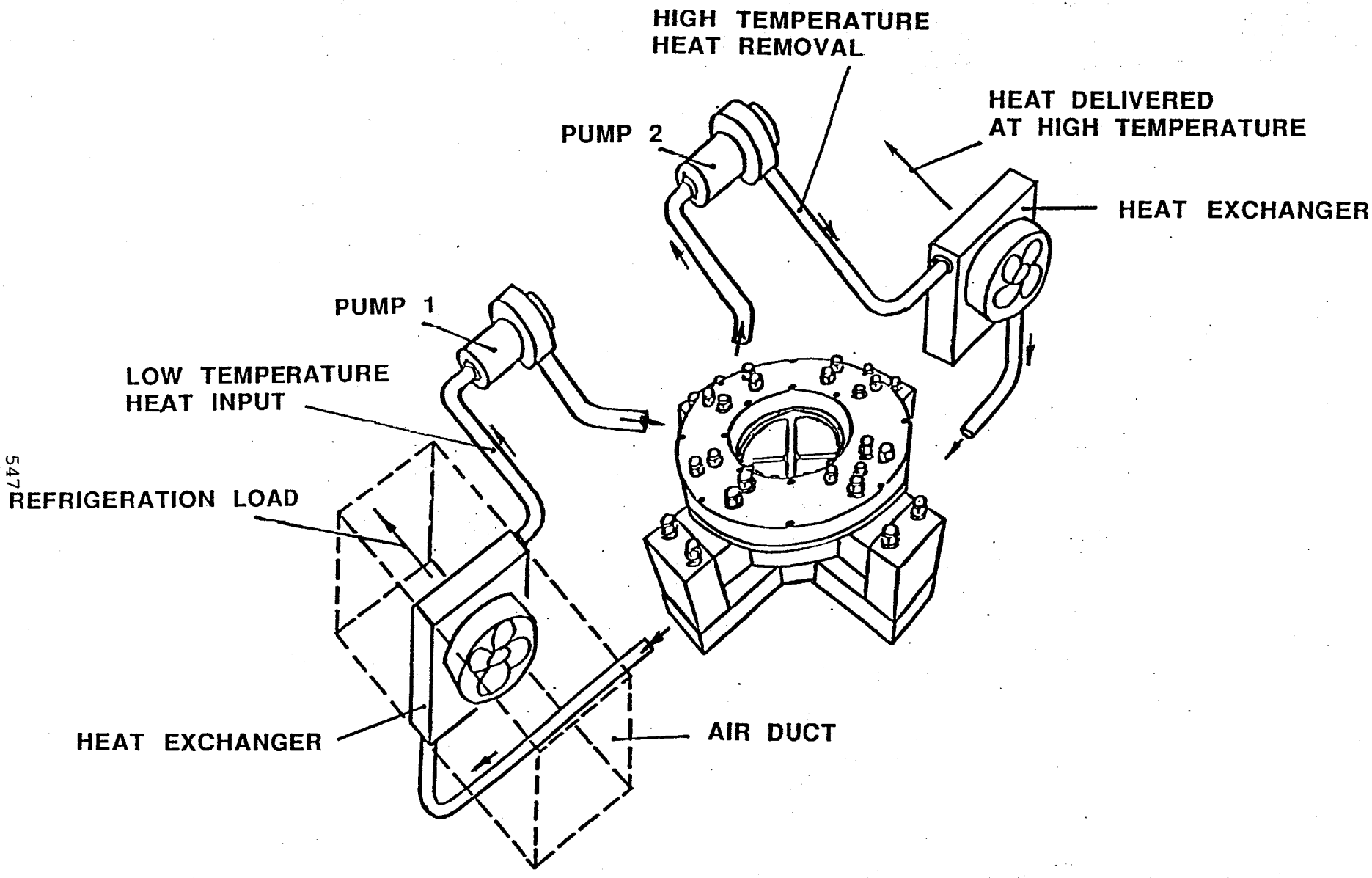

FIG 1 - SKETCH OF MAGNETIC HEAT PUMP

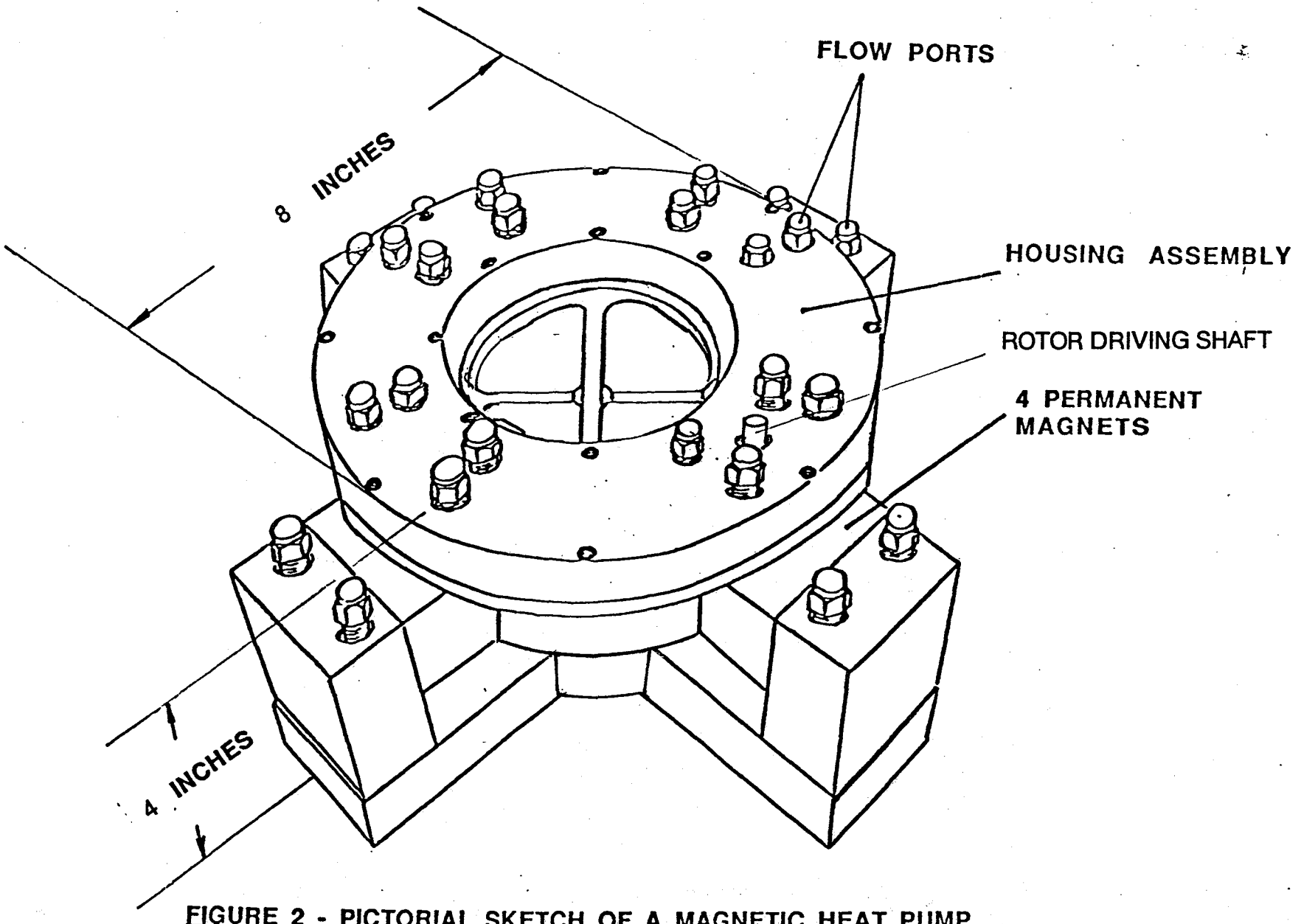

FIGURE 2 - PICTORIAL SKETCH OF A MAGNETIC HEAT PUMP HOUSING ASSEMBLY

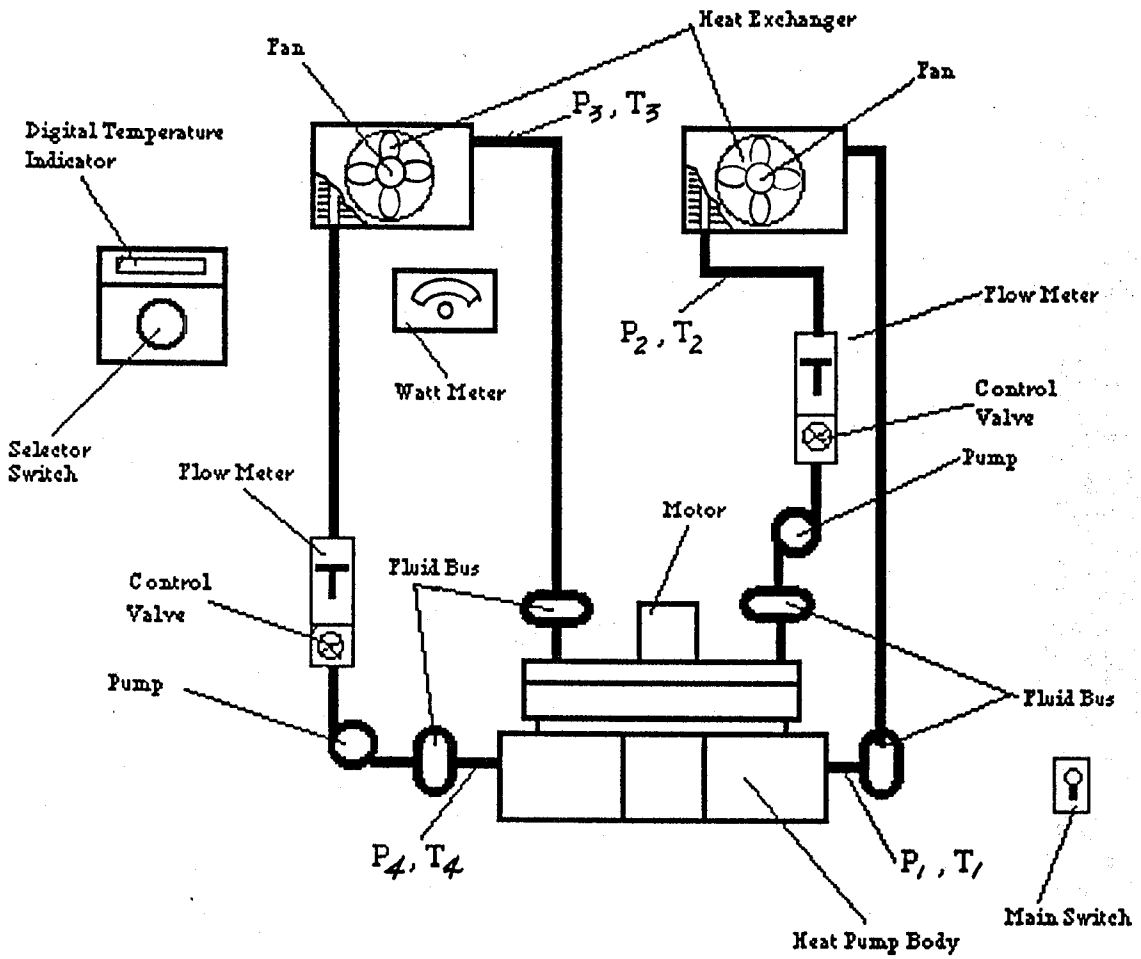

FIG. 3 MODULE ASSEMBLY

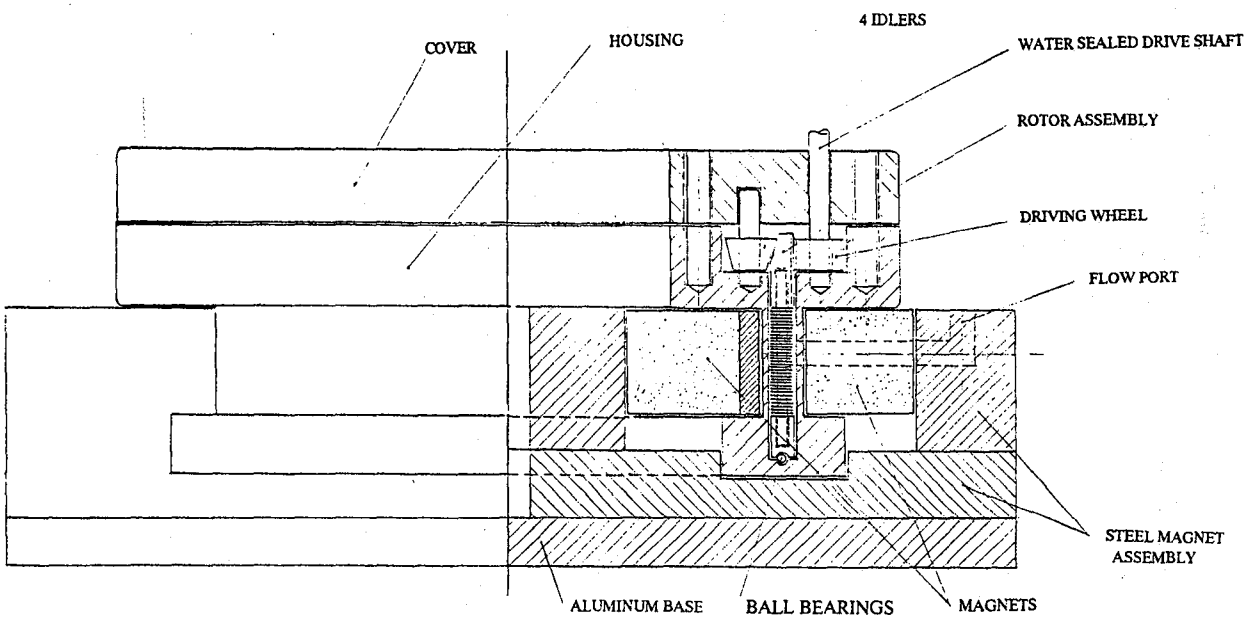

TOLERANCES (EXCEPT AS NOTED)	REVISIONS NO	DATE	BY	MAGNETIC HEAT PUMP ASSEMBLY		
DECIMAL ±	1					
	2					
FRACTIONAL ±	3			DRAWN BY	SCALE	MATERIAL
ANGULAR ±	4			CHK'D	DATE	DRAWING NO 1
	5			TRACED	APP'D	

TELEDYNE POST 18AE-08 -11X17

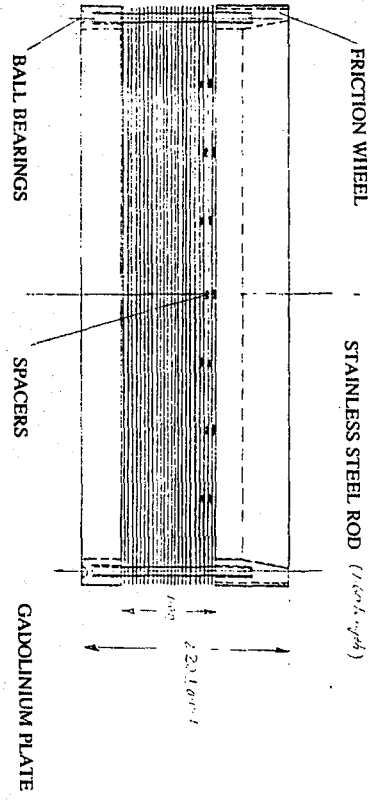

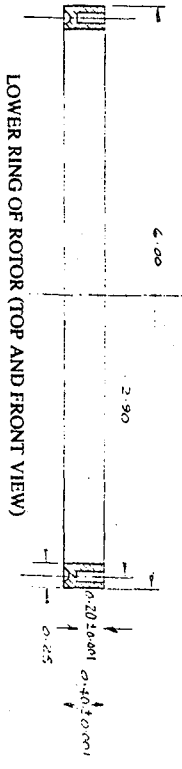

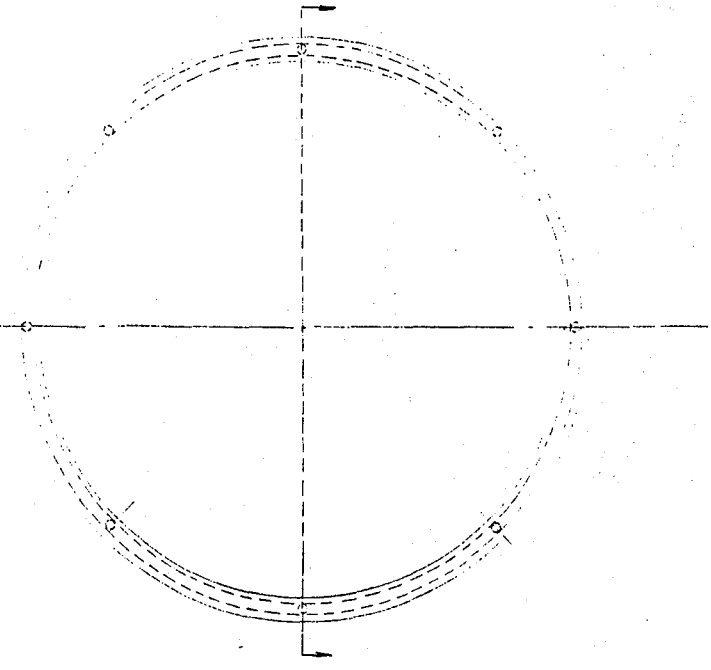

TOLERANCES (EXCEPT AS NOTED)	REVISIONS			ROTOR ASSEMBLY		
DECIMAL ± 0.001 in	NO.	DATE	BY			
FRACTIONAL ±	1					
ANGULAR ±	2					
	3			DRAWN BY	SCALE	MATERIAL
	4			CHK'D	DATE	DRAWING NO 2
	5			TRACED	APP'D	

TELEDYNE POST 18AE-08 -11X17

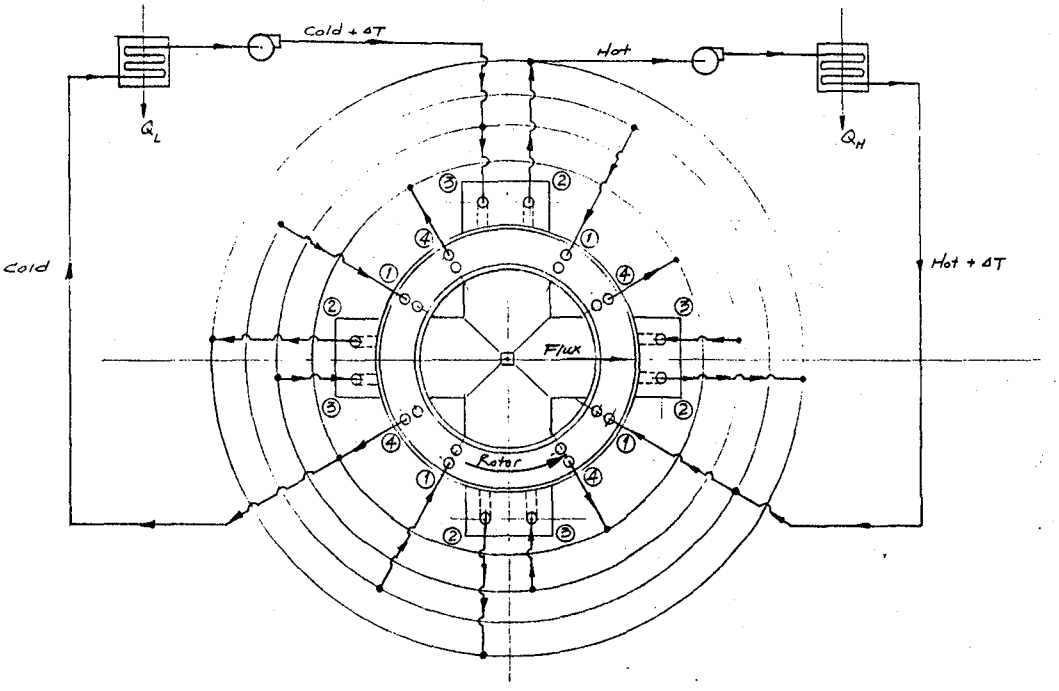

TOLERANCES (EXCEPT AS NOTED)	REVISIONS			FLUID FLOW CHART		
	NO	DATE	BY			
DECIMAL ±	1					
	2					
FRACTIONAL ±	3			DRAWN BY	SCALE	MATERIAL
	4			CHK'D	DATE	DRAWING NO. 3
ANGULAR ±	5			TRACED	APP'D	

TELEDYNE POST 18AE-08 -11 X17

REFERENCES

1. Harry J. Sauer and Ronald H. Howell, "Heat Pump Systems", John Wiley & Sons, New York 1983
2. G. V. Brown, "Basic Principles and Possible Configurations Magnetic Heat Pumps", ASHRA Transactions, 87, Pt 2, 1981
3. G. V. Brown, "Magnetic Heat Pumping Near Room Temperature", J. Appl. Phys., 47, 3673-3680, 1976
4. John R. Hull and Kenneth L. Uherka, "Magnetic Heat Pumps", Intersociety Energy Conversion Engineering Conf., Denver, August 1988

1991 NASA/ASEE SUMMER FACULTY FELLOWSHIP PROGRAM

JOHN F. KENNEDY SPACE CENTER
UNIVERSITY OF CENTRAL FLORIDA

EVALUATION AND ANALYSIS OF THE ANSI X3T9.5 (FDDI) PMD AND PROPOSED SMF-PMD AS INFLUENCED BY VARIOUS FIBER LINK CHARACTERISTICS

PREPARED BY:	Dr. M. Chris Wernicki
ACADEMIC RANK:	Associate Professor
UNIVERSITY AND DEPARTMENT:	SUNY - Maritime/NYIT Electrical Engineering
NASA/KSC	
DIVISION:	Networks Lab
BRANCH:	Communications
NASA COLLEAGUE:	Dr. Perry Rogers Mr. Jerry Barnes
DATE:	August 1, 1991
CONTRACT NUMBER:	University of Central Florida NASA-NGT-60002 Supplement: 6

Acknowledgement

The author would like to acknowledge the assistance and cooperation of a number of people at KSC without whom this research effort would not have been possible.

Dr. Perry Rogers for valuable assistance and genuine interest. Jerry Barnes, who suggested the program and provided valuable support along the way. Bryan Boatright for helping to provide laboratory space and testing equipment. Po. T. Huang for FDDI test procedures. Daniel Beavers for practical suggestions related to FDDI testing. Dr. Harry Bates -a visiting professor-for valuable computer support and the moral encouragement. In the laboratory, the Boeing Aerospace Personnel F. Houston Galloway and Bob Swindle were also most helpful in providing technical assistance. The Hewlett Packard representative, Bob Thompson who on a short notice provided a loan of the Network analyzers HP 8702 and HP 8703 for the fiber bandwidth measurements. Last but not least, I would like to thanks to Dr. Ray Hosler of UCF who managed the Summer Faculty Program and provided a great deal of support in the labs as well as outside KSC.

Abstract

The purpose of this project is to evaluate the parameters of operations outlined in the ANSI X3T9.5 (FDDI) Physical Medium Dependent (PMD) and Single Mode Fiber PMD standards based on conditions present in the KSC fiber optic cable plant. From the KSC fiber profile, it would be necessary to develop the modifications needed in existing FDDI PMD and proposed SMF-PMD standards to provide for FDDI implementation and operation at KSC. This analysis should examine the major factors that influence the operating conditions of the KSC fiber plant. These factors would include, but are not limited to the number and type of connectors, attenuation and dispersion characteristics of the fiber, non-standard fiber sizes, modal bandwidth, and many other relevant or significant fiber plant characteristics that effect FDDI characteristics. This analysis needed to gain a better understanding of overall impact that each of these factors have on FDDI performance at KSC.

Summary

This report evaluates the parameters of operations outlined in the ANSI X3T9.5 FDDI PMD standards and provides results based on the conditions present in the KSC Fiber Optic Cable Plant. This involves the development of an average link profile for KSC including limits for the multimode fiber links in the LC39 and industrial area as well as between them. The profile of the KSC Fiber is examined through the major factors that influence the operating conditions of the KSC Fiber Plant. These factors include the number and the type of connectors, non-standard fiber sizes, modal bandwidth and all other significant fiber plant characteristics that effect FDDI performance. The performance results for the Fiber Optic Plant at KSC are summarized and future research suggestions are given. Finally, the recommendation for the hardware purchases relevant to FDDI bandwidth performance testing is stated.

List of Acronyms

KSC- Kennedy Space Center

ANSI- American National Standards Institute

FDDI- Fiber Distributive Data Interface

PMD- Physical Medium Dependent

MMF- Multi Mode Fiber

SMF- Single Mode Fiber

LAN- Local Area Networks

OSIRM- Open System Interconnection Reference Model

MAC- Medium Access Protocol

BER- Bit Error Rate

Table of Contents

List of Figure

I. Introduction

I. 1. FDDI Background

1980's lack of standards hampered the growth of the short-to medium- distance fiber optic market, including LAN's and private point-to-point premise communication. In Oct. 1982 ANSI committee X3T9.5 was chartered to develop a high speed data networking standard that specified a packet switching LAN backbone that transported data at highthroughput rates over a variety of fiber. The FDDI grew out of the need for high speed interconnections among a mainframes, minicomputer and associated peripherals. The FDDI specifications encompass a token passing network enveloping two pairs of fibers operating at 100 Mb/s. The 1991-1992 standard covers the first two layers of OSIRM, through the MAC Sublayer. The optical based FDDI-LAN was design to enjoy the same type of serial interconnection provided by LAN's while providing a high bandwidth, inherent noise immunity and security offered by fiber. The FDDI is meant to provide inexpensive connectivity, thus, it focuses on the 100 Mb/s rates. The FDDI accommodates asynchronous and,in the future synchronous data transmission and is designed as a fiber optic network. This involve standardization in the following areas.

1. Duplex Optical Connectors
2. Fiber Characteristics
3. Optical bandwidth
4. Bypass relays
5. Cable assemblies

The FDDI ring is designed on overall BER < 10 to -9. The Network can tolerate up to 11dBm between the stations, and can support a total cable distance of 100 Km around the ring with 500 attachments (1000 physical connections for a total fiber path of 200 km). The intrinsic topology of FDDI is a counter-rotating token-passing ring . At least part of the reason why FDDI employs a ring topology is based on the characteristics of the optical communication. Bus and passive star topologies would require the optical transmission to be detected at several sources simultaneously. Although, practical fiber optical taps are beginning to become available, the attenuation is still such that number of nodes is relatively limited. Because the fiber optical transmission is best handled with a point-to-point configuration this aspect is included in FDDI's definition.

I. 2. FDDI requirementsoptical test performance-Multimode Fibers I. 2.1. Attenuation

Required attenuation less than 1dB/km at 1300 nm transmission measuring standard subject to EIA standard RS-455; FOTP-46 or FOTP-53.

Attenuation uniformity no greater than O.2dB at 1300 nm using OTDR per EIA standard RS-455, FOTP-59.

I. 2.2. Multimode bandwidth:

At- 3dB optical bandwidth for each optical fiber in the cable

y=1,.B-L product > 1GHz-km at 1300 nm +- 50 nm

EIA standard RS-455,FOTP-30 (frequency domain)

EIA standard RS-455,FOTP-51 (time domain)

I. 2.3. Numerical aperture, N.A:

N.A. equal to 0.2 +- 0.02 at 1300 nm optical spectrum window

EIA standard RS-455, FOTP-47 at 1300 nm.

I. 2.4. Multimode Chromatic Dispersion

Zero-dispersion wavelength point at 1300 +- 13 nm range with zero-dispersion slope no greater than 0.101 ps/nm2.km

EIA standard RS-455,FOTP-167 test method.

I. 3. KSC Fiber Optics Cable Plant.

At the present, KSC lab has as shown in Fig. 1, a number of optical communication lines installed for a single mode and multi-mode transmission. The MMF utilizes the 1300 nm carrier wavelength with a theoretical fiber bandwidth in excess of 1000 GHz.

The current FDDI requirement of 125 Mbs at the 1300 nm window utilizes only a small percentage of this.

Fig. 2 (Thanks to Dr. H. Bates) shows the actual testing diagram for the fiber loop between EDL facility and Banana River Repeater Station of a total distance of 12.4 Km.

This configuration has 12 independent fiber links and utilizes the biconic connectors for fiber jumpers and testing equipment.

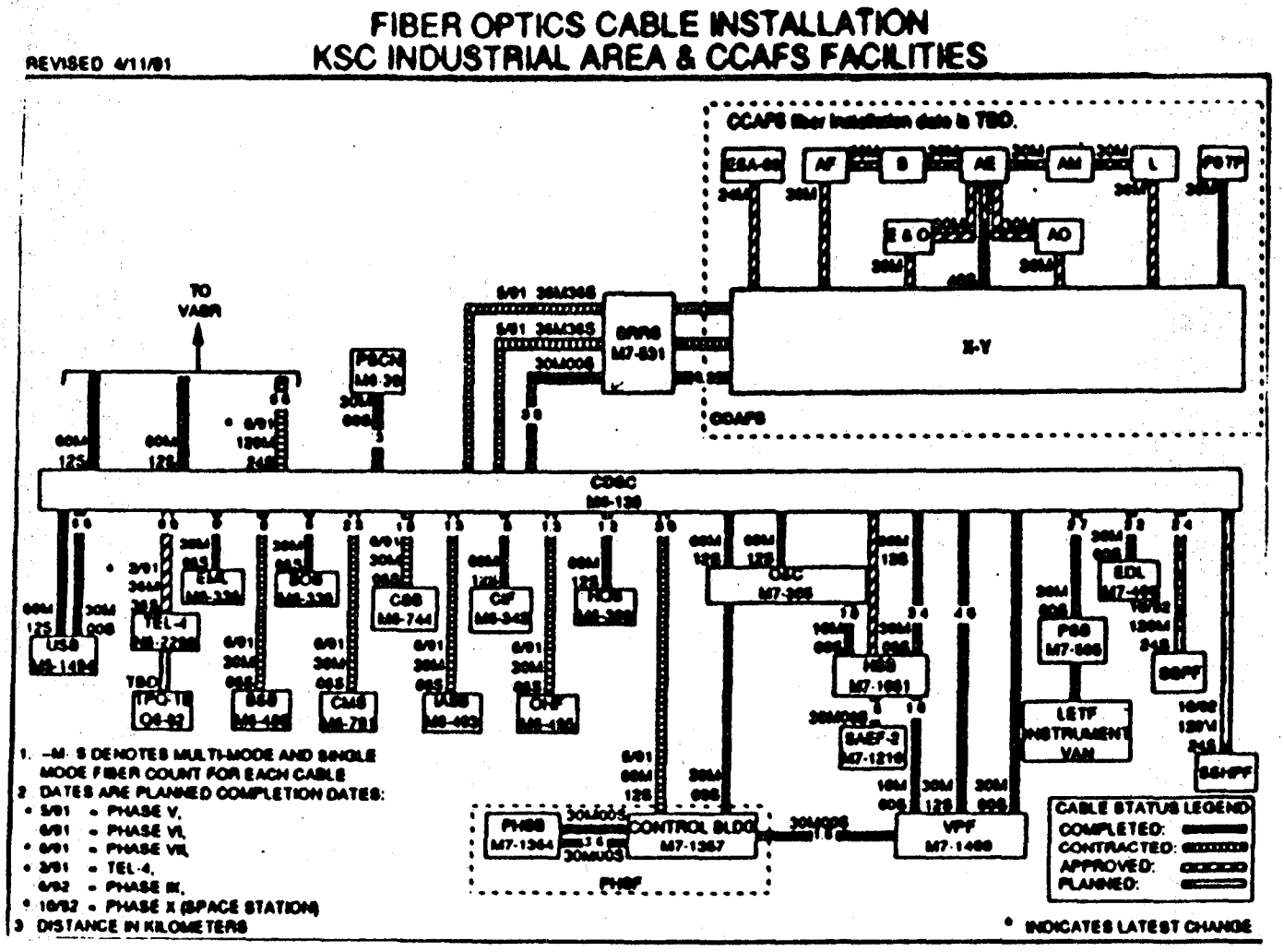

Fig.1 Fiber Optics Cable Installation at KSC

This configuration has 12 independent fiber links and utilizes the biconic connectors for fiber jumper and testing equipment.

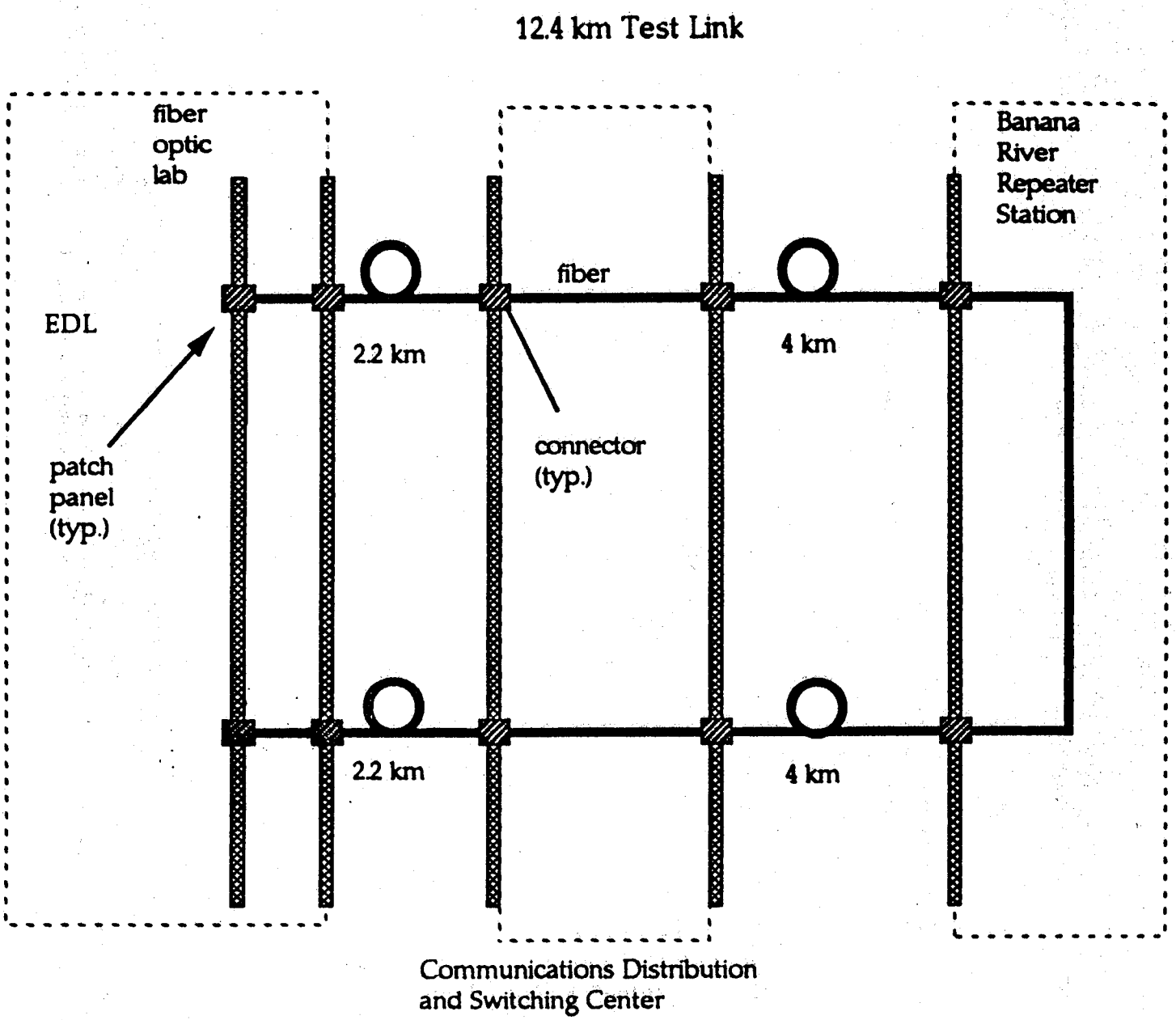

Fig. 2 The 12.4 Km Test Link

II. Laboratory test equipment

2.1. Optical Time Domain Reflectometer (OTDR)

In order to test the multimode fiber Bandwidth subject to the relevant EIA standard the TD - 9960 Local Area Network Optical Time Domain Reflectometer was used. The 9960 system consist of the main frame and large variety of plug-in optical modules, plus a fully buffered four inches digital X-Y plotter. This instrument incorporates a number of technical advances such as N-point averaging for rapid data acquisition, log transformations performed in software eliminating the linearity and temperature problem associating with analog techniques, etc. Splice loss measurements are extrapolated using curve fitting techniques for greater accuracy. Help facility is also incorporated into the instrument via the CRT display to provide instant access to information on every aspect on the use of the TD-9960(Appendix A for spects).

2.2. Optical Spectrum Analyzer

An ANRITSU optical spectrum analyzer model : MS 9001 B/BI was used to perform spectral analysis of the coherent sources used in testing the fiber. The optical spectrum analyzer is a high-speed accurate instrument design to measure the luminous spectra of Laser diodes or LED's in the range of 0.6 to 1.75 nm. Its features include wide-dynamic range and excellent linearity,high-speed measurements, high sensitivity,

guaranteed level accuracy, auto-ranging function half-bandwidth autoreading function , etc.

2.3. Lightwave Component Analyzer

The Fiber optic channels were tested using the Hewlett Packard light-wave component Analyzers HP 8702 and HP 83410 B with optical accessories: light wave source; HP 8301 A, and lightwave receiver; HP 83410 B and RF 11889 A interface kit.(provided by H.P. Company). The HP 8702 analyzer is a measuring system that injects a modulated signal into a test device and compares this modulated input signal to the signal which is transmitted or reflected by the test device. This comparison of the reflected or transmitted signal to the incident signal results in a ratio measurement that characterizes the test devices' response. A light wave component analyzer, similar to a network analyzer, provides an electrical signal to modulate a light-wave source. It also provides an electrical receiver section that compares the transmitted and reflected (demodulated) electrical signal to the RF modulation signal. The HP 8702 also provides new calibration routines and measurement features for characterizing opto-electrical and electro-optical devices directly and conveniently.

3.1 Typical Fiber Test Link.

The Fiber optics laboratory in the EDL building has a series of a multi-mode and single-mode fiber optic links as shown in Fig. 3-1

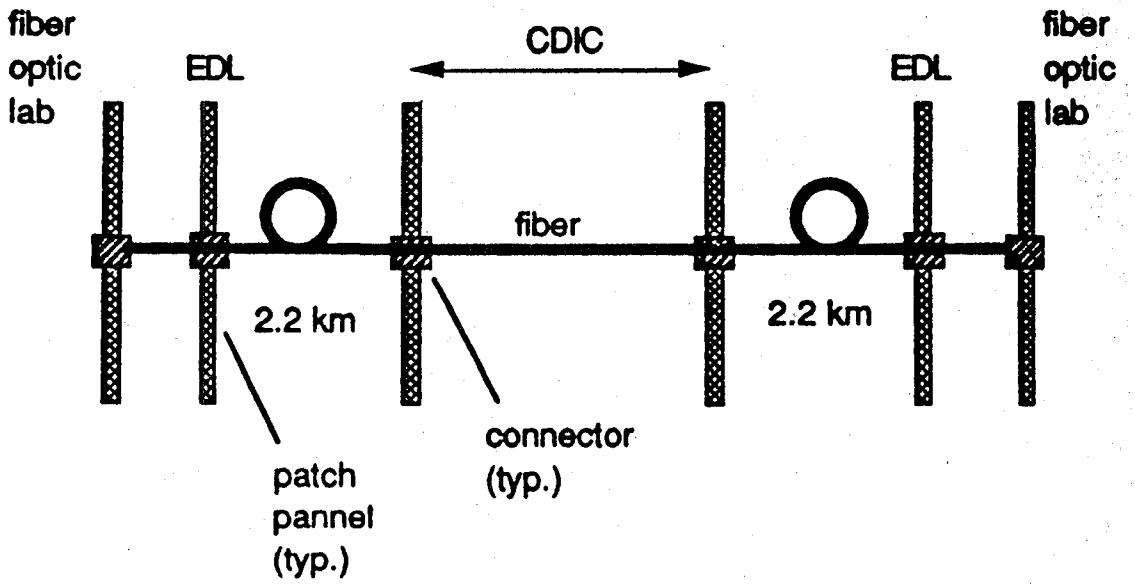

Fig 3.1 Fiber Optic Link at KSC

3.2. Attenuation Loss vs Fiber Links Length.

The attenuation loss of these links was measured as a function of the distance and number of connectors using the TD-9960 OTDR. Typical response shown in Fig. 3.2 for the link 1-2, indicates the attenuation loss in dB vs distance, loss on a biconic connectors and some reflective faults. (channels 3-12 in appendix B).

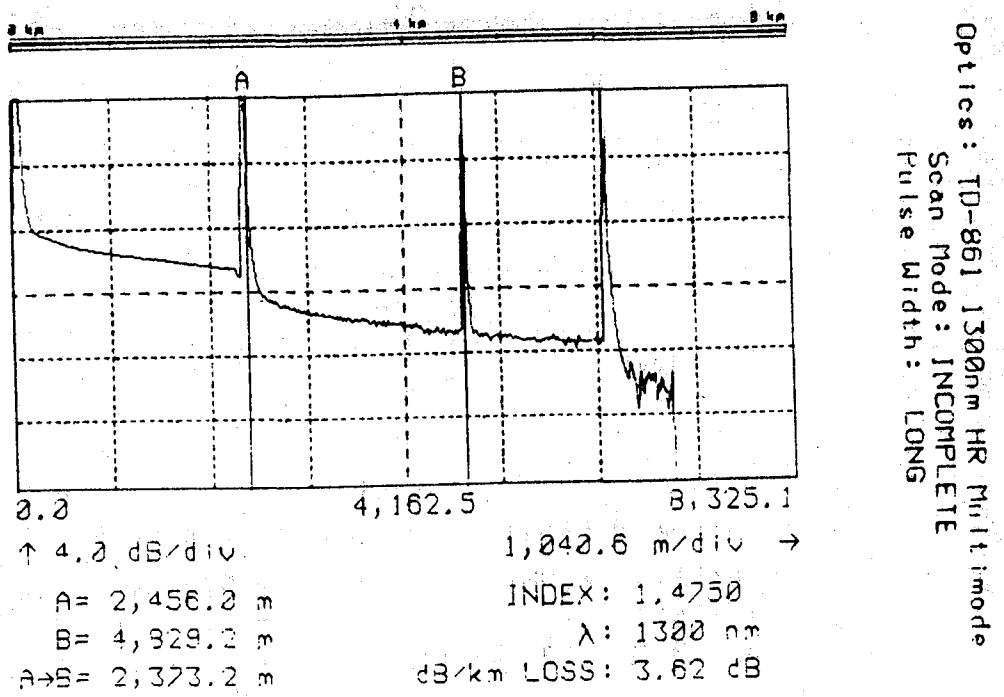

Fig. 3.2 Attenuation vs Length for MMF Link 1-2

Fig. 3.3 shows the attenuation for the link 2-1 (channels 3-12 in appendix B)

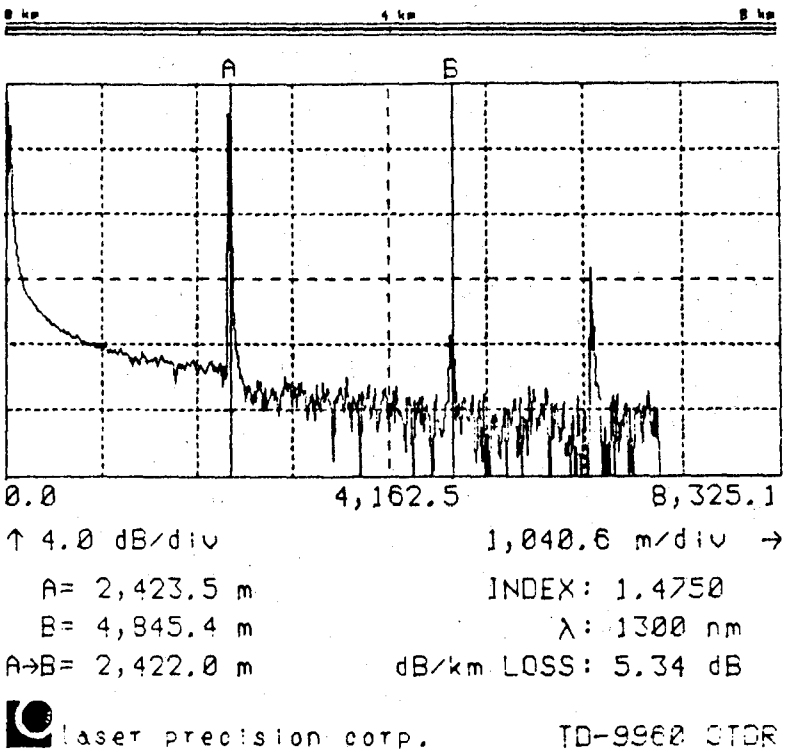

Pulse Width: SHORT

Fig 3.3 Attenuation for MMF Link 2-1

Fig. 3.4 shows the effect of an extra 1,410 m link with two additional biconic connectors. The reflective faults are shown to be a direct results of the biconic connectors.

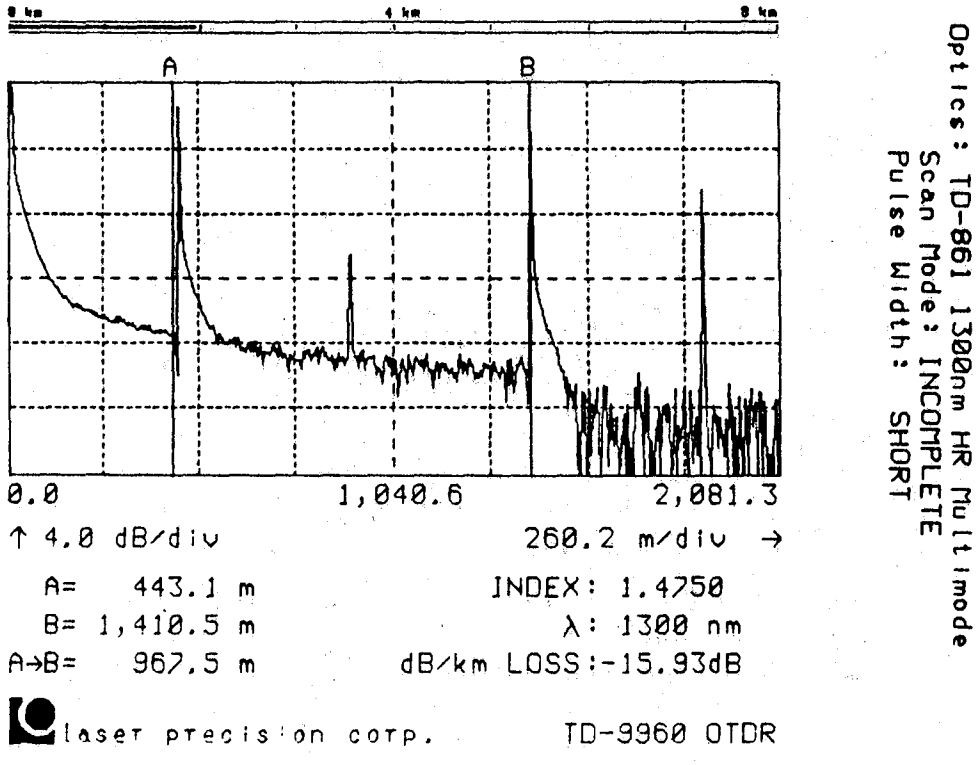

Fig. 3.4 Attenuation for 1410m MMF Link

Fig. 3.5 shows the spectral characteristics of the OTDR laser source at 1300 nm range for the future references.

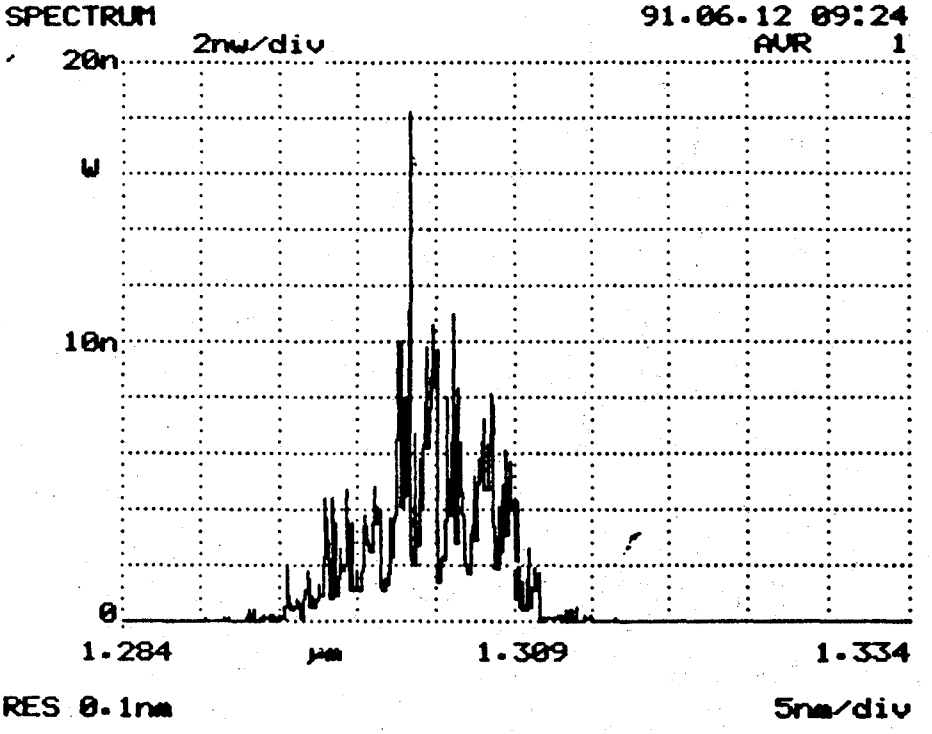

Fig. 3.5 Spectral Characteristic for OTDR Laser Source

3.3 Bandwidth Performance For KSC Fiber Link.

The lightwave component analyzer HP 8702 was used to measure the bandwidth performance of the KSC Fiber Link. The standard laser source HP 83401 A was used as a light source. The spectral characteristic of HP 83401 A is shown in Fig. 3.6

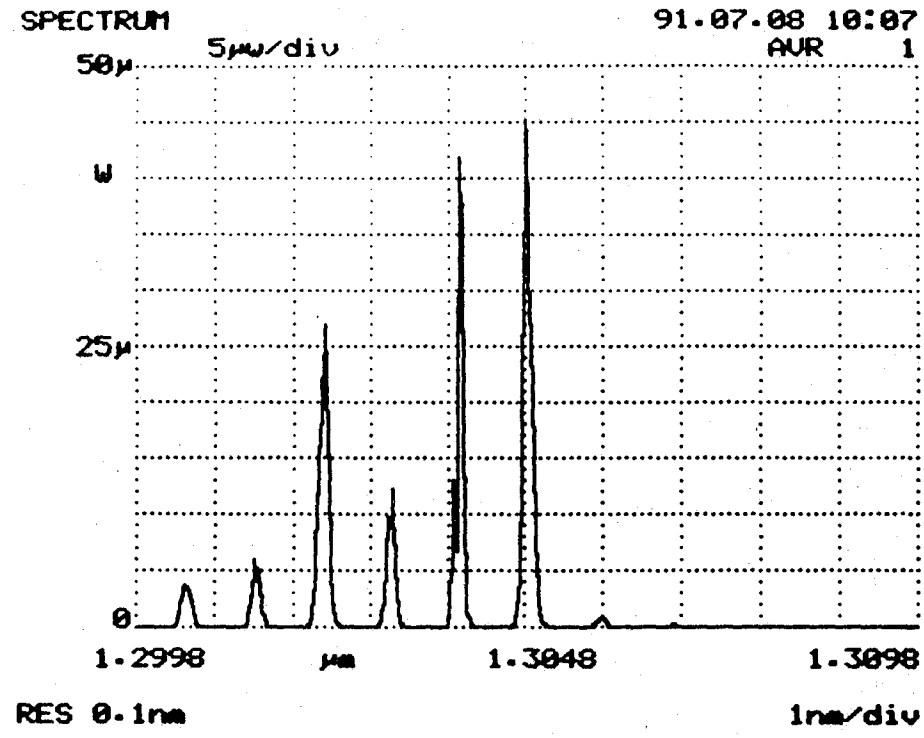

Fig. 3.6. HP 83401A Laser Source Spectral characteristic.

The warmup process and instability of HP Laser source as a function of time is shown in appendix C.

The bandwidth response for the KSC fiber Link 1-2 is shown in fig. 3.7. The -3dB bandwidth indicated by marker 1 suggest the 443.5 MHz optical bandwidth

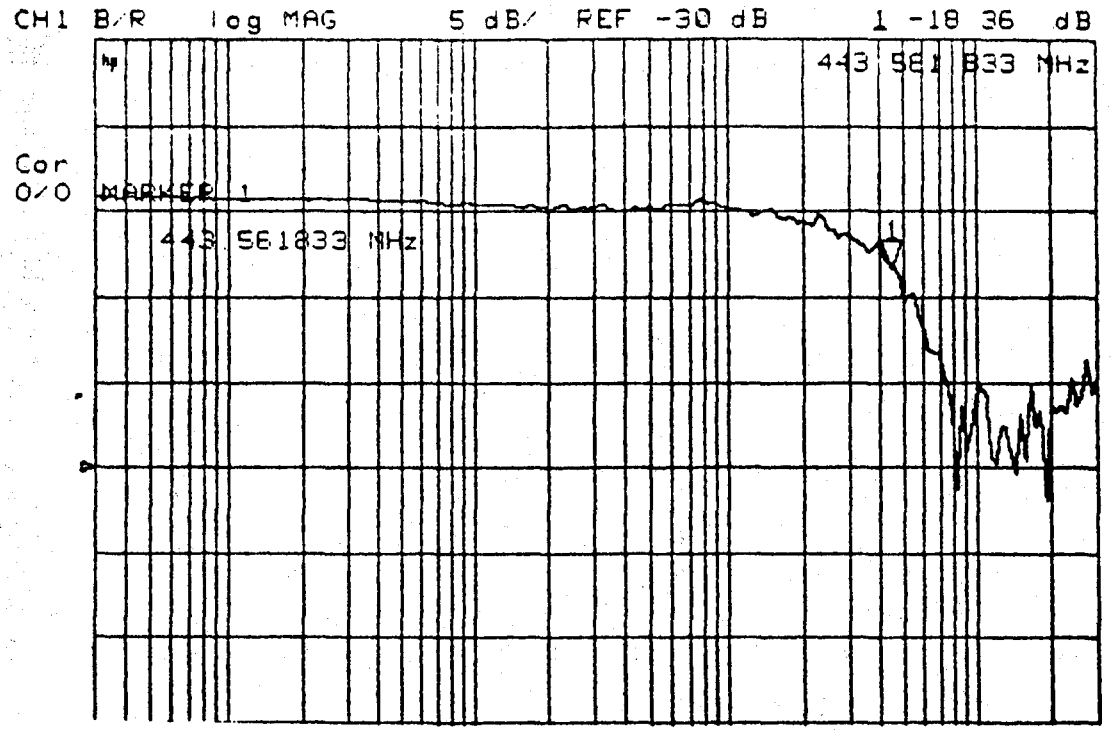

Fig.3-7 Gain vs. Frequency for the KSC link 1-2

The bandwidth response for the link 3-12 is shown in appendix D.

Fig 3.8 shown the bandwidth degradation with increased fiber link length and the -3dB cutoff at 343.8 MHz.

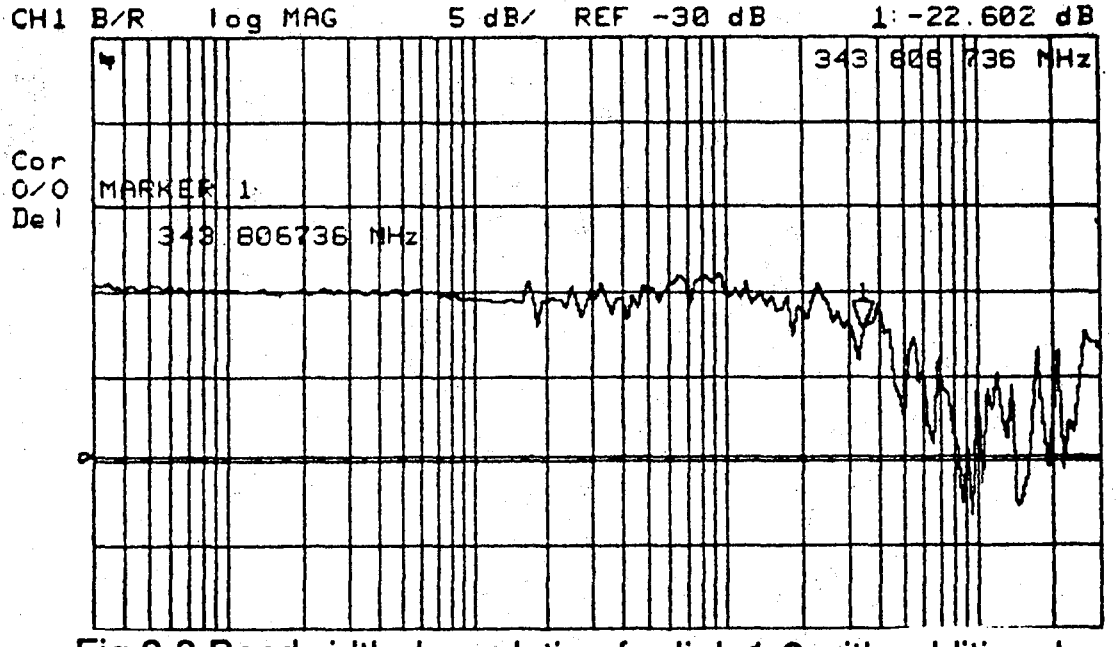

Fig 3.8 Bandwidth degradation for link 1-2 with additional 1.4km MMF length.

The effect of an extra biconic connectors is examined in Fig. 3.9. The 7 additional connectors were placed between the Laser source and the link 1-2. showing no noticeable degradation in the bandwidth .

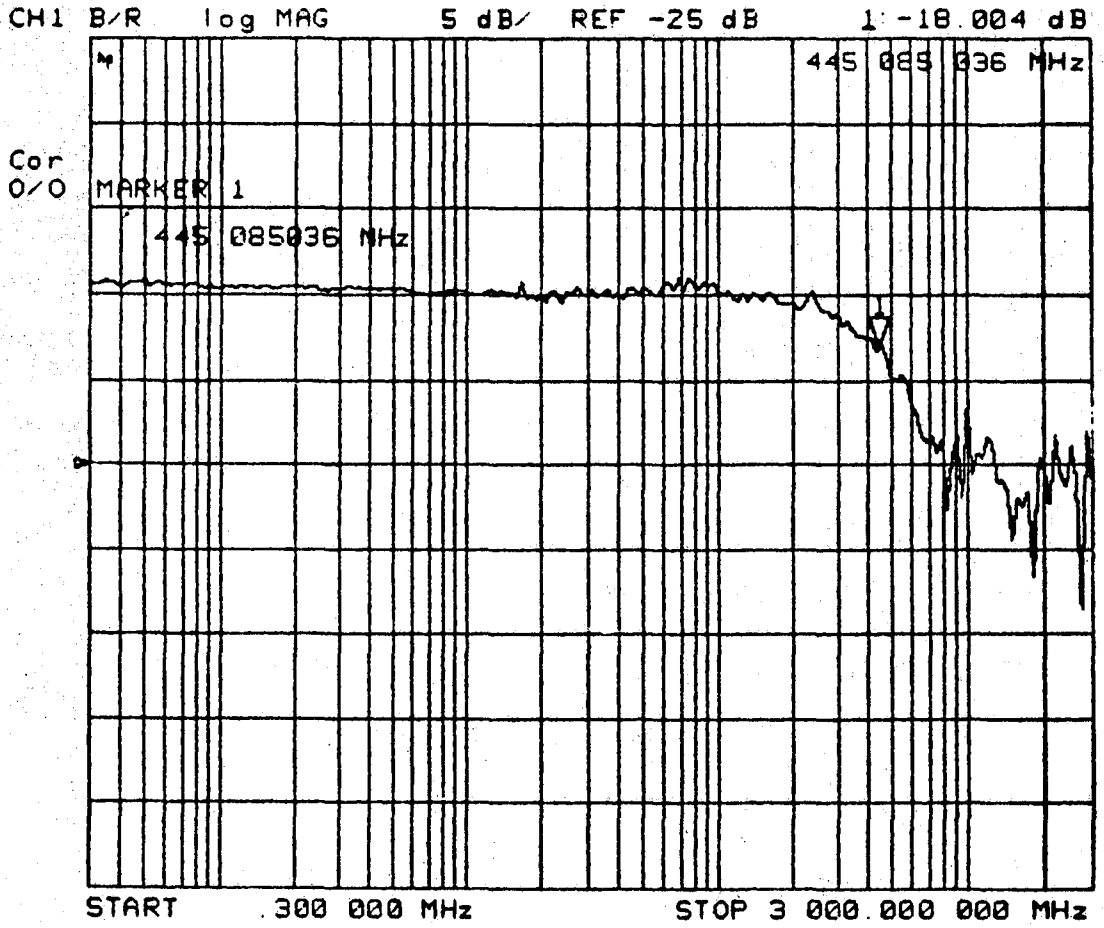

Fig. 3.9 Bandwidth response vs. additional biconic connectors

Fig.3.10 shows the bandwidth performance for the link 1-2 with additional 7 biconic connectors placed between link an optical detector. As in Fig. 3.9. there was no visible degradation in system performance. In appendix E, the effect of additional biconic connectors placed at the detector end for links 3-12 is shown. As previously observed, there was no degradation in the system performance (bandwidth) as a result of these additional biconic connectors.

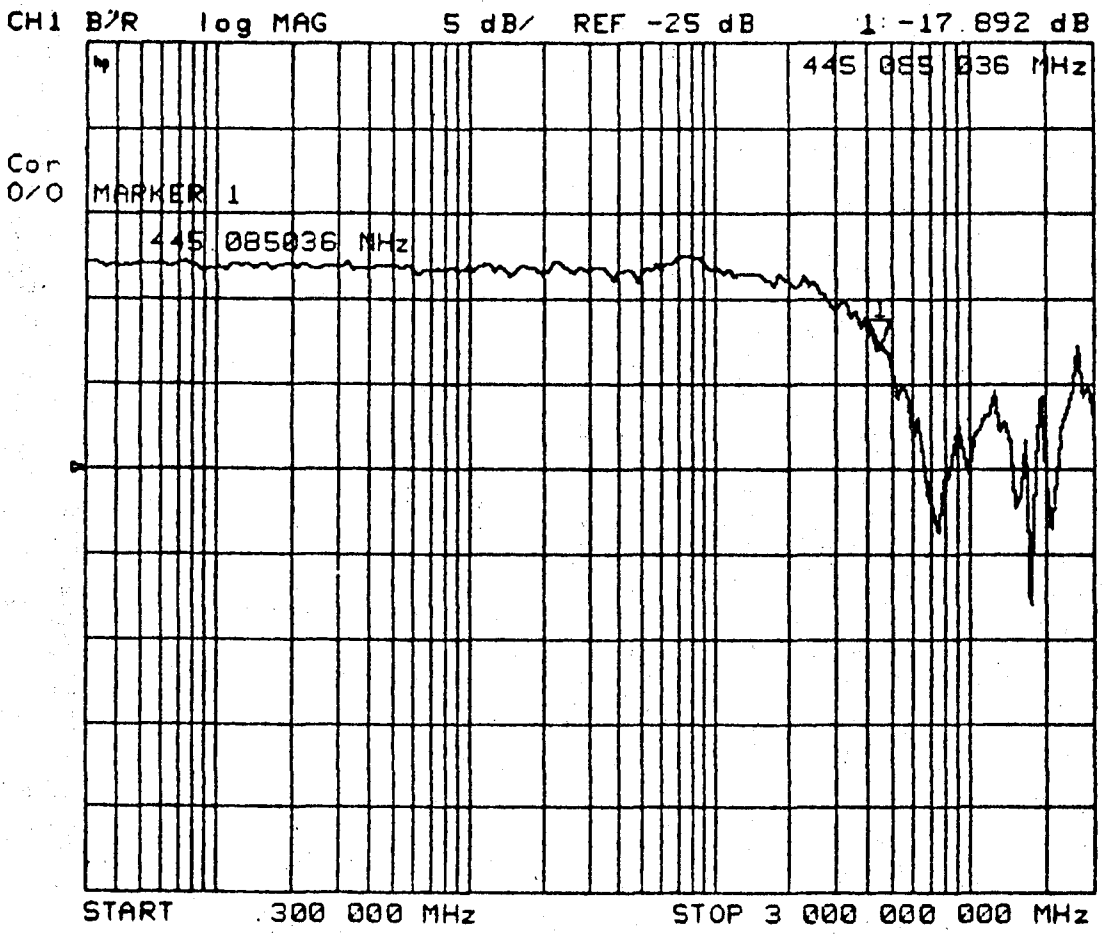

Fig. 3.10 Bandwidth vs additional biconic connectors at receiving end of the optical channel.

IV Conclusions.

The main goals of this research project were met. The KSC Fiber Optic Plant link was analyzed subject to ANSI X3T9.5 standards. Particular stress was placed on the system attenuation, and the bandwidth measurements for the multimode 50/125 micro meters fibers installed at KSC Plant. In order to assure quality measurements the optical source used in all tests were scrutinized using optical spectrum analyzer. In addition, a considerable amount of data was collected characterizing the biconic connectors and the effect they have on the overall channel transmission.The bandwidth of all 12 fiber optic test links in conjunction with a different interconnection of the biconic connectors was tested using the HP 8702 and 8703 Network analyzers (on a loan from Hewlett Packard). In conclusion, the current status of the KSC Fiber Optic Plant MMF mode will support the FDDI standard transmission data network. However, the effect of the biconic connectors, and the length of the KSC links, limits any future system expansion or improvements.

V. Future Research Suggestions.

In order to improve the performance of the FDDI at KSC the following is suggested:

5.1. Further analysis of the Biconic connectors in conjunction with large number of links at KSC.

5.2. Wave Form Fidelity

The pulse envelope measurement: the optical pulse shape output when measured through the Precision Test Fiber, shall fit within the boundaries of the pulse envelope in Fig. 5.1. For the rise and fall time measurements a minimum bandwidth range of 100 KHz to 750 MHz is required to evaluate the pulse envelope.

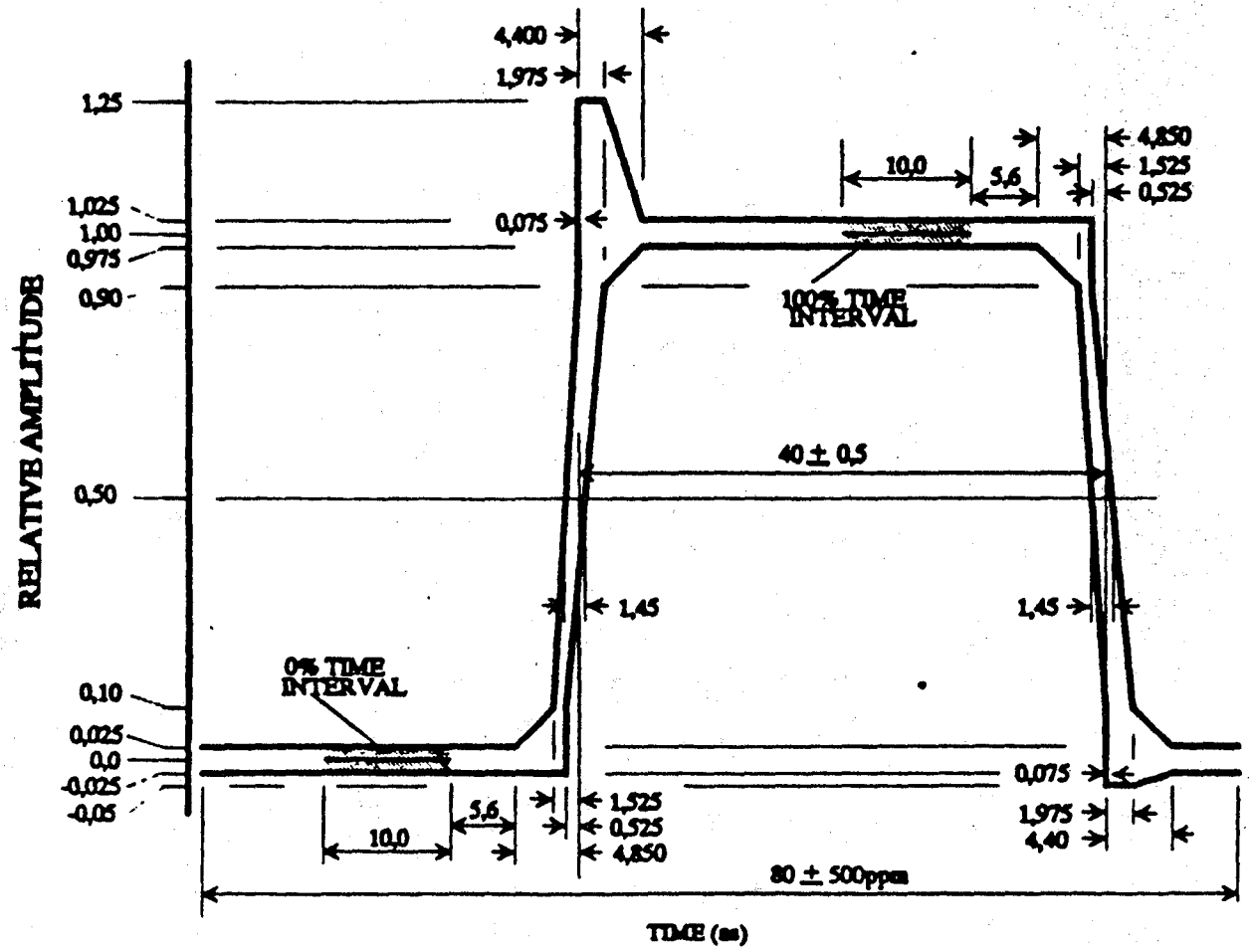

Fig.5.1 Pulse Envelope

5.3 The KSC link should be tested with FDDI Bridge FX 8210 and repeaters for a required EIA standard.

VI. Recommendation

All the bandwidth measurements for this project were done using a loaner from Hewlett Packard the Lightwave component analyzers (HP 8702 & 8703) with a Lightwave Source Module HP 83401 A and Lightwave receiver HP 83410 B with RF 11889 A interface kit. Therefore, it is recommended for the future measurements this equipment is placed permanently in the KSC Fiber Laboratory.

References:

1. Daniel Minoli, "Telecommunications Technology Handbook". Artech House 1991

2. Robert J. Ross. Fiber Optic Communications- Design Handbook Prentice Hall, 1990.

3. Chai Yeh " Handbook of Fiber Optics-theory & applications Academic Press 1990.

4. Serge UNGAR "Fiber Optics -theory & applications J. Wiley 1990.

5. Terry Edwards "Fiber-Optic Systems- Networks applications" J. Wiley 1989 .

6. N.B. Jones Jr. "Introduction to Optical Fibers Communication Systems. " HRW 1988.

7. Frederick C. Allard " Fiber Optics Handbook for scientist and engineers ". McGraw Hill 1989.

8. Amphenol Fiber Optic Products Catalog 1991

9. Hewlett Packard 1991 Tests and Measurements Catalogs

Appendix

A. Optical Time Domain Reflectometer TD-9960 Instrument Specifications.

1.2 Instrument Specifications

Data Acquisition Time (For 132 km display)	0.3 sec, Real Time 5 sec, Fast Scan 91 sec, Slow Scan Module Dependant
Readout Resolution	0.1 m, Module Dependant
Distance Scale Factors	4, 8, 16, 32, 64, 128, 256, 512, 1024, 2048, 4096, 8192, 16384 m/div. Module Dependant.
Vertical Scale Factors	0.25, 0.5, 1.0, 2.0, 4.0 dB/division
Vertical Resolution	0.01 dB
Vertical Linearity	0.04 dB/dB
Distance Accuracy	All modules except TD-860: ± 0.01 % of distance, ±4 m TD-860: ± 0.01 % of distance, ±1 m
CRT Display	7 inch, high-contrast green phosphor, raster scan, 512x480 resolution
Cursors	Dual independent with lock functions, automatic centering in expanded modes
Help Button	On line instructions and application notes which may be printed on the plotter
Video Output	NTSC Composite Video, (1V p-p 75 Ω) BNC Connector
Refractive Index	5 significant digits, range 1.0001 to 1.9999 digital entry, values retained in nonvolatile memory for each optical module.

Loss Modes	2 point- Relative loss between any two points in the fiber dB/km-Distance normalized fiber loss between any two points in the fiber Splice-Least square approximation of splice loss
Loss Resolution	0.01 dB
dB Accuracy	Digital logarithmic transformation, 0% temperature drift
Optical Modules Available (See Optical Module Specs.)	850 nm (± 30 nm) Multimode 1300 nm (± 30 nm) Multimode 1300 nm (± 30 nm) Single Mode 1520 nm (± 30 nm) Single Mode Dual 1300/1520 nm Single Mode
Interfaces	NTSC Composite Video Output (standard) RS-232C (DCE) Serial Interface (optional) GPIB (IEEE-488) Interface (optional)
Hardcopy Option	Plug-in 4 inch digital X-Y Plotter
Power Requirements	90-132 VAC, 47-63 Hz 180-260 VAC, 47-63 Hz 95 V.A. maximum
Dimensions	8" x 20.1" x 21.3"
Weight	38 pounds
Operating Temperature	-15 °C to 45 °C, ≤ 95 % Relative Humidity non-condensing (0 °C to 40 °C for rated specifications)
Storage Temperature	-20 °C to 60 °C
Laser Product Classification	21 CFR Class I, all optical modules

Accessories Provided	Power Cord Set of Fuses 2 m Fiber Optic Pigtail Instruction Manual

1.3 Optical Module Specifications

Optical Module	Wavelength Tolerance	Pulse Widths	Range For Scattering*	Maximum Range	Optical Connectors
TD-860 850 nm Multimode	± 30 nm	4 ns 40 ns	Min- 20 dB Typ- 23 dB	32 km	FC Standard Deutsch, SMA, Diamond, Biconic Available
TD-861 1300 nm Multimode	± 30 nm	10 ns 100 ns	Min- 17 dB Typ- 19 dB	64 km	FC Standard Deutsch, SMA Diamond, Biconic Available
TD-953 1300 nm Single Mode	± 30 nm	200 ns 630 ns 2 µs	Min- 20 dB Typ- 22 dB	132 km	PC Standard Biconic, D4, Diamond Availabl
TD-954 1520 nm Single Mode	± 30 nm	200 ns 630 ns 2 µs	Min- 18 dB Typ- 19 dB	132 km	PC Standard Biconic, D4, Diamond Availa
TD-955 1520/1300 Dual Single Mode	± 30 nm	200 ns 630 ns 2 µs	1300/1520nM Min- 20/17.5 dB Typ- 21/18.5 dB	132 km	PC Standard Biconic, D4, Diamond Availabl
TD-963 1300 nm Hi Res Single Mode	± 30 nm	25 ns 170 ns 1 µs	1300 nM Min- 16 dB Typ- 18 dB	64 km	PC Standard Biconic Available

Laser Safety Classification: 21 CFR Class 1

* Single-way dynamic range for a Signal to Noise ratio of 1.

1.4 Optional Equipment Available

TD-952	Fully buffered 4 inch digital X-Y Plotter, front panel plug-in.
TD-952C	4 color version of TD-952.
TD-232	RS-232C (DCE) Serial Interface for driving external HP-GL Compatible plotters. 50 to 19.2 k baud. Front panel plug-in.
TD-488	GPIB Interface for computer control. Functions: SH1, AH1, T5, L4, SR0, PP0, DC0, DT0, C0. Factory installed.
TD-910	Bare Fiber Adapter. Multimode.
TD-914	Bare Fiber Adapter. 1300 nm Single mode.
TD-960	Rugged Transit Case.

B. Attenuation Loss vs Fiber Link Length

B.1. Channels 3-12.

CH. 3-4

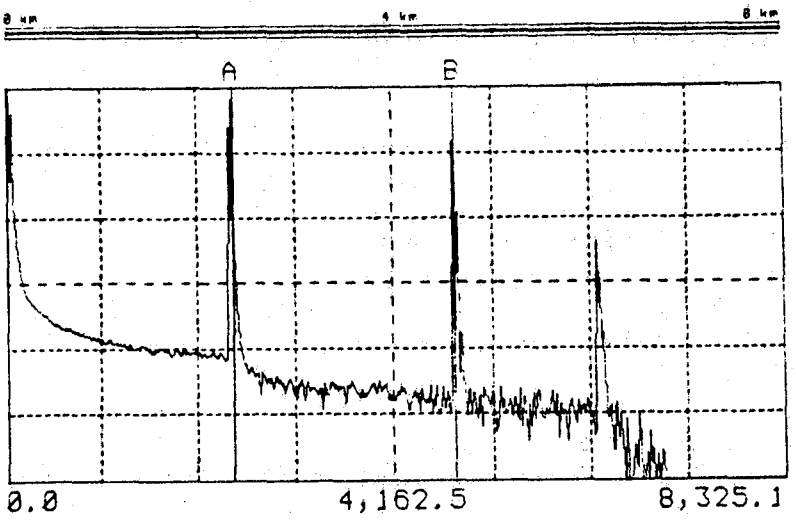

Optics: TD-861 1300nm HR Multimode
Scan Mode: SLOW
Pulse Width: SHORT

Ch. 5-6

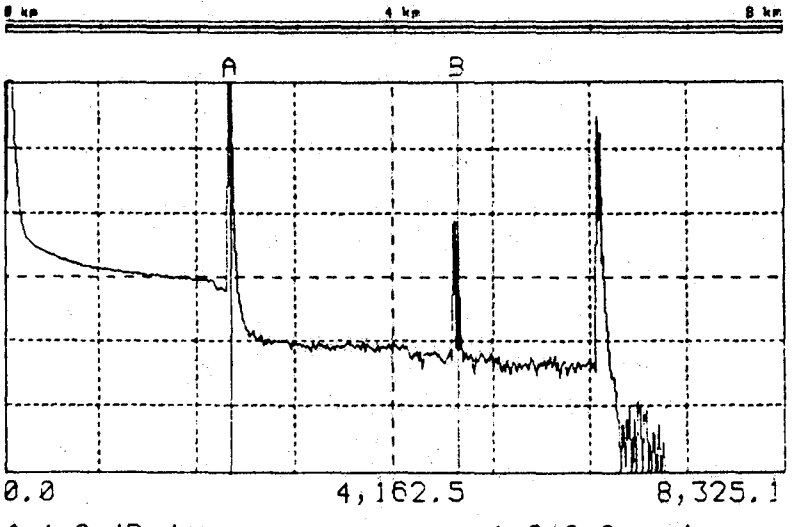

Optics: TD-861 1300nm HR Multimode
Scan Mode: INCOMPLETE
Pulse Width: LONG

Ch. 7-8

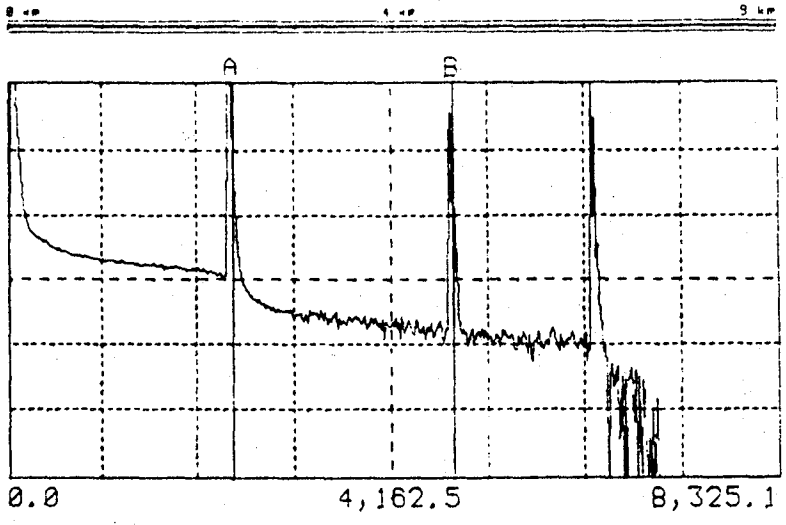

↑ 4.0 dB/div 1,040.6 m/div →

A= 2,461.0 m
B= 4,845.4 m
A→B= 2,384.5 m

INDEX: 1.4750
λ: 1300 nm
dB/km LOSS: 1.51 dB

Optics: TD-861 1300nm HR Multimode
Scan Mode: INCOMPLETE
Pulse Width: LONG

Ch.9-10

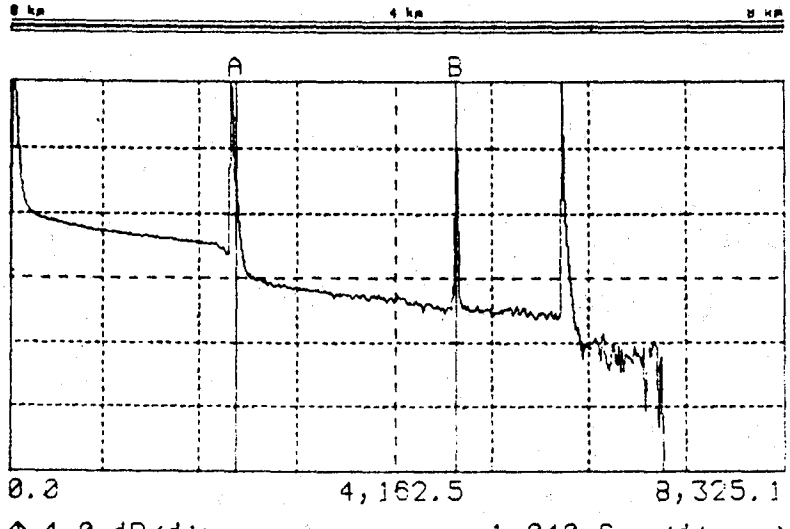

↑ 4.0 dB/div 1,040.6 m/div →

A= 2,465.0 m
B= 4,845.4 m
A→B= 2,380.4 m

INDEX: 1.4750
λ: 1300 nm
dB/km LOSS: 0.19 dB

Optics: TD-861 1300nm HR Multimode
Scan Mode: INCOMPLETE
Pulse Width: LONG

Ch. 11-12

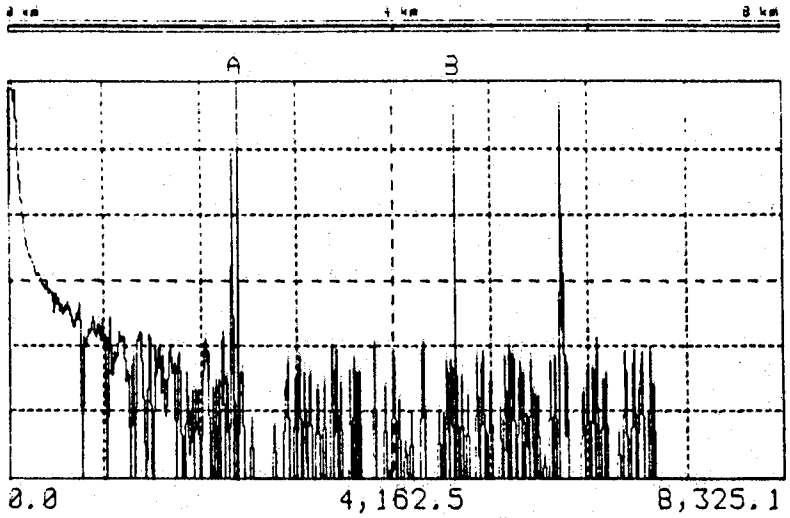

↑ 4.0 dB/div 1,040.6 m/div →

A= 2,465.0 m
B= 4,845.4 m
A→B= 2,380.4 m

INDEX: 1.4750
λ: 1300 nm
dB/km LOSS:-0.46 dB

Optics: TD-861 1300nm HR Multimode
Scan Mode: INCOMPLETE
Pulse Width: LONG

B.2. Channels 12-3

Ch.4-3

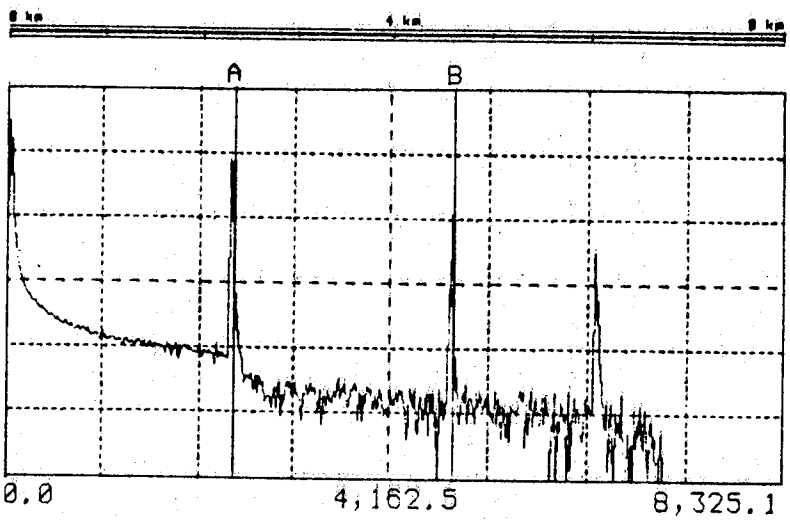

↑ 4.0 dB/div 1,040.6 m/div →

A= 2,433.7 m
B= 4,845.4 m
A→B= 2,405.7 m

INDEX: 1.4750
λ: 1320 nm
dB/km LOSS: 2.39 dB

Optics: TD-861 1300nm HR Multimode
Scan Mode: INCOMPLETE
Pulse Width: SHORT

Ch. 6-5

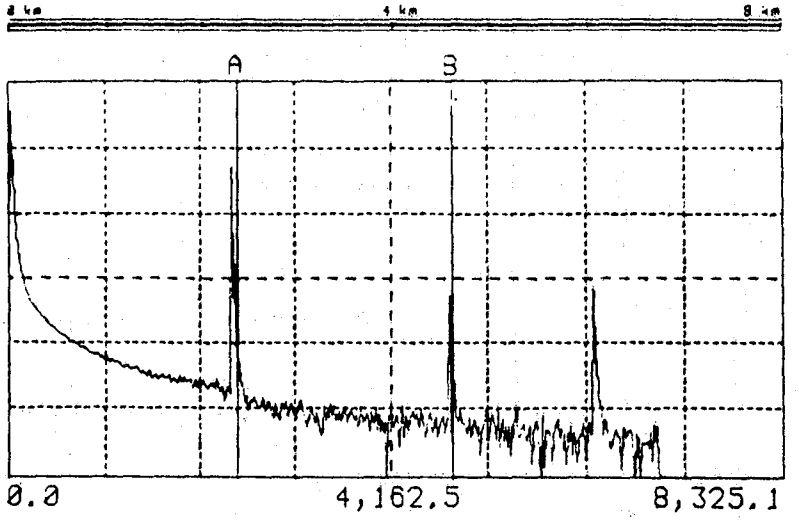

A= 2,455.2 m
B= 4,829.2 m
A→B= 2,373.9 m

INDEX: 1.4750
λ: 1300 nm
dB/km LOSS: 2.90 dB

Optics: TD-861 1300nm HR Multimode
Scan Mode: INCOMPLETE
Pulse Width: SHORT

Ch. 8-7

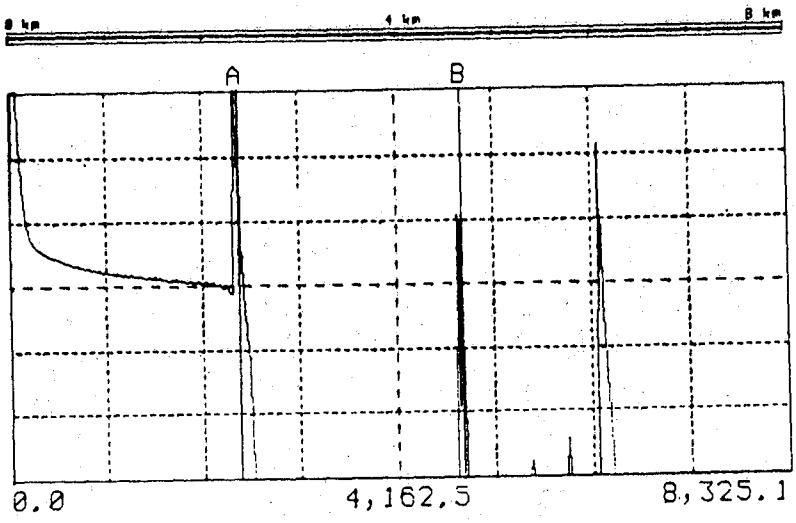

A= 2,439.7 m
B= 4,861.7 m
A→B= 2,422.0 m

INDEX: 1.4750
λ: 1300 nm
2-POINT LOSS:15.02 dB

Optics: TD-861 1300nm HR Multimode
Scan Mode: INCOMPLETE
Pulse Width: LONG

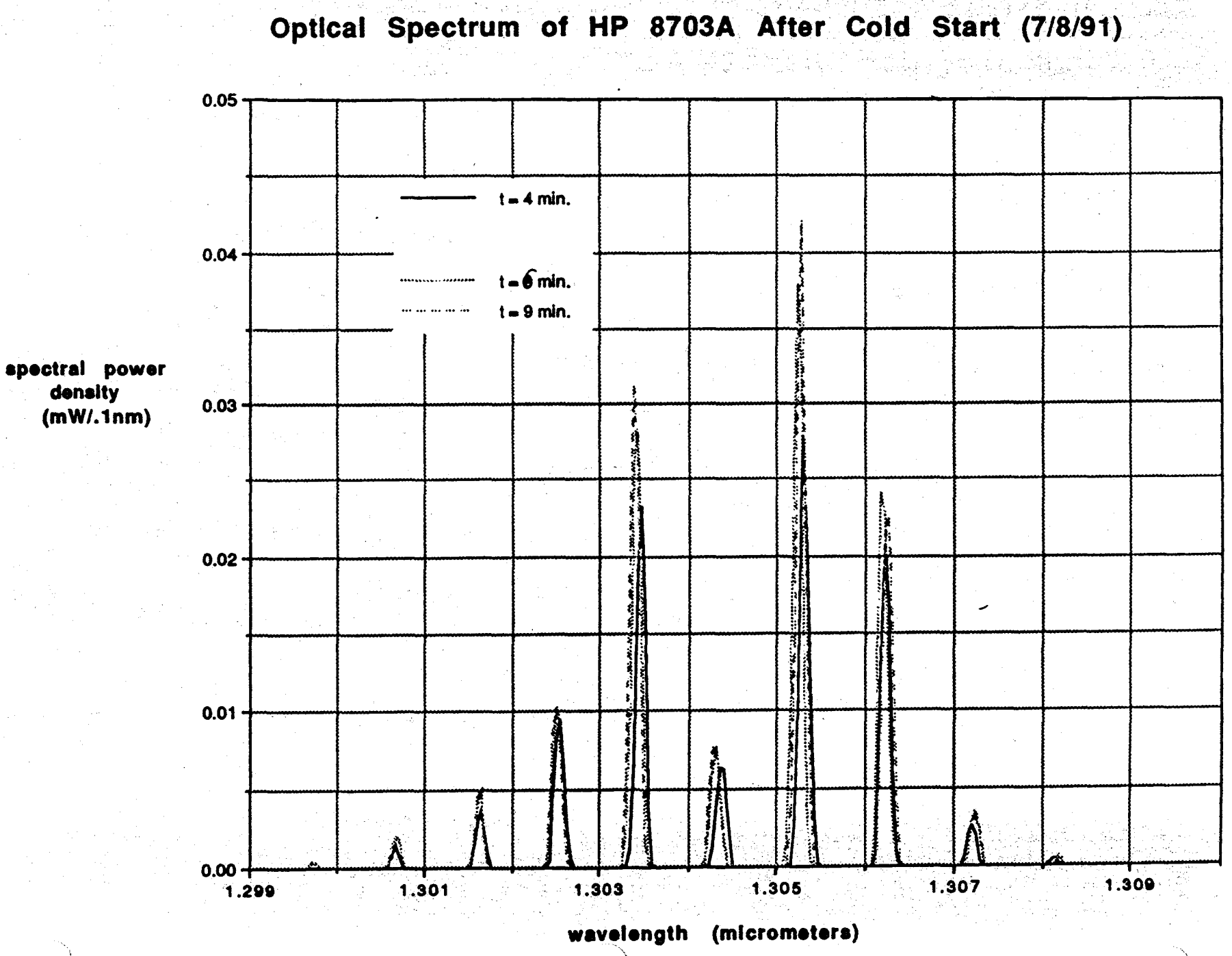
Optical Spectrum of HP 8703A After Cold Start (7/8/91)
spectral power density (mW/.1nm)
0.05
0.04
0.03
0.02
0.01
0.00
t = 4 min.
t = 6 min.
t = 9 min.
1.299
1.301
1.303
1.305
1.307
1.309
wavelength (micrometers)

D. Gain vs Frequency for the KSC Links 3-12

Ch. 3-4

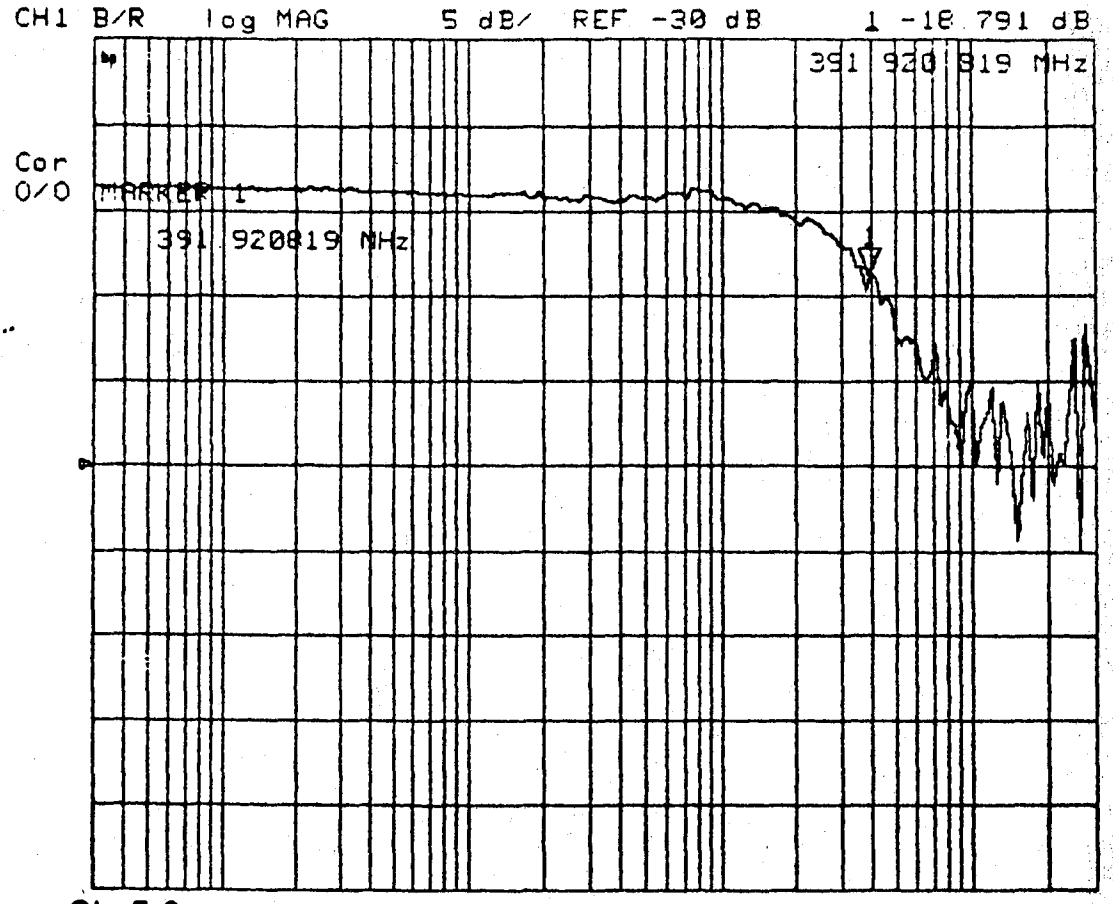

Ch. 5-6

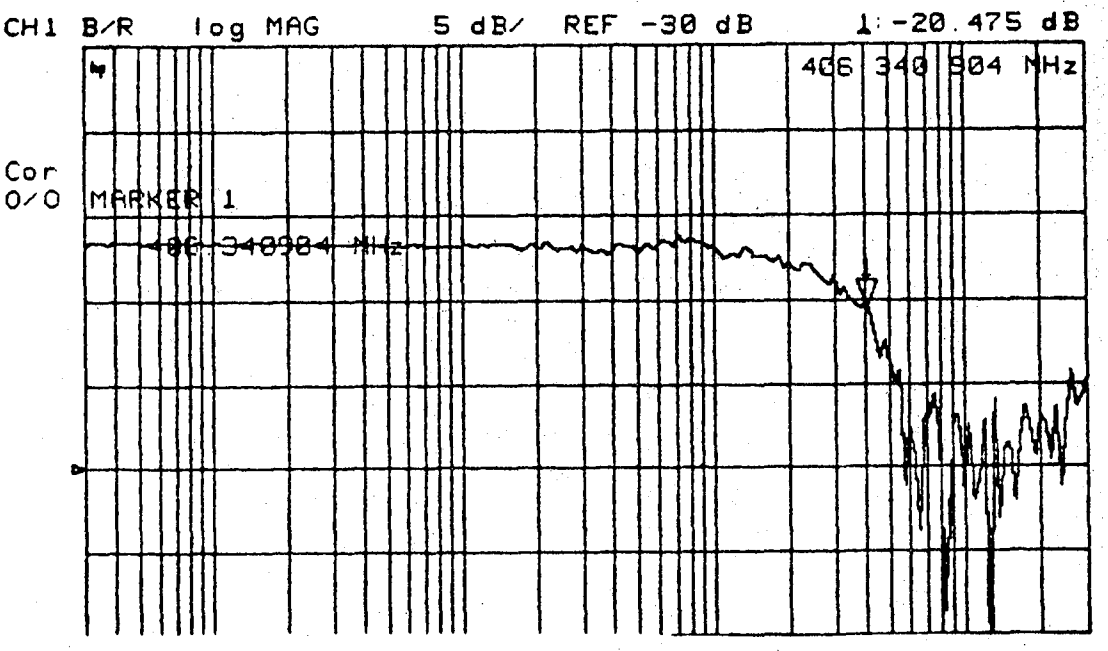

Ch. 7-8

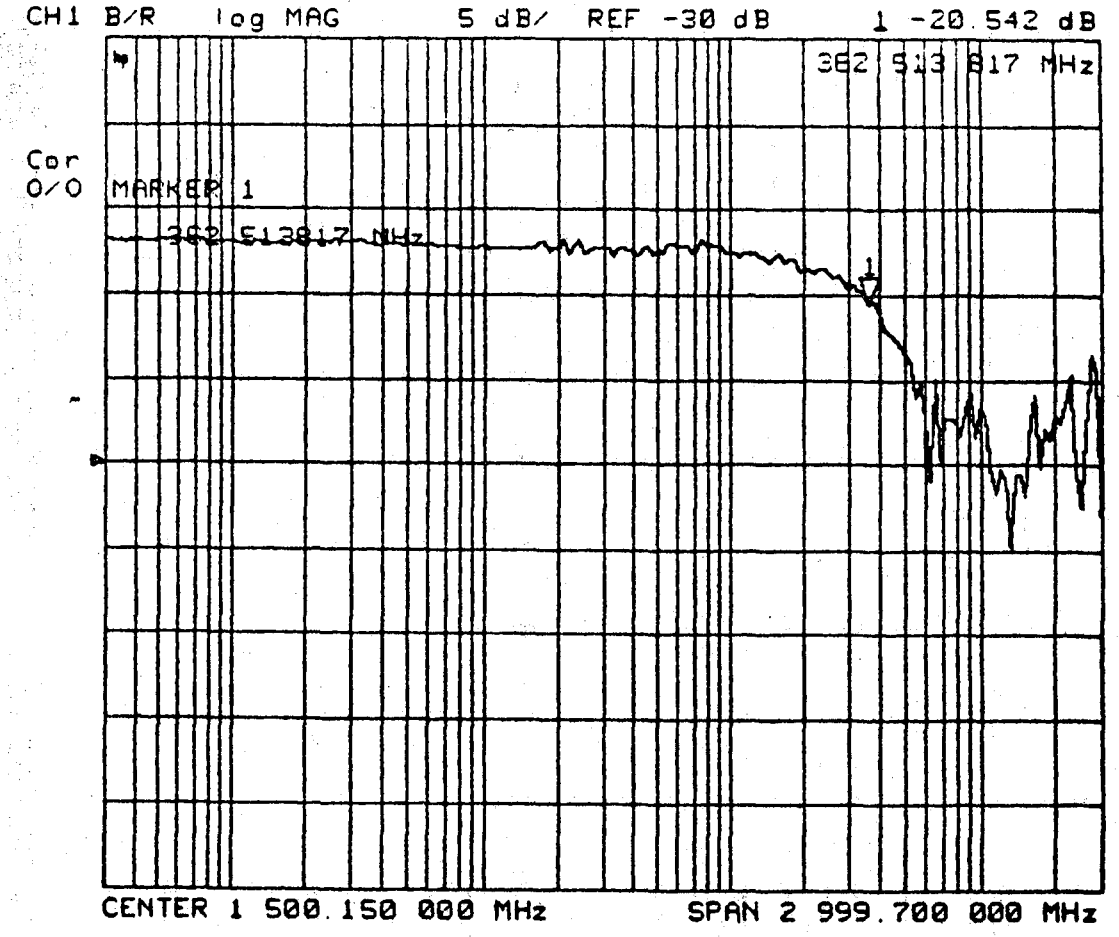
CH1 B/R log MAG 5 dB/ REF -30 dB 1 -20.542 dB
382 513 817 MHz
Cor
0/0
MARKER 1
382.513817 MHz
CENTER 1 500.150 000 MHz
SPAN 2 999.700 000 MHz

Ch. 9-10

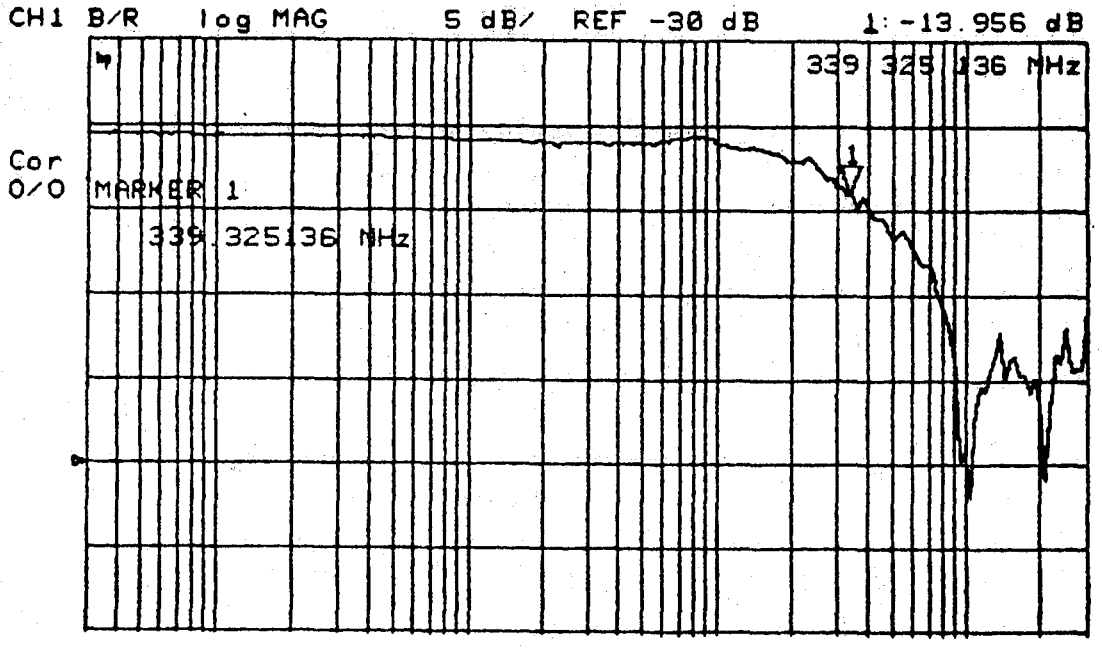
CH1 B/R log MAG 5 dB/ REF -30 dB 1: -13.956 dB
339 325 136 MHz
Cor
0/0
MARKER 1
339.325136 MHz

Ch.11-12

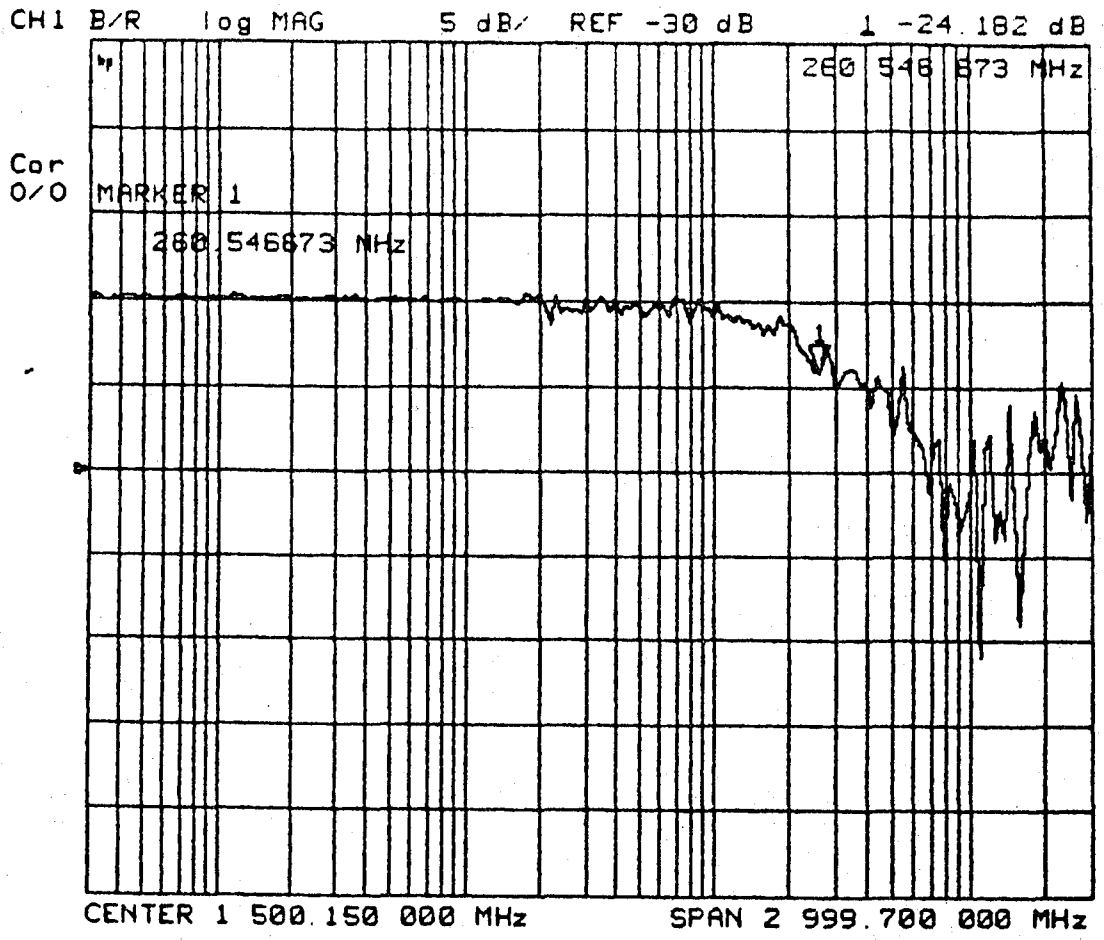
CH1 B/R log MAG 5 dB/ REF -30 dB 1 -24.182 dB
260 546 873 MHz
Cor
0/0
MARKER 1
260.546873 MHz
CENTER 1 500.150 000 MHz
SPAN 2 999.700 000 MHz

Appendix E

Effect of a biconic connectots on the KSC Fiber Plant placed at the detector end for Limks 3-12

Ch. 3-4

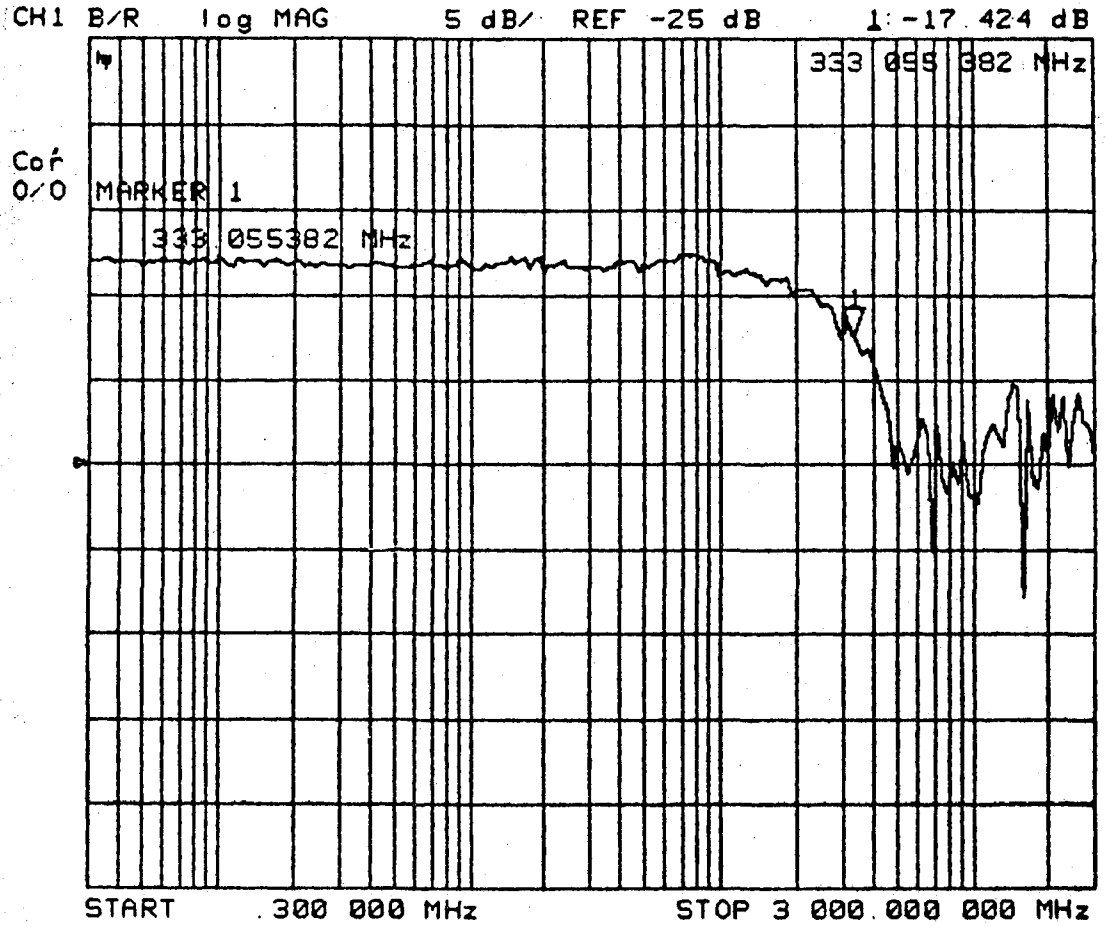

Ch. 5-6 plus additional biconic connectors

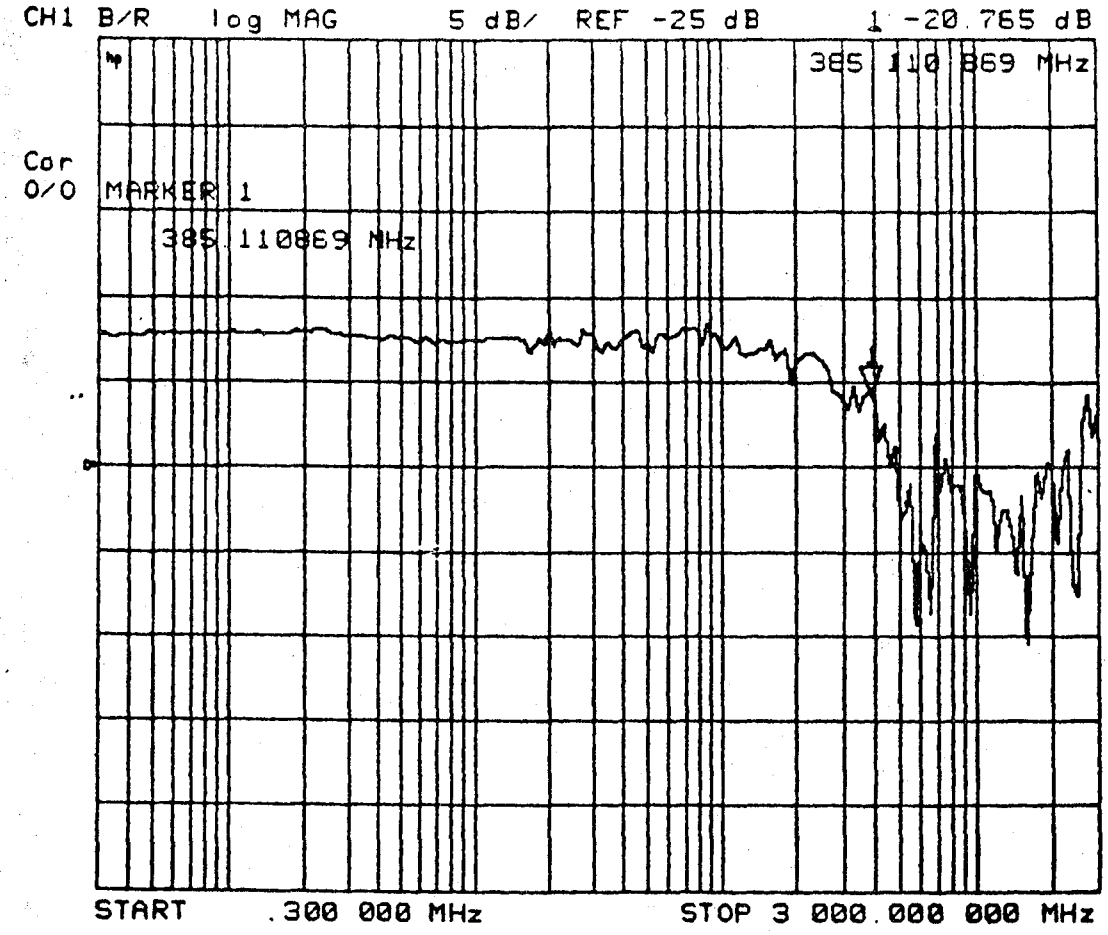

Ch. 7-8

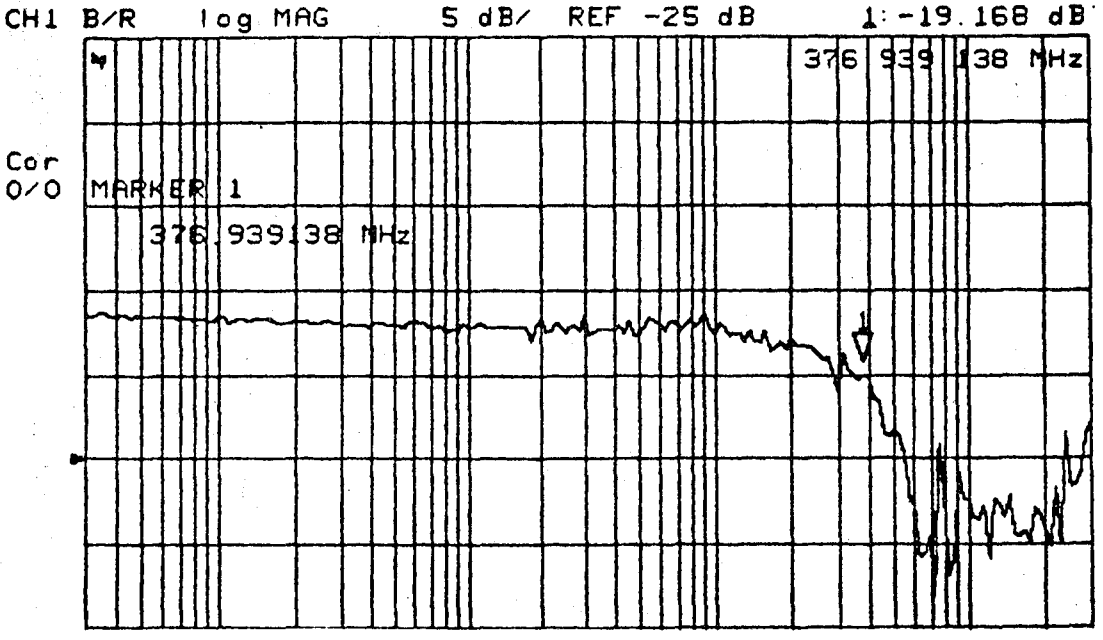

Ch. 9-10

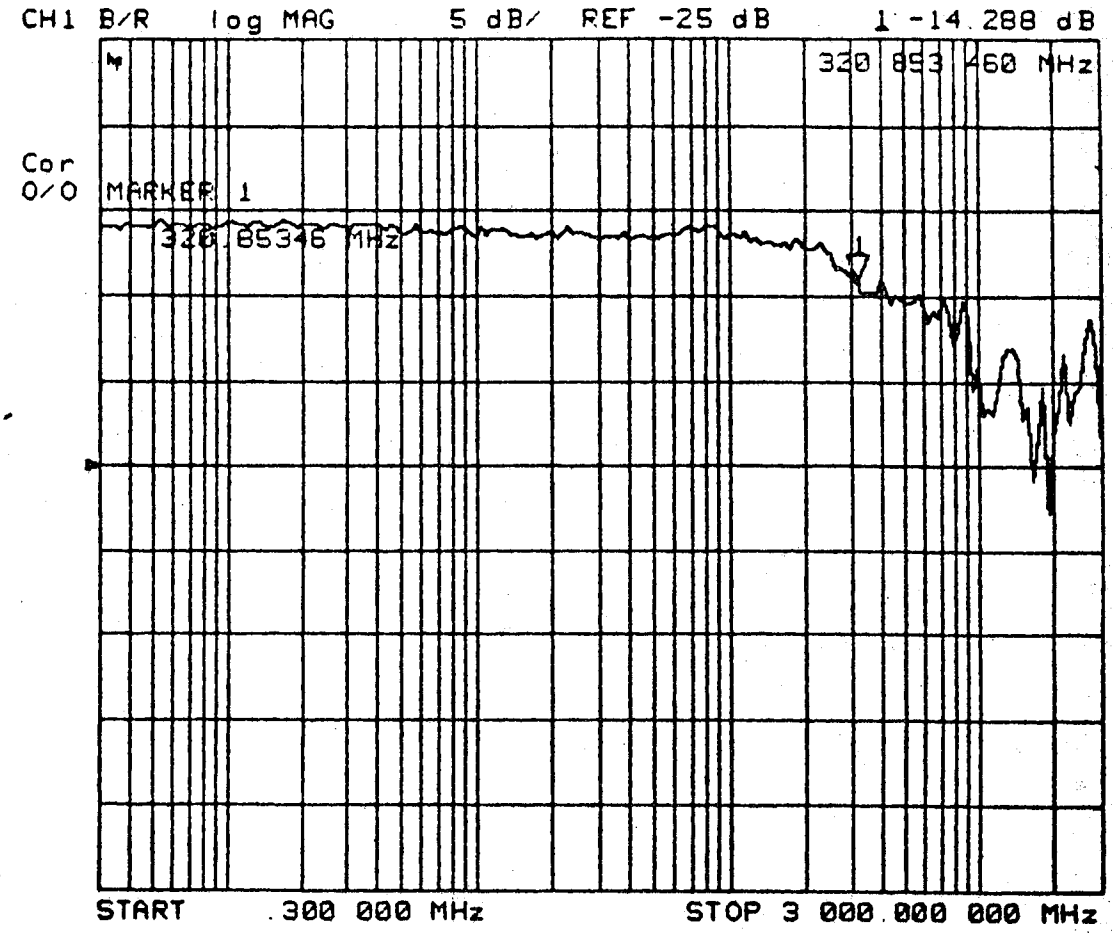

Ch.11-12